ISSN : 2349-6495(P) | 2456-1908 (O)

International Journal of Advanced Engineering Research and Science

(IJAERS)

An Open Access International Journal

Journal DOI: 10.22161/ijaers

Issue DOI: 10.22161/ijaers/3.11

AI PUBLICATIONS

Vol.- 3 | Issue - 11 | November , 2016

editor@ijaers.com | http://www.ijaers.com/

Editorial Board

Dr. Sambit Kumar Mishra
Specialization Database Management Systems
BE, ME, Ph.D,Professor, Computer Science Engineering
Gandhi Institute for Education and Technology, Baniatangi, Khordha, India

Dr. M. Venkata Ramana
Specialization in Nano Crystal Technology
Ph.D,Professor, Physics,Andhara Pradesh, INDIA

DR. C. M. Velu
Prof. & HOD, CSE, Datta Kala Group of Institutions, Pune, India

Dr. Rabindra Kayastha
Associate Professor, Department of Natural Sciences
School of Science, Kathmandu University, Nepal

Vol-3, Issue-11, November, 2016

International Journal of Advanced Engineering Research and Science (IJAERS) *[Vol-3, Issue-11, Nov- 2016]*
https://dx.doi.org/10.22161/ijaers/3.11.1 *ISSN: 2349-6495(P) | 2456-1908(O)*

Effect of Toxins (Microcystines, Shiga & Botulinum) on Liver Functions

Moghira Badar[1*], Qamar Mahmood K[1], Fatima Batool[2]

[1]Department of Environmental Management, National College of Business Administration and Economics, Lahore
[2]National Centre of Excellence in Molecular Biology, University of the Punjab, Lahore

Abstract— *Lfts (liver function tests) and Rfts (renal functions tests) values of patients show abnormalities and it is confirmed swelling of liver and poor filtration rate of kidneys. So, drinking water treatment is most needed.*

All the blood samples were taking under controlled environment to keeping the good quality and standards that support real data for final analysis. LFTs tests are taking by drawing blood samples from infected persons with the help of testing machines, it shows average value of ALT and SGOT is very high as 50 u/l and 53u/l that is not good sign for liver health due to high value of toxins in human blood stream which is confirmed by toxins medical laboratory tests. All these problems is mainly due to taking bio contaminated food and unsafe drinking water, so if we make assure the security and safety about our taking the food as essential component of life.

Keywords— LFTs, Toxins, Liver Functions, Blood sampling, Medical tests.

I. INTRODUCTION

Microcystins are 200 times more toxic and poison than cyanide metal. This toxin has structural variants include amino acid substitutions and alterations such as methylation and demethylation. Drinking water supplies contaminated with Cyanobacteria toxins is a main cause of a health hazard for human beings, domestic animals both large and small, and wildlife animals [1].

Pakistani population is the world's fastest increasing population and it may exceed to 180 million is observed by now; it is still growing with an alarming speed about 2.8% yearly. Current century gives a revolution for improvement in utilization of water and food. We must need to change our cultivation method and life living styles. Concurrently the water quality of underground and surface is poor, further it is deteriorating for the reason is unchecked disposal of untreated industrial and municipal wastes mix in natural sources. In this study, we are identifying the toxins in drinking water and blood and then removing from drinking water [2].

It is proved from study, the diffusion between activated carbon and toxins improve the taste and ordure. In order to test the effect of reducing raw water pH on the nature of the adsorption process value decreases. This increase in the adsorption capacity can be explained as toxins are predominately negatively charged; therefore, decreasing the pH values the negatively charged organic molecules more neutral. According to mechanism of reaction, it is less soluble the neutral molecule in water due to no charged on atoms or molecule, so increasing in pH values is very helpful to remove organic molecules from sample of drinking water [3].

The parameters like light, temperature and humidity are responsible for water quality as taste, natural and colour and their effects are showed the presence of organic matter in water reservoirs because these parameters increase with the dissociation and degradation characters of dissolved organic compound in drinking water such as toxins and other nitrogen based compounds [4].

Conversely, observations due to microcystins toxins from laboratory results presented the toxins which are created by the cyanobacteria specious as found slow growing. The major aspects in measuring for the removal of cyanobacteria toxin from water treatment which includes removing the soluble and suspended substance removes. Previous studied are showing the some like microcystins, botulinum toxins and shiga toxin resolvable in water [5].

The aim of this study is to detect the toxins in human blood samples and their harm effects on liver performing functions.

II. MATERIALS AND METHODS

Human Blood sampling

Collect the random human blood sampling from different places were with the frequency of samples (n= 116). All samples were collected by syringe in sterilized blood vessel used as container and blood sample 5 ml collected by volume and actual capacity of container was 5 ml. The temperature of the day when collect the samples was 16 ^{0}C.

Serums of samples were collected after mechanical centrifugation of the samples blood, and start the analysis of

https://dx.doi.org/10.22161/ijaers/3.11.1 *ISSN: 2349-6495(P) | 2456-1908(O)*

blood samples. It was used the Chemical reagent (in form kits) to determine concentrations of following parameters in the serum [6].

Microcystins Toxin Testing Method

The technique involved by the adding of 50 µL of negative control, each calibrator with each sample put in the wells and get 50 µL of microcystin with added assay diluent and was incubated for 30 minutes on a shaker. Next, added 100 µL of microcystins enzyme conjugate to each well and once again wells for 30 minutes were incubated, after then the wells four times with wash solution.

The step solution was added of substrate to each well and further for 30 minutes incubated. 100 µL of the stop solution was added to each well after incubation, the contents of the wells change into yellow and measured their optical density with Microplate Reader at 450 nm. The optical density values given by the reader and toxin concentration in the samples was calculated from the standard curve from the 3 Calibrators [7].

Testing Method of Botulinum Toxin

The procedure of testing is involved the following steps for investigating liquid samples for the identification of botulinum toxin, Dilution buffer of 50: 1L was added to all wells that hold a sample, Test sample of 50: L was added to the dilution buffer and incubated the plates for one hour at 25 ^{0}C temperature. Washed three times Plates with 200: 1L of ELISA washes buffer per Well. Detect antibody, was added of 100: L to each sample well and incubated the plates for one hour at 25 ^{0}C temperature [8].

Testing Method of Shiga Toxins

The concentration of residual Shiga toxins after heat treatment was determined by using ELISA, the Premier TM EHEC ELISA kit (Meridian Bioscience, Cincinnati, OH). Multi-point standard curves as well as positive and negative controls were performed to reduce variations among ELISA testing. The cut-off concentration according to the manufacturer's instructions was OD=0.18.

The Premier EHEC test kit utilizes monoclonal anti-Shiga toxin capture antibodies absorbed onto the bottom of micro wells. When testing, 100 µL samples were added to each well mixed thoroughly with the pipette and incubated at room temperature (RT) for 1 hourof the 96-well plates. Then Wells were washed according to manufacturer's instructions. Volumes of 100 µL of polyclonal anti-Shiga toxin antibodies provided by the kit were added into each well, mixed well as before, and incubated at RT for 30 min. Wells were washed again to remove unbound antibody. Aliquots of 100 µL of enzyme-conjugated anti-IgG polyclonal antibody was added into each well, mixed and incubated at RT for 30 min [9].

Liver functions Tests

Collected blood samples were homogenised by using the anticoagulant EDTA vial. Analysis the concentrations of blood parameters like, Protein, Alkaline phosphatase(ALP), Total Bilirubin, Direct bilirubin, Aspartate amino- transferase (AST), Alanine amino transferase (ALT), G-glutamyl transferase (GGT) [10].

III. RESULTS

Concentration of toxins in the blood

All the nations of world are very conscious on drinking water quality, so effective efforts in form of research and study make on this issue. E. coli related with Coliform family which is basic indicator of faecal contamination that also known as disease causing pathogen. Microbial quality is totally depending on presence of coliform group E. Coli. recognized as pathogenic microbes and their metabolise chemical known as toxins. In figure 1, it is clearly shown that all the toxins as microcystins, botulinum and shiga have high values in blood samples due to eating the contaminated food as well as drinking water linked with high absorption of toxins in blood samples.

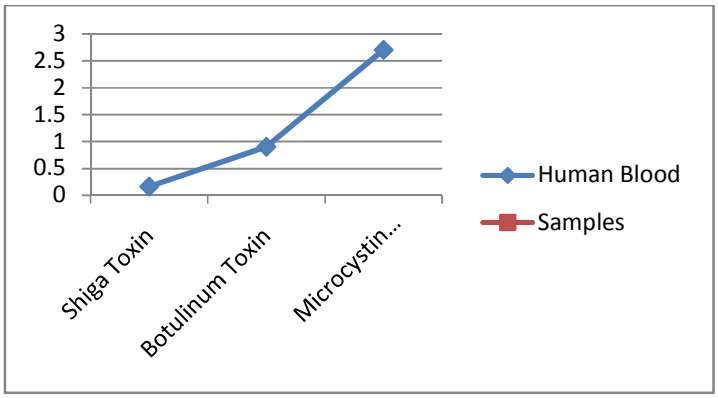

Fig.1: Chemical Analysis of Toxins in Blood (Humans) Samples

Effect of toxins on Liver Function Values

Liver damage situation is a very serious health issue across world due to drinking of bad quality water. Liver function tests are usually represent and recognized as the reliable indicator of liver performance of detoxification function. Inside the liver, enzymatic activity have been raised up, this is may be due to synthesis of enzymes, their low levels indicate that the enzymatic inhibition due to liver injury without specific regeneration. In figure-2, among liver enzymes, amylase GOT, GPT and ALT were elevated in the samples of human's blood, it was showing acute liver damage (hepatitis),

https://dx.doi.org/10.22161/ijaers/3.11.1 *ISSN: 2349-6495(P) | 2456-1908(O)*

while in samples of blood, all these enzymes were inhibited showing hypocondition or dysenzymia.

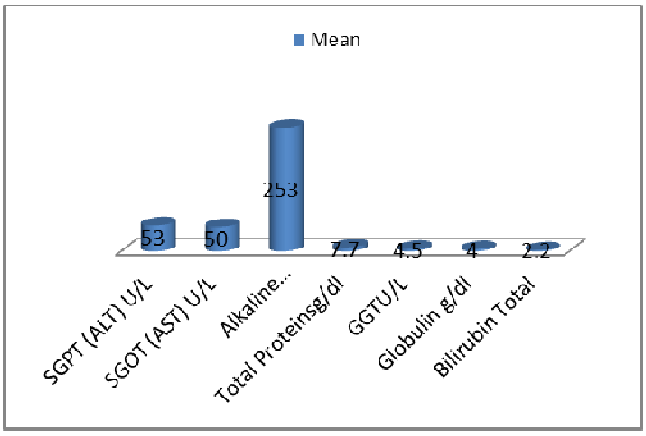

Fig.2: Live Function Clinical Test of Humans

Toxins accumulating within the blood were responsible for other end-organs being damaged. Some of these factors may be due to changes in the cellular component of blood, but many of these deleterious effects are due to changes in the humoral component of circulating blood. These toxins may arise either as a consequence of a failure of normal hepatic functions, or elsewhere in the body as an importance of simple liver disease. These toxic factors in the blood affect the function of many organ systems, such as the systemic and portal vasculature and the brain, as well as the liver itself. The exact nature of these toxins is unknown and may be different and multiple for each organ system damaged. Ammonia, aromatic amino-acids, tryptophan, indoles, mercaptans and endogenous benzodiazepines are implicated in the development of hepatic encephalopathy [11].

Effect of high values of liver functions on human health

Water sources treatment is only solution of these problems; in this case we use the coagulation process with ferric chloride solution of different doses. In this study, it has proved that microcystins are removed using the concentration of ferric chloride dose is 16 mg/l. Liver function tests were also played very important role to know the actual working positions of liver function, so values of Rfts indicated the abnormalities of liver in cows and buffaloes due to continues taking the microcystin toxins from water and food sources.

Results clear about amylase activity in the present investigation increased in both of samples of cows. Amylase is secreted by the exocrine region of pancreas in mammalians system by help of liver function. The increased activity may be due to pancreatitis or due to the damage of the amylase secretary cells inside body. There is also the possibility that greater amounts of amylase were secreted into the intestine, which causes the consequently enhanced starch digestion, and transferred itself to the degradation products into portal blood, and then into liver and hepatic cells through assimilation, which may also be caused for hyperglycemic response in animals.

IV. DISCUSSIONS

In developed countries water treatment and sanitation has removed the problem of diseases such as typhoid and cholera. These diseases, however, among other water related issues, remain a serious problem in developing countries. Modern water treatment processes control the spread of water related disease; remove numerous contaminants, such as organic chemicals and heavy metals, producing safe water. However the presence of pharmaceutical residues, disinfection by-products, and the possibility of disease causing agents as Cryptosporidium, which are unaffected by common water purification processes and so, need of new treatment technologies for this purposes. The single largest consumer issue affecting potable water under developing states is off-flavour. Off-flavour is caused by compounds in water that are known for their undesirable taste and odour characteristics. A survey conducted of more than 800 water usages in the America and Canada found the 16 % of utilities experience the serious taste and odour problems, spending approximately 4.5 % of their total budget for taste and odour control [12].

Whereas, prostanoids, inflammatory cytokines, nitric oxide and oxidative stress, are all considered to be important factors in the development of the haemodynamic and renal changes seen in liver failure. It is, however, the substances that are directly hepatotoxic that are particularly important in terms of recovery, as they may perpetuate liver injury invoking a downward spiral with further reduction in functional liver mass and increased toxin load. It is notable that many of the suggested toxins are insoluble in water and exist in the circulation bound to albumin [13].

Previous research and studies have been showing that one solution of treatment of drinking water is to measure the mass of activated carbon first and then put it into a prepared bottle, used as vessel. A thrilling bar put inside the bottle then it was sealed with cover of aluminium. On weighing machine, it was calculated the mass of activated carbon, bottle and stirring bar. Then 27 ml of ultra-pure water was added to each of bottle and boiled them for 3 minutes for remove air from the activated carbon bottle. After some time, cooling down the bottle to normal temperature and then it was measured total weigh difference after and before boiling process. To added the one litre of samples of different water and Then mass of the bottle calculated and recorded on data book, finally [14].

https://dx.doi.org/10.22161/ijaers/3.11.1 *ISSN: 2349-6495(P) | 2456-1908(O)*

Aluminium sulphate dosed at 20 mg/l without polymer addition removed about 80 percent of the toxicity from neurotoxic bloom of microcystins, Coagulation had an ability to eliminate the toxins in water samples in several studies. These studies tested the coagulant as Aluminium sulphate in different concentrations. Coagulation and clarification studies have had mixed results on cell lysis and the subsequent release of cyanobacterial algal toxins [1].

Nitrogen based biological compound inside samples of canal water can be detached by aluminium sulphate setting if the matter is based on organic compound a minor in quantity, Pietsch et al. (2001) initiate that the removal of nitrogenous matter is problematic to attain with simple coagulation in some cases and the nitrogen based compound are detached by microbial degradation and zonation processes [15, 16].

For this purpose, use the activated carbon filtering process is used in this research. It is achieved toxins removal by help with using the drinking water filtration process under filtered drinking water have normal values that given by WHO standards of drinking water guidelines.

V. CONCLUSIONS

In present study, it is investigate the toxins in drinking water samples from microbe's activities, very harmful health effect on humans and especially their liver functions disturb badly. Liver abscesses have a major economic and social impact on the health issues.

All these problems is mainly due to taking bio contaminated food and unsafe drinking water, so if we make assure the security and safety about our taking the food as essential component of life.

REFERENCES

[1] Abenavoli L, G Aviello, R Capasso, N Milic and F Capasso. Milk thistle for treatment of nonalcoholic fatty liver disease. Hepat Mon., vol. 11, pp. 173-177, 2011.

[2] Ayers, T, Williams, I. Outbreak Net Team: Electronic Foodborne Reporting System (eFORS) and National Outbreak Reporting System (NORS). Presented for the CDC Enteric Diseases Epidemiology Branch Program Plans. Atlanta, GA. (2008).

[3] Bakoyiannis, A., Delis, S., Triantopoulou, C. Dervenis, C. Rare cystic liver lesions: A diagnostic and managing challenge. Wbrld. J. Gastroenterol.,vol. 19(43), pp. 7603-7619, 2013.

[4] Bernuau J. Acute liver failure: avoidance of deleterious co-factors and early specific medical therapy for the liver are better than late intensive care for the brain (review). J. Hepatol., vol. 41, pp. 152-155, 2004.

[5] da Hora VP, Conceição FR, Dellagostin OA, Doolan DL. Non-toxic derivatives of LT as potent adjuvants. Vaccine, vol. 29, pp.1538-1544, 2011.

[6] de la cruz, A. Can we effectively degrade Microcystins? Implications on Human Health. Anti-Cancer Agents in Medical Chemistry, vol. 11, pp. 19-37, 2011.

[7] Ho, L., Lambling, P., Bustamante, H., Duker, P., Newcombe, G.. Application of powdered activated carbon for the adsorption of cylindrospermopsin and microcystin toxins from drinking water supplies. Water Res, vol. 9, pp. 2954–2964, 2011.

[8] Lehman, E.M. Seasonal occurrence and toxicity of Microcystis in impoundments of the Huron River, Michigan, USA. Water Res., vol. 4, pp. 795–802, 2007.

[9] Lequin, R. M. Enzyme immunoassay (EIA)/enzyme-linked immunosorbent assay (ELISA). Clin. Chem., vol. 51, pp. 2415-2418, 2005.

[10] Lucena, M.I.; García-Cortés, M.; Cueto, R.; Lopez-Duran, J.L. & Andrade, R.J. Assessment of drug-induced liver injury in clinical practice. Fundamental & Clinical Pharmacology , vol. 5, pp. 141-158, 2008.

[11] McKaigeny, C. Hepatic Abscess: Case report and review. Whst. J. Emerg. Med., vol.14, pp. 154-157, 2013.

[12] O'Connell, T.M. & Watkins, P.B. The application of metabolomics to predict druginduced liver injury. Clin. Pharmacol. Ther., vol. 3, pp. 394-399, 2010.

[13] Scott, P. Diagnosis and treatment of liver abscesses in cattle. Livest. Sci., vol. 18, pp. 20-23, 2013.

[14] Tehrani, A., Javanbakht, J., Hassan, M., Zamani, M., Rajabian, M., Akbari, H. Shafe, R. Histopathological and Bacteriological Study on Hepatic Abscesses of Herrik Sheep. J. Med. Microb. Diagn., vol. 1, pp. 115-119, 2012.

[15] Westrick, J., Szlag, D., Southwell, B. and Sinclair, J. A review of cyanobacteria and cyanotoxins removal/inactivation in drinking water treatment. Anal. Bioana.. Chem., vol. 397(11), pp. 1705-1714, 2010.

[16] Wu, W.W., Benjamin, M.M., Korshin, G.V. Effects of thermal treatment on halogenated disinfection by-products in drinking water. Water Res., vol. 15, pp. 3545–3550, 2001.

International Journal of Advanced Engineering Research and Science (IJAERS) *[Vol-3, Issue-11, Nov- 2016]*
https://dx.doi.org/10.22161/ijaers/3.11.2 *ISSN: 2349-6495(P) | 2456-1908(O)*

Microbiological Botulinum Toxins Removing From Drinking Water Sources by Treatment of Coagulation Process

M Badar[1*], Irshad Khokhar[1], Fatima Batool[2], Muhammad Idrees[3], Yasir Ch.[1]

[1]Department of Environmental Management, National College of Business Administration and Economics, Lahore
[2]Centre of Excellence in Molecular Biology, University of the Punjab, Lahore
[3]Departement of Computer Science & Engineering, University of Engineering and Technology, Lahore

Abstract— *Water is a very important nutrient and responsible to maintain good health as well as proper performing the body functions, Water can remove the harmful toxins from the body.*

Infective disease produced by pathogenic microbes like bacteria, parasites and viruses including their metabolites as toxins are the known as most common and common health risk which connected with unsafe drinking water. It is expected; around 1.1 billion people worldwide have to drink unsafe drinking water per day. More than 95 % of these deaths are possible in low-income countries, where numerous causes like malnutrition, poor hygiene and sanitation create the immune deficiencies and specially factor such as unsafe drinking of water strongly affected on it.

In the present study, C. Botulinum as bacterial specious and its related toxin botulinum toxins are detected in samples of ground water, water storage tanks and canal water but low values of toxins present in ground water sample and high values find in canal water sample.Coagulation process is used for removing the Botulinum toxins from drinking water source and giving the amazing results as show 92-97% toxins removes from drinking water samples by using the coagulant aluminium sulphate.

Keywords— Botulinum Toxin, Coagulation process, C. Botulinum, Removing toxin, Aluminium Sulphate.

I. INTRODUCTION

C. Botulinum was first discovered by E. van Ermengem in 1897 afterward his study on foodborne microbes and disease in Ellezelles, Belgium. Botulism is Foodborne microbe and found rare, but contaminated products with this may exposed to humans and animals. C. Botulism can produce a neuroparalytic illness causing by the contamination with it. Foodborne botulism can create an emergency of a medical and a public health and to avoiding this problem need effective messaging between clinicians and public health departments [1].

The types of C. Botulinum from A to G are different by only the antigenic characteristics found in the neurotoxins which they produced. C. Boulinum with Types A, B, E, and only F in rare cases found which cause illness in humans and animals. Especially C. Bolulinum with Types C and D cause illness in mammals and birds and type G are identified in 1970 which cause of infection in humans or animals [2].

The word of Botulism read from the language Latin as botulus, and its meanings is sausage. Botulism word was first time familiar in Europe and several cases were registered which caused by house fermented sausages. Historically importance, four different forms of botulism can observe, but depending on the mode of reaction of these toxins. Wound infection botulism is produce by c. botulinum that multiplies and then produce toxin in a contaminated wound of human or animals. Botulism is due to the harmful production of toxins by spores of C. Botulinum in the intestine, and Teen-ager or adult infected mostly [3, 4].

Botulism is a thoughtful and unusual, paralytic disease which caused by neurotoxins produced by the common bacterium specious as name Clostridium Botulinum, C. Botulinum found all over the world in samples of soil and ocean sediment. Usually, the bacterium can survive in the special environment as a resting spore. On the other hand, in low oxygen environments (anaerobic) such as in case of canned foods, intestinal tract, deep wounds and spores germination convert into active bacteria, then it multiply with passage of time and produce neurotoxin. C. Botulinum creates 8 types of different toxins (from A to H), which are known as the most strong toxins. Botulinum toxin is produced by Clostridium Botulinum which is a gram-positive anaerobic bacterium group. Clinical disease related to botulism can take place with ingestion of contaminated food and then settlement of bacterial growth inside the gastrointestinal tract. The infection

https://dx.doi.org/10.22161/ijaers/3.11.2 *ISSN: 2349-6495(P) | 2456-1908(O)*

due to c. botulinum as wound infection can also cause of spores transformation from person to person [5, 6].

Our study goal is to identify botulinum toxins in different samples and remove the toxins of botulinum species using coagulation method with economical ways.

II. MATERIALS AND METHODS

Area of Study

Sheikhupura is a city of Punjab, Pakistan which is located about 36 Km from Lahore. Sheikhupura lies 31° 42' 51.16 "N latitude and 73° 59' 3.49" E longitude. The city is well connected with its surrounding big urban centres like Faisalabad 94 Km, Sargodha 143 Km and Gujranwala 54 Km. Sheikhupura is also a railway junction. Importance of Sheikhupura city is due to its commercial zones and large number of industrial units which can contaminate water.

Ground water sampling

Random ground water samples were collected from different houses by water pump with power capacity 1 horse power and the frequency of samples (n= 116). In this area ground water 70 feet below from earth surface. All sample collect in sterilized PVC bottles. The bottles were filled up to 100 % of the volume capacity (1 L). The temperature was 20 ^{0}C at the time of sample collection [7].

Sampling from water storage tank

Random water samples were collected from different water storages tanks of houses with the depth of 0.5m and frequency of samples (n= 116). The average height of storage tanks was 7±0.9 feet and width 3±0.4 feet and the temperature of the day at sampling was 27 ^{0}C. All samples were collected in sterilized PVC bottles and were filled 100% of the volume capacity (1 L).

Canal water sampling

Random canal water samples were collected from different source points and the frequency of samples (n= 10). All samples were collected in sterilized PVC bottles which were filled 100 % of the volume capacity and actual capacity of the bottle was 1 L. The temperature of sampling day was 16 ^{0}C.

Analytical methods

Parameters like turbidity and colour were analysed on a spectrophotometer (Shumedzu 2011), according to the recommended procedure by the Standard Methods (APHA, 2005). pH was determined by using a pH digital meter (coloria 2011), operating under the manufacturer's methodology . Removal of toxins was examined by using the Utermöhl method (1958), which includes the sediment organisms counting on an especial chamber under an inverted microscope of good quality [1].

Isolation and Identification of C. Botulinum

Agar Base Media composition is used and media solution is prepared as the Suspension prepared by dissolving 37 grams media components in 500 ml ionized water and then heat it to its boiling state for complete mixed medium. Sterilize at 121°C by autoclaving at pressure 16 lbs at time 15 minutes and then keep the temperature from 50-55°C to avoid microbe's contamination, aseptically add sterile 50 ml of Egg Yolk as Emulsion. Allow mixing well and transferring into sterile Petri plates for microbial growth [7].

Incubated the Petri plates at 37 °C for the period of 24 hours. This process was repeated to other water samples for this test. Appears the colonies after incubation on the nutrient agar and number of positive (NP) samples recoded for this research. Final confirmation was made by biochemical reaction.

Confirmatory Biochemical Tests for C. Botulinum growth

Further confirmatory test for C. Botulinum growth in avoiding the any error in this research, conduct the biochemical and physical tests as below.

Catalase and in dole Tests

C. Boulinum confirmatory test method is involved standard test method as When bacterial growth mixed with reagent, if reaction give colour red to yellow, test will be positive and indicate presence of microbial growth [8].

Gram Staining

The microbial growth from media was spread and fixed on a clean glass slide and stained by putting the colour dye named as crystal violet on slid for 30 seconds and then washed it with distilled water. Then Gram's iodine was added on it for 10 seconds, after this, washed with tap water and uses decolourised as 95% Acetone alcohol solution and added finally safranin as secondary dye for 30 seconds. Final step was washed with tap water and dried in normal air. It is observed the slide under microscope with oil immersion objective of power 100X [9].

Aluminium Sulphate (AS)

Aluminium sulphate with a chemical formula $Al_2(SO_4)_3 \cdot 14H_2O$ was used in these experiments. Different composition of solutions (5 to 30mg/l) was prepared using AS as calculated amount of salt dissolved in deionised water. The flocculation/coagulation process under condition of rapid mixing regents and chemicals on (116 rpm) for mixing time (7 min) and for slow mixing use (27 rpm) and , time duration (11 min) [10].

Toxins Detection Methods

Only ELISA method is used for toxins analysis which still very useful and reliable in analytical testing field. The samples were analysed inside Chemical Bio-Tech laboratories, staffed with technicians and they skilled to handle the safely about botulinum toxin. Every day, fresh reagents were prepared

https://dx.doi.org/10.22161/ijaers/3.11.2 *ISSN: 2349-6495(P) | 2456-1908(O)*

from standards solutions in distilled water. Prepared the each sample was in its own container and labelled with identification number of sample that also noted in a laboratory record book with particulars of the sample preparation. Before analysis of each sample, the verification of staff recorded about the sample identification with number on a sample data sheet. After complete the analysis, sample results recorded on the sample data sheet. All test samples were three times repeated for analysis [11].

III. RESULTS

Microbe C. Botulinum detection and Toxins Analysis in drinking water samples

Toxins concentrations in the canal Water samples, water storage tanks samples and ground water samples were monitored using ELISA method which is very reliable for a detection toxin from microbes. To find the different concentrations of toxin level in different samples and there was seen that in canal water samples the toxins with very high values as Botulinum toxin (10.5±0.7) mg/l with range of 9-11.5 as shown in table-1. The toxins with very low values was observed in ground water samples as botulinum toxin (1.2±0.1) mg/l and in range 0.5-1.4, respectively as shown in tables 1&2.

Table.1: Detection of Microbes in Different Water Samples Analysis

Microbe	*Water Storage Tanks samples (%)*		*Ground Water samples (%)*		*Detection in Canal water Samples (%)*	
	Mean±S.D	*Rang*	*Mean±S.D*	*Rang*	*Mean±S.D*	*Rang*
C. Botulinum	*49±1.2*	*47-52*	*40±1.2*	*38-43*	*92±2*	*90-95*

Several factors contribute to the production the toxins like environmental condition and nutritional requirement, so C. botulinum can grow in surface water as faster and toxin botulinum produced quickly. Only microcystins toxin limit is 1 mg/l under the WHO in drinking water but other toxins like botulinum have no standard limit given in quality of drinking water. Water temperature varied from 11 to 20 ^{0}C, during our study due to extreme change in weather condition about 16 to 20 ^{0}C, such changes temperature are characteristic for this area. Table-2 was showed the concentration of Botulinum toxins found in different types of drinking water samples that depend on presence of microbe C. btulinum in quantity but these values of toxins are not in normal range.

Table.2: Water Analysis Data of different Samples

Sampling Type	Botulinum Toxin	
	Mean±S.D	Range
Canal water samples (mg/l)	10.5±0.7	9-11.5
Storage Tanks water samples (mg/l)	1.2±0.1	0.3-1.9
Ground Water samples (mg/l)	1.2±0.1	0.5-1.4

Effect of coagulant aluminium sulphate on Botulinum toxins removing

In **table-3**, could be seen that aluminium sulphate create good results to remove the toxins from canal water samples by using high dose of coagulant because canal water observed often time highly contaminated with carbon based dissolved solid like as microbes biomass and their metabolites as toxins. However, these organic materials have great capacity to be dissolved in water and make the source of contamination commonly in canal water.

Table.3: Data of Aluminium Sulphate as Coagulant Doses for Removing Toxins from Canal Water Samples

Coagulant Dose (mg/l)	Botulinum toxin(mg/l) (Actual value)		Botulinum toxin (mg/l) (after treatment)		Botulinum toxin after treatment (%)	
	Mean	Range	Mean	Range	Mean	Range
5	10.5	9-11.5	9	5-10	85.71	83-86
10	10.5	9-11.5	7	3-8.5	66.66	63-68
15	10.5	9-11.5	5	1-7	47.61	45-49
20	10.5	9-11.5	3	0.5-5	28.57	26-29
25	10.5	9-11.5	1	0.5-2	9.52	7-11

It is clearly seen in table-3 that value of Botulinum toxins had 1 % values with range 2-3 at AS dose 10 mg/l and 9.52 % values with range 7-11 respectively found at same coagulation dose 25 mg/l. it means that percentage of above given values show removal efficiency of different toxins by using the Aluminium Sulphate coagulation and further idea is created that need of high dose for proper coagulation process in canal water samples.

During sampling process, It was came into our notice that all the animals and some human use canal water as direct source of drinking and domestic purpose. The high level of confederation of toxin in canal water is the basically source of disease of liver, skin and disorder stomach function for equally both animals and humans as well.

https://dx.doi.org/10.22161/ijaers/3.11.2 *ISSN: 2349-6495(P) | 2456-1908(O)*

Gradually used the aluminium sulphate in different dose for removing of toxins because here objective was to find optimum dose value for treatment of water to drinking purpose. Increase the dose of aluminium sulphate step wise is the chance to minimise error in these batch experiments. Actually, in under developing countries facing the problems related with water treatment is badly effected due to mismanagement of handling the chemical dose in coagulation process which may show un- effected results on water treatment properly and appears the toxic effects on public health by drinking.

In general, organic molecules as toxins removed 95-97% in these results with treatment of coagulant aluminium sulphate using the different dose that depend on concentration of toxins in drinking water as seen in tables (3,4&5) in different Samples.

Table.4: Data of Aluminium Sulphate as Coagulant Doses for Removing Toxins from Storage Tank Water Samples

Coagulant Dose (AS) (mg/l)	Botulinum toxin(mg/l) (Actual value)		Botulinum toxin (mg/l) after treatment		Botulinum toxin after treatment (%)	
	Mean	Range	Mean	Range	Mean	Range
2	1.2	0.3-1.9	1.1	0.8-1.5	91.66	89-93
4	1.2	0.3-1.9	0.9	0.6-1.2	75	74-76
6	1.2	0.3-1.9	0.7	0.5-0.9	58.33	56-60
8	1.2	0.3-1.9	0.2	0.3-0.5	16.66	14-18
10	1.2	0.3-1.9	0.1	0.1-0.2	2.5	2-3

In table-5, it had significantly observed the low values of toxins seen in ground water drinking samples and these values were much correlated with table-4 because ground water stored in water storage tanks.

Table.5: Data of Aluminium Sulphate as Coagulant Doses for Removing Toxins from Ground water samples

Coagulant Dose (mg/l)	Botulinum toxin(mg/l) (Actual value)		Botulinum toxin (mg/l) after treatment		Botulinum after treatment (%)	
	Mean	Range	Mean	Range	Mean	Range
1	1	0.5-1.2	0.9	0.5-1.1	90	89-92
1.5	1	0.5-1.2	0.7	0.4-0.9	70	68-72
2	1	0.5-1.2	0.5	0.3-0.7	50	47-53
2.5	1	0.5-1.2	0.2	0.1-0.4	20	18-22
3	1	0.5-1.2	0.0	0-0.2	1	0.5-1.7

The greatest toxins reduction was observed in the water storage tanks samples and ground water samples, where 95.0 % and 97.0 % toxins removal (figure 1,2&3) were found with aluminium sulphate (4 to10 mg/l) by concentration. Even uses of Aluminium sulphate with Lower dosages effective for the destabilization of toxins and other organic materials because of amino groups in the toxins have high charge density.

Figures (1, 2&3) were gave a critical picture in which this research came on one point that hazards toxins in drinking water sources were able to remove using the different chemical treatment process but aluminium sulphate dosing could be applied in control range for getting the maximum removing efficiency. And dosing of aluminium sulphate depends on nature of toxins concentration in different types of drinking water sample.

The treated water was observed as lowest values in the canal water as (0.7-0.8 mg/l), water storage tanks as 0.5-0.21 mg/l, ground water as 0.31-0.1 mg/l previous up and low values of treated water as seen in tables (3,4 & 5). The removal of dissolved organic carbon as toxin and other organic matter was increased with the removal of turbidity and colour and it is reported the presence of toxins and dissolved organic carbon can be removed effectively with treated the aluminium sulphate as a coagulant in high concentration.

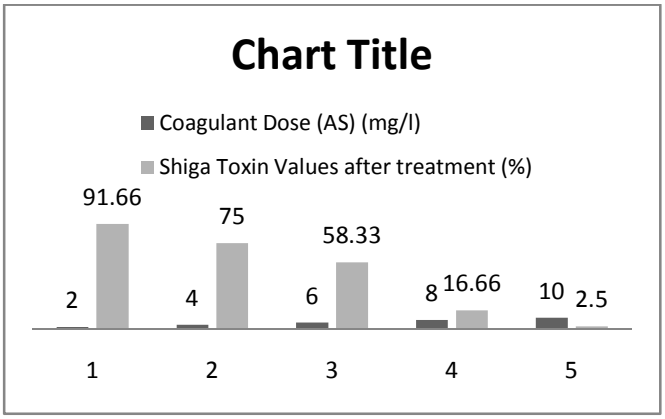

Fig.1: The graph shows the different dose effect on removing toxins in samples of drinking water storage tank

Given the results in tables (3,4 & 5) indicate that remove of toxins with organic matter of low molecular weight depends on the coagulant concentration and need to use this strong

https://dx.doi.org/10.22161/ijaers/3.11.2 *ISSN: 2349-6495(P) | 2456-1908(O)*

coagulant for canal water treatment for drinking purposes. The organic compound maximum removals observed in the samples of canal, ground water and water storage tanks samples waters with low values of Botulinum as shown in figure 1, 2 & 3 and it is also reported that the removal efficiency of coagulant depend on its molecular weight.

The results in tables (1&2) showed the presence of bacterial C. Botulinum and toxins was noted higher in canal water as compare to water storage tank and ground water samples. So, detection of bacterial group in a large number implies that the contaminated drinking water may be responsible for increasing number of water borne diseases in the country. It is evident from the study that water quality further deteriorated at the consumer level [14].

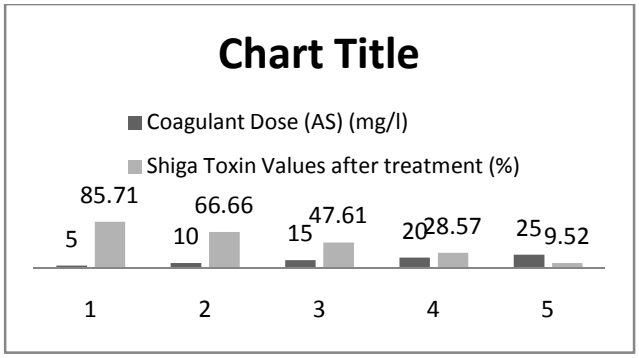

Fig.2: The graph shows the different dose effect on removing toxins in samples of Canal water

After the coagulation treatment with aluminium sulphate with high dose, the toxin decreased about 0.8 mg/l in most all samples of the treated water. Figure 2&3 showed that the drinking water is fusible is useful for drinking and other domestic uses.

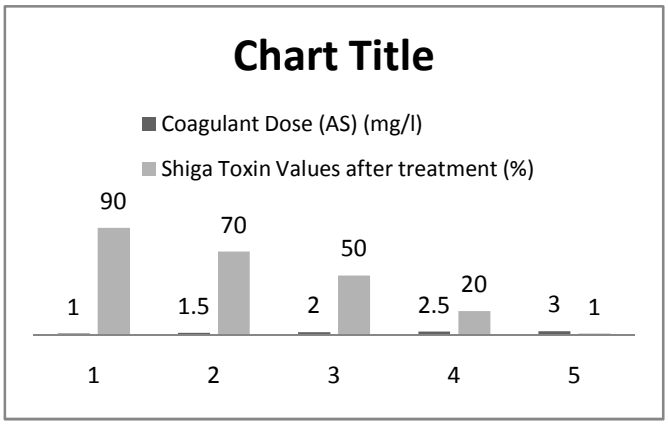

Fig.3: The graph shows the different dose effect on removing toxins in ground water sample

This is also formation in literature that by-products chlorinated water likes as trihalomethanes therefore will be less but organic matter mostly found in non-humic form with low weight.

IV. DISCUSSIONS

Identification of C. botulinum in water samples from area of city Sheikhupura was not thinkable due to non-professional way to control the quality of drinking water. Physical condition of temperature, light and humidity is very effective on producing water borne pathogens and their metabolites toxins. In the study, the pathogenic Microbe C Boulinum in samples of potable water is relative to sources of contamination [12, 13].

In the present study, these results had showed some similarities observed as in under developing countries like rural area of Pakistan has not correct quality of drinking sources of water for domestic purposes. Same results derived as given by the study's results from Brooks *et al*. (2011), it reported that in most of the developing countries, the quality of drinking water very not good as find some bacterial specious as per 100 ml of potable water used in domestic purpose. The recommend drinking water values of all limits under WHO guidelines is 100 ml per sample for detecting the total coliform group [15].

Toxins removes from drinking water samples by using the coagulant water treatment and boiling is also give more than 95% result for toxins removing. The diseases i.e. Diarrhoea, Dysentery, Gastroenteritis, Typhoid fever and Cholera and other water related nosocomial infection in health care setting may be the result of consumption of such polluted water [16].

The spores due to C. Botulinum, present in soil and then germinate for the produce of toxins and it caused by injecting the drugs that are contaminated by spores. Wound botulism is very common form in the UK and There have 100 clinical cases diagnosed of wound botulism from 2002 to 2007, but All related cases are illegal injecting drugs [17].

Infected injection is one cause of accidental botulism in pharmaceutical preparations may cause of botulinum neurotoxin, Such as four cases registered in December 2004 in state of Florida, cosmetic injection with contaminated with botulinum toxin that was not allowed for human purposes. It is not cases reported in the UK, but Inhalation of botulism has confirmed as three cases reported by veterinary technicians in Germany in 1962. C. boulinum toxin is a high possible route for releasing. Botulism due to Water borne may also be produce by ingestion of toxin. Accidental inhalation botulism, three cases were registered [18].

https://dx.doi.org/10.22161/ijaers/3.11.2 *ISSN: 2349-6495(P) | 2456-1908(O)*

This group is belong to bedrail specious and produce the Botulinum toxins, Our findings reveal the presence of C. Botulinumin 67% in drinking water samples collected from water storage tanks and 45 % detect in ground water in this study as given in table-1. The C. Botulinum and its toxins represented as faecal pollution of potable water and this is also an indicator organism as pathogenic if detected in raw sea foodstuff and any other foods. C. Botulinum denotes asrisk alarm of public health and C. Botulinum knows as pathogenic bacterium [19].

In case when the long-time abdominal infection and catheterization of bladder toxicities feeling is already reported due to producing C. Botulinum and their toxin. The isolation rate of C. Botulinums was significantly greater in summer months than in winter months in drinking water all samples from khanpur rural area in city sheikhupura, respectively. Samples of the study area were contaminated with C. Botulinum during three successive study years and displayed some toxicity level in blood samples as given in table-1. The always occurrence of organism and their toxins show the unhygienic condition of quality of drinking water in specific region. Both anthropogenic and from animals are the main source of contamination of this microorganisms due to the drinking water reservoirs was remained unprotect and open and facing activities of animals and human. Moreover, the chlorine treatment of potable water for domestic purposes was insufficient before the proper chlorine treatment [20, 21].

Botulinum toxins producing rate depend on C. Botulinum bacteria, high concentration of botulinum toxins seen in canal water as see table-2. Botulinum toxins effected on paralysis disease directly both male and female, and this was seen during interviews before sampling [22].

V. CONCLUSION

Almost the world's population now presently facing the deficiencies of potable water with better quality, with using of correct and applicable technology or water purifications above methods for domestic water are a wonder full solution of these problems with very low prices.

The removal of toxins inform of organic matter was manage to minimise the toxicity in the experimental steps from drinking water samples. Coagulation experiments conducted to know actual effective and improved dose used to optimise for coagulation process for maximum removal of toxins from drinking water. Selected aluminium sulphate coagulation dosing (10mg-27mg) for treating the contaminated drinking water from different samples canal water, water storage tanks and ground water, this dose does not causes of toxicity to human and animal health as the aluminium residues present in drinking water supplies.

Hygiene information is very important for better utilization of safe water drinking. Moreover, the procedure involved for drinking water management system and how to store at the domestic level, it is need to increase knowledge of individual and community about the awareness of water hygiene and public health.

REFERENCES

[1] Brooks C, E, Clarke H, J, Finlay D, A, McConnel Graham D, A, Ball H, J. Culture enrichment assists the diagnosis of cattle botulism by a monoclonal antibody based sandwich ELISA. Veterinary Microbiology, vol. 144, pp. 226-230, 2010.

[2] Brooks C, E, Clarke H, J, Graham D, A, Ball H, J. Diagnosis of botulism types C and D in cattle by a monoclonal antibody-based sandwich ELISA. Veterinary Record, vol. 30, pp. 168-174, 2011.

[3] Brooks J, T, Sowers E, G, Wells J, G, Greene K, D, Griffin P, M, Hoekstra R, M, Strockbine N, A. Non-O157 Shiga toxin-producing Escherichia coli infections in the United States, 1983-2002. The Journal of Infectious Diseases, vol. 192(8), pp. 1422-1429, 2005.

[4] CDC. Preliminary Food Net Data on the Incidence of Infection with Pathogens Transmitted Commonly Through Food---10 States, 2007. Morbidity and Mortality Weekly Report, Centres for Disease Control and Prevention, pp. 366-370, 2008.

[5] da Hora VP, Conceição FR, Dellagostin OA, Doolan DL. Non-toxic derivatives of LT as potent adjuvants. Vaccine, vol. 29, pp.1538-1544, 2011.

[6] Eisenberg D, J, Soller R, Sakaji A, Olivieri. A methodology to evaluate water and wastewater treatment plant reliability. Water Science and Technology, vol. 43, pp. 91–99, 2001.

[7] EPA, Regulations 2007 A handbook on the Implementation of the Regulations for Water Service Authorities for Public Water Supplies, (2010); European Communities (Drinking Water, No. 2)

[8] Evans J, Knight H, I, Smith A, W, Pearce M, C, Hall M, Foster G, Low J, C, Gunn G, J, Cefixime-tellurite rhamnose MacConkey agar for isolation of Vero cytotoxin-producing Escherichia coli serogroup O26 from Scottish cattle and sheep faeces. Letters Applied Microbiology, vol. 47(3), pp. 148-152, 2008.

[9] Ho¨rman A, R, Rimhanen-Finne L, Maunula C, von Bonsdorff J, Rapala K, Lahti M-L, Ha¨nninen.

https://dx.doi.org/10.22161/ijaers/3.11.2 *ISSN: 2349-6495(P) | 2456-1908(O)*

Evaluation of the purification capacity of nine portable, small-scale water purification devices. Water Science and Technology, vol. 50, pp. 179–183, 2004.

[10] Hoeger S, J, D, R, Dietrich B, C, Hitzfeld. Effect of ozonation on the removal of cyanobacterial toxins during drinking water treatment. Environmental Health Perspective, vol. 110, pp. 1127–1132, 2002.

[11] Josko D. Botulin toxin: a weapon in terrorism. Clinical Laboratory Science, vol. 17, pp. 30–34, 2004.

[12] Khan A, S, D, L, Swerdlow D, D. Juranek. Precautions against biological and chemical terrorism directed at food and water supplies. Public Health Reports, vol. 116. pp. 3–14, 2001.

[13] Mukul K, K, M, Atul.. Water and Sanitation in South Asia in the Context of the Millennium Development Goals. South Asia Economic Journal, vol. 6, pp. 99–115, 2005.

[14] Nkurunziza T, Nduwayezu J, B, Banadda E, N, Nhapi I. The effect of turbidity levels and concentration on the effectiveness of coagulation in water treatment. Water Science and Technology, vol. 59(8), pp. 1551-1558, 2009.

[15] Rapala J, K, Lahti L, A, Ra¨sa¨nen A, L. Esala, S. I. Niemela¨, and K. Sivonen.. Endotoxins associated with cyanobacteria and their removal during drinking water treatment. Water Res., vol. 36, pp. 2627–2635, 2002.

[16] Lequin R, M. Enzyme immunoassay (EIA)/enzyme-linked immunosorbent assay (ELISA). Clinical Chemistry, vol. 51, pp. 2415-2418, 2005.

[17] De Jong A, E, Rombouts F, M, Beumer R, R. Effect of cooling on Clostridium perfringens in pea soup. Journal of Food Protection, vol. 67(2), pp. 352-6, 2004.

[18] Carlin F, Broussolle V, Perelle S, Litman S, Fach P. Prevalence of Clostridium botulinum in food raw materials used in REPFEDs manufactured in France. International Journal of Food Microbiology, vol. 91(2), pp. 141-5, 2004.

[19] Andersen K.G, Hansen T, B, Knochel S. Growth of heat-treated enterotoxin-positive Clostridium perfringens and the implications for safe cooling rates. Journal of Food Protective, vol. 67(1), pp. 83-9, 2004.

[20] Whitby M, A, C, Street T, A, Ruff F, Fenner. Biological agents as weapons 1: smallpox and botulism. Medical Journal of Australia, vol. 176, pp. 431–433, 2002.

[21] Singh A, Ghosh S & Pankaj S. Water quality management of a stretch of river Yamuna: An interactive fuzzy multi-objective approach. Water Resources Management, vol..21, pp. 515 – 532, 2007.

International Journal of Advanced Engineering Research and Science (IJAERS) *[Vol-3, Issue-11, Nov- 2016]*
https://dx.doi.org/10.22161/ijaers/3.11.3 *ISSN: 2349-6495(P) | 2456-1908(O)*

Design and Thermal Analysis of Segmental baffle and Helical baffle in Shell and Tube Heat Exchangers using Kern method

Y. Aruna Prasanthi

M.Tech Student, Mechanical Engineering, Vishveshwarya Institute of Technology, Dadri, UP,India

Abstract— *Shell and Tube Heat exchangers are the most common type of heat exchanger widely used in oil refineries, automobiles, aerospace applications because it suits for high pressure applications. An effort is made in this paper to design Shell and Tube Double Pass Heat Exchanger with helical baffle and comparing with segmental baffle using kern method. The helixangle of baffle is varying from 0 to 50 degrees .The paper also consists of thermal analysis of a heat exchanger with helical baffles using the Kern method, which has been modified to approximate results for different helical angles. The result obtained shows us a clear idea that the Overall heat coefficient is maximum in helix changer as compared to segmental baffle. The pressure drop decreases with the increase in helix angle. Helix angle of 6 degree has better heat transfer than the one with an angle of 18 degree as it expenses pumping cost.*

Keywords— Kern method, helical baffle heat exchanger, helix angle, heat transfer coefficient, pressure drop, shell and tube heat exchanger.

I. INTRODUCTION

Generation of Motive Power was the Mother of Heat Exchanger Invention. The role of heat exchanger is to serve in a straight forward manner i.e. controlling the system's temperature by adding or removing the thermal energy. In other words, a heat exchanger is a device in which heat transfer from one fluid to another fluid occurs. The heat transfer device, used since the dawn of civilization, is a simple boiler for preparation of food, placed above an open fire. A good Heat exchanger is a true Mediator. It mediates the process by doing the action called heat transfer. The elementary steam boiler is considered as the first heat exchanger. There are different types of heat exchangers which are classified on the basis of nature of heat exchange process, relative direction of fluid motion, design and constructional features and physical state of fluids. Heat exchangers being one of the most important heat & mass transfer apparatus in industries like oil refining, chemical engineering, electric power generation etc. are designed with preciseness for optimum performance and long service life.

A. Shell and Tube Heat Exchanger:

Highest Thermal performance is the key factor determining the efficiency of any shell and Tube Heat exchanger [1]. Shell and Tube Heat Exchanger (STHE) consists bundle of tubes enclosed with in cylindrical shell pass through the tubes and second fluid flows between the tube and shells. The basic components of a shell and tube heat exchangers are tubes, tube sheets, shell and shell Nozzles, tube side channels and nozzles, channel covers, pass divider, baffles etc. Most commonly used STHE have large heat transfer surface area-to-volume ratios to provide high heat transfer efficiency in comparison with others. Shell and tube heat exchangers with segmental baffles have low heat transfer co-efficient due to the segmental baffle arrangement causing high leakage flow by passing through the heat transfer surface and high pressure drop that causes a big problem for industries as the pumping costs increases.

B. Developments in Shell and Tube Heat exchangers:

Shell-and-tube heat exchangers (STHXs) are widely used in many industrial areas, such as power plant, chemical engineering, petroleum refining, and food processing, etc. The developments for shell and tube exchangers focus on better conversion of pressure drop into heat transfer i.e. higher Heat transfer co-efficient to Pressure drop ratio, by improving the conventional baffle design. With single segmental baffles, most of the overall pressure drop is wasted in changing the direction of flow. This kind of baffle arrangement also leads to more grievous undesirable effects such as dead spots or zones of recirculation which can cause increased fouling, high leakage flow that bypasses the heat transfer surface giving rise to lesser heat transfer co-efficient, and large cross flow. The cross flow not only reduces the mean temperature difference but can also cause potentially damaging tube vibration. To overcome the

https://dx.doi.org/10.22161/ijaers/3.11.3 *ISSN: 2349-6495(P) | 2456-1908(O)*

above-mentioned drawbacks of the conventional segmental baffle, a number of improvements or structures were proposed to obtain higher heat transfer coefficient, low possibility of tube vibration, and reduced fouling factor with a mild increase in pumping power. The improvement process includes use various types of baffles such as deflector baffles, disk-and-donut configura- tion, spacing-optimized baffles (Mukherjee, 1992; Saffar-Avval and Damangir, 1995; Li and Kottke, 1998; Stehlik and Wadekar, 2002; Bell, 2004; Soltan et al., 2004). While maintaining a reasonable pres- sure drop across the heat exchangers, the principal shortcomings of the conventional segmental baffle still remain in above-mentioned improvements. Further improvement is to adopt a new type of baffle, called helical baffle, which is the major concern of the present paper. This type of baffle was first proposed by Lutcha and Nemcansky (1990) and then enhanced by Stehlik et al. (1994) and Kral et al. (1996).

C. Helical baffle Heat Exchanger: The baffles are of primary importance in improving mixing levels and consequently enhancing heat transfer of shell-and-tube heat exchangers. However, the segmental baffles have some adverse effects such as large back mixing, fouling, high leakage flow, and large cross flow, but the main shortcomings of segmental baffle design remain [5]

Compared to the conventional segmental baffled shell and tube exchanger Helix changer offers the following general advantages. [6]

1. Increased heat transfer rate/ pressure drop ratio.
2. Reduced bypass effects.
3. Reduced shell side fouling.
4. Prevention of flow induced vibration.
5. Reduced maintenance

Research on the helix changer has forced on two principle areas.

1. Hydrodynamic studies and experimentation on the shell side of the Heat Exchanger
2. Heat transfer co-efficient and pressure drop studies on small scale and full industrial scale equipment.

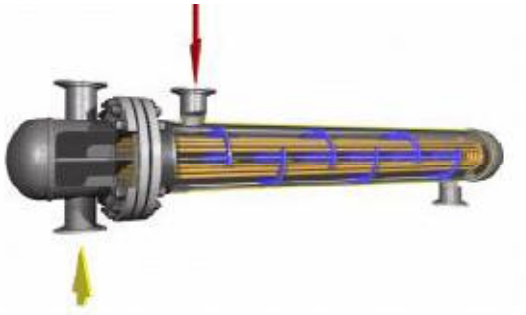

Fig.1: Helical baffle shell and tube Heat Exchanger

D. Kern Method

The first attempt is to provide methods for calculating shell-side pressure drop and heat transfer coefficient were those in which correlations were based on experimental data for typical heat exchangers. One of these methods is the well-known Kern method, which was an attempt to correlate data for standard exchangers by a simple equation analogous to equations for flow in Tubes. However, this method is restricted to a fixed baffle cut (25%) and cannot adequately account for baffle-to-shell and tube-to-baffle leakages. However, the Kern equation is not particularly accurate; it does allow a very simple and rapid calculation of shell-side coefficients and pressure drop to be carried out and has been successfully used since its inception.

E. Literature Review: Lutcha and Nemcansy upon investigation of the flow field patterns generated by various helix angles used in helical baffle geometry found that the flow patterns obtained in their study are similar to plug flow condition which is expected to decline pressure at shell side and increase heat transfer process significantly. Stehlik et al studied the effect of optimized segmental baffles and helical baffles in heat exchanger based on Bell-Delaware method and demonstrated the heat transfer and pressure decline correction factors for a heat exchanger.

Gang yong Lei et al [1] have showed the effects of baffle inclination angle on flow and heat transfer of a heat exchanger with helical baffles, where the helical baffles are separated into inner and outer parts along the radial direction of the shell. While both the inner and outer helical baffles baffle the flow consistently, smoothly and gently, and direct flow in a helical fashion so as to increase heat transfer rate and decrease pressure drop and impact vibrations, the outer helical baffle becomes easier to manufacture due to its relatively large diameter of inner edge.

Kral et al (1996) discussed the performance heat exchangers with helical baffles based on test results of various baffles geometries. A comparison between the test data of shell side heat transfer coefficient versus shell-side pressure drop was provided for five helical baffles and one segmental baffle measured from a water–water heat exchanger. A gain the case of 40^0 helix angle behaved the best. Wang (2002) measured the flow field in STHXs with helical baffles using laser Doppler anemometry. He pointed out that the optimum helix inclination angle depends on the Reynolds number of the working fluid on the shell side of the heat exchanger. Dr.B.Jayachandriah et al compared the segmental baffle with the helical baffle and found that the effects of helix angles on pressure drop are small when helix angle greater

https://dx.doi.org/10.22161/ijaers/3.11.3 *ISSN: 2349-6495(P) | 2456-1908(O)*

than 18 degree. Shinde et al, [6] has done analyses the conventional segmental baffle heat exchanger by using the modified formulas of Kern method with varied shell side flow rates. He evaluated form his results High Heat Transfer Co-efficient and lower pressure drop are more effectively obtained in a Helix changer. The flow pattern in the shell side of the continuous helical baffle heat exchanger is rotational & helical due to the geometry of continuous helical baffles results in significant increase in heat transfer coefficient.

II. OBJECTIVE OF THE PAPER

This paper contains comparison of helical baffle heat exchanger with segmental baffles. The Main objective of this paper is to show that the helical baffle inside the STHE has greater heat transfer coefficient and can be operated with lower pressure than the segmental baffle.

III. DATA COLLECTION

Table.1: Fluid properties

Property	Symbol	Unit	Cold water (Tube)	Hot Water (Shell)
Specific heat	C_p	KJ/Kg.K	4.178	4.179
Thermal Conductivity	K	w/m k	0.608	0.618
Viscosity	μ	Kg/m.sec	9.040×10^{-4}	7.74×10^{-4}
Prandtls number	Pr	-	6.11	5.31
Density	ρ	Kg/m^3	1000	1000

Table.2: Geometrical parameters-Shell Side

S.NO	DESCRIPTION	UNIT	VALUE
1.	No. of Passes	-	2
2.	Shell inner Diameter , D_i	m	0.387
3.	Shell outer Diameter, D_o	m	
4.	Tube inner diameter, d_i	m	0.0254
5.	Tube outer diameter, d_o	m	0.0220
6.	Number of tubes N_t	-	40
7.	Tube pitch (Triangular) P_t	m	0.031
8.	Baffle inclination angle θ	Deg	0 to 30
9.	Baffle spacing B	m	0.2322
10.	Baffle cut	-	25%
11.	Mean Bulk Temperature	Deg	31.6
12.	Tube length, l	m	6

Table.3: Geometrical parameters-Tube Side

S.NO	Quantity	Symbol	Value
1.	Tube side fluid		Water
2.	Tube side mass flow rate	$\dot{m}_t$	35.28 Kg/sec

https://dx.doi.org/10.22161/ijaers/3.11.3 *ISSN: 2349-6495(P) | 2456-1908(O)*

3.	Tube outer diameter	d_o	0.0254 m
4.	Tube thickness	-	0.00124 m
5.	Number Tubes	N_t	41
6.	Mean Bulk Temperature	MBT	25.3

IV. MATHEMATICAL ANALYSIS

A. Thermal Analysis of Segmental Baffle

1. Tube Clearance (C)

$$C = P_t - d_{ot}$$

= 0.0238 – 0.0190

= 0.00475m

2. Bundle Cross-flow Area (AS)

$$A_s = (D_{is} \cdot C \cdot B) / P_t$$

= (0.038 · 0.023 · 0.304)/ 0.023

= 0.0235 m^2

3. Equivalent Diameter (D_e)

$$D_e = 4\left|(p_t^2\sqrt{3}/4) - (d_o^2 \cdot \Pi/8)\right| - [\Pi \cdot d_0/2]$$

=4[(0.0238^2.0.433)-(0.019^2 .0.392)]-0.029

=0.0131 m

4. Maximum Velocity (V_{max})

V_{max}= m_s /ρ.A

=0.187 m/sec

5. Reynolds's number (Re)

Re=ρ .V_{max}. D_e /μ

=1000. 0.187. 0.0131/(7.74×10$^{-4)}$

=3163.76

6. Prandtl Number Pr = $\mu_s C_p / k_s$

=5.23

7.Heat Transfer coefficient (h_s)

h_s= (0.36.K_s .Re$^{0.55}$.Pr$^{0.99}$)/D_e

= (0.36 . 0.6181 . 3163.76$^{0.55}$ .5.23$^{0.99}$)/D_e

=7353.91 W/m^2k

8. Number of Baffles (N_b)

N_b= L/B

=6/0.3048

=19.68

= approx 20

9. Pressure Drop (ΔP_s)

ΔP_s= [f_s.G_s^2.(N_b+1) D_s]/2ρDeϕ$_s$

=0.384.937.02^2.(20+1).0.387/(2 . 1000 .0.0131 .1)

=104.58 Kpa

B. Thermal Analysis of Helical Baffle Heat Exchanger

1. Tube Clearance (C)

$$C = P_t - d_{ot}$$

= 0.0238 – 0.0190

= 0.00475m

2. Baffle spacing (L_b)

L_b=Π .D_{is} .Tanϕ

=Π.0.384.Tan (18^0)

=0.3919

2. Bundle Cross-flow Area (AS)

$$A_s = (D_{is} \cdot C \cdot L_b) / P_t$$

= (0.038 · 0.0047 · 0.3919)/ 0.0238

= 0.030 m^2

3. Equivalent Diameter (D_e)

$$D_e = 4\left|(p_t^2\sqrt{3}/4) - (d_o^2 \cdot \Pi/8)\right| - [\Pi \cdot d_0/2]$$

=4[(0.0238^2.0.433)-(0.019^2 .0.392)]-0.029

=0.0131 m

4. Shell Side Mass Velocity (Gs)

Gs= m_s / A_s

=22.02/0.030

=734 Kg/m^2.sec

5. Reynolds's number (Re)

Re=D_e.Gs/μ_s

= 0.0131.734 /(7.74×10$^{-4)}$

=12422.99

6. Prandtl Number Pr = $\mu_s C_p / k_s$

=5.23

7.Heat Transfer coefficient (h_s)

h_s= (0.36.K_s .Re$^{0.55}$.Pr$^{0.99}$)/D_e

= (0.36. 0.6181. (12422.99)$^{0.55}$. 5.23$^{0.99}$)/D_e

=15603.82 W/m^2k

8. Number of Baffles (N_b)

N_b= L/B

=6/0.3919

=15.3

= approx 15

9. Pressure Drop (ΔP_s)

ΔP_s= [f_s.G_s^2.(N_b+1) D_s]/2ρDeϕ$_s$

=0.384.734^2.(15+1).0.387/(2 . 1000 .0.0131 .1)

=37.39 Kpa

C. Thermal analysis for Tube Side:

1. Tube Clearance (C)

$$C = P_t - d_{ot}$$

= 0.0238 – 0.0190

https://dx.doi.org/10.22161/ijaers/3.11.3 *ISSN: 2349-6495(P) | 2456-1908(O)*

= 0.00475m

2. Mass Velocity (G_t)

$G_t = m_t / a_t$

=35.28/0.0172

=2051.162 kg/m^2.sec

3. Reynolds number (Re_t)

$Re_t = d_i.G_t/\mu_t$

$= (0.01656 \times 2051.162)/(9.040 \times 10^{-4})$

=37574.38

4. Nusselt Number(Nu)

$Nu=0.023 .Re^{0.8}.Pr^{0.4}$

$=0.023.37574.303^{0.8}.6.213^{0.4}$

=218.206

5. Heat Transfer (h_t)

$h_t = (Nu.k_t)/d_i$

$= (218 \times 206 \times 0.60812)/0.01656$

=8013 w/m^2k

OVERALL HEAT TRANSFER COEFFICIENT (U_o)

Over All Heat Transfer Coefficient for both shell side & tube side is given by

$1/U_o = [1/h_o] + [1/h_i .d_o/d_i] + [r_o \ln(r_o/r_i)/K_t$

U_o =3578.329 w/m^2k

V. RESULTS

A. Shell Side: The Table.3 shows the results of Overall heat transfer coefficient, Pressure drop at various helix angles of Helical Baffles including Segmental Baffle.

Helix Angle (deg)	Heat Transfer Coefficient W/m^2k	Over all heat transfer coefficient W/m^2k	Pressure drop Kpa
Segmental	7353.91	3578.32	104.58
6	29106.83	5640.15	291.82
12	19715.70	5147.74	80.8
18	15603.82	4816.02	37.39
24	13111.41	4549.17	21.15
30	11312.43	4311.27	13.20
40	9256.33	3975.19	6.72
50	7634.63	3642.45	3.56

GRAPH PLOTS:

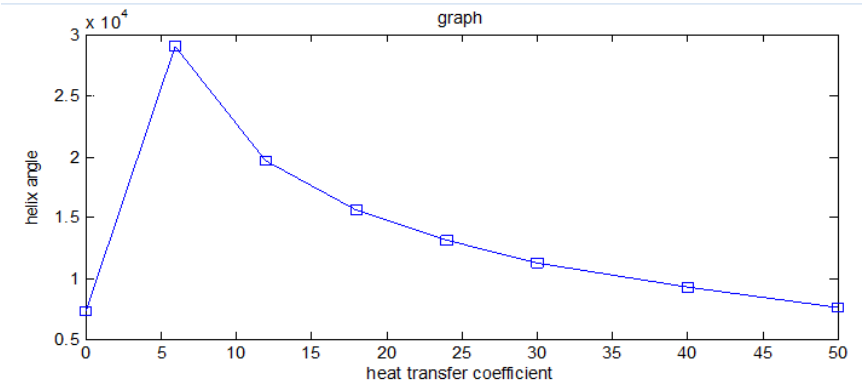

Graph.1:Heat Transfer coefficient VS Helix Angle

https://dx.doi.org/10.22161/ijaers/3.11.3 *ISSN: 2349-6495(P) | 2456-1908(O)*

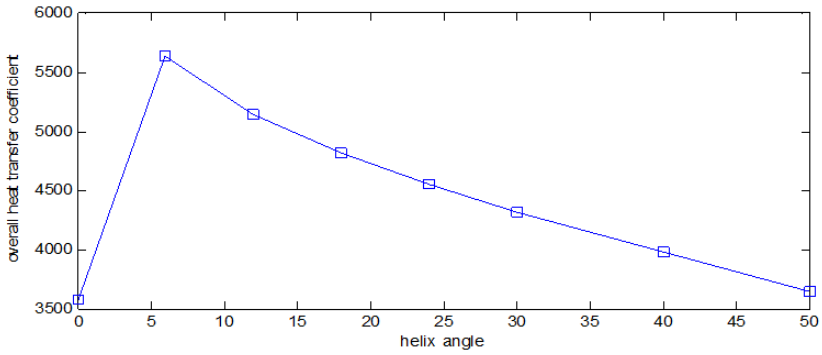

Graph.2: Overall heat transfer coefficient VS Helix Angle

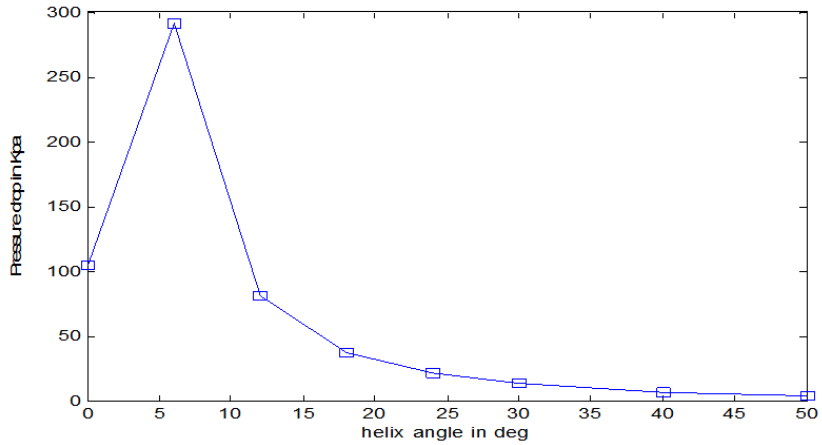

Graph.3: Pressure drop vs. helix angle

VI. CONCLUSIONS

- In the present study, an attempt has been made to modify the existing Kern method for continuous helical baffle heat exchanger, which is originally used for segmental baffles Heat Exchanger.
- The above graph plots give us a clear idea that the helical baffle Heat Exchanger has far more better heat transfer coefficient than the conventional segmental Heat Exchanger.
- The above graph plots also indicate that the pressure drop ΔP_s in a helical baffle heat exchanger is appreciably lesser than the segmental baffle heat exchangers due to increased cross flow area resulting in lesser mass flow. The pressure drop decreases with the increases of helix angle in all the cases considered. However, the effects of helix angles on pressure drop are small when helix angle is greater than 18 degree.
- From the graph plots shown , there is an increase of overall heat transfer in 6 deg helix angle than 0 deg segmental baffle.
- Suitable helix angle may be selected based upon the desired output and industrial applications. Helix angle of 6° may provide better heat transfer than the one with an angle of 18°, however at the expense of pressure drop.

REFERENCES

[1] Gang yong Lei, Ya-ling He and Rui Li, Ya-Fu Gao , **"**Effects of baffle inclination angle on flow and heat transfer of a heat exchanger with helical baffles", Science Direct-Chemical Engineering and Processing, (2008), 1-10.

[2] Master B.I, Chunagad K.S. Boxma A.J. Kral D, Stehlik P, Most frequently used Heat exchangers from pioneering Research to Worldwide Applications, vol. No.6, (1996), 1-8.

[3] Wang Qui, Dong Chen GUI, Xuging, Pengji Yan, "Design of Shelland- Tube Heat Exchanger With Continuous Helical Baffles," ASME journal, 132/101801, (2010).

https://dx.doi.org/10.22161/ijaers/3.11.3 *ISSN: 2349-6495(P) | 2456-1908(O)*

[4] Dr.B.jayachandraiah and V.Vinay Kumar," Design of helical Baffle in shell and tube heat exchanger and comparing with segmental baffle using kern method", Volume 3,Issue 2-March 2015,IJETCSE.

[5] Lutcha J, et al, "Performance improvement of tubular heat exchangers by helical baffles," Chemical Engineering Research and Design, 68, 263- 270 (1990)

[6] Sunilkumar Shinde, Mustansir Hatim Pancha, **"**Comparative Thermal Performance Analysis Of Segmental Baffle Heat Exchanger With Continuous Helical Baffle Heat Exchanger using Kern method," (IJERA) Vol.2,Issue4,July-August 2012,pp.2264-2271

[7] Peng B, Wang Q.W., Zhang C., An experimental Study of shell and tube heat exchangers with continuous helical baffles, *ASME Journal of Heat transfer*, (2007).

[8] Prithiviraj, M., and Andrews, M. J, Three Dimensional Numerical Simulation of Shell-and-Tube Heat Exchangers, *Foundation and Fluid Mechanics, Numerical Heat Transfer Part A - Applications, 33(8)*, 799–816, (1998).

International Journal of Advanced Engineering Research and Science (IJAERS) *[Vol-3, Issue-11, Nov- 2016]*
https://dx.doi.org/10.22161/ijaers/3.11.4 *ISSN: 2349-6495(P) | 2456-1908(O)*

The Influence of Biostimulator in the Remediation of Petroleum Sludge Polluted Clay Soil: *The Concept of Moringa Application*

Onu C[1], Kamalu C.I.O[2], Nwakaudu M. S[3], Onyelucheya O.E[4], Anyanwu E.E[5]

[1,2,3,4]Department of Chemical Engineering, Faculty of Engineering, Federal University of Technology, P.M.B. 1526, Owerri, Imo State, Nigeria
[5]Department of Mechanical Engineering, Faculty of Engineering, Federal University of Technology, P.M.B, Owerri, Imo State, Nigeria

Abstract— *The Bioremediation of Petroleum Sludge (PS) in a clay soil environment of the Niger Delta region of Nigeria using Moringa Seed oil extract (MO) as a Biostimulator (BS) has been investigated, with a view to studying the mitigation impact on the total petroleum hydrocarbon (TPH) content of the petroleum sludge. Two Bioreactors labeled R_1 (with MO treatment) and R_2 (control: No treatment) containing 3.0kg of clay soils were polluted with 300ml of petroleum sludge. 50ml of MO was added to R_1 as a biostimulator. R_2 received no form of treatment. Bioremediation extent monitoring was carried out bi-weekly by sampling of the bioreactors contents and analyzing for the individual petroleum hydrocarbon using a gas chromatography (GC). Analysis of the samples at two weeks intervals for a period of 12 weeks reveals that bioremediation occurred in the treatment reactor and the control reactor to which no biostimulator was added. Most of the Hydrocarbon degradation occurred within the first four weeks of the experiment. It was found that moringa seed oil extract was very effective and suitable for remediation of petroleum sludge polluted clay soils due to the high degradation rates of the individual hydrocarbons recorded in the biostimulated reactor against the low degradation rates of those of the control reactor with no form of bio-treatment.*

Keyword— Bioremediation, Biostimulation, Petroleum Sludge, Clay Soil, Moringa Seed Oil Extract.

I. INTRODUCTION

At Petroleum Refineries, flow stations and crude oil ocean terminals, petroleum is stored in various storage tanks before refining processing and shipment to various locations outside the shores of Nigeria. During this period of storage, petroleum sludge generation is inevitable due to the settlement of suspended solids. In addition to the grandiose manpower requirement and waste management issues associated with petroleum sludge handling, its presence in storage tanks reduces the oil storing capacities of the tanks with the increasing possibility of tank corrosion. Hence, the continual removal of the petroleum sludge from storage tanks becomes a necessity.

Nkeng and Nkwelang (2012) have stated that one of the major problems faced by the petroleum industries is the safe disposal of petroleum sludge in the environment since many of the constituent of petroleum sludge are toxic and carcinogenic. Petroleum sludge when improperly disposed to soil environment, alters the physical and chemical properties of the soil resulting to much changes in soil characteristics (Robertson et al., 2007; Kamalu et al., 2016). According to the finding of Al-Mutari (2008), the petroleum sludge contaminated soil may create nutrient deficiency, inhibit seed germination and cause restricted growth or demises of plants on contact.

Detoxification of petroleum sludge contaminated soils is therefore essential prior to soil re-use for agricultural and other purposes. Various physicochemical treatment techniques have been developed to clean up petroleum sludge polluted soils such as incineration, thermal desorption and chemical oxidation. In general, such treatments according to Alamri (2009) are very expensive, energy intensive and not sustainable with respect to their environmental impact which includes damage to the soil structures and toxicity issues associated with chemical additives. These limitations have been the basis of search for more economical and environmentally sound approaches to the clean up of petroleum sludge contaminated soils. Biological (Bioremediation) treatment of organic pollutants is a promising field of research which gives reliable, simple and cheap technologies over the

https://dx.doi.org/10.22161/ijaers/3.11.4 *ISSN: 2349-6495(P) | 2456-1908(O)*

chemical and physical process (Thayer, 1991; Kamalu et al., 2016).

Bioremediation has been defined as any process that uses microorganisms, fungi, green plants or their enzymes to return the natural environment altered by contaminants to its original condition (Ukpaka, 2007, Daugulis and McCracken, 2003; Leahy and Cohwell, 1990; Atlas, 1981; Adebuso *et al*., 2007; and Das and Mukherjee, 2007). Ukpaka (2012) in a study on the effects of functional parameters on the microbial characteristics in crude oil degradation has concluded that the use of microorganisms with appropriate metabolic capacities is the first step to achieving a successful bioremediation. In the present study, Ex-Situ biostimulation of the indigenous microbes by the addition of moringa seed oil extract was conducted to reclaim the petroleum sludge contaminated clay soil by evaluating its response to the degradation of individual hydrocarbons present in the petroleum sludge.

II. MATERIALS AND METHODS

MATERIALS:

The materials used includes: petroleum sludge (PS) obtained from Nigerian Agip Oil Company (NAOC) tank farm, Brass, Bayelsa State, Nigeria; clay soil collected from Rumuche-Emohua, Rivers State, Nigeria; Moringa seed oil extract purchased at Yenagoa Local Government Area Council office, Yenagoa, Bayelsa State, Nigeria; Glass beakers, measuring cylinder, weighing scale, mercury in glass thermometer; plastic buckets, trowel, masking tapes and gas chromatography (GC).

III. EXPERIMENTAL PROCEEDURE

Bioremediation mitigation experiment was conducted in two conic plastic buckets of seven litres capacity each. These containers served as the treatment reactors. 3.0kg of the experimental soil (clay) was measured into each of the treatment reactors labeled R_1 and R_2. 300ml of the petroleum sludge was measured into each of the plastic containers. Biostimulation method of Bioremediation was employed to enhance the microbial degradation of the hydrocarbon contaminants in the petroleum sludge polluted clay soils using moringa seed oil extract (MO) as the microbial biostimulant. 50.0ml of the moringa seed oil extract was measured out and poured into reactor R_1. Reactor R_2 which is the control received no Biostimulant. The contents of the reactors, after the addition of the biostimulant were properly stirred and transferred to a secluded hall away from sunlight and down pour, for a 90 day experimental period.

3.1 BIOREMEDIATION EXTENT MONITORING

The Bioremediation mitigation process was monitored by periodically analyzing samples of the petroleum sludge polluted clay soils undergoing remediation. Samples of the soils from the two reactors were collected at intervals of 15 days after proper mixing of the soils with trowel. The collected samples were analyzed for individual petroleum hydrocarbon content at SpringBoard Laboratories, Road 3, House 1, Udoka Housing Estate, Awka, Anambra State.

3.2 DETERMINATION OF INDIVIDUAL PETROLEUM HYDROCARBON IN THE SOIL SAMPLES

Reagents: Hexane, Acetonitrile

Apparatus: Buck 530 gas chromatography

Individual petroleum hydrocarbon presented in the PS polluted soil samples were extracted with 200ml of hexane. The mixture was separated using a separating funnel with the hexane layer concentrated in a rotary evaporator. 1ml of acetonitrile was added into a vial and placed into a Buck 530 gas chromatograph equipped with an on-column, automatic injector, electron capture detector, HP 88 capillary column (100m x 0.254m film thickness). The individual petroleum hydrocarbons present in the samples were then displayed in the visual unit of the gas chromatograph.

IV. RESULTS AND DISCUSSION

The results of the experiment with respect to the degradation of the individual petroleum hydrocarbons in the petroleum sludge polluted clay soil mitigation process are presented in tables 1, and 2 as shown in the appendix. From the experimental results, most of the petroleum hydrocarbons were not detected and so were skipped in tables 1 and 2, either because their concentrations were below the detection limits (<0.01mg/kg) of the gas chromatography used (Bulk 530 gas equipped with an on-column, automatic injector, electron capture detector) or they are not present in the petroleum sludge.

The profile of the bioremediation from the biostimulated reactor (R_1) and the control reactor (R_2) are shown in figures 1 and 2 below.

https://dx.doi.org/10.22161/ijaers/3.11.4 *ISSN: 2349-6495(P) | 2456-1908(O)*

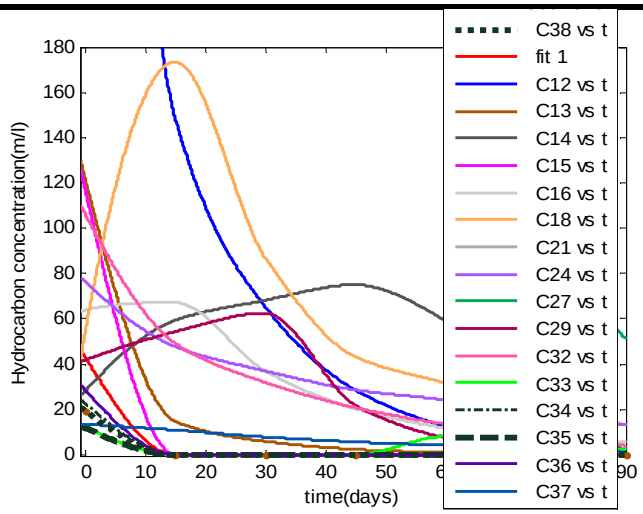

Fig.1: Hydrocarbon concentration bioremediation ersus time in days of bioremediation (biostimulated reactor).

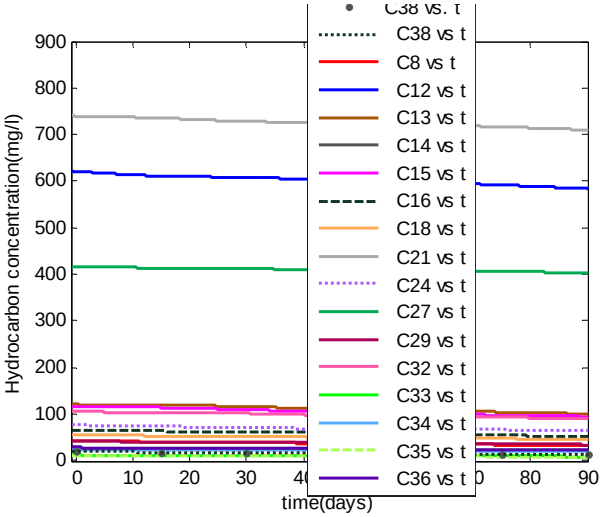

Fig.2: Hydrocarbon concentration bioremediation versus time in days of bioremediation (control).

The profiles from the biostimulated reactor (R_1) as depicted in figure 1 shows evidence of bioremediation of the individual petroleum hydrocarbon components of the petroleum sludge. Significant reductions from the initial concentration of the petroleum hydrocarbons were achieved. Most of the hydrocarbons degraded completely (100%) in the course of the mitigation experiment. It was observed from the profiles of most hydrocarbons such as C_{14}, C_{16}, and C_{18} increased in concentration. The sudden increase in concentrations of these hydrocarbons were due to fresh hydrocarbon formations due to the degradation of higher molecular weight hydrocarbons in the reactor, which also later degraded in the course of the experiment. The profiles shown in figure 2 are those of the control reactor with no biotreatment. From the profiles, slight degradations were recorded from the initial concentrations of the hydrocarbons. The slow rate of degradation is an indication that natural attenuation is not a suitable process for large scale bioremediation.

OCTANE (C_8)

Complete mineralization (100% degradation) of the octane component of the petroleum sludge occurred in reactor R_1, from the second week of the experiment. The complete degradation of the octane in the treatment reactor is attributed to the fact that the biostimulator (moringa seed oil extract) used contains certain nutrients in the form of phosphates and nitrates that are very important in the bioremediation process. The moringa seed oil extract supplies its nutrients to the soil, stimulating the indigenous microbes which in turn feed on the hydrocarbons present in the soil. The percentage degradation of octane in the control reactor (R_2) was 23.5934%. The slight reduction in the concentration of octane in the control reactor was due to the absence of a biostimulator in the degradation process. The result of the control reactor further validates the fact that bioremediation can proceed naturally (natural attenuation) without any form or soil amendment.

DODECANE (C_{12})

There was significant reduction in Dodecane in the treatment reactor (R_1) with the exception of the control reactor (R_2) which was only slightly reduced. From an initial concentration of 621.5731mg/l, Dodecane reduced to 1.9753mg/l (99.6822% degradation in the biostimulated reactor (R_1) and 583.8485 mg/l (6.0692% degradation) in the control reactor (R_2).

The significant reduction of the Dodecane fraction of the petroleum sludge in R_1 attests to the effectiveness of the bioremediation process using moringa seed oil extract as a biostimulator.

TRIDECANE (C_{13})

The initial concentration of the Tridecane detected was 120.9383mg/l before the biostimulation of the PS polluted clay soils. The final results obtained at the end of the 90 day experiment shows complete degradation (100%) of the Tridecane from the 75th day of the experiment in the treatment reactor, R_1, and 16.5999% (100.8626mg/l) reduction in the control reactor (R_2)

PENTADECANE (C_{15})

Pentadecane degraded completely in the treatment reactor (R_1) due to the activities of microorganisms (Hydrocarbon

https://dx.doi.org/10.22161/ijaers/3.11.4 *ISSN: 2349-6495(P) | 2456-1908(O)*

utilizing bacteria) being stimulated by the nutrient – rich biostimulator (moringa seed oil extract).

The degradation recorded in the control reactor (18.1369%) is insignificant in comparison to the complete mineralization recorded in the treatment reactor R_1 (biostimulated with moringa seed oil extract). This result is an indication that large scale bioremediation cannot be handled by natural attenuation.

HEXADECANE (C_{16})

Hexadecane increased from an initial concentration of 63.7382mg/l to 67.1647mg/l (5.3759% increase) within the first two weeks of the mitigation experiment in the treatment reactor (R_1). This increase in concentration is a function of the degradation of heavier ($>C_{16}$) molecular weight hydrocarbons in the treatment reactor. Response to microbial degradation of the Hexadecane component of the petroleum sludge was noticed on the 30th day of the experiment, reducing from 67.1647mg/l to 36.9406mg/l. Subsequent bi-weekly results of sample analysis showed continual reduction of hexadecane. At the end of the 90 day experiment, Hexadecane has degraded to 5.3803mg/l (91.5588%) in the treatment reactor R_1. Within the experimental period, Hexadecane, degraded to 53.2825mg/l (16.4041% reduction) in the control reactor R_1. The slight reduction is an indication that natural attenuation is not an effective method of bioremediation.

OCTADECANE (C_{18})

The reduction in concentration of octadecane within the 90 day experimental period in the treatment reactor (R_1) was 13.4185mg/l from initial concentration of 55.1684mg/l (75.6772% reduction). Tremendous increase in concentration of octadecane occurred in the first two weeks of the experiment in R_1 as was observed on the 15th day (173.390mg/l). This increase in concentration is accounted for by the breakdown of higher molecular weight hydrocarbons ($>C_{18}$) in the treatment reactor. From the 30th day, result of analysis showed degradation of octadecane. The percentage reduction of the octadecane in the control reactor (R_2) was 19.5764%. This value is low compared to that of the treatment reactor R_1, due to the non-application of a biostimulator.

HENEICOSANE (C_{21})

The results obtained from the bioremediation experiment for Heneicosane degradation in the petroleum sludge polluted clay soil shows that biostimulation is a useful tool in microbial degradation of hydrocarbons. The total concentration of Heneicosane measured prior to the commencement of the experiment was 740.2861mg/l. At the end of the 90 day experiment, the initial concentration of Heneicosane has reduced to 220.2769mg/l in the treatment reactor (R_1) and 710.4419mg/l in the control reactor (R_2). The above results accounts for the effectiveness of the bioremediation process and the efficiency of the moringa seed oil extract applied in stimulating the indigenous microbes in the polluted soils. R1 remediation by 70.2 and R_2 4.0314%.

TETRACOSANE (C_{24})

Analysis of samples revealed that bioremediation of Tetracosane occurred in both reactors R_1, (with a biostimulator) and R_2 (without stimulator). Percentage reduction of Tetracosane in the treatment reactor, R_1 was 82.5096% and 16.1966% in the control reactor, R_2. The result of the treatment reactor in comparison to the control reactor compliments the fact that moringa seed oil extract is an effective biostimulator and suited for bioremediation of petroleum sludge.

HEPTACOSANE (C_{27})

Heptacosane component of the petroleum sludge was very high at initial measurement compared to other hydrocarbon components present in the petroleum sludge. In the course of the bioremediation mitigation, heptacosane reduced from an initial concentration of 416.7177mg/l to 5.1362mg/l in the treatment reactor R_1, and 403.1791mg/l in the control reactor, R_2. The high rate of degradation of the Heptacosane component in the treatment reactor (R_1) was due to the high metabolic activities of the resident microorganisms stimulated by moringa seed oil extract. The low reduction (3.2489%) in the control reactor was because of natural attenuation (without stimulation).

NONACOSANE (C_{29})

Complete mineralization of the Nonacosane component of the petroleum sludge was achieved in the treatment reactor, R_1 (100% degradation) in the last two weeks of the experiment. Nonacosane increased in concentration in the first four weeks of the experiment. This increase in concentration was caused by the degradation of heavier hydrocarbons ($>C_{29}$) in the treatment reactor, R_1. Further analysis of samples gave results with indication of occurrence of bioremediation from the 45th day to a complete mineralization of the Nonacosane at the end of the experiment. The control experiment R_2 recorded 17.3961% degradation within the 90 day remediation period. The high degradation rate of C_{29} in the MO stimulated reactor was due to the enhancement of C_{29} bioavailability by moringa seed oil extract.

DOTRIACONTANE (C_{32})

Dotriacontane fraction of the petroleum sludge showed grandiose reduction in concentration in the course of the

https://dx.doi.org/10.22161/ijaers/3.11.4 *ISSN: 2349-6495(P) | 2456-1908(O)*

mitigation. A percentage reduction of 96.2134 % took place in the treatment reactor, R_1, and only 14.9019% in the control reactor, R_2, which was unaided with bionutrient carriers. This results shows the effectiveness of the impact of moringa stimulator in accelerating petroleum sludge degradation.

TRITRIACONTANE (C_{33})

Tritriacontane was degraded completely (100%) in the treatment reactor, R_1 within the first two weeks of the remediation, with slight reduction of 27.2231% in the control reactor, R_2. Complete mimeralization of the Tritriacontane compoinent of the petroleum sludge was maintained till the 6th week of the remediation. At the 8th week, there was fresh formation (8.0749mg/l) of Tritriacontane in the treatment reactor, due to degradation of higher molecular weight components (>C_{33}) in the reactor. The formed Tritriacontane was significantly degraded to 2.4451mg/l within the last four weeks of the experiment, corresponding to 69.7197% degradation of the formed tritriacontane component.

Within the same experimental time, the reduction in the control reactor (R_2) was minimal (27.2231%) compared to the reactor with a biostimulator. The low degradation rate recorded in the control reactor is an indicator of the unreliability of natural attenuation in petroleum sludge bioremediation.

TETRATRIACONTANE (C_{34})

TPH analysis of samples of the petroleum sludge polluted clay bioremediation reveals 100% (complete) degradation for Tetratriacontane component in the moringa stimulated bioreactor (R_1). Complete degradation of the C_{34} component within the first two weeks of the experiment gives credibility to the adequacy of the use of moringa seed oil extract in the mitigation of petroleum sludge polluted clay soils of the Niger Delta Environment. In the control reactor, R_2, which was not biostimulated, the C_{34} component degraded to 19.5301mg/l from an initial concentration of 22.8800mg/l, representing 14.6412% degradation within the 90 day experimental period.

PENTATRIACONTANE (C_{35})

Pentatriacontane (C_{35}) degraded completely (100%) from an initial concentration of 11.7860mg/l within the period of the experimental investigation in the biostimulated reactor, R_1 observed that the moringa seed oil extract in addition to being a microbial stimulant was responsible for the bioavailability of the heavier substrates to microbial consumption. In comparison to the non-MO stimulated bioreactor, R_2, a total of 23.1724% within the experimental period. The low degradation was due to the non – enhancement of the bioavailability of the heavier substrates in the control reactor to microbial consumption as in the MO stimulated reactor.

HEXATRIACONTANE (C_{36})

Initial concentration of the C_{36} component of the petroleum sludge was 28.3650mg/l prior to the bioremediation mitigation experiment within the period of the experimental investigation, results of sample analysis indicates occurrence of bioremediation in the reacted (R_1) and untreated (R_2) reactor. In the treated reactor (with MO stimulation), C_{36} degraded completely (100%). While in the untreated reacted, C_{36} component slightly degraded to 24.5848mg/l (13.3270% degradation), the low degradation rate was as a result of the fact that the remediation in the control reactor proceeded on natural attenuation without any form substrate bioavailability enhancement and microbial stimulator.

HEPTATIACONTE (C_{37})

Heptatriacontane (C_{37}), a heavier component of the petroleum degraded slightly, from an initial concentration of 13.4670mg/l to 10.8788mg/l in the MO treated reactor, R_1, within the first two weeks of the experiment. This initial slow rate of degradation was due to the time taken for the C_{37} degrading microbes to adapt in the reactor, consuming C_{37} as a new source of energy. By the end of the 90 day experimental period, results of sample analysis show 100% degradation of the C_{37} component in the moringa treated bioreactor, R_1.

The untreated reactor, R_2 (without addition of MO) on record 17.0944% degradation of the C_{37} component, reducing to 11.1649mg/l from an initial concentration of 13.4570mg/l. the low degradation rate of C_{37} component in the control reactor validates the claim that natural attenuation cannot effectively remediate hydrocarbon polluted environments within a short period as in the experimental investigation period.

OCTATRIACONTANE (C38)

Initial petroleum sludge characterization prior to commencement of bioremediation mitigation gave octatriacontane initial concentration as 19.2760mg/l. Results of sample analysis indicated that bioremediation occurred in moringa stimulated bioreactor (R_1) as well as the control reactor (R_2) without any form of biostimulation. Percentage reduction of octatriacontane component in the MO treated reactor was 100% and 26.5454% in the control reactor. The results of the treated reactor in comparison with the untreated reactor shows the reliability of biostimulation in achieving effective bioremediation of petroleum sludge in a record time.

https://dx.doi.org/10.22161/ijaers/3.11.4 *ISSN: 2349-6495(P) | 2456-1908(O)*

V. CONCLUSION

From the experimental study, it is concluded that the reduction in the total Petroleum Hydrocarbon (TPH) in the course of the remediation was due to the presence of TPH–degrading microbes in the polluted soil, whose growth and degrading capabilities were a direct function of the effectiveness of the biostimulator (moringa seed oil extract) applied in the experimental process. The moringa seed oil extract(biostimulator) was responsible for the enhancement of substrates and microbial activation in the treated reactor. The results of the individual petroleum hydrocarbon degradation in the control reactor, R_2, in comparison to those of the treatment reactor, R_1, were very low varying between 11% to 27% (percentage reduction). The result from the control reactor is an indicator that bioremediation can occur naturally without any form of soil amendment. The drawback to the natural attenuation is that the rate of natural bioremediation is very slow. Hence, large scale in-situ or ex-situ bioremediation cannot be reliably and successfully carried out in a record time.

REFERENCES

[1] Al-mutari, N., Burfasan, A and Al-Rukaibi, S (2008): Ecorisk evaluation and treatability potentials of soils contaminated with petroleum hydrocarbon based fuels. Chemosphere. 74; 142-148.

[2] Alamri, S. A (2009): use of microbiological and Chemical methods for assessments of enhanced hydrocarbon bioremediation. Journal of Biological Sciences, 9; 37-43.

[3] Atlas, R. M. (1981): Microbial degradation of petroleum hydrocarbons: an environmental perspective. Microbial Reviews.45(1)180-209.

[4] Adebusoye, S. A, Ilori, M. O, Amund, O. D, Teniola, O. D, and Olatope, S. O (2007): Microbial degradation of petroleum hydrocarbons in a polluted tropical stream. World J. Microbial and Biotechnol. 23(8) 1149-1159.

[5] As, K and Mukherjee, A.K (2007): Crude petroleum oil biodegradation efficiency of Bacillus subtilis and pseudomonas aeruginosa streams isolated from a petroleum oil contaminated soil from North-East India. Bioresource Technology. 98(7); 1339-1345.

[6] Daugulis, A.J and McCracken, C.M (2003): Microbial degradation of high and low molecular weight polyaromatic hydrocarbons in a two-phase partitioning bioreactor by two strains of sphingomonas SP. Biotechnology letter, 25(17) 1441-1444.

[7] Kamalu C10, Nwakaudu A.A, Onyelucheya OE, Uzondu FN, Ko,men FL, Nwakaudu M.S, Obijiaku JC(2016) Curve – Fitting of Bioremediation of Polycyclic Aromatic Hydrocarbons (PAHS) by Co-composting using Roost Manure. Int'l J. of Emerging Technologies in Engr. Research. Vol. 4 (7) p. 156-164

[8] Leahy J.G. and Colwell, R.R (1990): Microbial degradation of hydrocarbons in the environment. Microbiological review, 54 (3) 305-315.

[9] Nkeng, G. E. and Nkwelang G. (2012); Bioremediation of the petroleum refinery oil sludge in tropical soil. Open access scientific reports. 1 (2);1-4

[10] Reobertson, S.J., McGrill, W.B., Massiocotte, H.B and Rutherford, P.M. (2007): Petroleum Hydrocarbon contamination bored forest. Biol. Rev. 82; 213-240

[11] Thayer, A. M (1991): Bioremediation: Innovative Technology for cleaning up hazards waste. Chem. Eng. News 69 (34); 23-44.

[12] Ukpaka, C.P (2007): Modeling the microbial thermal kinetics system in Biodegradation of n-paraffins. J. Modeling, simulation and control (AMSE).67(1) 61-84.

[13] Ukpaka, C. P. (2012): The effect of functional parameters on microbial characteristics in crude oil degradation. Journal of Research in Environmental Science and Toxicology. 1(4); 66-90.

APPENDIX 1

Table.1: TPH BIOREMEDIATION EXTENT FOR PS POLLUTED CLAY SOIL IN R_1 (WITH THE ADDITION OF MORINGA SEED OIL EXTRACT)

Parameters (Mg/L)		**TIME (DAYS)**						
		0	**15**	**30**	**45**	**60**	**75**	**90**
Octane	C8	42.7640	0.0000	0.0000	0.0000	0.0000	0.0000	0.0000
Dodecane	C12	621.5731	147.8045	65.0339	28.6150	12.7154	5.5399	1.9753
Tridecane	C13	120.9383	14.7158	5.8863	2.3545	0.9418	0.0000	0.0000

https://dx.doi.org/10.22161/ijaers/3.11.4 *ISSN: 2349-6495(P) | 2456-1908(O)*

Tetradecane C14	28.2899	59.2994	68.1943	75.0137	59.2250	17.7675	2.6651
Pentadecane C15	116.1860	0.0000	0.0000	0.0000	0.0000	0.0000	0.0000
Hexadecane C16	63.7382	67.1647	36.9406	20.3173	11.7168	6.1460	5.3803
Octadecane C18	55.1684	173.3906	86.6953	43.3477	31.6586	20.8369	13.4185
Heneicosane C21	740.2861	703.2965	555.6042	438.9273	346.7526	273.9345	220.2769
Tetracosane C24	76.5193	47.7428	36.9874	28.5955	23.0360	16.1662	13.3835
Heptacosane C27	416.7177	187.5274	93.7802	42.2754	18.9572	10.4976	5.1362
Nonacosane C29	41.8416	54.3140	62.4611	21.8613	7.6515	2.6780	0.0000
Dotriacintane C32	105.9294	49.2215	31.9937	20.7961	13.5175	8.7864	4.0111
Triacontane C33	12.3700	0.0000	0.0000	0.0000	8.0749	5.4337	2.4451
Tetratriacontane C34	22.8800	0.0000	0.0000	0.0000	0.0000	0.0000	0.0000
Pentatriacontane C35	11.7860	0.0000	0.0000	0.0000	0.0000	0.0000	0.0000
Hexatriacontane C36	28.3650	0.0000	0.0000	0.0000	0.0000	0.0000	0.0000
Heptatriacontane C37	13.4670	10.8788	7.8327	5.6396	4.0605	1.9236	0.0000
Octatriacontane C38	19.2760	0.0000	0.0000	0.0000	0.0000	0.0000	0.0000

Table.2: TPH BIOREMEDIATION EXTENT FOR 12 PS POLLUTED CLAY SOIL IN R_2 (CONTROL: WITHOUT ADDITION OF MORINGA SEED OIL EXTRACT)

Parameters (Mg/l)	**TIME (DAYS)**						
	0	**15**	**30**	**45**	**60**	**75**	**90**
Octane C8	42.7640	40.6754	39.5026	37.0508	36.8355	34.4990	32.6745
Dodecane C12	621.5731	611.4850	608.1138	603.0853	598.0640	591.7980	583.8485
Tridecane C13	120.9383	119.4854	116.3640	110.9094	108.5590	104.6251	100.8626
Tetradecane C14	28.2899	28.1456	26.6129	25.9935	25.6369	23.8414	23.3651
Pentadecane C15	116.1860	114.4850	109.4592	104.9422	101.2067	97.9320	95.1134
Hexadecane C16	63.7382	63.4850	61.2598	60.3708	57.2781	54.2808	53.2825
Octadecane C18	55.1684	53.5861	52.4319	50.2023	49.7815	47.9298	44.3684
Heneicosane C21	740.2861	735.4850	728.5468	725.2148	721.7541	716.5787	710.4419
Tetracosane C24	76.5193	73.8970	70.4718	69.4482	68.6258	66.7319	64.1258
Heptacosane C27	416.7177	413.9485	411.8519	410.8292	409.7163	406.0806	403.191
Nonacosane C29	41.8416	40.4950	39.5198	38.2926	36.9633	36.2012	34.5628
Dotriacintane C32	105.9294	103.3850	101.8658	97.5359	96.8555	93.1513	90.1439
Triacontane C33	12.3700	11.8515	11.1121	10.6129	10.0718	9.5331	9.0025
Tetratriacontane C34	22.8800	22.6508	22.3650	21.9621	20.9338	20.1291	19.5301
Pentatriacontane C35	11.7860	11.0936	10.7490	10.4419	9.6122	9.1183	9.0549
Hexatriacontane C36	28.3650	27.7795	27.3131	25.9471	25.0052	24.9392	24.5848
Heptatriacontane C37	13.4670	13.4351	13.1835	12.8243	12.0194	11.5165	11.1649
Octatriacontane C38	19.2760	18.5401	18.0132	16.6269	15.0293	14.8599	14.1591

International Journal of Advanced Engineering Research and Science (IJAERS) *[Vol-3, Issue-11, Nov- 2016]*
https://dx.doi.org/10.22161/ijaers/3.11.5 *ISSN: 2349-6495(P) | 2456-1908(O)*

Multi-objective Economic Emission Load Dispatch using Grey Wolf Optimization

Nitish Chopra[1], Gourav Kumar[2], Shivani Mehta[3]

[1]Department of Electrical & Electronics Engineering, CTIT, Jalandhar, Punjab, India
[2]Department of Electrical Engineering, KC College of Engineering & I.T., Nawanshahr, Punjab, India
[3]Department of Electrical Engineering, D.A.V.I.E.T., Jalandhar, Punjab, India

Abstract*—This paper presents grey wolf optimization method for solving multi-objective economic emission load dispatch (EELD) problem in diverse test power systems. Grey Wolf Optimization (GWO) is a new meta-heuristic motivated from grey wolf. Diverse emission gases considered for the case studies are SOx, NOx and COx. GWO is applied on diverse test cases for finding EELD solution. Comparison of the obtained results is carried out with other techniques stated in literature which shows that GWO is effective to solve EELD.*

Keywords*— *Economic emission load dispatch, GWO, penalty factor, fuel cost, emission.

I. INTRODUCTION

The chief goal of EELD is to get optimum output of thermal generators in power system subjected to several constraints to diminish the operating costs. The thermal power plant operation is dependent upon incineration of fossil fuel which generates SOx, NOx and COx emission. The increasing pollution is a matter of environmental concern worldwide which has led to formation of international standards for emissions from industries and power plants. Different acts have been made which forces the industries to modify their principles to follow the environment-emission standards strictly. Therefore it is significant to consider emission constraint in economic dispatch. The economic & emission dispatch are contradictory in character and both must be considered together to find optimal dispatch. The problem is formulated as a multiobjective economic emission load dispatch (EELD) problem in which both the objectives (emission and economy) have to be minimized.

Earlier traditional methods like Newton's method, gradient approach and linear programming [1] were used for solving ELD problem. In the last years different techniques have been used for solving EELD. Nanda et.al [2] applied goal programming techniques for solving EELD. Song et.al [3] solved environmental/economic dispatch with genetic algorithm controlled by fuzzy logic. Abido [4] used genetic algorithm for the EELD to find out pareto-optimal solutions. Ah King [5, 6] applied improved non-dominated sorting genetic algorithm (NSGA-II) for creating pareto-optimal front for EELD. Thenmozhi [7] solved EELD using hybrid genetic algorithm. Perez [8] solved environmental/economic dispatch using differential evolution. Hong [9] applied immune genetic algorithm for EELD. Hazra [10] proposed bacteria foraging algorithm for emission constrained economic dispatch. Hemamalini [11] solved non convex EELD by applying particle swarm optimization.Bhattacharya.et.al [14] presented a BBO technique to solve EELD of thermal generators with different emission substances (SOx, NOx, & COx). Similarly there are many other techniques like teaching learning based algorithm [15,firefly algorithm (FFA) [16] and artificial neural networks [17],NSGA [21], SPEA [22],PSO[23], bacterial foraging algorithm with fuzzy logic[24] and Ant lion optimization[27] which have been successfully used to solve EELD problem.GWO has been earlier applied to solve single objective ELD [26].

In this paper combined emission and economic dispatch problem has been transformed to single objective problem by using cost penalty factors. After that grey wolf optimization (GWO) is used to solve the modified problem.

II. PROBLEM FORMULATION

2.1 Economic Load Dispatch

Aim for economic dispatch is to reduce the operating (fuel) cost of thermal generators satisfying some limits[27]. The objective function is given by:

$$C = \sum_{i=1}^{NG}(a_i P_{gi}^2 + b_i P_{gi} + c_i) \quad \ldots (1)$$

Where a_i, b_i, & c_i are the fuel-cost coefficients and P_{gi} is power output for the ith generating unit among NG total committed generating units.

The constraints to be considered are:

a) Energy equality constraint

https://dx.doi.org/10.22161/ijaers/3.11.5 *ISSN: 2349-6495(P) | 2456-1908(O)*

The overall generation by the entire generators should be equal to the sum of whole power demand (P_d) & system's real power loss (P_L).

$\sum_{i=1}^{NG} P_{gi} - P_d - P_L$ ... (2)

The power loss P_L is calculated by using generator power output and B coefficients:

$P_L = \sum_{i=1}^{NG}\sum_{j=1}^{NG} P_i B_{ij} P_j + \sum_{i=1}^{NG} B_{0i} P_i + B_{00}$ … (3)

b) Generator inequality constraint

Output power of each generator must lie between its lower P_{gi}^{min} and upper P_{gi}^{max} operating limits.

$P_{gi}^{min} \le P_{gi} \le P_{gi}^{max}$ i=1,2…NG … (4)

2.2 Economic Emission Dispatch

EED objective is to diminish the entire pollution ejection from combustion of coal or gas for producing electricity. The emission function consist of the summation of different types of emissions (i.e. COx, NOx and SOx)with appropriate pricing for every pollutant discharged[27]. The problem of EED for COx, NOx and SOx emissions can be defined by as :

$E_N = \sum_{i=1}^{NG}(d_{iN}P_{gi}^2 + e_{iN}P_{gi} + f_{iN})$

… (5)

$E_S = \sum_{i=1}^{NG}(d_{iS}P_{gi}^2 + e_{iS}P_{gi} + f_{iS})$

… (6)

$E_C = \sum_{i=1}^{NG}(d_{iC}P_{gi}^2 + e_{iC}P_{gi} + f_{iC})$

… (7)

Where E_N ,E_S & E_C are the total amount of NOx, SOx and COx emission from the power plant in (kg/hr.).

The power balance & generator limit restrictions are given by Eq. (2 & 4) respectively.

2.3 Economic emission Load dispatch (EELD) problem

The emission and economic dispatch are contradictory in character and they both have to be considered together to find optimal dispatch. The problem is expressed as a multiobjective EELD problem in which both objectives (emission and economy) [27] have to be minimized.

The objective function is given by: FC (C, E_N, E_S & E_C)

… (8)

Where C denote fuel cost objective and E_N,E_S & E_C denote emission objectives.

The multiobjective EELD can be transformed to single objective problem by using cost penalty factors (cpf) denoted by "k". When fuel cost and NOx emissions are considered objective function becomes:

$FC = C + k_N(E_N)$ … (9)

When fuel cost, NOx & SOx emissions have to be considered together, the final objective function can be defined as

$FC = C + k_N(E_N) + k_S$

… (10)

When fuel cost, NOx, SOx & COx emissions have to be considered together, the final objective function can be defined as

$FC = C + k_N(E_N) + k_S(E_S) + k_C(E_C)$ … (11)

Where k_N ,k_S & k_C are price penalty factors for the NOx , SOx & COx emissions ,that combines respective emissions cost with fuel cost.

The steps to calculate price penalty factors for SOx, NOx and COx [19, 25] are given below:

(a) Calculate fuel cost of every generating unit at its highest output, i.e.,

$C = \sum_{i=1}^{NG}(a_i P_{gi\,max}^2 + b_i P_{gi\,max} + c_i)$ ... (12)

(b) Calculate the SOx, NOx & COx emission discharge for each generator at its max output, i.e.,

$E_N = \sum_{i=1}^{NG}(d_{iN}P_{gi\,max}^2 + e_{iN}P_{gi\,max} + f_{iN})$ … (13)

$E_S = \sum_{i=1}^{NG}(d_{iS}P_{gi\,max}^2 + e_{iS}P_{gi\,max} + f_{iS})$ … (14)

$E_C = \sum_{i=1}^{NG}(d_{iC}P_{gi\,max}^2 + e_{iN}P_{gi\,max} + f_{iC})$ … (15)

(c) k_N [i], k_S [i] & k_C [i] ,(i = 1, 2, …. , NG) is calculated for every generator

$$k_N[i] = \frac{\sum_{i=1}^{NG}(a_i P_{gi\,max}^2 + b_i P_{gi\,max} + c_i)}{\sum_{i=1}^{NG}(d_{iN}P_{gi\,max}^2 + e_{iN}P_{gi\,max} + f_{iN})} \quad \text{... (16)}$$

$$k_S[i] = \frac{\sum_{i=1}^{NG}(a_i P_{gi\,max}^2 + b_i P_{gi\,max} + c_i)}{\sum_{i=1}^{NG}(d_{iS}P_{gi\,max}^2 + e_{iS}P_{gi\,max} + f_{iS})} \quad \text{… (17)}$$

$$k_C[i] = \frac{\sum_{i=1}^{NG}(a_i P_{gi\,max}^2 + b_i P_{gi\,max} + c_i)}{\sum_{i=1}^{NG}(d_{iC}P_{gi\,max}^2 + e_{iN}P_{gi\,max} + f_{iC})} \quad \text{... (18)}$$

(d) Organize k_N [i], k_S [i] & k_C [i] in increasing direction.

(e) Add max output of every generator (Pi max) single at a time, start from minimum k_N [i], k_S [i] & k_C [i] for NOx , SOx & COx emissions until $\sum P_{i\,max} \ge P_d$

(f) On this point k_N [i], k_S [i] & k_C [i] related with final generator in the procedure are the price penalty factor k_N, k_S & k_C for the NOx, SOx & COx emission for that demand P_d.

III. GREY WOLF OPTIMIZATION

In this section grey wolf optimization (GWO) is discussed for solving multiobjective EELD problem. Mirjalili et al [25] proposed GWO algorithm which was inspired by social and hunting behavior of grey wolf. The head of pack are a male and female, called alphas (α). The alpha is generally responsible for taking decisions about hunting, time to

https://dx.doi.org/10.22161/ijaers/3.11.5 *ISSN: 2349-6495(P) | 2456-1908(O)*

wake, sleeping place, and so on. Fascinatingly, the alpha is not essentially the strongest member in the pack but the greatest in terms of supervision of the pack. This shows that the discipline and organization of a pack is of a great deal than its strength. In the hierarchy of grey wolves the second level is beta. The betas are secondary wolves that help the alpha in making decisions or other activities of the pack. It maintains discipline in the pack and acts as an advisor to the alpha. The reinforcing of the alpha's orders is done by beta all through the pack and provides feedback to the alpha. Delta (δ) wolves are the third in social hierarchy of grey wolves and they have to submit to betas and alphas, but they govern the omega. Sentinels, scouts, hunters, elders, and caretakers belong to this group. Sentinels shield and promise the protection of the pack. Scouts are accountable for watching the borders of the territory of the pack and warn the pack in case of any threat. Elders are the knowledgeable wolves who used to be beta or alpha. Hunter's assist the betas and alphas when hunting prey plus providing food to the pack. Lastly, the caretakers are in charge for caring for the frail, sick, and injured wolves of the pack. The omega(ω) is ranked lowest among grey wolves. The omega acts like a scapegoat. Omega wolves always have to surrender to all the other governing wolves and are the last wolves that are permitted to eat.

In the mathematical model of the social hierarchy of the grey wolves, alpha (α) is considered as the fittest solution. Accordingly, the second best solution is named beta (β) and third best solution is named delta (δ) respectively. The candidate solutions which are left over are taken as omega (ω). In the GWO, the optimization (hunting) is guided by alpha, beta, and delta. The omega wolves have to follow these wolves.

During hunting prey is encircled by grey wolves which can be modeled mathematically as following equations[25]:

$$\vec{D} = \left|\vec{C}.\vec{X}_p(t) - \vec{X}(t)\right| \quad \text{... (19)}$$

$$\vec{X}(t+1) = \vec{X}_p(t) - \vec{A}.\vec{D} \quad \text{... (20)}$$

Where $\vec{A}$ and $\vec{C}$ are constant vectors, $\vec{X}_p$ is prey's location vector, $\vec{X}$ denotes grey wolf's location vector and 't' is present iteration.

$\vec{A}$ and $\vec{C}$ vectors are computed as follows [25]:

$$\vec{A} = 2.\vec{a}.\vec{r}_1.\vec{a} \quad \text{….. (21)}$$

$$\vec{C} = 2.\vec{r}_2 \quad \text{... (22)}$$

'$\vec{a}$ 'is reduced linearly from 2 to 0 during iterations and r1, r2 are random vectors in [0, 1] gap. Wolves are forced to attack upon the prey when |A| < 1 and diverge from the prey when |A| > 1 to optimistically find a better prey.

The hunt is normally directed by alpha, beta and delta, which have greater knowledge about the feasible site of prey. The other wolves must amend their position according to best wolf position. The equations used for wolves position updating are given below [25]:

$$\begin{bmatrix} \vec{D}_\alpha = \left|\vec{C}_1.\vec{X}_\alpha - \vec{X}\right| \\ \vec{D}_\beta = \left|\vec{C}_2.\vec{X}_\beta - \vec{X}\right| \\ \vec{D}_\delta = \left|\vec{C}_3.\vec{X}_\delta - \vec{X}\right| \end{bmatrix} \quad \text{… (23)}$$

$$\begin{bmatrix} \vec{X}_1 = \vec{X}_\alpha - \vec{A}_1.(\vec{D}_\alpha) \\ \vec{X}_2 = \vec{X}_\beta - \vec{A}_2.(\vec{D}_\beta) \\ \vec{X}_3 = \vec{X}_\delta - \vec{A}_3.(\vec{D}_\delta) \end{bmatrix} \quad \text{…. (24)}$$

$$\vec{X}(t+1) = \frac{\vec{X}_1+\vec{X}_2+\vec{X}_3}{3} \quad \text{…… (25)}$$

IV. SIMULATION TESTS AND RESULTS

In this paper multi-objective economic load dispatch has been solved for three different test systems. In all cases, the constraints of operating limit and power balance are considered. The program was written in MATLAB (R2009b).The population (i.e. number of grey wolves) taken in each case was 30 and maximum number of iterations performed were 500.

1) Test system 1

In this case system having 3 generating units considering NOx emissions is tested to reveal effectiveness of GWO.Theinput data, such as cost &emission coefficients, loss data, generation restrictions, istaken from [19]. The power demands are 300,500 and 700 MW. The best negotiating results achieved from GWO are shown in table 1 and their comparison with other techniques is shown in table 2.

Table.1: EELD with NOx emission for 3-unit system

	Load Demand		
	300	**500**	**700**
Unit 1	49.31	128.82	182.61
Unit 2	130	191.47	270.36
Unit 3	125	191.38	270.35
j_N (Rs/Kg)	43.1703	44.8063	47.8218

https://dx.doi.org/10.22161/ijaers/3.11.5 *ISSN: 2349-6495(P) | 2456-1908(O)*

Fuel cost(Rs/hr)	16378.37	25494.84	35462.78
Emission(Kg/hr)	135.24	311.12	651.50
Power loss(MW)	4.318	11.67	23.33
Total cost(Rs/hr)	22218.372	39435.338	66619.07

Table.2: Comparison of results for 3-unit system for 700MW load demand

Pf_N (Rs/Kg)	Performance	Conventional Method [12]	SGA [12]	RGA [12]	FFA[20]	GWO
47.8218	Fuel cost, Rs/hr	35485.05	35478.44	35471.4	35464	35462.78
	Emission, kg/hr	652.55	652.04	651.60	651.5	651.50
	Power loss, MW	23.37	23.29	23.28	23.36	23.33
	Total cost, Rs/hr	66690	66659	66631	66622.6	66619.07

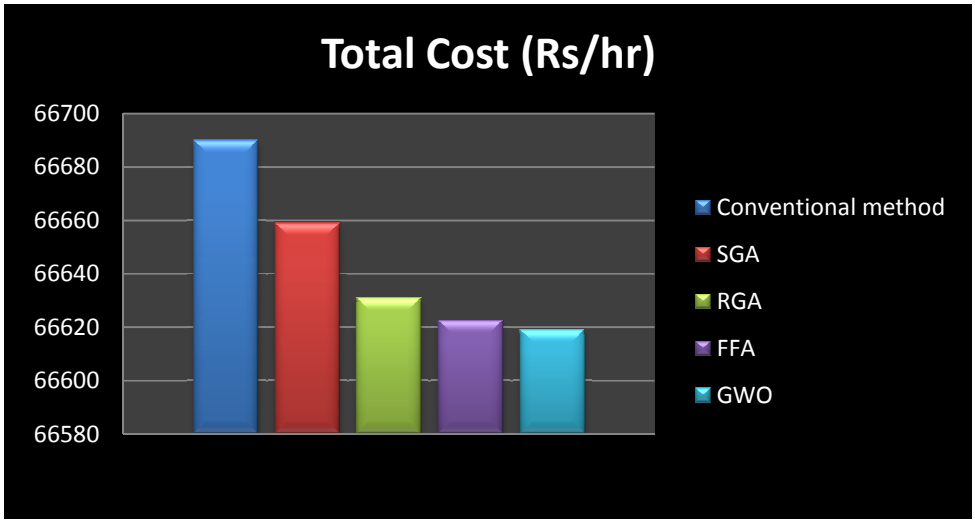

Fig.1: Comparison results for 3-Unit system with 700MW demand

2) Test system 2

In this test case a system with 6 generating units with NOx emissions is used to reveal the effectiveness of GWO for this type of system. The unit's data, such as cost & emission coefficients, B-loss coefficients, generation limits, are given in [19]. The load demands are 500,700 and 900 MW. The best compromising results achieved from GWO are shown in table 3 and their comparison with other techniques is shown in table 4.

Table.3: Best compromise solution of fuel cost and NOx emission for six-generator system

	Load Demand		
	500	**700**	**900**
Unit 1	33. 137	61.855	92.352
Unit 2	26. 821	61.382	98.373
Unit 3	89.928	120.030	150.087
Unit 4	90.553	119.577	148.457
Unit 5	135.805	178.564	220.423

https://dx.doi.org/10.22161/ijaers/3.11.5 *ISSN: 2349-6495(P) | 2456-1908(O)*

Unit 6	132.689	175.654	218.320
Pf_N (Rs/Kg)	43.1533	43.8983	47.822
Fuel cost(Rs/hr)	27612.23	37493.95	48350.41
Emission(Kg/hr)	263.03	439.764	693.79
Power loss(MW)	8.93	17.064	28.013
Total cost(Rs/hr)	38963.10	56798.88	81529.18

Table.4: Comparison of best compromise solution of fuel cost and NOx emission for six-generator system(900 MW demand)

Performance	Conventional Method [13]	RGA [13]	Hybrid GA [13]	Hybrid GTA [13]	FFA[20]	GWO
Fuel cost, Rs/hr	48892.900	48567.7	48567.5	48360.9	48353.4	48350.41
Emission, kg/hr	701.428	694.169	694.172	693.570	693.729	693.79
Power loss, MW	35.230	29.725	29.718	28.004	28.004	28.013
Total cost, Rs/hr	82436.580	81764.5	81764.4	81529.1	81529.01	81529.1

3) Test system 3

In this case system having 3 generating units considering NOx and SOx emissions is tested. The input data for generating units is taken from [5]. The power demandis 850MW. The best negotiating results achieved from GWO and its comparison with NSGA-II [5] is shown in table 5.

Table.5: EELD with NOx& SOxemission for 3-unit system with load demand of 850 MW

	Combined economic emission dispatch solution	
Unit Power Output	**NSGA-II [6]**	**GWO**
P1(MW)	496.328	506.7511
P2(MW)	260.426	252.0804
P3(MW)	108.144	105.9419
Total power output(MW)	864.898	864.7734
Ploss (MW)	14.898	14.769
Fuel Cost ($/hour)	8358.896	8364.148517
SOX Emission (Ton/hour)	8.97870	8.9743
SOX Price Penalty Factor($/Ton)	970.031570	970.0316
NOX Emission (Ton/hour)	0.09599	0.095925
NOX Price Penalty Factor($/Ton)	147582.78814	147582.78814
Total Cost ($/hour)	31234.99029	31226.91617

https://dx.doi.org/10.22161/ijaers/3.11.5 *ISSN: 2349-6495(P) | 2456-1908(O)*

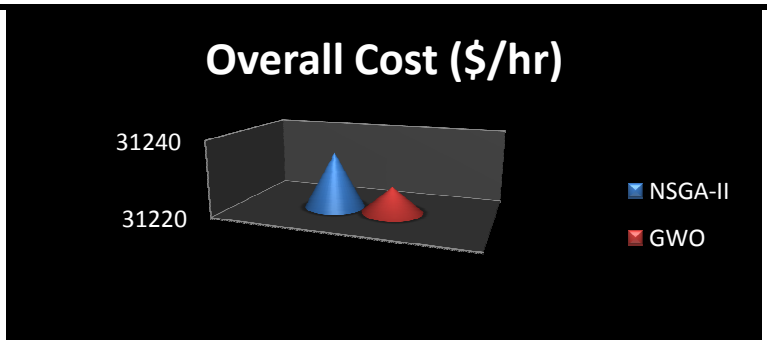

Fig.2: Comparison results for 3-generating units with NOx & SOx emission

4) Test system 4

A system with 6 generating units considering SOx, COx and NOx emissions is tested .The input data for generating units is taken from [18]. The power demand is 1800 MW. The compromised results achieved from GWO and its comparison with PSO [18] and BBO [14] is shown in table 6.

Table.6: EELD with SOx, NOx and COx emission for 6-unit system with load demand of 1800 MW

Unit power output	Combined economic emission dispatch solution		
	PSO [18]	BBO[14]	GWO
P1 (MW)	279.19	270.398419	270.4809687
P2 (MW)	350.52	299.351832	299.4672109
P3 (MW)	467.90	538.382133	538.2400654
P4 (MW)	176.26	139.632475	139.6657591
P5 (MW)	394.74	452.562062	452.3213489
P6 (MW)	256.20	245.197113	245.3152183
Total power output (MW)	1924.81	1945.524034	1945.490571
P loss (MW)	124.81	145.524034	145.490571
Fuel cost ($/hr)	18689.01	18934.704952	18934.20964
NOX emission (kg/hr)	2432.25	2416.130219	2415.944898
NOX PPF ($/kg)	9.362740	9.362740	9.362740
SOX emission (kg/hr)	14620.07	13491.924811	13492.71155
SOX PPF ($/kg)	1.670211	1.670211	1.670211
COX emission (kg/hr)	62856.00	68817.333954	68804.24931
COX PPF ($/kg)	0.244623	0.244623	0.244623
Total cost ($/hr)	81256.159388	80924.967912	80925.01058

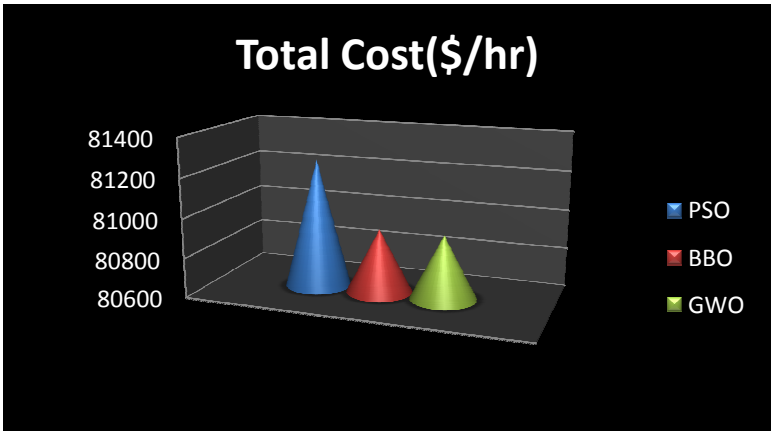

Fig.3: Comparison results for 6 generating units considering SOx, Cox & NOx emissions

https://dx.doi.org/10.22161/ijaers/3.11.5 *ISSN: 2349-6495(P) | 2456-1908(O)*

V. CONCLUSION

The GWO algorithm is effectively applied for solving multi-objective EELD problem. It is apparent from the obtained results that the proposed GWO algorithm can evade the deficiency of early convergence of the genetic algorithm and particle swarm optimization methods to get superior solutions. The results confirmed that GWO was able to give competitive results in comparison to GA, hybrid GA, PSO, FFA and BBO. The novel probabilistic model of searching, encircling and hunting the prey handle the trouble of early convergence. Because of simplicity and effectiveness of the GWO method, it can be useful for searching better results in difficult power system problems in future.

REFERENCES

[1] Wood, A. J. and Wollenberg, B. F., Power Generation, Operation, and Control, 1996, Wiley, New York, 2nd Ed.

[2] Nanda, J., Khotari, D. P., and Lingamurthy, K. S., “Economic-emission load dispatch through goal programming techniques,” IEEE Trans. Energy Conversion, Vol. 3, No. 1, pp. 26–32, March 1988.

[3] Song, Y. H., Wang, G. S., Wang, P. Y., and Johns, A. T., “Environmental/economic dispatch using fuzzy logic controlled genetic algorithms,” IEE Proc. Generat. Transm. Distrib., Vol. 144, No. 4, pp. 377–382, July 1997.

[4] Abido, M. A., “A niched Pareto genetic algorithm for multi-objective environmental/economic dispatch,” Elect. Power Energy Syst., Vol. 25, No. 2, pp. 79–105, February 2003.

[5] Rughooputh, H.C.S.; Ah King, R.T.F., "Environmental/economic dispatch of thermal units using an elitist multiobjective evolutionary algorithm," Industrial Technology, 2003 IEEE International Conference on , vol.1, no., pp.48,53 Vol.1, 10-12 Dec. 2003

[6] R. T. F. Ah King and H. C. S. Rughooputh, “Elitist Multi-objective Evolutionary Algorithm for Environmental/Economic Dispatch,”Congress on Evolutionary computation, vol. 2, pp. 1108-14, 8-12 Dec.2003.

[7] Thenmozhi, N.; Mary, D., "Economic emission load dispatch using hybrid genetic algorithm," TENCON 2004. 2004 IEEE Region 10 Conference, vol.C, no., pp.476,479 Vol. 3, 21-24 Nov. 2004 doi: 10.1109/TENCON.2004.1414811

[8] Perez-Guerrero, R.E.; Cedeno-Maldonado, J.R., "Differential evolution based economic environmental power dispatch," Power Symposium, 2005. Proceedings of the 37th Annual North American , vol., no., pp.191,197, 23-25 Oct. 2005

[9] Hong-da Liu; Zhong-li Ma; Sheng Liu; HaiLan, "A New Solution to Economic Emission Load Dispatch Using Immune Genetic Algorithm," Cybernetics and Intelligent Systems, 2006 IEEE Conference on , vol., no., pp.1,6, 7-9 June 2006

[10] Hazra, J.; Sinha, A.K., "Environmental Constrained Economic Dispatch using Bacteria Foraging Optimization," Power System Technology and IEEE Power India Conference, 2008. POWERCON 2008. Joint International Conference on , vol., no., pp.1,6, 12-15 Oct. 2008

[11] Hemamalini, S.; Simon, S.P., "Emission constrained economic dispatch with valve-point effect using particle swarm optimization," TENCON 2008 - 2008 IEEE Region 10 Conference , vol., no., pp.1,6, 19-21 Nov. 2008

[12] M. Sudhakaran, S.M.R Slochanal, R. Sreeram and N Chandrasekhar, “Application of Refined genetic Algorithm to Combined Economic and Emission Dispatch” J. Institute Of Engg. (India) volume-85, Sep. 2004pp. 115-119.

[13] M. Sudhakaran and S.M.R Slochanal, “Integrating Genetic Algorithm and Tabu Search for Emission and Economic Dispatch Problem” J. Institute of Engg. (India) volume-86, June.2005, pp-22-27.

[14] Bhattacharya, Aniruddha, and P. K. Chattopadhyay. "Application of biogeography-based optimization for solving multi-objective economic emission load dispatch problems." Electric Power Components and Systems 38, no. 3 (2010): 340-365.

[15] Niknam, T.; Golestaneh, F.; Sadeghi, M.S., " - Multiobjective Teaching–Learning-Based Optimization for Dynamic Economic Emission Dispatch," Systems Journal, IEEE , vol.6, no.2, pp.341,352, June 2012

[16] Abedinia, O.; Amjady, N.; Naderi, M.S., "Multi-objective Environmental/Economic Dispatch using firefly technique," Environment and Electrical Engineering (EEEIC), 2012 11th International Conference on , vol., no., pp.461,466, 18-25 May 2012

[17] Kumarappan, N.; Mohan, M.R.; Murugappan, S., "ANN approach applied to combined economic and emission dispatch for large-scale system," Neural Networks, 2002. IJCNN '02. Proceedings of the 2002 International Joint Conference on , vol.1, no., pp.323,327, 2002

https://dx.doi.org/10.22161/ijaers/3.11.5 *ISSN: 2349-6495(P) | 2456-1908(O)*

[18] AlRashidi, M. R., and El-Hawary, M. E., "Emission-economic dispatch using a novel constraint handling particle warm optimization strategy," Canadian Conference on Electrical and Computer Engineering 2006, pp. 664–669, Ottawa, Canada, 7–10 May 2006.

[19] Gaurav Prasad Dixit, Hari Mohan Dubey, ManjareePandit, B. K. Panigrahi, "Artificial Bee Colony Optimization for Combined Economic Load and Emission Dispatch", International Conference on Sustainable Energy and Intelligent System (SEISCON 2011) ,Dr.M.G.R. University, Maduravoyal, Chennai, Tamil Nadu, India. July.20-22, 2011.

[20] Dinakara Prasad Reddy P, J N Chandra Sekhar ,"Application of Firefly Algorithm for Combined Economic Load and Emission Dispatch" International Journal on Recent and Innovation Trends in Computing and Communication, Vol.2 , No.8(2014):2448-2452

[21] Abido MA. A novel multiobjective evolutionary algorithm for environmental economic power dispatch. Electr Power Syst Res 2003;65(1):71–81.

[22] Abido MA. Environmental/economic power dispatch using multiobjective evolutionary algorithms. IEEE Trans Power Syst 2003;18(4):1529–37

[23] Abido MA. Multiobjective particle swarm optimization for environmental economic dispatch problem. Electr Power Syst Res 2009;79(7):1105–13.

[24] Hota PK, Barisal AK, Chakrabarti R. Economic emission load dispatch through fuzzy based bacterial foraging algorithm. Int J Electr Power Energy Syst 2010;32(7):794–803.

[25] Mirjalili, Seyedali, Seyed Mohammad Mirjalili, and Andrew Lewis. "Grey wolf optimizer." Advances in Engineering Software 69 (2014): 46-61.

[26] Dr.Sudhir Sharma, Shivani Mehta, Nitish Chopra, "Economic Load Dispatch using Grey Wolf Optimization"Vol.5-Issue 4(April-2015),International Journal Of Engineering Research and Applications(IJERA),ISSN:2248-9622,www.ijera.com

[27] N. Chopra and S. Mehta, "Multi-objective optimum generation scheduling using Ant Lion Optimization," 2015 Annual IEEE India Conference (INDICON), New Delhi, 2015, pp. 1-6.doi: 0.1109/INDICON.2015.7443839.

https://dx.doi.org/10.22161/ijaers/3.11.6 *ISSN: 2349-6495(P) | 2456-1908(O)*

Accurate and Efficient Query Processing at Location-Based Services by using Route APIs

K. Bhavana[1], Dr. K. Venugopala Rao[2]

[1]M. Tech Student, Department of CSE, G. Narayanamma Institute of Technology and Science, Mandal Shaikpet, District Hyderabad, Telangana, India.

[2]Professor, Department of CSE, G. Narayanamma Institute of Technology and Science, Mandal Shaikpet, District Hyderabad, Telangana, India.

Abstract— *Efficient query processing system provides best search results to user by gathering user point of interest. Mobile users required a Location based server (LBS) to search the spatial related data. Existing system provided route results but it takes more time to execute the query and does not gives the accurate results means traffic related travel timings. The proposed system is a fastest processer for location search users. Here, LBS obtain route travel times from online route API. So it gives the accurate results to user by preventing number route request and query execution time. We use range query algorithm to reduce the number of route request and Parallel Scheduling Techniques to reduce the query execution time. Our experimental result shows that the proposed system is more efficient than existing processer.*

Keywords— Location based Server, Query Processing, Query Execution Time, Range Query, Spatial Data.

I. INTRODUCTION

Based on user point of interest, user may search the data related to street and restaurant data with location based Services. By using location based Services, a route API can find out exact travel times. Finding an optimal route in a road network between specified source and destination nodes (i.e., based on user point of interest) is one of the important things in real-world applications [10]. But whenever using route API, it takes more time to access the route. So we can reduce this problem by using Parallel Scheduling Techniques in LBS. LBS find exact results by using lower/upper bound techniques. This approach was recently shown to be very effective if lower bounds are computed using Parallel Scheduling Techniques [10]. The resulting lower bound could be used for distinguishing local and global queries for guiding local search.

Location-based server(LBS) use real-time geo-data from a mobile device or Smartphone or Computer device to provide data to user. Some services allow user to "check in" at restaurants, coffee shops, book stores, concerts, and other places or events. Often, businesses offer a reward prizes, coupons or discounts to people who check in Google Maps and Facebook Places are among the more popular services. Location-based services use a smartphone's GPS technology to find a person's location, if that person has opted-in to allow the service to do that. User can identify her area with using smartphone GPS technology without the need for manual work.

II. LITERATURE SURVEY

Web search is common in our daily lives. Caching method has been extensively used to reduce the query execution time of the search system and reduce the travel time on a road network. Another form of location related web search, known as online shortest path search, is enhanced approach due to advances in geo-positioning. However, existing caching techniques are ineffective for shortest path queries. This is due to several crucial differences between web search results and shortest path results, in relation to query matching, cache item overlapping, and query execution time. So we can manage those things by using Parallelized route requests.

If we are using LBS, It must be satisfied two things a) exact query result (i.e., exact travel timing, exact directions and exact map between sources to destination) b) less query execution time.

In Existing System **SMashQ** (Spatial mash up framework for k-NN queries) is used for best results. The k-nearest-neighbor (k-NN) query is one of the well known spatial query types for location-based services (LBS). It focus on k-NN queries in time-based road networks, where the travel time between source and destination locations may changes significantly at different time of the day [3]. In practice, it is difficult for a LBS provider to gather travel timing to find the correct route for a user to a spatial object of interest. So, we design SMashQ, a server-side spatial mashup framework that enables a database server to efficiently evaluate k-NN queries using the route data and travel time accessed from an external Web mapping service, e.g., Microsoft Bing Maps, Google API Direction. Because of the expensive cost and limitations of accessing such unnecessary external information, we propose three shared execution optimizations for

https://dx.doi.org/10.22161/ijaers/3.11.6 *ISSN: 2349-6495(P) | 2456-1908(O)*

SMashQ, to reduce the number of external route requests and provide highly accurate query answers. But it is not possible with SMashQ [13]. So here we are using range query search for accurate travel timings and less query execution time.

Use the Routes API to create a route and map that includes two or more locations and to create routes from major roads for security purpose. We can create driving or walking mode routes. Route data consists of a graphical representation of the route, a detailed turn-by-turn route description, travel times and exact directions. It enables mapping applications to provide the geographical representation of the route together with the map data, so that the route is displayed on the map to user. The Routing API is customizable so that the route calculation and additional route data can be adapted to both consumer and enterprise applications and specific application use cases. Here Routing API calculates routes between two or more points based on user interest [1] and it provides to the LBS and finally LBS send the additional route-related information like exact Direction and Travel timings to users.

III. SYSTEM DESIGN

The proposed query processing system is client-server architecture and it uses a Google route API with clients as mobile device (or) computer device and server on a computer device. This system is used to reduce query response time and number of route requests. The architecture need to meet the necessary conditions for implementing the whole system.

- First, User sends the point of interest to Location based services and this LBS integrated with route API [1].
- Second, This LBS uses the range search for accurate lower/upper bound travel time.
- Finally, It uses the parallelize route request to reduce the query response time.

System flow of the query processing can be identified as shown in Fig.1.The process initiates with a client issues a user query request. Each user having different point of interest so user search the hotels based on interest. First user send query to the location based services then these LBS's return the results with the help of Google route API. In LBS a range search algorithm is used for accurate query results (i.e., exact travel timings and directions) and less query execution time. A user sends area to server for Search the hotel. Based on area it showing the number of best hotels, map button showing the route map, travel timings and directions to the hotel, after selecting the hotel.

$$\overline{cw}(e)=dist(e)/V_{MAX} \quad (1)$$

$$p.t_c^{-}=spt_{cw}-(q,p) \quad (2)$$

In second step, LBS find out the lower/upper bound travel timings with using above equations (1), (2).Where $\overline{cw}(e)$ means lower bound travel time of a edge and V_{MAX} means maximum speed.

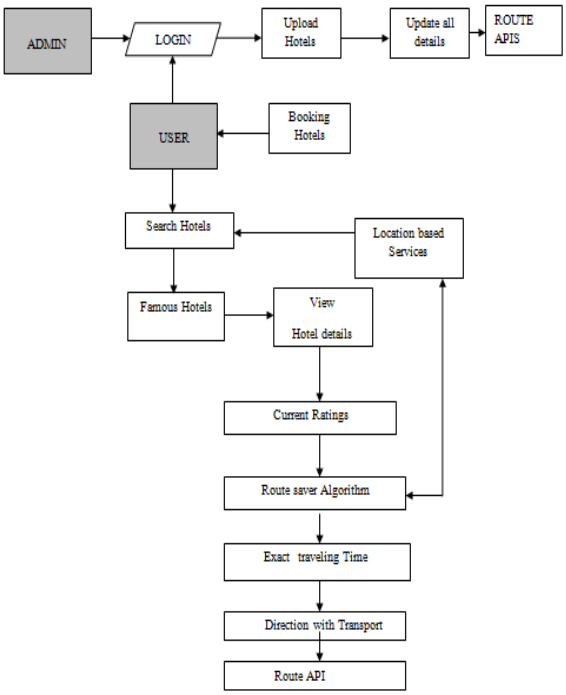

Fig.1: System flow of query processing system.

IV. FRAMEWORK

To implement the complete system the procedures section is introduced. The procedural section is examined in various sections which are:

4.1 Location based Server

This LBS takes the input as query from user and send the route request to online route API. LBS contains 3 parts and those are point of interest, route log and road network. It finds out user point of interest based on given query by using point of interest field. It sends the user interest as route request to route API. This route API provides a shortest path to LBS [8]. It stores exact routes and travel timings by using route log. Finally, it forwards the results to user.

4.2 Parallel Scheduling Techniques

Our aim is to reduce the query response time and this paper proposes advanced method for minimum query response time through parallel scheduling techniques. We can reduce the query response time by reducing number of route request. Here we use two techniques to reduce the customer response time and number of route request. Customer response time takes the more time than time spent on route request [4]. So we are considering query response time from route API's. However, Existing parallel scheduling methods having some problems related to route request because it takes extra route

https://dx.doi.org/10.22161/ijaers/3.11.6 *ISSN: 2349-6495(P) | 2456-1908(O)*

requests. Here we have two parallelization techniques to avoid the extra route requests. In first method, Greedy parallelization takes less execution time but it does not gives the exact result and another method Direction-based parallelization takes less execution time and gives the exact travel timings.

4.3 Range Query Algorithm

In this case, it presents our Route-Saver algorithm for processing a range query. It applies the travel time bounds discussed above to reduce the number of route requests. To guarantee the accuracy of returned results, it removes all expired routes in route log L. The algorithm first conducts a distance range search for P on G [6] to obtain a set C of candidate points. This algorithm consists of two phases to process the candidate points in C and store the query results in the set R. The first phase aims to shrink the candidate set C, so as to reduce the number of route requests to be issued in the second phase. First, we execute Dijkstra on G two times, using edge weight respectively.

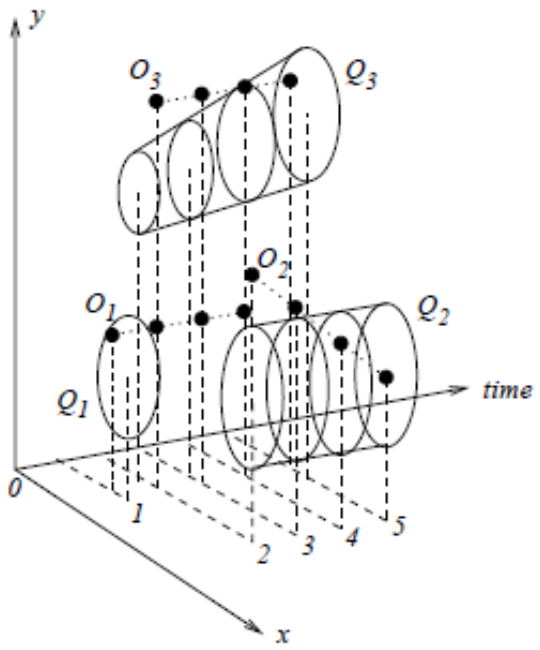

Fig.2: Predictive range query.

In predictive range query, there are three kinds of queries are distinguished based on the time span and the region they specify. Similarly, we distinguish three kinds of queries for the predictive range query: timeslice query, time-interval query and moving query. The above figure shows examples of the three kinds of predictive range queries in a 2-dimensional space. Together with the time dimension, the coordinate space is 3-dimensional. We use point objects in these examples for ease of presentation, although the following discussions also apply to objects with extents [11]. Q1 is a timeslice range query at timestamp 1. Its query region is a disk. Object O1 is in it, while O2 or O3 is not in it. Therefore the answer to Q1 is O1. *Q*2 is a time-interval range query spanning the period [2,5]. Its query region is a cylinder. At timestamp 2, no object is in *Q*2. Object *O*2 is moving and it moves into *Q*2 at timestamps 4 and 5. Objects *O*1 and *O*3 are not moving and they stay outside of *Q*2 all the time. Therefore the answer to *Q*2 is *O*2. *Q*3 is a moving range query spanning the period [2,5]. The center and radius of *Q*3 are both changing during the querying period. The query region of *Q*3 is a leaning truncated cone. No object is in *Q*3 at timestamp 2. Although *O*3 does not move, it is in *Q*3 at timestamps 4 and 5 because of the movement of *Q*3. The other two objects are outside of *Q*3 all the time. Therefore the answer to *Q*3 is *O*3. From these examples, we can see that the relative movements of objects and time are important factors to determine answers [11]. So the below route saver algorithm is used to reduce the number of route request.

Input: function Route-Saver-RANGE (Query (q,T), Data set P)

- The first phase aims to shrink the candidate set C, so as to reduce the number of route requests to be issued in the second phase.
- It execute Dijkstra on G two times so its compute the bounds p.t $_{G}^{-}$, p.t $_{G}^{+}$ and p.t $_{G}$ for every candidate p € C.
- Next, for each candidate p remaining in C, its compute exact travel time p.t $_{L}$ using optimal sub path property in L and use p.t $_{L}$ to detect true result.
- In the second phase, it issue route requests for the remaining candidates in C then insert the returned route into the route log L.
- This route provides not only the exact travel time for p, but also potential information for updating the bounds for other candidate p [1].

Output: This algorithm returns result set R to the user with accurate query result.

V. EXPERIMENTAL RESULTS

The mobile system or any system required an online route API to answer location related query and this route API integrated with location based server to provide a best search relevancy of results. However, it shows exact map between source and destination along with query execution time and here we can select the traveling mode. It shows exact travel timing based on traveling mode. Finally, it shows exact route direction to user.

https://dx.doi.org/10.22161/ijaers/3.11.6 *ISSN: 2349-6495(P) | 2456-1908(O)*

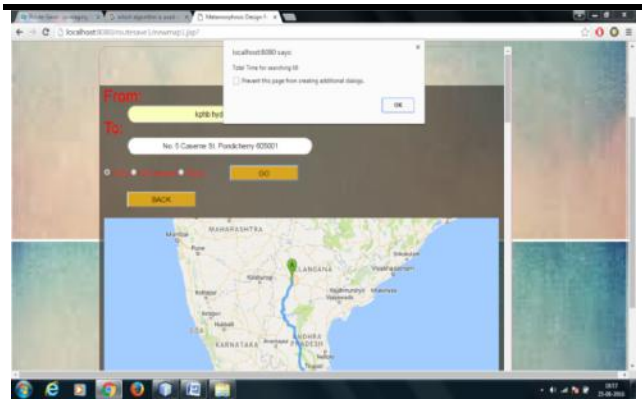

Fig.3: Showing map result

If user clicks map button in showing hotel details page then it shows the map between source and destination.

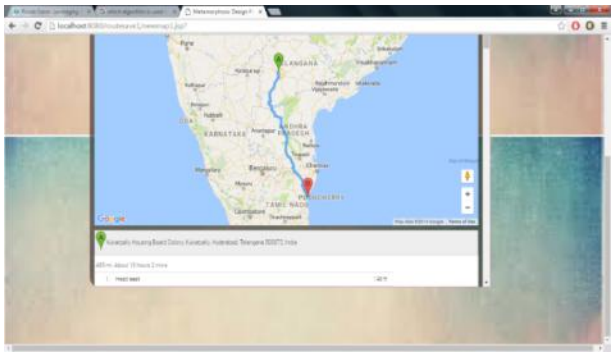

Fig.4: Showing travel times

It shows exact travel timing from user location to particular hotel.

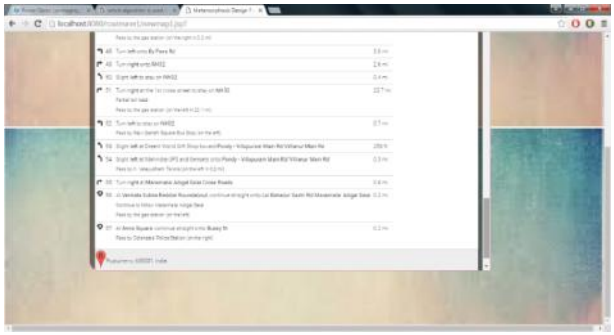

Fig.5: Showing exact directions

It shows exact direction from user location to particular hotel.

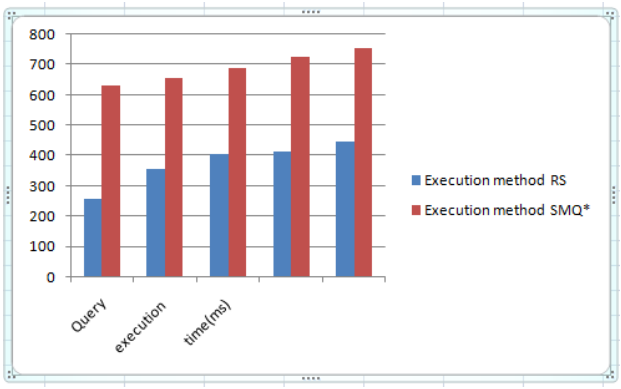

Fig.6: Showing different queries execution times

Our experiment shows the query execution time in Route saver method. We find out SMQ* query execution time based on survey. The above bar chart shows that query response time of a two execution methods and it express that route saver is more efficient than SMQ* in the point of query response time.

VI. CONCLUSIONS AND FUTURE SCOPE

It proposes a solution for the LBS to process range queries such that the query results have accurate travel times and the LBS incurs few number of web mapping requests. The time-tagged road network G and the route log L to derive lower and upper bounds of travel times for data points. During query processing, it exploits those routes to derive effective lower-upper bounds for saving web mapping requests, and examines the candidates for queries in an effective order. This solution shows that Route-Saver is more efficient than SMashQ.

In future, it can be enhanced to investigate automatic tuning the expiry time d based on a given accuracy requirement. This would help the LBS guarantee its accuracy and improve their users' satisfaction.

REFERENCES

[1] Yu Li and Man Lung Yiu, "Route-Saver: Leveraging Route APIs for Accurate and Efficient Query Processing at Location-Based Services," 2015, pp. 235-249.

[2] D. Papadias, J. Zhang, N. Mamoulis, and Y. Tao, "Query processing in spatial network databases," in Proc. 29th Int. Conf. Very Large Data Bases, 2003, pp. 802–813.

[3] D. Zhang, C.-Y. Chow, Q. Li, X. Zhang, and Y. Xu, "SMashQ: Spatial mashup framework for k-NN queries in time-dependent road networks," Distrib. Parallel Databases, vol. 31, pp. 259–287, 2012.

[4] E. Kanoulas, Y. Du, T. Xia, and D. Zhang, "Finding fastest paths on a road network with speed patterns," in Proc. Int. Conf. Data Eng., 2006, p. 10.

[5] E. P. F. Chan and Y. Yang, "Shortest path tree computation in dynamic graphs," IEEE Trans. Comput., vol. 58, no. 4, pp. 541–557, Apr. 2009.

[6] Google Directions API. (2013). [Online]. Available:https://developers.google.com/maps/documentation/directions/

[7] H. Samet, J. Sankaranarayanan, and H. Alborzi, "Scalable network distance browsing in spatial databases," in Proc. ACM SIGMOD Int. Conf. Manage. Data, 2008, pp. 43–54.

[8] J. R. Thomsen, M. L. Yiu, and C. S. Jensen, "Effective caching of shortest paths for location-based services," in Proc. ACM SIGMOD Int. Conf. Manage. Data, 2012, pp. 313–324.

[9] Pankaj K. Agarwal, "Range Searching", Available:https://www.cs.duke.edu/~pankaj/publications/surveys/.

https://dx.doi.org/10.22161/ijaers/3.11.6 *ISSN: 2349-6495(P) | 2456-1908(O)*

[10] Peter Sanders and Dominik Schultes," Robust, Almost Constant Time Shortest-Path Queries in Road Networks", Available: http://algo2.iti.kit.edu/schultes/hwy/hhTransit.pdf

[11] Rui Zhang1, H. V. Jagadish2, Bing Tian Dai3, Kotagiri Ramamohanarao4," Optimized Algorithms for Predictive Range and KNN Queries on Moving Objects", Available: http://www.ruizhang.info/publications/IS_MovingRangeKnn.pdf.

[12] U. Demiryurek, F. B. Kashani, C. Shahabi, and A. Ranganathan, "Online computation of fastest path in time-dependent spatial networks," in Proc. 12th Int. Symp. Adv. Spatial Temporal Databases, 2011, pp. 92–111.

[13] Wan D. Bae1 , Shayma Alkobaisi1 , Seon Ho Kim1 , Sada Narayanappa1, "Supporting Range Queries on Web Data Using *k*-Nearest Neighbor Search", Available: http://infolab.usc.edu/DocsDemos/w2gis.pdf .

International Journal of Advanced Engineering Research and Science (IJAERS) *[Vol-3, Issue-11, Nov- 2016]*
https://dx.doi.org/10.22161/ijaers/3.11.7 *ISSN: 2349-6495(P) | 2456-1908(O)*

Experimental Study of Convective Heat Transfer in a Horizontal Tube Using Nanofluids

Anurag Hatwar [1], V.M.Kriplani[2*]

Vishwabharti academy College of Engineering, Ahemednagar, India
Professor, G.H.Raisoni College of Engineering, Nagpur, India

Abstract*—Experimental analysis of heat transfer characteristics of Al_2O_3/water and CuO/water nanofluids flowing inside a horizontal circular tube heated with uniform heat flux is conducted at Reynolds number range of 2800 to 5000. Al_2O_3 and CuO nanoparticles of 45 nm average size dispersed in distilled water to form stable nanofluids. The volume concentration range of both nanofluids was 0.1% to 0.7%. The result indicates that heat transfer coefficient of both nanofluids increase as compared to base fluid, water. The heat transfer coefficient of CuO/water nanofluid is higher than that of Al_2O_3 nanofluid for the same concentration and same Reynolds number. In case of CuO/water nanofluid the percentage increase in heat transfer coefficient at Reynolds number 4800 was 40% as compared to water (at 0.1 vol. %) while in case of Al_2O_3/water nanofluid it was 22.2%. Further, the pressure drop by using nanofluids was not noticeable.*

Keywords*— Enhancement, Heat transfer, heat exchanger, nanofluid, thermal conductivity.

Nomenclature

A Outer surface area of the experimental tube (m^2)
Cp specific heat of fluid (J/kg K)
d_{hyd} hydraulic diameter of experimental tube (m)
h heat transfer coefficient (W/m^2K)
k thermal conductivity (W/m K)
m mass flow rate of the fluid (kg/s)
Nu average Nusselt number = (h_{exp} d_{hyd}) / k
P tube periphery (m)
Pr Prandtl number = μ Cp/k
Q heat transfer rate (W)
Re Reynolds number = ρ u d_{hyd} / μ
S cross- sectional area of the experimental tube
T temperature (K)
U fluid velocity (m/s)

Greek letters

ρ Density (kg/m^3)
μ Viscosity (kg/m s)
Ø Volume fraction

Subscripts

b bulk
exp. experimental
in inlet
nf nanofluid
out outlet
p particle
w wall

I. INTRODUCTION

In the last few decades we have seen unprecedented growth in electronics, communication and computing technologies and will continue to grow at the faster rate. Thermal management of high power systems like hybrid electric vehicles (HEV), aerospace applications, microprocessors heat fluxes etc. are challenging issues. Electronic devices, lasers, high-power x-rays, and optical fibers are integral parts of today's computation, scientific measurement, medicine, material synthesis, and communication devices all these require high performance compact cooling techniques. Enhancement of heat transfer and reduction of energy losses is most important to deal with the energy wastage problems. Extended surfaces technologies such as fins, micro channels are reaching to their limits. Therefore, new technologies which have potential to improve the thermal properties of cooling fluids are of great interest to the researchers. Conventional fluids such as water, ethylene glycol and mineral oils possess poor thermal conductivity. A possible effective way of improving heat transfer performance on conventional fluids is to suspend small solid particles, such as metallic (e.g. Cu, Ag) and non-metallic (e.g. CuO, Fe_2O_3, Al_2O_3, TiO2) particles in conventional fluids. Recent developments in nanotechnology and related manufacturing techniques have made possible to manufacture the nanosized particles. Fluids with nanoparticles (diameter less than 100 nm) suspended in conventional fluids are called nanofluids, as coined by Stephen U.S.Choi and J.A.Eastman [1] early in 1995, Argonne National Laboratory, U.S.A., to increase the

https://dx.doi.org/10.22161/ijaers/3.11.7 *ISSN: 2349-6495(P) | 2456-1908(O)*

heat transfer characteristics. Nanofluid due to its molecular chain behavior, nanoparticles properly dispersed in the base fluid achieved major benefits such as higher heat conduction, microchannel cooling without clogging, reduced chances of erosion and pumping power with enhancement in thermal conductivity and stability of mixture. Heat transfer takes place at the surface of particles and therefore it is desirable to use particle size with a large surface area. Nanoparticles have extremely large surface areas and therefore much higher heat transfer. Particles having size less than 20 nm carry 20% of their atoms on their surface [13] making them available instantaneously for thermal interaction. In general the above features of nanofluids provide us the new area of research in nanofluid technology, plays an important role to improve heat transfer and energy efficiency in several areas including vehicular cooling in transportation, power generation, defense, nuclear, space, microelectronics and biomedical devices.

C.J.Ho et al.[2] experimentally investigated the forced convective cooling performance of a copper microchannelheat sinkwith Al_2O_3/water nanofluid as the coolant, Reynolds number ranging 226 to 1676. Results showed that the nanofluid-cooled heat sink have significantly higher average heat transfer coefficient and therby lower thermal resistance, friction factor was found slightly increased. Zeinali Heris et al. [3] experimentally investigated convective heat transfer of Al_2O_3 nanofluid in laminar flow through circular tube with constant wall temperature. The results indicate that heat transfer coefficient of nanofluids increases with Peclet number as well as nanoparticles concentration. Thermal conductivity may not be the only reason for heat transfer enhancement in nanofluids. Dispersion and chaotic movement of nanoparticles Brownian motion and particle migration may also cause the enhancement. S. M. Peyghambarzadeh et al. [4] convective heat transfer in Al2O3/water nanofluid has been experimentally compared with that of pure water in automobile radiator. Concentration range used was 0.1 to 1.0 vol.%, liquid flow rate 2 – 5 liters/min., turbulent flow range $9x\ 10^3 < Re < 2.3\ x10^4$. In addition the effect of inlet temperature of $37 – 49^0C$ to the radiator on heat transfer analysed. Results demonstrate that flow rate increase improve the heat transfer performance while flow inlet temperature to the radiator has trival effects. S.M.Fotkian et al.[5] experimentally investigated turbulent heat transfer and pressure drop of Al_2O_3/water nanofluid in a circular tube. The volume fractions of nanoparticles in base fluid were 0.03%, 0.054%, 0.067% and 0.135%. Results indicated the enhancement of heat transfer, but increasing the volume fraction of nanoparticles in the range used in their work did not show much effect on enhancement of heat transfer. Pressure drop observed was much grater than base fluid. Experimental results were compared with the existing correlations. .Mangrulkar C.K., Vilayatrai M.Kriplani [6] reviewed the work of the researchers. K.B.Anoop et al. [7] an experimental investigation on convective heat transfer characteristics in the developing region of tube flow with constant heat flux was carried out with alumina-water nanofluids to evaluate the effect particle size on convective heat transfer in laminar developing region. Average particle size of 45 nm and 150 nm were used. Nanofluid with 45 nm particles showed higher heat transfer coefficient than that with 150 nm particles in laminar developing region than developed region. M.H.Kayhani et al. [8] Experimental analysis of turbulent convective heat transfer of Al2O3/water nanofluid flowing inside uniformly heated horizontal tube with Al2O3 nanoparticles 40 nm size, volume concentration 0.1, 0.5, 1.5 and 2.0% was conducted. Results show that convective heat transfer enhancement for 2.0% volume concentration Nusselt number increased by 22% ar Re no. 13500.Comparaison between experimental results with existing correlations was also done. Ahmed Elsayed et al. [10] their work presents a numerical study to investigate the combined effect of using helical coils and nanofluids on heat transfer characteristics and pressure losses in turbulent flow regime. Combine effect of Al2O3nanofluid and tube coiling could enhance the heat transfer coefficient by up to 60% compared with that of pure water in straight tube at the same Reynolds number. Pressure drop in helical coils using Al2O3/water for volume fraction of 3% was six times that of water in straight tube (80% of pressure drop increase due to nanoparticles addition). M.Naraki et al.[11] experimentally investigated the overall heat transfer coefficient of CuO/water nanofluid under laminar flow ($100 \leq Re \leq 1000$) in a car radiator. Results indicate the increase in overall heat transfer coefficient with increase in nanofluid concentration (0 to 0.4 vol.%). However, it decreases with increase in nanofluid temperature from 50 to 80^0C.In the developing region, the heat transfer coefficients show higher enhancement than in developed region. At concentration of 0.15 and 0.4 vol.% of CuO nanoparticles, he overall heat transfer coefficient enhancements compared with the pure water are 6% and 8%.

The main objective of work was experimental investigation of heat transfer enhancement in horizontal tube using naofluids. The nanoparticles, Al_2O_3 and CuO, were selected, as metallic oxides are cheaper than metallic one,

https://dx.doi.org/10.22161/ijaers/3.11.7 *ISSN: 2349-6495(P) | 2456-1908(O)*

though metals have much higher thermal conductivity than metallic oxides and therefore, higher heat transfer enhancement. Base fluid chosen was distilled water.

II. NANOFLUID PREPARATION

The first step in experimental studies is the preparation of nanofluids. Preparation of a stabilized nanofluid is of great importance in heat transfer applications of nanofluids. Poorly prepared nanofluids will render biphasic heat transfer (i.e. solid-liquid). Dispersant or surfactant was not added as they may change the properties of the nanofluid. Nanofluids were prepared with nanoparticles Al_2O_3 and CuO (average size 45 nm) with deionized water as base fluid. The nanoparticles were purchased from Sigma Aldrich, Germany.

Specific quantities of nanoparticles were mixed with distilled water as the base fluid for both and stirred with magnetic stirrer for about eight hours. The stirred nanofluid was kept for about 24 hrs. And no sedimentation was observed. Immediately the experiment was started.

Table.I: Properties of Al_2O_3 and CuO nanopowders

Properties	Al_2O_3	CuO
Diameter (nm)	45	45
Density (kg/m3)	3700	800
Sp.Heat (J/kg-K)	880	660
Thermal Conductivity (W/m-K)	46	62

III. NANOFLUID PROPERTIES

Thermophysical properties of the nanofluid must be known before using for experimental test. The nanoparticles are assumed to be well dispersed in the base fluid and concentration of nanoparticles is assumed to be uniform in the tube. The thermo-physical properties of prepared nanofluids are calculated from water and nanoparticles characteristics at mean inlet and outlet bulk temperatures. The following correlations for thermal conductivity, density, specific heat, viscosity are used.

The density of nanofluids can be predicted by the mixing theory as:

$$\rho_{nf} = (1- \emptyset)\, \rho_{bf} + \emptyset\, \rho_{np} \qquad (1)$$

$$k_{nf} = [\{k_{np} + (n-1)\, k_{bf} - \emptyset(n-1)(k_{bf} - k_{np})\} / \{k_{np} + (n-1)\, k_{bf} + \emptyset(k_{bf} - k_{np})\}]\, k_{bf} \qquad (2)$$

The following relationship is used for calculation of specific heat which is same approach as the mixing theory of ideal gases:

$$Cp_{nf} = \emptyset\, Cp_{np} + (1-\emptyset)\, Cp_{bf} \qquad (3)$$

$$\mu_{nf} = \mu_{bf}\, (123\, \emptyset^2 + 7.3\, \emptyset + 1) \qquad (4)$$

In the above equations, the subscripts "nf", "np" and "bf" refer to the nanofluid, nanoparticle and base fluid respectively. $\emptyset$ is the volume fraction of the nanoparticles added to base fluid. 'n' is the imperial shape factor given by $n = 3/\psi$, and ψ is the particle sphericity, defined as the ratio of the surface area of a sphere with volume equal to that of the particle, to the surface area of the particle, and in this paper n considered to be 3.

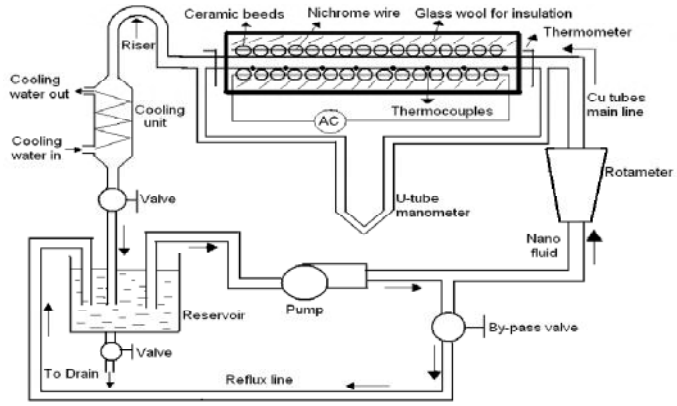

Fig.1: Experimental set up

IV. EXPERIMENTAL APPARATUS

An experimental apparatus is designed and constructed to investigate the convective heat transfer of nanofluids in a horizontal circular tube heated with uniform heat flux (Fig.1). The test section is a smooth horizontal copper tube, inner diameter (ID) 9.5 mm, 1 mm thick and length 1.0 meter. Electrically insulated nickrome heating wire was uniformly wound along the length of the tube. The terminals of the nickrome wire were connected to the variac transformer. Thermocouples were tapped along the tube wall for monitoring the local temperatures of the surface tube wall. The heating tube and thermocouples were covered with insulation to minimized heat loss to surrounding. The pump gives constant flow rate. The flow rate in the test section is regulated by adjusting the bypass valve located in the reflux line Thermometers will measure the inlet and outlet temperatures of working fluid, rotameter to measure required flow rates of the fluid. Cooling unit at

https://dx.doi.org/10.22161/ijaers/3.11.7 *ISSN: 2349-6495(P) | 2456-1908(O)*

the exit of test section will cool the test fluid to the inlet temperature. To measure the pressure drop along the test section a manometer was used. Readings were taken after the system reached the steady state condition.

V. DATA ANALYSIS

Observations were taken at steady state conditions. Initially experiment was performed with distilled water at various mass flow rates and then for Al_2O_3/water and CuO/water nanofluids with volume concentrations 0.1- 0.7%. Flow rates were same for all three fluids. Constant heat flux was maintained in all the cases. According to the Newton's law of cooling,

$Q=h_{exp}A(Tw–Tb)$ (5)

Where mean bulk temperature is given by

$Tb = (Tin+Tout)/2$

Where Tin = inlet temperature of fluid

Tout = outlet temperature of fluid

Heat transfer rate,

$Q=mCp_{nf}(Tout–Tin)$ (6)

Equating (5) & (6)

$h_{exp} A (Tw – Tb) = m Cp_{nf} (Tout–Tin)$

$h_{exp}=[mCp_{nf}(Tout–Tin)]/[A(Tw-Tb)]$ (7)

$Nu = (h_{exp} D_{hyd}) / k$

$D_{hyd} = 4S/P$

All the physical properties are evaluated at bulk mean temperature Tb, of the fluid.

VI. RESULT AND DISCUSSION

Experimental results are compared with Dittus-Boelter (eq.8) and Gnielinsky (eq. 9) correlations

$Nu=0.023Re^{0.8}Pr^{0.4}$ (8)

$Nu= [(f/8) (Re – 1000) Pr]/ [1+12.7 (f/8)^{0.5} (Pr^{2/3} – 1)]$ (9)

$3000 \leq Re \leq 5 \times 10^6$ and $0.5 \leq Pr \leq 2000$

Where from Petukhov, 1970, friction factor f, was calculated using equation (10)

$f = (0.79 \ln Re – 1.69)^{-2}$ (10)

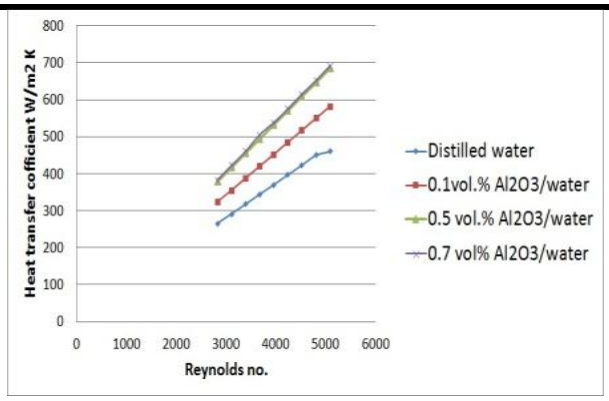

Fig. 2 Heat transfer coefficient Vs Reynolds number

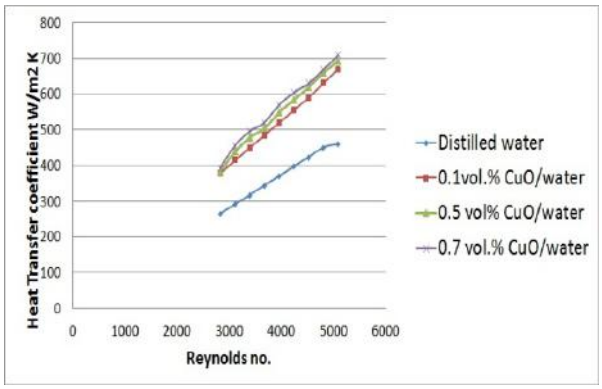

Fig. 3: Heat transfer coefficient Vs Reynolds number

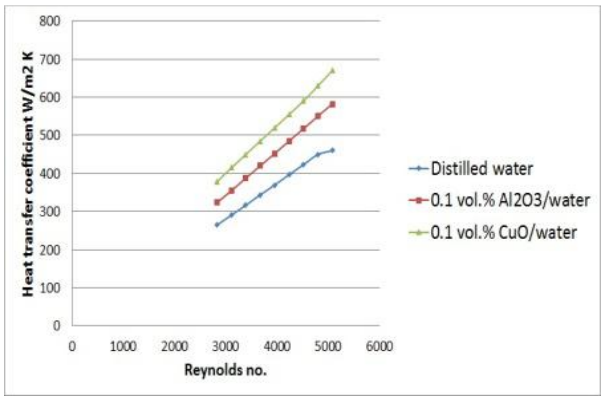

Fig. 4: Heat transfer coefficient Vs Reynolds number

https://dx.doi.org/10.22161/ijaers/3.11.7 *ISSN: 2349-6495(P) | 2456-1908(O)*

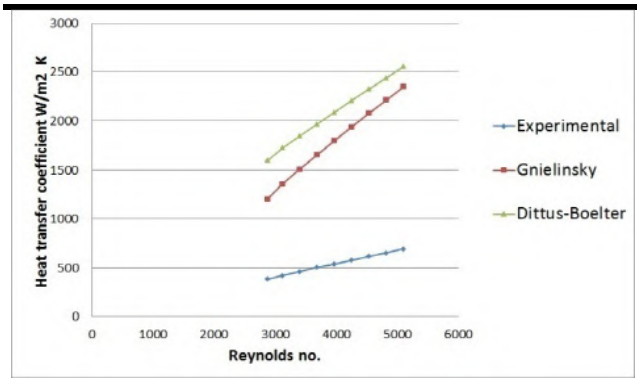

Fig. 5: Heat transfer coefficient Vs Reynolds number, 0.7 vol.% Al_2O_3/water

To validate the heat transfer coefficient enhancement of nanofluids experiment was performed on distilled water. Experimental results of heat transfer coefficient of nanofluids with varying volume concentrations were compared with that of base fluid, distilled water. Also experimental results were compared with that of predictions of Dittus-Boelter and Gnielinski correlations [5].

Heat transfer coefficient increases with Reynolds number and with increase in volume concentration of nanoparticles. In case of Al_2O_3/water nanofluid (Fig.2), increase in heat transfer coefficient at volume concentration of 0.7% and at Reynolds no. 4800, is 44.8% as compared with distilled water. Similarly in case of CuO/water nanofluid (Fig.3), at volume concentration 0.7% and Reynolds no. 4800, it is 48.8%. Fig.4 shows the increase in heat transfer coefficient for Al_2O_3/water and CuO/water nanofluids as compared with distilled water. At Reynolds no. 4800 and 0.1vol. %, increase is 22.2% and 40% for Al_2O_3/water and CuO/water nanofluid respectively. Experimental values of heat transfer coefficient (Fig.5) are compared with that of predicted by Dittus-Boelter and Gnielinsky correlations (8, 9). At Reynolds no. 4800 and 0.7vol. %, heat transfer coefficient increase predicted is 2.39 times and 2.74 times with Gnielinski and Dittus-Boelter correlations respectively. Enhancement of heat transfer in nanofluid is due to much higher thermal conductivity of nanoparticles dispersed in base fluids. Nanofluid concentration results increase in effective thermal conductivity. Heat transfer enhancement is associated with particle motion in the form of Brownian motion [13] by which particles move through liquid and possible collide, enabling direct solid to solid transporting of heat from one to another, and expecting increase in thermal conductivity. Other possible concept in nano-convection of fluid around particles due to their motion, particle transport some of the amount of heat transferred through agitation in the liquid. Yet another concept is liquid layering around the particle may give path for rapid thermal conduction. A liquid shell around the particles behave like solids, is assumed [13].

Concluding remarks

Nanofluid with enhanced thermal conductivity brings about enhanced heat transfer. However, in addition, with other suitable conditions such as nanoparticles material and size, appropriate particle concentration range, additives to maintain the stability may achieve higher heat transfer coefficients. However, thermal conductivity is not the sole reason for heat transfer enhancement. Suspended nanoparticles increase the surface area and the thermal conductivity of suspensions increases with the ratio of the surface area to volume of the particle, hence increase in heat transfer rate. As volume concentration of nanoparticles increases the heat transfer enhancement increases.

Metals (Al, Cu, and Ag) have higher thermal conductivity and therefore experiments with metallic nanofluids be performed. Lesser the particle size greater will be heat transfer enhancement. This is because of increase of heat transfer area. Size of nanoparticles should be small, as large particles tend to quickly settle out of suspension and thereby causing severe clogging while passing through microchannels and increase pressure drops considerably. Further large size particles may damage the equipment, such as pump, piping etc.

REFERENCES

[1] Stephen U.S.Choi, and J.A. Eastman, “Enhancing Thermal Conductivity of Fluids with Nanoparticles”, Energy Technology Division and Material Science Division, Argonne National Laboratory, Argonne, Illinois, Oct. 1995.

[2] C. J. Ho, L.C. Wei, Z.W. Li “An experimental investigation of forced convective cooling performance of a microchannel heat sink with Al_2O_3/water nanofluid”Applied Thermal Engineering 30(2010) 96-103.

[3] S.Zeinali Heris, M. Nasr Esfahany, S.Gh. Etemad, “Experimental investigation of convective heat transfer of Al2O3/water nanofluid in circular tube” International Journal heat and fluid flow 28(2007) 203-210.

[4] S.M. Peyghambarzaeh, S.H. Hashemabadi, S.M. Hoseini, M. Seifi Jamnani “Improving the cooling performance of automobile radiator with Al2O3/water

nanofluid" Applied Thermal Engineering 31(2011) 1833-1838.

[5] S.M. Fotukian, M. Nasr Esfahany, "Experimental investigation of turbulent convective heat transfer of dilute Al2O3/water nanofluid inside a circular tube" Intl. J. of Heat and Fluid Flow 31 (2010) 606-612

[6] Chidanand K Magrulkar, Vilayatrai M. Kriplani "Nanofluid Heat Transfer – A Review", International Journal of Engineering and Technology, U K, Volume 3 No. 2, February, 2013.

[7] K.B.Anoop et.al.,"Effect of particle size on the convective heat transfer in nanofluid in the developing region", Intl. J. of Heat and Mass Transfer,52(2009) 2189-2195.

[8] M.H. Kayhani, M. Nazari, H. Soltanzadeh, M. M. Heyhat, F. Kowsary, "Experimental analysis of turbulent convective heat transfer and pressure drop of Al2O3/water nanofluid in horizontal tube", Micro and nano Letters, 2012, vol. 7,Iss. 3, pp. 223-227.

[9] Ahmed Elsayed , Raya K. Al-dadah, Saad Mahmoud, Ahmed Rezk , "Numerical investigation of turbulent glow heat transfer and pressure drop of Al2O3/water nanofluid in helically coiled tubes", Intl. Journal OF Low-Carbon Technologies , February 9, 2014 1-8

[10] Khwanchit Wongcharee, Smith Eiamsa-ard, "Enhancement of heat transfer using CuO/water nanofluid and twisted tape with alternate axis", International Communication in Heat and Mass Transfer, March 2011.

[11] M. Naraki, S.M. Peyghambarzadeh, S.H. Hashemebadi, Y. Vermahmoudi, "Parametric study of overall heat transfer coefficient of CuO/water nanofluis in a car radiator" ,International Journal of Thermal sciences, 66 (2013) 82-99.

[12] S. Suresh, K.P.Venkitaraj, P. Selvakumar, M. Chadrasekar. "A comparison of thermal characteristics of Al2O3/water and CuO/water nanofluids in transition flow through a straight circular duct fitted with helical screw tape inserts", Experimental Thermal and Fluid science 39 (2012) 37-44.

[13] P. Keblinski, S.R. Phillpot, S.U.S. Choi, J. A. Eastman, "Mechanism of heat flow in suspensions of nano-sized particles (nanofluids)" International Journal of Heat and Mass Transfer 45 (2002) 855-863.

https://dx.doi.org/10.22161/ijaers/3.11.8 *ISSN: 2349-6495(P) | 2456-1908(O)*

The Comparison of Characteristics in Tin Doped Indium Oxide (ITO) Synthesized via Nonaqueous Sol-Gel and Solvothermal Process

Khuong Anh Nguyen Quoc[1], Hien Hau Vo Thi[1], Long Giang Bach[2], Van Thi Thanh Ho[1*]

[1]Hochiminh City University of Natural Resources and Environment
[2]NTT Institute of High Technology, Nguyen Tat Thanh University, Ho Chi Minh City, Vietnam

Abstract— *Tin doped indium oxide nanoparticles were synthesized by nonaqueous sol-gel method and solvothermal process from indium acetylacetonate ($In(acac)_3$) and tin bis(acetylacetonate)dichloride ($Sn(acac)_2Cl_2$) in oleyamine as the starting materials. The structure and morphology of ITO samples were analyzed by XRD and TEM. The electrical conductivy and specific surface area of both ITO samples were also determined and compared to each other. The ITO prepared via solvothermal method showed better results that prepared by nonaqueous sol-gel method.*

Keywords— ITO, Tin doped Indium Oxide, nanoparticles, nonaqueous sol-gel, solvothermal.

I. INTRODUCTION

There is continuing interest in Tin-doped Indium oxide (ITO) for a variety of applications including liquid crystal displays, optoelectronic devices, heat reflecting mirrors, and sensors. [1-7] More recently, nanoparticles (NPs) made of ITO have been investigated as emerging materials for catalyst support in fuel cell applications due to high conductivity of indium oxide as well as its stable durability in acid at oxygen reduction reaction (ORR) relevant potentials. [8] In addition, the serious problems involved in reducing the Pt utilization such as carbon corrosion of the support substrate, [9] Pt sintering, [10] Pt dissolution [11] are also overcome by reason of combining Pt nanoparticles with the SnO_2. [12,13]

It is evident that for nanoparticle synthesis, in which size and shape have a crucial influence on the properties of the materials. Therefore, preparation of ITO powder with nano size, excellent dispersibility, high crystalline and homogenous shape is the key requirement to bring about the good characteristic of ITO materials include electrical conductivity and specific surface area. Metal oxides NPs can be synthesized by a variety of solution-based techniques such as coprecipitation, sol–gel chemistry, microemulsion, hydrothermal/solvothermal processing and template syntheses. Among them, the nonaqueous sol-gel method and the solvothermal method are particularly attractive routes which enables the formation of metal oxides at low temperatures and overcomes the aggregation of particles. [14]

In this manuscript, we report the solvothermal and sol-gel synthesis of ITO NPs from indium acetylacetonate ($In(acac)_3$) and tin bis(acetylacetonate)dichloride ($Sn(acac)_2Cl_2$) in oleyamine. The comparison of the structure and morphology of the materials in two methods is described. The conductivity and surface area of ITO Nps prepared by these methods are compared to each other.

II. MATERIALS AND METHOD

2.1. Materials

All reagents and solvents are commercially available and used without further purification . Indium(III) acetylacetonate (In(acac)3, 99,99%), oleyamine (70%) were purchased from Acros – Belgium. Tin(IV) bis(acetylacetonate)dichloride (98%) were purchased from Sigma – Aldrich. Ethanol (99,7%) were obtained from Xilong – China.

2.2. Preparation

2.2.1. Nonaqueous sol-gel synthesis process of ITO NPs

A total of 0.2699 g of $In(acac)_3$ and 0.026 g of $(Sn(acac)_2Cl_2)$ were combined with 4 ml of oleyamine in a three-neck flask connected with a condenser. This solution was continuously stirred and heated at 235^oC for 3h in air. After the dark yellow suspension was produced, grey crystals were collected by centrifugation, washed many times with ethanol and dried at 80^oC for 24 h in air.

2.2.2. Solvothermal synthesis process of ITO NPs

The starting materials, 0.2699 g of $In(acac)_3$ and 0.026 g of $(Sn(acac)_2Cl_2)$ were first dissolved in 4 ml of oleyamine under constantly magnetic stirring at 500 rpm for 1 hour. The mixtures were added to Teflon-lined stainless autoclave of 100 mL capacity, which was heated and maintained at 220^oC for 24 h, and then gradually cooled to room temperature. The resultant precipitate was collected by centrifugation, washed with ethanol for

https://dx.doi.org/10.22161/ijaers/3.11.8 *ISSN: 2349-6495(P) | 2456-1908(O)*

several times and dried at 80 °C for 12 h in air. The final ITO powders were blue.

2.3. Characterization

Powder X-ray diffraction (XRD) patterns of ITO nanosupport-catalysts were obtained with XRD – D8 Advance – Bruker AXS (Germany) measurements using CuKa X-ray tube emitting at 1.54 Å. The data were collected from 20° to 80° in 2θ scale in step size of 0.03° with a scan rate of 2°. min-1.

Transmission electron microscopy (TEM) images were performed at 100 kV on a field-emission instrument of the type JEOL JEM-1010 with an ultrahigh resolution pole piece, providing a point resolution about 2 Å.

The specific surface area of the ITO nanoparticles was measured by multi-point Brunauer, Emmett and Teller adsorption (BET, Quantachrome Instruments Nova 2200e) with nitrogen gas at 77K.

Conductivity measurements were performed on ITO pellets (6 mm in diameter) prepared from about 120 mg of powder in an evacuated press under a pressure of 2 tons on Manual 12 Ton SpectroPress® instrument.

Resistance across the pellet was measured by a digital multimeter (manufactured by Faculty of Physics and Engineering Physics - University of Science HCM city) in a four-probe mode for eliminating the undesired resistance of the measuring circuit. The specific conductivity σ was calculated from the measured resistance R as $\sigma = \delta/RS$, where S is the electrode area and δ is the pellet thickness.

III. RESULTS AND DISCUSSION

The measured X-ray powder diffraction spectrum in the range of angles (2□) between 20° and 80° for the Tin doped indium oxides nanoparticles is presented in **Figure 1**. All diffraction peaks match the JCPDS 06-0416 database for the cubic bixbyite In_2O_3. No diffraction due to SnO_2 phases are observed, suggesting that Sn is incorporated into the In_2O_3 nanoparticles. The peaks of ITO2 NPs prepared via solvothermal method are stronger and narrower than that of ITO1 NPs prepared by sol-gel synthesis, indicating that the solvothermal method produces high crystalline materials. It has been found that Sn^{4+} doping induces the shifted peaks of ITO to the higher 2θ values comparing to pure In_2O_3 due to a smaller ionic radius of Sn^{4+}. The ITO2 NPs prepared via solvothermal method show this clearly than ITO1 NPs prepared by sol-gel route. The result suggests that the doping level of ITO2 NPs synthesized via solvothermal is better. In addition, the color of ITO products (Figure 2) have the following change: white as In_2O_3 NPs, gray as ITO1_solgel and blue as ITO2_solvothermal. This observation can be explained that the doping level of Sn into the structure of In_2O_3 NPs is higher, the free-electron concentrations are more, which influences the UV vis transmission spectra of ITO NPs. [15,16]

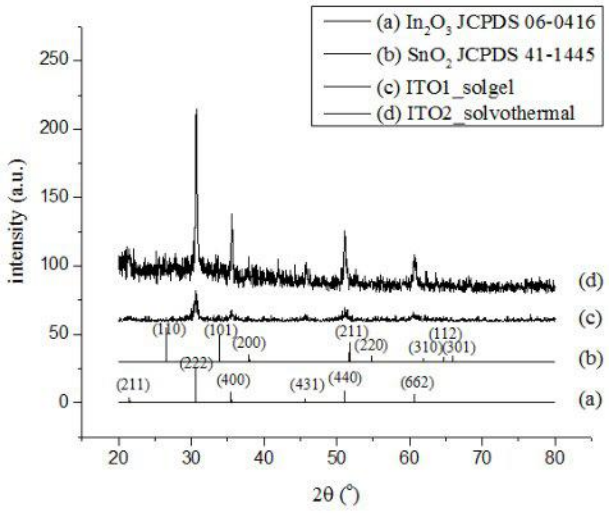

Fig.1: XRD patterns of tin-doped indium oxide (ITO) NPs with the different synthesis methods.

Fig. 2: The color of In_2O_3 sample (a), ITO1_solgel (b) and ITO_2_solvothermal (c).

TEM micrographs of ITO1 sample without using calcination process are presented in **Figure 3** shows the TEM images of ITO1_solgel and ITO2_solvothermal. Surprisingly, ITO1_solgel NPs are isolated as flowerlike clusters with size distribution in the range of 7 to 14 nm while ITO1_solvothermal NPs shows the spherical shapes and the high crystallinity of the particles with relatively uniform sizes of ca. 50 nm, in good agreement with XRD results determined by the Scherrer's formula. The morphology of ITO1 and ITO2 are completely different because the surface of ITO1_solgel is covered by organic ligand whereas the organic coverage is broken by solvothermal process. [17]

https://dx.doi.org/10.22161/ijaers/3.11.8 *ISSN: 2349-6495(P) | 2456-1908(O)*

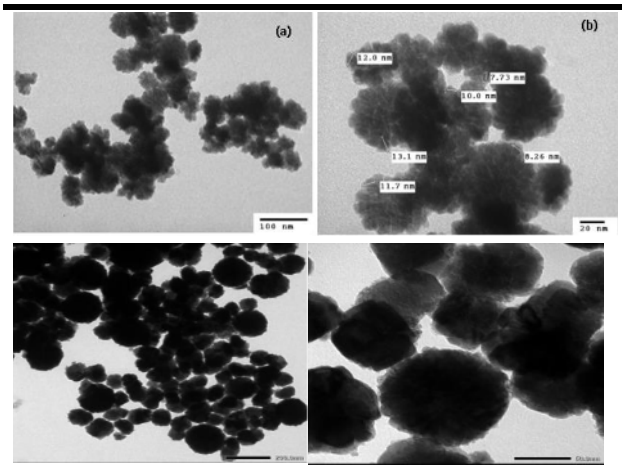

Fig.3: TEM micrographs of ITO samples: the overview of ITO1_solgel (a) and ITO2_solvothermal (c); the high resolution of ITO1_solgel (b) and ITO2_solvothermal (d).

Sample	EC (S/cm)	BET (m^2/g)
ITO1_solgel	0.089	63.568
ITO2_solvothermal	1.25	17.369

There were nearly four times as much the surface area value of ITO1_solgel (63.568 m^2/g) as that of ITO2_solvothermal (17.369 m^2/g). On the other hand, ITO2_solvothermal shows the higher electrical conductivity value than the other sample, respectively 1.25 S/cm and 0,089 S/cm. The results are consistent with good crystalline structure and high doping level of ITO2 prepared via solvothermal method. However, its surface area value is quite small because the particles size is relatively large.

IV. CONCLUSIONS

In summary, the ITO NPs have been successfully synthesized by both methods include sol-gel and solvothermal process. The solvothermal route show the properties such structure, shape, and electrical conductivity of ITO materials are superior to the sol-gel synthesis. However, the particles size is the major drawback of ITO NPs prepared via solvothermal method. The as-prepared ITO samples can be further investigated for noncarbon support of Pt in PEMFC.

ACKNOWLEDGEMENTS

We are grateful for finacial support from The National Foundation for Science and Technology Development (NAFOSTED) given under a special program for Basic Research Projects in Natural Science 2014 (Grants No. 104.03-2014.92) supported for this work.

REFERENCES

[1] Kim, H., Gilmore, C. M., Pique, A., Horwitz, J. S., Mattoussi, H., Murata, H., Kafafi, Z.H., and Chrisey, D.B. - Electrical, Optical, and Structural Properties of Indium–Tin–Oxide Thin Films for Organic Light-Emitting Devices, Journal of Applied Physics. 86 (1999) 6451 – 6461.

[2] Osaz, K., Ye, T., and Aoyagi, Y. - Deposition of Thin Indium Oxide Film and Its Application to Selective Epitaxy for In Situ Processing, Thin Solid Films. 246 (1994) 58 – 64.

[3] Hambergend, I., and Granquist, C.G. - Evaporated Sn-doped In2O3 Films: Basic Optical Properties and Applications to Energy-Efficient Windows, Journal of Applied Physics. 60 (1986) R123 – R160.

[4] Dijaoued, Y., Phong, V.H., Badilescu, S., Ashrit, P.V., Girouard, F.E., and Truong, V.V. - Sol-gel-Prepared ITO Films for Electrochromic Systems, Thin Solid Films. 293 (1997) 108 – 112.

[5] Mattox, D. M. - Sol-gel Derived, Air-Baked Indium and Tin Oxide Films, Thin Solid Films. 204 (1991) 25 – 32.

[6] Copra, K.L., and Das, S.R. - Thin film solar cell, NewYork: Plenum, 1983, pp. 480.

[7] Luff, B.J., Wilkinson, J.S., and Perrone, G. - Indium Tin Oxide Overlayered Waveguides for Sensor Applications, Applied Optics. 36 (1997) 7066 – 7072.

[8] Nguyen, A.Q.K, Huynh, T.T., Bach, G.L, and Ho, V.T.T. - Preparation and Characterization of Indium Doped Tin Oxide (ITO) via a Non-aqueous Sol-gel, Molecular Crystals and Liquid Crystals. 635 (2016) 8 – 15.

[9] Ho, V.T.T., Pan, C-J., Rick, J., Su, W-N., and Hwang, B-J. - Nanostructured Ti0.7Mo0.3O2 Support Enhances Electron Transfer to Pt: High-Performance Catalyst for Oxygen Reduction Reaction, Journal of the American Chemical Society. 133 (2011) 11716 – 11724.

[10] Ho, V.T.T., Nguyen, N.G, Pan, C-J., Cheng, J-H., Rick, J., Su, W-N., Lee, J-F., Sheu, H-S., and Hwang, B-J. - Advanced Nanoelectrocatalyst for Methanol Oxidation and Oxygen Reduction Reaction, Fabricated as One-Dimensional Pt Nanowires on Nanostructured Robust Ti0.7Ru0.3O2 Support, Nano Energy. 1 (2012) 687 – 695.

[11] Nguyen, T.T, Ho, V.T.T, Pan, C-J., Liu, J-Y., Chou, H-L., Rick, J., Su, W-N., and Hwang, B-J. - Synthesis of Ti0.7Mo0.3O2 Supported-Pt Nanodendrites and Their Catalytic Activity and Stability for Oxygen Reduction Reaction, Applied Catalysis B: Environmental. 154 – 155 (2014) 183 – 189.

https://dx.doi.org/10.22161/ijaers/3.11.8 *ISSN: 2349-6495(P) | 2456-1908(O)*

[12] Ho, V.T.T, and Nguyen, N.G. - Advanced Nanostructure Ti0.7In0.3O2 Support Enhances Electron Transfer to Pt: Used as High Performance Catalyst for Oxygen Reduction Reaction, Molecular Crystals and Liquid Crystals. 635 (2016) 1 – 7.

[13] Saha, M.S., Li, R., Cai, M., and Sun, X. - High Electrocatalytic Activity of Platinum Nanoparticles on SnO2 Nanowire-Based Electrodes, Electrochemical and Solid-State Letters. 10 (2007) B130 – B133.

[14] Niederberger, M., and Garnweitner, G. - Organic Reaction Pathways in the Nonaqueous Synthesis of Metal Oxide Nanoparticles, Chemistry – A European Journal. 12 (2006) 7282 – 7302.

[15] Ito, D., Yokoyama, S., Zaikova, T., Masuko, K., and Hutchison, J.E. - Synthesis of Ligand-Stabilized Metal Oxide Nanocrystals and Epitaxial Core/Shell Nanocrystals via a Lower-Temperature Esterification Process, ACS Nano. 8 (2014) 64 – 75.

[16] Jianhua, B., Dina, F.R., Armin, F., Torsten, B., Igor, D., Michael, W., and Markus, N. - Nonaqueous Synthesis of Uniform Indium Tin Oxide Nanocrystals and Their Electrical Conductivity in Dependence of the Tin Oxide Concentration, Chemistry of Materials. 18 (2006) 2848 – 2854.

[17] Narayanaswamy, A., Xu, H., Pradhan, N., Kim, M., & Peng, X. - Formation of Nearly Monodisperse In2O3 Nanodots and Oriented-Attached Nanoflowers: Hydrolysis and Alcoholysis vs Pyrolysis, J. Am. Chem.

https://dx.doi.org/10.22161/ijaers/3.11.9 *ISSN: 2349-6495(P) | 2456-1908(O)*

Solar Powered Vulcanizer: An Innovation

Eduardo Zeta Ramis, Ed Carlo De Guia Ramis

Technology Department, College of Engineering, University of Eastern Philippines, University Town, Catarman, Northern Samar, Philippines

Abstract— *This experimental research design was developed to a Solar Power Vulcanizer (SPV) in all serviceable aspects to save time, investment, manpower and the environment.*

This study is all about the utilization of the nature's power - the SUN'S POWER that means no brownout in vulcanization operation. SPV is designed for greening the world to be lived by from generation to generation.

The result of the three vulcanizer has the best temperature at 60°C in which the gum was bonded exactly to the rubber tire. Solar vulcanizer's rate of energy consumption of 0.0033 and an efficiency of 85.22%, while Class B gum, rate of energy consumption is Php 0.0067 and an efficiency of 85.22%. Portable electronic vulcanizer's rate of energy consumption at Php 0.0757 and an efficiency of 85.22%, while the Class B gum the rate of energy consumption at Php 0.15 and an efficiency of 85.22%.

Conventional vulcanizer's rate of energy consumption at Php 1.08 and efficiency of 43.38%, while Class B gum's rate of energy consumption at Php 1.52 and with an efficiency of 78.08%.

This study concluded that the usage of nature's power resulted to a continuous power supply to the vulcanizer; and the accurate temperature and duration of the vulcanizing process using the SPV which eliminates the problem of gas emission (carbon dioxide) produced by the conventional (gas fired) vulcanizer of about 2.772 kg of carbon dioxide for 1 liter of diesel fuel and/or 2.331 kg of carbon dioxide for 1 liter of petrol into the atmosphere.

Keywords— solar vulcanizer, portable vulcanizer, electronic vulcanizer, electric vulcanizer, conventional vulcanizer.

I. INTRODUCTION

This study is all about the utilization of the nature's power - the SUN'S POWER that means no brownout in vulcanization operation. This solar power operated vulcanizer is a green machine and environmentally-friendly equipment. Its design is considered for greening the world to be lived by from generation to generation. The modernization of this gadget is introduced for the benefit of mankind.

Renewable energy dramatically lowers pollution emissions, reduces environmental health risks, and slows the depletion of finite natural resources. Renewable energy is derived from sun, wind, water, or the earth's core. It can also be derived from biomass—or plant matter—which is grown, harvested, and transferred into energy by one of a number of processes.

Therefore, as a green machine, it is an "environment friendly" product. The radiant light and heat from the sun, has been harnessed by humans since ancient times using a range of ever-evolving technologies.

A. Rationale

This electronic vulcanizer and the conventional vulcanizer (carbon dioxide emitting apparatus) have a common problem. In electric vulcanizer, if power supply is cut down during vulcanization, the process is not completed and will result to damage and an uncured vulcanization results. To solve the aforementioned problems and for environmental concern, (gas emission), this innovative technology (solar power vulcanizer) is studied which is expected to be applied over time as technology changes.

B. Flow Chart of the Study

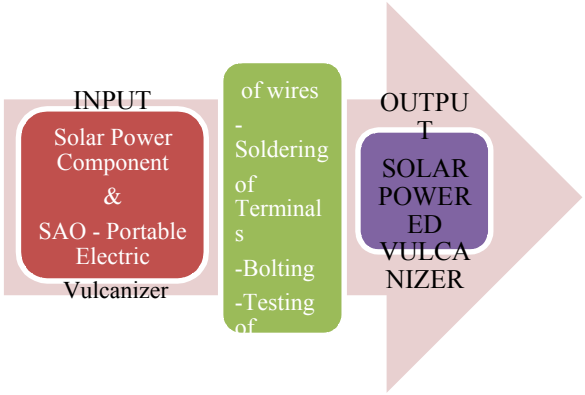

Fig. 1: Flow Chart of the Study

Fig. 1 shows the construction methods of this solar power machine in three steps.

C. Objectives

Specifically, this study was conducted to:

1. identify the design of a solar power vulcanizer (SPV);
2. determine the material component for the solar power electronic vulcanizer (SPV);

https://dx.doi.org/10.22161/ijaers/3.11.9 *ISSN: 2349-6495(P) | 2456-1908(O)*

3. find out the efficiency solar power vulcanizer (SPV) in terms of vulcanization operation; and
4. find out the economic feasibility of the solar power electronic vulcanizer.

II. REVIEW OF RELATED LITERATURE

The work environment refers to the aggregate of surrounding things and conditions that affect the quality of work, life and the individual itself being an employee or an entrepreneur.

The Technical Education Skills Development Authority (TESDA) reported the government's quest to realign technician education program to be of paramount importance. Mismatch problems of the education sector and industry are vital issues as regards the graduates of colleges and universities, wherein most of them cannot find jobs because of lack of skills needed by the industry. Hence, graduates of technical courses have wider range of employment compared to those graduates of white collar profession[1].

The technological development begins with basic research when a scientist discovers some new phenomena or advances new theory. Other reaches to examine the breakthrough for its potential utility. If further development leads to a prototype and engineering refinement makes commercial exploitation practical. Then, the technology that is finally put to use and may be widely adopted[2].

Technological changes take place in many directions at once; that is, it is multi-lineal. Bar codes, for example, are used to track items not only in grocery stores but also in warehouses, assembly lines, shipping docks, libraries, even in the Department of Defense. Technological changes are also nonlinear; developments take irregular directions. There are many dead ends, and each highly visible advance may depend on a host of small developments (including failures)[3].

Renewable technologies are designed to capture and store this energy. They include:

- Photovoltaic solar panels convert sunlight directly into electricity.
- Wind turbines capture wind to turn rotors, which turn a generator and creates electricity.
- Transpired solar collectors use sunlight to preheat air for heating purposes.
- Solar hot water heaters use the sun to heat water for domestic applications.
- Small-scale hydroelectric power plants flow water over turbines, which turn a generator and create electricity.
- Fuel cells combine hydrogen and oxygen to produce electricity and heat.
- Ground source heat pumps transfer heat to the ground in summer and extract heat from the ground in winter.
- Green power is electricity generated from renewable sources such as wind, solar, geothermal, biomass, and landfill gas.

Solar Power Tower Design (also known as 'central tower' power plants or 'heliostat' power plants) capture and focus the sun's thermal energy with thousands of tracking mirrors (called heliostats) in roughly a two square mile field. A cost/performance comparison between power tower and parabolic trough concentrators was made by the NREL which estimated that by 2020 electricity could be produced from power towers for 5.47 ₡/kWh and for 6.21 ₡/kWh from parabolic troughs. The capacity factor for power towers was estimated to be 72.9% and 56.2% for parabolic troughs[4].

Levelised Cost. Given the fact that solar thermal power is reliable, can deliver peak load and does not cause pollution, a price of US$0.10 per kWh starts to become competitive. Although a price of US$0.06 has been claimed[5]. With some operational cost a simple target is 1 dollar (or lower) investment for 1 kWh production in a year.

Related Studies

The Philippines today must recognize the present educational technologies status that these may be used whenever possible to enhance and equalize the opportunities in this field of technical education, like in the engineering field, considering that license professional engineers undermine the people who graduated technical education only, even though that these people are sometime more skillful than them. The problem of mismatch does not only embrace from technology graduates but they are included for some do not carry practical skills.

Former President Fidel V. Ramos [6], stressed that the living condition of the people in every sector of society can be improved by initiating family investment or group. He wanted the Philippines to be a New Industrialized Country (NIC) in Asia and the Pacific by 2000 and beyond. Thus, Executive Order No. 318, s. 1991, was passed to reinforce functional program in the implementation toward industrial reform and development.

Vulcanization Methods[7]

A variety of methods exist for vulcanization. The economically most important method (vulcanization of tires) uses high pressure and temperature. A typical vulcanization temperature for a passenger tire is 10 minutes at 170 °C.

Vulcanization is the chemical process by which the physical properties of natural or synthetic rubber are

https://dx.doi.org/10.22161/ijaers/3.11.9 *ISSN: 2349-6495(P) | 2456-1908(O)*

improved; finished rubber has higher strength and resistance to swelling and abrasion, and elastic over a greater range of temperature. In its simplest form, heating rubber with sulfur brings about vulcanization.

The Discovery of Vulcanization

Vulcanizing gum is a ready-made natural rubber that is vulcanized to bond the rubber tire. Therefore, vulcanization of rubber is a curing process of rubber that involves high heat and the addition of sulfur or other equivalent curatives[8].

Rubber

Vulcanizing gum is classified according to its texture, bonding temperature and the content of accelerators. The three classes of the gum are as follows[9]:

Class A – usual bonds on the rubber 30°C-70°C and is smooth;
- Use for small punctured and cracks in the inner tube rubber tire.

Class B – usual bonds on the rubber 35°C-80°C and is moderately rough;
- Use for medium or punctured holes and cracks/scars in the inner tube rubber tire.

Class C – usually bonds on the rubber 45°C to 90°C and is very rough;
- Seldom available in the market and is used in tire repairing big and busted with cracks/scars in the inner tube rubber tire and mostly used for tire recapping.

In modern practice, temperature of about $140^0 – 180^0$ C is deployed, and in addition to sulfur and accelerations, carbon black oxides are usually added, not merely as an extender, but improve further the qualities of the rubber. Vulcanizing gum, which is a classified "ready to heat" rubber, is now utilized to repair worn out interior/exterior rubber tires with the help of vulcanizing equipment. Certain problems such as inaccuracy of the product are evident to third-world countries as the first-world never used some[10].

Other Related Studies

Solar power uses the sun's energy to produce electricity. A number of solar technologies are currently available or under development, like a Solar PV is the most familiar solar technology. Photovoltaic's use semiconductor materials—most frequently silicon—to convert sunlight directly into electricity.

The use of fossil fuels like coal and oil cause long term damage to our world. They not only cause air pollution, but reduce the ozone layer and contribute to the greenhouse effect which is causing global warming. They also cause untold damage to the environment.

Solar energy is clean and free of side effects to the environment. Solar panels require little maintenance and usually last 25 or 30 years. Solar panels are made to withstand the elements of the northern climate, such as snow, sleet and hail. Solar increases the value of one's property[11].

The technological development begins with basic research, when a scientist discovers some new phenomenon or advances new theory. Others reach and examine the breakthrough for its potential utility. If further development leads to a prototype, and engineering refinement makes commercial exploitation practical's, then, the technology is finally put to, use may be widely adopted[12].

Engineering and Technology Education goes hand in hand to the rapid pace of globalization which pressures nations to be competitive in order to survive. In this field of education its ushers the freer permeability of human resources among countries. While it poses as a huge challenge to the survival of Filipino workforce in the global market, it yields various opportunities. This challenge pushes for the continuing development and replenishment of manpower through this field of education in order to ensure that there are workers of the right quality and right quantity for jobs that are made available at any given instance. Further, it urges for a stronger labor market intelligence and technology development. Lastly, it encourages transformation of the Filipino workforce to be knowledge-based and adaptable to shifting skills or even occupations [13].

The Philippines today must recognize the present educational technologies status that these may be used whenever possible to enhance and equalize the opportunities in this field of technical education, like in the engineering field, considering that license professional engineers undermine the people who graduated technical education only, even though that these people are sometime more skillful than them. The problem of mismatch does not only embrace from technology graduates but they are included for some do not carry practical skills.

III. MATERIAL AND METHODS

This chapter discusses the processes that were done during the experiment and the tools that were used during the experiment.

A. Rationale

The study utilized experimental research method which includes the new design, selection and identification of materials, assemblage or fabrication, and testing process.

B. Materials

The materials to be used in the assemblage of the SPV for construction were the following:

A. Materials:

https://dx.doi.org/10.22161/ijaers/3.11.9 *ISSN: 2349-6495(P) | 2456-1908(O)*

Solar panels, charge controllers, storage batteries, wires and cables, system meters and monitors, solar array disconnect, battery charge controller, deep cycle batteries, solar power converter/inverters, backup power, angle bars, steel bars, and bolts and nuts.

B. Tools & Equipment

Portable electric drill, electric soldering rod, soldering lead, multi tester(digital/analog), welding machine, hacksaw, and ball-pen hammer.

These are the materials to be used to shape up the Solar Power Vulcanizer. The parts is to be collected, measured and welded, boring of holes for bolt and spring placement and assembled as the new semi-auto-open portable electronic vulcanizer.

Fig. 2 shows the schematic diagram of the solar power electronic vulcanizing equipment.

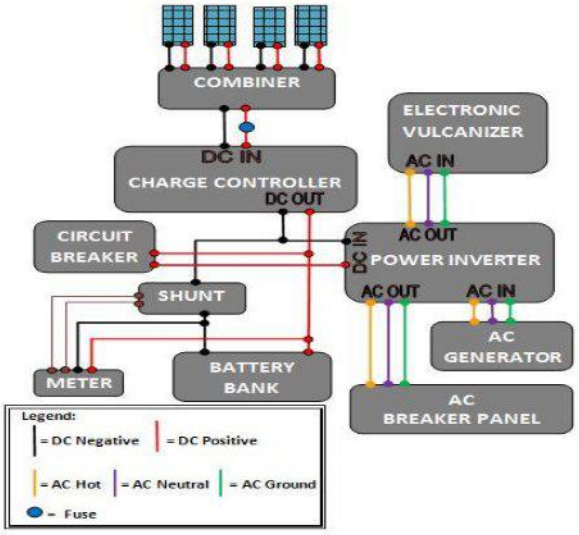

Fig. 2: Schematic diagram of solar power electronic vulcanizing equipment

C. Timetable of Research

This study was conducted during the school year 2013 - 2015 in the Technology Department, College of Engineering, University of Eastern Philippines, University Town, Northern Samar.

.

IV. RESULTS AND CONCLUSIONS

The study utilized experimental research method which included the new design, selection and identification of materials, assemblage or fabrication, and testing process:

1. ***New design.*** The new design of the solar power vulcanizer (SPV) vulcanizing equipment was based on the power supply shortage that hampers the vulcanization operation. The following features of this SPV machine are as follows:

1. Vulcanizing Machine

a. The vulcanizing machine weighs 9.25 kilograms; total length of 49 cm, height of 33.5 cm, back width (panel board) of 22 cm with front width (front base) of 14 cm, and environment-friendly.

b. Its body configuration is like a letter L configuration. A movable arm is like a letter J appearance is bolted at the top of the base, that is made of GI pipe schedule, 40 x 49cm in length x 6,3cm in diameter, and attached to it is a detachable vulcanizer head of 15.5cm in length x 6.5cm in width x 1.5cm in thickness.

c. The base was made of channel bar with dimension of 47cm in length x 9cm in width x 6.5cm in height and thickness of 0.30cm that served as foundation of the equipment;

d. A flat type 300 watts mica heating element is attached to the vulcanizer head and a box type panel board of 22 cm in length x 27cm in width x 8cm in thickness.

e. Cost of the vulcanizer machine is Php 8, 786.00

2. **Solar panel components:**

i. Solar panel 250 watts @P15,000/set
-3 sets ---------- Php 45,000.00

ii. Deep Cycle Battery 12volts 150 AH
@ P9,600/unit – 3 units---------- 28,000.00

Industrial inverter 1,500 watts
-1 set (pure sine wave) ---------- 7,200.00

iii. Controller 30 ampere ---------- 2,500.00

iv. Accessories (wiring, switches,
Holders bolt and nuts, etc.) -------- 8,900.00

Total --------- Php 91,600.00

Total Project Cost ---------- Php 100,386.00

3. ***Selection and identification of materials.*** Selection and identification of materials was seriously considered for this study.

4. ***Fabrication.*** Based on the plans and design,

5. ***Testing process.*** Testing of the machine was undertaken to determine the workability of the machine.

The design of this solar power electronic vulcanizer is due to intermittent brownout in the province.

The function of the component parts of the SPV machine comprises seven (7) basic main components, namely:

1. **Solar Panels** - One can order discount photovoltaic cells online, and assemble these into complete 80W, 200W, or 500W solar panels.

2. **Solar Array Disconnect** - This is basically just an electrical switch but is an important part of the system. It allows disconnection and cutting off the DC power output from solar panels and array should any repairs be required or if there is a problem with the solar system.

3. **Battery Charge Controller** - The battery charge controller ensures that a consistent amount of electrical

https://dx.doi.org/10.22161/ijaers/3.11.9 *ISSN: 2349-6495(P) | 2456-1908(O)*

power is sent to the batteries so that they are not over charged, and to ensure that the backup batteries do not discharge back through the system at night.

4. **Deep Cycle Batteries** - Deep cycle storage batteries for solar systems are more robust and are designed for the type of charging and discharging cycles they need to endure.

5. **System Power Meter** - Help improve the system to gain the maximum efficiency from solar installation as well as having the advantage of letting neighbors know how much money a solar system saves.

6. **Solar Power Converter** - The solar power converter converts the solar energy from the panels into usable energy in the home by providing the DC to AC conversion using electronic switching techniques.

7. **Backup Power** - This is used when the sun does not shine and the batteries are empty. Most systems will include some sort of backup power. In a stand-alone installation this would generally be a diesel generator. In a grid-tied system the utility grid itself would provide the backup power through the converter.

Data on TABLE 1 & 2 shows that the three vulcanizers had the best temperature at 60°C in which the gum was bonded exactly to the rubber tire. For solar vulcanizer the rate of energy consumption of 0.0033 and an efficiency of 85.22%, while the Class B gum, the efficiency of 85.22%. For electronic vulcanizer the rate of energy consumption at Php 0.15 and an efficiency of 85.22%.

For the conventional vulcanizer, the rate of energy consumption at Php 1.08 and an efficiency of 43.38%, while the Class B gum, the rate of energy consumption at Php 1.52 and with an efficiency of 78.08%.

Table.1: Time/Temperature/Power/Fuel Consumption/ Solar Power/Electronic/Conventional Vulcanizer

Type of Vulcanizer	**Table Column Head**					
	Time in Minutes		***Temperature in °C***		***Power/Fuel Consumed***	
	Class					
	A	B	A	B	A	B
Solar	1	2	60	60	0.005kw-hr	0.10 kw-hr
Electronic[a]	1	2	60	60	0.005kw-hr	0.10 kw-hr
Conventional[a]	5	10	60	60	20ml	30ml

a. Ramis. E.Z. Efficiency of Portable Electronic Vulcanizer, World Journal of Engineering and Technology, Volume 3, No. 1. February 2015. ISBN: 2331- 4222.

Table.2: Efficiency and Rate of Energy Consumed of Solar Power/Electronic/Conventional Vulcanizer

Type of Vulcanizer	***Cost in Kw-hr/ Gas-ml***		***Rate of Energy Consumption***		***Results***		***Efficiency (%)***	
	Class							
	A	B	A	B	A	B	A	B
Solar	Php 0.0067		Php 0.0033	Php 0.0067	Best bonding		85.22%	
Electronic[a]	Php 0.0067		Php 0.0757	Php 0.15	Best bonding		85.22%	
Conventional[a]	Php 0.054		Php 1.08	Php 1.52	Good bonding		43.38%	78.08%

a. Ramis. E.Z. Efficiency of Portable Electronic Vulcanizer, World Journal of Engineering and Technology, Volume 3, No. 1. February 2015. ISBN: 2331- 4222.

Fig. 3 shows that the conventional vulcanizer is also five (5) times behind the operation compared to the solar and electric vulcanizer for both Class A vulcanizing gum. It consumed 20ml of fuel for class A. The efficiency of 43.38% for Class A gum. The solar power vulcanizer was five (5) times efficient Class A and B gum compared to the conventional vulcanizer. It shows also that the cost per kw-hr was only Php 0.0067 for both gums and an efficiency of 85.22% for Class A gum.

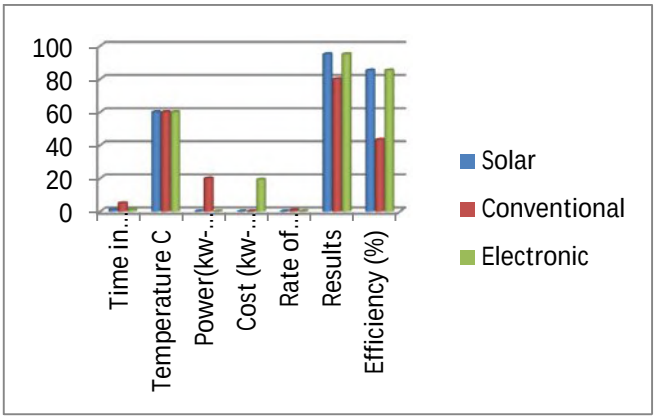

Fig.3:The Solar, Conventional, & Electronics vulcanizers using Class A vulcanizing gum

Fig. 4 shows that the electronic vulcanizer was also five (5) times efficient for Class A and B gum compared to the conventional vulcanizer. It shows also that the power consumed at Php 0.010 kw-hr for Class B gum and cost per kw-hr was only Php 0.0067 for Class B gum. The

https://dx.doi.org/10.22161/ijaers/3.11.9 *ISSN: 2349-6495(P) | 2456-1908(O)*

rate of energy was Php 0.15 for class B gum with an efficiency of 85.22%

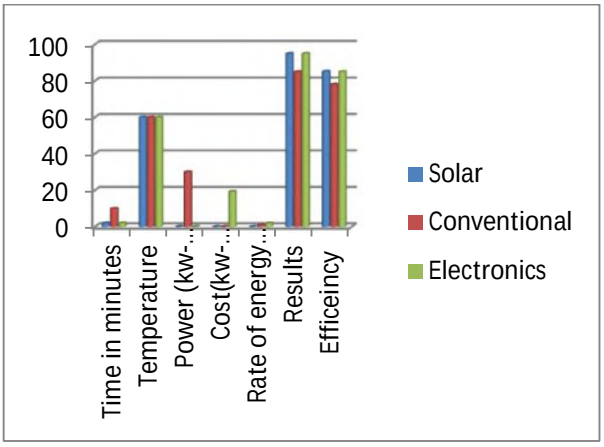

Fig.4: The Solar, Conventional, & Electronics vulcanizers using Class B vulcanizing gum

This study concluded that the usage of nature's power resulted a continuous power supply to the vulcanizer and the accurate temperature and duration of the vulcanizing process using the electronic vulcanizer which eliminates the problem of gas emission[14] (carbon dioxide) produced by the conventional (gas fired) vulcanizer of about 2.772 kg of carbon dioxide for 1 liter of diesel fuel and/or 2.331 kg of carbon dioxide for 1 liter of petrol into the atmosphere.

V. CONCLUSION

This study concluded that the usage of nature's power resulted a continuous power supply to the vulcanizer and the accurate temperature and duration of the vulcanizing process using the electronic vulcanizer which eliminates the problem of gas emission[14] (carbon dioxide) produced by the conventional (gas fired) vulcanizer of about 2.772 kg of carbon dioxide for 1 liter of diesel fuel and/or 2.331 kg of carbon dioxide for 1 liter of petrol into the atmosphere.

The findings of this study have an important implication for future enhancement and improvement of the study. More tires can be vulcanized in a short period of time; therefore increase income over time.

It is suggested that this solar power vulcanizer should be adopted in welding, automotive and machine shops to save time and investment in their operations;

Small time businesses like vulcanizing shops in the Philippines are encouraged to provide this solar power vulcanizing machine so that they can save money and labor in their operation;

It is suggested also that this study be innovated thru additional features like automatic release of vulcanizer head after the vulcanization process.

ACKNOWLEDGEMENTS

This research work would not have been realized without the guidance of the Almighty God.

Sincerest appreciation and gratitude are likewise extended to the following persons:

Dr. Pio P. Tuan, R & D Director, and all Members of R & D In- House Review panel, for their guidance, intellectual insights and valuable suggestions in the completion and success of this study; Prof. Villa C. Carpio, for her untiring support and editing this manuscript; Dr. Rem N. Laodeno, VP Administration and Finance; Dr. Benjamin D. Varela, Dean, College of Engineering; Engr. Jose Ariel Geriane, Director, Center for Computer Studies; Engr. Constantine F. Merida, Chair, Mechanical Department, Engr. Leo M. Sauro, Coordinator, College of Engineering Extension Unit; Prof. Joel J. Tejano and Prof. Nelito E. Getalado for their moral support .

Dr. Rolando A. Delorino, President, University of Eastern Philippines (UEP), University Town, Catarman, Northern Samar, for his valuable suggestion and encouragement in this field of endeavor;

To those who contributed much for the success of this study, particularly my wife, Guadalupe and children, my friends & colleagues.

REFERENCES

[1] *Congressional Commission on Education, Making Education Work: An Agenda for Reform.* Congress of the Republic of the Philippines, Manila, Quezon City, (1993).

[2] Compton's Encyclopedia, 1995 edition.

[3] Ramis, Eduardo Zeta. "Professionalism of Graduate School in Region VIII, Philippines. LAP Lambert Academic Publishing Inc. Germany, ISBN 978-3-659-70840-4.

[4] Google's Goal: Renewable Energy Cheaper than Coal November 27, 2007" Accessed January 2014. http://www.google.com/intl/en/press/pressrel/2007_green.html

[5] Development of Two Solar-thermal Electronic Hybridized Power Plant Debuts in Southern California International Energy Agency. Technology Roadmap: Solar photovoltaic energy." October 2010. Accessed August 2, 2014. http://www.newswiretoday.com/news/25722/

[6] Executive Order No. 318, s. 1991, Pres. Fidel V. Ramos.

[7] http://www.answers.com/tyopic/vulcanization#ixzz1SL6NkxBq Retrieved March 2014, Accessed April 29, 2014.

[8] Compton's Encyclopedia, 1995 edition.

[9] Encyclopedia Britannica, 15th Edition.

[10] IEA Technology Roadmap 2010. Technology deployment strategic goals and milestones." Accessed November 19, 2013.

https://dx.doi.org/10.22161/ijaers/3.11.9 *ISSN: 2349-6495(P) | 2456-1908(O)*

http://www.eia.doe.gov/cneaf/solar/renewable/page/solarreport/table2_10html

[11] Ramis, Eduardo Zeta. "Professionalism of Graduate School in Region VIII, Philippines. LAP Lambert Academic Publishing Inc. Germany, ISBN 978-3-659-70840-4.

[12] Ramis. Eduardo Zeta, paper presentation "Efficiency of Portable Electronic Vulcanizer" during the 3rd WIETE Annual Conference on Engineering and Technology Education on February 6-10, 2012 at Pattaya, Thailand.

[13] U.S. Environmental Protection Agency (EPA), Accessed April 5, 2009.

https://dx.doi.org/10.22161/ijaers/3.11.10 *ISSN: 2349-6495(P) | 2456-1908(O)*

Characterizing the Bistable Flow, of BWR, as a Bifurcation (Pitchfork Type) in the Navier-Stokes' Equation Solution

Dr. Carlos J. Gavilan Moreno

Cofrentes NPP. Iberdrola Generación Nuclear, Paraje el Plano S/N. Cofrentes 46625. Valencia. Spain.

Abstract— *Many nuclear power plants have undertaken power uprate processes, increasing recirculation, feed water and steam flow rates. With regards to recirculation flow, adverse scenarios,may arise where the flow varies autonomously between two values, a phenomenon known as bistable flow.Although this phenomenon is typically related to power uprate processes, some plants experience it when they reach high flow values, especially at the end of the cycle.*

This study proves empirically the existence of a Pitchfork-type bifurcation in the bistable flow situation.The parameter determining bifurcation will be Flow Control Valve (FCV) position in recirculation loop. This choice is made considering that it is the only variable during recirculation loop operation, because under stable operation and constant power the remaining variables (Geometry, Combustible, Differential Core Pressure, Pump Turning Speed (r.p.m.), etc.), are considered constant.

Keywords— ***Bifurcation, pitchfork, bistable, recirculation, FCV, flow.***

I. INTRODUCTION

In 1985, an electrical power fluctuation was detected at the Leibstadt Nuclear Power Plant during startup and load tests at 100%. Loop "A" fluctuation ranged between 2.5% and 3%, whereas in loop "B" it was between 3% and 3.5%. It was concluded that recirculation flow fluctuations were caused by a bistable flow pattern in the pump discharge header.

In the year 1986, the first regulatory reference on abnormal performance of recirculation loop flows was written. (USNRC IE IN No. 86-110). This document determines that fluctuations vary from station to station and even within the loops of the sameunit. This document also concludes that this phenomenon does not impact safety.

In July 1988, General Electric issued a letter (General Electric Energy, Nuclear SIL No. 467) establishing that the problem affects Boiling Water Reactors BWR from generation 3 to 6 and is detected at the manifoldsof pipes supplying jet pumps. (Figure 1).

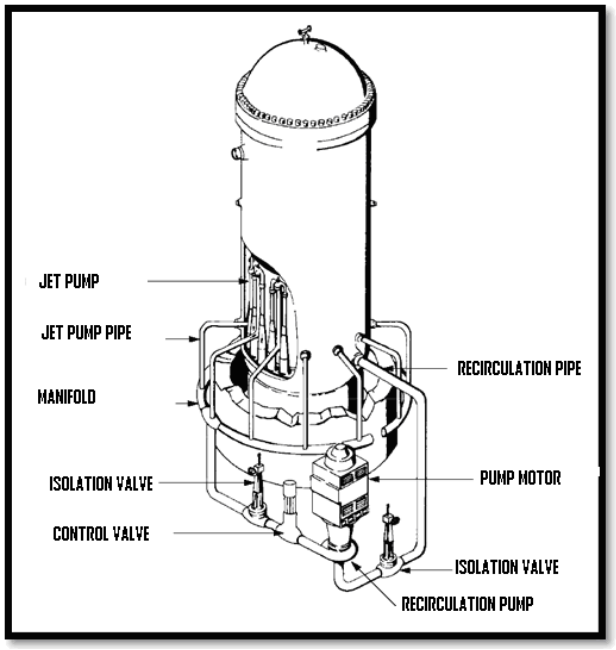

Fig.1: Recirculation loop scheme in a Generation 6 BWR.

In Japan, between1986 and1989 a group of researchers applied various hydraulic models to replicate (Miura et al 1986), characterize (Miura et al 1987) and propose compensatory measures (Ohki, A. et al 1988) to the bistable flow.

In 2006, a bistable flow phenomenon analysis was presented at Laguna Verde nuclear power plant in México. (Nuñez Carrera et al., 2006).

After 2008, new research (Gavilan Moreno, C.J. 2008), concluded that the bistable flowcan be described as a noise-induced transition mechanism (Horstheme & Lefever (2005)). In this theory, noise is identified as flow turbulence under high Reynolds values.

In 2009, bistable flow analyses continued, using mathematical techniques such as wavelets (Nuñez-Carrera et al., 2009) and codes for fluid dynamics. These were used to replicate the results of hydraulic models from the 80s. (Gavilan Moreno, C.J. 2009).

https://dx.doi.org/10.22161/ijaers/3.11.10 *ISSN: 2349-6495(P) | 2456-1908(O)*

In 2011, a new 3D CFD model confirmed the existence of two states and the non-convergence of the stable condition at specific Reynolds values. (Gavilán Moreno, C.J. 2011)

In line with the above mentioned in this section, the state of the art in bistable flow can be summarized as Unpredictable, fluctuating hydraulic phenomenon, characterized by high turbulence.

In the following paragraphs,the Pitchfork type bifurcationconcept is introduced and justified.

Supposed a dynamic system, a bifurcation occurs when a small smooth change made to the parameter values of a system causes a sudden qualitative or topological change in its behavior. The name "bifurcation" was first introduced by Henri Poincare in 1885, in the first paper in mathematics showing such a behavior.

It is normal to divide bifurcations into two classes: Local bifurcations and Global Bifurcations. A local bifurcation occurs when a parameter change, causes the stability of equilibrium or fixed point to change. Examples of local bifurcation include: Saddle-node bifurcation, Transcritical bifurcation, Pitchfork bifurcation, Hopf bifurcation and Neimark-Sacker bifurcation. In continuous dynamical systems described by Differential Equations (DE)—i.e. flows—pitchfork bifurcations occur generically insystems with symmetry.Pitchfork bifurcationshave several types – supercritical, transcritical and subcritical.Normally solving the DE´s can be found that, for depending on some parameters values, the system has one stable equilibrium point, or an unstable pointor two stable equilibria points.This last status is the key to identify the bistable flow with the pitchfork bifurcation.

The recirculation system, of a BWR, is a hydraulic system, whose behavior is described by the equation of Navier Stokeswhich can be seen in Equation (1). The recirculation system is a symmetric system. So the solution of the Partial Derivatives Equation (PDE), could present Pitchfork type bifurcation. A deeperanalysis is done to justify the bifurcation.

$$\frac{D\vec{u}}{Dt} = \vec{F} - \nabla P + \frac{\mu}{\rho}\left(\frac{1}{3}\nabla(\nabla\vec{u}) + \nabla^2\vec{u}\right) \quad (1)$$

The equation (Eq. 1) has the following vectors: u (speed), P (pressure), μ (viscosity) and ṕ (fluid density). Since the system has a constant section and there are no fluid sumps or sources, integrated fluid speed is similar to the scalar flow value. Likewise, pressure variation only depends on FCV opening. Thus, Equation (1) can be reformulated as Equation (2):

$$\frac{dq}{dt} = F(q, A) \quad (2)$$

Where q=flow rate and A= FCV position.

Additional information regarding this equation and systemis:

- The fluid is in an incompressible state.
- The fluid is at a constant temperature.
- The system responds with an equation similar to q=q(A).
- Primary derivatives are determined by Equation (3), with notation and secondary derivatives being simplified in Equation (4):

$$\frac{\partial F(q,A)}{\partial q} = F_q \; y \; \frac{\partial F(q,A)}{\partial A} = F_A \quad (3)$$

$$\frac{\partial F^2(q,A)}{\partial q^2} = F_{qq} \; ; \; \frac{\partial F^2(q,A)}{\partial A^2} = F_{AA} \; y \; \frac{\partial F^2(q,A)}{\partial qA} = F_{qA} \quad (4)$$

The stability analysis results from establishing a null time derivative. In other words, if the system does not change and FCV opening and other conditions do not vary, flow remains the same. Mathematically, this is seen in equation (5).

$$\frac{dq}{dt} = 0 = F(q, A) \quad (5)$$

So, analyzing bifurcations in Equation (4) is the same as analyzing specific F curve points (q, A) on the FCVopening-flow plane. Considering these parameters, the points that confirm the equation (7) are considered unique and can be classified as follows: Regular Points, Regular Inflexion Points, Unique Points, Double Curve Point, Double Inflexion Points and Peak Points.

The Double Curve Point generates two solutions and a curve running through the unique point that has two slopes. Although there are multiple potential shapes, the one selected provides two stable results as it is coherent with bistable conditions.

In the case of double point bifurcation, there is anequilibriumpoint with two curves and two different slopes. (Ioos, G; Joseph, P.D. 2001). Curve tangents conform to Equation (6)

$$\begin{bmatrix} \frac{dq^{1)}}{dA} \\ \frac{dq^{2)}}{dA} \end{bmatrix} = \begin{bmatrix} q_A^{1)} \\ q_A^{2)} \end{bmatrix} = -\frac{F_{qA}}{Fqq}\begin{bmatrix}1\\1\end{bmatrix} - \sqrt[2]{\frac{D}{F_{qq}}} \cdot \begin{bmatrix}1\\-1\end{bmatrix} \quad (6)$$

Where "D" is determined by equation (7):

$$D = F_{qA}^2 - F_{AA} \cdot F_{qq} \quad (7)$$

Slope analysis results from analyzing the value of parameter D. If D<0, there are no real tangential lines on the point, which means the existence of a double point and two slopes can only be justified when D>0. In this case, if specific concepts are renamed, flow curve slopes in relation to FCV opening are determined by equation (8):

$$\frac{dq}{dA}(A_0) = q_A(A_0) = -K_1 \pm \sqrt[2]{K_2} \quad (8)$$

For this equation to be true, the condition of F_{qq} not being null must be satisfied,. The other condition for conformance to D>0 is the verification of equation (9):

$$F_{qA} > \sqrt[2]{F_{AA} \cdot F_{qq}} \quad (9)$$

https://dx.doi.org/10.22161/ijaers/3.11.10 *ISSN: 2349-6495(P) | 2456-1908(O)*

To conclude this theoretical development, the requirements for existence of a double point bifurcation are mathematically confirmed because F_{qq} is not null and D can, under specific conditions, be higher than zero. And as the solution existence theorem says, if F(q,A) is continuous, then at least one solution of the Equation 1 exist. (Existence and not uniqueness).

II. METHODOLOGY

The methodology used in this study has foursteps. The Analysis is done based on recorded recirculation flow rate (%) and FCV position (%) data for a full 24-month cycle at an operating station.

S1. Determine the curve for recirculation flow (%) vs. FCV position (%). Using the data from the plant computer a third order polynomial is fitted with a 99.99% of confidence interval. The polynomial order is determined by the recirculation system designer. This step will demonstrate that a continuous and derivable function (Flow rate (%)-FCV position(%)) exists. This is a prerequisite to have a bifurcation.

S2. The error is calculated as difference between fitted curve values and real data for a given FCV position (%). (Equation 10)

$$Error(FCV\ Position) = Measured\ Flow(\%) - Calculated\ Flow(\%) \quad (10)$$

The analysis, of the equation (10) results, is the starting point of the bifurcation study.

S3. Taken the FCV (%) error-position data, Figure 3 and Equation (10), the bifurcation map is built. The bifurcation start point and two branches that characterize the pitchfork bifurcation are identified. The FCV position is considered as bifurcation parameter and will be the abscissa axe.

The bifurcated parameter is the recirculation flow rate. To enhance the graphic representation, a linear conversion will be done. So instead of recirculation flow rate (%) analysis, the error (Eq. 10) analysis will be done. The analysis will be as follows:

- A time period, in which the FCV position (%) is stable and constant, is selected. TheFCV position (%) values selected for this task are 29, 62, 62.3, 63, 64, 68, 72, 77 and 82%. The reason is because the FCV position is not continuous nor a differentiable as time function.
- New time series are recorded. Now, the time between records is 1 s. The time series are again, recirculation flow rate (%) and FCV position (%).
- Using equation 10 and table 2, the error is calculated from the recirculation flow rate time series built from previous step.
- A histogram with the error data is built. New variable named τ (tau) is built. The value of τ will be the error value in which the histogram has a maximum (most expected value) but if there are two maximums, then τ+ and τ- will be recorded.
- Based on τ (τ+, τ-) and FCV position (%) the bifurcation map is built.

2.1. Development

FCV position (%) and recirculation loop flow rate(%) are interrelated time series with which a bifurcation diagram will be developed. This approach is aligned with previous works which use time series as a starting point contributing to determinate bifurcation states. (Bagariano, E. et al, 1998 & 2000). It is also important to take into consideration that used time series are noisysignals.

The analysis of recirculation loop flow signal under bistable conditions has a number of phases aimed at determining flow signal features. Once this information is obtained, the entire system is analyzed, with a special focus on the relationship between recirculation loop flow rate and FCV position. The idea, suggesting bifurcation existencewill appear at this point.

2.1.1. Flow control Valve (FCV) position (%)-Flowrate(%) curve analysis (S1).

The studied NPP is a BWR 6 reactor, has two recirculation loops, each with its own flow control valve (FCV). (Figure 1)Figure 2shows records during a 24-month operating cycle, of the recirculation flow rate (%) and the FCV position (%).

A morphological analysis of the points cloud reveals that after a 60% opening approximately, the cloud begins to widen and after 62% it has a new width which remains constant until the end.

https://dx.doi.org/10.22161/ijaers/3.11.10 *ISSN: 2349-6495(P) | 2456-1908(O)*

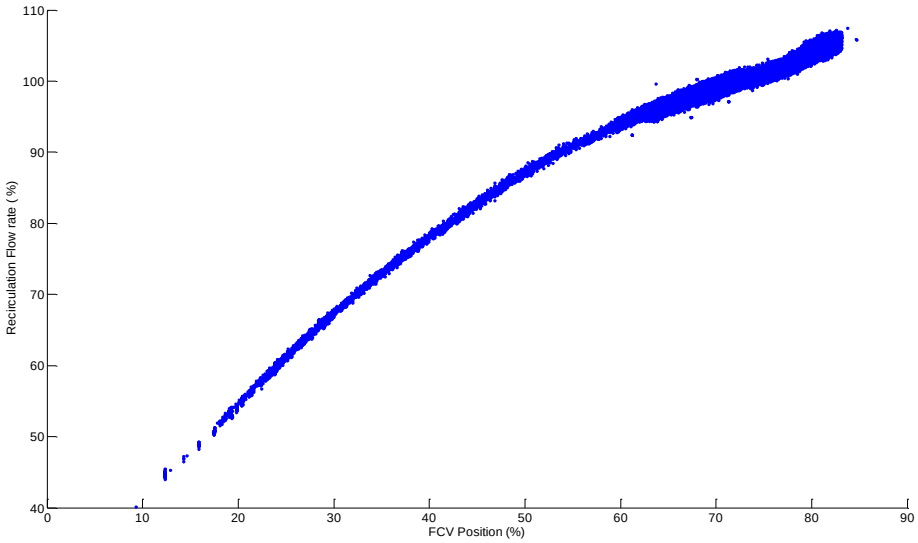

Fig.2: Operational points plot. (Recirculation Flow rate % vs. FCV position%).

The system designer fitted a third degree polynomial for the flow equation based on FCV position. This fit, with a confidence level of 99.999%, provides the coefficients shown in table 2.

Table.2: Polynomial coefficients for the theoretical curve fittedwith actual data.

	$Calculated\ Flow\ (\%) = a * (FCV_{POS})^3 + b * (FCV_{POS})^2 + c * (FCV_{POS}) + d$			
	a	B	c	d
FLOW RATE-FCV POSITION ADJUSTMENT	$6.5801 \cdot 10^{-5}$	-0.0188	2.1469	18.5307

So it is confirmed that there is a continuous and derivable function that stablish a relationship between flow rate (%) and FCV position (%). Based on that, the existence of Navier-Stokes´equation solution is clear, but the uniqueness is not ensured. So the bifurcation is possible.

2.1.2. Error analysis (S2).

Error (Equation (1)) is established as the difference between the measured flow value (%) and the fittedcurve value, as seen in table 2 parameters.(Figure 3.)

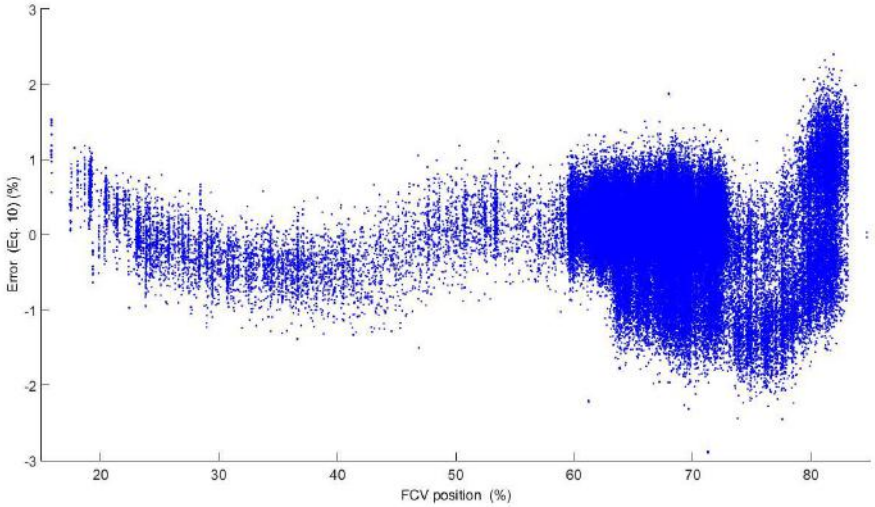

Fig.3: Error vs FCV position (%).

https://dx.doi.org/10.22161/ijaers/3.11.10 *ISSN: 2349-6495(P) | 2456-1908(O)*

Figure 3confirms the idea that there is some kind of phenomenon is changing flow patterns when FCV positionis 60% or above. This is because the error value, changes in shape and values. Error varies from about 0% with a +-0.5% band to a +-1.5% band. Even for values exceeding 80%, there is a clearly strong, differentiated bias with regards to flow behavior at this FCV position.

A histogram is created to analyze the overall error. Figure 4shows the Error (Equation 1) histogram. The histogram when analyzed leads to the conclusion that the average error tends to positive values and with a certain level of asymmetry for negative values. The histogram showed in figure 4, could be explained as the superposition of two normal distribution functions. The principal one has an expected value or maximum on 0.1 and the secondary has the expected value or maximum about 1%.

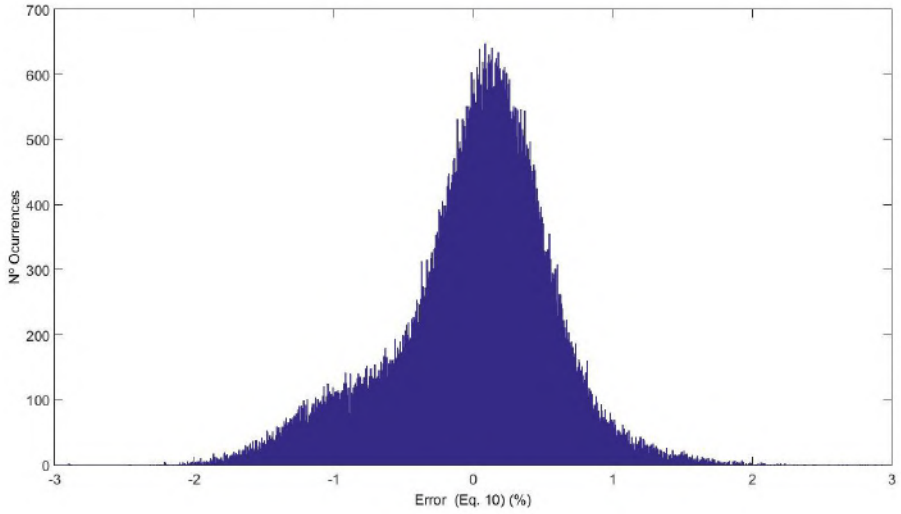

Fig.4: Error (Equ. 10)histogram

2.2. BifurcationCharacterization

The existence of a bifurcation structure will be demonstrated in this phase through the selection of FCV positionas the bifurcation parameter because isthe only one variable parameter in the system.

This section is focused on characterizing the pitchfork-type bifurcation for recirculation flow under bistable conditions. The coordinate parameterwill be tau (τ), whereas the abscissa is the FCV position (%). The initial bifurcation point will be FCV position at 62, 3 and τ=0. The FCV position and tau values canbe seen on table 3.

Table.3: tauand FCV position (%)values.

FCV Position (%)	*Tau (-)*	*Tau (+)*	*Reference figure*
30,3	-0.577	-0.577	
62,3	0	0	Figure 5
63,75	-0.674	0.293	
64	-0.675	0.294	
66	-0.728	0.306	
68	-0.785	0.313	
72	-0.863	0.256	
77,5	-0.955	0.287	Figure 6
82	0	1.3	

The graphical representation of values in table 3 is seen in figures 5and 6. These values are used to create the bifurcation map. (Figure 7).

https://dx.doi.org/10.22161/ijaers/3.11.10 *ISSN: 2349-6495(P) | 2456-1908(O)*

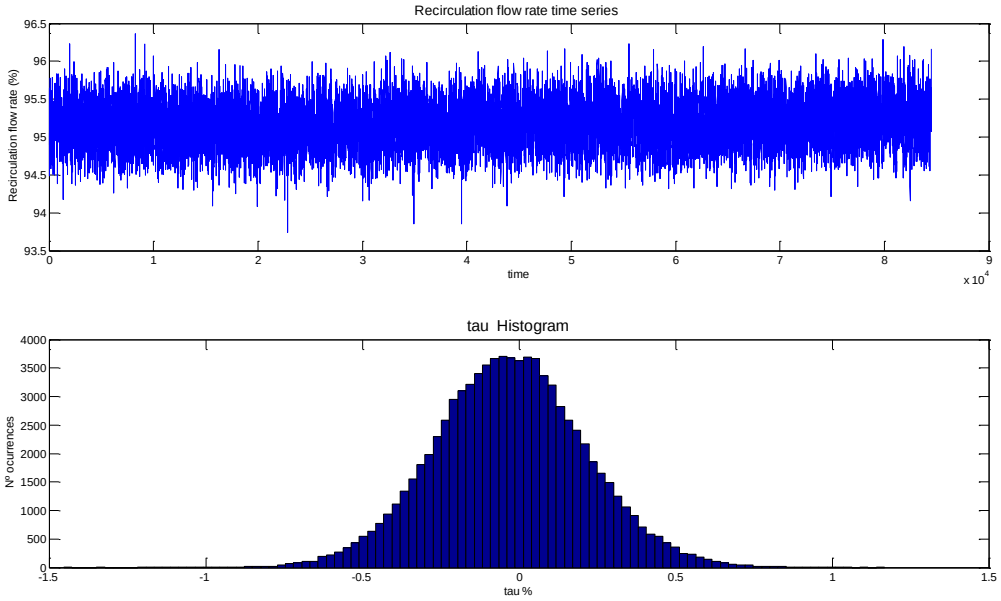

Fig.5: Recirculation flow evolution with FCV position value at 62,3 %.

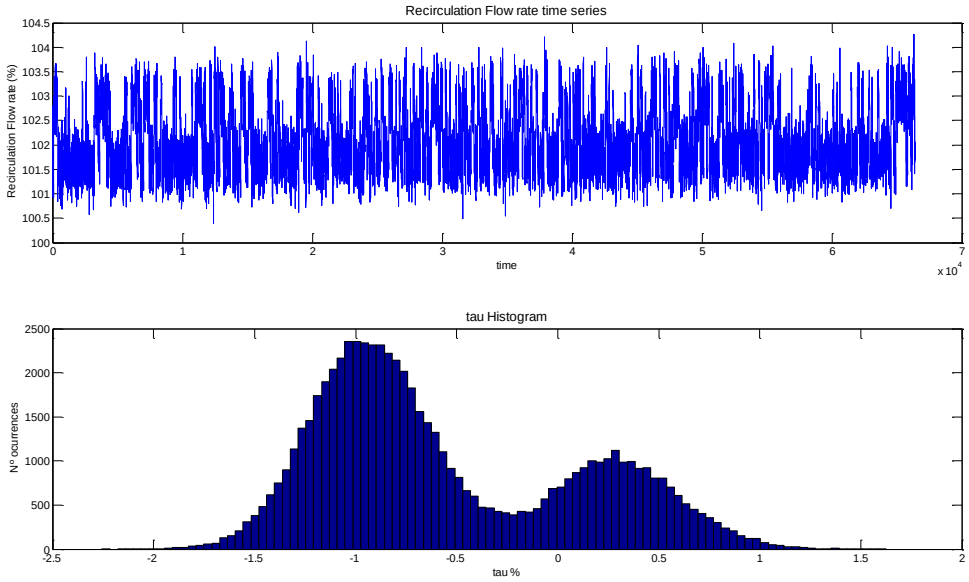

Fig.6: Recirculation flow evolution with FCV positionvalue at 77,5 %.

https://dx.doi.org/10.22161/ijaers/3.11.10 *ISSN: 2349-6495(P) | 2456-1908(O)*

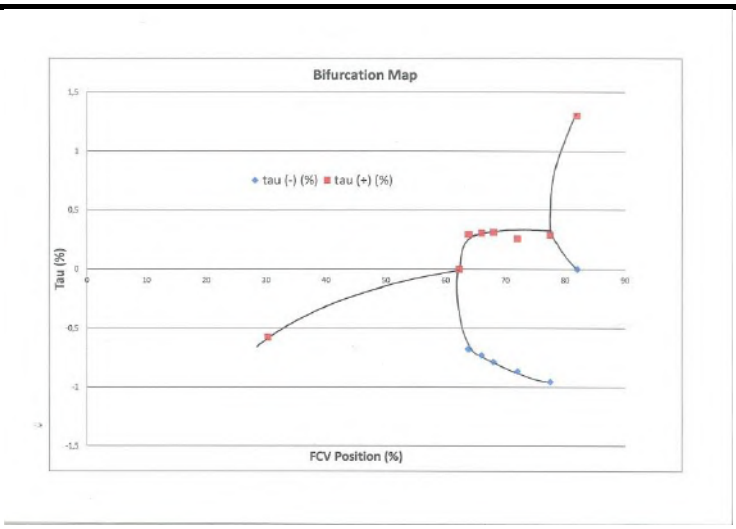

Fig.7: Taubifurcation diagram. Continuous lines represent the values of stable and expected solutions (feasible)

The data in table 3 is used to create a set of points on plane FCV position-τ. The result is seen in the graph of figure 7. An analysis of the graph in figure 8reveals the evident existence of bifurcation on point (62,3,0), which corresponds to a bifurcation of the pitchfork-type .

Deeper analysis shows that there are two consecutive bifurcations and two bistable states. The first bistable state is limited to FCV positionvalues ranging between 62,3and77(pitchfork bifurcation), whereas the second bistable state occurs whenFCV position values are larger than 77(secondary pitchforkbifurcation).

All the bifurcation analysis and results about tau(τ) are applicable to recirculation loop flow rate, because tau(τ) is a variable linearly dependent of recirculation flow rate(%). So the recirculation flow rate has the same bifurcation map, than tau(τ) .

III. RESULTS ANALYSIS

In section 2.2 a bifurcation diagram is created in response of the behavior of recirculation loop in a BWR6 unit, which is the system under analysis.

The existence of bistable flow is proven as a physical reality of the mathematical bifurcation concept. However, it is necessary to relate flow states with mathematical states and their physical meaning. This interpretation is based on the results of this work and those of the hydraulic model (Miura et al, 1986, 1987) and computational fluid flow models (CFD). (Gavilán Moreno, C.J. 2009).

The recirculation flow rate can have three stable states, grouped in twos. The first two states, corresponding to FCV positionvalues between 62.3% and 77%, are defined by the vortex dynamics of flow adaption in the so-called cross-piece. These states cause the following effects:

Vortex formation on the side legs of the manifold, in normal operation.

The newly formed vortexes cause flow to take two forms: one for direct inlet at high flow and the other for helical current at low flow. (Figure 8, Low Flow Pattern and High Flow Pattern)

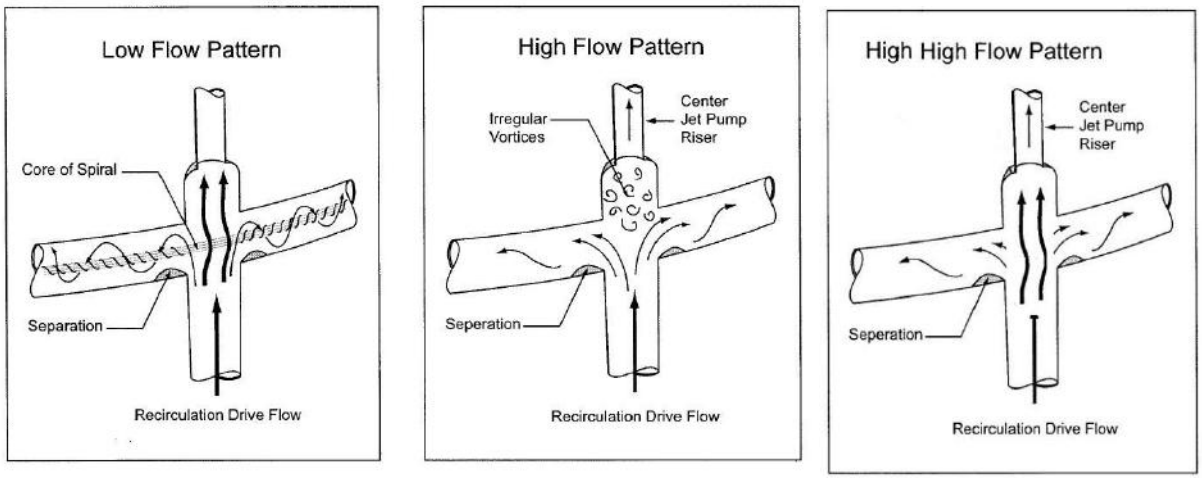

Fig.8: Recirculation loop cross-piece flow conditions for first bifurcation.

https://dx.doi.org/10.22161/ijaers/3.11.10 *ISSN: 2349-6495(P) | 2456-1908(O)*

In the first flow shape, pressure loss is as designed and flow is quite similar to its theoretical value (Figure 8 High Flow Pattern). In the second flow shape, pressure loss is higher since helical flow has more internal fluid friction and pipe wall friction, causing flow to be lower (Figure 8. Low Flow Pattern).

The next bistable scenario occurs when FVC position is 77%. In this case, flow equals rated values and some slightly higher (1%). In this state, flow takes two shapes: one of direct inlet at high flow (coinciding with the former high flow Pattern) and the other free of central connection vortexes (which are dragged by the high flow), hence reducing internal friction and enhancing flow. (Figure 8 High High Flow Pattern).

IV. CONCLUSIONS

The conclusions of this work are the following:

The bistable flow is a real flow situation in symmetric dynamic systems. The recirculation flow rate has two main values, but the FCV position just one.

The control system is not creating the bistable situation, because there is no variation of any parameter. There is no anomalous behavior of the recirculation system, because the real curve of recirculation loop flow rate vs FCV position fits very well with the theoretical one.

The Navier Stokes fluid flow equation, formally, allows and justified the pitchfork type bifurcation. There are situationswhere the solution, of the Navier Stokes equation,is double, so this equation has two solutions that comply with the system characteristics and boundary conditions.

A bifurcation map has been built, and the bifurcation is demonstrated. There are two bifurcations one at 62,3% FCV position and other at 77% of FCV position. Both of them arepitchfork type bifurcations.

The mathematical and real bifurcation has been correlated with the fluid flow behavior in the recirculation loop. More exactly the bifurcation is correlated with the fluid flow behavior in the crosspiece and the turbulence regime inside.

REFERENCES

[1] USNRC IN No. 86-110. (United Stated Nuclear Regulatory Commission) “Anomalous behavior of recirculation loop flow in jet pump BWR plants”, Washington. December 1986

[2] General Electric, Nuclear SIL.467 (1988) “Recirculation System bi-stable flow in jet pump BWRs”.

[3] Miura et al. (1986) “Unstable Phenomenon in Flow through a Pipe system with a cross pipe.(1st report, Generation of flow instability and its condition” Journal of Japan Society of Mechanical Engineers, No 86-127B, pp 35-39.

[4] Miura, S. et all (1987) “Unstable Phenomenon in Flow through a Pipe system with a cross pipe. (2nd report, The influence of the branching discharge ratio and structural factor of a pipe upon the unstable discharge phenomenon)” Journal of Japan Society of Mechanical Engineers, No 87-1251 B, pp 1067-1610.

[5] Ohki, A. et al (1989) “Unstable Phenomenon in Flow through a Pipe system with a cross pipe. (3rd report, Investigation of flow stabilizing structure of a pipe for the unstable discharge phenomenon)” Journal of Japan Society of Mechanical Engineers, No 88-1677 B, pp 3040-3043.

[6] A Nuñez Carrera, E. Martinez-Mendez, G. Espinosa Paredes, Analyses of the bistable flow phenomenon at Laguna Verde Nuclear Power Plant: Proceedings of the 2006 International LAS/ANS Congress of Buenos Aires(in Spanish).

[7] Gavilán Moreno, C.J. (2008) “Analysis and simulation of the flow signal in the recirculation loop of a nuclear power station during a bistable flow event.” Nuclear Engineering and Design.

[8] Horsthemke&Lefever (2005). “Noise Induced Transitions”. Ed. Springer series in Synergetics.

[9] Nuñez-Carrera, A; Prieto-Guerrero, A; Espinosa-Martínez, E.-G; Espinosa-Paredes, G. (2009) “Analysis of a signal during bistable flow events in Laguna Verde Nuclear Power Station with wavelets techniques” Nuclear Engineering and Design. Vol. 239, Iss. 12, pp. 2942-2951.

[10] Gavilán Moreno, C.J. (2009) “Hydraulic Study on recirculation loops using computational fluid dynamics (CFD). Design optimization and turbulence reduction” Nuclear Engineering and design.Vol. 239, Iss. , pp. 434-441.

[11] Gavilán Moreno, C.J. (2011) “The Bistable flow in a nuclear Power Plant. A bifurcation in the fluid flow in the recirculation loop, modeling and simulation” Proc. Bifurcation in Fluid Dynamics. CIMNE. Barcelona

[12] Poincare, H. (1885) “L’Equilibre d’une masse fluide animée d’un mouvement de rotation” Acta Mathematica, T.7 pp 259-380.

[13] Ioos, G; Joseph, D.D. (1997) “Elementary stability and bifurcation theory”. Ed. Springer.

[14] Bagarinao, E. et al. (1998) ”Generalized once-parameter bifurcation diagram reconstruction using time series” Physica D, Vol. 124, pp. 258-270.

[15] Bagariano, E. et al. (2000) “Reconstructing Bifurcation diagrams o dynamical systems using measured time series” Method Inform. Med, Vol. 39, pp. 146-149.

International Journal of Advanced Engineering Research and Science (IJAERS) *[Vol-3, Issue-11, Nov- 2016]*
https://dx.doi.org/10.22161/ijaers/3.11.10 *ISSN: 2349-6495(P) | 2456-1908(O)*

Characterizing the Bistable Flow, of BWR, as a Bifurcation (Pitchfork Type) in the Navier-Stokes' Equation Solution

Dr. Carlos J. Gavilan Moreno

Cofrentes NPP. Iberdrola Generación Nuclear, Paraje el Plano S/N. Cofrentes 46625. Valencia. Spain.

Abstract— *Many nuclear power plants have undertaken power uprate processes, increasing recirculation, feed water and steam flow rates. With regards to recirculation flow, adverse scenarios,may arise where the flow varies autonomously between two values, a phenomenon known as bistable flow.Although this phenomenon is typically related to power uprate processes, some plants experience it when they reach high flow values, especially at the end of the cycle.*

This study proves empirically the existence of a Pitchfork-type bifurcation in the bistable flow situation.The parameter determining bifurcation will be Flow Control Valve (FCV) position in recirculation loop. This choice is made considering that it is the only variable during recirculation loop operation, because under stable operation and constant power the remaining variables (Geometry, Combustible, Differential Core Pressure, Pump Turning Speed (r.p.m.), etc.), are considered constant.

Keywords— ***Bifurcation, pitchfork, bistable, recirculation, FCV, flow.***

I. INTRODUCTION

In 1985, an electrical power fluctuation was detected at the Leibstadt Nuclear Power Plant during startup and load tests at 100%. Loop "A" fluctuation ranged between 2.5% and 3%, whereas in loop "B" it was between 3% and 3.5%. It was concluded that recirculation flow fluctuations were caused by a bistable flow pattern in the pump discharge header.

In the year 1986, the first regulatory reference on abnormal performance of recirculation loop flows was written. (USNRC IE IN No. 86-110). This document determines that fluctuations vary from station to station and even within the loops of the sameunit. This document also concludes that this phenomenon does not impact safety.

In July 1988, General Electric issued a letter (General Electric Energy, Nuclear SIL No. 467) establishing that the problem affects Boiling Water Reactors BWR from generation 3 to 6 and is detected at the manifoldsof pipes supplying jet pumps. (Figure 1).

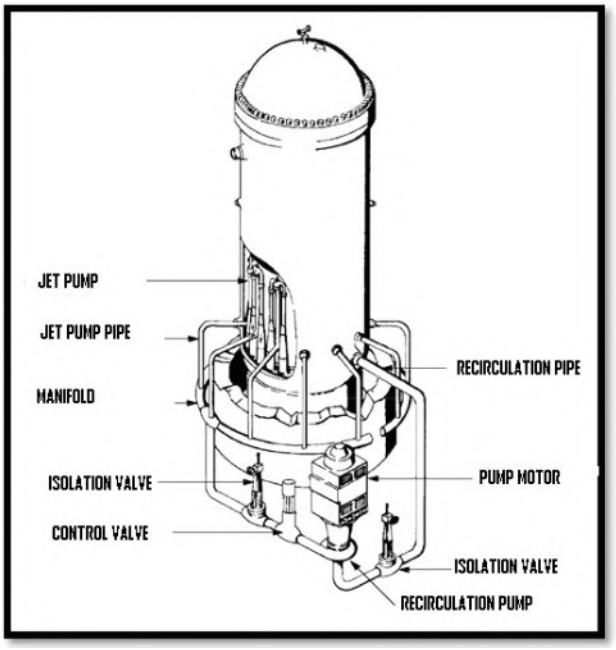

Fig.1: Recirculation loop scheme in a Generation 6 BWR.

In Japan, between1986 and1989 a group of researchers applied various hydraulic models to replicate (Miura et al 1986), characterize (Miura et al 1987) and propose compensatory measures (Ohki, A. et al 1988) to the bistable flow.

In 2006, a bistable flow phenomenon analysis was presented at Laguna Verde nuclear power plant in México. (Nuñez Carrera et al., 2006).

After 2008, new research (Gavilan Moreno, C.J. 2008), concluded that the bistable flowcan be described as a noise-induced transition mechanism (Horstheme & Lefever (2005)). In this theory, noise is identified as flow turbulence under high Reynolds values.

In 2009, bistable flow analyses continued, using mathematical techniques such as wavelets (Nuñez-Carrera et al., 2009) and codes for fluid dynamics. These were used to replicate the results of hydraulic models from the 80s. (Gavilan Moreno, C.J. 2009).

https://dx.doi.org/10.22161/ijaers/3.11.10 *ISSN: 2349-6495(P) | 2456-1908(O)*

In 2011, a new 3D CFD model confirmed the existence of two states and the non-convergence of the stable condition at specific Reynolds values. (Gavilán Moreno, C.J. 2011)

In line with the above mentioned in this section, the state of the art in bistable flow can be summarized as Unpredictable, fluctuating hydraulic phenomenon, characterized by high turbulence.

In the following paragraphs,the Pitchfork type bifurcationconcept is introduced and justified.

Supposed a dynamic system, a bifurcation occurs when a small smooth change made to the parameter values of a system causes a sudden qualitative or topological change in its behavior. The name “bifurcation” was first introduced by Henri Poincare in 1885, in the first paper in mathematics showing such a behavior.

It is normal to divide bifurcations into two classes: Local bifurcations and Global Bifurcations. A local bifurcation occurs when a parameter change, causes the stability of equilibrium or fixed point to change. Examples of local bifurcation include: Saddle-node bifurcation, Transcritical bifurcation, Pitchfork bifurcation, Hopf bifurcation and Neimark-Sacker bifurcation. In continuous dynamical systems described by Differential Equations (DE)—i.e. flows—pitchfork bifurcations occur generically insystems with symmetry.Pitchfork bifurcationshave several types – supercritical, transcritical and subcritical.Normally solving the DE´s can be found that, for depending on some parameters values, the system has one stable equilibrium point, or an unstable pointor two stable equilibria points.This last status is the key to identify the bistable flow with the pitchfork bifurcation.

The recirculation system, of a BWR, is a hydraulic system, whose behavior is described by the equation of Navier Stokeswhich can be seen in Equation (1). The recirculation system is a symmetric system. So the solution of the Partial Derivatives Equation (PDE), could present Pitchfork type bifurcation. A deeperanalysis is done to justify the bifurcation.

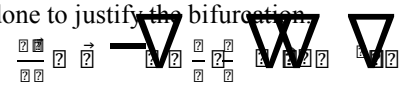

(1)

The equation (Eq. 1) has the following vectors: u (speed), P (pressure), μ (viscosity) and ṕ (fluid density). Since the system has a constant section and there are no fluid sumps or sources, integrated fluid speed is similar to the scalar flow value. Likewise, pressure variation only depends on FCV opening. Thus, Equation (1) can be reformulated as Equation (2):

(2)

Where q=flow rate and A= FCV position.

Additional information regarding this equation and systemis:

- The fluid is in an incompressible state.
- The fluid is at a constant temperature.
- The system responds with an equation similar to q=q(A).
- Primary derivatives are determined by Equation (3), with notation and secondary derivatives being simplified in Equation (4):

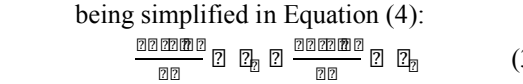

(3)

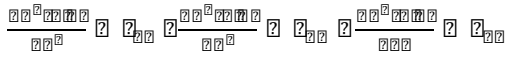

(4)

The stability analysis results from establishing a null time derivative. In other words, if the system does not change and FCV opening and other conditions do not vary, flow remains the same. Mathematically, this is seen in equation (5).

(5)

So, analyzing bifurcations in Equation (4) is the same as analyzing specific F curve points (q, A) on the FCVopening-flow plane. Considering these parameters, the points that confirm the equation (7) are considered unique and can be classified as follows: Regular Points, Regular Inflexion Points, Unique Points, Double Curve Point, Double Inflexion Points and Peak Points.

The Double Curve Point generates two solutions and a curve running through the unique point that has two slopes. Although there are multiple potential shapes, the one selected provides two stable results as it is coherent with bistable conditions.

In the case of double point bifurcation, there is anequilibriumpoint with two curves and two different slopes. (Ioos, G; Joseph, P.D. 2001). Curve tangents conform to Equation (6)

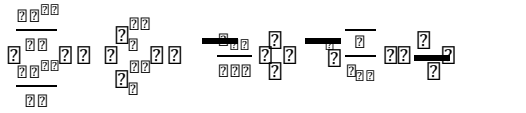

(6)

Where “D” is determined by equation (7):

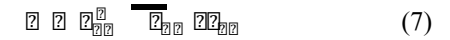

(7)

Slope analysis results from analyzing the value of parameter D. If D<0, there are no real tangential lines on the point, which means the existence of a double point and two slopes can only be justified when D>0. In this case, if specific concepts are renamed, flow curve slopes in relation to FCV opening are determined by equation (8):

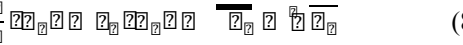

(8)

For this equation to be true, the condition of F_{qq} not being null must be satisfied,. The other condition for conformance to D>0 is the verification of equation (9):

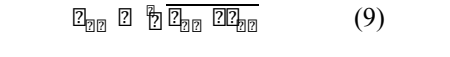

(9)

https://dx.doi.org/10.22161/ijaers/3.11.10 *ISSN: 2349-6495(P) | 2456-1908(O)*

To conclude this theoretical development, the requirements for existence of a double point bifurcation are mathematically confirmed because F_{qq} is not null and D can, under specific conditions, be higher than zero. And as the solution existence theorem says, if F(q,A) is continuous, then at least one solution of the Equation 1 exist. (Existence and not uniqueness).

II. METHODOLOGY

The methodology used in this study has foursteps. The Analysis is done based on recorded recirculation flow rate (%) and FCV position (%) data for a full 24-month cycle at an operating station.

S1. Determine the curve for recirculation flow (%) vs. FCV position (%). Using the data from the plant computer a third order polynomial is fitted with a 99.99% of confidence interval. The polynomial order is determined by the recirculation system designer. This step will demonstrate that a continuous and derivable function (Flow rate (%)-FCV position(%)) exists. This is a prerequisite to have a bifurcation.

S2. The error is calculated as difference between fitted curve values and real data for a given FCV position (%). (Equation 10)

(10)

The analysis, of the equation (10) results, is the starting point of the bifurcation study.

S3. Taken the FCV (%) error-position data, Figure 3 and Equation (10), the bifurcation map is built. The bifurcation start point and two branches that characterize the pitchfork bifurcation are identified. The FCV position is considered as bifurcation parameter and will be the abscissa axe.

The bifurcated parameter is the recirculation flow rate. To enhance the graphic representation, a linear conversion will be done. So instead of recirculation flow rate (%) analysis, the error (Eq. 10) analysis will be done. The analysis will be as follows:

- A time period, in which the FCV position (%) is stable and constant, is selected. TheFCV position (%) values selected for this task are 29, 62, 62.3, 63, 64, 68, 72, 77 and 82%. The reason is because the FCV position is not continuous nor a differentiable as time function.
- New time series are recorded. Now, the time between records is 1 s. The time series are again, recirculation flow rate (%) and FCV position (%).
- Using equation 10 and table 2, the error is calculated from the recirculation flow rate time series built from previous step.
- A histogram with the error data is built. New variable named τ (tau) is built. The value of τ will be the error value in which the histogram has a maximum (most expected value) but if there are two maximums, then τ+ and τ- will be recorded.
- Based on τ (τ+, τ-) and FCV position (%) the bifurcation map is built.

2.1. Development

FCV position (%) and recirculation loop flow rate(%) are interrelated time series with which a bifurcation diagram will be developed. This approach is aligned with previous works which use time series as a starting point contributing to determinate bifurcation states. (Bagariano, E. et al, 1998 & 2000). It is also important to take into consideration that used time series are noisysignals.

The analysis of recirculation loop flow signal under bistable conditions has a number of phases aimed at determining flow signal features. Once this information is obtained, the entire system is analyzed, with a special focus on the relationship between recirculation loop flow rate and FCV position. The idea, suggesting bifurcation existencewill appear at this point.

2.1.1. Flow control Valve (FCV) position (%)-Flowrate(%) curve analysis (S1).

The studied NPP is a BWR 6 reactor, has two recirculation loops, each with its own flow control valve (FCV). (Figure 1)Figure 2shows records during a 24-month operating cycle, of the recirculation flow rate (%) and the FCV position (%).

A morphological analysis of the points cloud reveals that after a 60% opening approximately, the cloud begins to widen and after 62% it has a new width which remains constant until the end.

https://dx.doi.org/10.22161/ijaers/3.11.10 *ISSN: 2349-6495(P) | 2456-1908(O)*

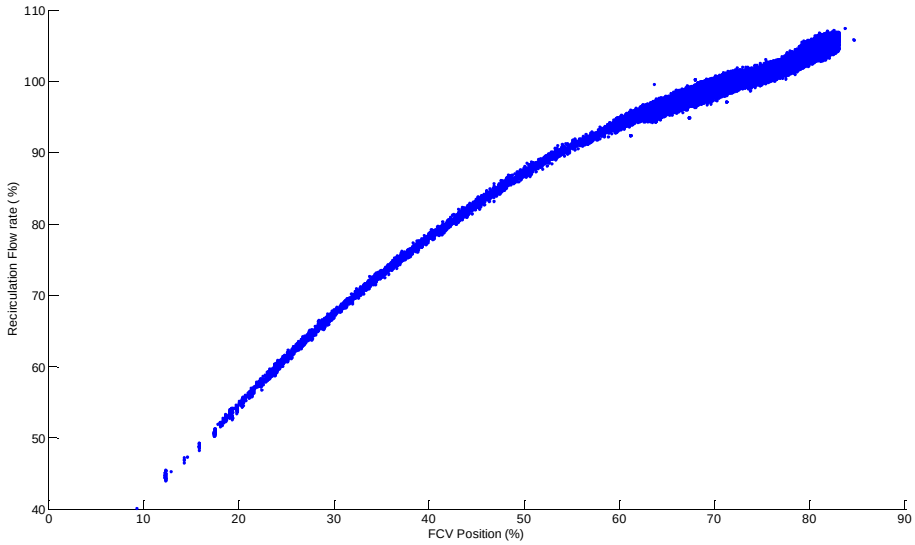

Fig.2: Operational points plot. (Recirculation Flow rate % vs. FCV position%).

The system designer fitted a third degree polynomial for the flow equation based on FCV position. This fit, with a confidence level of 99.999%, provides the coefficients shown in table 2.

Table.2: Polynomial coefficients for the theoretical curve fittedwith actual data.

	[illegible]			
	a	B	c	d
FLOW RATE-FCV POSITION ADJUSTMENT	$6.5801 \cdot 10^{-5}$	-0.0188	2.1469	18.5307

So it is confirmed that there is a continuous and derivable function that stablish a relationship between flow rate (%) and FCV position (%). Based on that, the existence of Navier-Stokes´equation solution is clear, but the uniqueness is not ensured. So the bifurcation is possible.

2.1.2. Error analysis (S2).

Error (Equation (1)) is established as the difference between the measured flow value (%) and the fittedcurve value, as seen in table 2 parameters.(Figure 3.)

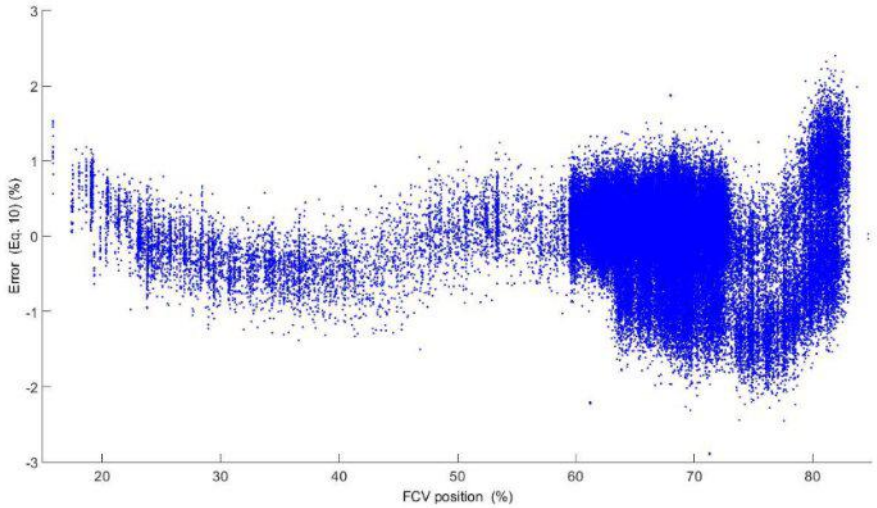

Fig.3: Error vs FCV position (%).

https://dx.doi.org/10.22161/ijaers/3.11.10 *ISSN: 2349-6495(P) | 2456-1908(O)*

Figure 3confirms the idea that there is some kind of phenomenon is changing flow patterns when FCV positionis 60% or above. This is because the error value, changes in shape and values. Error varies from about 0% with a +-0.5% band to a +-1.5% band. Even for values exceeding 80%, there is a clearly strong, differentiated bias with regards to flow behavior at this FCV position.

A histogram is created to analyze the overall error. Figure 4shows the Error (Equation 1) histogram. The histogram when analyzed leads to the conclusion that the average error tends to positive values and with a certain level of asymmetry for negative values. The histogram showed in figure 4, could be explained as the superposition of two normal distribution functions. The principal one has an expected value or maximum on 0.1 and the secondary has the expected value or maximum about 1%.

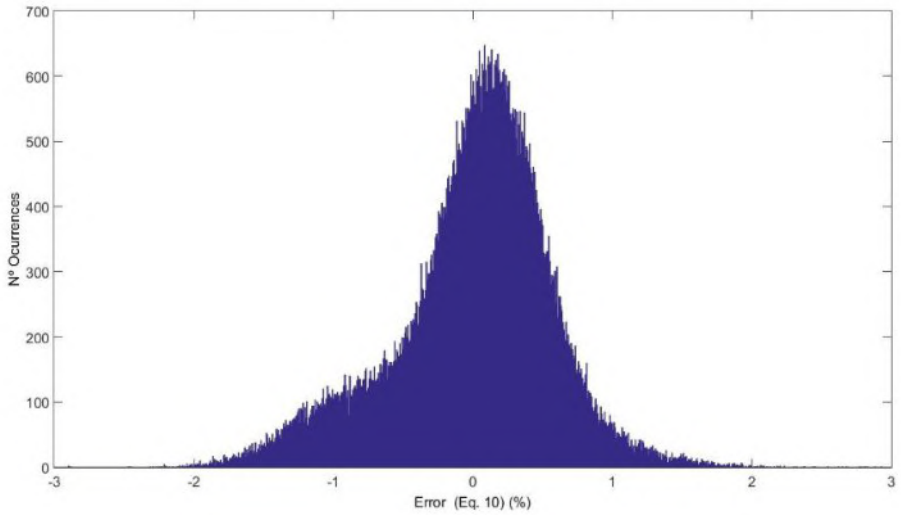

Fig.4: Error (Equ. 10)histogram

2.2. BifurcationCharacterization

The existence of a bifurcation structure will be demonstrated in this phase through the selection of FCV positionas the bifurcation parameter because isthe only one variable parameter in the system.

This section is focused on characterizing the pitchfork-type bifurcation for recirculation flow under bistable conditions. The coordinate parameterwill be tau (τ), whereas the abscissa is the FCV position (%). The initial bifurcation point will be FCV position at 62, 3 and τ=0. The FCV position and tau values canbe seen on table 3.

Table.3: tauand FCV position (%)values.

FCV Position (%)	*Tau (-)*	*Tau (+)*	*Reference figure*
30,3	-0.577	-0.577	
62,3	0	0	Figure 5
63,75	-0.674	0.293	
64	-0.675	0.294	
66	-0.728	0.306	
68	-0.785	0.313	
72	-0.863	0.256	
77,5	-0.955	0.287	Figure 6
82	0	1.3	

The graphical representation of values in table 3 is seen in figures 5and 6. These values are used to create the bifurcation map. (Figure 7).

https://dx.doi.org/10.22161/ijaers/3.11.10 ***ISSN: 2349-6495(P) | 2456-1908(O)***

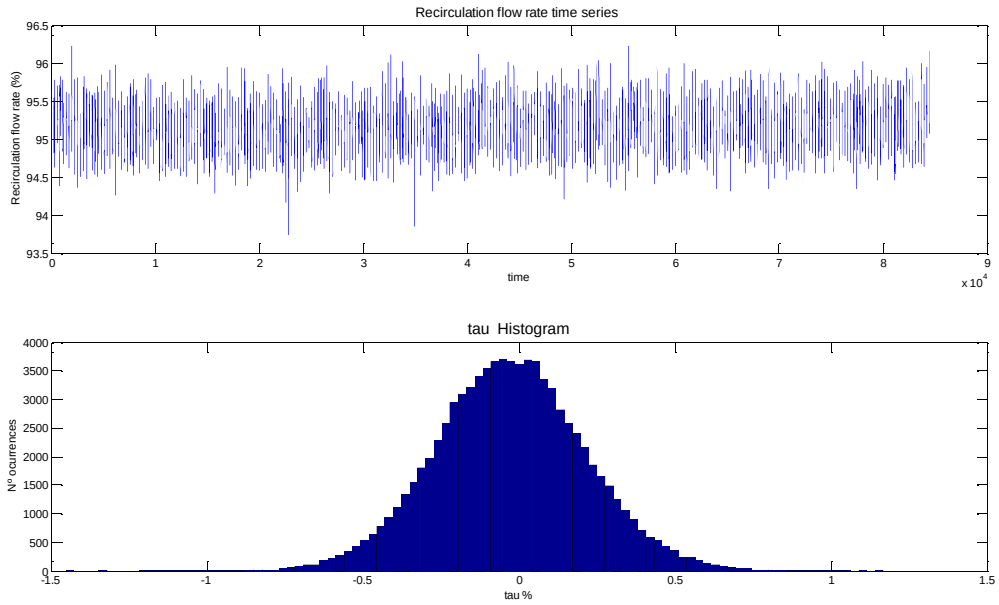

Fig.5: Recirculation flow evolution with FCV position value at 62,3 %.

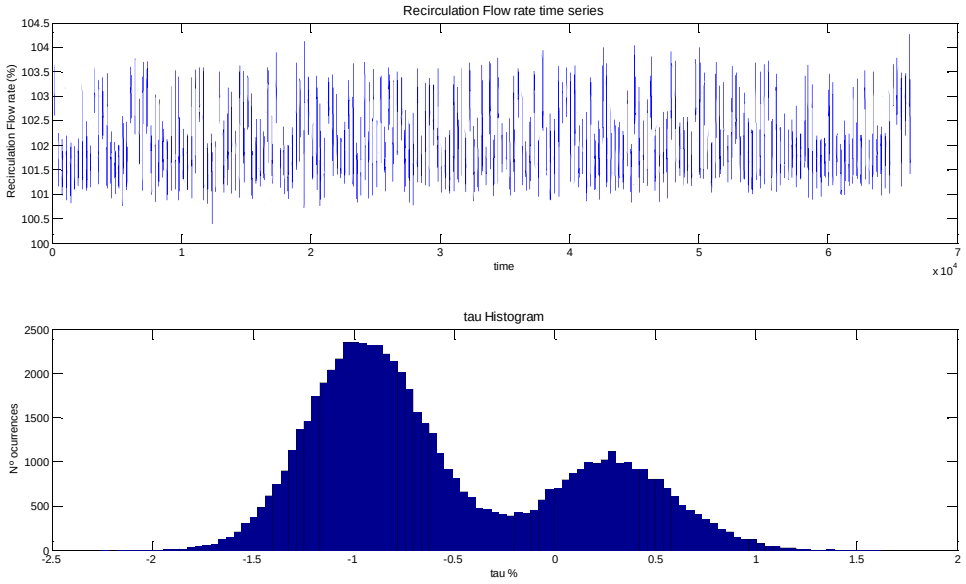

Fig.6: Recirculation flow evolution with FCV positionvalue at 77,5 %.

https://dx.doi.org/10.22161/ijaers/3.11.10 *ISSN: 2349-6495(P) | 2456-1908(O)*

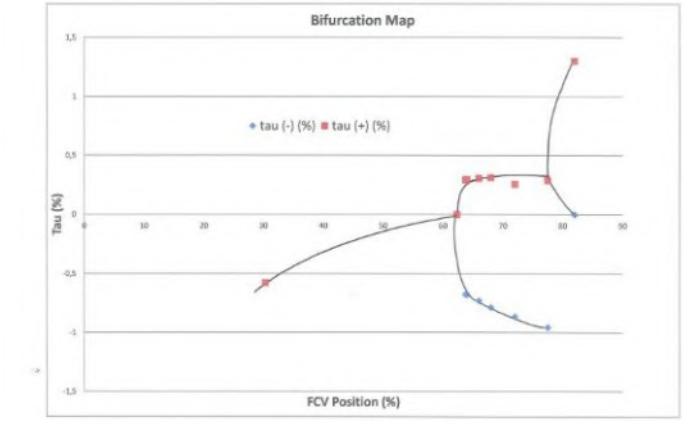

Fig.7: Taubifurcation diagram. Continuous lines represent the values of stable and expected solutions (feasible)

The data in table 3 is used to create a set of points on plane FCV position-τ. The result is seen in the graph of figure 7. An analysis of the graph in figure 8reveals the evident existence of bifurcation on point (62,3,0), which corresponds to a bifurcation of the pitchfork-type .

Deeper analysis shows that there are two consecutive bifurcations and two bistable states. The first bistable state is limited to FCV positionvalues ranging between 62,3and77(pitchfork bifurcation), whereas the second bistable state occurs whenFCV position values are larger than 77(secondary pitchforkbifurcation).

All the bifurcation analysis and results about tau(τ) are applicable to recirculation loop flow rate, because tau(τ) is a variable linearly dependent of recirculation flow rate(%). So the recirculation flow rate has the same bifurcation map, than tau(τ) .

III. RESULTS ANALYSIS

In section 2.2 a bifurcation diagram is created in response of the behavior of recirculation loop in a BWR6 unit, which is the system under analysis.

The existence of bistable flow is proven as a physical reality of the mathematical bifurcation concept. However, it is necessary to relate flow states with mathematical states and their physical meaning. This interpretation is based on the results of this work and those of the hydraulic model (Miura et al, 1986, 1987) and computational fluid flow models (CFD). (Gavilán Moreno, C.J. 2009).

The recirculation flow rate can have three stable states, grouped in twos. The first two states, corresponding to FCV positionvalues between 62.3% and 77%, are defined by the vortex dynamics of flow adaption in the so-called cross-piece. These states cause the following effects:

Vortex formation on the side legs of the manifold, in normal operation.

The newly formed vortexes cause flow to take two forms: one for direct inlet at high flow and the other for helical current at low flow. (Figure 8, Low Flow Pattern and High Flow Pattern)

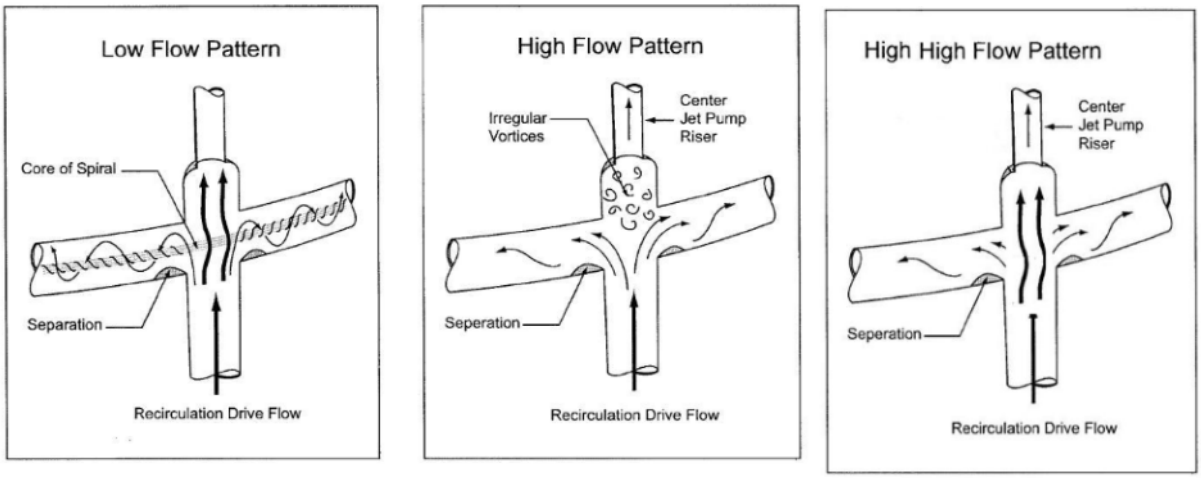

Fig.8: Recirculation loop cross-piece flow conditions for first bifurcation.

https://dx.doi.org/10.22161/ijaers/3.11.10 *ISSN: 2349-6495(P) | 2456-1908(O)*

In the first flow shape, pressure loss is as designed and flow is quite similar to its theoretical value (Figure 8 High Flow Pattern). In the second flow shape, pressure loss is higher since helical flow has more internal fluid friction and pipe wall friction, causing flow to be lower (Figure 8. Low Flow Pattern).

The next bistable scenario occurs when FVC position is 77%. In this case, flow equals rated values and some slightly higher (1%). In this state, flow takes two shapes: one of direct inlet at high flow (coinciding with the former high flow Pattern) and the other free of central connection vortexes (which are dragged by the high flow), hence reducing internal friction and enhancing flow. (Figure 8 High High Flow Pattern).

IV. CONCLUSIONS

The conclusions of this work are the following:

The bistable flow is a real flow situation in symmetric dynamic systems. The recirculation flow rate has two main values, but the FCV position just one.

The control system is not creating the bistable situation, because there is no variation of any parameter. There is no anomalous behavior of the recirculation system, because the real curve of recirculation loop flow rate vs FCV position fits very well with the theoretical one.

The Navier Stokes fluid flow equation, formally, allows and justified the pitchfork type bifurcation. There are situationswhere the solution, of the Navier Stokes equation,is double, so this equation has two solutions that comply with the system characteristics and boundary conditions.

A bifurcation map has been built, and the bifurcation is demonstrated. There are two bifurcations one at 62,3% FCV position and other at 77% of FCV position. Both of them arepitchfork type bifurcations.

The mathematical and real bifurcation has been correlated with the fluid flow behavior in the recirculation loop. More exactly the bifurcation is correlated with the fluid flow behavior in the crosspiece and the turbulence regime inside.

REFERENCES

[1] USNRC IN No. 86-110. (United Stated Nuclear Regulatory Commission) “Anomalous behavior of recirculation loop flow in jet pump BWR plants”, Washington. December 1986

[2] General Electric, Nuclear SIL.467 (1988) “Recirculation System bi-stable flow in jet pump BWRs”.

[3] Miura et al. (1986) “Unstable Phenomenon in Flow through a Pipe system with a cross pipe.(1s^{t} report, Generation of flow instability and its condition” Journal of Japan Society of Mechanical Engineers, No 86-127B, pp 35-39.

[4] Miura, S. et all (1987) “Unstable Phenomenon in Flow through a Pipe system with a cross pipe. (2nd report, The influence of the branching discharge ratio and structural factor of a pipe upon the unstable discharge phenomenon)” Journal of Japan Society of Mechanical Engineers, No 87-1251 B, pp 1067-1610.

[5] Ohki, A. et al (1989) “Unstable Phenomenon in Flow through a Pipe system with a cross pipe. (3rd report, Investigation of flow stabilizing structure of a pipe for the unstable discharge phenomenon)” Journal of Japan Society of Mechanical Engineers, No 88-1677 B, pp 3040-3043.

[6] A Nuñez Carrera, E. Martinez-Mendez, G. Espinosa Paredes, Analyses of the bistable flow phenomenon at Laguna Verde Nuclear Power Plant: Proceedings of the 2006 International LAS/ANS Congress of Buenos Aires(in Spanish).

[7] Gavilán Moreno, C.J. (2008) “Analysis and simulation of the flow signal in the recirculation loop of a nuclear power station during a bistable flow event.” Nuclear Engineering and Design.

[8] Horsthemke&Lefever (2005). “Noise Induced Transitions”. Ed. Springer series in Synergetics.

[9] Nuñez-Carrera, A; Prieto-Guerrero, A; Espinosa-Martínez, E.-G; Espinosa-Paredes, G. (2009) “Analysis of a signal during bistable flow events in Laguna Verde Nuclear Power Station with wavelets techniques” Nuclear Engineering and Design. Vol. 239, Iss. 12, pp. 2942-2951.

[10] Gavilán Moreno, C.J. (2009) “Hydraulic Study on recirculation loops using computational fluid dynamics (CFD). Design optimization and turbulence reduction” Nuclear Engineering and design.Vol. 239, Iss. , pp. 434-441.

[11] Gavilán Moreno, C.J. (2011) “The Bistable flow in a nuclear Power Plant. A bifurcation in the fluid flow in the recirculation loop, modeling and simulation” Proc. Bifurcation in Fluid Dynamics. CIMNE. Barcelona

[12] Poincare, H. (1885) “L’Equilibre d’une masse fluide animée d’un mouvement de rotation” Acta Mathematica, T.7 pp 259-380.

[13] Ioos, G; Joseph, D.D. (1997) “Elementary stability and bifurcation theory”. Ed. Springer.

[14] Bagarinao, E. et al. (1998) ”Generalized once-parameter bifurcation diagram reconstruction using time series” Physica D, Vol. 124, pp. 258-270.

[15] Bagariano, E. et al. (2000) “Reconstructing Bifurcation diagrams o dynamical systems using measured time series” Method Inform. Med, Vol. 39, pp. 146-149.

https://dx.doi.org/10.22161/ijaers/3.11.11 *ISSN: 2349-6495(P) | 2456-1908(O)*

An Approach of Automated Electronic Voting Management System for Bangladesh Using Biometric Fingerprint

M. Mesbahuddin Sarker[1], Md. Ariful Islam Shah[1], Tajim Md. Niamat Ullah Akhund[1], Md. Sharif Uddin[2]

[1]Institute of Information Technology Institute, Jahangirnagar University, Savar, Dhaka.
[2]Dept. of Mathematics Jahangirnagar University, Savar, Dhaka.

Abstract— *The existing system of election is running manually and the piloted electronic voting using electronic voting machine (EVM) has many limitations in its mechanism. In this paper we have proposed an automated biometric electronic voting system, where a four layered network system has been used for sending the votes from client to the main database, and there exist three application servers and a client. That means, the proposed systems starts with automated registration system that would provide the secured database of the voters' information, and voter details will be stored against their finger prints in the main database. Finally, at the end of the day, casted votes will be counted automatically which would take lesser time than the manual system and the result would be accurate, faster and reliable, and thus minimize the corruption.*

Keywords— *Electronic Voting, Biometric, EVM, SEIR.*

I. INTRODUCTION

A biometric system is a technological system that uses information about a person (or other biological organism) to identify that person. Biometric systems rely on specific data about unique biological traits in order to work effectively. In general, biometrics is any use of biological data in technology. Biometric methods provide identification by using specifications such as fingerprints, face, hand shape, iris, retina, voice track and signature. These specifications vary from person to person. Biometric solutions are generally client/server solutions, giving system administrators the ability to audit usage, manage security levels, and remove unauthorized users [Adem et. al, 2011]. In this study, biometric election system is aimed instead of traditional election systems. By developing the deficiencies of the present system, biometric based election system has been developed and gives the details of requirements, design and implementation of a generic and secure electronic voting system where voters can cast their votes any-time, anywhere and mainly to cast a vote to that person to whom voter want to cast a vote using a number of electronic devices.

The system that exists currently in Bangladesh is totally paper based except very few centers consider EVM. This EVM is a simple electronic device used to record votes in place of ballot papers and boxes which were used earlier in conventional voting system. It is a simple machine that can be operated easily by both the polling personnel and the voters. Being a standalone machine without any network connectivity, nobody can interfere with its programming and manipulate the result. It has mainly two units: Control unit and Ballot unit. The Control Unit is the main unit which stores all data and controls the functioning of EVM. The program which controls the functioning of the control unit is burnt into a microchip on a "one time programmable basis" [Sarker, 2013]. Once burnt it cannot be read, copied out or altered. The EVMs use dynamic coding to enhance security of data transmitted from ballot unit to control unit. The new EVMs have also real time clock and date-time stamping facility which enables them to record the exact time and date whenever a key is pressed. The existing election system in Bangladesh is pictured below:

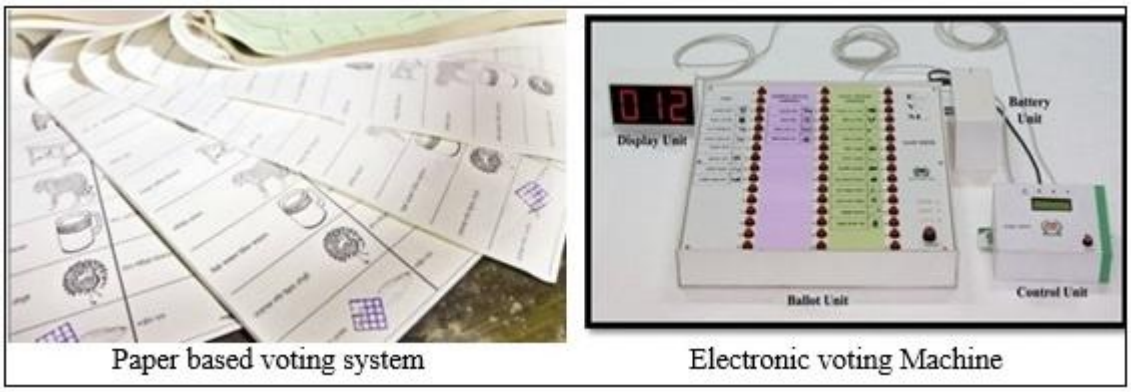

Fig.1: Existing election system in Bangladesh

https://dx.doi.org/10.22161/ijaers/3.11.11 *ISSN: 2349-6495(P) | 2456-1908(O)*

II. PURPOSE OF THE RESEARCH

A close election in 1998 in the Australian Capital Territory (ACT) found numerous problems in the state's hand-counting system, when two candidates were separated by only three or four votes [Thomos, 2004]. After recounting, officials discovered that out of 80,000 ballots, they had made about 100 mistakes. Ultimately, the ACT Electoral Commission adopted a new system known as eVACS, or Electronic Voting and Counting System. The system was created (by a company called Software Improvements) to run on Linux, which is a widely used, freely available open-source operating system [AEC's, 2007].

Recently, over 100 million mobile phone SIMs have been re-registered with the biometric details of subscribers[1]. A Bangladeshi Higher Court has declared that ongoing biometric SIM registrations using fingerprints is legal[2]. The Bangladesh government has assured mobile phone users that their privacy would not be in jeopardy after they undergo biometric registration of their SIM cards and if there is any misuse of their personal data, carriers could be fined up to Tk. 300 crore ($38.3M USD). "The cabinet has assured that there is no scope for misuse of the fingerprints of the subscribers and they need not be worried to this end[3]".

The government decided to undertake voter registration along with their photographs, finger print and signature. The Bangladesh army commenced the creation of suitable people identification system to give the voter registration process a head start. International and local firms, academic institutions offered solutions. On invitation Dohatec[4] proposed a solution for gathering voter data on laptops with web cam, finger print scanner and signature pad to the army. Dohatec solution comprises of the electronic Voter Registration and ID software - 'eRegistry' and the higher level matching software – 'Biometrics Fusion Server' [Akan]. Microsoft examined the system and found it a robust solution and gave it worldwide focus. The Pilot Project went off successfully. Large scale matching solution has been provided since. Moreover many universities and organizations using biometric registrations and security systems all over the Bangladesh. For a democratic country public opinion is the most important determinant to establish a government and voting is the process through which people display their opinion and help to setup a democratic government. So the voting system should be reliable, accurate and it must be transparent. But the existing system has lot of limitations listed as below:

a. The manual system that takes lots of time and the government has to bear the financial expenses for this purpose every election year.
b. The election commission gets on pressure to prepare new and previous voter into the voter list. So it may contain numerous fake voters in voter list.
c. Sometimes people ruin their votes by stamping on two or more signs mistakenly.
d. While casting the votes the acting officers present in the centers marks a voter with a black ink on his or her nail but it is removable. So there is a chance for casting illegal votes.
e. Manually checking voter list by poling agents takes long time whereas 100% vote cast is challenging.
f. These votes are counted manually so the process becomes a gradual one which may be inaccurate as well.
g. In Electronic voting machine has no reporting system whereas voter cannot understand his/her vote is casted or not.
h. Anyone can press the button and give the vote. Device has no authentication process.

All these limitations together made people think about inventing a new system that will reduce corruption, increase accuracy and fast paced. The concept of electronic voting system comes from this necessity.

III. PROPOSED SYSTEM

In this system voter will select his/her preferable candidate by providing his/her opinion on a touch screen where all candidates' voting sign is displayed. Four layered network system is used for sending the votes from client to the main database, where there are three application server and a client are existed. Among them one application server works as dispatcher. The encrypted votes will be sent from the client to the dispatcher through an application server and this layer will send those votes to main database through another application server. The category "Biometric electronic voting" is potentially broad, referring to several distinct possible stages of electronic usage during the course of an election. The different phases of the proposed system are described below:

3.1 Registration

Here registration system has been proposed to be automated. Two different databases are used to make this system to be automated. One is NID database and another is voter database. People will be enlisted in the NID database. Voter database will contain only the people who are existing voters. The NID database people have to give their details and finger prints (who are equal to or over 18 years) to the authority.

[1] 31 May, 2016: bdnews24.

[2] 13 April, 2016: biometricupdate.com.

[3] 4 April, 2016: Bangladesh Cabinet.

[4] Dohatec CA is a trusted, qualified and licensed CA and issues Digital Certificates according to Bangladesh Law.

https://dx.doi.org/10.22161/ijaers/3.11.11 *ISSN: 2349-6495(P) | 2456-1908(O)*

3.2 Candidate

Candidate is an important process in this system. A candidate can participate in the poll from a party or he can compete alone. On the polling session each candidate will have a sign on the touch pad where the voters give their opinion. The final result depends on the result of each candidate since the system has to keep an eye on the candidate's result of each area.

3.3 Checking

During registration when the fingerprint of the voters will be collected then a hash function will be generated for each finger print. Each voters detail will be laid under this hash function. When a vote will be cast the system will read the packet with the hash function and will verify the constituents then the system will check whether the ID is blocked or not. If it is not blocked then the vote will be counted otherwise access denied.

3.4 Data Manipulation

All the data should be manipulated or updated to maintain good database management. When NID database will be updated then central database will be updated. The synchronization process depends on the database administrator and management. In that process all servers sync with central database and servers are always updated.

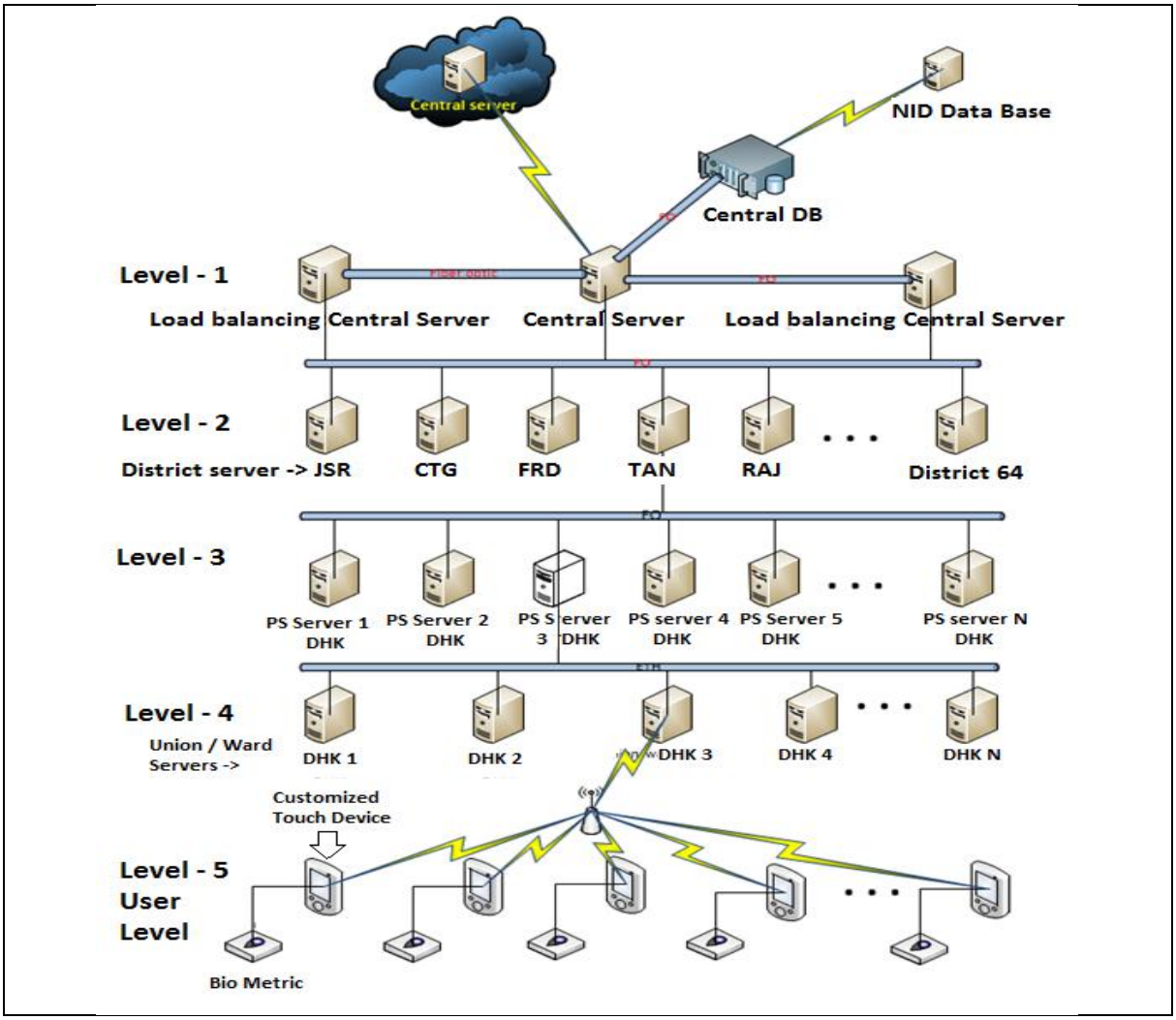

Fig.2: Four Layered Network for Proposed System

3.5 Accessibility

The election commission authority is not getting the supreme power to do whatever they want to do with the voter list or the voter details. They have the accessibility to the details but any kind of modifying or changing they will need the finger print of that voter.

3.6 Casting

The id of a voter will be blocked just after casting his/her vote, he/she can vote again but it won't be counted. So it is ensured that only one process will be cast for a single voter. The voter will cast a vote by giving his/her identification with his/her finger print and vote on a touch screen.

3.7 Counting

The votes will be counted constitute wise. After finishing the voting session the votes stored constitute wise will be counted. Each constitute will pick only

https://dx.doi.org/10.22161/ijaers/3.11.11 *ISSN: 2349-6495(P) | 2456-1908(O)*

the votes it won't think about the id. It will just pick the votes of each sign and then count them.

3.8 View Report

Report will show which candidate sign got how many votes from which constitute. Main database have the name of the candidates so the system will be able to publish the result for each candidate. From this result the system will also publish the final result that which sign win getting how many constitute. When voter cast his/her vote than he/she get one report successful report but this is not encourage because of time consuming and other resource (printers) is dependent. If anyone challenge the system is wrong than report will be generate with given charges.

IV. SYSTEM PERFORMANCES

Electronic voting system using fingerprint provides a high performance with high security to the voting system. The proposed system has covered the following areas:

4.1 Database Maintenance Efficiency

Database is mainly divided into two parts - Local NID database and Central Voter database. After entering all existing people in to the database, system will collect new entry from local NID database. Central database has two segments: Primary and Secondary database. Primary database keeps the record of that part of population. Moreover if anyone wants to change his/her information it is possible by using their fingerprint. So there is no chance to make double entry. Primary database is used specially during the election period. When the election comes the people who are voter, their record upgrade from NID database to Central (Voter) database. At that time this database will distribute the voter list according to their area ID [Vishal, 2014].

4.2 Biometric Fingerprint maintenance system

Most efficient and effective part of this system is fingerprint, which is a unique identification for any voter. At the registration period when anyone gives his/her information, the system will generate an ID against that information. When any voter wants to cast his/her vote, the system will at first find his/her fingerprint at the database. Then the system will check whether the specific ID is block or unblock. When system find ID block it will reject that vote otherwise it will cast that vote and preserve that against that fingerprint [Akyildiz]. So the system will provide single vote for single person.

In the "Finger print scanner technology" the sensor has been optimally designed with SEIR (Surface Enhanced Irregular Reflection), incorporating high resolution and endurance (scratches, chemical corrosion, ESD, physical impacts). Its compact size and outstanding durability has made it one of the most advanced products in the world to successfully eliminate the optical defect of image distortion [Ravi, 2009].

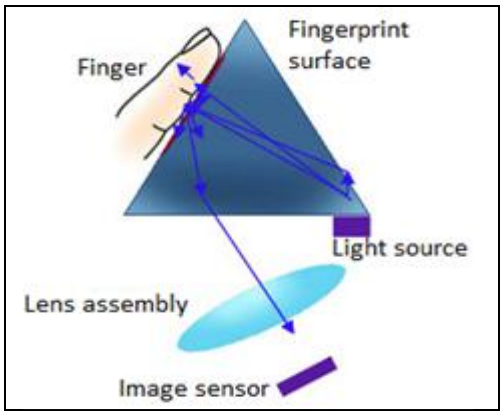

Fig.3: Finger print scanning

- Optimally designed with SEIR (Surface Enhanced Irregular Reflection)
- High resolution and endurance (scratches, Chemical corrosion, ESD, Physical, impacts).
- Superior optical design realizes small sized device without distortion, a defect of optical instruments.
- Patent registration number 79115, 341738.

4.3 Temporarily takes voter picture

When voter can press his/her finger in to the biometric device then system can automatically takes picture from voter. If any polling agent wants to give objection regarding any voter. Polling officer can easily generate report of specific voter.

4.4 Network Issues

A three tiered network system has been proposed here for implementation of this electronic voting system. There will be a number of clients in the most root level (Police Station level or sub-district level of a country). In the district level there will be a dedicated application server for those police station or sub-district clients under that district. These clients together make a cluster. In the district level there will be some dispatchers. There will be a layer of application server layer after the dispatcher through which the dispatcher will pass the encrypted vote to the main database. The encrypted vote will be checked first to see whether the ID of the voter is locked or not [A. Fujioka, 1992]. The encrypted vote will be passed to that server and after that it will be directly passed to main database. Here from dispatcher to the main database, a fiber optic network will be used as the dispatcher has to handle millions of packets at a time, so it will need a better paced as well as secured network system [D.W & W.L, 1984]. At every layer the system

https://dx.doi.org/10.22161/ijaers/3.11.11 *ISSN: 2349-6495(P) | 2456-1908(O)*

make some queues to back up data. This type of network structure will also preserve time.

V. SYSTEM ALGORITHM

The system proposed here for electronic voting has two active actors. One is the administrator and another one is the voter. The administrator has the supreme power to manipulate the voter details even the candidate details. The main responsibility of the administrator is to registration of the voters. Administrator is authorized to view the details of the candidate and also voters although he is not authorized for modifying the details without the fingerprint of the voter or the candidate. An administrator is allowed to view all the reports like candidate result, area result or even political party result. He is also responsible for publishing the result. Voter is responsible for only casting the vote. If there comes any change in the voter details it is voter's responsibility to go to the authority and let them know so that the officials can modify the details taking the finger prints of that voter. An overview of the total system by use case diagram and flow chart is given below:

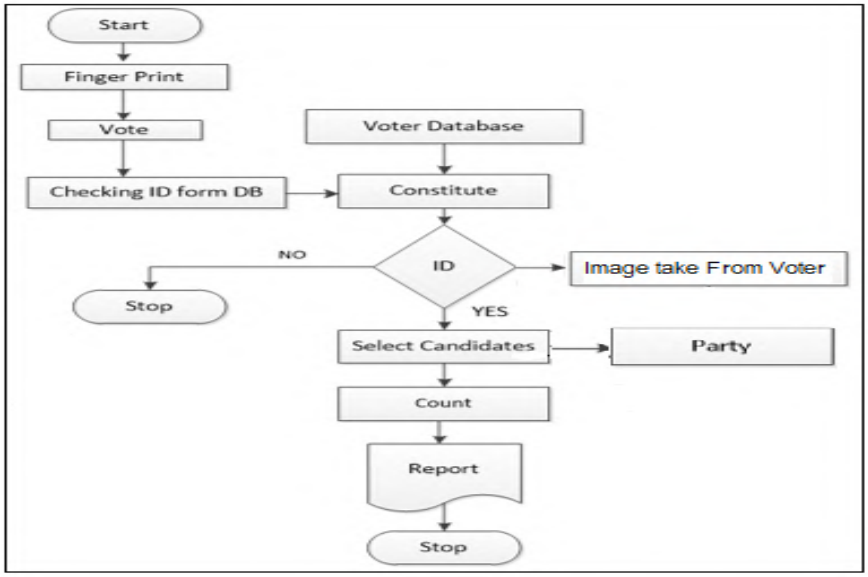

Fig.4: Use case diagram

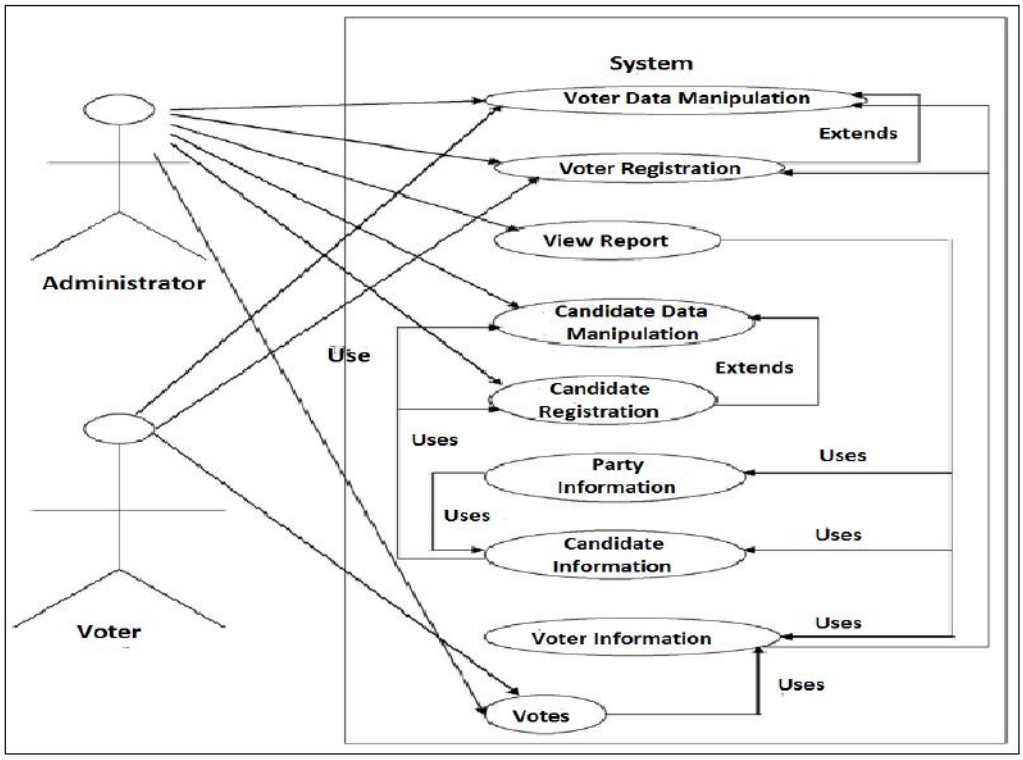

Fig.5: Voting process algorithm & system flowchart

https://dx.doi.org/10.22161/ijaers/3.11.11 *ISSN: 2349-6495(P) | 2456-1908(O)*

VI. SIMULATION STUDY

A simulation model has been built in order to justify and examine the system performance, where it is useful for providing proper guidance on configuring the e-Voting system in terms of server requirements, configuring, networking, voting station and the like. The simulation process includes a database system for voters and candidates with their personal information, authentication and locality of both. Valid casted votes are stored and invalid voters are rejected properly (Fig. 6, 7). This is obviously one of the main advantages of the proposed systems.

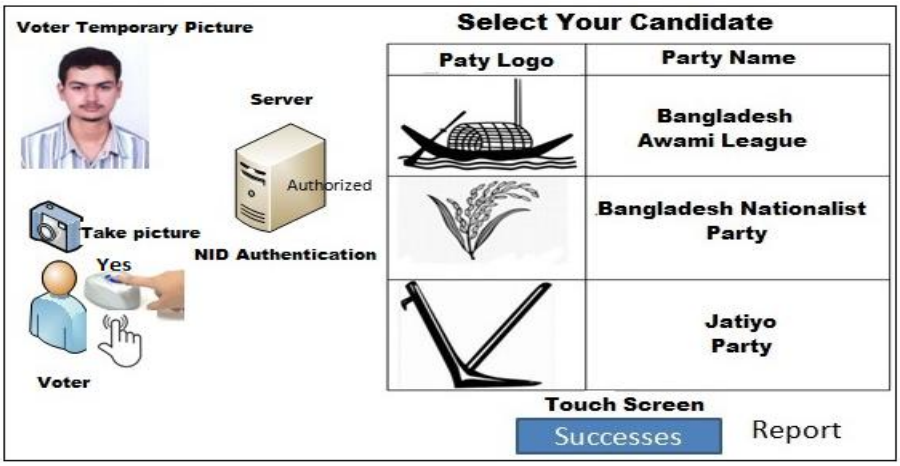

Fig.6: Voting process for valid voter

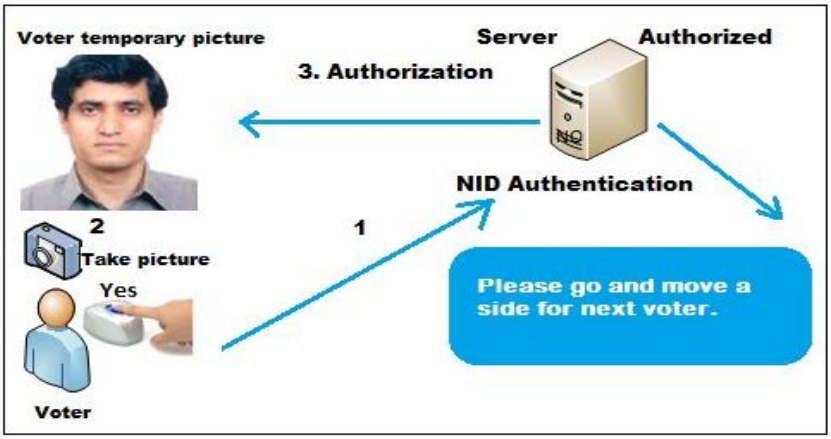

Fig.7: Voting process for invalid voter

Voters	Status
	Success
	Not authorized
	Success

Fig. 8: Voting dashboard

VII. CONCLUSION AND FUTURE WORKS

E-voting systems have many advantages over conventional systems but it still has to solve many hurdles before becoming coming to fruition [Rohan, 2015]. Bangladesh's majority population is rural and illiterate. Also there is shortage of power and inadequate network between cities and villages. This system requires good bandwidth and high speed internet connection for operating, but it is still a distant reality in many rural areas. However conditions are improving with the onset of education in rural areas and with increasing urban population this project may soon become a reality. On the

https://dx.doi.org/10.22161/ijaers/3.11.11 *ISSN: 2349-6495(P) | 2456-1908(O)*

other hand, biometric electronic voting system is very challenging work. Moreover, fingerprints have been one of the most highly used methods for human recognition; automated biometric systems have only been available in recent years. Because fingerprints have a generally broad acceptance with the general public, law enforcement and the forensic science community, they will continue to be used with many governments' legacy systems and will be utilized in new systems for evolving applications that require a reliable biometric. However, the proposed system is highly reliable and secure and is designed for more secure and transparent for every people. In the long run the maintenance cost is very less when compared to the present systems. The citizens can be sure that they alone can choose their leaders, thus exercising their right in the democracy. Though in this project we don't consider the outside voter of Bangladesh for security concern. Our further work include outside voter can join any local and national election.

REFERENCES

[1] Adem Alpaslan ALTUN1 and Metin BĐLGĐN (2011), "Web based secure e-voting system with fingerprint authentication", Scientific Research and Essays Vol. 6(12), pp. 2494-2500, 18 June, 2011.

[2] AEC's, 2007: "Audit of AEC'S electronics voting machine for blind and vision impaired voters", Technical Report by Australian Electoral Commission, 23 August 2007.

[3] Akan: Akyildiz I. F., Akan O. B., Chen C., Fang J., and W. Su, "Biometrics Internet" State-of-the-art and research challenges.

[4] A. Fujioka, 1992: A.Fujioka, T. Okamoto and K. Ohta (1992): "A practical secret voting scheme for large scale elections, In Advances in Cryptology – ASIACRYPT", 1992, LNCS, Springer-Verlag, 1992; 718, 244–251.

[5] D.W & W.L, 1984: D. W. Davies and W.L. Price (1984): "Security for Computer Networks: An Introduction to Data Security in Teleprocessing and Electronic Funds Transfer", Second Edition, John Wiley & Sons, New York, 1984.

[6] Ravi, 2009: Ravi. J, K. B. Raja, Venugopal K. R, (2009): "FINGERPRINT RECOGNITION USING MINUTIA SCOREMATCHING", International Journal of Engineering Science and Technology Vol. 1(2), 2009.

[7] Rohan, 2015: Rohan Patel, Vaibhav Ghorpade , Vinay Jain and Mansi Kambli (2015): "Fingerprint Based e-Voting System using Aadhar Database", INTERNATIONAL JOURNAL FOR RESEARCH IN EMERGING SCIENCE AND TECHNOLOGY, VOLUME-2, ISSUE-3, MARCH-2015.

[8] Sarker, 2013: Sarker M. M. (2013). "E-VOTING EXPERIENCE IN BANGLADESH BY USING ELECTRONIC VOTING MACHINES (EVMS)", International Journal of Engineering Science and Technology (IJEST), ISSN: 2278-9510, Vol. 5 No.5, 2013, p: 1143-1148.

[9] Thomos, 2004: Thomos M. Buchsbaum (2004): "E-Voting: International developments and lesson learnt", Technical Report by Australian Federal Ministry for Foreign Affairs, 2004.

[10] Vishal, 2014: Vishal Vilas Natu (2014): "E-Voting Using Biometric", International Journal of Emerging Technology and Advanced Engineering Website: www.ijetae.com, Volume 4, Issue 6, 672, June 2014.

International Journal of Advanced Engineering Research and Science (IJAERS) *[Vol-3, Issue-11, Nov- 2016]*
https://dx.doi.org/10.22161/ijaers/3.11.12 *ISSN: 2349-6495(P) | 2456-1908(O)*

Optimization of Drilling Process Parameters on Die Steel (H13) using Carbide Coated Drill by Design of Experiment Concept

J. Ganesh [1], P.Renukadevi[2], P.Vijayakumar[3], T.T.M.Kannan[4]

[1]P.G.Scholar, Department of Mechanical Engineering Prist University, Thanjavur, India
[2,3]Assistant professor, Department of Mechanical Engineering Prist University, Thanjavur, India
[4]Associate professor,Department of Mechanical Engineering, Indra Ganesan college of Engineering, Trichy, India

Abstract—*This experimental work presents the optimization of process parameter of surface roughness with using coated carbide drill on H13 steel. Taguchi design of experiments was implemented for executing the process parameter of Drilling process on H13 steel plates. The drilling parameters including 2 Factors such as spindle speed (rpm) and feed rate (mm/min) are optimized using response performance characteristic of surface roughness of H13 die steel plates.H13 steel play an important role in many applications such as Shaft, axle, gears and fasteners due to their strength to weight ratio. The process parameters of spindle speed and feed rate are influenced by machining accuracy during drilling process. The main objectives of experimental works have been identified by lower roughness during drilling process of H13 steel plates. Orthogonal array (L_{16}) of Taguchi Design of experiments and Analysis of Variance (ANOVA) are utilized to analyze the effect of drilling parameters on Quality of drilled holes. The result of experiments indicate is a dominating parameter of surface roughness of H 13 steel plates in Drilling process.*

Keywords— *H13, Drilling Parameters, Taguchi, DOE, S/N ratio, ANOVA.*

I. INTRODUCTION

Drilling is a process used to produce holes from surface to inside solid parts. The tool is rotated and also moved in the axial direction. Drilling is used to create a round or an oval hole. It is accomplished by a rotating tool that usually have two or four helical cutting edges. The tool is fed in a direction parallel to the axis of rotation into the work piece to form the round shaped hole. Drilling is an operation in which holes are produced or refined by bringing a rotating cutter with cutting edges at the lower extreme end is in contact with the work piece.

II. EXPERIMENTAL DETAILS

2.1 H 13 steel

In this Experimental work H13 die steel is used as work piece .Generally H13 steel are hard and tough to be machined. The chemical composition and Mechanical properties of H13 steel plates are shown in Table 1 and 2.

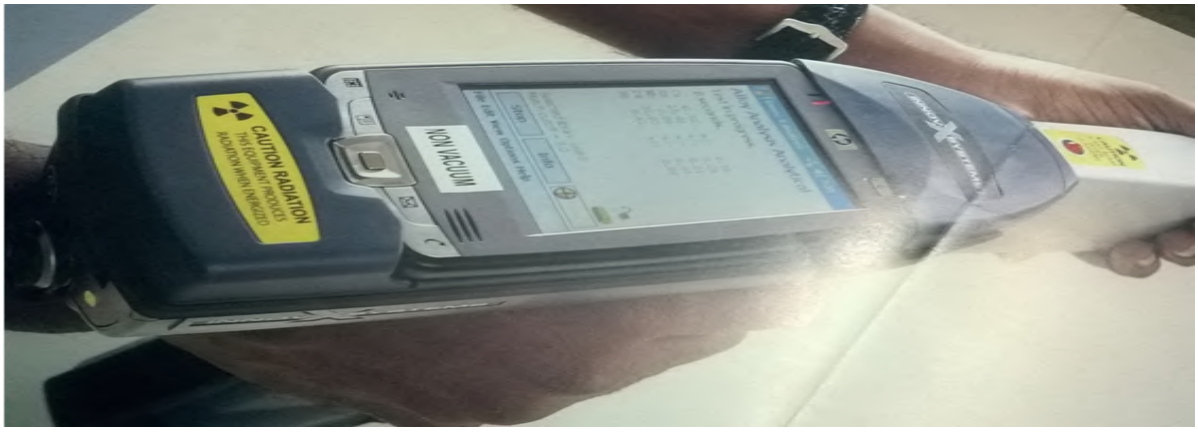

Fig.1: Innovox portable Metal Analyzer

https://dx.doi.org/10.22161/ijaers/3.11.12 *ISSN: 2349-6495(P) | 2456-1908(O)*

H13 die steel is widely used in the tool and die industry because of its resistance to wear at high-temperature it remains in temper. It has high thermal fatigue and ability to be hardened at high temperature. These properties make it is a material of choice for hot working application such as die-casting upset dies, inserts, cores, ejector pins, plunger, sleeve, slide, forging die, extrusion die, dummy blocks and mandrels. In particular, die-casting is the process of producing metal part by forcing molten metal into a mold or die which is usually made of metal. Over a period, the part produced by this process may be unacceptable because of failure of the die primarily due to fatigue, erosion and reaction of the molten material with the die material.

H13 tool steel is a versatile chromium-molybdenum hot work steel that is wide utilized in hot working die and cold work die tooling applications. The recent hardness (hot strength) of H13 resists more thermal fatigue and cracking that happens as the results of, cyclic heating and cooling process in hot work tool and die applications. Due to its wonderful combination of high toughness and resistance to thermal fatigue, cracking (also called heat cracking) H13 is used for additional hot work in tooling application it performs better than the other tool steel material. Because of its high toughness and really sensible stability in heat treatment, H13 die steel is additionally utilized in a spread of cold work tooling applications. In these applications, H13 provides higher hardenability and higher wear resistance than common alloy steels like H11,H12 materials

Table .1: CHEMICAL COMBINATION OF H13 GRADE DIE STEEL

C	Mn	P	S	Si	Cr	V	W	Mb	Fe
0.37%	**0.71%**	**0.01%**	**0.013%**	**0.94%**	**4.88%**	**0.96%**	**0.17%**	**1.68%**	**99.63%**

Table.2: MECHANICAL PROPERTIES OF H13 DIE STEEL

Young's Modulus	Poisson's ratio	Density	Modulus of Elasticity	Bulk modulus
210 GPa	0.29	7.8 g/cm^3	220 GPa	150 GPa

2.2 Machine details The drilling operations have been carried out on a CNC MILL MT250 Machining Center, (Make-MTAB Educational equipment ltd,(India) is shown in fig1. The CNC vertical machining centre equipped with a range of variable spindle speed up to 4000 rpm, and 2HP motor drive was used for experimentation

The process parameters that were chosen for experimentation are given as under:

1) Spindle speed (rpm)
2) Feed (mm/rev.)

Fig.1: CNC vertical machining centre

https://dx.doi.org/10.22161/ijaers/3.11.12 *ISSN: 2349-6495(P) | 2456-1908(O)*

Fig.2: H13steel drilled specimen (L_{16})

Coated carbide drill bit of 12mm diameter is used to making drill hole on H13 steel plates are shown in fig 2.The drill is having a flute helix angle of 118˚degree.The tool of double helical flute is used.

2.4 Taguchi design of experiment

Taking Spindle speed and feed rate are as an input parameter and surface Roughness is taken as response parameter of drilling process of H13 steel plates. Here 2factors and 4 levels of drilling process parameter are used as design of experiment in L $_{16}$ orthogonal array is shown in table 3

Table.3: L 16 Orthogonal Array

Spindle speed	Feed
1	1
1	2
1	3
1	4
2	1
2	2
2	3
2	4
3	1
3	2
3	3
3	4
4	1
4	2
4	3
4	4

III. RESULT AND DISCUSSION

The experimental work conducted on H13 Die steel with various process parameters as per design of experiment. The drilling process are performed by Carbide coated drill. The result of drilling process parameter are analyzed by signal to Noise ratio.The surface roughness values are measured by Surface roughness tester the corresponding values are shown in table 4.

Table.4: Taguchi L_{16} OA with Surface Roughness values of H 13 Die Steel

SPINDLE SPEED	FEED	SURFACE FINISH	SNRA1
1	1	7.32	-17.2902
1	2	5.86	-15.3580
1	3	6.86	-16.7265
1	4	6.54	-16.3116

https://dx.doi.org/10.22161/ijaers/3.11.12 *ISSN: 2349-6495(P) | 2456-1908(O)*

2	1	3.58	-11.0777
2	2	3.47	-10.8066
2	3	3.39	-10.6040
2	4	3.18	-10.0485
3	1	6.24	-15.9037
3	2	5.94	-15.4757
3	3	4.93	-13.8569
3	4	4.52	-13.1028
4	1	4.64	-13.3304
4	2	4.48	-13.0256
4	3	4.24	-12.5473
4	4	4.02	-12.0845

After conducting experiment on H 13 steel plates in drilling process. The most important and influence parameter are represent by response table (Table 5).It indicate spindle speed is an influence parameter of H13 die steel for achieving lower surface roughness in drilling process.

Table.5: Response table of H13 Die steel drilled plates

Level	Spindle speed	Feed
1	-16.42	-14.40
2	-10’63	-13.67
3	-14.58	-13.43
4	-12.75	-12.89
DELTA	5.79	1.51
RANK	1	2

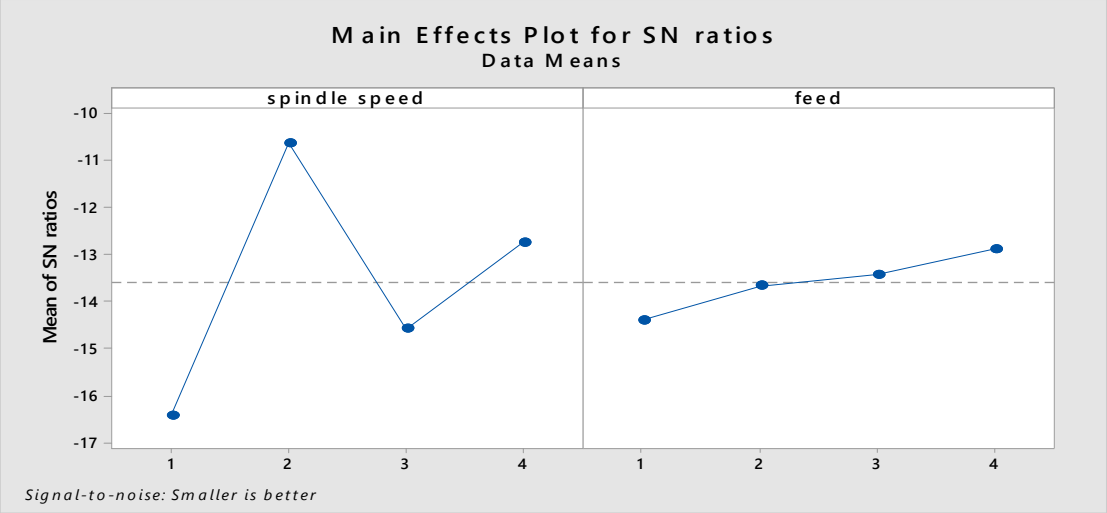

Fig.3: S/N ratio for H13 die steel

Figure 3 represents signal to noise ratio of H 13 die steel plates during drilling process. It also indicate 2 nd level of spindle speed and 4 th level of feed rate produce lower surface roughness. The H 13 steel plates is suitable for manufacturing dies with high accuracy and toughness.

https://dx.doi.org/10.22161/ijaers/3.11.12 *ISSN: 2349-6495(P) | 2456-1908(O)*

Table.6: Analysis of variance value of Surface roughness of H13 Die steel

Source	D F	ADJ SS	ADJ MS	F-VALUE	P-VALUE
Spindle speed	3	23.342	7.7805	38.49	0.000
Feed	3	1.610	0.5366	2.65	0.112
Error	9	1.819	0.2021		
Total	15	26.770			

Table 6 shows that Spindle speed is a dominating parameter in drilling process on H13 die steel plates based on higher value of F value. It produce better surface finish and dimensional tolerance by using carbide coated drill. The R sq values (93.20 %) indicate the most significant of process parameter and experiments are conducted in efficient method.

The contour plot shows (fig 5) that lower surface roughness is achieved in drilling process with significant.

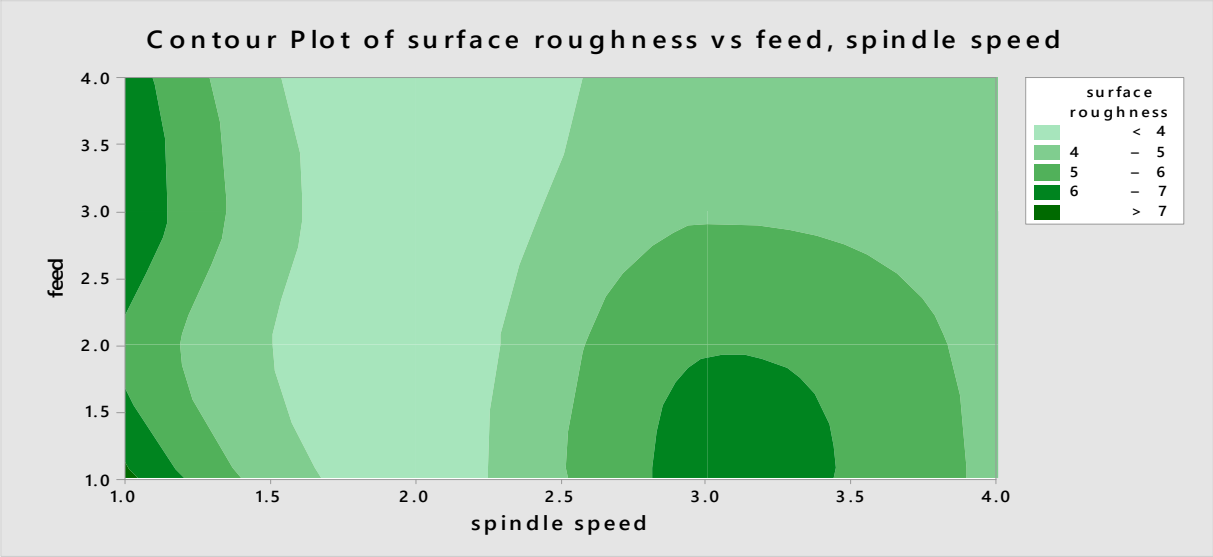

Fig.5: Contour plot of surface roughness of H13 die steel

IV. CONCLUSION

In this experiment work of H13 die steel on drilling process, it conclude the following

- H13 provide good machinablity property and produce reasonable surface roughness.
- Drilling parameter is optimized by signal to noise ratio and analyzed by in Anova.
- Drilling parameter of H13 steel are dependent on the implement in hot die making process.
- H13 steel may used in production of heavy machinery, Power machinery die works and press tools.
- The optimum parameter of H13 steel on drilling process are the second speed (600rpm) and fourth feed rate (0.016mm/rev) and a response parameter of surface roughness of 3.18 microns

REFERENCES

[1] Paul, A.; Kappor, S.G. & Devor R.E. (2005). Chisel Edge and Cutting Lip Shape Optimization for Improved Twist Drill Point Design, International Journal of Machine Tools & Manufacture, 45, pp.421-431.

[2] RP Rampersad, Hareland, G., and Boonyapaluk, P.: "Drilling Optimization Using Drilling Dataand Available Technology," paper SPE 27034 presented at the SPE LAPEC Conference, Buenos Aires, 27-29 April, 2009.

[3] B.Y. Lee, H.S. Liu and Y.S. Tarng, (2006). Modeling and Optimization of Drilling Process. Department of Mechanical Manufacture Engineering, National Huwei Institute of Technology, Huwei, 632, pp. 1-9.

[4] C. Sanjay, M.L. Neema and C.W. Chin, (2005). Modeling of Tool Wear in Drilling by Statistical Analysis and Artificial Neural Network, Journal of Materials Processing Technology, 170, pp. 494–500.

[5] Chandrasekharan V., Kappor S.G. and DeVor R.E, A Mechanistic Approach to Predicting the Cutting Forces in Drilling: with Application to Fiber-Reinforced Composite Materials, ASME J. Eng. Ind., (117),559–570.

https://dx.doi.org/10.22161/ijaers/3.11.12 *ISSN: 2349-6495(P) | 2456-1908(O)*

[6] Paul, A.; Kappor, S.G. & Devor R.E. (2005). Chisel Edge and Cutting Lip Shape Optimization for Improved Twist Drill Point Design, International Journal of Machine Tools & Manufacture, 45, pp.421-431.

[7] RP Rampersad, Hareland, G., and Boonyapaluk, P.: "Drilling Optimization Using Drilling Data and Available Technology," paper SPE 27034 presented at the SPE LAPEC Conference, Buenos Aires, 27-29 April, 2009.

[8] B.Y. Lee, H.S. Liu and Y.S. Tarng, (2006). Modeling and Optimization of Drilling Process. Department of Mechanical Manufacture Engineering, National Huwei Institute of Technology, Huwei, 632,pp. 1-9.

[9] Kadam M.S., Pathak S.S.Experimental Analysis and Comparative Performance of Coated and Uncoated Twist Drill Bit Dry Machining International Journal of Research in Mechanical Engineering and Technology Vol. 1, Issue 1, Oct. 2011.

[10] S.A. Jalali and W.J. Kolarik, (2001). Tool life and Mach Inability Models for Drilling Steels, International Journal of Machine Tools & Manufacture, 31 (3), pp. 273–282.

https://dx.doi.org/10.22161/ijaers/3.11.13 *ISSN: 2349-6495(P) | 2456-1908(O)*

The Overview of Avionics Full-Duplex Switched Ethernet

Karthik.S[1], Vinodh.S[2]

[1]Assistant Professor, Department of ECE, Mahendra Institute of Technology, Namakkal, India
[2]Assistant Professor, Department of Aeronautical, Mahendra Engineering College, Namakkal, India

Abstract—*This paper deals about basic preface about superior avionic system AFDX. Avionics Signalling and communication in avionics have been significant topics ever since electronic devices were first used in aerospace systems. To deal with the challenges introduced by the extensive use of general purpose computing in marketable avionics, standards like ARINC 419 and later on 429 were available and adopted by the trade. AFDX combines confirmed safety and accessibility functionality with recent Ethernet technology to be able to handle today's needs. These papers outlines two of the most fundamental avionics network architectures and aims at depicting the development of networking concepts and wants over the course of the past 30 years. It mainly focuses on ARINC 429 and AFDX, the most important current and past standards, but also covers two other attractive past protocols.*

Keywords—AFDX, ARINC 664, ARINC 429, Ethernet, MIL-STD-1553, avionics, fault tolerance, security, safety.

I. INTRODUCTION

Today, ARINC 429 can be found in most active and retired aircraft series. While it is well-established in the industry, it has been adapted and extensive little since the initial specifications were formulated in the late 1970s. In dissimilarity to avionics standards, multiple technological revolutions have happened in the computer industry at a fast pace. Networking of computers aboard aircraft may have been preposterous in 1970, whereas modern aircraft without any networked computers are very unusual. Legacy avionics communication standards still reflect past views on computing. eventually, a modern networking structural design for avionics use should offer a maximum of safety, the sack and security, as well as apply failsafe defaults. The ensuing infrastructure should be economically maintainable, flexible and offer a solid foundation for software development.

More recent standards reflect these demands, though few saw broader use across the industry. In contrast to the Internet, security and cost efficiency are not the key objectives in avionics; rather safety is. However, most modern networking standards are aimed at achieving traditional PC-world security objectives and only indirectly address safety requirements (by fulfilling traditional security objectives) .In ARINC 664 Part 7, also referred to as AFDX, standard Ethernet technology is extended and design objectives are built around safety.

Two of the most vital network architectures in the avionics manufacturing are outlined in this paper, and we aim at depicting the evolution of networking concepts and requirements over the course of the past 30 years. It mainly is focused on the most prominent current and past standards, ARINC 429 and 664, but also covers two other significant standards (MIL-STD-1553 and ARINC 629). These standards introduced important features into aerospace net- working design and are used as intermediate steps in this paper even though AFDX evolved originally .In this paper, a deeper considerate of Ethernet is thought; the reader should be general with redundancy and failover concepts, as well as information-security. The OSI layer model is used throughout this paper, even though it is not used within the cited avionics standards. When referring to layer 2 (L2) frames, Ethernet or AFDX frames at the data link layer are meant, while L3 and L4 refer to data structures used in the respective protocol at the network and transport layers.

Within the next segment, the most extensive standard, AR- INC 429, is explained in detail. In Section 3, the transition from federated network architectures, such as 429 to modern Integrated Modular Avionics, is depicted. Then, an investigation of the orientation operating system planned in ARINC 653 for use with included architectures is conducted. In segment 2 ARINC 629 and Mil-Std-1553, two more recent networking standards are briefly introduced. Section 5 is focused on the networking standard AFDX.

The importance is on the enhancements to Ethernet required to comply with the desires of avionics applications. The final chapter is dedicated to summarizing the advantages and disadvantages of the main two named architectures.

https://dx.doi.org/10.22161/ijaers/3.11.13 *ISSN: 2349-6495(P) | 2456-1908(O)*

II. A BRIEF HISTORY OF ARINC 664

As an evolved standard, 429 had many limitations, but it is a confirmed and normally used protocol. As time progressed and technology advanced, more bandwidth, more elastic topologies and new challenges like incorporated Modular Avionics emerged and were beyond ARINC 429's capabilities .ARINC 664 (Part VII) was initially developed by the EADS Airbus partition as Avionics Full-Duplex Ethernet switching (AFDX). however previous aircraft already deployed fully electronic fly-by-wire systems, wiring using previous principles could no longer meet the desires of modern day state-of-the-art aircraft. In the case of AFDX, the Airbus A380 prompted for a new technical base to be realize; thus, AFDX was created. Later on, Airbus' AFDX was distorted into the actual ARINC model. Figure 9 shows a simple AFDX-based Network.

III. FROM ETHERNET TO AFDX

Architectural Changes

Ethernet has been in use for decades outside of the aerospace industry and proved to be a robust, low-cost, extensible and flexible technology. However, it cannot offer indispensable functionality required for high availability and reliability. Thus, it is not directly suitable for avionics. 664 offers mod- ern day transfer rates, while construction on top of the previously much-loathed Ethernet standard 802.3 . AFDX inherits parts of the MIL-STD-1553 terminology and overall setup. Devices transmitting data via the network are called sub- systems, which are attached to the network via end systems. The full-duplex network itself is called AFDX Interconnect ; in Ethernet terms, this includes all passive, physical parts of the network, but not switches and other active devices .

The mainly well-known hindrance for using Ethernet network- ing in avionics is Ethernet's non-determinism. A single laid off MIL-STD-1553 bus network with hardware and device roles predefined for provisioning second fail-over bus C. paths. In highly heaving setups, switches may even drop packets on purpose if buffer limits have been reached2 .

In Ethernet, collisions are handled via CSMA/CD, but up- per layers may encounter packet loss. There, protocols (e.g. TCP, SCTP, etc) in the operating system's network stack have to deal with packet loss . However, this is not a viable solution in safety-critical environments. convinced applications require bandwidth guarantees, while others may demand timing performance to remain within strict borders. Neither can be offered by Ethernet. No hard quality of ser- vice guarantees are available in vanilla Ethernet, and soft scheduling is only offered through protocol extensions such as Ethernet-QOS IEEE 802.1p.

The same applies to band- width allocation, which can not be guaranteed in Ethernet on a per-flow level, but is implemented using various dissimilar algorithms. While there are several proprietary approach for making Ethernet usable in real-time environments, none of these principles is directly usable in avionics. Thus, the new standard requisite determinism to make it usable in avionics .Upper layers, such as a station's operating system or applications, are supposed to handle these issues by de- sign. If a message is lost or corrupted during agenda, it will simply be begrudge or its loss fully mitigated.

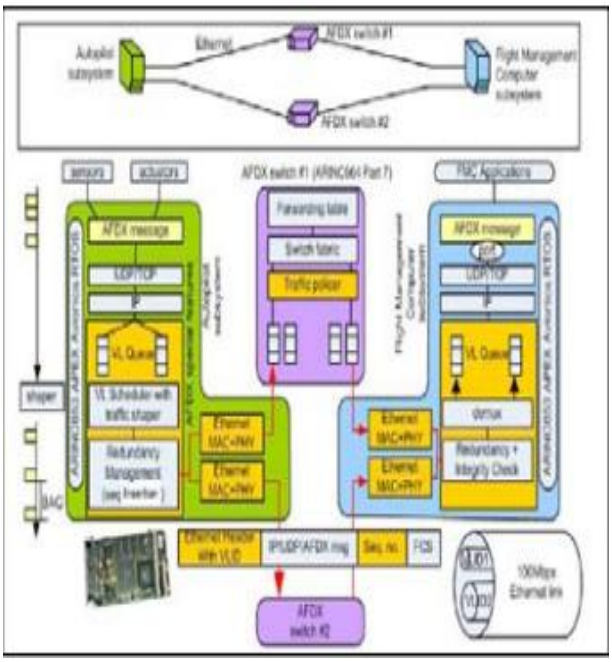

Fig .1: Redundancy in AFDX Network

When sending data on a non micro segmented network, collisions may occur in each segment, forcing all stations involved in the collision to resend. Transmission of packets is retired after a random time interval by whichever station starts first. Again, a smash may occur which may lead to next to in- distinct repeating, and this may subsequently result in a jammed bus .Another variable feature of Ethernet networking and subsequently ARINC 664, are switches/bridges.

While they add flexibility to networking, additional non-determinism is introduced, as frames may be reordered or manipulated in transit. Switches offer micro-segmentation of network segments, but in turn also increase the number of hops a frame takes from source to destination.

https://dx.doi.org/10.22161/ijaers/3.11.13 *ISSN: 2349-6495(P) | 2456-1908(O)*

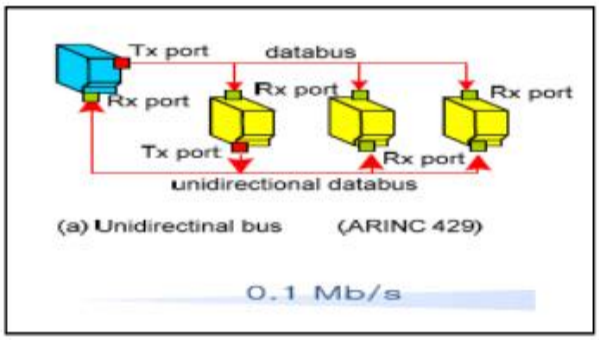

Fig .2: ARINC 429 STD Unidirectional Bus

Virtual Links are designated using so called Virtual Link Identifiers (VLID). The VLID replaces MAC-address based delivery, occupying the bits normally used for the destina- tion MAC. To retain compatibility with Ethernet, AFDX splits the destination-MAC field into several parts: the initial bits are set to reflect a locally administered MAC- address (site-local), the final 16 bits store the VLID .Only one subsystem may send data using a given VLID, thus Virtual Links are again unidirectional.

As in ARINC 429, a subsystem can assume different roles in multiple VLs using different ports (see below), and multiple recipients may contribute in a Virtual Link. Subsystems are not clearly addressed, as in common Ethernet where MAC addresses are used, but the meaning of a Virtual Links identifier is defined Sampling ports have committed buffer-spaces in which one single memo can be read and stored. If a new message arrives, previous data will be overwritten. A queuing port's buffer may contain up to a fixed number of messages that are stored in a FIFO queue; upon reading the oldest message, it is removed from the queue. Handler services for communication ports need to be provided according to the ARINC 653 specifications . BAGs and LMAX of a VL should be set accordingly to the collective requirements of all ports participating in a link .

Virtual Links

Ethernet is independent of physical connections and allows logical endpoints to be defined. Multiple physical or virtual devices may thus share one link, supporting virtual sub- systems or virtual machines in IMA [12, 13, 18]. Multiple applications or devices may require different timing charac- teristics or a fixed minimal amount of bandwidth .

Virtual point-to-point connections implement the same con- cept as used in ARINC 429. In contrast to 429, they do not exist physically, but as logical links. They are implemented as Virtual Links (VL) on top of the AFDX Ethernet layer. An example of virtual channels is given in Fig. To a certain degree, VLs are quite similar to VLAN tagging as defined in IEEE 802.1Q , but offer additional information in addition to network remoteness. Each virtual channel has three properties besides its channel ID: the Bandwidth Allocation Gap, the maximum L2 frame size, called LMAX or Smax, and a bandwidth limit .

LMIN and LMAX are used to set a predefined smallest and largest common Ethernet frame size along the path a packet 2 In a properly laid out AFDX network, buffer overruns should never actually occur. The network parameters are configured based on values calculated during the planning phase of an aircraft using a mathematical support.

Redundancy

High availability environments also require redundancy on the bus as well as within stations. Again, Ethernet does not offer any sort of fail-over by default, however, optional link aggregation as defined in IEEE 802.1AX can of- fer such functionality. 664 by design specifies sophisticated redundancy concepts for end stations as well as cabling by providing two dedicated networks (network A and B). After scheduling of Ethernet frames, redundancy is introduced.

Each AFDX subsystem has two interfaces called end systems. Redundancy is added transparently by sending each frame via both end systems, applying the frame sequence number . Assuming no transmission errors occurred, one spare will arrive at the destination for each frame transmitted .

AFDX Switches

Most features AFDX consists of can also be implemented using regular Ethernet hardware, if special AFDX-stack implementations are run. While purely software-based implementations exist , these solutions can not guarantee determinism. They cannot keep jitter within boundaries im- posed by AFDX and are useful for basic interoperability testing only. To achieve determinism, specialized hardware to enforce the Virtual Link rules, which are based on the VL parameters. introduced by ARINC 664 is needed.

AFDX switches fill this role and enforce latency, bandwidth constraints for VLs and provide a dependable, fixed configuration. This set is read at boot up and remains constant at run time to avoid fluctuations in the network's topology and provide uniform timing behaviour. For honesty reasons, store-and-forward circuit switching is used when relaying packets, in contrast to most mod- ern day high-speed Ethernet switches, which perform cut- through switching The configuration for all Virtual Links (LMIN, LMAX, BAG, priority) and switch parameters should be set according to a one of the mathematical proofing models in use today .

https://dx.doi.org/10.22161/ijaers/3.11.13 *ISSN: 2349-6495(P) | 2456-1908(O)*

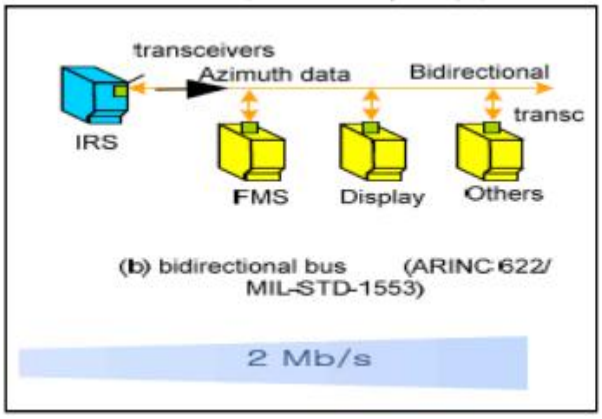

Fig. 3: Full Duplex Ethernet Network

By fixing network parameters at boot-up, changes at run-time are prevented and the network retains constant timing properties and a static layout throughout operation. Non- fault generated deviations off default settings may not hap- pen and are taken into account when calculating global parameters mathematically . Switches isolate Virtual Links from each other and execute scheduling for passing-through frames based on their VLID. Other parameters specified in switch and system configuration include priority, LMIN (equivalent to LMAX) and jitter for Virtual Link. Ports have a fixed maximum delay and buffer-size .

Impact On OSI-Layer 3 and Above

AFDX adderes to the OSI layer model and is based on common protocols from the Internet-world. Subsequently, familiar protocols like IP, UDP and IP-multicast are used. Alien networking environments, such as ARINC 429 links, can be transported within a Virtual Link transparently to the individual applications, thereby reducing development effort. In fact, virtually any previous network standard which does not exceed ARINC 664 in capabilities can be implement on top of it .At Layer 3, the IPv4 protocol is deployed, though the fields usually used for source and destination IP-addresses have been reassigned, as depicted in Figure 12. The top packet- version shows an IP packet being directed to an individ- ual system using the VLID, while the bottom packet uses multicast-addressing. The 32 bits of the source IP address field are separated into:

- The single bit class identifier,
- 7 bit private address,
- User-defined 16 bit ID,
- As well as an 8 bit partition identifier.

The partition identifier is used to address virtual subsystems in a virtualized IMA environment .The Destination IP is either used to designate a multicast IP address, or contains a field of 16 bits prefixed to the VLID. The first 16 bits contain a fixed number (specified by the standard), while the second part contains the VLID, if direct IP-addressing and IMA is used .Due to the guarantee provided by AFDX, certain features usually introduced at higher OSI layers (e.g. packet-loss handling and reordering of packets) are already implemented by the underlying L2/3-networking structure. In business networking, protocols such as TCP or SCTP are used to provide this functionality. In AFDX, transmission control and integrity is already provided at the lower layers, thus, UDP was chosen to be the default protocol in AFDX .

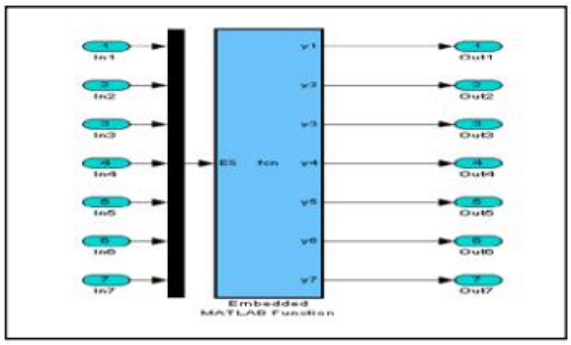

Fig. 4: Full Duplex Ethernet Network

AFDX-Ports are mapped directly at UDP's source and destination port fields. AFDX-flows are identified by using a combination of the following parameters:

- Destination MAC address (containing the VLID),
- Source and destination IP address,
- Source and destination UDP port,

Due to architectural restrictions, the minimum payload size for packets transmitted inside a AFDX-L3 packet is 144 bits. If an UDP packet's length drops below this limit, padding is added at the end of the L4 packet .The standard also defines monitor to be performed via SNMP, and intra-component data transfer through TFTP. Payload transferred inside the L4-structure usually has no fixed predetermined meaning, in contrast to earlier standards. However, ARINC 664 defines a number of common data structures, such as floating point number formats and booleans. These do have no direct impact on network pay- load, but offer common ground for software development.

IV. CONCLUSION

ARINC 429 was developed at a time when the use of consistent, programmable subsystems aboard aircraft was simply not reasonable due to aspects such as size, energy spending, fragility and hardware cost. 429 solely treats data transfer between systems at a per-device level, interconnecting systems on a pin level. Though it has advantages over more modern standards, it clearly had reached its confines once multipurpose computers are interconnected. However, AFDX combines proven safety and ease of use functionality with modern technology to be able to handle today's re- quirements.

https://dx.doi.org/10.22161/ijaers/3.11.13 *ISSN: 2349-6495(P) | 2456-1908(O)*

It adheres to the OSI-layer-model and outlines a well-matched stack architecture, while allowing to emulate previous communication standards on top. Besides, the In- ternet Protocols Suite (IP/UDP) and Ethernet are used and only slight alterations to the individual data structures are applied, which lowers the bar for designing hardware and developing software in avionics considerably. For certain parts of an AFDX network, COTS hardware can be used in coincidence with matching software, though AFDX hardware implementations must be used to retain determinism. Still, by adding standard Ethernet hardware in conjunction with an AFDX-stack implementation in the op- erating system, non-AFDX hardware could be used without further alterations Changes to the overall network layout do not negatively im- pact individual Virtual Links or ports of the individual end- and subsystems, due to the added abstraction.

REFERENCES

[1] P. Frodyma and B. Waldmann. ARINC 429 Specification Tutorial. AIM GmbH, 2.1 edition, 2010. Working Group. ARINC 615, P2: ARINC Airborne Computer Data Loader. Technical Report 1,Aronautical Radio, INC, June 1991.

[2] P. Frodyma, J. Furgerson, and B. Waldmann.MIL-STD-1553 Specification Tutorial. AIM GmbH,2.3 edition, 2010.

[3] L. Buckwalter. Avionics Databuses, Third Edition.Avionics Communications Incorporated, 2008.

[4] Miguel A. Sa´nchez-Puebla and Jesu´s Carretero. A new approach for distributed computing in avionics systems. In Proceedings of the 1st international symposium on Information and communication technologies, ISICT 2003, pages 579 – 584. Trinity College Dublin, 2003.

[5] N. Thanthry and R. Pendse. Aviation data networks: security issues and network architecture. Aerospace and Electronic Systems Magazine, IEEE, 20(6):3 – 8, June 2005.

[6] T. Schuster and D. Verma. Networking concepts comparison for avionics architecture. In Digital Avionics Systems Conference, 2008. DASC 2008. IEEE/AIAA 27th, pages 1.D.1–1 – 1.D.1–11, October 2008.

[7] J. Craveiro, J. Rufino, C. Almeida, R. Covelo, and P. Venda. Embedded Linux in a partitioned architecture for aerospace applications. In Computer Systems and Applications, 2009. AICCSA 2009. IEEE/ACS International Conference on, pages 132 –138, May 2009.

[8] M.J. Morgan. Integrated modular avionics for next-generation commercial airplanes. In Aerospace and Electronics Conference, 1991. NAECON 1991., Proceedings of the IEEE 1991 National, pages 43 – 49 vol.1, May 1991.

International Journal of Advanced Engineering Research and Science (IJAERS) *[Vol-3, Issue-11, Nov- 2016]*
https://dx.doi.org/10.22161/ijaers/3.11.14 *ISSN: 2349-6495(P) | 2456-1908(O)*

A Seismic Channel Model: The San Ramon Fault

Hector Torres-Silva[1], Diego Torres Cabezas[2]

[1] Escuela Universitaria de Ingeniería Eléctrica-Electrónica. Universidad de Tarapacá. Avda. 18 de Septiembre 2222, Casilla Postal 6-D. Arica, Chile.
[2] Departamento Tecnologías de Información. Dirección del Trabajo, Agustinas 1253, Of. 509. Santiago, Chile.

Abstract— *Although seismic waves have been studied for many years, their soliton structure has only recently studied. Deformation solitons propagate along earthquake faults and can induce large earthquakes. Rotation solitons are generated in earthquake sources and propagate throughout the Earth. The conclusion to be reached from our paper is that the research on seismic solitons is essential for investigating the propagation of seismic waves and helps understand mechanisms triggering earthquakes. This paper discusses the development of elastodynamics equations similar to Maxwell's equations in a chiral -mode which is applied to a seismic channel, which is dispersive and nonlinear. The chirality is described in terms of the formalism proposed by Born-Fedorov. The nonlinearity is Kerr-type, and dispersion of the medium is taken into account explicitly through the Taylor series expansion. Through numerical calculations these theoretical results allow us analyze the soliton propagation of S-seismic pulses which can induce strong earthquakes. The numerical calculation is applied to the San Ramon Fault localized in Santiago City, Chile which is a seismically active fault that is a main element to be considered in any study on seismic hazard assessment for this city.*

Keywords—chirality, S waves, San Ramon Fault, earthquake, soliton.

I. INTRODUCTION

Paleoseismic studies of a prominent fault scarp at the west flank of the Andes in Santiago, Chile (The San Ramón Fault) were published recently. The San Ramón Fault (SRF) has been recently identified like a geologically active fault which can produce large magnitude crustal earthquakes, in the range of M_W 6.9 – 7.4 [1-6]. Figure 1 shows the geomorphologic map of the San Ramón fault. Seismic moment can be estimated with a fixed rupture width of 30 km, consistent with the structure of the SRF at depth (Armijo et al., 2010; Pérez et al., 2013) and 5 m of average slip. In that case, assuming that the fault scarp is either 15 km long, according to the most emergent part of the scarp, or 35 km long if considering the entire well-recognized SRF (Armijo et al., 2010), predicts M_W 7.25 and M_W 7.5, respectively. Those magnitude estimates would imply surface rupture and significantly stronger ground motion (and destructive effects) for Santiago (Pérez et al., 2013; Pilz et al., 2011).

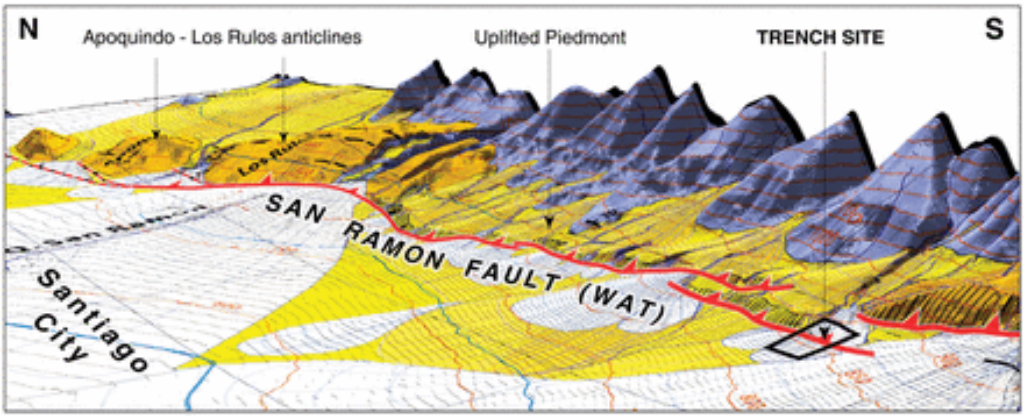

Using 5 m

Fig.1: The San Ramón fault scarp, Chile (WAT—west Andean thrust). The geomorphologic map (Armijo et al., 2010) is draped over a 9 m digital elevation model. The San Ramón fault forms a continuous scarp that limits to the west the uplifted piedmont covered with Quaternary alluvium and incised by streams (early-middle Pleistocene in yellow tones, late Pleistocene–Holocene in white).

https://dx.doi.org/10.22161/ijaers/3.11.14 *ISSN: 2349-6495(P) | 2456-1908(O)*

To further investigate site conditions in the Santiago basin we must consider different locations of possible hypocentres along the San Ramón Fault, a multikilometric frontal thrust at the western front of the Main Cordillera, which has been shown to pose a significant seismic hazard for the city (Armijo *et al*. 2010). The best surface expression of the San Ramón Fault is found along an around 15 km long segment with a sharp fault trace in the 25 km long part separating the rivers Mapocho and Maipo along the San Ramón mountain front (see Fig. 1).

In this paper we propose a model to estimate the magnitude of earthquakes along the fault of the SRF which acts as a seismic channel which develops a soliton pulse acting as earthquake source. Rotational motions in earthquake sources naturally generate rotational seismic waves [7-10].

The difference in speed of travel of P-waves and S-wave is vital to transmit energy of seismic wave. The P wave is a *longitudinal* wave or a *compression* wave. Force is applied in the direction that the wave is travelling. In S wave, the medium is displaced in a *transverse* (up and down - compared to the line of travel) way, and the medium must *shear* or "move away" from the material right next to it to cause the shear and transmit the wave. This take more time, and this is why the S wave moves more slowly than the P wave in seismic events. Here we model the SRF like a seismic channel using a chiral approach [11-13].

There are two types of tectonic solitons which can be excited in the earthquake source and propagating along the fault: longitudinal self-distortion (plastic) solitons and shear self-distortion solitons. The Earth's interior is modeled as an elasto-plastic continuum and elastoplastic waves [9, 10], that describe elastic longitudinal and plastic shear distortion solitons. We apply similar method in order to determine the solitons propagating along the fault SRF. The type of soliton studied here is seismic shear self-distortion Schrödinger's solitons which may propagate slowly along the fault and trigger new strong earthquakes. Our main results (equation 20) is obtained under the chiral approach [11-13].

The chirality was first observed as optical activity and corresponds to the rotation of the plane of polarization in linear isotropic materials. The Born-Fedorov equations for electromagnetic system are given by [14, 15].

$$D = \varepsilon\left(\vec{E} + T_c \nabla \times \vec{E}\right) \quad (1)$$

$$B = \mu\left(\vec{H} + T_c \nabla \times \vec{H}\right) \quad (2)$$

The pseudoscalar T_c represents the measure of chirality and has units of length. The validity of equations (1) and (2) has been demonstrated in studies of chiral electrodynamics [11] and from an electromagnetic point of view, chiral soliton pulse can be described by specific equations [12]-[13]. By analogy between elastodynamics and electrodynamics in this work we use these Born-Fedorov equations which are the most suitable to study SRF like a seismic channel. Here the electric permittivity is equivalent density of matter $\varepsilon \to \rho$, the magnetic permeability is equivalent to the inverse of the Lamé parameter $\mu \to 1/\mu_S$. The speed of transversal seismic S- waves is given by $\sqrt{\rho/\mu_S}$ [14, 15] and changes of the polarization of transverse seismic waves are take into account during their propagation through the SRF.

II. BASIC EQUATION FOR ROTATIONAL PROPAGATION.

Using equations (1) and (2), we obtain in the analogous framework under this section the nonlinear Schrödinger equation for a chiral seismic channel. (S-type waves)

$$D_S = \rho_n \vec{E}_S + \rho T_c \left(\nabla \times \vec{E}_S\right) \quad (3)$$

$$B_S = 1/\mu_S (\vec{H}_S + T_c \left(\nabla \times \vec{H}_S\right)) \quad (4)$$

These equations are symmetric under duality transformations and temporal reversibility, ρ_n is the density of matter and T_c the chiral rotational seismic coefficient. The corresponding like Maxwell equations are

$$\nabla \times \vec{H}_S = \frac{\partial\left(\rho_n \vec{E}_S\right)}{\partial t} + \sigma \vec{E}_S + \frac{\partial}{\partial t} T_c \left(\nabla \times \vec{E}_S\right) = \frac{\rho_n \partial \vec{E}_S}{\partial t} + \sigma \vec{E}_S + \rho T_c \nabla \times \frac{\partial \vec{E}_S}{\partial t} \quad (5)$$

$$\nabla \times \vec{E}_S = -\frac{\partial \vec{B}_S}{\partial t} = -(1/\mu_S)\frac{\partial \vec{H}_S}{\partial t} - (1/\mu_S) T_c \frac{\partial\left(\nabla \times \vec{H}_S\right)}{\partial t} \quad (6)$$

Taking the rotational of the equation (6) and considering the following approximations

$$\nabla \cdot D_S \; 0 = \rho_n \nabla \cdot \vec{E}_S + \rho T_c \nabla \cdot \nabla \times \vec{E}_S \; ; \; \nabla \cdot \vec{E}_S \cong 0 \to \nabla \rho_n \to 0$$

.

$$\nabla \cdot B_S = 0 \Rightarrow \nabla \cdot \vec{H}_S = 0$$

We obtain the following wave equation

$$\nabla^2 \vec{E}_S + (1/\mu_S)\rho T_c^{\,2} \frac{\partial^2}{\partial t^2} \nabla^2 \vec{E}_S = (1/\mu_S)\rho_n \frac{\partial^2 \vec{E}_S}{\partial t^2}$$
$$+(1/\mu_S)\sigma \frac{\partial \vec{E}_S}{\partial t} + \left((1/\mu_S)\rho_n T_c + (1/\mu_S)\rho\right) T_c \nabla \times \frac{\partial^2 \vec{E}_S}{\partial t^2} \quad (7)$$
$$+(1/\mu_S)\sigma T_c \nabla \times \frac{\partial \vec{E}_S}{\partial t}$$

Here we assume that the chiral seismic medium is of a Kerr nonlinearity type, described by a refractive index such that the seismic permittivity is

$$\rho_n = \rho_S + \rho_2 \left|\vec{E}_S\right|^2 \quad (8)$$

https://dx.doi.org/10.22161/ijaers/3.11.14 *ISSN: 2349-6495(P) | 2456-1908(O)*

where ρ_S is the linear part and ρ_2 is the nonlinear component respectively of ρ_n σ is the rock conductivity loss. Past studies have demonstrated that the slip type or style of faulting is potentially significant for correlating earthquake magnitude and rupture parameters. To categorize the dominant slip type for SRF in this paper, we use a simple scheme based on equation (8).

From equation (8) we can be inferred easily the expression for the index of refraction as in [8]. Replacing ρ_n into equation (7) we obtain

$$\begin{aligned}&\nabla^2\vec{E}_S+(1/\mu_S)\rho_S T_c^{\,2}\frac{\partial^2\vec{E}_S}{\partial t^2}\nabla^2\vec{E}_S=(1/\mu_S)\rho_S\frac{\partial^2\vec{E}_S}{\partial t^2}\\&+(1/\mu_S)\sigma\frac{\partial\vec{E}_S}{\partial t}+(1/\mu_S)\rho_2\left|\vec{E}_S\right|^2\frac{\partial^2\vec{E}_S}{\partial t^2}+\\&2(1/\mu_S)\rho_S T_c\nabla\times\frac{\partial^2\vec{E}_S}{\partial t^2}+(1/\mu_S)T_c\rho_2\left|\vec{E}_S\right|^2\nabla\times\frac{\partial^2\vec{E}_S}{\partial t^2}\\&+(1/\mu_S)T_c\sigma\nabla\times\frac{\partial\vec{E}_S}{\partial t}\end{aligned}\qquad(9)$$

Assuming that $\vec{E}_S$ represents a localized waveform, which propagates in the z direction, it has

$$\vec{E}_S(\vec{r},t)=(\hat{x}+j\hat{y})\Psi(\vec{r},t)e^{-j(kz-\omega_0 t)}=\vec{\Psi}e^{-j(kz-\omega_0 t)}\qquad(10)$$

where $\vec{\Psi}$ represents the complex envelope. To solve the equation (9) the property of the Fourier transform $\partial^2/\partial t^2\leftrightarrow-\omega_0^2$ is applied, and then we determine the operators ∇^2 and $\nabla\times$.

After several algebraic manipulations the result is as follows

$$\begin{aligned}&\left(1-T_c^{\,2}k_0^2\right)\left(-2jk_0\frac{\partial\vec{\Psi}}{\partial z}-k_0^2\vec{\Psi}\right)\\&-\frac{1}{v^2}\left(2j\omega_0\frac{\partial\vec{\Psi}}{\partial t}-\omega_0^2\vec{\Psi}\right)=\\&2\zeta k_0^3\vec{\Psi}+j\omega_0\alpha\left(1-T_c k_0\right)\vec{\Psi}\\&-\beta\omega_0^2\left|\vec{\Psi}\right|^2\left(1-T_c k_0\right)\vec{\Psi}\end{aligned}\qquad(11)$$

where $v_S^2=\mu_S\frac{1}{\rho_S}$; $\alpha=(1/\mu_S)\sigma$; $k_0 v=\omega_0$; $\beta=(1/\mu_S)\rho_2$, $j=\sqrt{-1}$. To get to the equation (13) the approximation of small amplitudes is also considered, given by

$$\left|\frac{\partial^2\vec{\Psi}}{\partial z^2}\right|\square\left|j2k\frac{\partial\vec{\Psi}}{\partial z}\right|,\left|\frac{\partial\vec{\Psi}}{\partial t}\right|\square\left|j\omega_0\vec{\Psi}\right|,\left|\frac{\partial^2\left|\vec{\Psi}\right|^2\vec{\Psi}}{\partial t^2}\right|\square\left|j\omega_0\frac{\partial\left|\vec{\Psi}\right|^2\vec{\Psi}}{\partial t}\right|\square\left|j\omega_0\left|\vec{\Psi}\right|^2\vec{\Psi}\right|$$

To illustrate the difference between the high frequency and the low frequency in an earthquake we show the figure 2, which corresponds to the strong earthquake February 27, 2010, Chile. Here we have a set of measurements of high-frequency energy radiation. The upper, middle and lower traces are an observed seismogram, the squares of the band-pass (2-4 Hz) filtered seismogram, and its smoothed time series (normalized by the maximum value), respectively. "A" and "F" in the lower trace denote the arrival of P-wave and estimated end of high frequency energy radiation, respectively (ω_0 have correspondence with the upper signal of high frequency> 10 radians/seg and $\frac{\partial}{\partial t}$ have correspondence with the lower signal of slow frequency) [14, 18]. In our analysis we assume that a possible earthquake in San Ramon Fault waveforms can be similar but of lower amplitude to those shown in Figure 2

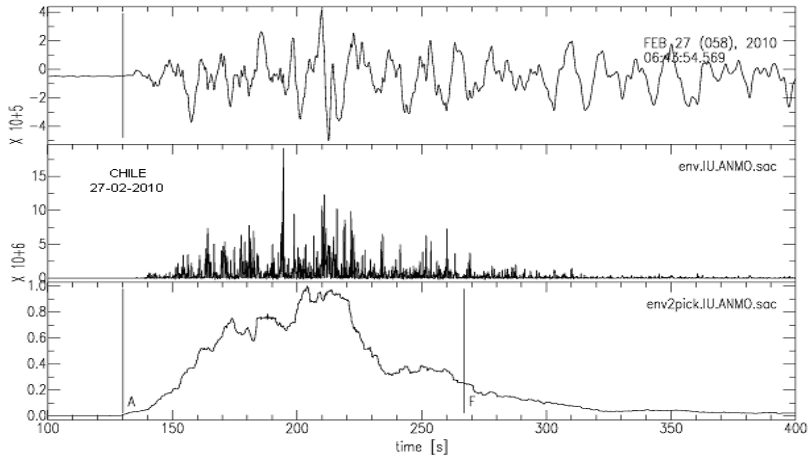

Fig.2: A measurement of high frequency energy radiation of the February 27, 2010 Chile Earthquake, the bottom graph shows the low frequency signal which is the envelope of the high frequency wave. In the next section this envelope is modeled as a Gaussian pulse.

https://dx.doi.org/10.22161/ijaers/3.11.14 *ISSN: 2349-6495(P) | 2456-1908(O)*

The effect of dispersion is included heuristically. Making the change of variables $\phi = 2k_0\vec{\Psi}$ y $z^* = \frac{z}{1-T_c^2 k_0^2}$ and rearranging the terms of equation (11) we obtain

$$j\left[\frac{\partial\phi}{\partial z^*}+\frac{1}{v}\frac{\partial\phi}{\partial t}\right] = -(1-k_0T_c)\frac{j\omega\alpha}{2k}\phi$$
$$-\frac{\beta\omega_0^2}{(2k)^3}(1-k_0T_c)|\phi|^2\phi \qquad (12)$$
$$+k_0^2T_c\left(1-\frac{k_0T_c}{2}\right)\phi$$

As the envelope $\Psi(z,t)$ is a slowly varying function of in z and t, the dispersion relation $k = k(\omega)$ can be transformed to the domain of spatial variations by means of $\Delta\omega = \omega - \omega_0$, which is a small deviation of the sideband frequency with respect to ω_0, and through $\Delta k = k - k_0$, which represent the corresponding wave number.

Using the Fourier transform for Δk, $\Delta\omega$, approximating $\frac{1}{v} \approx \frac{\Delta k}{\Delta\omega}$, and using the Taylor series we obtain

$$\Delta k = \frac{1}{v}\frac{\partial}{\partial t} = \frac{\partial k}{\partial\omega}\frac{\partial}{\partial t} - j\frac{1}{2}\frac{\partial^2 k}{\partial\omega_0^2}\frac{\partial^2}{\partial t^2} + \ldots = \frac{k_0}{\omega_0}\frac{\partial}{\partial t}$$

By substituting this operator in equation (14), we obtain

$$j\frac{\partial\phi}{\partial z^*}+\frac{1}{v_g}\frac{\partial\phi}{\partial t}+\frac{1}{2}k''\frac{\partial^2\phi}{\partial t^2}+(1-k_0T_c)\frac{j\omega\alpha}{2k_0}\phi-(1-k_0T_c)\frac{\beta\omega_0^2}{(2k)^3}|\phi|^2\phi$$
$$+\left(1-\frac{k_0T_c}{2}\right)T_c k_0^2\phi = 0 \qquad (13)$$

where

$$k' = \frac{\partial k}{\partial\omega} = \frac{1}{v_g};\ k'' = \frac{\partial^2 k}{\partial\omega^2};$$

Equation (13) describes the propagation of pulses in a chiral, rotational, dispersive and non linear channel [13].

The first term represents the evolution of the pulse with distance. The second, and third terms represents the scattering of a seismic chiral channel $k'\left(=\frac{1}{v_g}\right)$ and k'' corresponds to the chromatic dispersion k', indicating that the pulse moves with the group velocity, while the dispersion of the group velocity (GVD) is represented by k'', which alters the relative phases of the frequency components of pulse widening, producing its temporal expansion. The fourth is associated with attenuation (α), in this case such losses are weighted by the seismic chirality. The fifth term $|\phi|^2\phi$ represents nonlinear effect, like a Kerr effect, which is characterized by having a refractive index dependent on the seismic field intensity and related to the slip type that can alter and widen the spectrum of frequency. This term also depends on the chiral factor. Finally, the last term is clearly associated with the chirality of the seismic channel.

III. ANALYSIS AND SIMULATIONS

In order to ease up the solution of the propagation equation the following change of variables is introduced: $t^* = t - \frac{Z}{v_g}$,

$z^* = Z$

Defining

$$v_S^2 = \mu_S\frac{1}{\rho_S};\ \alpha = (1/\mu_S)\sigma;\ k_0 = \frac{\omega_0}{v};\ \beta = (1/\mu_S)\rho_2$$
$$C = 1-k_0T_c \qquad (14)$$

$$q = 2k_0\phi,\ Z = \frac{z}{1-\zeta^2k_0^2},\ k_0 = \frac{\omega_0}{v},\ v_g = \frac{1}{k'} = \frac{1}{\partial k/\partial\omega},$$
$$k'' = \frac{\partial^2 k}{\partial\omega^2}, \qquad (15)$$

We have

$$j\frac{\partial q}{\partial Z} = -\frac{1}{2}k''\frac{\partial^2 q}{\partial t^{*2}} - j\frac{\omega_0\alpha C}{2k_0}q + \frac{\beta\omega_0^2\alpha}{(2k_0)^3}|q|^2 q \qquad (16)$$

Finally, is useful normalize the Eq. (16) by introducing

$$\tau = \frac{t^*}{t_0} \qquad (17)$$

Let us model heuristically the relationship between the wave amplitude and the initial seismic power as follows

The normalized amplitude q (equation 16) is proportional to $\sqrt{\frac{P_S}{P_{ref}}}$ or $\sqrt{\frac{P_S t_S}{P_{ref} t_{ref}}} = \sqrt{\frac{E_S}{E_{ref}}}$

Where P_S is the power earthquake, P_{ref} is the power reference and t_S is the time duration of the earthquake, $t_S = t_{ref}$, so using the empirical equation of Gutemberg and Richer [16] which is useful for magnitude of shallow, small-moderate nearby earthquakes

$$\log E_S = 11.8 + 1.5M \qquad (18)$$

We have

$$\frac{E_S}{E_{ref}} = e^{\sqrt{0.12(M_S - M_{ref})}}$$

https://dx.doi.org/10.22161/ijaers/3.11.14 *ISSN: 2349-6495(P) | 2456-1908(O)*

We use this empirical equation because this theory gives a relationship between the magnitude M_S and the energy released E_S which only tends to saturate for really great earthquakes.

Thus we can model the S-wave q through the transformation

$$q(Z,\tau) = e^{\sqrt{0.12(M_S - M_{ref})}} e^{-\frac{\alpha\omega_0 C}{2k_0} Z} U(Z,\tau) \quad (19)$$

where M_S is the peak magnitude of the soliton and M_{ref} is the reference magnitude for a weak seism which acts as calibration standard. Finally the expression (16) can be scaled as

$$j\frac{\partial U}{\partial Z} = -\frac{1}{2}\frac{k''}{t_0^2}\frac{\partial^2 U}{\partial \tau^2} + \frac{\beta\omega_0^2}{(2k_0)^3} e^{\sqrt{0.12(M_S - M_{ref})}} e^{-\frac{\alpha\omega_0}{k_0} CZ} |U|^2 U \quad (20)$$

To our knowledge this is the first time that the magnitude M_S of earthquake is considered into the nonlinear Schrodinger equation. Through numerical calculations these theoretical results (eqs 14-20), would allow analyze the effects of chirality on the attenuation of equation (20) for propagation of S-seismic pulses. Also we take into account the magnitude M_S of moderate earthquakes along the SRF which can trigger strong earthquakes in Santiago City.

To solve the pulse propagation in nonlinear dispersive media we use the split-step Fourier method. The relative speed of this method compared with most FD methods can be attributed in part to the use of finite-Fourier-transform (FFT) algorithm [17]. In general, linear and nonlinear parts of equation (19) act together along the length of the earthquake. The split-step method obtains an approximate solution by assuming that in propagation the seismic field over a small distance Δz, is carried out in two steps. In the first step, from $Z = Z_0$ to $Z = Z_0 + \Delta Z/2$, the linear part acts alone, and the non linear part is zero. In the second step, the nonlinearity acts alone in the point $\Delta Z/2$, (linear part is null).

For the simulation we consider an average of velocity v_S because the bedrock of SRF is layered with $v_S = 2.500 m/s$ between 0 and 2.2 km depth, $v_S = 3.300 m/s$ between 2.2 km and 8 km depth (Barrientos et al. 2004) [19]. The frequency w_0 was set to $> 10 radians/s$ in this simulation. The wave comes to 8 km deep in the bedrock.

Figure 3. shows the Intensity U calculated numerically from equation (20). The parameters correspond to a weak earthquake with $M_S = 1$, M_{ref} is the reference magnitude for a weak seism which acts as calibration standard to nonlinear Schrodinger equation with $M_s > 1$.Here $T_c = 0$, $C = 1$ the chiral effect is not considered. The angle θ between the plane which contains U and axis Z, $\theta = 0$ .The normalized attenuation $\frac{\alpha\omega_0}{k_0}$ is neglected for short distance, $Z \square 30km$.

The equation (20) is reduced to

$$j\frac{\partial U}{\partial Z} = -\frac{1}{2}\frac{k''}{t_0^2}\frac{\partial^2 U}{\partial \tau^2} + \frac{\beta\omega_0^2}{(2k_0)^3}|U|^2 U$$

Which is the typical result obtained by other authors [7, 9].

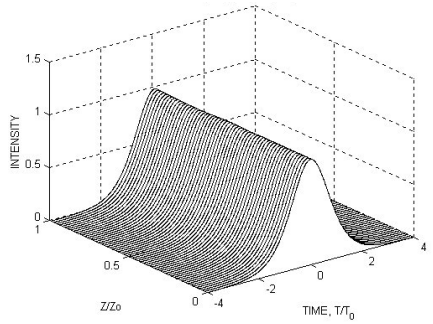

Fig.3: Parameters of a weak earthquake; $M_{ref} = 1$, $M_S = 1$, $k_0 v_S = w_0$, $T_c = 0$, $C = 1$ $\sqrt{\rho/\mu_S} = 3km/s$ $\rho_S = 4g/cm\wedge 3$ $\rho_2 = 10^{-4}$ $Z_0 = 30km$, $\beta = (1/\mu_S)\rho_{2\,=\,10^{-3}}$, $C = 1$, $\theta = 0$, depth = 8km

The propagating shear wave is represented by a Gaussian pulse simulating the bottom graph of figure 2

Figure.4. shows the envelope of U for a strong earthquake with $C = 1 - k_0 T_c = 0.3$, nearly of $Z = 30km$ we have a peak of U, which it indicates that the maximum of U can trigger a major earthquake. From equation (20) we can obtain $M_S - M_{ref} \approx 6.4$, that is $M_S \approx 7.4$. This value agrees with the estimations of Vargas, Armijo y Pérez [1, 2, 3] respectively who are used the Wells – Coppersmith's semi empirical approach [6]. We note that in this paper $M_W \square M_S$ because M_S only tends to saturate for really great earthquakes $M_W > 8.0$. The properties of rock in the seismic wave travel path are important because they directly influence the amplitudes of seismic waves. Rock is normally considered to be stable with respect to seismic amplification, but here we show that this is not always the case. The wavelength of a seismic wave of a given frequency is proportional to its velocity. $v_g = v_S = \lambda f$. If a shear wave passes into a lower velocity medium, it will reduce its wavelength so to conserve

https://dx.doi.org/10.22161/ijaers/3.11.14 *ISSN: 2349-6495(P) | 2456-1908(O)*

energy, the wave is amplified. Sedimentary basins have lower velocities than bedrock and can therefore produce intense amplification of incoming seismic waves. As seismic wave travel faster through harder denser rocks and compact sediments than through soft rocks and loose sediments.The change in velocity also changes the rate at which seismic energy is amplified. As a wave travels up to the layer with sediment (nearly of $Z = 30km$), density decreases (as does the impedance), therefore the shear wave velocity also decreases. If Energy is to remain constant when wave approaches the surface, the particles velocity must increase to compensate the decrease in density and shear wave velocity producing a large effect on the basin layer. Sediment impedance affects the amplitude of earthquake ground motion. When $Z > 30km$, the S-wave along the rock layer decreases due to the drastic change of impedance between the rock and the sediment layer. Impedance is the product of the density (ρ_S), the shear wave velocity (v_S) and the cosine of the angle of incidence which is defined as the angle between the vertical and the direction of seismic wave propagation. In terms of angle θ_S the change in impedance is expressed with the impedance contrast $I_C = \rho_S V_S \sin\theta_S / \rho_b V_b$. At $Z_0 = 30km$ the reflection coefficient is $r_C = \rho_S V_S \sin\theta_S - \rho_b V_b / (\rho_S V_S \sin\theta_S + \rho_b V_b)$ with $I_C = \rho_S V_S \sin\theta_S / \rho_b V_b >> 1$ the S-wave has a peak with $M_S > 7$, that is the energy E reaches a maximum that is transferred to the basin layer where seismic waves are trapped and begin to reverberate.

Thus we can see that the chiral factor C contributes to the S wave to be amplified. Consequently the S wave travels further along the fault.

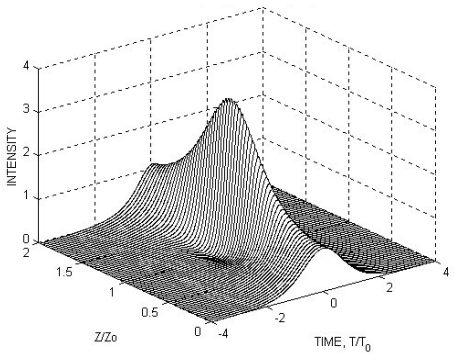

Fig.4: Parameters of a strong earthquake, Peak of $M_S > 7$,

$M_{ref} = 1$, $C = 1 - k_0 T_C = 0.3$

$\sqrt{\rho/\mu_S} = 3km/s$, $\rho_S = 4g/cm\wedge 3$, $\rho_2 = 10(-4)$ $Z_0 = 30km$, $w > 10$ radians/s. $\theta = 15^o$, depth = 8km

As we can see, rotational tectonic waves can propagate along the fractured tectonic fault like SFR with a speed of 2-4 km per second. These waves may have a form of rotational seismic solitons and can trigger major earthquakes. Thus, the research on rotational seismic solitons is essential for investigating the propagation of seismic waves and helps understand mechanisms triggering earthquakes. Chiral rotational seismic waves propagate faster in solid rocks and much slower in fractured media along tectonic faults. A rupture breaking the free surface is another important element to keep in mind in order to improve future kinematic rupture scenarios for the SRF region. Indeed. In this model further improvements should include local site/soil effects and basin/topographic effects.

IV. CONCLUSIONS

In this paper we have obtained the Schrödinger nonlinear equation for a channel whose core is chiral, dispersive and has nonlinear behavior. The effect of chirality is manifested by the terms associated with the loss of the chiral channel and the nonlinear coefficient. The most significant result of our work is that to use the chirality of S waves can cancel out the losses and nonlinearities of the channel, which would allow us to modify radically their behavior as channel of seismic soliton. Numerical calculation of the equation was obtained, to model by soliton in the SRF. We propose that the San Ramón Fault is not only a geologically active fault, but also it presents seismicity that can be associated with this structure at and resulting in a seismically active fault too. As seismic waves travel though the ground, they travel faster through hard rock than soft soil. As a result, when the waves move from hard rock to soft soil, the amplitude (largeness) of the waves needs to increase to be able to carry the same amount of energy, creating stronger shaking. This same principle accounts for the site effects of sediment thickness. The deeper the sediment above bedrock, the more soft soil there is for seismic waves to travel through, therefore creating stronger amplifications. This is a main element to be considered in any study on seismic hazard assessment for the city of Santiago, Chile. Through numerical calculations our theoretical results would allow analyze the propagation of S-seismic pulses that can trigger strong earthquakes in this city.

ACKNOWLEDGEMENT

One of us is grateful to Professor Raul Sanhueza of EIEE the fruitful discussions on this subject.

REFERENCES

[1] Vargas G et al, 2014, Probing large intraplate earthquakes at the west flank of the Andes, Geology,

published on line on 17 October 2014 as doi: 1130/35741.1.

[2] Armijo R., et al ,2010, The West Andean thrust, the San Ramón fault and the seismic hazard for Santiago, Chile: Tectonics, v. **29**, TC2007.

[3] Pérez A et al, 2013,Improving seismotectonics and seismic hazard assessment along the san Ramón fault at the eastern border of Santiago city, Chile: Natural Hazards, v. **71**, p.243–274.

[4] Brooks B.A., et al, 2011, Orogenic-wedge deformation and potential for great earthquakes in the central Andean backarc: Nature Geoscience, v. **4**, p. 380–383.

[5] Pilz M et al 2011, Modelling basin effects on earthquake ground motion in the Santiago de Chile basin by a spectral element code: Geophysical Journal International, v. **187**, p. 929–945.

[6] Wells D and Coppersmith K, (1994) New Empirical Relationships among Magnitude, Rupture Length, Rupture Width, Rupture Area, and Surface Displacement, Bulletin of the Seismological Society of America, Vol. 84, No. 4, pp. 974-1002,

[7] Teisseyre K P, (2007), Analysis of a group of seismic events using rotational components, Acta Geophys. 55, 535–553.

[8] Teisseyre, R. (2009). New developments in the physics of rotational motions, Bull. Seismol. Soc. Am. 99, no. 2B, 1028–1039.

[9] Erofeyev VI (2003) Wave processes in solids with microstructure. World Scientific, Singapore

[10] Teisseyre R, Yamashita T (1999) Splitting stress motion equations into seismic wave and fault-related fields. Acta Geophys Pol **47**: 2, 135-147

[11] Lakhtakia A, et al 1985. "Time-Harmonic Electromagnetic Fields in Chiral Media" Lecture Notes in Physics 335, Springer-Verlag.

[12] Torres Silva H, 2003, Effect of Chirality on Soliton in Optical Fiber, The Journal Mathematics and Computers in Simulation, vol 62, pp 149-161.

[13] Torres-Silva H, 2004, Non-linear polarization and chiral effects in birefringent solitons, Pramana Journal of Physics Vol. 62 Nº 1 Pág. 37.

[14] Torres-Silva H and Lopez-Bonilla J L(2011). Early Prediction and detection of Strong Earthquakes through Chiral Radiation Waves, Journal of Vectorial Relativity, 6, 2, 1-11.

[15] Torres-Silva H, Torres Cabezas D (2013), Chiral Seismic Attenuation with Acoustic Metamaterials, Journal of Electromagnetic Analysis and Applications**,**Vol.5 No.1,

[16] Gutemberg B and Richer C F, (1956), Ann. Geoph.9, 1.

[17] Agrawal G, Nonlinear Fiber Optics, Academic Press, Inc., 1995.

[18] Torres-Silva H et al, (2015), Chiral ratio of the compressional and shear velocity for the determination of strong earthquake, Journal of Science, Engineering and Technology, Vol. 11, No. I, pp 20-28.

[19] Barrientos, S et al (2004): Crustal seismicity in central Chile, Journal of South American Earth Sciences 16, 759-768.

https://dx.doi.org/10.22161/ijaers/3.11.15 *ISSN: 2349-6495(P) | 2456-1908(O)*

Thermal and Elastic Properties of Thin Films

Francisco C. Marques

Physics Institute, State University of Campinas, 13083-859, Campinas – SP, Brazil

Abstract*—Optical, electronical and structural properties of thin films have been largely reported on literature. On the other hand, thermal properties have received little attention. Here we adopted two different techniques to determine thermal and elastic constants of thin films. The first was the bending beam technique, based on a deflection of a laser beam, used to determine the radius of curvature of the film/substrate composite, allowing extracting the stress of thin films. By making these measurements in substrates with different coefficient of thermal expansion we can also obtain a mixed elastic constant (biaxial modulus) involving a combination of the Young´s modulus and the Poisson´s ratio. Combining these results with a second technique, i.e., nanoindentationmeasurements, we demonstrate that one can obtaina total of 5 different thermal and elastic properties of thin films: stress, hardness, coefficient of thermal expansion, Young´s modulus and Poisson´s ratio. The procedure was used to obtain these parameters of hydrogenated diamond-like carbon (DLC) thin films.*

***Keywords*—Coefficient of thermal expansion, Young´s modulus, Poisson´s ratio, stress, hardness.**

I. INTRODUCTION

Mechanical and structural properties of amorphous carbon are largely reported in literature. However, there are few works reporting the thermal properties, such as the coefficient of thermal expansion (CTE) [1-4]. It is well known that amorphous carbon tends to have high stress [5,6] that hinders the measurements of properties that require relatively thick material, such as the measurement of thermomechanical properties. The high stress limits the production of stable thin films with thickness of few microns, which is necessary for the measurement to the CTE using the bending beam technique.

Here we report on a combination of the measurement of two properties, stress and nanoindentation (nanohardness), that allow the determination of 3 additional thermal and elastic properties of thin films, *i.e.*, the coefficient of thermal expansion, Young´s modulus andPoisson´sratio. This procedure was adopted to determine those parametersofamorphous hydrogenated diamond-like carbon (DLC), a-C:H.

II. EXPERIMENTAL

The DLC films were prepared by plasma enhanced chemical vapor deposition (PECVD) on the cathode electrode at high bias (800V) following description of reference [7].The films were deposited at room temperature using a flow of methane (CH_4) and keeping the pressure constant at 1.0Pa.

The measurement of the stress was performed by the thermally induced bending (TIB) technique, which comprise of the deflection a double beam laser (created with two mirrors) from the surface of the film. This procedure allows the determination of the curvature of the film/substrate sample from which one can obtain the stress of the film. By making the measurement as a function of temperature one also determines the thermal expansion coefficient of the film. Detailed description is found in reference [3]. The hardness of the films deposited on a silicon substrate was measured using a Berkovich diamond tip from a NanoTest-100 system and adopting the Oliver and Pharr method [8].

III. THEORY

The stress (s) of the films were determined using the bending beam technique, which consist in determining the curvature of a film/substrate composite before and after the film deposition using the Stoney equation [9,10]:

$$s = \left(\frac{E_s}{1-v_s}\right)t_s^2/6t_f\left(\frac{1}{R}-\frac{1}{R_0}\right) \quad (1)$$

where E_s, v_s and t_s are the Young´s modulus, Poisson´s ratio and thickness of the substrate, respectively, R and R_0 are the radius of curvature of the film/substrate composite and the blank substrate, respectively, and t_f is the film thickness.

For the determination of the coefficient of thermal expansion one needs to perform measurements of the stress as a function of temperature, as illustrated in Figure 1a. The slope of the stress withtemperature is related to the thermal expansion coefficient of the film (α_f) and substrate (α_s) by the equation [9,10]:

https://dx.doi.org/10.22161/ijaers/3.11.15 *ISSN: 2349-6495(P) | 2456-1908(O)*

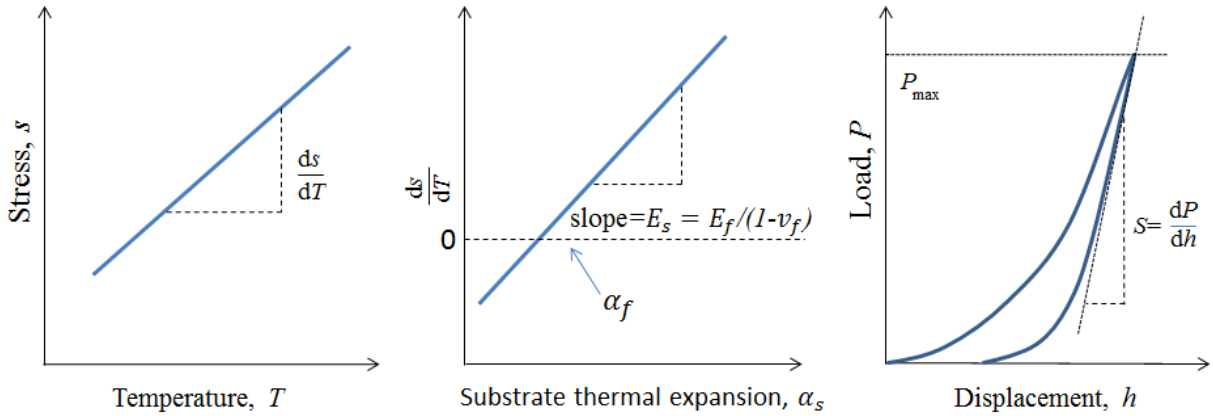

Fig.1: Schematic diagrams of (a) stress (s) of thin film as a function of temperature, (b) variation of stress with temperature (ds/dT) as a function of the coefficient of thermal expansion of the substrate (α_s) and (c) load as a function of tip displacement in typical nanoindentation measurements.

$$\frac{ds}{dT} = \left(\frac{E_f}{1-v_f}\right)(\alpha_s - \alpha_f) \qquad (2)$$

whereE_f and v_f are respectively the Young´s modulus and Poisson´s ratio of film. Thus, if one performs measurements of stress as a function of temperature in different substrates, eq. 2 shows that the ds/dT versusα_s is a linear relation, where the intersection with the abscissa axis is the coefficient of thermal expansion (α_f) and the slope (E_s) is the biaxial elastic modulus of the films, *i.e.:*

$$E_s = \frac{d\left(\frac{ds}{dT}\right)}{d\alpha_s} = E_f/(1-v_f) \qquad (3)$$

The hardness of thin films has been usually determined using nanoindentation techniques with Berkovich diamond tips and adopting the Oliver and Pharr model [8]. Figure 1c displays a sketch showing the main characteristics of the indentation process. A load placed on the indenter is measured as a function of the tip penetration (displacement). The final load is determined by the user and kept constant for a short period and then the indenter is unloaded. The hardness, *H*, is then determined by:

$$H = \frac{P_{max}}{A} \qquad (4)$$

where P_{max} is the maximum load applied to the film and *A* is the indented area of the diamond tip. The measurement also allows the determination of the elastic constant by using the slope (stiffness, *S*) extracted from the upper part of the unloading curve, which is given by [8]:

$$S = \frac{dP}{dh} = \frac{2}{\sqrt{\pi}} E_r \sqrt{A} \qquad (5)$$

whereE_r, is the reduced modulus given by:

$$\frac{1}{E_r} = \frac{(1-v_f{}^2)}{E_f} + \frac{(1-v_i^2)}{E_i} \qquad (6)$$

WhereE_i and v_i are the Young´s modulus and Poisson´s ratio of the indenter (diamond tip).
Since the properties of the diamond tip are known and the area can be determined by the tip geometry and indentation depth, one can obtain the reduced modulus determined by the nanoindentation process,E_H, as [6]:

$$\frac{1}{E_H} = \frac{(1-v_f{}^2)}{E_f} = \frac{1}{E_r} - \frac{(1-v_i^2)}{E_i} \qquad (7)$$

or

$$E_H = \frac{E_f}{(1-v_f^2)} \qquad (8)$$

In summary, from stress as a function of temperature and nanohardness measurements one obtains 5 thermal and elastic properties of thin films: stress (*s*), hardness (*H*), coefficient of thermal expansion (α_f), and two reduced elastic modulus, one obtained from stress vs. temperature measurements $(E_s = E_f/(1-v_f)$, eq. (3) and the second from hardness measurement $(E_H = E_f/(1-v_f^2)$, eq. (8). Note that both reduced elastic modulus are different in the exponent of the Poisson´s ratio, which is 1 for the reduced modulus obtained from stress and 2 for hardness measurement. That is an interesting result since the two equations are independents, so they allow us to extract separately both the Young's modulus (E_f) and the Poisson´s ratio (v_f) of the film by solving the system of equations (3) and (8). A similar procedure for determining separately the Young´s modulus and Poisson´s ratio have also been proposed by Ferrari *et al.* [11], but using Brillouin scattering in place of the bending beam technique used here.

https://dx.doi.org/10.22161/ijaers/3.11.15 *ISSN: 2349-6495(P) | 2456-1908(O)*

IV. RESULTS AND DISCUSISION

The above procedure was adopted to determine the thermal and elastic properties of diamond-like (DLC) film. Figure 2 displays the stress (*s*) as a function of temperature of a DLC film deposited in 2 different substrates: Precision glass 211 and Corning glass 7059.The negative value of the stress indicates the stress is compressive, which has usually been observed in amorphous carbon film [5,6]. The value is relatively low since the film was prepared at high bias producing a material with high concentration of sp^2 bonds. The positive slope (*ds/dT)*of those curves indicates that the thermal expansion coefficient of the film is smaller than those of the substrates, and the higher the difference the higher the slope.

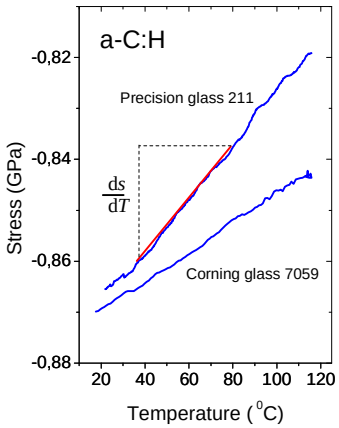

Fig.2: Stress as a function of temperature of a-C:H films deposited in two different substrates (Precision glass 211 and Corning glass 7059).

The slope of the measurements displayed in Fig. 2 can be plotted as a function of the coefficient of thermal expansion of the substrates. In Fig. 3 we show an example of this procedure using a-C:H films deposited on 5 different substrates (silicon and germanium (111), sapphire, Precision glass 211 and Corning glass 7059). One can observe that it follows a linear relation with the coefficient of thermal expansion of the substrate. A linear fitting of the data gives a slope ($E_s = d(ds/dT)/d\alpha_s = E_f/(1-v_f)$ equal to 95GPa, and the intersection with the abscissa gives the coefficient of thermal expansion of the film (α_f)equal to2.2x10^{-6} C^{-1}, according to equation (2).

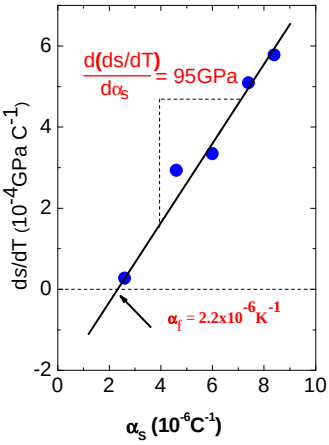

Fig.3: Slope of stress versus temperature as a function of the coefficient of thermal expansion of the substrates

Table 1 presents the results obtained for the stress and hardness measurementsof a-CH films deposited on (111) silicon substrates. The reduced biaxial modulus determined by stress was E_s=*95*GPa (Fig. 2), whereas the reduced elastic modulus determined by nanoindentationwasE_H=GPa. The difference is due to the fact that these reduced elastic moduli are different. By adopting the procedure described in the theory section, one can use this difference to extract separately the pure Young´s modulus (E_f=77GPa) and the Poisson´s ratio (v_f=0.19) of the a-CH film using equations (3) and (8).

Table.1: Thermal and elastic properties determined through stress as a function of temperature and nonoindentation and using the procedure described in the text.

Stress	0.87GPa
Hardness	14 GPa
Thermal expansion coefficient	2.2x10^{-6} C^{-1}
Biaxial modulus, *E/(1-v)*	95 GPa
Reduced modulus, *E/(1-v^2)*	80 GPa
Young´s modulus	77 GPa
Poisson´s ratio	0.19

V. CONCLUSION

Measurements of stress as a function of temperature of thin films deposited on substrates with different coefficient of thermal expansion supply an elastic modulus different from the one obtained by nanohardnessmeasurements. In this work we present a procedure using these two techniques to obtain separately the Young´s modulus and the Poisson´s ratio of thin films.Thus, by adopting these two techniques one can determine 5 thermal and elastic properties of thin films:

https://dx.doi.org/10.22161/ijaers/3.11.15 *ISSN: 2349-6495(P) | 2456-1908(O)*

stress, hardness, coefficient of thermal expansion, Young´s modulus and Poisson´s ratio. The procedure was adopted to obtain those data from hydrogenated diamond-like (DLC) carbon films, a-C:H.

ACKNOWLEDGMENT

This work was financially supported by the Brazilian research finance agencies: FAPESP, CAPES, CNPq and INCT/INES.

REFERENCES

[1] J. S. Wang, Y. Sugimura, A. G. Evansand W. K. Tredway, "The mechanical performance of DLC films on steel substrates",Thin Solid Films, 325, pp. 163-174, July 1998.

[2] F. Demichelis,C. F. Pirri,A. Tagliaferro, G. Benedetto, L.Boarino,R. Spagnolo, E. Dunlop,J. Haupt, W. Gissler, "Mechanical and thermophysical properties of diamond-like carbon (DLC) films with different sp3/sp2 ratios", Diamond and Relat. Mater.,2,pp. 890-892, 1993.

[3] M. M. de Lima Jr.,R. G. Lacerda,J.Vilcarromero and F. C. Marques, "Coefficient of thermal expansion and elastic modulus of thin films", J. of Applied Physics, 86 (9), pp. 4936-4942, Nov. 1999

[4] F. C. Marques,J. Vilcarromero,R. G.Lacerda, "Thermomechanical properties of amorphous hydrogenated carbon-germanium alloys", Applied Physics A, 71(6), pp. 633-637, Dec. 2000.

[5] J. Robertson,"Diamond-like amorphous carbon", Materials Science and Engineering R 37, pp. 129-281, 2002.

[6] Grill, A. "Diamond-like carbon: state of the art", Diamond and Related Materials 8, pp. 428-434, March 1999.

[7] F. C. Marques,R.G. Lacerda, G. Y. Odoand C. M. Lepienski,"On the hardness of a-C:H films prepared by methane plasma decomposition", Thin Solid Films, 332, pp.113-117, Nov. 1998.

[8] W. C. Oliver andG. M.J. Pharr, "An improved technique for determining hardness and elastic modulus using load and displacement sensing indentation experiments", G. M. J. Mater. Res., 7, pp. 1564-1583, June 1992.

[9] G. G. Stoney, "The tension of metallic films deposited by electrolysis", Proc. R. Soc. London, Ser. A, 32, pp.172-177, May 1909.

[10] R. W. Hoffman,Physics of Non-Metallic Thin Films, Vol. B-14, New York: Plenum, 1970.

[11] A. C. Ferrari, J. Robertson, M. G. Beghi, C. E. Bottani, R. Pastorelli, "Elastic constants of tetrahedral amorphous carbon films by surface Brillouin scattering", Appl. Phys. Lett. 75, pp. 1893-1898.July 1999.

International Journal of Advanced Engineering Research and Science (IJAERS) *[Vol-3, Issue-11, Nov- 2016]*
https://dx.doi.org/10.22161/ijaers/3.11.16 *ISSN: 2349-6495(P) | 2456-1908(O)*

Design and Analysis of Brake and Gas Pedal

Ajinkya Bhonge[1], Prashant Gunai[2], Kaushal Joshi[3]

[1]Department Of Mechanical Engineering, LTCOE, Mumbai University, India

Abstract*—The requirement of pedal mount have become increasingly complex in recent years due to the expansion of global markets and diversification of the conditions under which vehicles are used in different parts of the world. It is also becoming increasingly important to ensure that vehicles offer adjustability, ergonomical for the driver, light weight, serviceability, secure and better braking effect which are expected by drivers, but can also provide less aggressive feel to driver while severe braking. We designed it with keeping all the requirements of pedal system and driver in mind. The chances of condition of pedal fail is also reduced in ours design and also the weight of whole assembly is very less than the conventional ones. The aim of this study is to design and analyse the brake pedal and accelerator using Solidworks and ANSYS software*

Keywords*—Automotive brake pedal, accelerator, Light weight, adjustable.

I. INTRODUCTION

An automobile or other road vehicle may have two to three pedals. They can be either hanging from the firewall (bulkhead) or standing on the floor; the latter is usually used in off-road vehicles and sports car. The arrangement is the same for both right- and left-hand traffic. From left to right:

- Normally operated by the left foot:

Parking brake pedal (in some newer vehicles, in place of a hand brake lever)

- Normally operated by the right foot:

Throttle (known as the accelerator or gas pedal), controls fuel and air supply to the engine. It is usually narrow and close to the floor allowing the drivers heel to rest on the floor. It has a fail-safe design in that it automatically returns to the idle position when not depressed by the driver.

1.Floor Mounted Pedals

If the pedals are mounted at the floor then the only adjustment would be the length of the pedals and you may compromise driver ergonomics if you make the pedals too short or too long.

2. Advantage of floor mounted pedals

- Lower CG is obtained.
- It has more natural foot movement.
- Floor mounted assemblies are typically more compact (out of necessity).
- It provides simpler line routing
- Floor mounted assemblies typically has less mounting options.

II. PURPOSE

- The essential purpose of the brake and throttle systems of the vehicle are extremely simple. The throttle needs to make the car accelerate at the driver's will, and the brake system needs to make the car decelerate at the driver's will. However, the overall capability of the system transcends this simple definition.
- Other considerations that must be taken into account in a braking and throttle system is are ergonomics and component interference.
- In terms of ergonomics, the driver must be able to comfortably use the brake and throttle pedals for an extended period of time.

III. WORKING

1.Brake System:-When you push the brake pedal it depresses a piston in the master cylinder, forcing fluid along the pipe The fluid travels to slave cylinders at each wheel and fills them, forcing pistons out to apply the brakes. Fluid pressure distributes itself evenly around the system. The combined surface 'pushing' area of all the slave pistons is much greater than that of the piston in the master cylinder. Consequently, the master piston has to travel several inches to move the slave pistons the fraction of an inch it takes to apply the brakes. This arrangement allows great force to be exerted by the brakes, in the same way that a long-handled lever can easily lift a heavy object a short distance.

2. Accelerator system:-The gas pedal in your car is connected to the throttle valve -- this is the valve that regulates how much air enters the engine. So the gas pedal is really the air pedal. When you step on the gas pedal, the throttle valve opens up more, letting in more air. The engine control unit (ECU, the computer that controls all of the electronic components on your engine) "sees" the throttle valve open and increases the fuel rate in anticipation of more air entering the engine.

https://dx.doi.org/10.22161/ijaers/3.11.16 *ISSN: 2349-6495(P) | 2456-1908(O)*

IV. MATERIAL

After performing detailed study of the different materials that have been used in the pre-existing pedal mount, we formulated the properties that were required to be possessed by the material chosen for our pedals.

- It should possess high fatigue strength.
- It should have good machining properties.
- It should have high strength.
- It should possess resistance to corrosion.
- It should be cheap and easily available

After detailed research of all kinds of material which fit properly in the above properties, we decided upon our material which could be used for our turbine.Aluminium alloy 7075 as our pedal material because it possessed the perfect balance between corrosion strength, cost, machinability and fatigue ability possesses, less density (i.e. low weight) than that of stainless steel and is less costly than stainless steel.

Table.1 : Properties

Properties	Values
Hardness, Brinell	150
Ultimate Tensile Strength	572 MPa
Tensile Yield Strength	503 MPa
Modulus of Elasticity	71.7 GPa
Fatigue Strength	159 MPa
Poisson's Ratio	0.33
Shear Strength	331 MPa

V. METHODOLOGY

The design of the pedal is carried out as per the flow chart given in fig. In this flow chart, the initial step starts with the material information, machine specifications, geometric dimensions and tolerances required to be achieved on the component, and different parts of the head end sub-assembly and their cad drawings which are modeled using the software Solidworks.

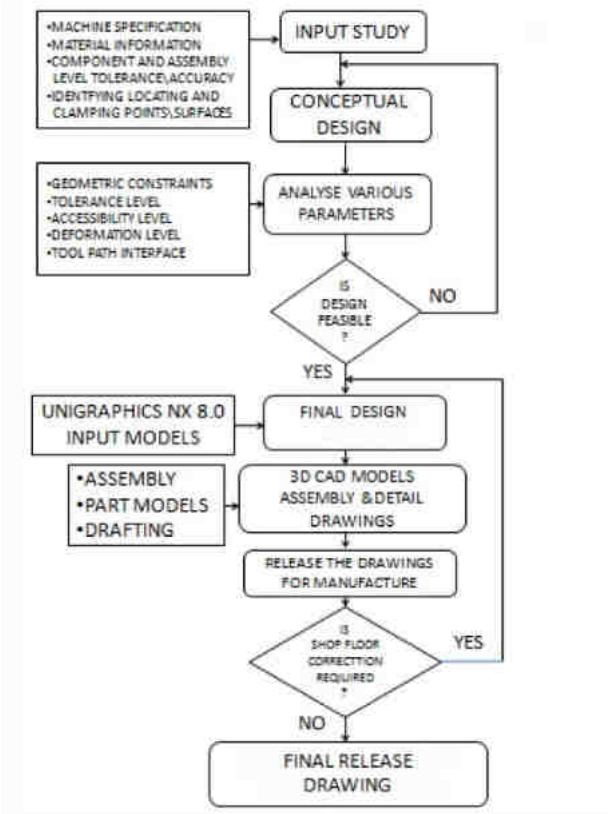

Fig 1:-Methodology

Before the design of the pedal, some requirements have to be considered.

Pedal design Requirement:-

1.Size: In view of the limited space available for the driver's feet, the dimensions should be small as possible but must comply with safety and ergonomics standards. For dimensional reference, existing model of Wilwood pedal is taken.

2. Weight: In view of reducing the weight of accelerator pedal, it should have minimum weight.

3. Safety: The component must be free from sharp edges. The system must comply with all relevant parts of India and international legislation. The maximum force on the accelerator pedal is 40 N with a maximum deflection of 10 mm.

4. Environment: The accelerator pedal must be capable of use in all weather conditions and should be non corrosive. It must be resistant to fuel slippage, greases and should not degrade by ultra violet radiation.

5. Ergonomics: The distance between steering wheel and accelerator pedal are kept sufficeintly. The return force should be between 40-60 N. The dimensions of pedal should not be too short so that drivers feel difficult to

https://dx.doi.org/10.22161/ijaers/3.11.16 *ISSN: 2349-6495(P) | 2456-1908(O)*

depress the pedal. The design must provide comfort and enough space installing and removal of the pedal. Design dimension should account factors for easy accessibility and women driving with high heeled shoes

6. Brake pedal ratio:-Pedal assembly ratio, or mechanical leverage, is the ratio calculated as the length from the pivot point of the pedal to the center of the foot pedal (A), divided by the length from the pivot point to the master cylinder pushrod. Mechanical leverage is simply a means of increasing the brake force without increasing your leg effort. the mechanical leverage increases brake force without pushing harder on the pedal.

Fig 2:-Holes for variable pedal ratios

7. Balancing bar: The balance bar is an adjustable lever (usually a threaded rod), that pivots on a spherical bearing and uses two separate master cylinders for the front and rear brakes. Most balance bars are part of a pedal assembly that also provides a mounting for the master cylinders. When the balance bar is centered, it pushes equally on both master cylinders creating equal pressure, given that the master cylinders are the same size bore. When adjusted as far as possible toward one master cylinder it will push approximately twice as hard on that cylinder as the other.

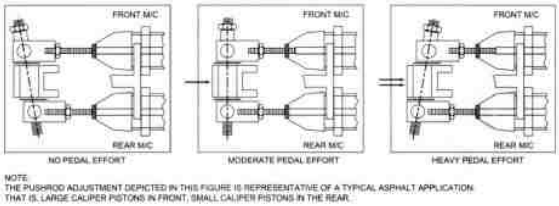

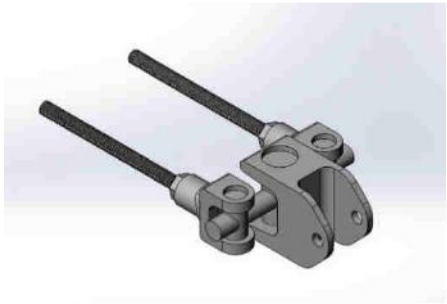

Fig 3:-Balancing Bar

VI. RESULTS

1.Brake Pedal:-

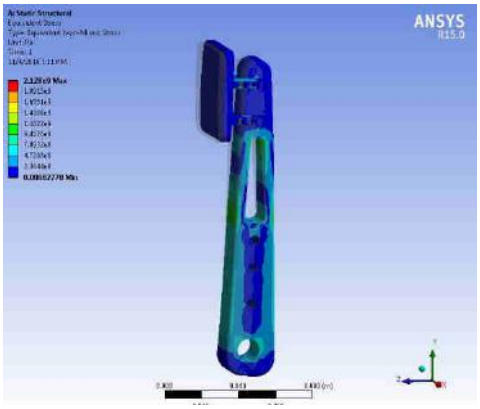

Fig 4:-Equivalent Stress

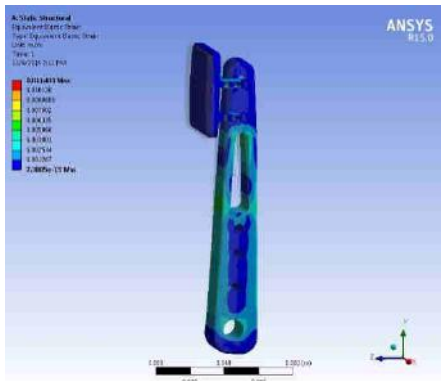

Fig 4:-Equivalent Strain

https://dx.doi.org/10.22161/ijaers/3.11.16 *ISSN: 2349-6495(P) | 2456-1908(O)*

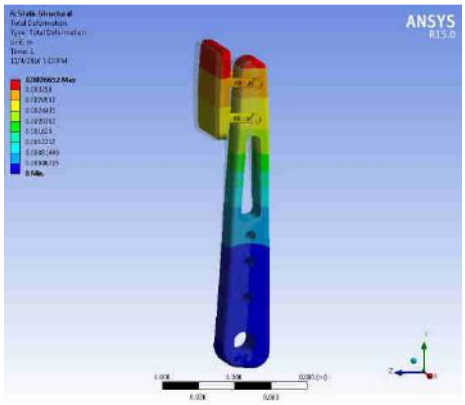

Fig 6:-Total deformation

Table.2: Results for Brake Pedal

	Maximum	Minimum
Equivalent Stress	2.128e+009 Pa	8.2778e-004 Pa
Equivalent Strain	1.1403e-002 m/m	7.3885e-015 m/m
Total Deformation	3.6652e-003 m	0 m

2. Gas Pedal:-

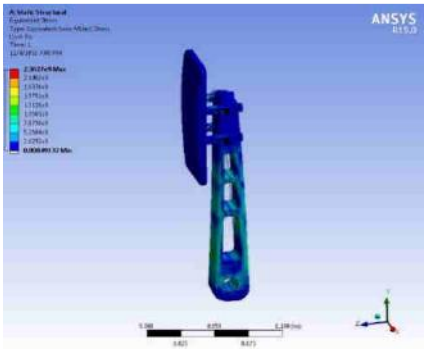

Fig 7:-Equivalent Stress

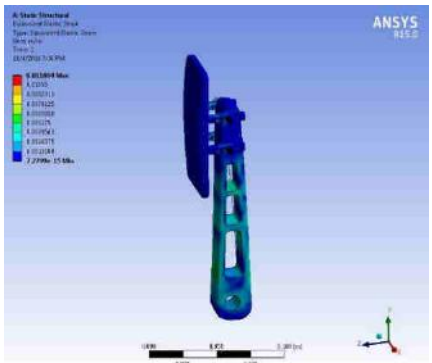

Fig 8:-Equivalent Strain

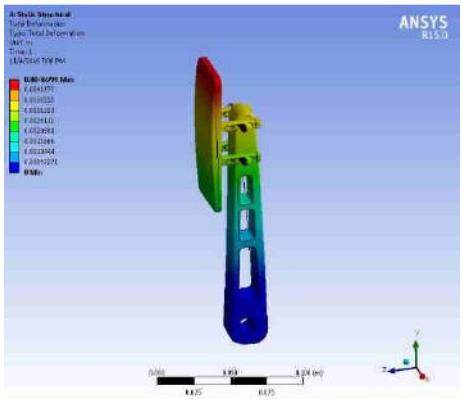

Fig 9:-Total deformation

Table.3: Results for Gas Pedal

	Maximum	Minimum
Equivalent Stress	2.3627e+009 Pa	4.9132e-004 Pa
Equivalent Strain	1.1869e-002 m/m	7.2799e-015 m/m
Total Deformation	4.6999e-003 m	0 m

VII. CONCLUSION

The development process of pedal has been carried to replace the existing Standard pedal for various benefits. It is observed that there weight reduction of Due to use of aluminum alloy 7075. It is produced as a single unit so gives lower manufacturing complexities, better fit and better finish. Moreover, it is also found to be dimensional stable that makes it suitable for usage in a wide range of temperature. It is non-corrosive and could be worked without requirement paint coatings. It has an inherent resistance to fuel, oil and greases suitable for usage. It is inherently better sound insulator than steel.

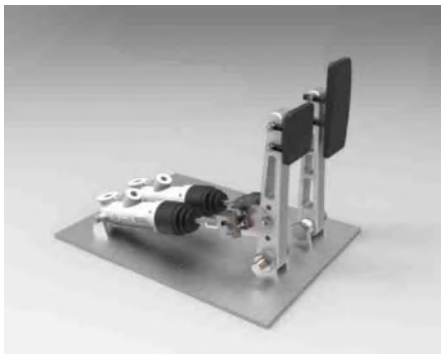

https://dx.doi.org/10.22161/ijaers/3.11.16 *ISSN: 2349-6495(P) | 2456-1908(O)*

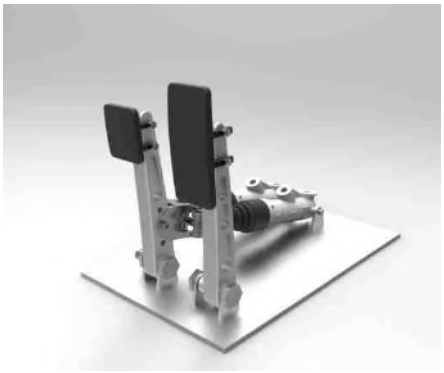

Fig 10:-Final Assembly

REFERENCES

[1] Dr Hosseinsaidpour "Light weight high performance material for car body structure" NTI Technology conference CEME, Ford Motors Company 16June2004

[2] Hansmann, J. and Baitezak, A, (1991). Clutch and brake pedal made of plastics. Kunststoffie German Plastics81:26-28

[3] Jurgen Hirsch "Aluminium in Innovative Light-Weight Car Design" Material Transactions, Vol. 52, No.5 (2011) pp. 818 to 824 Special Issue on Aluminium Alloys 2010 # 2011 the Japan Institute of Light Metals Hydro Aluminium Deutschland GmbH, R&D. P. O. Box 2468-53117 Bonn, Germany

[4] Adrian. X.: Simon. S.-P.; Tlieo. F.: A comparison of concept selection in concept scoring and axiomaticdesign methods. Presented to Canadian Congress 011 Engineering Education. Canada. Paper No. 69. 22 – 24 July, 2007

[5] Bowonder. B.: Concurrent engineering in an Indian automobile firm: the experience of Tata. International Journal of Manufacturing Technology and Management, 6(3/4), 2004.

[6] McMahon, C.-D.; Scott, M.-L.: Innovative techniques for the finite element analysis and optimization of composite structures, 23rd International Congress of Aeronautical Sciences, Toronto. Canada Page No. 61. 8-13 September. 2002.

International Journal of Advanced Engineering Research and Science (IJAERS) *[Vol-3, Issue-11, Nov- 2016]*
https://dx.doi.org/10.22161/ijaers/3.11.17 *ISSN: 2349-6495(P) | 2456-1908(O)*

Design Analysis Fabrication and Testing of Progressive Air Suspension Strut

Ajinkya Bhonge[1], Sunnel Daniel[2], Saurabh Bhandare[3], Kaushal Joshi[4]

[1]Department of Mechanical Engineering, LTCOE, Mumbai University, India

Abstract—*Ride comfort and adjustability has always been deprived on low budget suspensions. The main problems faced in the current market shocks are that, they being heavy and having no adjustability. There should be a way to provide the masses with a highly efficient shock absorber for a very low price. The project aims to provide the reader an ideal way to design, analyze, simulate and manufacture a non-conventional shock absorber having adjustability in the ride parameters.*

Keywords—Venturi effect, Damping, Air as Spring, Adjustable, Serviceability.

I. INTRODUCTION

Suspension is the system of tires, tire air, springs, shock absorbers and linkages that connects a vehicle to its wheels and allows relative motion between the two. Suspension systems serve a dual purpose — contributing to the vehicle's road holding/handling and braking for good active safety and driving pleasure, and keeping vehicle occupants comfortable and a ride quality reasonably well isolated from road noise, bumps, vibrations, etc. These goals are generally at odds, so the tuning of suspensions involves finding the right compromise. It is important for the suspension to keep the road wheel in contact with the road surface as much as possible, because all the road or ground forces acting on the vehicle do so through the contact patches of the tires.

The job of a car suspension is to maximize the friction between the tires and the road surface, to provide steering stability with good handling and to ensure the comfort of the passengers. In this article, we'll explore how car suspensions work, how they've evolved over the years and where the design of suspensions is headed in the future.

II. PURPOSE

The main purpose of an automobile is to transport man, his livestock, machinery and equipment from one place to other. This transport has to be done with utmost care as the ride has to be safe and smooth to reduce fatigue on the in transit goods, people and also on the automobile as road shocks can cause collateral damage to the automobile parts as well as human body joints and spine. Hence there is a need to eliminate such road shocks and make the ride less bumpy.

III. PROBLEM STATEMENT

The suspension systems that are currently used in most automobiles have steel springs to store the energy and hydraulic oil passes through shims to damp these oscillations.These springs made of steel are heavy and increase the unsprung mass, the characteristics of the spring remain same irrespective of road profiles. The longitudinal length of these struts are huge and there is no adjustability until the strut is unmounted from the vehicle and the spring has been replaced. This job was tedious and requires a professional hence it consumes time, increases cost and hence is not a feasible idea as the ride parameters cannot be changed in real time.

Ethereal suspension strut combines air and hydraulic oil in a single assembly wherein the air acts in spring and being naturally progressive in nature and has the capability to store energy. Hydraulic oil passes through the orifice where the velocity and pressure of the oil changes and damps the oscillation. Changing the amount of air in gas chamber changes the stiffness of the suspension and by simple clicks on the knob the damping can be changed as it varies the area of the orifice.

IV. WORKING

1. Air as Spring-

1.1.Breakaway Force:-When a spring is compressed, it exerts a force against whatever is compressing it. This is called a breakaway force. In order to further compress the spring, the breakaway force must be overcome.

https://dx.doi.org/10.22161/ijaers/3.11.17 *ISSN: 2349-6495(P) | 2456-1908(O)*

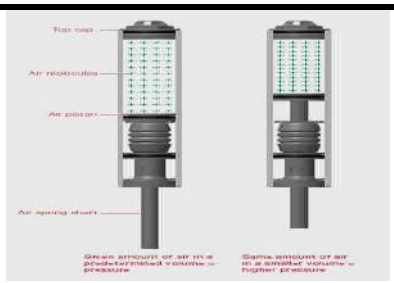

Fig.1:- Air Springs Sectional View

1.2. Breakaway force in an air spring

Pressurized air in a chamber creates force against all surfaces inside the chamber. The force acting against the piston creates a breakaway force. Because of this, an air spring can feel firm at the beginning of the stroke, similar to a preloaded coil.

1.3. Preload

A coil spring at rest is not under pressure and creates no break away force. Preloading a coil spring compresses the spring without initiating stroke. This results in a breakaway force and stiffer spring feel.

1.4. Air Spring

An air spring is the result of a sealed chamber filled with air that has one or more of the chamber walls able to move in and out of the chamber. In suspension, the moving wall is called the air piston. During the compression stroke, the air piston presses against the air as it moves into the chamber. The amount of air molecules in the chamber remains the same but the volume of the chamber is reduced. The result is an increase of air pressure in the chamber. Any air pressure creates a proportional amount force against the piston, opposing the force pushing the piston into the chamber. Pressure in an air spring is determined by the ratio of air in the chamber and the volume of the chamber. The pressure at any point in the stroke can be calculated by using the overall length of the air chamber and the air pressure at top out as a baseline; the percentage of change is the result of the amount of piston movement through the length of the air chamber. For example: Take an air chamber that is four inches long and pressurize it to 100 psi. Move the piston into the air chamber two inches. This reduces the volume of the air chamber by 50%, which doubles the pressure. The remaining chamber length is two inches. Move the piston into the chamber one inch. This reduces the remaining volume of the air chamber by 50%, which doubles the pressure again. Continue to repeat this process of reducing the volume by half and doubling the pressure. The result is an exponential increase in air pressure throughout the stroke.

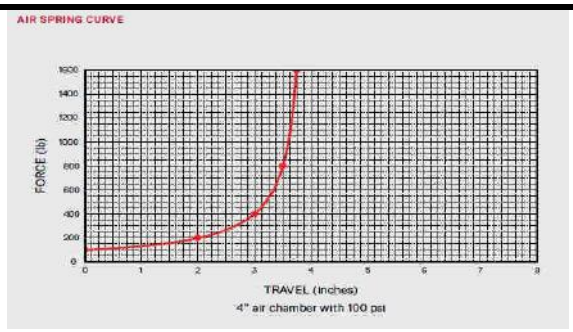

Fig 2:-Air Spring curve- Force vs Travel

1.5. Pressure vs. force

A common misconception is that the pressure in an air chamber is equal to the amount of force required to initiate compression. A simple way to think about the relationship between input forces and spring pressure is to look at a common way that pressure is expressed, pounds per square inch. In this case, pounds is a measure of force and square inches is a measure of the surface area of the piston. By determining the area of the piston surface, taking into account any curvature of the surface, and dividing the force by the result, the amount of pressure required to counter the force can be calculated as follows : Pressure = Force/area

2. DAMPING

2.1. Damping- is an influence within or upon an oscillatory system that has the effect of reducing, restricting or preventing its oscillations. In physical systems, damping is produced by processes that dissipate the energy stored in the oscillation. Examples include viscous drag in mechanical systems, resistance in electronic oscillators, and absorption and scattering of light in optical oscillators. Damping not based on energy loss can be important in other oscillating systems such as those that occur in biological systems.

The damping of a system can be described as being one of the following:

Over damped ($\zeta > 1$)

The system returns (exponentially decays) to equilibrium without oscillating. When $\zeta > 1$, the system is *over-damped* and there are two different real roots.

Critically damped ($\zeta = 1$)

The system returns to equilibrium as quickly as possible without oscillating. When $\zeta = 1$, there is a double root γ (defined above), which is real. The system is said to be *critically damped*. A critically damped system converges to zero as fast as possible without oscillating (although overshoot can occur).

Underdamped ($0 \leq \zeta < 1$)

The system oscillates (at reduced frequency compared to the *undamped* case) with the amplitude gradually

https://dx.doi.org/10.22161/ijaers/3.11.17 *ISSN: 2349-6495(P) | 2456-1908(O)*

decreasing to zero. Finally, when $0 < \zeta < 1$, γ is complex, and the system is *under-damped*. In this situation, the system will oscillate at the natural damped frequency ω_d, which is a function of the natural frequency and the damping ratio.

Undamped

The system oscillates at its natural resonant frequency (ω_o) without experiencing decay of its amplitude.

V. METHODOLOGY

1. Problem definition.

The problem of the suspension was noted down and the bump force and cornering force was calculated. The basic consideration was that the vehicle of 300kg is moving over a bump of 8 inches at a speed of 60 kmph. Accordingly the ride parameters were set. The amount of forces acting on the suspension was calculated and the gas pressures were noted.

2. Calculation for spring rate.

The spring ratio was calculated at all pressures and the pressure was noted down depending on the ride parameters needed viz. soft or hard. For off road terrains the suspension needs to be soft and the pressure of gas tube was calculated, for perfect tar and cement concrete roads the suspension needs to be hard so that it can work at high speeds and the pressure was calculated.

3. Calculation for volumn ratio.

The volume ratio was calculated for the required travel of 6 inches and the volume inside each of the tubes was calculated. Through this the diameter of the tubes and the length of the tubes were calculated keeping the eye to eye length as constant. the basic physical dimension of the strut was hence derived.

4. Market survey.

Market survey for standard size bearings and seals was done so that they could be readily available at cheap rates at common stores around the locality. Standard size helps to finalize the physical dimension of the components as having to order a nonstandard part increases cost and also increases lead time of the production.

5. Designing.

- Based on available bearing and seals (viz. v-groove seal, viper seal) sizes design the inner diameter of the central housing, the outer diameter of the gas tube was designed.
- From outer diameter of gas tube was assumed and a suitable wall thickness and conclude the inner diameter of the gas tube.
- Based on standard available size of piston seal, the piston grove was designed for the piston. The outer diameter of the piston seal should be compatible with inner diameter of gas tube.
- From the inner diameter of gas tube the basic dimensions for orifice was derived.
- Using the inner diameter of central housing the outer diameter for the oil tube was derived.
- The inner diameter of oil tube was found to be greater than the outer diameter of gas tube.
- The outer diameter for oil tube should be the driving dimension for the bottom cap
- The outer diameter for gas tube should be the driving dimension for the top cap
- Use the dimension of standard radial bearing to derive the hole size on the cap.
- Based on the size of bolt to be used to mount the suspension, the spacers for both ends were designed.
- Using the newly achieved dimension verify the strut travel through the volume ratio, if the travel is approximately 6 inches then finalize the dimensions.

6. CAD modelling

Use computer aided tools such as Solidworks® to model these dimension using the standard procedure depending on the modelling software being used.

7. CAE

Import the cad model into an analytical software, here Ansys® to check

A. effect of internal pressure on the tube
B. thermal effect on the tubes
C. effect of forces on the threads

On achieving satisfactory results confirm all dimensions

8. Simulation

Using the newly achieved dimensions calculate the spring rate and check all ride parameters on Lotus®

9. Drafting

Create a 2D sketch of all components which would include all basic views and an isometric view. Provide necessary tolerance where ever required.

10. Procurement

Procure the raw materials for all components keeping a minimum of 2 mm clearance to remove quality and to bring proper finishing to components. The test certificate of each material is to be collected from suppliers. Procure all the standard components required for assembling the suspension strut.

11. Manufacturing

- Using the 2D drawings start the manufacturing process.

https://dx.doi.org/10.22161/ijaers/3.11.17 *ISSN: 2349-6495(P) | 2456-1908(O)*

- Turn the components on lathe and achieve a proper finish on the components. after threading the components check for proper fit.
- Honing process is to be carried out on the inner surface of the gas tube.
- The outer surface of the gas tube has to be ground.
- Mill the top and bottom caps post turning.
- Drill the top and bottom caps to incorporate the radial bearing.
- Machine the piston as per drawings.
- The orifice is a critical part and has to be dealt with utmost care.
- Mill the inner surfaces at angles to facilitate the movement of the shims.
- Conduct a quality check on all the parts

12. SUB-ASSEMBLY

Assemble the orifice together and screw the two parts.
Fix all bearings and seals to their respective positions.
Screw the valve on the top cover

13. Assembly

- Cap the oil tube securely and apply liquid sealant between threads.
- Fill the oil tube with oil to the predetermined level.
- Screw the orifice to the tube and insert the gas tube into the oil tube.
- Put the piston into the gas tube and open the bleed port.
- Bleed out all the air in the oil and seal the bleed port.
- Screw the top cap on gas tube.
- Fill in air through the valve at a predetermined pressure.
- Place the inserts

14. ON Road Testing

Mount the suspension strut on the vehicle and it is ready to race.

VI. RESULTS

1. THREAD ANALYSIS:-

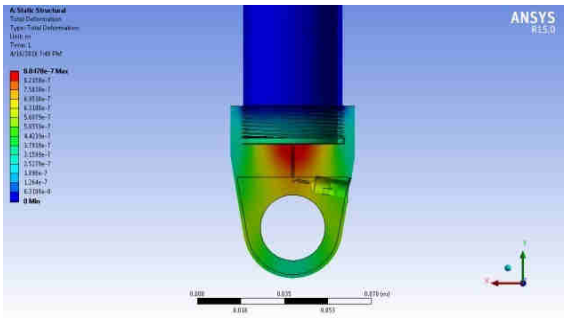

Fig.3 : Deformation

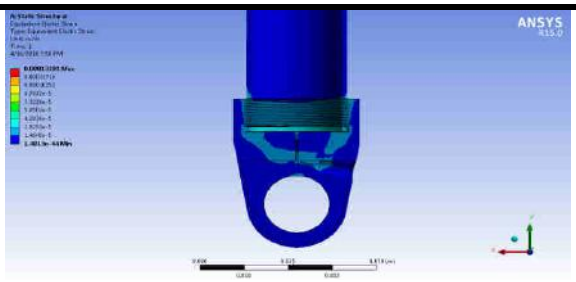

Fig.4 : Equivalent Elastic Strain

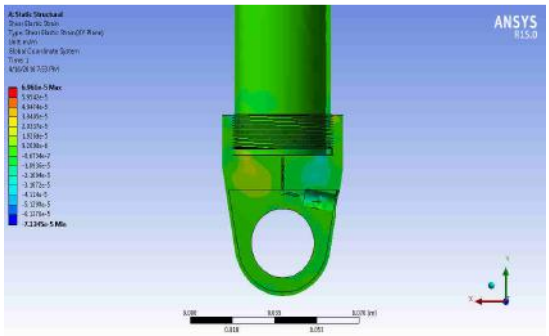

Fig.5 :Equivalent Stress

2. FATIGUE ANALYSIS:-

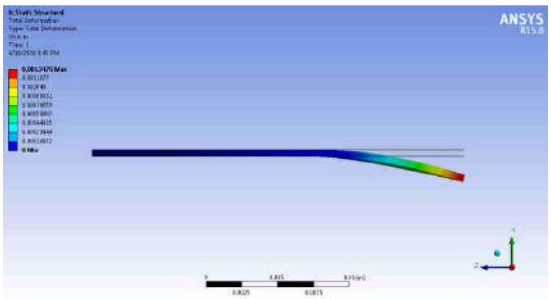

Fig 6 :Deformation

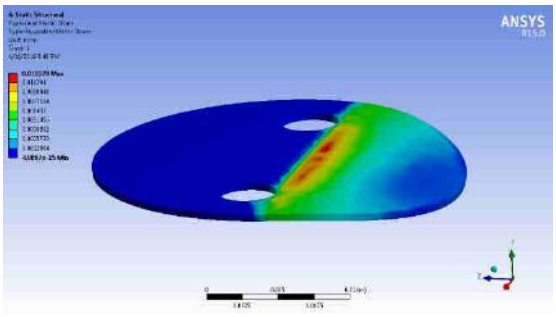

Fig.7 :Elastic Strain

https://dx.doi.org/10.22161/ijaers/3.11.17 *ISSN: 2349-6495(P) | 2456-1908(O)*

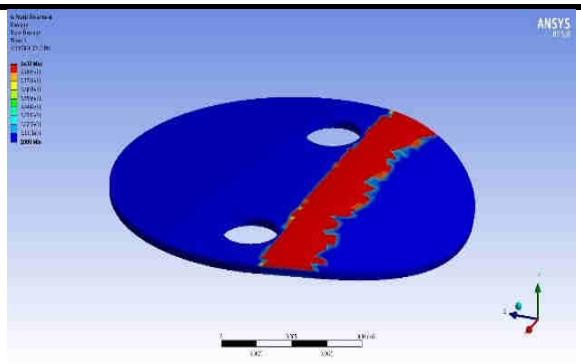

Fig.8 : Life

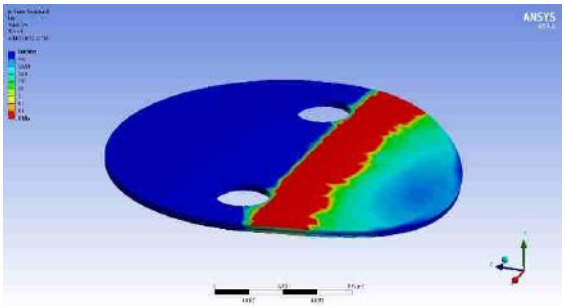

Fig.9 : Damage

3. FLUID SOLID INTERFACE:-

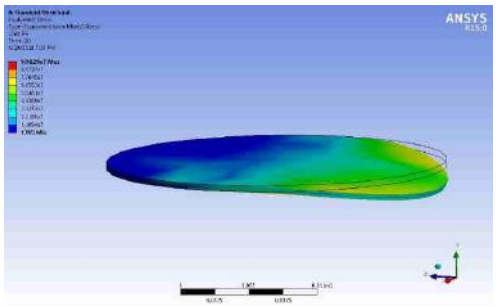

Fig.10 : Total Deformation

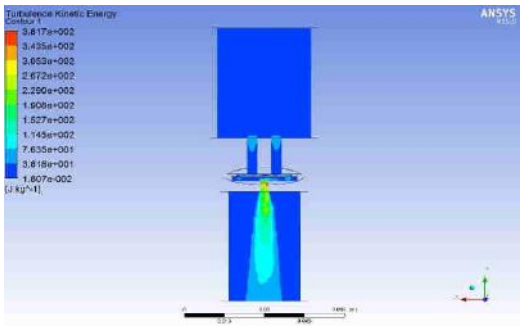

Fig.11 : Pressure

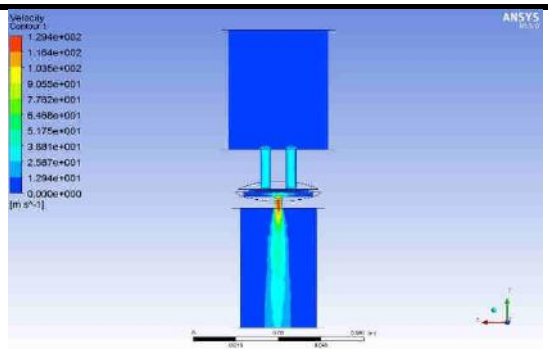

Fig.12 : Velocity

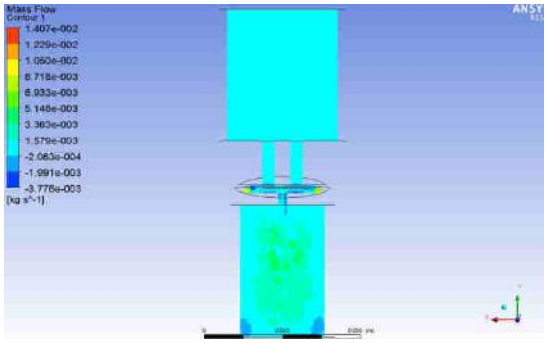

Fig.13 : mass flow rate

4. STATIC ANALYSIS:-

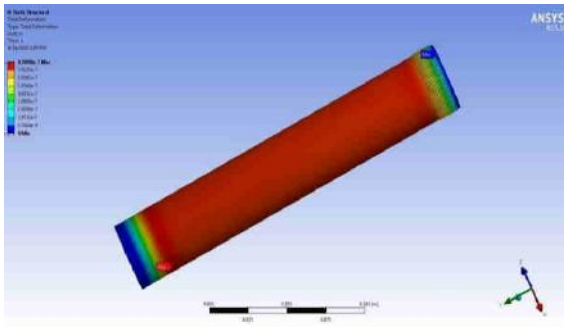

Fig.14 :Déformation

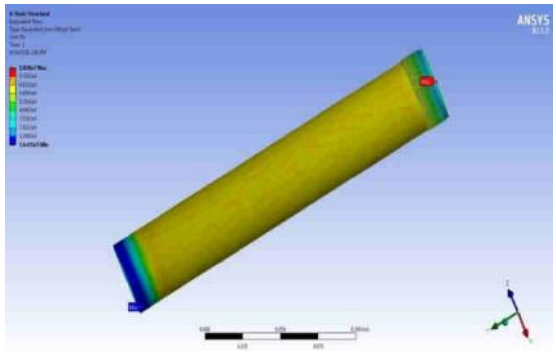

Fig.15 :Stress

https://dx.doi.org/10.22161/ijaers/3.11.17 *ISSN: 2349-6495(P) | 2456-1908(O)*

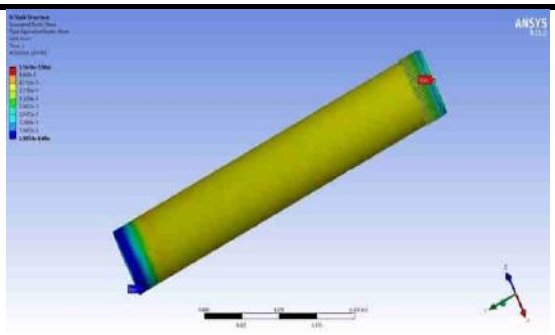

Fig.16:Strain

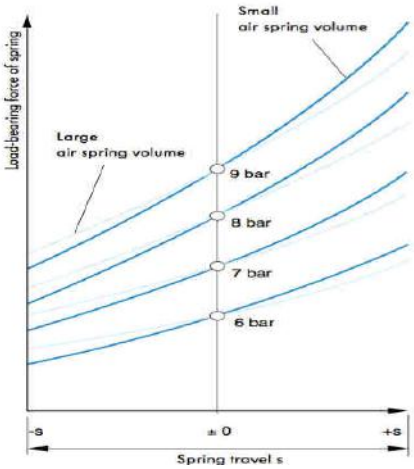

Fig.17:Déformation

Input	Input	Input
Mass, m[kg]=	100	Kg
Damper Travel, x[m]=	0.0700	M
Time taken, s[sec]=	5	S
Coefficient of damping, c[Ns/m]	350.16	Ns/m

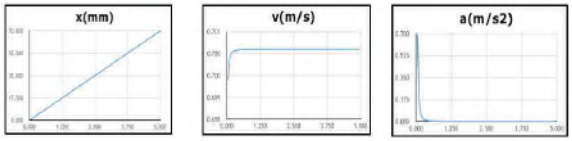

Fig.18 : Load result

Input	Input	Input
Mass, m[kg]=	2	Kg
Damper Travel, x[m]=	0.1200	M
Time taken, s[sec]=	4.5	S
Coefficient of damping, c[Ns/m]	351.06	Ns/m

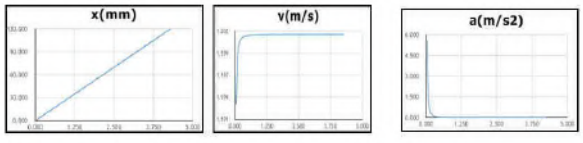

Fig.19 : Load result

Input	Input	Input
Mass, m[kg]=	3	Kg
Damper Travel, x[m]=	0.1540	M
Time taken, s[sec]=	3.7	S
Coefficient of damping, c[Ns/m]	352.73	Ns/m

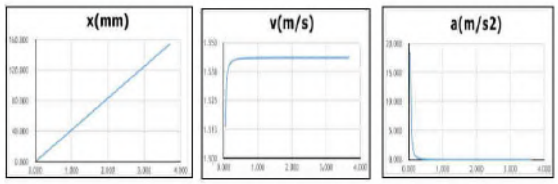

Fig.20 : Load result

VII. CONCLUSION

1. Adjustability

Ethereal shocks have a very high level of adjustability. A few clicks on the knob and Ethereal is ready to pounce on the track. The simple aim that any common person should be able to adjust the ride parameters has been achieved.

2. Low cost

An upgrade to Ethereal shocks cost merely one fifth of the cost of most available after market suspensions offered in the global market. Being low in cost Ethereal hasn't compromised on the quality and safety aspects and it has raised the standards for comfort and drivability.

3. Light weight

F=m x a. This law clearly brings to light that lower the mass of the vehicle higher the acceleration of the car. Ethereal has come out with a light weight and highly efficient solution into one of the major weight defaulter. Ethereal weighs under 2 Kilograms which is 7 times lighter than the conventional steel spring suspension which in any ways has no susceptibility to adjustability.

4. Serviceability

Ethereal shocks are an assembly of simple components and has no component fastened to each other by permanent mechanical connections. Each component is fastened through threads and the service time for Ethereal is minimal. It takes under 12 minutes to assemble a complete Ethereal strut from stage scratch.

VIII. FUTURE SCOPE

The quest to improve and rise each day never ends. By the addition of sensors the strut can adapt to the road conditions. The next generation Ethereal shocks will be equipped with sensors that would read the road conditions and understand the terrain, calculate the spring and damper parameters and adjust accordingly. Depending on the terrain it would also increases or decreases the riding height of the vehicle.

https://dx.doi.org/10.22161/ijaers/3.11.17 *ISSN: 2349-6495(P) | 2456-1908(O)*

By adding a few extensions in the orifice rebound adjustability can be achieved.

Few more designs incorporations are aimed and when achieved would make the ride quality even more self-indulgent. The new add ones would provide adjustability in the bounce and jounce characteristics.

REFERENCES

[1] Mohamed EssamShalabi, Ahmed I. Abdel-Aziz and Nabila ShawkyElnahas, "Performance of Automotive Air Suspension Control System" , International Journal of Engineering Research & Technology (IJERT), ISSN: 2278-0181, Vol. 4 Issue 09, September-2015

[2] Mark R. Easter , "Adjustable rate air spring" US patent 5413316 A, May 9, 1995

[3] Shubham Dhar Dwivedi , AK Akshay , SaurabhShrivastav , GajendraPadwa, "Study of Dependency of Temperature on Kinematic Viscosity for Blended Oils" , International Journal of Engineering Research & Technology (IJERT), ISSN: 2278-0181, Vol. 4 Issue 10, October-2015

[4] Tod Johnson, Andrew Tarshis, George Goldberg, "Market survey data collection method" US patent 4355372 A ,Oct 19, 1982

[5] William E. Howard, Joseph musto, "Introduction to Solid Modeling Using Solid Works 2012" ,ISBN:0073402443

[6] M. Aravind ,Dr. S. Periyasamy, "Optimization of Surface Grinding Process Parameters By Taguchi Method And Response Surface Methodology " ,International Journal of Engineering Research & Technology (IJERT), ISSN: 2278-0181 ,Vol. 3 Issue 5, May - 2014

[7] B. Praveen kumar, P. Sampath Rao, " Investigation on Reduction in Premature Failure of Locomotive Coil Springs" , International Journal of Engineering Research & Technology (IJERT), ISSN: 2278-0181 ,Vol. 3 Issue 9, September- 2014

International Journal of Advanced Engineering Research and Science (IJAERS) *[Vol-3, Issue-11, Nov- 2016]*
https://dx.doi.org/10.22161/ijaers/3.11.18 *ISSN: 2349-6495(P) | 2456-1908(O)*

Numerical Analysis of Crosss Flow Hydokinetic Turbine by Using Computational Fluid Dynamics

Prashant Gunai, Ajinkya Bhonge, Kaushal Joshi

LTCOE, University Of Mumbai, India

Abstract*—The invention of cross flow turbine industry from straight blades of the Darrieus turbine was modified by Alexander Gorlov into helical shape. There have been several research projects dealing with the design and analysis for tidal applications. This paper deals with the Numerical analysis of a cross flow hydrokinetic turbine (CFHT) with helical blades. Static analysis with optimum blade velocity and constant pressure conditions was performed for the blade with fixed pitch by using Computational Fluid Dynamics (CFD) in Fluent 15. Solidworks was used to carry out 3D modeling of the turbine. The hydrofoil shape of NACA 0018 was created by the airfoil coordinate database. Two different turbulence models Spalart-Allmaras (One-Equation model) and sst-k (Two –Equation model) were employed to compute and compare the results. Pressure profiles, drag and lift coefficients are calculated under a steady flow of 1.5 m/s.*

Keyword—Naca0018, hydrofoil, Spalart-Allmaras, sst-k, CFHT.

I. INTRODUCTION

Cheap and efficient manner is the main motive of today's generation of electricity in every country. Each country develops the best possible method of electricity and renewables have become the primary source
of power generation with the rapid consumption of conventional fuel. The flow potential of water currents in rivers, oceans, estuaries is thus studied as an immaculate and environmentally amiable source. Hydroelectricity is electricity produced from hydropower. In 2015 hydropower generated 16.6% of the world's total electricity and 70% of all renewable electricity, and was expected to increase about 3.1% each year for the next 25 years. There is a huge demand renewable form of energy. Gorlov turbine provides that alternative. Turbine rotates at twice speed as of water flow and in the same direction independent of water flow direction. The turbine is can be operated horizontally and vertically that reduces its construction and can be used widely in any open water flow along with shaft and generator arrangement. Hydrokinetic turbines are in early stage of developed on the reference of wind turbine theory.
The NACA 0018 hydrofoil used as the blade profile is symmetric and has an 18% width-to-thickness ratio. This symmetrical hydrofoil shape helps in balancing the forces generated during the rotation of the turbine, as the direction of forces changes after 180º of rotation. Static analysis refers to velocity, pressure, shear stress distribution, turbulent kinetic energy. Present work highlights the design and analysis for a model of helical blade cross flow turbine (CFHT). The analysis was done for a model of height 1500 mm, 4 bladed turbine with 58.49º inclination angle. Pressure contours, drag and lift coefficient are calculated under a steady flow of 1.5 m/s using CFD solver fluent 15. CFD simulations do not need any external data (experimental lift & drag) and can include separation from foils and drag induces vortices from turbine's shaft. CFD modeling is a powerful tool for complex geometries. However, CFD simulations for tidal turbines still suffer from high computational cost and time, thus it is very important to analyze the problem first. We have solved till 200 iterations for each turbulent model independently. When a blade rotates, its angle of attack (α) (angle between local relative velocity and chord) changes leading to variable hydrodynamic forces. Spalart-Allmaras model is a one equation model which solves a transport equation for a viscosity like variable ν. This may be referred to as the Spalart-Allmaras variable. The SST k-ω turbulence model is a two-equation eddy-viscosity model which has become very popular. The shear stress transport (SST) formulation combines best of two worlds. The use of a k-ω formulation in the inner partsof the boundary layer makes the model directly usable all the way down to the wall through the viscous sub-layer. The SST formulation also switches to a k-ε behavior in the free-stream and thereby avoids the common k- ω problem that the model is too sensitive to the inlet free-stream turbulence properties.
Figure 1 shows orientation of the hydrofoil geometry at different positions and angles.

https://dx.doi.org/10.22161/ijaers/3.11.18 *ISSN: 2349-6495(P) | 2456-1908(O)*

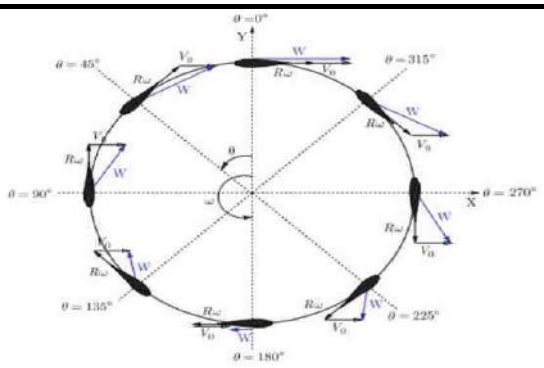

Fig.1: Turbine Positioning

II. CAD MODEL AND MESHING DETAILS OF THE TURBINE

The helical profile of the turbine blade was created using the data points obtained from UIUC Airfoil Coordinate database. A reference model, a spherical channel was created and the continuum used is water. The CAD model is shown in figure 2 and the details of the geometry are mentioned in Table 1

Fig.2: 3D CAD model

In figure '3' turbine is placed inside the channel which was developed in ANSYS 15 workspace .It is used as a duct through which water at normal atmospheric conditions will flow, thus water act as a continuum

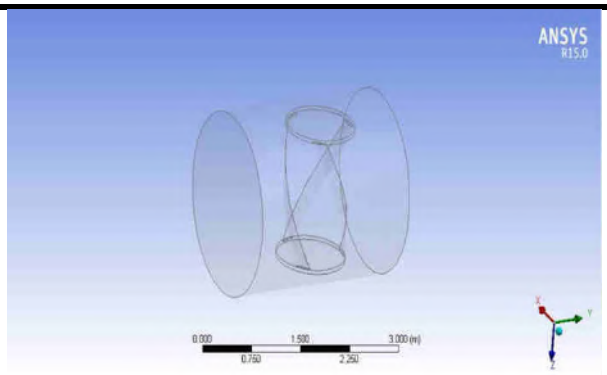

Fig.3: Turbine inside the channel

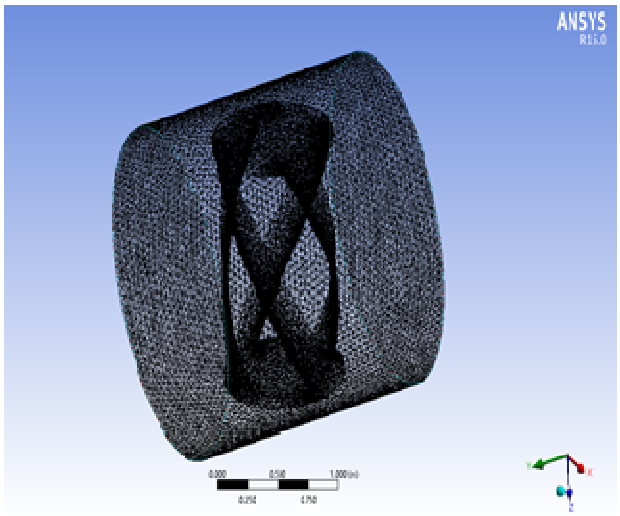

Fig.4: Meshing of the turbine

The CAD model of the turbine consists of four helical blades, two circular plates each 50mm thick and a central shaft that would be coupled with generator. The meshing was done with fine relevance center as shown in fig. 4. The meshed model consists of 3, 27, 697 nodes and 2, 48, 341 elements. The sweep in the helical blade geometry is given by the inclination angle which is a measure of inclination of the blade with respect to the horizontal plane. In general, the close the inclination angle is to 90º the better is the efficiency of the turbine**.**

Table.1: Blade and turbine parameters

S. No	Turbine Parameter	Magnitude
1	Blade profile	NACA0018
2	Number of blades, N	4
3	Chord length, c	274.889mm

https://dx.doi.org/10.22161/ijaers/3.11.18 *ISSN: 2349-6495(P) | 2456-1908(O)*

4	Diameter	1000mm
5	Height of turbine	1500mm
6	Inclination angle	58.49º
7	Aspect ratio (A.R)	1.5
8	Solidity Ratio (σ) for 4 blade	0.35
9	Plate thickness	50mm

III. MATERIAL PROPERTIES AND BOUNDARY CONDITIONS

There are a wide variety of materials by which turbine blades are manufactured. We have considered 5086 marine grade aluminum, primarily alloyed with magnesium. It has good corrosion resistance properties and it has a density of 2,660 kg/m3 slightly less dense than aluminum. Boundary conditions employed in computations consists of a constant velocity inlet of 1.5 m/s on left side, a constant pressure outlet of 104268 Pa on right, wall conditions include no slip condition at the bottom surface and zero shear stress condition at the free channel surface with 5 % turbulent intensity.

IV. CFD ANALYSIS AND FLUENT SETT INGS

Computational Fluid Analysis (CFD) is a branch of fluid mechanics that deals with numerical simulation methods and makes use of different algorithms to solve and analyze the fluid flow problems. Fluent requires various settings like pressure velocity coupling, discretization schemes and relaxation factors. These important parameters are mentioned in Table 2

Table.2: Simulation parameters

Pressure-Velocity Coupling	**SIMPLE**
Discretization of Gradient	Green Gauss Node Based
Discretization of Pressure	Second Order
Discretization of Momentum	Second order Upwind
Discretization of Turbulent Kinetic Energy	Second order Upwind
Discretization of Specific Dissipation Rate	Second order Upwind
Pressure Under-relaxation Factor	0.2
Momentum Under-relaxation Factor	0.6

V. RESULTS AND DISCUSSION

The Residuals curves, Pressure profiles, drag coefficient and lift coefficient curves for turbine are evaluated using Fluent 15 solver. It is clearly evident from fig.6 and fig.7 that coefficient of lift (Cl) converges towards zero with increasing number of iterations for both the turbulent models the reason being that the hydrofoil NACA0018 has zero camber i.e. it is symmetrical thus it generates zero lift at zero angle of attack.

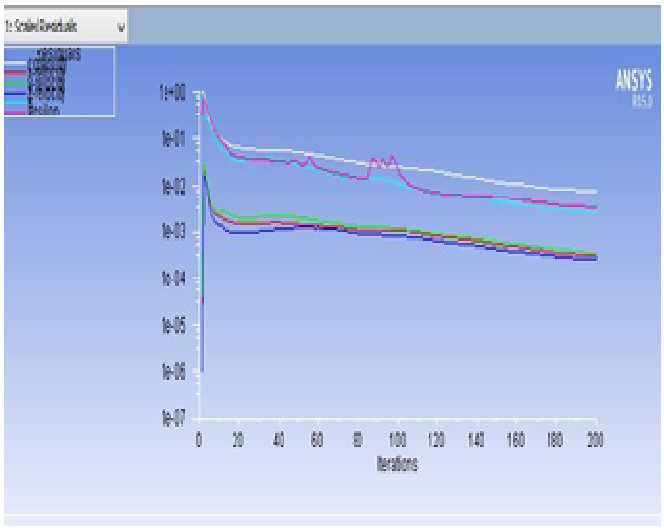

Fig.5: Scaled residuals

The scaled residuals curve shows that the solution obtained is converging to exact solution and after nearly 20 iterations the curve is constant showing very small variation in the obtained solution

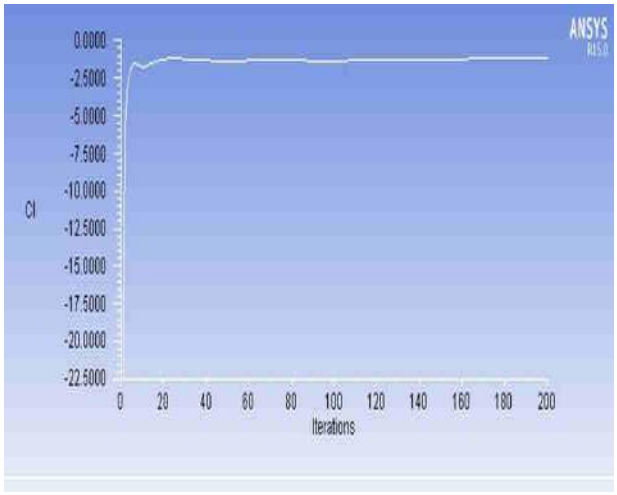

Fig.6: Coefficient of Drag (Cd) convergence

https://dx.doi.org/10.22161/ijaers/3.11.18 *ISSN: 2349-6495(P) | 2456-1908(O)*

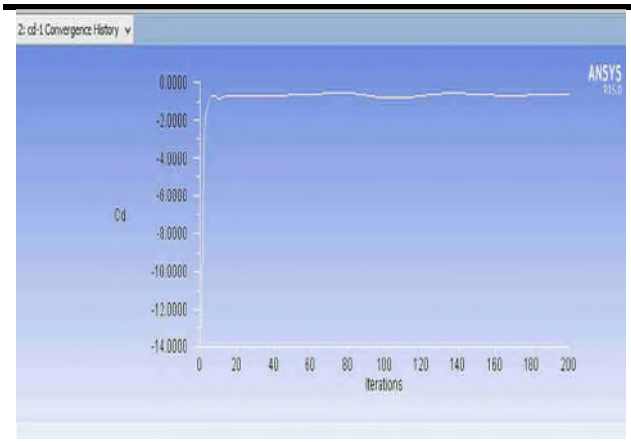

Fig.7: Coefficient of Lift (Cl) convergence

Red region in figure.8 and figure.12 shows areas of maximum pressure region and similarly blue region shows profile of minimum pressure region. The results which states that the maximum pressure region in a turbine is along the thicker side and minimum pressure region is along the leading edge of the blade.

5.2. SST-k_ model plots

The following results are for SSTequations to find the approximate results. The results are similar to that were obtained by Spalart model.

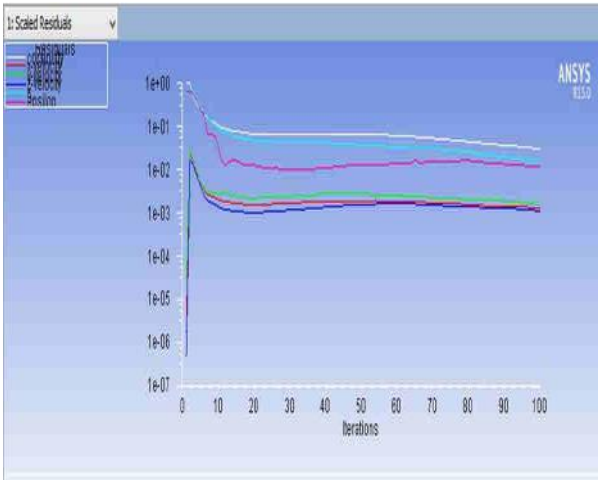

Fig.8: scale residual

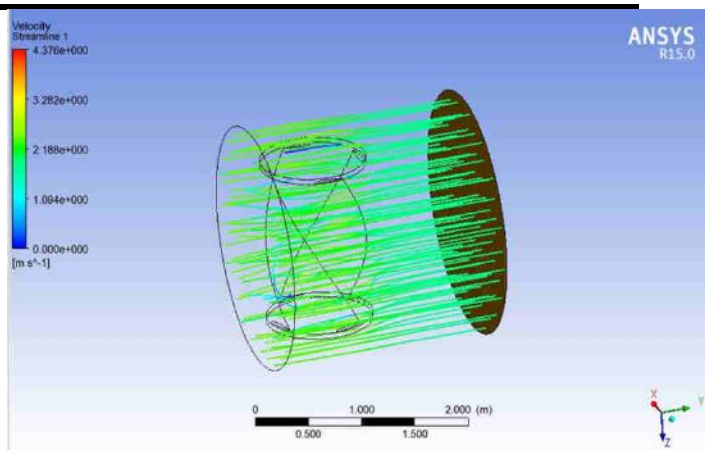

Fig.9: Velocity distribution

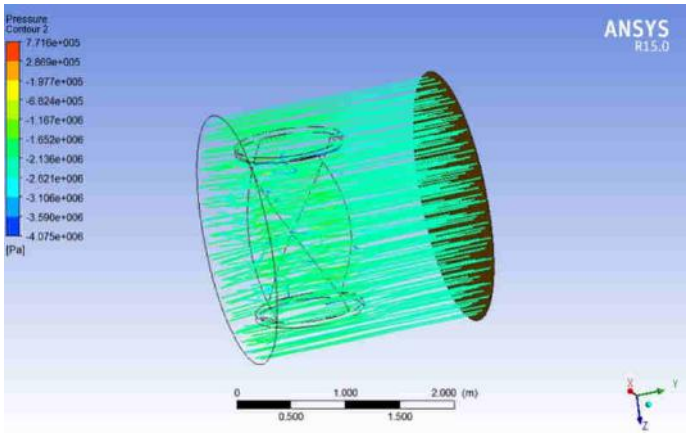

Fig.10: Pressure Distribution

Figure 9 & 10 represents velocity and pressure distribution of the water particle along the path. It also gives range of maximum velocity and pressure to minimum.

VI. CONCLUSION

The current work illustrate the simulation of pressure distribution around cross flow hydrokinetic turbine using CFD tool fluent 15, including underlying turbulence of fluid flow and also the viscous effects, without using tabulated drag and lift data. The primary objective of this research work was to develop an understanding of the pressure variation and profiles for the CFHT, as because of the limited literature available, this makes it very useful for novice in this field. The results obtained from both the models shows similar pressure variation and drag and lift convergence curves and are in accordance with the literature surveyed. India has many perennial and seasonal rivers with huge hydropower potential; installing such turbines in place of conventional turbines will not only

https://dx.doi.org/10.22161/ijaers/3.11.18 *ISSN: 2349-6495(P) | 2456-1908(O)*

reduce project cost but will help prevent destructions of forests and villages. Also the paper draws attention to a new method of hydropower generation which doesn't require construction of large dams and tunnels to store energy.

REFERENCES

[1] Oliver Paish, "Small hydro power: technology and current status", Renewable and Sustainable Energy Reviews 6 (2002)537–556
[2] Energy Alternatives India(EAI), http://www.eai.in/ref/ae/hyd/hyd.html
[3] http://www.gcktechnology.com/GCK/pg2.html
[4] Taylor Jessica Hall: Numerical simulation of a marine crossflow hydrokinetic turbine, University of Washington, (2012)
[5] Adam L. Niblick: Experimental and Analytical Study of Helical Cross-Flow Turbines for a Tidal Micropower Generation System, University of Washington, (2012)
[6] M.R. Castelli and E. Benini. Effect of Blade Inclination Angle on a Darrieus Wind Turbine. Journal of Turbomachinery-Transactions of the ASME, 134(3), (2012).
[7] http://airfoiltools.com/airfoil/details?airfoil=naca0018-il
[8] Menter: Zonal Two Equation kappa-omega Turbulence Models for Aerodynamic Flows (1993)

International Journal of Advanced Engineering Research and Science (IJAERS) *[Vol-3, Issue-11, Nov- 2016]*
https://dx.doi.org/10.22161/ijaers/3.11.19 *ISSN: 2349-6495(P) | 2456-1908(O)*

A Secured File Store in Cloud Environment Using Hierarchy Attribute-Based Encryption

M.Kiruthika[1], R.Mohanabharathi[2]

[1]PG Scholar, Department of Computer Science and Engineering, Selvam College Of Technology, Namakkal, India
[2]Assistant Professor, Department of Computer Science and Engineering, Selvam College Of Technology, Namakkal, India

Abstract—*Cloud Computing(CC) has been envisioned as the next production architecture of Information Technology (IT)Enterprise. In contrast to accepted solutions, anywhere the IT services are under proper physical, logical and personnel controls.CC moves the application software and databases to the max data centers, where the organization of the data and services may not be fully dependable. With CC and storage services, data is not only stored in the cloud, but routinely shared among a max number of users in a group. In this project, Hierarchy Attribute-Based Encryption(HABE) scheme is proposed for shared data with large groups in the cloud. Hash signatures are used to compute verification information on shared data, so that the authority is able to audit the correctness of shared data, but cannot reveal the identity of the signer on each block. Hash signature and Keys are generated by hierarchical access tree .Implementation of auditing scheme to perform efficient public to protect both identity and data privacy in cloud environments. Also users can access the data from data owner through cloud provider in real time dynamic cloud environment.*

Keywords—cloud data, cloud authority, security, cloud storage, auditing strategy.

I. INTRODUCTION

CC is an emerging technology which provider a lot of opportunities for online sharing of resources or services. One of the fundamental advantages of CC is pay-as you-go pricing model, where customers pay only according to their usage of the services. Cloud Computing is an internet oriented computing.

Fig.1: CC Architecture

It dynamically delivers all as a service over the internet base and on user demand, such as network, storage, operating system, hardware, software and resources. These are cloud services types:

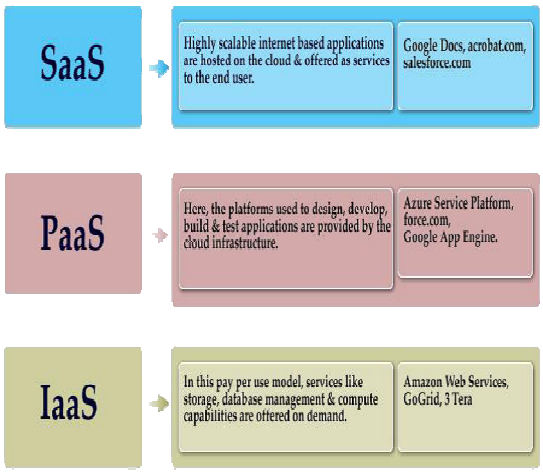

Fig.2: CC Services

https://dx.doi.org/10.22161/ijaers/3.11.19 *ISSN: 2349-6495(P) | 2456-1908(O)*

1.1 Software as a Service In this model, a full application is to be had to the customer, as a service on demand. Alone instance of the service runs on the cloud & multiple end users are serviced. On the patron's side, there is no need for open investment in servers or software license, while for the provider, the costs are lower, since only a single request needs to be hosted & maintained. Today SaaS is offered by company such as Google, Salesforce, Microsoft, Zoho, etc.

1.2 Platform as a Service Here, a layer of software or development environment is encapsulated & accessible as a service, upon which other top level of service can be built. The purchaser has the freedom to build his own application, which process on the provider's infrastructure. To meet manageability and scalability supplies of the applications, PaaS provider present a predefined group of OS and application servers, such as LAMP platform (Linux, Apache, MySql and PHP), Ruby etc. Google's App Engine, Force.com, etc are some of the popular PaaS examples.

1.3 Infrastructure as a Service IaaS provides basic resources and computing capability as standardized services over the network. Servers, storage space systems, networking equipment, data centre space etc. are shared and made available to handle workloads. The client would classically install his own software on the infrastructure. Some general examples are Amazon, GoGrid, 3 Tera, etc.

CC is application as three types such as Public, Private and Hybrid Clouds.

Public Cloud

Public clouds are owned and operate by third party; they distribute superior economies of range to patrons, as the infrastructure costs are reach among a mix of users, giving each character client an beautiful low-cost, "Pay-as-you-go" model. All clients share the same infrastructure pool with limited pattern, security protections, and ease of use variances. These are managed and support by the cloud provider. One of the compensation of a Public cloud is that they may be better than an enterprises cloud, thus providing the ability to scale effortlessly, on demand.

Private Cloud

Private clouds are built completely for a single project. They aim to address concern on data security and offer larger control, which is naturally lacking in a public cloud. There are two variations to a private cloud using follow:

- ✓ On-premise Private Cloud
- ✓ Externally hosted Private Cloud

On-premise Private Cloud.

On-premise private clouds, also known as familial clouds are hosted surrounded by one's own data center. This model provides a more even method and protection, but is limited in aspect of size and scalability. IT department would also need to incur the capital and prepared costs for the corporal resources. This is best right for applications which need complete control and configurability of the infrastructure and defense.

Externally hosted Private Cloud

This type of personal cloud is hosted externally with a cloud provider, where the provider facilitates an exclusive cloud setting with full agreement of privacy. This is best suited for enterprise that doesn't prefer a public cloud due to giving out of physical resources.

Hybrid Cloud

Hybrid Clouds connect equally public and private cloud model. With a Hybrid Cloud, examine providers can utilize 3rd party Cloud Providers in a full or partial manner thus increasing the suppleness of computing. The Hybrid cloud environment is capable of providing on-demand, on the exterior provisioned scale. The ability to enlarge a private cloud with the wealth of a public cloud can be used to administer any unexpected surges in workload.

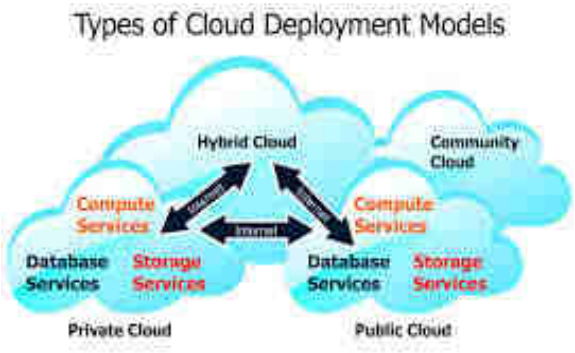

Fig.3: CC deployments

Cloud Storage system, is also recognized as Data storage as a service (DAAS), is the abstract of resources last an interface where resources can be administered on order. Cloud data resources works on distribution file systems because of its ability to handle a countless volume of data effectively. Storage can be limited or remote. Cloud computing is cost effective, safe and scalable but organization the load of random job available is a tricky work. Data ease of use means data is available when never it is request. Accessibility of data increases with augmentation in number of duplication of data. But after accomplishment a specific level of repetition, there occurs no growth in availability. So it is improved to find an optimum level of duplication. Availability and replication ratio also depends on node malfunction ratio. If failure probability is towering, more

https://dx.doi.org/10.22161/ijaers/3.11.19 *ISSN: 2349-6495(P) | 2456-1908(O)*

number of replication of that data is required. So if node breakdown ratio is less, less duplication number is necessary for maximum file availability.

CC BENEFITS

Enterprises would want to align their applications, so as to develop the architecture model that CC offers. Some of the classic benefits are listed follows:

- ✓ Reduced Cost
- ✓ Increased Storage
- ✓ Flexibility

Reduced Cost

There are a number of reasons to attribute Cloud technology with lesser costs. The billing model is pay as per usage; the infrastructure is not purchase thus lower maintenance. Initial cost and recurring fixed cost are much inferior than traditional computing.

Increased Storage

With the huge Infrastructure that is offered by Cloud provider today, storage & continuance of large volumes of data is a reality. Impulsive workload spike are also managed successfully & efficiently, since the cloud can scale dynamically.

Flexibility

This is an enormously important quality. With enterprises have to adapt, even more rapidly, to varying business conditions, speed to deliver is significant. Cloud computing stresses on getting application to market very rapidly, by using the majority appropriate building blocks compulsory for deployment.

II. LITERATURE SURVEY

2.1 Bethencourt J et al.[1] complex access control on encrypted data that is called as Cipher text-Policy Attribute-Based Encryption. By using these techniques encrypted data can be kept congenital even if the storage server is unfrosted; moreover, our methods are privacy against complexity attacks. Previous Attribute-Based Encryption systems used attributes to describe the encrypted data and built policy into user's keys while in our system attributes are used to describe a user's commendation and a revelry encrypting data determines a rule for who can decrypt. Thus, our methods are theoretically closer to traditional access manage methods such as Role-Based Access Control (RBAC). In addition, we provide an implementation of our system and give performance capacity

2.2 Goyal V et al.[2] In an ABE system, a user's keys and cipher texts are label with sets of descriptive attribute and a fastidious key can decrypt a particular cipher text only if there is a competition between the attribute of the cipher text and the user's key. The cryptosystem of Shay and Waters allowed for decryption when at least *k* attributes overlap between a cipher text and a private key. While this primitive was shown to be useful for error liberal encryption with biometrics, the lack of impressibility seems to limit its applicability to larger systems. In our cryptosystem, cipher texts are labeled with sets of attribute and private keys are connected with contact structure that manage which cipher texts a user is intelligent to decrypt. We disclose the applicability of our structure to sharing of audit log data and broadcast encryption. Our structure supports delegation of private keys which subsume Hierarchical Identity-Based Encryption (HIBE).

2.3 Joseph K. Liu et al.[4] In a fine-grained two-factor access control protocol for web-based cloud compute services, using a trivial security device. The device has the following properties:

(1) It can compute some light algorithms, e.g. hash and exponentiation; and

(2) It is tamper resistant, i.e., it is assumed that no one can smash into it to get the secret information stored inside.

With this device, our protocol provides 2FA privacy. First the user secret key (which is more often than not stored inside the computer) is required. In addition, the security device should be also coupled to the computer (e.g. through USB) in order to authenticate the user for access the cloud. The user can be granted access only if he has both items. Furthermore, the user cannot use his secret key with another device belong to others for the access. Our protocol chains fine-grained attribute-based access which provides a great suppleness for the system to set varied access policy according to different scenarios. At the same time, the privacy of the user is also preserved. The cloud system only knows that the user possesses some required attribute, but not the real identity of the user.

2.4 Tsz Hon Yuen et al.[7] ABE only deals with authenticated access on encrypted data in cloud storage service. It is not practical to deployed in the case of access control to cloud computing service: The cloud server may encrypt a chance message using the access policy and asks the user to decrypt it. If the user can successfully decrypt the cipher text, it is allowed to access the cloud computing service. Although this approach can fulfill the requirement, it is highly inefficient. In this new idea, a user can validate him/herself to the cloud calculate server incognito. The server only knows the user acquire some necessary attribute, yet it does not be common with the identity of this user. In supply a k-times edge for anonymous access control. That is, the member of staff serving at table may limit a meticulous

https://dx.doi.org/10.22161/ijaers/3.11.19 *ISSN: 2349-6495(P) | 2456-1908(O)*

set of user (i.e., person's users with the same set of quality) to access the system for a maximum k-times within a period or an event. Further other access will be denied. We also prove the privacy of our instantiation. Our success result shows that our scheme is practical.

2.5 Liang K et al.[3] To achieve more flexibility on re-encryption, many variants have been proposed Proxy Re-Encryption(PRE), Identity-Based PRE (IBPRE), and Attribute-Based PRE (ABPRE). CPRE allows an encryption connected with a condition to be converted to a new cipher text tagged with a new form. The technologies of IBPRE and ABPRE are rather similar, and a main difference between them is ABPRE enjoys more expressiveness in data sharing. Furthermore, the above encryption is allowed to be misshapen to another cipher text associated with a new string by a semi trusted proxy to whom a re-encryption key is agreed. Nonetheless, the proxy cannot gain access to the underlying plaintext. This new ancient can increase the flexibility of users to delegate their decryption rights to others. We also prove it as fully chosen cipher text secure in the standard model.

III. SYSTEM ARCHITECTURE

CC service provider requires a system which can handle a large number of requests at a time. For processing the huge cloud of requests for data access permission, services need to be very available. System keeps many copies of the blocks of data on different nodes by duplicate. A large number of replication strategies for management of replicas have been implemented in traditional system. As a result of replication, data replications are stored on different data nodes for high consistency and ease of use. Replication factor for each data block and replica placement sites need to be determined at first. In existing support data can be lost so in this paper propose improved secure perform in ABE to protect the data from loss. It present efficient constancy as a service model, where a group of data owners that compose service provider can verify whether the data cloud update the data or not and design user function table to change status of split files with different metrics and proposed in fig 1

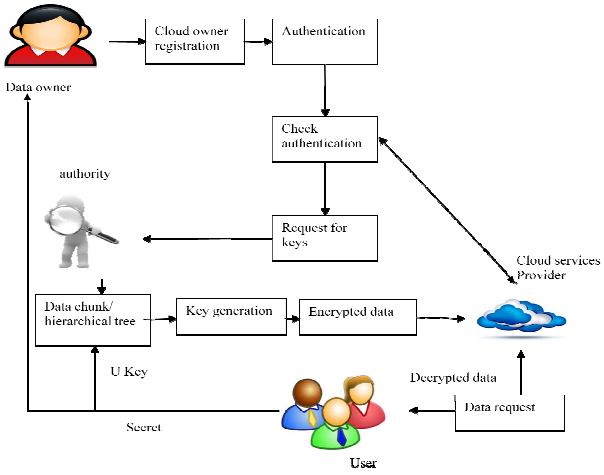

Fig.4: Improved Framework

IV. INDENTATIONS AND EQUATIONS

4.1 Setup ()

The setup algorithm take as input a privacy parameter λ and a small universe description U= {1, 2, 3…, ℓ}. It first runs G (λ) to obtain (p,G,G_T ,e), where G and and G_T are cyclic groups of prime order . It then chooses g,u,v,d ∑ G,and α,a ∑ Z_p^* uniformly at random,for each attribute i ∑ U. It chooses a random value Si ∑ Z* p and a collision-resistant hash function H:G⟶ Z_p^*,the public parameters PK = (G, G_T ,e,g,u,v,d,g^a , e(g, g)$^\alpha$,$T_i = g^{si}$ ∀ i ,H). It outputs a master public key and master secret key MSK= α.

4.2 KeyGen ()

The key generation algorithm randomly picks t ∑ Z* p

$K = g^\alpha g^{at}$

$K_o = g^t$

$K_i = T_i^t \ \forall\ i \in s$

It outputs a transformation key and decryption key.

4.3 Encrypt ()

The encrypt algorithm use the public parameters, message and access structure. Access structure consists of attributes and their mapping.

$$C = u^{H(M)} v^{H(M)} d$$
$$C_1 = M.e(g.g)^{\alpha s}$$
$$C_1^{'} = g^s$$
$$C_{1,i} = g^{a,A_i,v} T^{-r1,i} \rho(i)$$
$$D_{1,i} = g^{r1,i} \ \forall\ i \in \{1,2,\dots,1\}$$
$$C_2 = M.e(g.g)^{\alpha s}$$
$$C_2^{'} = g^s$$
$$C_{2,i} = g^{a,A_i,v} T^{-r2,i} \rho(i)$$
$$D_{2,i} = g^{r2,i} \ \forall\ i \in \{1,2,\dots,1\}$$

It output a cipher texts CT as,

Encrypted data CT=$((A, \rho), \hat{c}, C_1, C_1^{'}, C_{1,i}, D_{1,i}, C_2, C_2^{'}, C_{2,i}, D_{2,i})$

https://dx.doi.org/10.22161/ijaers/3.11.19 *ISSN: 2349-6495(P) | 2456-1908(O)*

4.4 Transform ()

This algorithm will generate the transformed cipher text. This algorithm takes as input the public parameters PK, cipher text CT, and the transformation key TKs to generate the transformed cipher text CT'. It send the transformed cipher text to the user.

$$T_1' = [e(c_1', \frac{K'}{[(\prod_{i\in I}(e(C_{1,i}, K_0').\, e(K'_{\rho(i)}, D_{1,i}))^{\omega i})}]$$

$$= [e(g,g)^{\alpha s/z} e(g,g)^{ats/z} / [\prod_{i\in I}(e(g,g)^{atAi.v\omega i/z}$$

$$= e(g,g)^{\alpha s/z}$$

$$T_2' = [e(c_2', \frac{K'}{[(\prod_{i\in I}(e(C_{2,i}, K_0').\, e(K'_{\rho(i)}, D_{2,i}))^{\omega i})}]$$

$$= [e(g,g)^{\alpha s'/z} e(g,g)^{ats'/z} / [\prod_{i\in I}(e(g,g)^{atAi.v'\omega i/z}$$

$$= e(g,g)^{\alpha s'/z}$$

4.5 Decrypt ()

Decrypt algorithm uses the public parameters, transformed cipher text, and decryption key. PK = $(G, G_T, e, g, u, v, d, g^a, e(g,g)^{\alpha}, T_i = g^{si} = g \forall i, H)$

CT=$((A,\rho), \hat{c}, \hat{c}, C_1, C_1', C_{1,i}, D_{1,i}, C_2, C_2', C_{2,i}, D_{2,i}, i)$

CT' = $(T=C, T_1 = C_1, T_1', T_2' = C_2, T_2')$.

RKs = z

4.6 Hierarchical Tree Algorithm

We present an implementation of the hierarchical tree algorithm on the individual time step algorithm (the Hermits scheme) for collision N-body simulations, running on GRAPE-9 system, a special future hardware accelerator for gravitational various body simulations. Such combination of the tree algorithm and the individual time step algorithm was not simple on the prior GRAPE system mainly as its recollection addressing scheme was limited only to sequential access to a full set of unit data. The present GRAPE-9 system has an indirect memory address unit and a particle memory big adequate to store all particle data and also tree nodes data. The indirect memory address unit stores dealings lists for the tree algorithm, which is construct on host computer, and, according to the contact lists, force pipelines calculate only the connections necessary. In our implementation, the interaction calculations are appreciably reduced compared to direct N^2 summation in the original Hermit scheme. For example, we can archive about a factor 30 of speedup (equivalent to about 17 teraflops) against the Hermits scheme for a simulation of $N=10^6$ system, using hardware of a peak speed of 0.6 teraflops for the Hermits scheme.

V. CONCLUSION & FUTURE WORK

In this paper, we currently enable data reliability proof and constancy services over multi cloud system using ABE which helps in informative violation as much as possible. The cloud reliability model and local auditing, global auditing that helps user to confirm the cloud service provider (CSP) provide the promised constancy or not and count the severity of the violations. Therefore system monitor consistency service model as well as level of data uploads which helps the user to get the data in updated version. User can recognize various sub servers in CSP. It is a considered to provide regular update mechanism to confirm fragments simply and provide the data to users after updation only.

REFERENCES

[1] J.Bethencourt, A.Sahai, and B.Waters, "Ciphertext-policy attributebased encryption," IEEE Symposium on Security and Privacy, pp. 321– 334, May 2007.

[2] V.Goyal, O.Pandey, A.Sahai, and B. Waters, "Attribute-based encryption for fine-grained access control of encrypted data," Proceedings of the 13th ACM conference on Computer and communications security, pp. 89–98, October 2006.

[3] K. Liang, M. H. Au, J. K. Liu, W. Susilo, D. S. Wong, G. Yang, T. V. X. Phuong, and Q. Xie, "A DFA-based functional proxy re-encryption scheme for secure public cloud data sharing," IEEE Transactions on Information Forensics and Security, vol. 9, no. 10, pp. 1667–1680, October 2014.

[4] J. K. Liu, M. H. Au, X. Huang, R. Lu, and J. Li, "Fine-grained twofactor access control for web-based cloud computing services," IEEE Transactions on Information Forensics and Security, vol. 11, no. 3, pp. 484–497, March 2016.

[5] A. Sahai and B. Waters, "Fuzzy identity-based encryption," Advances in Cryptology–EUROCRYPT, pp. 457–473, May 2005.

[6] X. Xie, H. Ma, J. Li, and X. Chen, "An efficient ciphertext-policy attribute-based access control towards revocation in cloud computing,"Journal of Universal Computer Science, vol. 19, no. 16, pp. 2349–2367,October 2013.

[7] T. H. Yuen, J. K. Liu, M. H. Au, X. Huang, W. Susilo, and J. Zhou, "ktimes attribute-based anonymous access control for cloud computing," IEEE Transactions on Computers, vol. 64, no. 9, pp. 2595–2608, September 2015.

International Journal of Advanced Engineering Research and Science (IJAERS) *[Vol-3, Issue-11, Nov- 2016]*
https://dx.doi.org/10.22161/ijaers/3.11.20 *ISSN: 2349-6495(P) | 2456-1908(O)*

Performance Analysis of Genetic Algorithm with PSO for Data Clustering

G.Malini Devi[1], M.Lakshmi Prasanna[2], Dr.M.Seetha[3]

[1]Asst.Professor, Department of CSE, G. Narayanamma Institute of Technology and Science, Hyderabad,
[2]M. Tech Student, Department of CSE, G. Narayanamma Institute of Technology and Science Hyderabad,
[3]Professor and HOD, Department of CSE, G. Narayanamma Institute of Technology and Science, Hyderabad,

Abstract*—Data clustering is widely used in several areas like machine learning, data mining, pattern recognition, image processing and bioinformatics. Clustering is the process of partitioning or grouping of a given set of data into disjoint cluster. Basically there are two types of clustering approaches, one is hierarchical and the other is partitioned. K-means clustering is one of the partitioned types and it suffers from the fact that that it may not be easy to clearly identify the initial K elements. To overcome the problems in K-means Genetic Algorithm (GA) and Particle Swarm Optimization (PSO) techniques came into existence. A Genetic Algorithm (GA) is one of hierarchical approach and can be noted as an optimization technique whose algorithm is based on the mechanics of natural selection and genetics. Particle Swarm Optimization (PSO) is also one of the hierarchical search methods whose mechanics are inspired by the swarming. The PSO algorithm is simple and can be developed in a few lines of code whereas GAs suffers from identifying a current solution but good at reaching a global region. Even though GA and PSO have their own set of strengths they have weaknesses too. So a hybrid approach (GA-PSO) which combines the advantages of GA and PSO are proposed to get a better performance. The hybrid method merges the standard velocity and modernizes rules of PSOs with the thoughts of selection, crossover and mutation from GAs. A comparative study is carried out by analyzing the results like fitness value and elapsed time of GA-PSO to the standard GA and PSO.*

Keywords*—*Clustering, GA-PSO, Genetic Algorithm, Particle Swarm Optimization.

I. INTRODUCTION

Clustering is a technique that is used to partition elements in a data set such that similar elements are grouped to same cluster while elements with different properties are grouped to different clusters as shown in “Fig 1” [7]. Clustering is a popular approach for automatically finding classes, concepts, or groups of patterns [4]. The reason behind clustering a set of data is to get a well structured data and expose this structure as a set of groups. It is used to perform efficient search of elements in a data set and is particularly effective in multi-dimensional data that may be otherwise difficult to organize in an effective manner. Such data is typically represented in the form of a floating-point number. We cannot use sorted arrays to search as they are multidimensional nature of data.

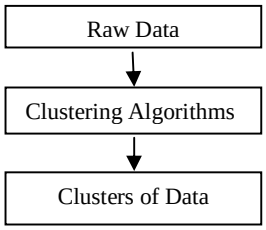

Fig.1: Clustering process.

Hash tables cannot be used because we may want to retrieve an item that is closest in properties to a specified item when the specified item does not exists in the data set. Clustering provides an elegant solution to this problem while providing a fast search capability for the same. Clustering widely used in areas like data mining [6, 9] image processing.

Most clustering algorithms belong to two groups: hierarchical clustering and partitioned clustering [3]. One of the partitioned clustering techniques in the literature is the K-means clustering method In this technique, clustering is based on the identification of K elements in the data set that can be used to create an initial representation of clusters[4]. These K elements form the cluster seeds. The remaining elements in the data set are then assigned to one of these clusters. Even though the method seems to be straightforward, it suffers from the fact that it may not be easy to clearly identify the initial K elements. To overcome

https://dx.doi.org/10.22161/ijaers/3.11.20 *ISSN: 2349-6495(P) | 2456-1908(O)*

the problem of partitioned clustering various heuristic algorithms have been proposed in the literature surveyed such as Genetic Algorithm (GA), and Particle Swarm Optimization (PSO) [8].

GA is one of the hierarchical clustering algorithms and is inspired by biological system's improved fitness through evolution [7]. Genetic algorithms are based on three operations selection, crossover and mutation. It evolves a population of chromosomes representing potential problem solutions encoded into suitable data structures. Genes holds a set of values for the optimization variables[12]. To simulate the natural survival of the fittest process, best chromosomes exchange information (through crossover or mutation) to produce offspring chromosomes. The offspring solutions are then evaluated and used to evolve the population if they provide better solutions than weak population members. Usually, the process is continued for a large number of generations to obtain a best-fit (near optimum) solution.

The particle swarm optimization (PSO)[10] is a kind of optimization tool based on iteration, and the particle has not only global searching ability, but also memory ability, and it can be convergent directionally [1]. PSO is based on the behavior of a flock of migrating birds trying to reach an unknown destination. In PSO, each solution is a 'bird' in the flock and is referred to as a 'particle'. A particle is analogous to a chromosome (population member) in GAs. Physically, birds looks in a specific direction (towards their destination) and during their communication, they identify the bird that is in the best location. Accordingly, each bird speeds towards the best bird using a velocity that depends on its current position. PSO algorithm had basic three steps, namely, generating particles' positions and velocities, velocity update, and finally, position update. Each bird investigates the search space from its new local position, and the process repeats until the flock reaches a desired destination.

The proposed GA-PSO algorithm combines the features of both GA and PSO. It takes both the stability of the genetic algorithm and the local searching capability of Particle Swarm Optimization. The result proves that this method outperformed the GA and pure PSO in clustering efficiency.

II. LITERATURE SURVEY

2.1 Genetic Algorithm:

Current knowledge and many successful experiments suggest that the application of GAs is not limited to easy-to-optimize unimodal functions this work was proposed by Emmanuel Sarkodie Adabor *et al* (2012). The method Asymmetric key Encryption using Genetic Algorithm proposed by Poornima G.Naik ,Girish R. Naik *et al* (2013), describes an attempt to exploit the randomness involved in crossover and mutation processes for generating an asymmetric key pair for encryption and decryption of message. Tung-Kuan Liu, Yeh-Peng Chen and Jyh-Horng *et al* (2014) Chou says that Over time, the traditional single-objective job shop scheduling method has grown increasingly incapable of meeting the requirements of contemporary business models.

2.2 Particle Swarm Optimization:

Chuang *et al* (2012), suggest fresh particle swarm optimization (CPSO) algorithms that discover the best SNP arrangement for cancer connection studies containing seven SNPs. Marinakis *et al* (2013), this introduce a fresh algorithmic environment inspired techniques that uses a hybridized Particle Swarm Optimization algorithm with a fresh neighborhood topology for effectively solving the Feature Selection Problem (FSP). Akhshabi *et al* (2014), propose a particle swarm optimization (PSO) based on Memetic Algorithm (MA) that hybridizes with a local look for technique for work out a no-wait flow scheduling difficulty.

2.3 GA-PSO:

Optimal location management in mobile computing with hybrid Genetic algorithm and particle swarm optimization was proposed by Lipo Wang and Guanglin Si *et al* (2012). Priya I. Borkar and Leena H. Patil *et al* (2013) present a model of hybrid Genetic Algorithm -Particle Swarm Optimization (HGAPSO) for Web Information Retrieval. Yue-Jiao Gong, Jing-Jing Li, Yicong Zhou *et al* (2015) proposed that social learning in particle swarm optimization (PSO) helps collective efficiency, whereas individual reproduction in genetic algorithm (GA) facilitates global effectiveness.

III. GENETIC ALGORITHM [GA]

Genetic Algorithms are based on the concepts of natural selection and natural evaluation techniques [1]. Through reproduction genetic algorithm (GA) represents the evolution and improvement of life, when each individual holds its own genetic information through which a new one with fitness to the environment and more surviving chances is build. It is an iterative process and the evolution usually starts from a population of randomly generated individuals. The fitness of every individual in the population is evaluated at each generation; the fitness depicts the value of the objective function in the optimization problem being solved. The individuals are selected from the current

https://dx.doi.org/10.22161/ijaers/3.11.20 *ISSN: 2349-6495(P) | 2456-1908(O)*

population which is having best fitness value, and a new generation is formed modifying each individual's genome.

The fitness value of each individual is computed by the following fitness function. The fitness value is the sum of the intra-cluster distances of all clusters. This sum of distance has a profound impact on the error rate.

Fitness =∑ | Xj - Zi | , i=1,…., K j=1,……,n

Where *K* and *n* are the numbers of clusters and data sets, respectively. *Zi* is the cluster center at point *i* and *Xj* is the cluster for data point *j*.

The new individuals are formed using three genetic operators selection, crossover, and mutation. In selection individuals are selected based on their fitness value to generate offspring. The crossover aim of this mechanism was swapping to yield better fitness. Mutation increases the diversity and additional modifications increase the population [2]. These new offsprings are then used in the next iteration of the algorithm. Termination of the algorithm is occurred when either a maximum number of generations have been produced, or a satisfactory fitness level has been reached for the population. The flow steps of genetic algorithm for finding a solution of a given problem may be summarized as follows.

01: Begin
02: t=0
03: Initialize population P (t)
04: Evaluate fitness of each particle
05: t=t+1
06: If termination criterion occurs go to step 11
07: Select P (t) from P (t-1)
08: Crossover P (t)
09: Mutation P (t)
10: Go to step 4
11: Best output
12 Next generation until stopping criterion
13: End

The Genetic Algorithm consumes more CPU time. Here the CPU time is total time required to optimize a complete dataset by undergoing all the three operations like selection, crossover and mutation. As the algorithm is containing many operations to be done it requires more.

IV. PARTICLE SWARM OPTIMIZATION [PSO]

PSO was originally designed and introduced by Eberhart and Kennedy [6]. The PSO is a population search algorithm where each individual, called particle, within the swarm is represented by a vector in a multidimensional search space. A velocity vector is assigned to each particle to determine the next movement of the particle. Each particle updates its velocity based on the current velocity, best personal position it has explored so far and the global best position explored by the swarm [2]. The fitness function used to in this technique is as follows.

Fitness =∑ | Xj - Zi | , i=1,…., K j=1,……,n

Where *K* and *n* are the numbers of clusters and data sets, respectively. *Zi* is the cluster center at point *i* and *Xj* is the cluster for data point *j*.

Each particle is updated by following two "best" values at every generation. The first one is the best solution that has been achieved so far. This value is called *pbest*. Another "best" value which is tracked by the particle swarm optimizer is the best value, obtained so far by any particle in the population. This value is a global best solution and called *gbest* [5]. After finding the two best values (*pbest* and *gbest*), the particle updates its velocity and position using the equations (1) and (2):

v(k+1) = *w* v(k) + c1 r1 (pbest(k) – pr(k)) + c2 r2 (gbest(k)- pr (k))….. (1)

pr(k+1) = pr(k) + v(k+1)…. (2)

where v(k) is the particle velocity; pr(k) is the current particle (solution) at the kth generation; r1 and r2 are two independent random numbers c1 and c2 are constants called acceleration coefficients; c1 controls the attitude of the particle of searching around its best location and c2 controls the influence of the swarm on the particle's behavior, and *w* is a constant known as inertia factor. Generally, the procedure for this algorithm is summarized as follows:

01: Begin
02: Initialize particles
03: While (number of iterations, or the stopping criterion is not met)
04: Evaluate fitness of each particle
05: For *n* = 1 to number of particles
06: Find *pbest*
07: Find *gbest*
08: For *d* = 1 to number of dimension of particle
09: Update the velocity and position of particles by equations (1) and (2)
10: Next *d*
11: Next *n*
12 Next generation until stopping criterion
13: End

The time taken to complete all the operations with a given number of iteration is known as CPU time. The PSO technique can execute a dataset with a satisfactory fitness value in less CPU time as the algorithm is simple and

https://dx.doi.org/10.22161/ijaers/3.11.20 *ISSN: 2349-6495(P) | 2456-1908(O)*

contains a very less operations like only updating the velocities current positional values.

V. HYBRID GENETIC ALGOTITHM WITH PSO [GA-PSO]

PSO often locates nearly optimal solutions at a fast convergence speed, but fails to adjust its velocity step size to continue optimization in the binary search space, which leads to premature convergence. In contrast, research has shown that genetic algorithms (GA) can adjust its mutation step size dynamically in order to better reflect the granularity of the local search area. However, GA suffers from a slow convergence speed. Although GAs have been successfully applied to a wide spectrum of problems, using GAs for large-scale optimization could be very expensive due to its requirement of a large number of function evaluations for convergence [11]. Therefore, hybrid GA-PSO has been proposed to overcome those problems and combine advantages of PSO and GA [13]. The basis behind this is that such a hybrid approach is expected to have merits of PSO with those of GA. One advantage of PSO over GA is its algorithmic simplicity. The idea behind GA is due to its genetic operator's crossover and mutation. The idea of combining GA and PSO is not new [5]. By applying crossover operation, information can be swapped between two particles to have the ability to fly to the new search area. Therefore, in our proposed hybrid GA-PSO, the crossover operation is also included, which can improve the diversity of individuals. Generally, the procedure for this algorithm is summarized as follows:

01: Begin
02: Initialize particles
03: While (number of iterations, or the stopping criterion is not met)
04: Evaluate fitness of each particle
05: For n = 1 to number of particles
06: Find *pbest*
07: Find *gbest*
08: Apply crossover and mutation operations
09: For d = 1 to number of dimension of particle
10: Update the velocity and position of particles by equations (1) and (2)
11: Next d
12: Next n
13 Next generation until stopping criterion
14: End Initialization

This hybrid approach consumes more CPU time because it need to perform all the operations of GA including the operations of PSO. But the fitness values generated by GA-PSO are more satisfactory than the other two approaches.

VI. EXPERIMENTAL RESULTS

In this section the three different optimization techniques are used to cluster ten different data sets and the results of GA-PSO are compared with standard GA and PSO algorithms in term of elapsed time and optimal fitness values. For the comparison purpose the stopping criteria that is number of maximum generations is taken same for all the three algorithms. Each algorithm will run 100 times.

Table.1: Results comparisons with Optimal Fitness Value

Datasets	**GA**	**PSO**	**GA-PSO**
Breast Cancer	1.90E+02	-154.3372	-185.9505
Concrete	1.49E+04	-122.7247	-147.2694
HayesRoth	8.233	-185.9505	-186.7039
HeartDisease	3.13E+04	-186.7309	-186.7039
Lung Cancer	5.34E+00	-122.8209	-144.3609
Seeds	-5.36E+00	-154.3372	-185.9003
Wine	1.87E+05	-28.885	-107.8089
Data	1.13E+04	-186.7309	-186.7309
Diabetic	1.33E+07	-184.4576	-185.6309
DataScience	2.01E+02	-185.1554	-185.1554

For the above Table 1 we can consider diabetic dataset as a best example because the GA-PSO can produce an optimized result than the other two and DataScience dataset is not performing well while using it with GA-PSO.

Table.2: Results comparisons with Time

Datasets	**GA**	**PSO**	**GA-PSO**
BreastCancer	32.560091	31.476014	48.668747
Concrete	31.573397	31.190026	31.452406
HayesRoth	31.254429	31.254429	32.744419
HeartDisease	49.111702	33.659704	51.12346
LungCancer	31.674727	31.453808	31.631851
Seeds	32.046989	31.816387	31.757602
Wine	32.956209	31.484516	32.359612
Data	169.634856	37.381394	140.483837
Diabetic	438.7682	224.48307	916.528801
DataScience	9797.553331	1592.40601	10876.302102

The above Table 2 stores the CPU time taken to complete the optimization for a dataset. Even though the GA-PSO gets the best optimized value it consumes more time.

VII. CONCLUSION

PSO works efficiently on large datasets by minimizing the time, utilizing the less parameter and gives the better

https://dx.doi.org/10.22161/ijaers/3.11.20 *ISSN: 2349-6495(P) | 2456-1908(O)*

performance than the GA by forming effective clusters. Proposed Hybrid (GA+PSO) methodology enhances the better performance results by incorporating the faster convergence and high computational speed than the individual comparison. The results show that the Hybrid of PSO and GA algorithms provides a performance that is significantly superior to that of other algorithm for these data sets. Genetic algorithm and particle swarm optimization are greatly related to their inherent parallel characteristics, both algorithms perform the function with a group of randomly created population, both have a fitness rate to calculate the population. PSO methodology is observed for document clustering limitation. It is found that the document clustering problem is successfully tackled with PSO methodology by optimizing for clustering process. A most useful advantage of the PSO is its capacity to cope with local optima by maintain, recombining and evaluation numerous candidate solutions concurrently. The Hybrid GA-PSO algorithm merges the capability of fast convergence of the PSO algorithm with the competence of ease to exploit preceding solution of GA for eliminating the early convergence.

REFERENCES

[1] Atul Garg, Dimple Juneja "A Comparison and Analysis of various extended Techniques of Query Optimization" *International Journal of Advancements in Technology, Vol. 3, No. 3, July 2012, ISSN 0976-4860, Page No.184-194.*

[2] Dr. Arvinder Kaur and Divya Bhatt "Hybrid Particle Swarm Optimization for Regression Testing" *International Journal on Computer Science and Engineering (IJCSE), Vol. 3, No. 5, May 2011, ISSN 0975-3397, Page No.1815-1824.*

[3] E. Mehdizadeh, S. Sadi-nezhad and R. Tavakkoli-Moghaddam "Optimization of fuzzy clustering criteria by a Hybrid PSO And Fuzzy C-Means clustering algorithm" *Iranian Journal of Fuzzy Systems, Vol. 5, No. 3, 2008, Page No. 1-14.*

[4] K. Premalatha "A New Approach for Data Clustering Based on PSO with Local Search" *Computer and Information Science, vol 1, No 4, November 2008, Page No.139-145.*

[5] Lipo Wang and Guanglin Si "Optimal location management in mobile computing with hybrid Genetic algorithm and Particle Swarm Optimization (GA-PSO)" *IEEE Trans. Information Theory*, vol. 39, Page No. 1877-1886.

[6] Min Chen and Simone A. Ludwig "Fuzzy Clustering Using Automatic Particle Swarm Optimizations" *IEEE International Conference on Fuzzy Systems (FUZZ-IEEE) July 6-11, 2014, Page No 1545-1552.*

[7] Navpreet Rupal 1, Poonam Kataria "Comparative Analysis of Clustering & Enhancing Classification Using Bio- Inspired Approaches" *(IJCSIT) International Journal of Computer Science and Information Technologies, Vol. 5, 2014, ISSN: 0975-9646, Page No.6453-6457.*

[8] Oluleye Babatunde, Leisa Armstrong, Jinsong Leng, and Dean Diepeveen "Comparative Analysis of Genetic Algorithm and Particle Swam Optimization: An Application in Precision Agriculture" *Asian Journal of Computer and Information Systems, Vol. 03, Issue 01, February 2015, ISSN: 2321 – 5658, Page No.1-12.*

[9] P.Vivekanandan, R. Nedunchezhian **"**A Fast Genetic Algorithm for mining classification rules in large datasets" *International Journal on Soft Computing (IJSC), Vol.1, No.1, November 2010, Page No. 10-20.*

[10] Rahul Sharma "Comparative Analysis of Clustering by using Optimization Algorithms" *(IJCSIT) International Journal of Computer Science and Information Technologies, Vol. 5, 2014, ISSN: 0975-9646, Page No. 1076-1081.*

[11] Sapna Katiyar "A Comparative Study of Genetic Algorithm and the Particle Swarm Optimization" *AKGEC International Journal of Technology, Vol. 2, No. 2, Page No: 21-24.*

[12] Sameh Bennour, Amin Sallem, Mouna Kotti, Emna Gaddour, Mourad Fakhfakh, Mourad Loulou "Application of the PSO Technique to the Optimization of CMOS Operational Transconductance Amplifiers" *International Conference on Design & Technology of Integrated Systems in Nanoscale Era, 2014, Page No 1-5.*

[13] Sundararajan S and Dr.Karthikeyan " An Hybrid Technique for Data lustering Using Genetic Algorithm with Particle Swarm Optimization" *International Journal of Advanced Research in Computer Science and Software Engineering, Volume 4, Issue 12, December 2014, ISSN: 0975-3397, Page No. 979-983.*

https://dx.doi.org/10.22161/ijaers/3.11.21 *ISSN: 2349-6495(P) | 2456-1908(O)*

Software Complexity Prediction by Using Basic Attributes

Rasha Gaffer. M. Helali

Sudan University of Science and Technology, Sudan

Abstract— *Software complexity is one of the important quality attribute that affect the success of software. Predicting such attribute is a difficult task for software engineers. Current used measures for computing complexity are not sufficient. Data mining can be applied to software data to explore useful interesting patterns. In this paper we present a simple data mining based prediction model to predict software complexity based on some basic attributes. The article starts by considering the correlation between different features that describes software code structure then selecting some of these features to be used for complexity prediction. Results reveal the ability to use branching count feature as strong predictor of complexity.*

Keywords— Software complexity, LOC, McCabe, halstead, branch count.

I. INTRODUCTION

Software complexity is "a natural byproduct of the functional complexity that the code is attempting to enable" [1]. In literature, software complexity has been defined differently by many researchers [2]. Z use defines software complexity as the difficulty to maintain, change and understand software. Others view it as difficulty to develop, test, debug and maintain [2].Therefore, no standard definition exits for the same in literature. However, knowledge about software complexity represents an indicator of development, testing, and maintenance efforts, defect rate, fault prone modules and reliability [2].With multiple system interfaces and complex requirements, the complexity of software systems sometimes grows beyond control, rendering applications overly costly to maintain and risky to enhance [1]. The complexity is affected by many factors former to software development [3]. Understanding, predicting and resolving complexity of software are critical tasks that affect the success of software.

Software complexity can be measured by Direct Measures which is also known as internal attributes and Indirect Measures which is also known as external attributes. Direct Measures are measured directly such as Cost, effort, LOC, speed, memory. Indirect Measures cannot be measured directly. Example - Functionality, quality, complexity, efficiency, reliability, maintainability [4]. The common used complexity measures are:

- The cyclomatic complexity v(G) has been introduced by Thomas McCabe in 1976.The McCabe complexity is one of the more widely - accepted software metrics, it is intended to be independent of language and language format.
- The McCabe's [5] software complexity introduces the concept of Cyclomatic Complexity. It combines the number of flow graph edges, nodes and predicate nodes to represent the complexity. The Cyclomatic Complexity of a source code is the linearly independent paths count through the source code.
- The Halstead [6] software complexity measures the complexity by counting number of operators and operands in software. It measures the software's ability to understand and estimates the effort required to develop a software algorithm. Halstead metrics are difficult to calculate and it is very hard to count the distinct and total operators and operands in a software program.
- Metrics Suite for Object Oriented Design [7] proposed by Chidambaram Kamerer to measures complexity of object oriented software based on coupling and coherence between class.

Recently, many researches focused on predicting complexity because complexity prediction can help in estimating many other quality attributes like testability and maintainability. The main goal of this paper is to build predictive model by using data mining techniques to find out which attribute/s can help predicting complexity more than others. The subsequence sections are organized as follows: section II contains what had been done in the area of complexity prediction. Section III describes the proposed predictive model and used data set. Then the following sections highlight analysis, results and validation. Finally, conclusion is presented.

II. RELATED WORK

A number of studies investigate software complexity either as attribute to be predicted or as predictor to other attributes. Software complexity commonly used as indicator to fault prone class/modules. Moreover, several studies focused on the relationship between software complexity and software reliability and maintainability. More complex software is,

https://dx.doi.org/10.22161/ijaers/3.11.21 *ISSN: 2349-6495(P) | 2456-1908(O)*

less maintainability and reliability is Usha Chhillar and Sucheta Bhasin, pointed out that there is a relationship between complexity and possibility of faults [8]. Graylin et.al.Constructed a model to find correlation between McCabe's Cyclomatic Complexity (CC) and lines of code (LOC). Their model successfully predicts roughly 90% of CC's variance by LOC alone. D. Francis Xavier Christopher and E. Chandra[9], addressed software Requirements Stability Index Metric (RSI) that helps to evaluate the overall stability of requirements and also keep track of the project status. Their study proposes Multi-criteria Fuzzy Based approach for findingOut the complexity weight based on Requirement Complexity Attributes such as Functional Requirement Complexity, Non – Functional Requirement Complexity, Input Output Complexity, Interface and File Complexity. The advantage of their model is that it is able to estimate the software complexity early which in turn predicts the Software Requirement Stability during the software development life cycle.

N. J. Pizzi et.al. [10] Investigated a computational intelligence based strategy, random feature selection, as a classification system to determine the subset of software measures that yields the greatest predictive power for module complexity. Sabharwal.et.al.In[11]discussed how to use fuzzy logic based approach to predict complexity.On the same direction M S. Dattathreya, and H Singh used Fuzzy logic techniques for developing, modeling and analyzing the software complexity prediction metric. The authors propose five non-technical factor metrics based on the current software development process to predict future Army Vehicle software complexity [3].

Some studies moved towards computing software complexity differently, Henry and Kafura [3] provide the measure of couplings between modules in terms of number of parameters, global variables and function calls. In[13] authors introduce The Entropy software complexity measure based on the average information content of each operator in a software program's source code. An attempt was made by Jingqiu Shao and Yingxu Wang [3] to models the software complexity based on the cognitive functional size of the software. Although, many studies considered software complexity, still much research is required. Above literature leads to a conclusion that we need to find a way to use current available measures of software attributes to give an indicator to how software complexity is. We describe the proposed software complexity prediction model in a step wise manner as follows:

1- Data set and feature selection
2- Find correlation between software attributes.
3- Applying data mining techniques to predict complexity.

III. COMPLEXITY PREDICTIVE MODEL

Our analysis is divided into two main steps. The first step is to determine the software attributes (metrics) that can yield acceptable predictability then find the correlation between these attributes to select the most related attributes to complexity. The second step is using the selected attributes to build prediction models. These two steps/ phaseswere presented in the following two subsections.

- **Feature selection**

The study investigates the ability to use some basic attributes that describe software code to predict its expected complexity. The features/ attributes that are suggested simply including LOC, number of operatorsand number of operands, branch count, an estimation of complexity and used programming Language. We tried to find dataset including these features to be used for prediction purpose. The data used in this study is retrieved from online public repository PROMISE [14]. The original data is made available by Software Research Laboratory of Bogazici University [15]. The utilized data sets areembedded software products implemented in C. It contains the measurements of 21 static code attributes (complexity metrics) and 1 defect information (false/true) of tens tohundreds of modules. Module attributes were collected using "Prest Metrics Extraction and Analysis Tool" [15]. The collected attributes contains:

%
% 1.loc : numeric % McCabe's line count of code
% 2.v(g) : numeric % McCabe "cyclomatic complexity"
% 3.ev(g) : numeric % McCabe "essential complexity"
% 4.iv(g) : numeric % McCabe "design complexity"
% 5.n: numeric % Halstead total operators + operands
% 6.v: numeric % Halstead "volume"
% 7.l: numeric % Halstead "program length"
% 8.d: numeric % Halstead "difficulty"
% 9.i: numeric % Halstead "intelligence"
% 10.e: numeric % Halstead "effort"
% 11.b: numeric % Halstead
% 12.t: numeric % Halstead's time estimator
% 13.lOCode: numeric % Halstead's line count
% 14.lOComment : numeric % Halstead's count of lines of comments
% 15.lOBlank : numeric % Halstead's count of blank lines
% 16.lOCodeAndComment: numeric
% 17.uniq_Op: numeric % unique operators
% 18.uniq_Opnd: numeric % unique operands
% 19.total_Op: numeric % total operators
% 20.total_Opnd: numeric % total operands
% 21: branch Count : numeric % of the flow graph

https://dx.doi.org/10.22161/ijaers/3.11.21 *ISSN: 2349-6495(P) | 2456-1908(O)*

% 22.defects:{false,true} % module has/has not one or more
% % reported defects

According to suggested features only 18 attributes were used from the above list. We omit 4 attributes (design complexity, essential complexity, and b and time estimator t). It is important to note that all attributes were measured by using traditional known metrics (LOC, McCabe and Halstead). Our goal here is to figure out which of the above attributes can be used to predict complexity. Spearman's Correlation is done between these attributes table "1" below shows correlation results.

Table.1: Correlation results

	Complexity v(g)	
	r-value	p-value
LOC (McCabe's line count)	.889	0.00
Design complexity	.826	0.00
total operators + operands	.869	0.00
Volume	.872	0.00
Length	**-0.832**	0.00
Difficulty	.861	0.00
Intelligence	.733	0.00
Effort	..883	0.00
Loc code (Halstead's line count)	.569	0.00
Locomments	.635	0.00
Loblank	.676	0.00
LOC and comments	**-0.062**	.170
uniq_Op	.887	0.00
Uniqu_oernd	.843	0.00
total_Op	.869	0.00
total_Opnd	.860	0.00
Branch_ count	.999	0.00
Defects	.169	0.00

By considering r- value it is obvious that the most related attributes to complexity estimation which measured by McCabe are branch count, LOC and unique operators. In contrast, 2 attributes are not related to complexity such as Length whichmeasured by Halstead and (LOCand commands)measure that appears from negative r value resulting from correlation process. So, both of negative attributes are omitted from selected features. Finally, the rest of attributes (16 attributes) were fed to predictive model.It is important to note that for prediction purpose we assign two classes for complexity the first class is "high"if complexity value is greater than 20, second class is "Low" if complexity is less than 20.

- **Proposed predictive model**

The proposed predictive model as mentioned above consists of two main phases: feature selection phase and analysis/ prediction phase. Data mining generally used to extract previously unknown patterns help to improve or even predict new knowledge[16]. Data mining are integrated in analysis / prediction phasethat classifyingsoftware data as high or low complexity based on labeled training data. If complexity estimation is less than 20 it labeled as low, if greater than 20 labeledhigh. Decision tree classification algorithm C5.0 is used to perform classification process.The decision trees algorithms are classification algorithms for use in predictive modeling. They build a data mining model by creating a series of splits in the tree [16].The C5.0 algorithm was chosen for the following reasons. Firstly, it's simplicity. Secondly, it has boosting feature that mean using multiple classifiers instead of one to provide better classification accuracy. The output of this phase is three sets of software data in addition to set of classification rules. Figure 1 bellow shows the proposed prediction model.

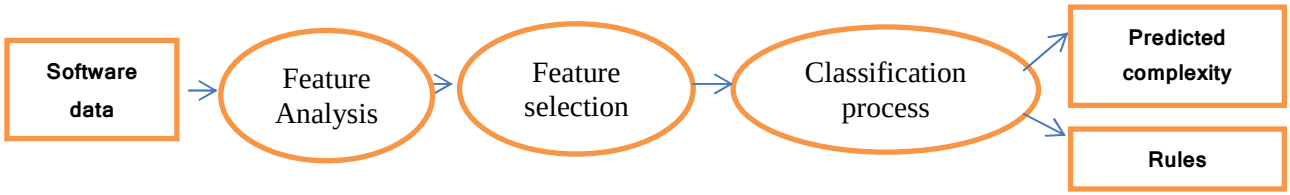

Fig.1: Prediction model

Total number of records fed to classifier is498records. Records are randomly split into two sets, a training set and a testing set. The training set used to create the mining model. The testing set used to check model accuracy.Trainingdata represents40% of total data/records. Results are listed in the following section.

IV. ANALYSIS AND RESULTS

Results confirm the existence of strong relation between branch count and complexity. C5.0 algorithm generates set of classification rules learned from training data as follows:

- If branch count between 1and 20 then complexity class is low.

https://dx.doi.org/10.22161/ijaers/3.11.21 *ISSN: 2349-6495(P) | 2456-1908(O)*

- If branch count is greater than 20 then complexity will be high.
- Special cases if branch count in [27 32 33 34 41 43 49 59 63 71] also complexity class Low

So, branch count can work as a good predictor to software complexity. Predication accuracy, prediction precision, and recall rate are commonly used metrics to evaluate the binary prediction models [14]. Classification accuracy is estimated by used mining algorithmequal to 100%. Table "2"presents the results after applying C5.0 to data.

Table.2: Prediction Results Details

	High	Low
Predicted high	24	0
Predicted Low	0	474

Accuracy =acc =100%
Probability of false alarm = pf = 0%
Probability of detection = pd = recall = 474/474=1
Precision = prec=474/474= 1

For validation purpose six programs are selected and tested according to the above rules. The selected programs are: stack,Gzip, print tokens, and arraysorting, binary search and replace programs. Branch count ismeasured for the five programs and also complexity estimated by using McCabe metric then rules are checked for validation.According to Validation results we can say branch count predict complexity correct 100%. Table 3 shows validation results.

Table.3: Validation Results

Program name	Branch count	Complexity v(G)	Class	Check
Stack	2	18	Low	correct
Gzip	100	1260	high	correct
Array sorting	2	6	Low	correct
replace	28	92	high	correct
Print tokens	61	79	high	correct
Binary search	2	4	low	correct

V. CONCLUSIONS

In this paper, a simple data mining based complexity prediction model were presented. Model depends on some attributes measured using traditional metrics from code structure.The most important aspect of the model was to figure out which attribute could be used as predictor to software complexity. Results find strong relation between complexity and branch count feature.

REFERENCES

[1] Application Analytics Software,What is Software Complexity:http://www.castsoftware.com/glossary/software-complexity.
[2] Chhillar, Usha, and SuchetaBhasin. "Establishing Relationship between Complexity and Faults for Object-Oriented Software Systems." IJCSI International Journal of Computer Science Issues 8.5 (2011).
[3] Dattathreya, Macam S., and Harpreet Singh."Army Vehicle Software Complexity Prediction Metric-Five Factors."
[4] Bhatnagar, Anurag, NikharTak, and Shweta Shukl. "A LITRERATURE SURVEY ON VARIOUS SOFTWARE COMPLEXITY MEASURES." International Journal of Advanced Studies in Computers, Science and Engineering 1.1 (2012): 1.
[5] McCabe, T.J. A Complexity Measure, IEEE Trans. On Software Engg., SE-2, 4, 1976, pp. 308-320
[6] Halstead, M.H. Elements of Software Science, New York: Elsevier North Holland, 1977.
[7] Jamali, Seyyed Mohsen. "Object oriented metrics." A survey approach Technical report, Department of Computer Engineering, Sharif University of Technology, Tehran, Iran (2006).
[8] Chhillar, Usha, and SuchetaBhasin. "Establishing Relationship between Complexity and Faults for Object-Oriented Software Systems." IJCSI International Journal of Computer Science Issues 8.5 (2011).
[9] International Journal of Software Engineering & Applications (IJSEA), Vol.3, No.6, November 2012 doi : 10.5121/ijsea.2012.360 8 101 prediction of software requirements stability based on complexity point measurement u sing m ulti – c riteria fuzzy approach d. francisxavierchristopher 1 and e.chandra
[10] N. J. Pizzi, "A Computational Intelligence Strategy for Software Complexity Prediction," Neural Networks, 2006.IJCNN '06. International Joint Conference on, Vancouver, BC, 2006, pp. 4727-4733. doi: 10.1109/IJCNN.2006.247127
[11] S. Sabharwal, R. Sibal and P. Kaur, "Software complexity: A fuzzy logic approach," Communication, Information & Computing Technology (ICCICT), 2012 International Conference on, Mumbai, 2012, pp. 1-6.
[12] Harrison, Warren. "An entropy-based measure of software complexity." Software Engineering, IEEE Transactions on 18.11 (1992): 1025-1029.
[13] S.W. QingWANG, L.I. Mingshu, Software defect prediction, J SoftwMaintEvol: Res Practice, 19 (7) (2008), pp. 1565–1580
[14] S. J. Sayyad and T. J. Menzies, The PROMISE Repository of Software Engineering Databases, School

https://dx.doi.org/10.22161/ijaers/3.11.21 *ISSN: 2349-6495(P) | 2456-1908(O)*

of Information Technology and Engineering, University of Ottawa, Can-ada, http://promise.site.uottawa.ca/SERepository.

[15] Graylin, J. A. Y., et al. "Cyclomatic complexity and lines of code: empirical evidence of a stable linear relationship." Journal of Software Engineering and Applications 2.03 (2009): 137.

[16] Yousef, Ahmed H. "Extracting software static defect models using data mining." Ain Shams Engineering Journal 6.1 (2015): 133-144.

https://dx.doi.org/10.22161/ijaers/3.11.22 *ISSN: 2349-6495(P) | 2456-1908(O)*

A Comparative Study of Text Summarization Based on Synchronous and Asynchronous PSO

R. Pallavi Reddy[1], Kalyani Nara[2], S. Sravani Reddy[3]

[1]Assistant professor, Dept of CSE, GNITS, Hyderabad, Telangana, India.
[2]Professor, Dept of CSE, GNITS, Hyderabad, Telangana, India.
[3]PG Scholar, Dept of CSE, GNITS, Hyderabad, Telangana, India.

Abstract*—Text summarization is the process of extracting the most important sentences from the original document without its meaning change. The paper focus on Extractive summarization technique which chooses the important sentences from the document and integrates into summary. An extractive summarization technique, Particle swarm Optimization performs arithmetic operations that enhances a problem, by iteratively trying to improve possible solution with regard to input data. It determines a problem by having a population of possible solutions moving around the search space according to arithmetic formulae over the particles position and velocity. The sequence of modernized particles of PSO can be categorized into Synchronous PSO (S-PSO) and Asynchronous PSO(A-PSO). In synchronous PSO, after calculating the whole performance, velocities and positions of the particles are modernized, this increases the performance. In A-PSO after calculating its performance, velocities and positions of the particles are modernized using partial data which leads to extreme analysis. The comparative study on the synchronous PSO and asynchronous PSO with the precision and recall values for different datasets is considered. Asynchronous PSO has higher precision and recall values compared to synchronous PSO. Asynchronous PSO leads to extreme analysis of data.*

Keyword—Text Summarization, particle swarm optimization, Synchronous PSO (S-PSO), Asynchronous PSO (A-PSO).

I. INTRODUCTION

Text summarization is the process of distilling the most important information from the source document to produce a abridged version of text. Automatic text summarization is to present the input text into a summary. The main advantage of using a summary is abating the reading time. Text summarization techniques can be classified into extractive and abstractive summarization. An extractive summarization method elites important sentences, paragraphs etc. from the original document and concatenating them into short data. An Abstractive summarization is an adapting of the main concepts in a document and then expresses those concepts in clear natural language.

Generally Extraction methods use sentence extraction technique to create the summary. In 1995 Kennedy and Eberhart introduced Particle swarm optimization (PSO) [1]. PSO is stochastic optimization algorithm depends on the swarm that simulate the social behavior of organisms such as birds and fishes. These organisms' benefits in search for food sources through distinctive work with neighbors. In PSO, the distinctive agents depicted by a swarm are called particles. The particles move within the search space to find the optimum solution by modernizing their velocity and position. These values are affected by the participation of the particles. PSO has drawn a lot of attentions from the researchers all over the world. PSO has sustained many evolutionary processes. Many variations of PSO have been proposed to improve the performance of the algorithm. The particles update sequence effects on the efficiency of PSO. In PSO, after evaluating the whole performance the best found solution is chosen as PBest from the Particle information. This method of PSO algorithm is known as synchronous PSO (S-PSO). The update method leads to the exploitation of the data.

In Asynchronous PSO (A-PSO), the position and velocity are modernized as soon as a particle's performance is evaluated. Therefore, a particle's search is directed by the partial or flawed information from its neighbor. This method leads to distinctness in the swarm [3]. In the beginning of iteration, the particles are updated using previous iterations while particles are updated at the end of the iteration based on the existing iteration [4]. A-PSO has been asserted to perform better than S-PSO. Xue et al. [8] reported that asynchronous update leads to a shorter execution time. Asynchronous method attempt on the incomplete information of the current best found solution communicated to the particles more slowly, thus lead to more exploration.

A comparative study is performed on the two algorithms to determine which algorithm support for a better summary. The paper is further organized as follows: The text summarization technique correspond to

https://dx.doi.org/10.22161/ijaers/3.11.22 *ISSN: 2349-6495(P) | 2456-1908(O)*

Preprocessing and Feature Extraction as their initial stage. These steps are briefly explained in section II. The synchronous PSO (S-PSO) algorithm is explained in detail in section III. The asynchronous PSO (A-PSO) algorithm is highlighted in section IV. Various input documents relating to different domains are given as input data. The results obtained from algorithms are used to calculate precision and recall values. The analysis of results are given in section V. The conclusions stated in section VI based upon the experimental evaluations from section V.

II. PREPROCESSING AND FEATURE EXTRACTION

A. Preprocessing:

Preprocessing is important as it provides summarization systems with a clean and adequate representation of source document. The pre-processing helps in interacting the most important information of a document. The text file is taken as the input document which is given for pre-processing. Pre-processing consists of four main steps: Segmentation, stop word removal, tokenization, stemming.

Sentence segmentation is the process of dividing the input file into number of sentences. The stop words such as I, a, the. .etc. are removed from the segmented lines. After stop word removal, each word is divided into tokens. base words are obtained by removing the prefixes and suffixes.

B. Feature Extraction

After Pre-processing, it is subjected to feature extraction by which the properties of the sentences are extracted to score the sentence. Eight features are considered. Values for each Feature are between 0 and 1.The eight features are:

Title Feature:

The sentences that contain title words are important as they are more relevant to theme. These sentences have a more chance of getting constituted in the summary. The title feature ($\mathbf{T_F}$) can be calculated as below:

$$\mathbf{T_F} = \frac{no\ of\ title\ words\ in\ sentence}{no\ of\ title\ words\ in\ title} \quad \textbf{(1)}$$

Sentence Length:

Sentence Length (S_L) is important in creating the summary. Short sentences such as names, date lines etc., are not added to the summary. This feature is used to isolate the short sentences.

$$\mathbf{S_L} = \frac{no\ of\ words\ in\ sentence}{no\ of\ words\ in\ longest\ sentence} \quad \textbf{(2)}$$

Term Weight:

The term occurrences within a document have often been used for calculating the weight of each sentence. The sentence score can be calculated as the sum of the score of words in the sentence. Each word weight is given term frequency. The term weight is given by:

$$\mathbf{Wt = tfi * isfi = tfi * \log \frac{n}{N}} \quad \textbf{(3)}$$

Tfi :Term Frequency of word i

N: Number of sentences in the document

ni :Number of sentences in which the Word i occur

The Total Term Weight (T_W) is given by the formula

$$\mathbf{T_W} = \frac{\sum_{i=1}^{k} Wi(s)}{Max(\sum_{i=1}^{k} wi(si))} \quad \textbf{(4)}$$

K: Number of Words in Sentences

Sentence Position:

The sentence position (S_P) also plays an important role in determining whether the sentence is appropriate or not. If there are 5 lines in document the sentence positions are given by

S_P= 5/5 for 1st, 4/5 for 2nd, 3/5 for 3rd, 2/5 for 4th, 1/5 for 5th **(5)**

Sentence to Sentence Similarity:

Similarity between the sentences is very important in generating the summary. The Similar sentences should not repeat in the summary that is to be generated.

$$\mathbf{SS_{sim}} = \frac{\sum sim(si,sj)}{Max(\sum sim(si,sj))} \quad \textbf{(6)}$$

Si: sentence i

Sj: sentence j

Sim (si, sj): is the similarity of 1 to n terms in sentence si and sj

Proper Noun:

The sentences which have more proper nouns are mostly to be included in the summary. The Proper noun(N_P) feature is calculated as below:

$$\mathbf{N_P} = \frac{no\ of\ proper\ nouns\ in\ sentence}{length\ of\ sentence} \quad \textbf{(7)}$$

Thematic word:

The terms that occur more frequently are more related to the topic. We consider top 10 most frequent words as thematic words. Thematic words(W_T) are calculated as below:

$$\mathbf{W_T} = \frac{no\ of\ thematic\ word\ in\ sentence}{Max(no\ of\ thematic\ words)} \quad \textbf{(8)}$$

Numerical Data:

This Feature is used to identify the statistical data in every sentence. Numerical data(D_N) is calculated as follows:

$$\mathbf{D_N} = \frac{no\ of\ numerical\ data\ in\ senence}{length\ of\ sentence} \quad \textbf{(9)}$$

III. PARTICLE SWARM OPTIMIZATION

Particle swarm optimization performs arithmetic operations which enhances a problem by iteratively trying to improve possible solution with regard to given input data. A conventional approach called synchronous method is a more precise natural model which increases the possibility of parallelization of an algorithm [7], [8].

https://dx.doi.org/10.22161/ijaers/3.11.22 *ISSN: 2349-6495(P) | 2456-1908(O)*

In PSO, the search for the optimum solution is directed by a swarm of P particles. At time t, the ith particle has a position, p(t), and a velocity, V(t). A solution is represented by the particle position and velocity. Velocity represents the rate of change from the current particle position to the next particle position. The position and velocity values are initialized by random numbers at the beginning. In consecutive iterations, the search process is directed by updating the position and velocity using the following equations:

$$V(t) = V_i(t-1) + c_1 r_1(pBest_i - x_i(t-1)) + c_2 r_2(gBest - x_i(t-1)) \quad (1)$$

$$x_i(t) = V(t) + x_i(t-1) . \quad (2)$$

To prevent the particles from attempting too far from the feasible region, the V(t) value is clasped to $\pm V$max. If the value of Vmax is too large, then the exploration range is too wide. Conversely, if the value of Vmax is too small, then the particles will favor the local search [10]. In (1), c_1 and c_2 are the learning factors that control the effect of the logical and social impact on a particle. Typically, both c_1 and c_2 are set to 2. Two independent random numbers r_1 and r_2 ranges from 0.0 to 1.0 are consolidated into the velocity equation. These random terms provide hypothetical behavior to the particles, thus strengthen them to explore a wider area.

A distinctive progress in PSO influenced not only by the particle's endeavor and experience but also by sharing the information to its neighbors. The particle's involvement is represented in equation (1) by pBest$i$, the best position which is found until, by the ith particle. The neighbors' influence is represented by gBest, the best position found by the swarm till the current iteration. The particle's position, $x_i(t)$, is updated using equation (2), in which a particle's next search is started from its previous position and the new search is involved by the past search[4]. Typically, $x_i(t)$ is limited to prevent the particles from searching in an infeasible region [5]. The quality of x(t) is appraised by a problem-dependent fitness function. Each particles is evaluated to determine its current fitness. If a new position fitness is better than the current fitness then gBest or pBest$i$ or both are found, then the new position value will accordingly be saved as gBest or pBest$i$; otherwise the old best values will remain same. This process continues till the stopping benchmark is met, when the maximum iteration limit, T, is attained or the target solution is accomplished. Therefore, the maximum number of fitness evaluation for a swarm with number of particles P in a run is (P×T).

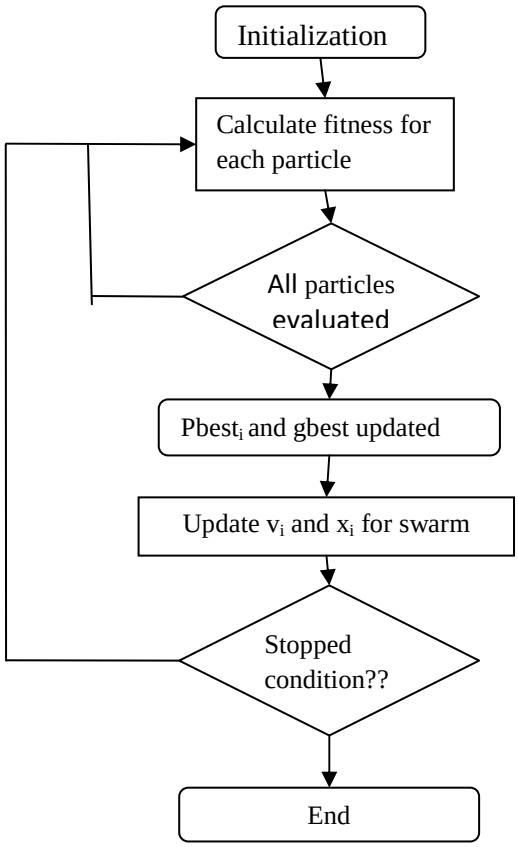

Fig.1: Synchronous PSO

The flowchart of figure 1 represents the original PSO algorithm. As shown in the algorithm, the updated values of the Best$i$ and gBest are evaluated after the fitness of all the particles has been evaluated. Therefore, this approach of PSO is known as Synchronous PSO (S-PSO). The pBest$i$ and gBest are modernized after all the particles fitness is evaluated, S-PSO assure that all the particles receive accurate and complete information about their neighbors , leads to a better choice of gBest and thus allowing the particles to exploit this information so that a better solution can be found. The summary is generated based the gBest values that are arranged in the descending order and the sentences are extracted from the source document and concatenated. However, this possibly leads the particles in S-PSO to converge faster, resulting in a untimely convergence.

IV. ASYNCHRONOUS PSO (A-PSO)

In S-PSO, a particle has to wait for the complete swarm to be evaluated before it can progress to a new position and continue its search. Thus, the particle is idle for the longest time after evaluating and waiting for the entire swarm to be modernized. A-PSO is an alternative approach to S-PSO, in which the particles are modernized based on the present state of the swarm. In A-PSO, A particle position, velocity, $p$best and $g$best are modernized as soon as its fitness is evaluated. The

https://dx.doi.org/10.22161/ijaers/3.11.22 *ISSN: 2349-6495(P) | 2456-1908(O)*

particle chooses *g*Best using a combination of information from the present and the prior iteration. In A-PSO, particle in the same iteration uses various values of *g*Best as it is preferred, based on the accessible information during a particle's updating process.

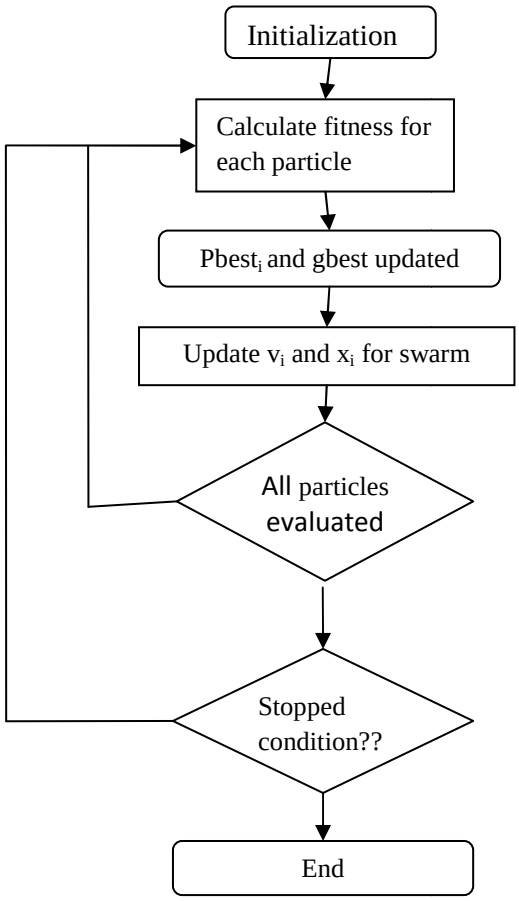

Fig.2: Asynchronous PSO

The flowchart in Figure 2 represents A-PSO algorithm. The flow of A-PSO is unlike S-PSO, however the fitness function is evaluated for *P* times per iteration, once for each particle. Therefore, the maximum number of iterations for fitness evaluation is (*P*×*T*).This is alike to S-PSO. Using the same equations as S-PSO, The velocity and position are evaluated.

Other than the type of information, the lack of coexistence in A-PSO resolves the issue of ineffective particles faced in S-PSO. An asynchronous update also allows the modernize sequence of the particles to alter dynamically or a particle to be modernized more than once.

V. ANALYSIS OF RESULTS

The analysis of the result is done considering the domains relating to Economy, Secularism, Earth, Nature, Forest, and Metadata. For every document, a manually generated relevant summary is compared to obtain the precision and recall values. Summary is generated using synchronous PSO and asynchronous PSO. Precision, recall and F-measure values are calculated for each document as shown in the below table1. In the graphs, precision, recall and F-measure values are represented to determine the performance of the systems.. The graph are drawn for each dataset as shown in the below. Recall is also known as sensitivity. Recall is gradually increasing as shown in the figure. The increase in recall suggests that the system performs better compared to other systems. Compared to synchronous PSO and Asynchronous PSO the recall value of Asynchronous PSO is higher than the Synchronous PSO. This leads to more exploration of data.

Table.1: values of Synchronous PSO(S-PSO) and Asynchronous PSO (A-PSO)

Data sets	Synchronous PSO			Asynchronous PSO		
	precision	Recall	F-measure	precision	Recall	F-measure
Nature	17.5	38.8	27	22.5	66.6	33
metadata	20	50	27.2	25.7	66.6	37
Forest	41	58	51	53	88	66
reservation	36	38	43	47	84	60
computer	26	46	34	34	61	44
economy	63.3	81	71	72	83	77

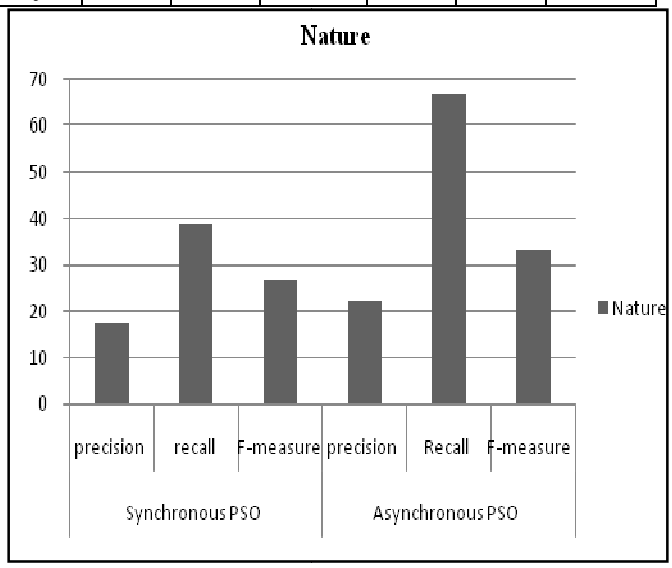

Fig.3: Comparison of S-PSO and A-PSO for Nature dataset

https://dx.doi.org/10.22161/ijaers/3.11.22 *ISSN: 2349-6495(P) | 2456-1908(O)*

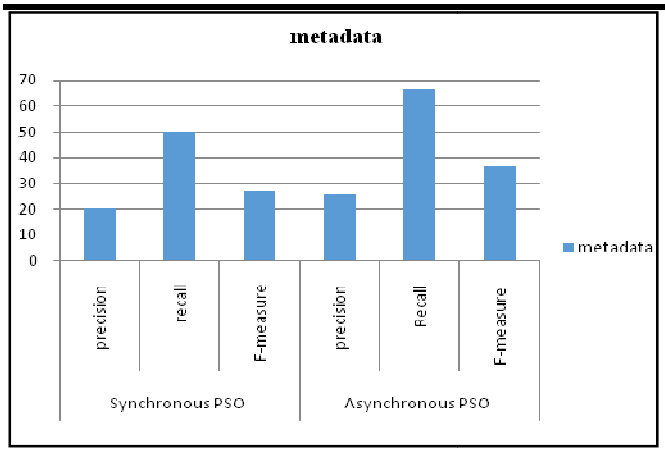

Fig.4: Comparison of S-PSO and A-PSO for Metadata dataset

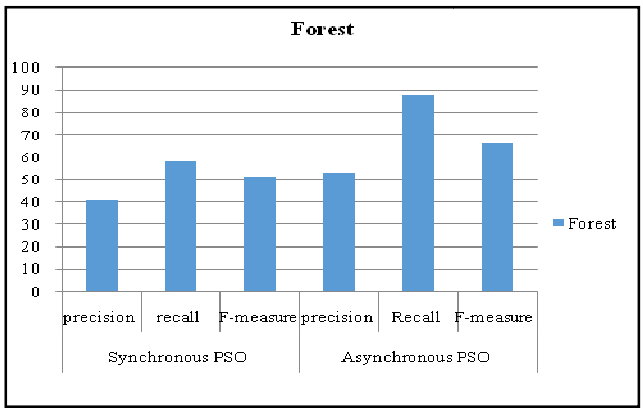

Fig.5: Comparison of S-PSO and A-PSO for Forest dataset

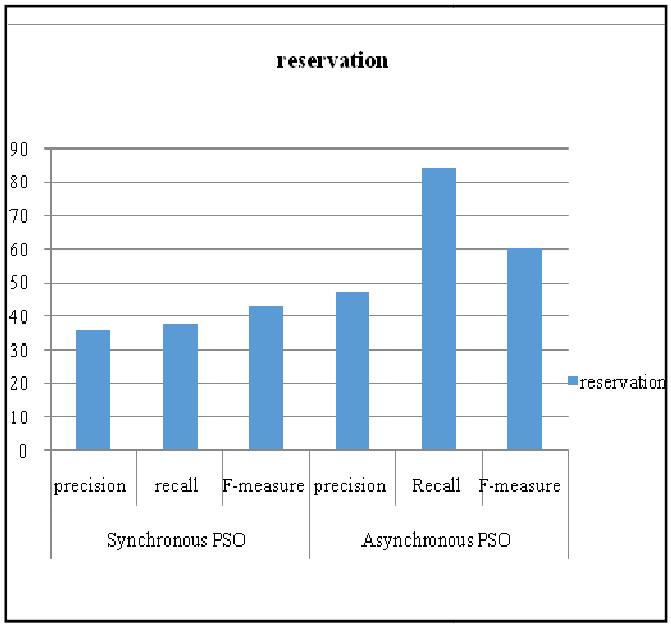

Fig.6: Comparison of S-PSO and A-PSO for Reservation dataset

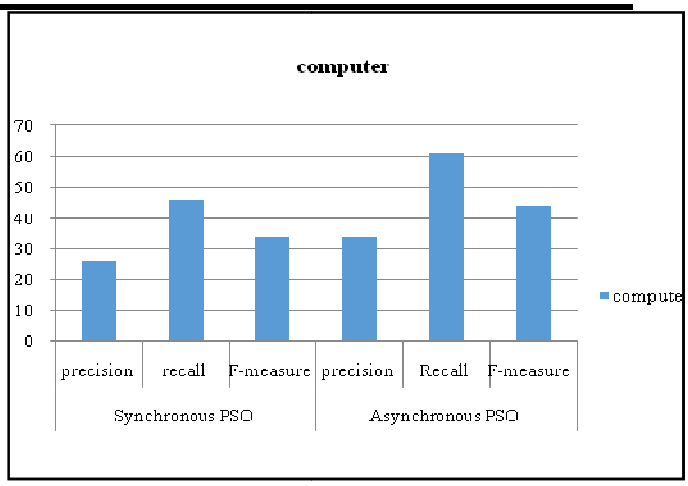

Fig.7: Comparison of S-PSO and A-PSO for Computer dataset

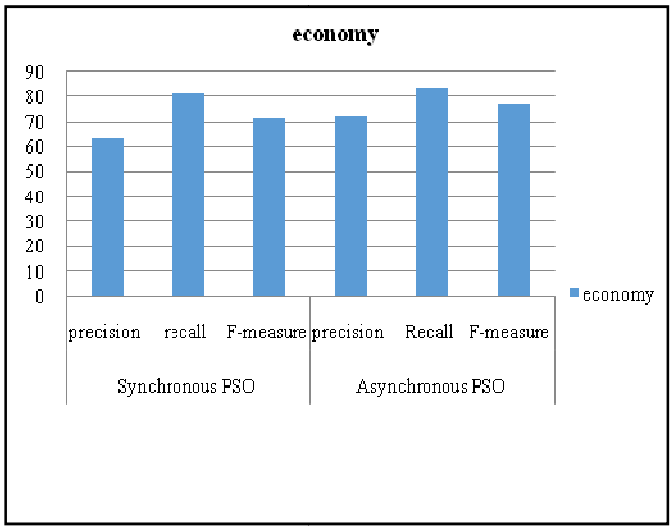

Fig.8: Comparison of S-PSO and A-PSO for Economy dataset

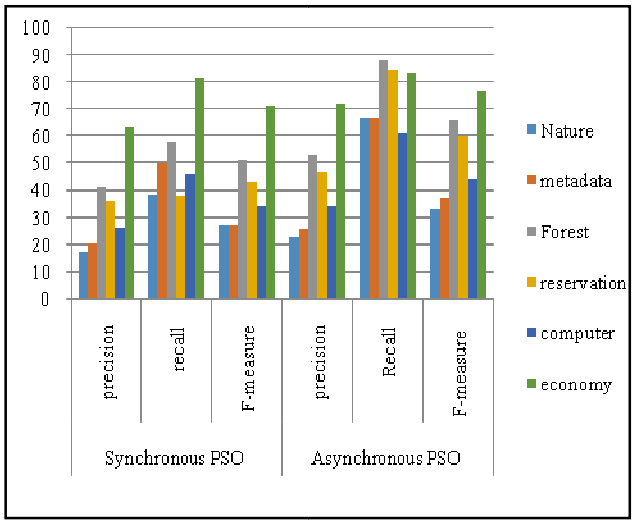

Fig.9: values of synchronous PSO(S-PSO) and asynchronous PSO(A-PSO)

https://dx.doi.org/10.22161/ijaers/3.11.22 *ISSN: 2349-6495(P) | 2456-1908(O)*

VI. CONCLUSION

Automatic summarization is a aggregate task that affects the performance to produce high quality summaries. A comparative study of synchronous PSO and asynchronous PSO summarization techniques are evaluated using different text documents related to different domains as inputs. In synchronous PSO, after calculating the entire performance the particles velocities and positions are modernized. This modernizing method improves the performances. In A-PSO after calculating the own performance, velocities and positions of the particles are modernized. Therefore, particles are modernized using partial data, leads to extreme exploration. The analysis of results show that the Asynchronous approach produces efficient results compared to Synchronous approach. The work can be further enhanced by using a hybrid approach which combines S-PSO and A-PSO.

REFERENCES

[1] J. Kennedy and R. Eberhart, "Particle swarm optimization,"in *Proceedings of the IEEE International Conference on Neural Networks (ICNN '95)*, vol. 4, pp. 1942–1948, Perth, Western Australia, November-December 1995.

[2] G. J. Rath, A. Resnick, and T. R. Savage, "The formation of abstracts by the selection of sentences" American Documentation, vol. 12, pp.139-143.1961.

[3] R. Juan, M. Zhang, and W. Seah, "A performance study on synchronous and asynchronous updates in Particle Swarm Optimization," in *Proceedings of the 13th Annual Genetic and Evolutionary Computation Conference (GECCO '11)*, pp. 21–28,July 2011.

[4] J. Rada-Vilela, M. Zhang, and W. Seah, Random asynchronous PSO," in *Proceedings of the 5th International Conference on Automation, Robotics and Applications (ICARA '11)*, pp. 220–225,Wellington, New Zealand, December 2011.

[5] B. Jiang, N. Wang, and X. He, "Asynchronous particle swarm optimizer with relearning strategy," in Proceedings of the 37th Annual Conference of the IEEE Industrial Electronics Society (IECON '11), pp. 2341–2346, November 2011

[6] Voglis C.A., Parsopoulos K.E., and Lagaris I.E. 2012. Particle swarm optimization with deliberate loss of information. Soft Computing. Vol. 16, No. 8, pp. 1373–1392.

[7] M. N. Ayob, Z. M. Yusuf, A. Adam et al., "A particle swarm optimization approach for routing in VLSI," in *Proceedings of the 2nd International Conference on Computational Intelligence, Communication Systems and Networks (CICSyN '10)*, pp. 49–53,Liverpool, UK, July 2010.

[8] Y. Shi and R. Eberhart, "A modified particle swarm optimizer," in *Proceedings of the IEEE International Conference on Evolutionary Computation and IEEE World Congress on Computational Intelligence*, (Cat.No. 98TH8360) , pp. 69–73, Anchorage, Alaska, USA, May 1998.

[9] M.A. Fattah and Fuji Ren, "Automatic Text Summarization" In proceedings of World Academy of Science, Engineering and Technology Volume 27. pp 192-195. February 2008.

[10] Shi Y. and Eberhart R. 1998. Parameter selection in particle swarm optimization. In Proceedings of the 7th International Conference on Evolutionary Programming VII (EP '98), V. William Porto, N. Saravanan, Donald E. Waagen, and A. E. Eiben (Eds.). pp. 591-600

[11] C. Tu, L. Chuang, J. Chang, and C. Yang, "Feature Selection using PSO-SVM". IAENG International Journal of Computer Science. 33(1), 2006, pp.138-143

[12] Y. Liu, Z. Qin, Z. Xu and X. He, "Feature Selection with Particle Swarms". In *Computational and Information Science, LNCS 3314*, J. Zhang, J.-H. He, and Y. Fu, Ed. Heidelberg: Springer-Verlag, 2004, pp. 425–430.

International Journal of Advanced Engineering Research and Science (IJAERS) *[Vol-3, Issue-11, Nov- 2016]*
https://dx.doi.org/10.22161/ijaers/3.11.23 *ISSN: 2349-6495(P) | 2456-1908(O)*

Development of ANFIS Control System for Seismic Response Reduction using Multi-Objective Genetic Algorithm

Tomar R S[1], Qureshi M F[2], Shrivastava S K[3]

[1]Department of Physics, Kirodimal Institute of Technology, Raigarh, Chhattisgarh, India
[2]Department of Electrical Engineering, Government Polytechnic, Dhamtari, Chhattisgarh, India
[3]Department of Physics, Dr C V Raman University, Kota, Bilaspur, Chhattisgarh, India

Abstract— *Adaptive neuro fuzzy inference system (ANFIS) and Genetic algorithm (GA) was proposed in this study to reduce dynamic responses of a seismically excited building. A multi-objective genetic algorithm (MOGA) was used to optimize the ANFIS+GA controller. Two MR dampers were used as multiple control devices and a scaled five-story building model was selected as an example structure. A fuzzy control algorithm was compared with the proposed ANFIS and ANFIS+GA controller.*

Adaptive neuro-fuzzy inference system (ANFIS) and Ganetic algorithm with several outputs was proposed. In case study, after numerical simulation, it has been verified that the ANFIS control algorithm can present better control performance compared to the fuzzy control algorithm in reducing both displacement and acceleration responses.

Keywords—Adaptive Neuro Fuzzy Inference System (ANFIS), Earthquake loads, Vibration control, Multi-objective optimization using MOGA, Ganetic algorithm (GA).

I. INTRODUCTION

Although significant studies have been conducted in recent years toward development and application of semi-active control schemes for vibration control of building structures in seismic zones, the application of intelligent controllers, including ANFIS controllers, has not been addressed extensively. As an alternative to classical control theory, ANFIS controller allows the resolution of imprecise or uncertain information. Because of the inherent robustness and ability to handle nonlinearities and uncertainties, Although ANFIS controller has been used to control a number of structural systems, selection of acceptable fuzzy membership functions has been subjective and time-consuming. To overcome this difficulty, a multi-objective genetic algorithm (MOGA) was used to optimize fuzzy rules and membership functions of ANFIS controller. In order to compare the control efficiency of the proposed MOGA-optimized ANFIS controller, a fuzzy control algorithm was considered as the baseline in this study

A neuro-fuzzy system is based on an inference system formed by a training algorithm derived from the neural theory. There exists several approaches to integrate artificial neuron systems and the fuzzy logic, and very often the choice depends on the application. Jang and Sun introduced the adaptive network-based fuzzy inference system ANFIS. ANFIS was later extended to generalize ANFIS for the modeling of a multivariable system. The proposed ANFIS is used to obtain peak or maximum responce of three functions i.e. displacement, drift and acceleration but our study is concentrated to only two parameters i.e displacement and acceleration.

II. ANFIS CONTROLLER

2.1 Adaptive Neuro-fuzzy Inference System

ANFIS is a neuro-fuzzy system whose structure is a multi-layer ANN see fig.4. It consists of three major parts i.e. IF-part, Rules + Norm-part and THEN-part for rule processing. It embeds fuzzy rules with the ANN and use a back-propagation-like algorithm to fine-tune the parameters of single-output, Sugeno-type fuzzy inference system. The learning algorithm combines least-squares and back-propagation (BP) gradient descent methods. This section introduces the basics of ANFIS network architecture and its hybrid learning rule.

Adaptive Neuro-Fuzzy Inference System is a feed forward adaptive neural network which implies a fuzzy inference system through its structure and neurons. Jang was one of the first to introduce ANFIS[Jang et all (1993)]. He reported that the ANFIS architecture can be employed to model nonlinear functions, identify nonlinear components on-line

https://dx.doi.org/10.22161/ijaers/3.11.23 *ISSN: 2349-6495(P) | 2456-1908(O)*

in a control system, and predict a chaotic time series. It is a hybrid neuro-fuzzy technique that brings learning capabilities of neural networks to fuzzy inference systems. The learning algorithm tunes the membership functions of a Sugeno-type Fuzzy Inference System using the training input-output data. For a first order Sugeno type of rule base with two inputs x, y and one output, the structure of ANFIS is shown in Fig.1

As we have already seen, fuzzy systems present particular problems to a developer:

- Rules:-The if-then rules have to be determined somehow. This is usually done by 'knowledge acquisition' from an expert. It is a time consuming process that is fraught with problems.
- Membership functions:-A fuzzy set is fully determined by its membership function. This has to be determined. If it's Gaussian then what are the parameters?

The ANFIS approach learns the rules and membership functions from data.

ANFIS is an *adaptive network*. An adaptive network is network of nodes and directional links. Associated with the network is a learning rule - for example back propagation. It's called adaptive because some, or all, of the nodes have parameters which affect the output of the node. These networks are learning a relationship between inputs and outputs.

An adaptive network covers a number of different approaches but for our purposes we will investigate in some detail the method proposed by Jang known as ANFIS.

The ANFIS architecture is shown below. The circular nodes represent nodes that are fixed whereas the square nodes are nodes that have parameters to be learnt.

A Two Rule Sugeno ANFIS has rules of the form:

$$If\ x\ is\ A_1\ and\ y\ is\ B_1 \quad THEN\ f_1 = p_1x + q_1y + r_1$$
$$If\ x\ is\ A_2\ and\ y\ is\ B_2 \quad THEN\ f_2 = p_2x + q_2y + r_2$$

For the training of the network, there is a forward pass and a backward pass. We now look at each layer in turn for the forward pass. The forward pass propagates the input vector through the network layer by layer. In the backward pass, the error is sent back through the network in a similar manner to back-propagation.

Layer 1: The output of each node is:

$$O_{1,i} = \mu_{A_i}(x) \qquad for\ i = 1,2 \ldots\ldots\ldots\ldots\ldots\ldots\ldots (1)$$
$$O_{1,i} = \mu_{B_i}(y) \qquad for\ i = 3,4 \ldots\ldots\ldots\ldots\ldots\ldots\ldots (2)$$

So, the $O_{1,i}(x)$ is essentially the membership grade for x and y.

The membership functions could be anything but for illustration purposes we will use the bell shaped function given by:

$$\mu_A(x) = \frac{1}{1 + \left|\frac{x - c_i}{a_i}\right|^{2b_i}} \ldots\ldots\ldots\ldots\ldots\ldots\ldots\ldots\ldots (3)$$

Where a_i, b_i, c_i are parameters to be learnt. These are the premise parameters.

Layer 2: Every node in this layer is fixed. This is where the t-norm is used to 'AND' the\ membership grades - for example the product:

$$O_{2,i} = w_i = \mu_{A_i}(x)\mu_{B_i}(y), \qquad i = 1,2 \ldots\ldots\ldots\ldots (4)$$

Layer 3: Layer 3 contains fixed nodes which calculate the ratio of the firing strengths of the rules:

$$O_{3,i} = w_i = \frac{w_i}{w_1 + w_2} \ldots\ldots\ldots\ldots\ldots\ldots\ldots\ldots\ldots\ldots (5)$$

Layer 4: The nodes in this layer are adaptive and perform the consequent of the rules:

$$O_{4,i} = \overline{w_i} f_i = \overline{w_i}(p_i x + q_i y + r_i) \ldots\ldots\ldots\ldots\ldots\ldots (6)$$

The parameters in this layer (p_i, q_i, r_i) are to be determined and are referred to as the consequent parameters.

Layer 5: There is a single node here that computes the overall output:

$$O_{5,i} = \sum_i \overline{w_i} f_i = \frac{\sum_i w_i f_i}{\sum_i w_i} \ldots\ldots\ldots\ldots\ldots\ldots\ldots\ldots\ldots (7)$$

This then is how, typically, the input vector is fed through the network layer by layer. We now consider how the ANFIS learns the premise and consequent parameters for the membership functions and the rules.

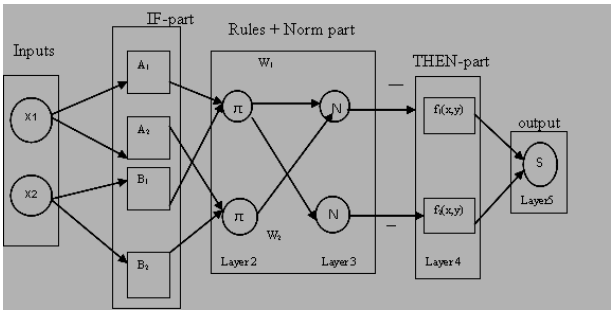

Fig.1: Structure of ANFIS

2.1.1 Operation of training

The MISO-ANFIS training paradigm uses a gradient descent algorithm to optimize the antecedent parameters, and a least squares algorithm to solve for the consequent parameters. The consequent parameters are updated first using a least squares algorithm, and the antecedent parameters are then updated by back-propagating the errors that still exist.

https://dx.doi.org/10.22161/ijaers/3.11.23 *ISSN: 2349-6495(P) | 2456-1908(O)*

2.1.2 The back-propagation of the gradient

In the stage of back-propagation, the signal of error is back propagated and local parameters are updated by the method of gradient descent. For the neuro-fuzzy system to an alone output *y*, we have:

$$a_{ij}(t+1) = a_{ij}(t) - \frac{h}{p}.\frac{\partial E}{\partial a_{ij}} \quad (13)$$

h: the training rate for *i a* ,

p : number of data of x (or *yd*),

The following rule is used to calculate partial derivatives, employed to update of the parameters of membership function *g*. (Zhenming et al. 2001).

$$\frac{\partial E}{\partial a_i} = \frac{\partial E}{\partial y}.\frac{\partial y}{\partial y_i}.\frac{\partial y_i}{\partial w_i}.\frac{\partial w_i}{\partial g}.\frac{\partial g}{\partial a_i} \quad (14)$$

$$E = \frac{1}{2}(y - y_d)$$

E: the quadratic cost function,

ANFIS system for three outputs as shown by Fig.1, possesses similar entry weights to these of ANFIS system for an alone output (therefore similar local parameters (a_i, b_i, c_i, d_i). The difference resides in consequent parameters. For MISO-ANFIS of single outputs, each output possesses these clean consequent parameters (p_i , q_i, r_i for y_a , p_i' , q_i' , r'_i for y_b and p_i" , q_i" , $r"_i$ for y_c). To make the local parameter correction, MISO-ANFIS of single outputs uses the sum of the gradient of the two errors of the two outputs:

$e_1 = y_a - y_{d1}$, $e_2 = y_b - y_{d2}$, $e_3 = y_c - y_{d3}$.

Such that

$$a_{ij}(t+1) = a_{ij}(t+1) - \frac{h}{p}\left(\frac{\partial E_1}{\partial a_{ij}} + \frac{\partial E_2}{\partial a_{ij}} + \frac{\partial E_3}{\partial a_{ij}}\right) \quad (15)$$

Where:

$$\frac{\partial E_1}{\partial a_{ij}} = f(e_1) \cdot \quad \frac{\partial E_2}{\partial a_{ij}} = f(e_2) \cdot \quad \frac{\partial E_3}{\partial a_{ij}} = f(e_3)$$

2.2 Application of ANFIS systems

To show the efficiency of the proposed ANFIS, we consider the approximation of the three following functions:

$$y_{d1} = .2*\sin(.3*x) \quad (16)$$

$$y_{d2} = .2*\sin(-.3*x); \quad (17)$$

$$y_{d3} = .2*\cos(.3*x); \quad (18)$$

The precision of ANFIS increases with the number of weight of inputs. For ANFIS of three outputs, it concerns three errors of estimation (for y_{d1} , y_{d2} and y_{d3}). To make the approximation of these three functions, we have used a ANFIS of three weights in the input (in first layer). Then, and so as to have best results of approximation, we have used a ANFIS with six weights in the input. Then we have made the comparison of the results of the approximation for the two ANFIS systems. Local parameters are initialed to small values that we have chosen to accelerate the convergence. The type of membership function of ANFIS that we have used is the trapezoidal function.

2.2.1 Scaled Building Model

In order to develop an MISO semi-active ANFIS for effective control of multiple MR dampers, a 5-story example building structure shown in Fig. 2 is employed. This example structure is developed based on a scaled 3-story shear building model used in the literature. As shown in this figure2, two MR dampers are rigidly connected to the first floor and the second floor of the structure, respectively.

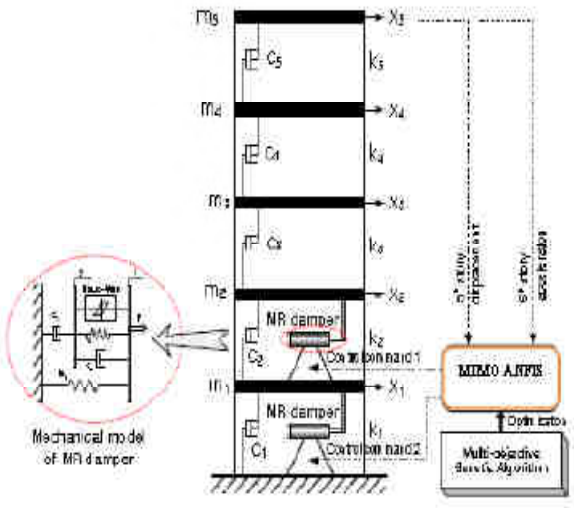

Fig.2: 5-story example building model

The first five natural frequencies of the example structure model are 4.12, 11.27, 17.14, 23.02 and 26.31 Hz, respectively. In this study, the modified Bouc-Wen model [ ] is used to describe how the damping force is related to the velocity and applied command voltage. The mechanical model for the MR damper based on the Bouc-Wen hysteresis model is shown in Fig. 2. The detailed description and the parameter values of the MR damper model are presented in Dyke *et al.*'s work [ ]. This MR damper model has a maximum generated force of about 1600 N depending on the relative velocity across the MR damper with a saturation voltage of 2.52 V. In numerical analysis, the model of the example structure is subjected to the SE component of the 1997 Gadha Jabalpur earthquake. Because the system under consideration is a scaled model, the earthquake has been reproduced at five times the recoded rate

Genetic Algorithm (GA)

The algorithm begins with a set of solutions (chromosomes) that are called the population. Solutions from one

https://dx.doi.org/10.22161/ijaers/3.11.23 *ISSN: 2349-6495(P) | 2456-1908(O)*

population are reproduced to create a new generation in the population. Mutations occur randomly in each population. ANFIS is applied for optimization of the premise parameters (input membership functions) and the consequent parameters (output membership function), GA algorithm will search for the best ANFIS configuration based on minimizing the least mean square error between the expected and real output of the network. The set of possible input membership function is {trimf, trapmf, gbellmf, gaussmf}, output membership function is {constant ($z=c_i$), linear ($z=p_iX+q_iY+r_i$)}, the number of membership functions for each input is in range from 2 to 6. Two groups of randomly selected chromosomes are generated and the chromosome with the best fitness function is picked up from each group. Then these two chromosomes with the offspring produced by crossover operator are sent to next generation. This process continues to fill the next generation completely.

Since the aim of GA is to optimize the membership functions of a predetermined ANFIS structure to reach the lower error; the fitness function is defined as the inversion of the model's MSE (mean square error) between the data and the model output. Thus trying to upraise the fitness value of the model, GA searches for better parameters to reduce the model error.

III. THE OPTIMIZATION OF ANFIS BASED ON GA

Traditional genetic algorithm has some inevitable defects, for example, the local optimum solution that produced too early can be concentrated and miss the global optimum solution. This paper introduced immune operator which is obtained from immune choice. Immune choice computes the individual density of some group. Through population Refreshing based on density and sufficiency test, the individual better than the parent generation is chosen into the next group. Traditional algorithm chromosome is monolayer and is easily subjected to following defect; the probability of actual intercrossing and variation of short gene in chromosome is long.

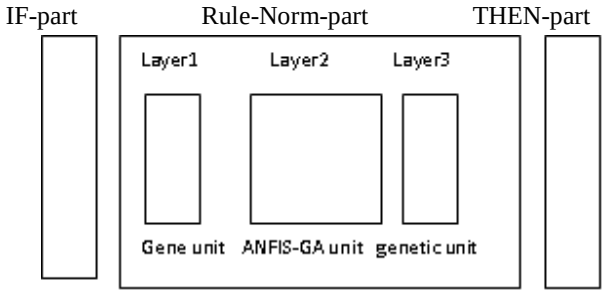

Fig.3: Chromosome structure

This paper proposed a chromosome structure with three layers as shown in Fig.3. The first layer is gene unit with Rules-Norm-part of Structure to represent the number of layer Rules-Norm-part in pre-feed backed genetic network. The second layer is ANFIS+GA unit to represent the number of neure under a Rules-Norm-part. The genetic unit of third layer used decimal code to represent all threshold of upper neuron.

IV. CASE STUDY

A numerical model of the 5-story example building structure with two MR dampers is implemented in SIMULINK and MATLAB. Using this numerical model, time history analyses of 15 seconds with a time step of 0.005 sec are performed in order to investigate the control performance of MR dampers controlled by the MOGA optimized MISO ANFIS. The MOGA based optimization is performed with the population size of 100 individuals. An upper limit on the number of generations is specified to be 1000. As the number of generations increases, the control performance of the elite (i.e. non-dominated) individuals is improved. After optimization run, a set of optimal solutions is obtained. Optimization results show that two objective function values of every solution in optimal record are less than 1. It means that the MOGA optimized MISO-ANFISs can provide better control performance in reducing both displacement and acceleration responses compared to the MIMO fuzzy controller.

Consequently, one controller, that can appropriately control both displacement and acceleration responses, has been selected among the optimal ANFISs. The values of two objectives of the selected ANFIS are both 0.75 and it means that the selected MIMO ANFIS can reduce both the peak 5th floor displacement and acceleration responses by 25%, compared to the MIMO fuzzy controller. The peak responses of the MIMO ANFIS, MIMO FLC controller, and uncontrolled case for the five floors of the seismic-excited example building structure are compared in Table 1.

Table.1: Comparison of peak story responses.

Story	Displacement (cm)				Acceleration (cm/sec^2)			
	Uncontrolled	fuzzy	ANFIS	ANFIS+GA	Uncontrolled	fuzzy	ANFIS	ANFIS+GA
1	0.340	0.101	0.115	0.1	620.6	570.3	294.8	270.5
2	0.601	0.198	0.181	0.17	712.1	387.5	338.9	300.3

https://dx.doi.org/10.22161/ijaers/3.11.23 *ISSN: 2349-6495(P) | 2456-1908(O)*

3	**0.754**	**0.273**	**0.250**	**0.23**	**512..3**	**401.2**	**251.6**	**161.5**
4	**0.901**	**0.345**	**0.272**	**0.25**	**588.8**	**342.6**	**271.8**	**205.1**
5	**0.970**	**0.376**	**0.288**	**0.26**	**904.7**	**398.7**	**298.5**	**197.6**

The peak displacement of the 5th floor of the uncontrolled case is 0.970 cm. On the other hand, the peak displacement of the 5th floor of the MIMO ANFIS is 0.288 cm, which is only 29 % of the uncontrolled case. The peak acceleration of the 5th floor of the MIMO ANFIS is reduced by 71 % compared to the uncontrolled case.

In the elastoplastic analysis of the structure with MR dampers, the frame structure is simulated by the trilinear stiffness degeneration model. The stiffness of each floor changes in the fold line path during the earthquake. The model structure parameters are the mass vector

$\boldsymbol{m}$ = [3.25 3.04 2.88 2.78 2.66] × 104 kg, the initial stiffness vector

$\boldsymbol{k}$ = [1.82 2.50 2.50 2.50 2.50] × 107 N m−1, the story height

$\boldsymbol{h}$ = [4 3.5 3.5 3.5 3.5] m, the inter-story cracking drifts

Δc = [6.3 4.9 4.2 3.87 3.75] mm, the inter-story yielding drifts

Δy = [21.8 18.9 17.2 14.5 11.8] mm.

In this example, the model of the structure is subjected to the south east component of the 1997 Gadha Jabalpur earthquake with 355 gal acceleration amplitude, and the sampling time is 0.025 s, i.e. the delay time. We developed a MATLAB program for the MOGA optimized MIMO-ANFIS control and elastoplastic analysis of the structure with MR dampers.

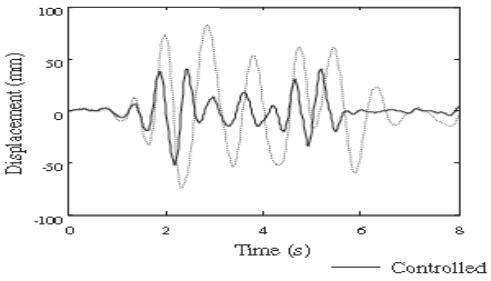

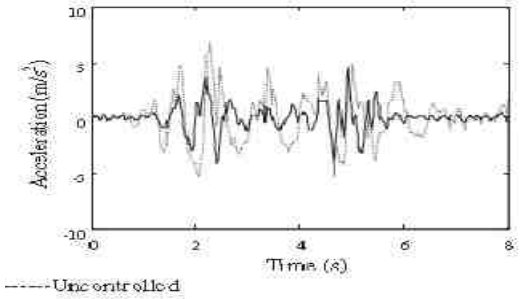

Fig.4: Response comparison of controlled and uncontrolled structure using MOGA optimized ANFIS+GA.

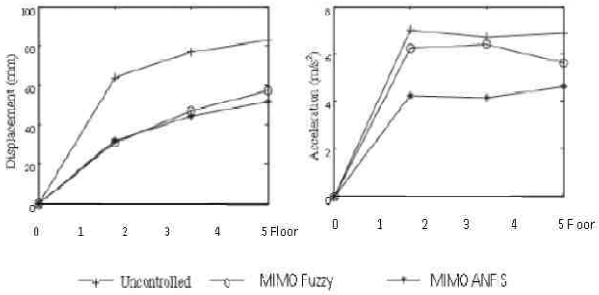

Fig.5: The maximum responses comparison of each floor.

The top-floor displacement and acceleration responses of the structure with the MR damper are compared with those of the structure without the MR damper, as shown in figure 4. Both the displacement and the acceleration responses of the controlled structure with the MR damper are reduced effectively. The maximum displacement of the uncontrolled structure is 0.970 cm, while the maximum displacement of the MIMO fuzzy controlled structure is 0.376 cm and of proposed MIMO-ANFIS controlled structure is 0.288 cm for fifth storey. The displacement response is reduced by 29%. The maximum acceleration of the uncontrolled structure is 6.86 m s^{-2}, while the maximum acceleration of the controlled structure is 904.7 cm s^{-2} for fifth storey. The peak acceleration of the 5th floor of the MIMO ANFIS is reduced by 71 % compared to the uncontrolled case. It can also be shown that the displacement responses are reduced more effectively than the acceleration responses. This is due to the fact that control forces produced by MR dampers are equivalent to increasing stiffness and damping of structures: both are beneficial to decreasing displacement responses, while increasing of stiffness will possibly increase acceleration responses. Figure 5 compares maximum displacement and maximum acceleration for the uncontrolled structure, the MIMO fuzzy controlled structure and the MIMO-ANFIS controlled structure. Both the displacement and the acceleration responses are reduced effectively when MR dampers are used. At the same time, it

https://dx.doi.org/10.22161/ijaers/3.11.23 *ISSN: 2349-6495(P) | 2456-1908(O)*

can be clearly seen that the MIMO-ANFIS method can reduce the dynamic responses of the structure more effectively than the uncontrolled structure, especially for the acceleration responses. Increasing the control forces blindly is equal to increasing the stiffness and the damping of the structure blindly, which will lead to increase of the dynamic responses, especially for acceleration responses.

V. CONCLUSIONS

This study investigates the control performance of the MIMO ANFIS optimized by an MOGA for control of a 5-story building subjected to earthquake. For comparison purpose, a MIMO fuzzy control algorithm is considered as the baseline. Based on numerical simulations, it can be seen that the MOGA-optimized MIMO ANFIS+GA can effectively reduce both displacement and acceleration responses of the building structure by 30% compared to the MIMO fuzzy control algorithm. After single optimization run using MATLAB Software, an engineer can simply select another ANFIS that satisfies the desired performance requirements from among a number of optimal solutions. It would be important characteristics of the MOGA based optimization compared to other optimization methods.

In a numerical example, a five-storey smart structure with a MR damper in the first floor is analyzed. Some conclusions can be drawn from the analysis.

(1) The MR damper is a kind of smart damper, and it can reduce the responses of structures effectively.

(2) The MOGA-optimized MIMO ANFIS real-time control method solves the problem of time delay. The responses of the structure with MR dampers by proposed method are smaller than those by the MIMO fuzzy method, especially for the acceleration responses.

REFERENCES

[1] Constantinou, M.C., Soong, T.T.: Passive and Active Structural Vibration Control in Civil Engineering. Springer-Verlag, New York (1994).

[2] Spencer, B.F., Jr., Nagarajaiah, S.: State of the art of structural control. Journal of Structural Engineering, ASCE, Vol. 129, pp. 845-856 (2003).

[3] Kim, H.S., Roschke, P.N.: GA-Fuzzy Control of Smart Base Isolated Benchmark Building using Supervisory Control Technique. Advances in Engineering Software, Vol. 38, pp. 453-465 (2007).

[4] Jansen, L.M., Dyke, S.J.: Semi-active Control Strategies for MR dampers: a Comparative Study. Journal of Engineering Mechanics, ASCE, Vol. 126, pp. 795-803 (2000).

[5] Dyke, S.J., Spencer, B.F., Jr., Sain, M.K., Carlson, J.D.: Modeling and Control of Magnetorheological Dampers for Seismic Response Reduction. Smart Mat and Struct, Vol. 5, pp. 565-575 (1996).

[6] Deb, K., Pratap, A., Agrawal, S., Meyarivan, T.: A Fast Elitist Non-dominated Sorting Genetic Algorithm for Multi-objective Optimization: NSGA-II. IEEE, Trans. Evol. Comput., Vol. 6, pp. 182-197 (2002).

[7] Hyun-Su Kim" Development of MIMO Fuzzy Control System for Seismic Response Reduction using Multi-Objective Genetic Algorithm" Advanced Science and Technology Letters Vol.32 (Architecture and Civil Engineering 2013), pp.50-53 http://dx.doi.org/10.14257/astl.2013.32.12

[8] J.S.R Jang, "*Neuro-Fuzzy and Soft Computing*", Prentice Hall, Upper Saddle River, NJ: 07458. [Jang, 1992, Jang and Gulley, 1995]

[9] J. Wesley, "*Fuzzy and Neural Approaches in Engineering*", Hines New York 1997.

[10] Hongxing Li, C.L. PhiliD Ghen, Han-Pang Huang,*"Fuzzy Neral Intelligent System: Mathematical foundation and the applications in engineering"*, by CRC Press LLC 2001.

[11] Yu.Hen.Hu, Jenq-Neng Hwang, *"Introduction to Neural Networks for Signal Processing "*, by CRC Press LLC 2002.

[12] Lakhmi C. Jain and Berend Jan van der Zwaag and Ajith Abraham. *"Innovations in Intelligent Systems Design, Management and Applications* ", Springer, 2004.

[13] Xuan F. Zha, *"Artificial Intelligence And Integrated Intelligent Information Systems-Emerging Technologies And applications* ", Idea Group Inc (IGI), 2006.

[14] M.F. Azeem, et al, "*Generalization of adaptive neuro-fuzzy inference systems*", IEEE Trans. Neural Networks 11, pp 1332 –1346 2000.

BIOGRAPHY

RAVINDRA SINGH TOMAR received the Bachelor Degree from the University of Harisingh Gaur, Sagar, Madhya Pradesh, in 1981, the Master of Science (Physics) degree from the University of Harisingh Sagar, Madhya Pradesh, in 1984. Currently, He is Director of Kirodimal Institute of Technology, Raigarh, Chhattisgarh, India. His teaching and research areas include application of soft-computing techniques in seismic vibration under Physics faculty. He is pursuing his Ph.D degree from Dr C V Raman University,Bilaspur,Chhattisgarh,India.

cgjjvp@rediffmail.com

https://dx.doi.org/10.22161/ijaers/3.11.23 *ISSN: 2349-6495(P) | 2456-1908(O)*

DR M F QURESHI received the B.E. degree in Electrical Engineering from Guru Ghasi Das Central University, Bilaspur, Chhattisgarh, in 1984, the M.E. degree in Electrical Engineering from Rani Durgavati University, Jabalpur, Madhya Pradesh, in 1998, and the Ph.D. degree in Electrical Engineering from the Guru Ghasi Das Central University, Bilaspur, Chhattisgarh, in 2004, respectively. Currently, He is Head of Department of Electrical Engineering at Govt. Polytechnic Dhamtari, Chhattisgarh, India. He has authored/co-authored a number of research papers published in many journals across the world. He has guided six M. Phil student and four Ph.D scholars.
mfq_pro@rediffmail.com

DR S K SHRIVASTAVA Currently, He is Professor of Physics department in Dr C V Raman University,Bilaspur,Chhattisgarh,India. His teaching and research areas include application of soft-computing techniques in seismic vibration under Physics faculty. He is pursuing his Ph.D degree from Dr C V Raman University,Bilaspur,Chhattisgarh,India

https://dx.doi.org/10.22161/ijaers/3.11.24 *ISSN: 2349-6495(P) | 2456-1908(O)*

Development of ANFIS Controller and PID Controller for Seismic Vibration Control of Structural System

Tomar R S[1],Qureshi M F[2], Shrivastava S K[3]

[1]Department of Physics, Kirodimal Institute of Technology, Raigarh, Chhattisgarh, India
[2]Department of Electrical Engineering, Government Polytechnic, Dhamtari, Chhattisgarh, India
[3]Department of Physics, Dr C V Raman University, Kota, Bilaspur, Chhattisgarh, India

Abstract *—In this paper, the problem of active vibration control of multi-degree-of-freedom structures is considered. ANFIS Controller and PID Controller are designed to suppress structural vibrations against earthquakes under the non-linear soil-structure interaction. The advantage of the ANFIS Controller and PID Controller approach is the ability to handle the non-linear behavior of the system. Non-linear behavior of the soil is modeled in the dynamics of the structural system with non-linear hysteric restoring forces. The ANFIS Controller and PID Controller are designed for getting the maximum response reduction under different types of earthquake excitations. A structural system was simulated against the ground motion of the destructive Gadha earthquake (Mw = 6.9) in Jabalpur, India on 21 May 1997. At the end of the study the time history of the storey displacements and accelerations and the frequency responses of both the uncontrolled and the ANFIS Controller and PID Controller based controlled structures are presented. These results show that the proposed ANFIS Controller and PID Controller have great potential in active structural control. In another situation two MR dampers were used as multiple control devices and a scaled five-story building model was selected as an example structure. A clipped-optimal control algorithm was compared with the proposed ANFIS Controller and PID Controller. After numerical simulation, it has been verified that the ANFIS Controller and PID Controller can present better control performance compared to the clipped-optimal control algorithm in reducing both displacement and acceleration responses. Also in this paper, conventional (MR Damper), PID controllers and ANFIS+PID controllers, respectively denoted by PID controllers and ANFIS+PID controllers, are designed to suppress vibrations of a three - story building against earthquake. The structural system is simulated against the ground accelerations of the Gadha-Jabalpur earthquake in India on May 21th, 1997; the Northridge earthquake in USA on January 17th, 1994 and the Kobe earthquake in Japan on January 16th, 1995. The control effects of PID controllers and ANFIS+PID controllers are compared via the time history of the story displacements of the structure.*

Keywords—Seismic vibration control, ANFIS Controller, PID Controller, non-linear structure, earthquake induced vibration.

I. INTRODUCTION

Natural hazards such as earthquakes and high winds pose a serious threat to multi-degree-of freedom structures. Recent earthquakes, such as the 1996 Gadha (Jabalpur), India, the 1994 Northridge, USA_ the 1995 Kobe, Japan and the 1999 Kocaeli, Turkey earthquakes resulted in extensive destructive damage to structures. A variable solution to safeguard the civil structures against these natural hazards is the use of structural control systems. Over the past few decades, a number of structural control strategies have been developed and practical applications have been realized. Schlacher et al. (1997) used a class of hybrid control systems for earthquake-excited high raised buildings, which consists of a base isolation and an additional active damper, and the mechanical model of building is a shear wall structure with non-linear hysteretic restoring forces. Al-Dawod et al. (2001, 2004) applied fuzzy logic control (FLC) for active vibration control of tall buildings in two papers. Yagiz (2001) applied sliding mode control for a multi-degree-of-freedom structural system. Guclu (2003) designed a fuzzy logic based controller and PD controller for an active control device considering a five degrees of freedom structure against the ground motion of the destructive earthquake. Yang et al. (2006) applied a neural network designed for system identification and vibration suppression in a building structure with an active mass damper. In this study, ANFIS Controller and PID Controller are proposed and designed to suppress structural vibrations against earthquake. This earthquake motion is obtained

https://dx.doi.org/10.22161/ijaers/3.11.24 *ISSN: 2349-6495(P) | 2456-1908(O)*

using the seismic data of the destructive Gadha(Jabalpur),India earthquake (M*w* = 6.9), which resulted in disaster in the vicinity of Jabalpur.

There are a couple of reasons to use ANFIS Controller and PID Controller in reducing earthquake excited structural response. It is well known that civil structures are complex and large structural system. They generally have distributed parameters and are of complex geometries making them difficult to model and analyze. They are subjected not only to static loading but also to a variety of complex dynamic loading, including winds, and earthquakes. The complexity in these structures generally arises from uncertainties in structural models, parameters and geometries. Some uncertainties are not random in nature. Normally, a precise mathematical model is difficult to be obtained for describing an entire large structural system. Conventional structural analysis models are built based on many simplifications and assumptions on structural system to reach the goal of precision. All these provide the motivation to use soft computing technique in design of earthquake resistant structures.

ANFIS Controller and PID Controller have the ability to handle this problem. It also takes into account uncertainty in loading and structural behavior. To evaluate the efficiency of the proposed control method, a 5-storey realistic shear building is used. The ANFIS Controller and PID Controller is designed for the first mode characteristics of the mentioned structure for getting the maximum response reduction under different types of earthquake excitations.

To illustrate the effectiveness of the proposed ANFIS Controller and PID Controller, data based simulation was implemented for a structural system in MATLAB/Simulink environments. It is shown that the controller provides robust performance when large parameter variations in structural system are presented. A numerical model of the 5-story example building structure with two MR dampers is implemented in SIMULINK and MATLAB. Using this numerical model, time history analyses of 12 seconds with a time step of 0.004 sec are performed in order to investigate the control performance of MR dampers controlled by the NAGA-II optimized ANFIS Controller and PID Controller. The NSGA-II based optimization is performed with the population size of 100 individuals. An upper limit on the number of generations is specified to be 1000. As the number of generations increases, the control performance of the elite (i.e. non-dominated) individuals is improved. After optimization run, Pareto-optimal front (a set of Pareto-optimal solutions) is obtained. Optimization results show that two objective function values of every solution in Pareto-optimal front are less than 1. It means that the NSGA-II optimized ANFIS Controller and PID Controller can provide better control performance in reducing both displacement and acceleration responses compared to the clipped-optimal controller.

In this paper, conventional (MR Damper), PID controllers and ANFIS+PID controllers, respectively denoted by PID controllers and ANFIS+PID controllers, are designed to suppress vibrations of a three - story building against earthquake. The structural system is simulated against the ground accelerations of the Gadha-Jabalpur earthquake in India on May 21th, 1997; the Northridge earthquake in USA on January 17th, 1994 and the Kobe earthquake in Japan on January 16th, 1995. The control effects of PID controllers and ANFIS+PID controllers are compared via the time history of the story displacements of the structure.

II. SCALED BUILDING MODEL

In order to develop an ANFIS Controller and PID Controller for effective control of multiple MR dampers, a 5-story example building structure shown in Fig. 1 is employed. This example structure is developed based on a scaled 3-story shear building model used in the previous research. As shown in this figure, two MR dampers are rigidly connected to the first floor and the second floor of the structure, respectively. A numerical model of the 5-story example building structure with two MR dampers is implemented in SIMULINK and MATLAB. Using this numerical model, time history analyses of 12 seconds with a time step of 0.004 sec are performed in order to investigate the control performance of MR dampers controlled by the NAGA-II optimized ANFIS Controller and PID Controller.

https://dx.doi.org/10.22161/ijaers/3.11.24 *ISSN: 2349-6495(P) | 2456-1908(O)*

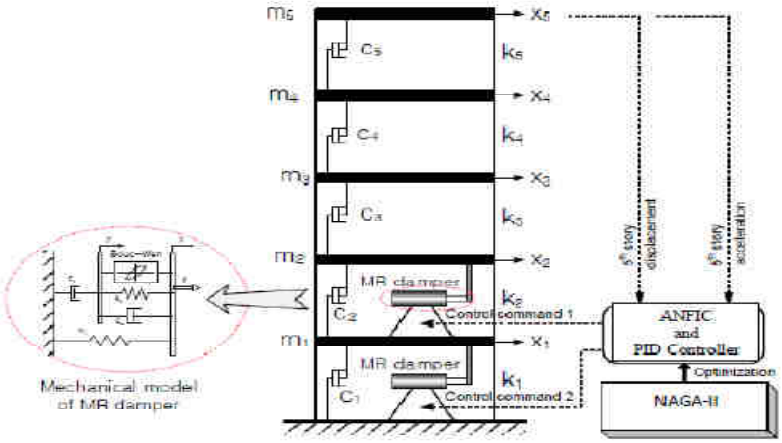

Fig.1: 5-story example building model

The first five natural frequencies of the example structure model are 3.62, 10.57, 16.94, 22.07 and 25.41 Hz, respectively. In this study, the modified Bouc-Wen model [18] is used to describe how the damping force is related to the velocity and applied command voltage. The mechanical model for the MR damper based on the Bouc-Wen hysteresis model is shown in Fig. 1. The detailed description and the parameter values of the MR damper model are presented in Dyke *et al.*'s work [18]. This MR damper model has a maximum generated force of about 1500 N depending on the relative velocity across the MR damper with a saturation voltage of 2.25 V. In numerical analysis, the model of the example structure is subjected to the NS component of the 1940 El Centro earthquake. Because the system under consideration is a scaled model, the earthquake has been reproduced at five times the recoded rate.

III. THE PID CONTROLLER

PID control has been widely used in industry. In general the closed loop diagram of the feedback system is shown in Figure 2. Here, $x_{r2}(t)$ is the desired value for the output of the system. $x_2(t)$ is the output and $e(t)$ is error.

$$e(t) = x_{r2}(t) - x_2(t). \quad (1)$$

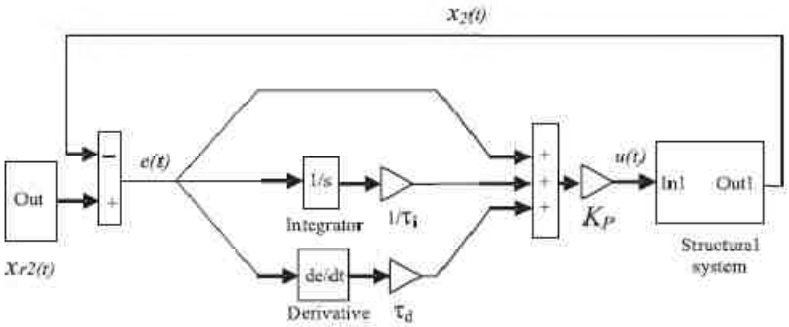

Fig.2: Closed loop block diagram with PID controller.

The control input u(t) is obtained as follows:

$$u(t) = K_P \left[e(t) + \frac{1}{\tau_i} \int_0^t e(t)d(t) + \tau_d \frac{de(t)}{dt} \right] \quad (2)$$

Where, *KP*, τ_i and τ_d are the proportionality constant, integral time and derivative time, respectively. These values are given in the Appendix.

IV. ANFIS ALGORITHM

ANFIS was introduced in1993. ANFIS is able to extract a set of fuzzy "if-then" rules and define the membership functions in order to establish the association between

https://dx.doi.org/10.22161/ijaers/3.11.24 *ISSN: 2349-6495(P) | 2456-1908(O)*

inputs and outputs. Its structure is shown in Figure 3. Basically, ANFIS suggests a method that, through the training procedure, can estimate the membership function parameters that serve the fuzzy inference system (FIS) to consequently specify the desired output for a certain given input.

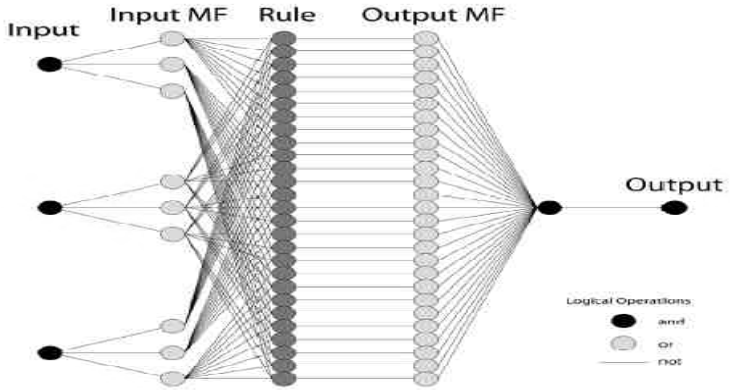

Fig.3: ANFIS structure.

ANFIS creates a fuzzy inference system in order to relate a certain input to the appropriate output. FIS interprets inputs into a set of fuzzy membership values and similarly the output membership functions to outputs. During the learning process, all parameters which define the membership functions will change. In order to optimize the model, these parameters are evaluated. Usually a gradient vector is used and an optimization routine could be applied in order to tune the parameters, so as to lead the model to a better generalization performance. In this work, 20 seismic parameters are used as input data to describe the damage caused by one seismic event, and a total of 200 seismic events are used to train the system. All 20 seismic features have been normalized to belong in the interval [0, 1]. The 200 seismic events are distributed equally to all four damage categories in order to create a uniform data set. First, inputs are related to membership functions (MFs), (Figure 4 shows the initial MF for one of the seismic parameters), to rules to outputs MFs, by using Fuzzy C-Means (FCM) technique [32, 33], which is analyzed later in this section. Next, the input/output data, which is a uniform set of 100 accelerograms, is used for training the model. The membership function parameters are tuned through the training process.

After the training, a model validation procedure is performed. During this procedure, an unknown input data set is presented to the trained fuzzy model for simulation. Thus, it can be evaluated the efficiency of the model. When a checking data set is presented to ANFIS, the fuzzy model selects the appropriate parameters associated with the minimum checking data model error. One crucial point with model validation, is selecting a suitable data set. This set must be representative of the data that the model is trying to simulate, and at the same time distinguishable from the training data. If a large amount of samples is collected, then all possible cases are contained and thus, the training set is more representative. In our case, a total number of 200 seismic excitations are considered as the data set. FCM is a wildly used data clustering technique. Each data point is assigned to a cluster with a membership grade that is specified by a membership grade. It provides a method that shows how to group data points that populate some multidimensional space into a specific number of different clusters.

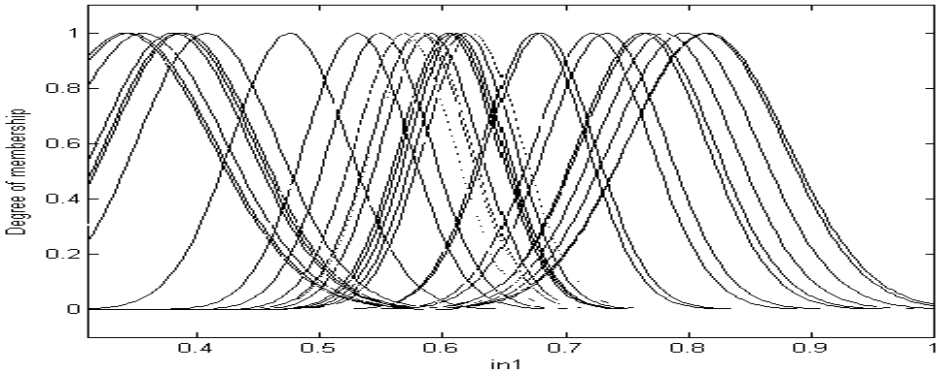

Fig.4: Initial membership function on input 1.

https://dx.doi.org/10.22161/ijaers/3.11.24 *ISSN: 2349-6495(P) | 2456-1908(O)*

The purpose of data clustering is to discover similarities between input patterns from a large data set, in order to design an effective classification system. At first, the FCM algorithm selects randomly the cluster centers. This initial choice for these centers is not always the appropriate. Furthermore, the variation of the cluster centers leads to different membership grades for each one of the clusters. Through the iteration process of the FCM algorithm, the cluster centers are gradually moved towards to their proper location. This is achieved by minimizing the weighted distance between any data point and the cluster centre. Finally, FCM function defines the cluster centers and the membership grades

or every data point.

A flow of hybrid active control system

In this paper, intelligent fuzzy control system and reflective fuzzy control system are combined. Intelligent fuzzy control consists of three systems which are already proposed: (1) prediction of earthquake input (2) structural identifucation (3)fuzzy maximizing decision [Bellman,R.E. and Zadeh,L.A., 1970]. On the other hand, conditioned fuzzy set rules are employed in fuzzy control system.

Figure 5 shows a flow chart of hybrid control system used in this research. This hybrid active control system has the following special and intelligent features,: 1) Objective and constraint conditions of active control are described with membership functions of fuzzy theory, 2) Prediction of earthquake input and the structural identification are performed in real time, 3) An optimal control variable is determined by means of fuzzy maximizing decision, and 4) Fuzzy control system is employed as the reflective fuzzy control system against unexpected large disturbance.

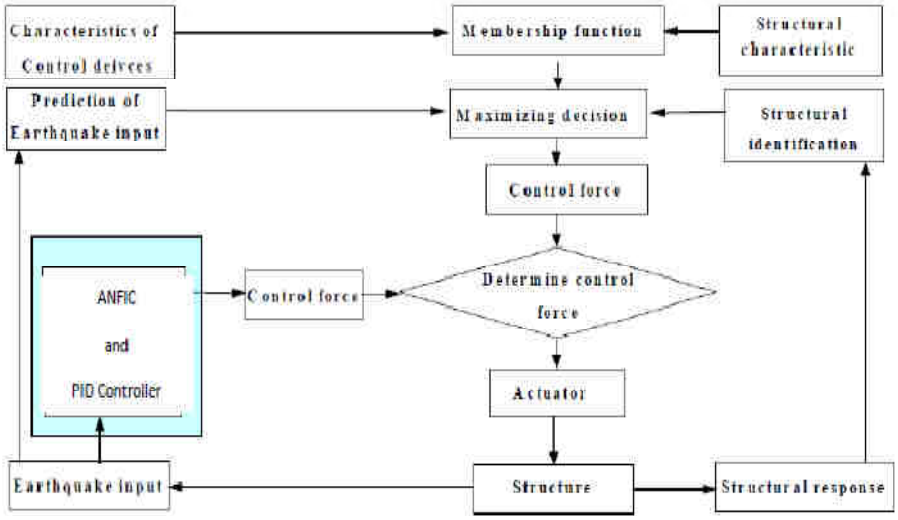

Fig.5: A flow chart of hybrid active control system

V. SIMULATION

Numerical Studies

A numerical model of the 5-story example building structure with two MR dampers is implemented in SIMULINK and MATLAB. Using this numerical model, time history analyses of 12 seconds with a time step of 0.004 sec are performed in order to investigate the control performance of MR dampers controlled by the NAGA-II optimized ANFIS Controller and PID Controller. The NSGA-II based optimization is performed with the population size of 100 individuals. An upper limit on the number of generations is specified to be 1000. As the number of generations increases, the control performance of the elite (i.e. non-dominated) individuals is improved. After optimization run, Pareto-optimal front (a set of Pareto-optimal solutions) is obtained. Optimization results show that two objective function values of every solution in Pareto-optimal front are less than 1. It means that the NSGA-II optimized ANFIS Controller and PID Controller can provide better control performance in reducing both displacement and acceleration responses compared to the clipped-optimal controller.

Consequently, one controller, that can appropriately control both displacement and acceleration responses, has been

https://dx.doi.org/10.22161/ijaers/3.11.24 *ISSN: 2349-6495(P) | 2456-1908(O)*

selected among the Pareto optimal ANFIS Controller and PID Controller. The values of two objectives of the selected ANFIS are both 0.8 and it means that the selected ANFIS Controller and PID Controller can reduce both the peak 5th floor displacement and acceleration responses by 20%, compared to the clipped optimal controller. The peak responses of the ANFIS Controller and PID Controller, clipped-optimal controller, and uncontrolled case for the five floors of the seismic-excited example building structure are compared in Table 1.

Table.1: Comparison of peak story responses. Story

	Displacement (cm)			Drift (cm)			Acceleration (cm/sec^2)		
Story	Uncontrolled	PID	ANFIS +PID	Uncontrolled	PID	ANFIS +PID	Uncontrolled	PID	ANFIS +PID
1.	0.324	0.096	0.113	0.324	0.096	0.113	497.8	469.8	283.6
2.	0.563	0.187	0.169	0.217	0.096	0.054	670.8	370.7	336.9
3.	0.723	0.255	0.233	0.203	0.093	0.085	486.8	387.9	245.7
4.	0.857	0.327	0.265	0.197	0.076	0.072	542.3	313.2	268.2
5.	0.950	0.045	0.242	0.123	0.054	0.043	840.3	368.3	296.3

ANFIS Controller and PID Controller are 20% smaller than those of the clipped optimal controller. The peak displacement of the 5th floor of the uncontrolled case is 0.930 cm. On the other hand, the peak displacement of the 5th floor of the ANFIS Controller and PID Controller is 0.218 cm, which is only 30 % of the uncontrolled case. The peak acceleration of the 5th floor of the ANFIS Controller and PID Controller is reduced by 65 % compared to the uncontrolled case. The story drifts of the ANFIS Controller and PID Controller are also about 20% smaller than those of the clipped-optimal controller.

Earthquake Excitation and the response of the structure

In this study, Matlab Simulink with ANFIS and PID Toolbox is used. The aim of the ANFIS control system for the structural system uses the errors in the second storey motion $(e = x_{r2} - x_2)$ and the derivatives of it as the input variable while the control voltage (u) are their outputs. Reference values are considered to be zero in Figure 6.

Table.2: Rule base for the ANFIS Controller and PID Controller.

Velocity of the error (de/dt)		VN	VZ	VP
Error (e)	XNB	UNB	UNM	UNS
	XNS	UNM	UNS	UZ
	XZ	UNS	UZ	UPS
	XPS	UZ	UPS	UPM
	XPB	UPS	UPM	UPB

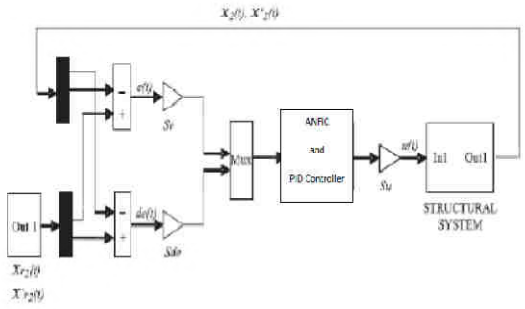

Fig.6: Closed loop model of the structure with ANFIS Controller and PID Controller.

A model of the two similar rule bases developed by heuristics with error in body bounce motion, pitch motion and velocity as input variables is given in Table 2, where P, N, Z, B, M, S represent Positive, Negative, Zero, Big, Medium and Small, respectively. A trial and error approach with triangular membership functions has been used to achieve a good controller performance. The membership functions for both scaled inputs (e, de) and output (u) of the controller have been defined on the common interval [–1, 1]. Scaling factors (Se, Sd, Su) are used to set e, de and u (Figure 6) (Mudi and Pal, 1999). The first rule in Table 2 is given below:

If e is *XNB and* de/dt is *V N THEN* u is *UNB.*

All the rules are written using the Mamdani method to apply to fuzzification. In this study, the centroid method is used in defuzzification. A structural system has been simulated against the earthquake ground motion of the

https://dx.doi.org/10.22161/ijaers/3.11.24 *ISSN: 2349-6495(P) | 2456-1908(O)*

destructive Gadha earthquake (M*w* =6.9). Earthquake ground motion is used as an input to a building structure. Accelerations were recorded at the Gadha (Jabalpur) Observatory and Earthquake Research Institute strong motion station at the IIT Rurki, India.

Table.3: Peak response and peak response reduction using different control systems in Gadha Earthquake

Floor	Peak response of displacement		Percentage response reduction (%)
	Uncotrolled	ANFIS+PID Control	
1	0.013	0.006	48.0
2	0.026	0.012	50.0
3	0.040	0.018	52.0
4	0.052	0.023	54.3
5	0.065	0.025	57.5

It is seen from the Table3 that ANFIS Controller and PID Controller reduces the uncontrolled peak displacement response of the top floor about 49% and 57.5 % for first and fifth storey respectively for the Gadha earthquake. This feature of ANFIS Controller and PID Controller is revealed in the time history responses of the top floor compared to uncontrolled response when subjected to Gadha earthquake.

Dynamic Model of the Structural System

In this paper, the simple structure model is used to study the control effect of ANFIS+PID in comparison with PID. The structure, which has three degrees of freedom all in a horizontal direction, is shown in Fig.7. In this paper, conventional (MR Damper), PID controllers and ANFIS+PID controllers, respectively denoted by PID controllers and ANFIS+PID controllers, are designed to suppress vibrations of a three - story building against earthquake. The structural system is simulated against the ground accelerations of the Gadha-Jabalpur earthquake in India on May 21th, 1997; the Northridge earthquake in USA on January 17th, 1994 and the Kobe earthquake in Japan on January 16th, 1995. The control effects of PID controllers and ANFIS+PID controllers are compared via the time history of the story displacements of the structure.

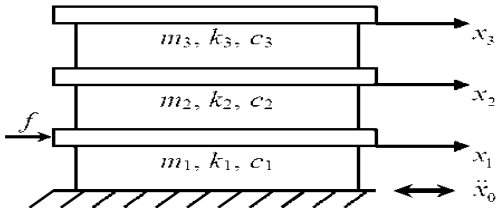

Fig.7: The structural system

The equations of motion of the system subjected to the ground acceleration ¨x0 (see
Fig. 8), with control force vector {F}, can be written as:

$$[M]\{\ddot{x}\} + [C]\{\dot{x}\} + [K]\{x\} = \{F\} - [M]\{r\}\ddot{x}_0 \quad (1)$$

where, $\{x\} = [x_1\ x_2\ x_3]^T$, $\{F\} = [-f\ 0\ 0]^T$, $\{r\} = [1\ 1\ 1]^T$. f is the control force,
the matrices [M], [C] and [K], respectively representing the structural mass, damping and
stiffness ones, are given as follow:

$$[M] = \begin{bmatrix} m_1 & 0 & 0 \\ 0 & m_2 & 0 \\ 0 & 0 & m_3 \end{bmatrix}, [K] = \begin{bmatrix} k_1 + k_2 & -k_2 & 0 \\ -k_2 & k_2 + k_3 & -k_3 \\ 0 & -k_3 & k_3 \end{bmatrix},$$

[C] = 0.1 × [M] + 0.003 × [K].

https://dx.doi.org/10.22161/ijaers/3.11.24 *ISSN: 2349-6495(P) | 2456-1908(O)*

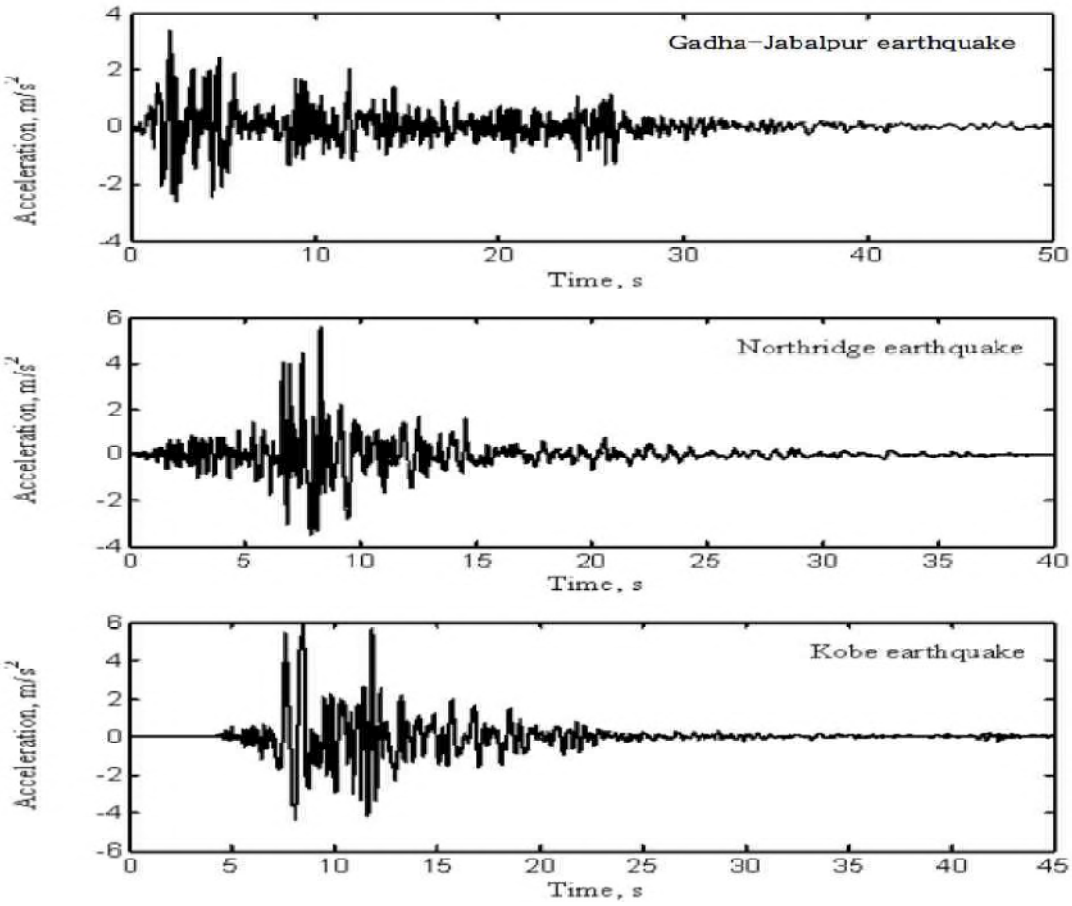

Fig. 8: The ground acceleration ¨x0, m/s²

VI. RESULTS AND DISCUSSION

The results include: time history of the storey displacements of the structure for both controlled and uncontrolled cases in order to compare control effect of PID and ANFIS+PID. Here m is structural mass and k is stiffness ones,

Results for the structure excited by the Gadha earthquake

In this subsection, the following data will be used: m1 = m2 = m3 = m0 = 4 ×10^5(kg); k1 = k2 = k3 = k0 = 2 × 10^8 (N/m).

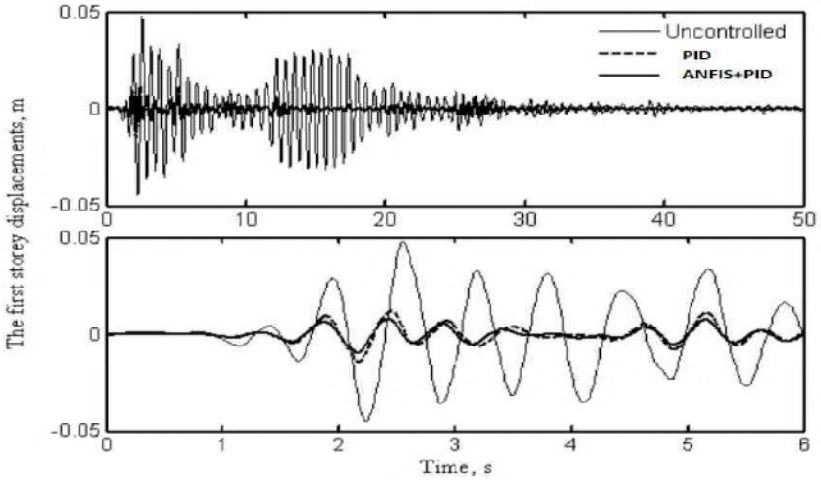

Fig. 9: Time responses of the first storey displacements - Gadha earthquake

https://dx.doi.org/10.22161/ijaers/3.11.24 *ISSN: 2349-6495(P) | 2456-1908(O)*

Figs 9 and 10 show the time responses of the first and top storey displacements, respectively. The maximum storey drifts are shown in Fig. 11. Comparison of the effectiveness of the two controllers is presented in Table 4.

Table.4: Comparison of the effectiveness of the three controllers - Gadha earthquake

Building Storey	Maximum uncontrolled displacement, m	Controlled to uncontrolled displacement ratio	
		PID	ANFIS+PID
1	0.047	0.3	0.2
2	0.084	0.55	0.5
3	0.107	0.60	0.53

Results for the structure excited by the Northridge earthquake

In this subsection, the structural data will be changed as follow: m1 = m2 = m3 = m0+ 10%m0; k1 = k2 = k3 = k0 - 10%k0.Figs 12 and 13 show the time response of the top storey displacement and the maximum storey drifts, respectively. Comparison of the effectiveness of the three controllers is presented in Table 5.

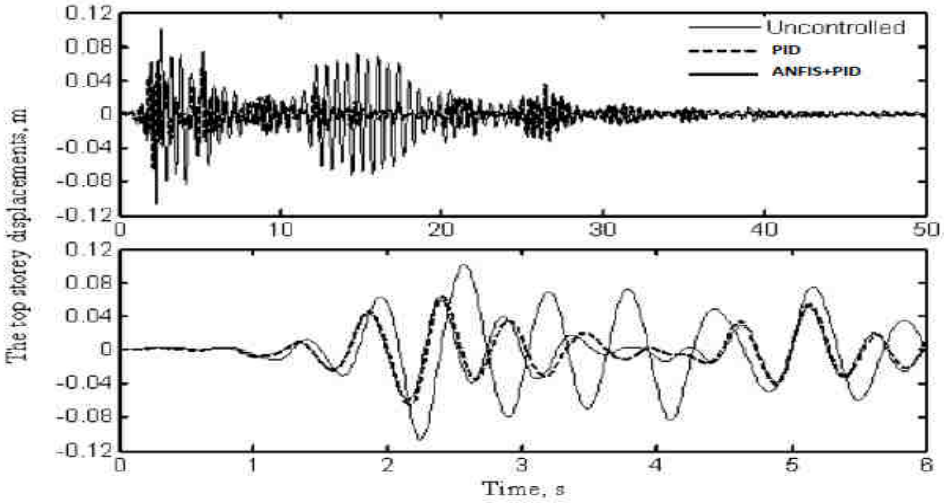

Fig. 10: Time responses of the top storey displacements - Gadha earthquake

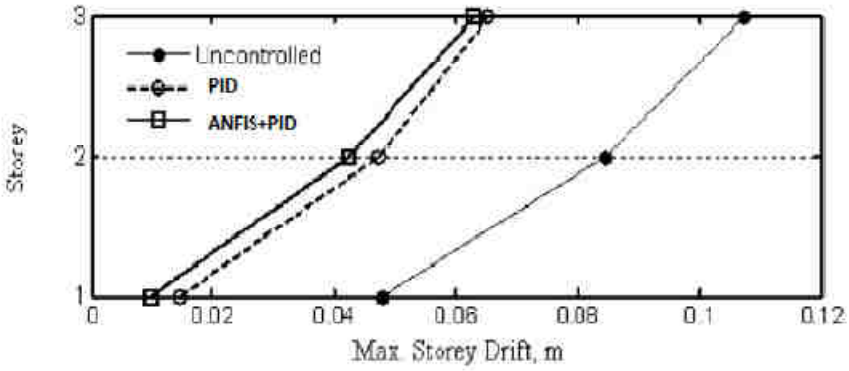

Fig. 11: The maximum storey drifts - Gadha earthquake

Table.5: Comparison of the effectiveness of the three controllers - Northridge earthquake

Building Storey	Maximum uncontrolled displacement, m	Controlled to uncontrolled displacement ratio	
		PID	ANFIS+PID

https://dx.doi.org/10.22161/ijaers/3.11.24 *ISSN: 2349-6495(P) | 2456-1908(O)*

1	0.070	0.223	0.156
2	0.135	0.456	0.45
3	0.157	0.567	0.534

Results for the structure excited by the Kobe earthquake

In this subsection, another structural parameter will be used as follow: m1 = m2 = m3 = m0 − 10%m0, k1 = k2 = k3 = k0 + 10%k0.

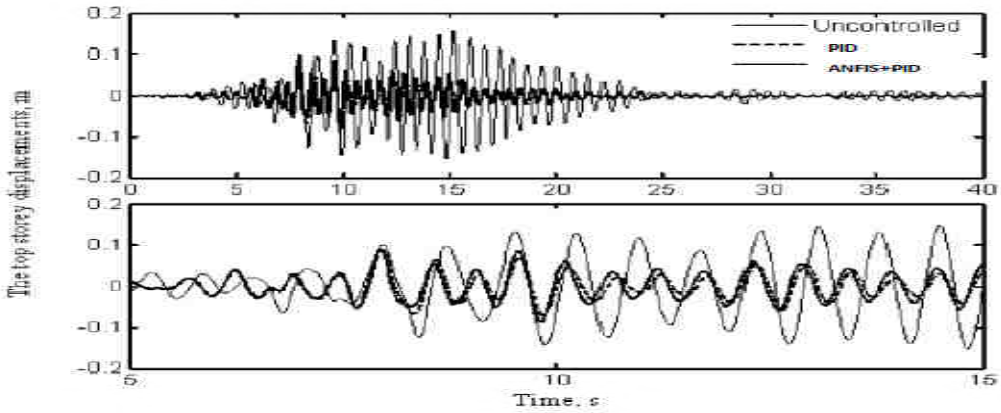

Fig.12: Time responses of the top storey displacements - Northridge earthquake

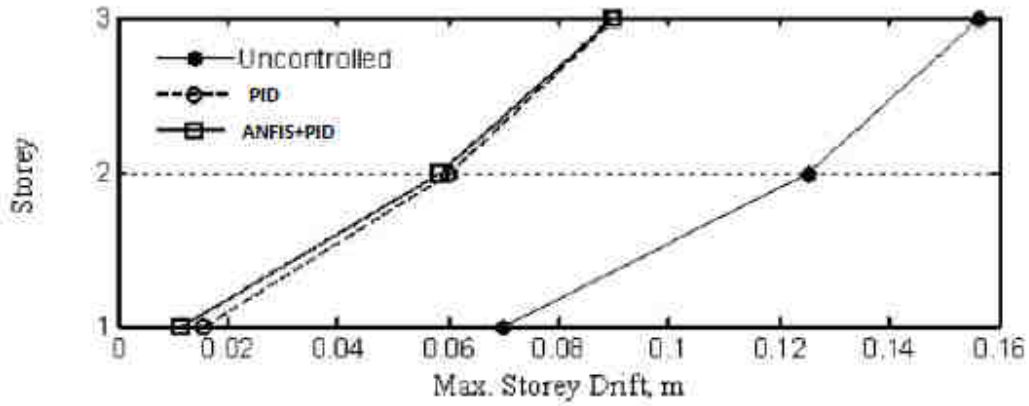

Fig. 13: The maximum storey drifts - Northridge earthquake

Figs 14 and 15 show the time response of the top storey displacement and the maximum storey drifts, respectively. Comparison of the effectiveness of the three controllers is presented in Table 6.

Table.6: Comparison of the effectiveness of the three controllers - Kobe earthquake

Building Storey	Maximum uncontrolled displacement, m	Controlled to uncontrolled displacement ratio	
		PID	ANFIS+PID
1	0.065	0.256	0.176
2	0.114	0.456	0.461
3	0.135	0.563	0.545

https://dx.doi.org/10.22161/ijaers/3.11.24 *ISSN: 2349-6495(P) | 2456-1908(O)*

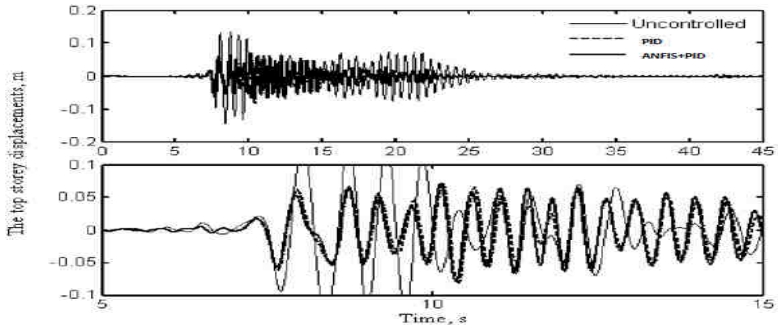

Fig.14: Time responses of the top storey displacements - Kobe earthquake

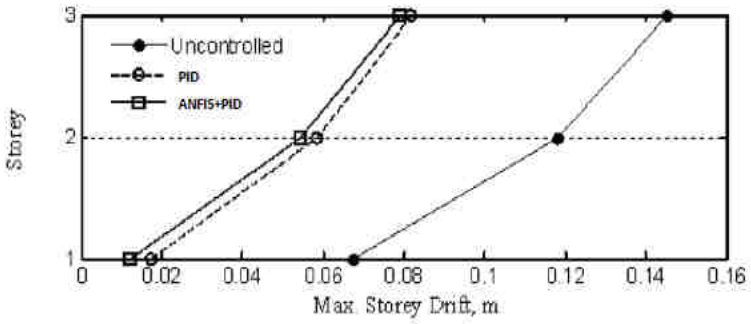

Fig. 15: The maximum storey drifts - Kobe earthquake

As shown in above - mentioned figures and tables, vibration amplitudes of the storeys are decreased successfully with PID and ANFIS+PID for the structure with the different structural data excited by three different earthquakes. It allows partially evaluating the stability and robustness capacities the proposed controller - ANFIS+PID. With the case of the Gadha earthquake, the reduction ratios (ratio of the con- trolled to uncontrolled response) for maximum displacement of the top floor of the structure are about 61% and 59% for the PID and ANFIS+PID, respectively (Fig. 11 and Table 5). Therefore, it is seen that the ANFIS+PID is more effective than the PID in view of reducing the displacement response of the structure. The effectiveness of two controllers in reducing the response of the structure due to other two earthquakes (Northridge and Kobe) is also shown for comparison in Figs. 13 and 15 and Tables 6 - 7. Almost the same behavior as for the Gadha earthquake can be observed for these earthquakes too.

A Simulink model of the system, which consisted of the selected building, was created and simulations were performed using MATLAB. It is seen from the Table 3 that ANFIS Controller and PID Controller reduces the uncontrolled peak displacement response of the top floor about 49% and 57.5 % for first and fifth storey respectively for the Gadha earthquake. This feature of ANFIS Controller and PID Controller is revealed in the time history responses of the top floor compared to uncontrolled response when subjected to Gadha earthquake.

VII. CONCLUSIONS

The safety of the structures mainly depends on the displacement response, while the comfort level of the occupants depends on the acceleration response. To ensure that both responses are within permissible limits, ANFIS controller and PID controller have been designed for a multi-degree-of-freedom system having the parameters of a real structure under the non-linear behavior of soil-structure interaction, and simulation results have been presented. The main idea behind proposing ANFIS controller is its success and the ability of using these types of controllers on structural systems. Because the destructive effect of earthquakes is a result of horizontal vibrations, in this study the degrees of freedom were assumed only in this direction. The system is modeled including the dynamics of a linear motor which is used as the active isolator, and the structural system is then subjected to Gadha earthquake vibration effects, which are treated as disturbance. The simulation results indicate that the implementation of ANFIS+PID controllers shows a good response as far as absorbing the vibration due to earthquake effects. Essential performance requirements for the safety of the structures and comfort level for the user are achieved. The displacements of the fifteenth storey are minimized successfully using the

https://dx.doi.org/10.22161/ijaers/3.11.24 *ISSN: 2349-6495(P) | 2456-1908(O)*

ANFIS+PID controller. The designed ANFIS+PID show high performance. A designed ANFIS+PID controller brought better active control performance than a PID controller. The improvement in resonance values and the decrease in vibration amplitudes support this result and the proposed fuzzy logic controller has great potential in active structural control.

This study investigates the control performance of the ANFIS Controller and PID Controller optimized by an NAGA-II for control of a 5-story building subjected to earthquake. For comparison purpose, a clipped-optimal control algorithm is considered as the baseline. Based on numerical simulations, it can be seen that the NAGA-II optimized ANFIS Controller and PID Controller can effectively reduce both displacement and acceleration responses of the building structure by 20% compared to the clipped optimal control algorithm. After single optimization run using NSGA-II, an engineer can simply select another ANFIS Controller that satisfies the desired performance requirements from among a number of Pareto optimal solutions. It would be important characteristics of the NSGA-II based optimization compared to other optimization methods.

REFERENCES

[1] Al-Dawod, M., Samali, B., Kwok, K., and Naghdy, F., 2004, "Fuzzy controller for seismically excited nonlinear buildings," *Journal of Engineering Mechanics* **130**(4), 407–415.

[2] Guclu, R., 2006, "Sliding mode and PID control of a structural system against earthquake," *Mathematical and Computer Modelling* **44**(1–2), 210–217.

[3] Li, N.H., Jia, Y., andWang, S.Y., 2004, "Theoretical and experimental studies on reduction for multi-modal seismic responses of high-rise structures by tuned liquid dampers," *Journal of Vibration and Control* **10**(7), 1041–1056.

[4] Battaini M, Casciati F, Faravelli L. Fuzzy control of structural vibration. An active mass system driven by a fuzzy controller, *Earthquake Engineering and Structural Dynamics*, No**.**11,**27**(2004)1267-76.

[5] Al-Dawod M, Samali B, Li J. Experimental verification of an active mass driver system on a five-storey model using a fuzzy controller, *Structural Control and Health Monitoring*, No**.**5, **13**(2006) 917-43.

[6] Pourzeynali S, Lavasani HH, Modarayi AH. Active control of high rise building structures using fuzzy logic and genetic algorithms, *Engineering Structures*, No**.** 3, **29**(2007) 346-57.

[7] Guclu R, Yazici H. Vibration control of a structure with ATMD against earthquake using fuzzy logic controllers, *Journal of Sound and Vibration*, No**.** 1–2, **318**(2008) 36-49.

[8] Li L, Song G, Ou J. Hybrid active mass damper (AMD) vibration suppression of nonlinear high-rise structure using fuzzy logic control algorithm under earthquake excitations, *Structural Control and Health Monitoring*, No**.** 6, **18**(2011) 698-709.

[9] Venanzi I, Ubertini F, Materazzi AL. Optimal design of an array of active tuned mass dampers for wind-exposed high-rise buildings, *Structural Control and Health Monitoring*, No**.** 6, **20**(2013) 903-17.

[10] Mendel JM, John RI, Liu F. Interval type-2 fuzzy logic systems made simple, *Fuzzy Systems, IEEE Transactions on*, No**.** 6, **14**(2006) 808-21.

[11] Mendel JM. Advances in type-2 fuzzy sets and systems, *Info. Sciences*, No**.** 1, **177**(2007) 84-110.

[12] *L.-Y.Lu, G.-L.Lin, T.-C.Kuo*, Stiffness controllable isolation system for near-fault seismic isolation. Engineering Structures, **vol. 30**, p. 747-765, 2008

[13] *S.M.Yang, C.J.Chen, W.L.Huang*, Structural Vibration Suppression by a Neural-Network Controller with a Mass-Damper Actuator. Journal of Vibration and Control, **vol. 12(5)**, p. 495-508, 2006

[14] *W.S.Oates, R.C.Smith*, Nonlinear Optimal Control Techniques for Vibration Attenuation Using Magnetostrictive Actuators. Jr. of Intelligent Material Systems and Structures, **vol. 19**, p.193-209, 2008

[15] *S.Pourzeynali, H.H.Lavasani, A.H.Modarayi*, Active control of high rise building structures using fuzzy logic and genetic algorithms. Engineering Structures, **vol. 29**, p. 346-357, 2007

[16] *I.Dumitrache*, Ingineria Reglarii Automate (Control Systems Engineering). Editura Politehnica Press, Bucharest, Romania, 2010

[17] *M.Bitaraf, O.E.Ozbulut, S.Hurlebaus, L.Barrosso*, Application of semi-active control strategies for seismic protection of buildings. Engineering Structures, **vol. 32**, p. 3040-3047, 2010

[18] Dyke, S.J., Spencer, B.F., Jr., Sain, M.K., Carlson, J.D.: Modeling and Control of Magnetorheological Dampers for Seismic Response Reduction. Smart Mat and Struct, Vol. 5, pp. 565-575 (1996).

[19] R.O. Duda, P.E. Hart, D.G. Stock, *Pattern classification*, 2nd edition, John Wiley and Sons, New York, 2001.

[20] Qureshi Mohd. Farukh, Jha Manoj, Sao Gopi,(2009)"Fuzzy interval theory based governing control and excitation control for stability of power

https://dx.doi.org/10.22161/ijaers/3.11.24 *ISSN: 2349-6495(P) | 2456-1908(O)*

system." Advances in Modelling C Automatic Control (theory and applications), Vol. 64, Issue 1,pp1-19.

[21] Qureshi M. F.,Bharti I.C. (2006) "Fuzzy based study and simulation of local heat transfer coefficient at Circumference of horizontal tube in free board region of fluidized bed" AMSE Journals, Modeling-B, Vol.75,Issue 2, pp1-20.

[22] Qureshi M.F.,Devangan P. and Devangan N.P. (2010) "Mamdani-ANFIS and its application of student's value" AMSE Journals,Modeling-D, Vol 31,issue 1,pp 65-74.

[23] Qureshi et.al. (2006) "Design of fuzzy rule-based classifier for data mining from library data warehouse using EMO algorithms".AMSE Journals, Advances-D, Vol.11, Issue 4, pp 31-42.

https://dx.doi.org/10.22161/ijaers/3.11.25 *SSN: 2349-6495(P) | 2456-1908(O)*

The Prediction of Tear Strength of plain weave fabric Using Linear Regression Models

Hisham E Eltayib[1], Akram H M Ali[2], Isam A Ishag[3]

[1]Open University of Sudan, Khartoum, Sudan
[2, 3]College of Engineering and Industries Technology, Sudan University of Science and Technology, Sudan

Abstract*—The aim of the study is to predict the tear strength of plain weave fabric by knowing the yarn count, yarn tensile strength and the fabric linear density. A total of nine fabric samples (produced of three different yarn counts which were 36.88, 29.50 and 9.83 tex) were produced in deferent densities at weft direction which were 4.33, 7.08 and 8.26 threads per cm, while the density was fixed at the warp direction in 9.84 ends per cm . Tensile strength was tested for these fabrics at warp and weft direction. The results were analyzed and incorporated in the Min-Tab program and the development of regression coefficients and correlation between variables to obtain equations to predict the tear strength at warp and weft direction.*

Keywords*— *Tear strength, yarn count, fabric linear density, warp, weft, regression coefficient.

I. INTRODUCTION

Strength of the fabric is an important property that decides and influences all other performance properties of the fabrics (Teli et al, 2008). The tear strength of a woven fabric is very important, since it is more closely related to serviceability of the fabric. Tearing can be described as the sequential breakage of yarns or groups of yarns along a line through a fabric. Tearing can be described as the sequential breakage of yarns or groups of yarns along a line through a fabric. It is one of the most common types of failure in textile materials and in many cases, serves to terminate their useful life. The tearing strength is often used to give a reasonably direct assessment of serviceability than the tensile strength and a fabric with low tearing strength is generally an inferior product. The studies on tearing strength began with *Krook* and *Fox* they named the triangular distortion at the active region of tearing as 'del'. They stated that fabric structure is more important, which determines the del shape in the region of tear and strongly affects the tear strength of the fabric.(Eryuruk, Kalaoğlu, 2015). The main factors that affect tear strength are yarn properties and fabric structure. The mechanism of fabric tearing is different from linear tensile failure and relates to the ability of individual yarns to slide, pack together or 'jam' into a bundle, increasing the tearing force. Thus an open fabric structure contributes to more yarn sliding and jamming, and higher tear strength. An increase in yarn density in a woven fabric will decrease the tear strength of a fabric as yarns are broken individually as they have more restriction; preventing yarn slide (HU, 2008). Tear strength is the tensile force required to start, strength test is often required for woven fabrics used for applications including army clothing, tenting, sails, umbrellas and hammocks. It may also be used for coated fabrics to evaluate brittleness and serviceability (HU, 2008).The mechanical properties which most often decide their application into a given fabric include unidirectional stretching, tear and elastic properties (Witkowska, Frydrych, 2004). Taylor in his study of tensile and tearing strengths of cotton fabrics, states that this usefulness of the test for fabric strength is one of assessment of quality and not one of assessment of serviceability. Nevertheless, when a demand for a minimum strength is added to the cloth specification, the manufacturer is restricted to a minimum quality fiber and yarn and to a range of twist factors. Therefore, a fall in strength may yield a valuable warning of a change in the quality of raw material or yarn or of deterioration in the control of finishing processes. (Devsrakondn, Pope, 1970). The main aim of this study is to predict the tear strength of the fabric by knowing the yarn count and yarn tenacity and fabric liner density. Prediction of the mechanical properties of fabrics has been studied by numerous authors. Theoretical and mathematical models have been proposed in these studies. However, one of the most common statistical approaches is the multiple regression method. (Fattahi, Ravandi, 2013). The decision made in this study based on the p-value compared to the significant level.

II. MATERIALS AND METHODS

In this study, nine different fabric samples were produced on **PANTE** Textile machine, model **E5X** in **SHENDI Weaving mill**. The study used three different yarn counts with different tenacities. These yarns were from 100% cotton. The yarns used were 36.88, 29.50 and 9.83 tex.

https://dx.doi.org/10.22161/ijaers/3.11.25 *SSN: 2349-6495(P) | 2456-1908(O)*

All the fabrics were woven in a plain weave structure, the weft densities were 4.33, 7.08 and 8.26 threads per cm, while the warp density were fixed in all the samples at 9.84 ends per cm. Tear strength properties were carried out in warp and weft direction in **Sur Military and Civil Clothing Factory** laboratory at standard weather conditions by **Elmtear2 (Digital Tear Tester 855.** From the test results which were two sets of data of yarns and fabrics in tear strength are used for warp and weft directions. One contains 30 results and the other 90. These two data from the laboratory (Table 1and 2) have been analyzed by using Mini-tab statistical analysis software to calculate the regression and relationship between the variables.

III. RESULTS AND DISCUSSION

The measurement of yarn tensile strength was illustrated in Table (1),

Table.1: Yarns Tensile strength

sample no.	Yarns Tensile strength (gf/tex)		
	36.88 tex	29.50 tex	9.83 tex
1	10.04	14.74	23.60
2	6.67	14.73	18.72
3	9.11	15.45	19.94
4	9.21	15.49	18.31
5	8.17	16.08	20.75
6	7.71	13.57	22.08
7	9.72	16.03	17.90
8	10.04	15.41	21.77
9	8.75	18.18	19.94
10	9.39	16.53	18.41
mean	**8.88**	**15.62**	**20.14**

While yarn counts and fabric densities and measurement of fabrics tear strength were illustrated in Table (2).

Table.2: Fabrics tear strength in warp and weft directions (kg)

Densities	Fabric tear strength produced of yarn 36.88 tex		Fabric tear strength produced of yarn 29.50 tex		Fabric tear strength produced of yarn 9.83 tex	
	warp direction	weft direction	warp direction	weft direction	warp direction	weft direction
11/25	0.41	1.01	1.40	1.05	3.67	2.69
	1.06	1.16	1.02	1.14	3.54	2.66
	1.14	0.95	2.28	1.18	3.52	2.77
	1.28	0.93	1.91	1.00	3.65	2.60
	1.45	1.04	1.62	1.13	4.05	3.11
mean	**1.07**	**1.02**	**1.65**	**1.10**	**3.69**	**2.77**
18/25	1.41	0.97	1.85	0.84	1.86	2.83
	1.61	1.03	1.62	0.82	1.95	2.73
	1.54	0.90	1.68	0.86	1.80	2.62
	1.62	0.94	1.69	0.84	1.92	2.66
	1.74	1.08	1.69	0.79	2.21	3.59
mean	**1.56**	**0.98**	**1.71**	**0.83**	**1.95**	**2.89**
21/25	1.13	1.13	1.40	0.82	1.83	3.03
	1.41	1.01	1.37	0.88	2.44	3.05
	1.37	0.88	1.33	0.87	1.33	2.71
	1.53	0.91	1.38	0.86	2.17	2.64
	1.41	0.98	1.45	0.87	2.55	2.65
mean	**1.37**	**0.98**	**1.39**	**0.86**	**2.06**	**2.82**

Table (3) illustrates the goodness of fit statistics of models for the fabric tear strength at the warp and weft direction.

Table.3: Goodness of fit statistics of models

statistical Parameter	R	R^2	Adj.R	SEE*
Fabric tear strength at warp direction	0.815	0.663	0.591	0.467
Fabric tear strength at weft direction	0.995	0.989	0.987	0.105

From table 3 the goodness of fit statistic of model, the (R) was 0.815 which means strong positive correlation between independent variables in the study and the dependent variable fabric tear strength at the warp direction. The simple coefficient of determination (R^2) was 0.663 which indicates a positive correlation between variables. The standard error of estimated was a low value which was 0.467. In the weft direction the correlation coefficient R was 0.995 which means strong positive correlation between independent variables in the study (yarn tenacity, yarn count (tex)) and the dependent variable tear strength. The simple coefficient of determination (R^2) was 0.989 which indicates a positive correlation between variables. The standard error of estimated was a low value which was 0.105.

https://dx.doi.org/10.22161/ijaers/3.11.25 *SSN: 2349-6495(P) | 2456-1908(O)*

IV. MODEL EQUITATION OF THE FABRIC TEAR STRENGTH AT THE WARP DIRECTION

Table.4: Analysis of variance (ANOVA) results

Source	DF	SS	MS	F	P
Regression	3	6.0213	2.0071	9.20	0.001
Residual Error	14	3.0540	0.2181		
Total	17	9.0752			

In table (4) the calculated F is 9.20 and the p-value equal 0.01 less than 0.05 which indicates high significant value.

Table.5: Regression coefficients, T-values and significance level of T-values of our linear regression model for fabric tenacity at the warp direction

Predictor	Coefficient	SD	T	P
Constant	1.81100	1.54400	1.17	0.260
Yarn Tensile strength	0.07603	0.07603	1.18	0.260
Fabric linear density	-0.04743	0.02632	-1.80	0.093
Yarn count	-0.01403	0.02106	-0.67	0.516

In Regression coefficients table (5) shows the degree of contribution of the different variables, where we find there is no effect for all variables (yarn tensile strength, fabric linear density, yarn count) where the p-value is 0.260 for the yarn tensile strength and 0.093 for the fabric linear density and 0.516 for the yarn count which bigger than 0.05. Therefore the model equation for the fabric tear strength at the warp direction is:

$$\mathbf{FTS_{wp} = 1.81 + 0.0760\ Y_t - 0.0474\ F_{ld} - 0.0140\ Y_c} \quad \text{... (1)}$$

Where:

FTS_{wp} fabrics tear strength at the warp direction, Y_{ts} Yarn tensile strength, F_{ld} fabric linear density and Yc Yarn count.

V. MODEL EQUITATION OF THE FABRIC TEAR STRENGTH AT WEFT DIRECTION

Table (3) illustrates the goodness of fit statistics of models of the fabric tear strength at the weft direction. From the table the correlation coefficient R equal 0.995 which means strong positive correlation between independent variables in the study (yarn tenacity, yarn count (tex)) and the dependent variable tear strength at the weft direction. The simple coefficient of determination R^2 equal 0.989 which indicates a positive correlation between variables. In table (6) the F calculated is 422.86 and the p-value equal 0.00 less than 0.05 which indicates high significant value.

Table.6: Analysis of variance (ANOVA) results

Source	DF	SS	MS	F	P
Regression	3	13.9198	4.6399	422.86	0.000
Residual Error	14	0.1536	0.0110		
Total	17	14.073			

Table (7) shows the degree of contribution of the different variables.

Table.7: Regression coefficients, t-values and significance level of T-values of our linear regression model for fabric tenacity at the weft direction

Predictor	Coefficient	SD	T	P
Constant	5.87110	0.346400	16.95	0.000
Yarn tensile strength	-0.12092	0.014510	-8.33	0.000
Fabric linear density	-0.011236	0.005903	-1.90	0.078
Yarn count	-0.096895	0.004724	-20.51	0.000

where we find the effect of the yarn tensile strength is -0.12092 and the p-value is 0.000 which means this variable have an effect on the tear strength at the weft direction, as in yarn count the effect is significant p-value is 0.00 and the degree of impact is 0.096895, while the fabric linear density is not significantly in the tear strength at the weft direction because p-value is 0.078 which is bigger than 0.05. Therefore the model equation of the fabric tear strength at the weft direction is:

$$\mathbf{FTS_{wf} = 5.87 - 0.121\ Y_{ts} - 0.0112\ F_d - 0.0969\ Y_c} \quad \text{..... (2)}$$

Where:

$\mathbf{FTS_{wf}}$ fabric Tear strength at the weft direction, Y_{ts} Yarn tensile strength, F_{ld} fabric linear density and Y_c Yarn count.

VI. CONCLUSION

Multiple linear regression equations were developed to predict the fabric tear strength in warp and weft direction as one of the most important fabric characteristics. For this aim nine samples of fabrics were produce by different linear densities and yarns 36.88, 29.50 and 9.83 tex were

https://dx.doi.org/10.22161/ijaers/3.11.25 *SSN: 2349-6495(P) | 2456-1908(O)*

used in this study. Yarn tensile strength was tested by **Titan2 Universal Strength** instrument and the fabric samples were tested by **Elmtear** (**Digital Tear tester 855**. The study tested the type of relationship between fabric tear strength and independent variables (i.e. yarn tensile strength, yarn count and fabric linear density) one by one. Tests indicated that there was a relationship between the variables and fabric tear strength. The study showed that the fabric tear strength was affected by the yarn tensile strength and yarns count at the weft direction while it was affected by the fabric linear density and yarn count at the weft direction. The study devised equations to predict the tensile strength in the warp and weft direction as illustrated in equation (1) and equation (2).

REFERENCES

[1] Devsrakondn, V. and Pope, C.*Clothing and Personal Life Support Equipment Laboratory*, U. S. Army Natick Laboratories, Massachusetts; 1970.
[2] Dubrovski, P. *Woven Fabric Engineering*, Sciyo , India; 2010.
[3] Eryuruk, S and Kalaoğlu, F. Autex Research Journal, Vol. 15, No 3, p 207;2015
[4] Fattahi S, and Hoseini R. Prediction and Quantitative Analysis of Yarn Properties from Fiber Properties Using Robust Regression and Extra Sum Squares, Fibers & Textiles in Eastern Europe; 21, 4(100): p 48-54;2013.
[5] HU, J. *Fabric testing*, Woodhead Publishing in Textiles: Number 76, p 92-99, England;2008.
[6] Teli, M and Khare, . Autex Research Journal, Vol. 8, No3,p 63-65,2008.
[7] Witkowska, B and Frydrych, I . Fibers & Textiles in Eastern Europe, Vol. 12, No. 2 (46), p 42-43,2004.

International Journal of Advanced Engineering Research and Science (IJAERS) *[Vol-3, Issue-11, Nov- 2016]*
https://dx.doi.org/10.22161/ijaers/3.11.26 *ISSN: 2349-6495(P) | 2456-1908(O)*

Evaluation and Optimization of Poly-aromatic Cationic Surfactant as Additive for Mineral base Oil

Moustafa, El-Abbas A.A.*,Enas.A.I.*, Omer, A.M.A.*, El-Adly, R.A.*

* Egyptian Petroleum Research Institute (EPRI), Nasr City, Cairo-Egypt.

Abstract— *In this research, evaluation and optimization of poly- aromatic cationic surfactant as modifier for base mineral oil. Different weight percent from this modifier was added to base mineral oil and assessed. Physicochemical properties mineral base oil and blended oil were carried out. The rheological behaviors of base mineral oil with and without modifier were investigated at different temperatures using Programmable Rheometer LADV-III Ultra-System. Yield stress and dynamic viscosity for these blended oils were determined. Optimization and modeling of the obtained data concerning dynamic viscosity was studied which the predicting of these data with different temperatures. It was found that the rheological behavior of these oils show Newtonian flow. The results revealed that the rheological behavior and pour point of base oil with and without poly-aromatic cationic surfactant depend on a large extant on the contents of the components in the base oil. It was concluded that the poly-aromatic cationic surfactant can be used as rheological and pour point modifier to such base mineral oil. The predicted of viscosity mineral base oil blank or with additive poly-aromatic cationic surfactant at temperature 130, 160 and 190^{o}C using Trend line modelingwhich as blended base oil samples show the poly- aromatic cationic surfactant is suitable as rheological modifier.*

Keywords—Mineral base Oil, viscosity, Poly-aromatic, and LADV-III.

I. INTRODUCTION

A lubricant is a substance that is used between two surfaces of moving materials to reduce the friction generated between them. There are many types of lubricants, including gases, liquids, solids, and grease. Among them, liquid lubricants are most often used. Liquid lubricants are mixtures that consist of about 90% base fluids and less than 10% chemical additives. The base fluids act as a lubricant primarily by separating the fluid layer from the moving surfaces and should easily remove any generated heat. The base oil, usually referred to as mineral oil, meets these requirements; thus, it is typically used as the base fluid(1, 2).

To improve the quality, lube oil always contains different types of additives are mixed to the lube oil to impart a new and desirable property which was not originally present in the oil. Sometimes additives amplify the property already present to some degree in the oil(1,2). The quantity and quality of the additives depend on the nature of the base oil and also on the purpose of their use. Types of additives are antioxidants, detergents and dispersants, corrosion inhibitors, viscosity index improvers (VIIs) and pour point depressants (PPDs), etc. of them VIIs and PPDs are the very important ingredients in modern lubricants.In addition, viscosity is a very important property of a lubricant(3,4).The viscosity of a liquid is a measure of its resistance to flow. High viscosity oil is less fluid than the one of low viscosity. At higher temperatures, the oil tends to thin out and flow more readily and vice versa(5). The change in viscosity with the variation of temperature is expressed by a parameter known as viscosity index (VI). Higher viscosity index of oil means the viscosity of the oil does not vary much with the variation of temperature. Viscosity modifiers (VMs) are added to the lubricating oil to improve the VI of the oil(2).

The rheological properties such as fluidity of the oil at low temperature, viscosity, and variation of viscosity with temperature govern the performance of lubricant base oils. To have effective performance at low as well as at high temperatures, an engine lubricant should be fluid at low temperature and should have minimum variations of its viscosity with temperature (2).

This has directed modern lubrication science toward the development of a new type of polymer additives with multifunctional activity and ability to improve their dispersant in addition to the control of viscosity properties(6.7,8).

Introducing the ability of dispersant into a polymer additive demands a carefully engineered incorporation of a strongly polar functional group to the main polymer backbone. The

https://dx.doi.org/10.22161/ijaers/3.11.26 *ISSN: 2349-6495(P) | 2456-1908(O)*

most commonly employed functional groups are amines, alcohols, or amides (8-10). Such formulated polymer additives will have the ability to keep insoluble combustion debris and oil oxidation products dispersed in the oil, which will prevent their deposition on the main part of the engine(11). This will have a direct effect on minimizing harmful engine exhaust emissions, increasing engine life, and controlling oil consumption by maintaining clean engine operation (12).

II. VISCOSITY AND MODELING EQUATIONS

The simplest of this rheology is the Newtonian viscous fluid. To under-stand the assumptions let us restrict attention to the determination of a viscous stress tensor at x, t, which depends only upon the fluid properties within a fluid parcel at that point and time. It is reasonable to assume that the forces dues to the rheology of the fluid are developed by the deformation of fluid parcels, and hence could be determined by the velocity field (12). The Newtonian viscous fluid is one where the stress tensor is linear in the components of the velocity derivative matrix, with a stress tensor whose specific form will depend on other physical conditions (13).

Dynamic viscosity or absolute viscosityis a measure of a fluid's resistance to deformation under shear stress. For example, crude oil has a higher resistance to shear than water. Crude oil will pour more slowlythan water from an identical beaker held at the same angle. This relative slowness of the oil implies a low "speed" or rate of strain(5,13).

The symbol used to represent viscosity is (μ).To understand the physics of viscosity, it is useful to refer back to solid mechanics and the concepts of shear stress and shear strain. Shear stress, τis the ratio of force/area on a surface when the force is aligned parallel to the area. However, the shear stress on a fluid element is proportional to the rate (speed) of strain, and the constant of proportionality is the viscosity (5, 13):

{Shear stress} = {Viscosity} × {Rate of Strain}

The rate of strain is related to the velocity gradient by(ϕ= *dV/ dy*), so the shear stress (shear force per unit area) is

$$\tau = \mu \frac{dV}{dy} \qquad Eq.\ 1$$

Where *V* is the fluid velocity and *y* is the distance measured from the wall. The velocity distribution shown is characteristic of flow next to a stationary solid boundary, the shear stress decreases with distance from the boundary. From Eq. (1) it can be seen that the viscosity μ is related to the shear stress and velocity gradient.

$$\mu = \frac{\tau}{dV/dy} = \frac{N/m^2}{(m/s)/m} = N.s/m^2\ Eq.2$$

A common unit of viscosity is the *poise*, which is 1 dyne-s cm^2 or $0.1N\cdot s/m^2$. The viscosity of water at 20°C is one centipoise (10^{-2} poise) or $10^{-3}N\cdot s/m^2$. The unit of viscosity in the traditional system is$lbf\cdot s/ft^2$.

III. EXPERIMENTAL WORK

First of all, Poly-aromatic cationic surfactant was prepared and structure confirmed on the basis of the presented method by to Omar et al. (1-2). The purity of this compound is about 94.85% with molecular weight 4500 gm/mol. This compound was evaluated as rheological modifier using base mineral oil and its effect of concentration was investigated by using 1.0 wt. %, 2.0wt. % and 3.0 wt. %.Second one; Mineral base oil was kindly supplied by Co-operative petrol. The characteristics of this base oil were carried out according to ASTM methods. Then, the evaluation of the poly-aromatic surfactant was as the rheological modifier for mineral base oil. The profile dynamic viscosity - shear rate of base oil contains the tested polymer was investigated at temperature 40, 70 and 100°C. Different concentrations 1.0, 2.0 and 3.0wt.% was used to explore the effect of concentration on rheological modification of mineral base oil.

Rheological measurements test was performed on a Brookfield programmable Rheometer HV DV-III UITRA used in conjunction with Brookfield software, RHEOCALC V.2, through RHEOCALC all Rheometer function (rotational speed, instrument % torque scale time interval, set temperature) are controlled by a computer. The corresponding shear stress, shear rate, dynamic viscosity, mathematical model and confidence of fit consistence index were also recorded by the software. Then, series of experimental was performed to determine the effect of prepared additives on the rheological properties of the mineral base oil at temperatures 40, 70 and 100 ºC.Finally, Prediction of viscosity values were obtained from applying of the trend lines or regression with different modeling till its choosing of the suitable model to excellent predict to viscosity at different temperature.

IV. RESULT AND DISCUSSION

The physicochemical characteristics and structural group analysis of the base mineral oil with and without poly-aromatic cationic surfactant were presented in **Table 1**. The

https://dx.doi.org/10.22161/ijaers/3.11.26 *ISSN: 2349-6495(P) | 2456-1908(O)*

base mineral oil without additive in this Table is characterized high pour point (+3) and high paraffinic carbon percentage (47% of CP**).** So that the base oil under investigation could be classified as paraffinic oil.

Data inthis **Table** show that the prepared modifier has significant effect on pour point and yield values of blended oil with modifier compared with the mineral oil without modifier; this indicate that the efficiency increases with increasing the concentration of prepared modifier. This may be due to the effect of the salvation power of the modifier on the paraffinic compounds, in particular wax content, of base mineral oil. Also, this modifier obstructs the lateral crystal growth at lower temperature. Accordingly, the poly-aromatic cationic surfactant can use as pour point depressant for base mineral.

In this respect, significant increases of the kinematic viscosity at 40 and 100^{o}C of blend base oil with increasing of poly-aromatic cationic surfactant were observed. This may be because of the fact that, at a higher temperature, while the lube oil viscosity gets decreased, the polymer molecules change from tight coil to expanded ones as a result of increase in the interaction between the additive molecule and the solvent molecule. This increase in volume causes an increase in the viscosity of the blend and offsets the normal reduction in viscosity of the oil with increasing temperature. The increase of concentration of the additive, from 1.0 to 3.0 wt. %, may be leads to an increase in total volume of surfactant micelles in the oil solutions. Consequently, a high concentration of additive will impart a high viscosity index rather than a low concentration of the additive

Rheology is the study of those properties of materials that govern the relationship between shear rate and shear stress. In general, the rheological program calculated and output the yield value using power low mathematical model. **Table 1** show calculated yield values data of base mineral oil with and without modifier. From this table in general, the yield value of base oil alone is higher compared with base oil contains additive. In this respect, the yield value decreases with increasing the concentration of the poly-aromatic cationic surfactant. This indicates that the additive compound is efficient as flow improver and rheological improver by decreasing yield value or yield stress. This view is in agreement with the dynamic viscosity data for base oil with and without additive. It may be explained that the poly-aromatic cationic surfactant tends to solvation power and reduces the attractive forces between the base mineral oil molecules. Accordingly, base mineral oil with additive is close to Newtonian behavior compared with base oil alone and is weekly dependent on temperature.

Dynamic viscosity-shear rate profiles for base oil with and without additives at temperatures 40^{o}C, 70^{o}C and 100^{o}C are presented in **Figures 1, 2 and 3**, respectively. These figures indicate that the flow behavior of base oil with and without additive obey Newtonian flow. Also, it is found that the dynamic viscosity of oil and oil blends with additive approaches low viscosity as the temperature increase. The increase of temperature, from 40^{o}C to 100^{o}C, tends to increase the molecular motion leads to reduce the attractive forces between molecules.

The correlation between yield stress in the **Table 1** and dynamic viscosity- shear rate profiles in **Figures 1, 2 and 3**, indicates highly Newtonian behavior with increasing weight percent of poly-aromatic cationic surfactant to base oil. Also, the viscosity variation with shear rate decreased with increasing temperature and the base oil with additive approach a more Newtonian behavior at high temperature 100^{o}C and high concentration 3.0 wt. % of additive. The obtained results showed that the flow behavior of base oil with additive increased with increasing the additive concentration. This reveals the important role of the additive to enhance the flow properties of the base oil.

Table.1: Physicochemical properties of mineral base oil with and without additives.

Properties	**Base oil**	**Base oil + 1.0 wt. % additives***	**Base oil + 2.0 wt. % additives***	**Base oil + 3.0 wt. % additives***	**Test method**
Density @ 15^{o}C	0.8911	0.8915	0.8917	0.8917	ASTM D-4052
Kinematic Viscosity					
@ 40^{o}C	53.8	59.5	65.1	75.4	ASTM D-445
@100^{o}C	9.10	10.6	12.0	13.9	ASTM D-445
Flash point,^{o}C					
Close	193	193	193.5	193.5	ASTM D-93
Open	215	215	215	215	ASTM D-93
Pour point,^{o}C	+3	-3	-10	- 16	ASDM d-97

https://dx.doi.org/10.22161/ijaers/3.11.26 *ISSN: 2349-6495(P) | 2456-1908(O)*

Cont'*Table.1: Physicochemical properties of mineral base oil with and without additives.*

Properties	**Base oil**	**Base oil + 1.0 wt. % additives***	**Base oil + 2.0 wt. % additives***	**Base oil + 3.0 wt. % additives***	**Test method**
Carbon residue, wt%	0.4	0.4	0.4	0.4	ASTM D-189
Structural group analysis					
Paraffin **% C_p**	47	---	---	---	n-d-M method
Aromatic**%C_A**	22	---	---	---	
Naphthenic**%C_N**	31	---	---	---	
Dynamic viscosity measured, by Rheometer HV DV-III UITRA					
@40^{o}C	418.84	440.69	459.45	461.74	with RHEOCALC V.2 program.
@70^{o}C	104.2	108.93	112.58	113.45	
@100^{o}C	39.08	40.12	42.83	44.12	
Yield value, D/cm^2					
@ 40^{o}C	10.5	7.5	3.2	2.1	
@ 70^{o}C	6.2	3.1	2.3	1.0	
@100^{o}C	4.4	2.1	0.0	0.0	

* Additives are weight percent of poly-aromatic cationic surfactant to base oil.

V. PREDICTION MATHEMATICAL MODELLING

The studied main task for work experimental was to develop models for the prediction of theviscosity of mineral base oil at high temperature (HT) conditions; in particular the implementation of reliable and accurate models for predicting viscosities of HT fluids and select of the best modelling for obtained the correct viscosity results at any value from temperature. Additionally, experimental data needed to be acquired on a set of selected fluids being representative of mineral base oil. A final task for the work was the validation of the models developed in order to test the accuracy of the results in a wide range of industrial applications. The need for the work followed from the fact that in the oil as well as other industries, theviscosity is one of the weakest predicted parameters.

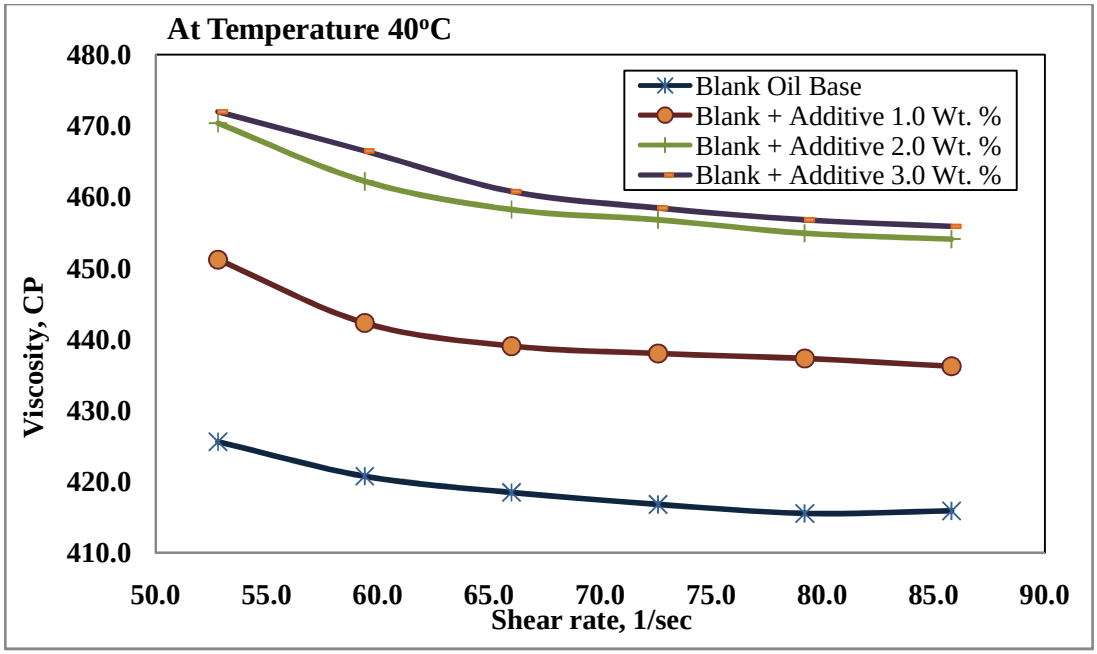

Fig. 1: Viscosity Measurement Versus Shear Rate at Temperature 40^{o}Cfor Blank and Different Concentration of Additives for co-polymers on mineral base oil.

https://dx.doi.org/10.22161/ijaers/3.11.26 *ISSN: 2349-6495(P) | 2456-1908(O)*

Thus, this study has been carried out as one of the main contributions of the ***Trendline Options*** group or **Regression Types** (Best types such as Exponential, Polynomial and power modelling) to this study focusing on the friction result for viscositymodeling predict values. As it is widely illustrated in next section, the modeling results obtainedwith this novel approach have been validated far beyond the high temperature conditionsconsidered in this work.The effect of temperature on viscosity is different for liquids. Thus, an increase in temperature causes a decrease in viscosity for liquids. An equation for the variation of liquid viscosity with temperature is (2):

$$\mu = Ce^{b/T} \qquad \text{Equation 1}$$

For example for calculating viscosity of liquid as a function of temperature, we can select for two value of viscosity measurement at different temperature. The following value of viscosity at temperature 40 and 70°C are shown below:

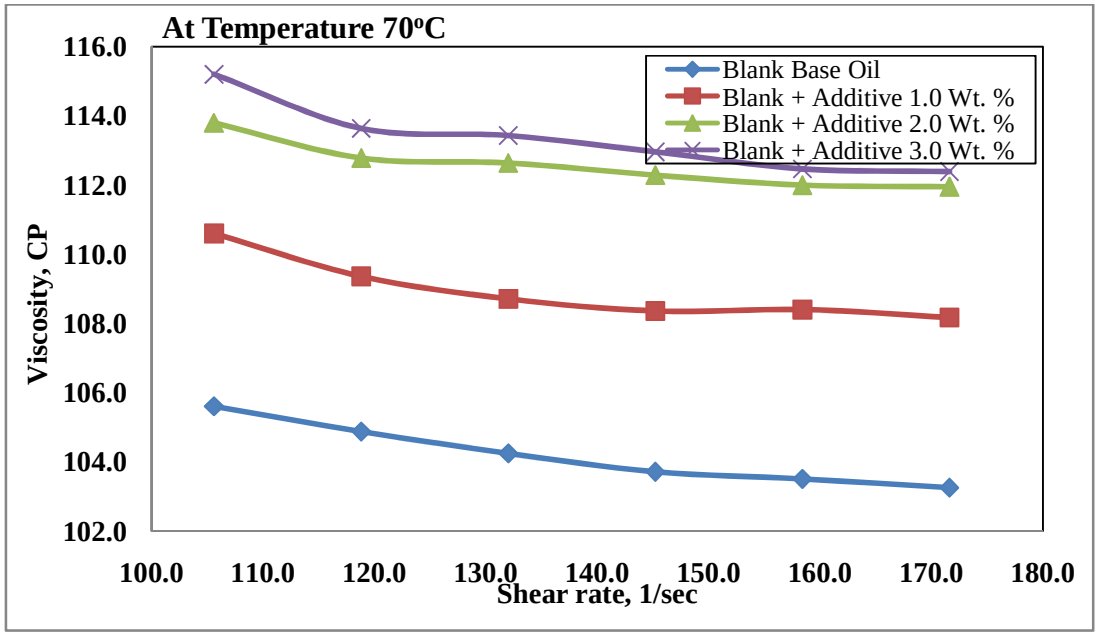

Fig.2: Viscosity Measurement Versus Shear Rate at Temperature 70°Cfor Blank and Different Concentration of Additives for co-polymers mineral base oil.

For Example, mineral baseoil viscosity (Blank sample) at 40°C is **418.84** CP and viscosity value at 70°C is 104.20 CP. We could use the below equation for calculate the constant value with the following steps:

1. Logarithm of Equation above ,

   $\ln\mu = \ln C + b/T$ Equation 2
2. Interpolation for two Equations of two value viscosity at 40 and 70°C,

   ln 424.18 = ln C + b/40

   6.050158 = ln C + 0.0250000 b

   ln 104.66 = ln C + b/70 4.640717 = ln C + 0.0142857 b
3. Solution for ln C and b

   ln C= ?????

   b= ?????

https://dx.doi.org/10.22161/ijaers/3.11.26 *ISSN: 2349-6495(P) | 2456-1908(O)*

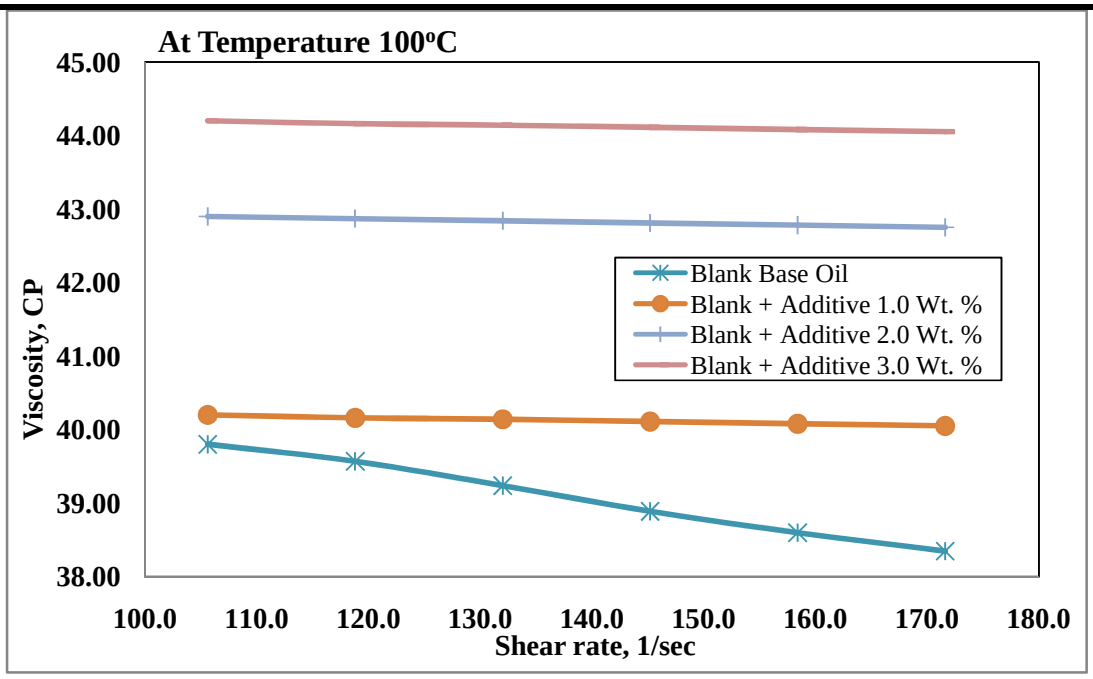

Fig.3: Viscosity Measurement Versus Shear Rate at Temperature 100°Cfor Blank and Different Concentration of Additives for co-polymers mineral base oil.

VI. ANALYSIS OF PREDICTION MATHEMATICS MODELLING

As a result, up to four different viscosity estimations, for each one of the reference sets of viscosities are derived for each measured temperature. The previous**Table 1 s**hows that the dynamic viscosity measurement of Mineral base oil blank and with different additives 1.0, 2.0, and 3.0% by weight concentration ofPoly-aromatic Cationic Surfactant at different temperature 40, 70 and 100°C. **Fig. 4** shows that measurement of dynamic viscosity for Mineral baseOil and different additives concentration on it versus different temperature. In addition to **Fig. 5** shows that measurement of dynamic viscosity for mineral baseOil versus different additives concentration of Poly-aromatic Cationic Surfactant at different temperature.

In order to predict the dynamic viscosities for Poly-Aromatic Cationic Surfactant mixtures, we havebeen used different mathematics models that only involve the viscosity data of the pure compounds of themixture. For pure poly-aromatic Cationic Surfactant mixtures, the experimental measurement for dynamic viscosity values between 40°C and 100°C has been taken from a Brookfield Viscometer. **Table 2** represents the Predict of viscosity value at different temperature from 40°C to 200°C formineral base Oil without additive (Blank sample),

https://dx.doi.org/10.22161/ijaers/3.11.26 ISSN: 2349-6495(P) | 2456-1908(O)

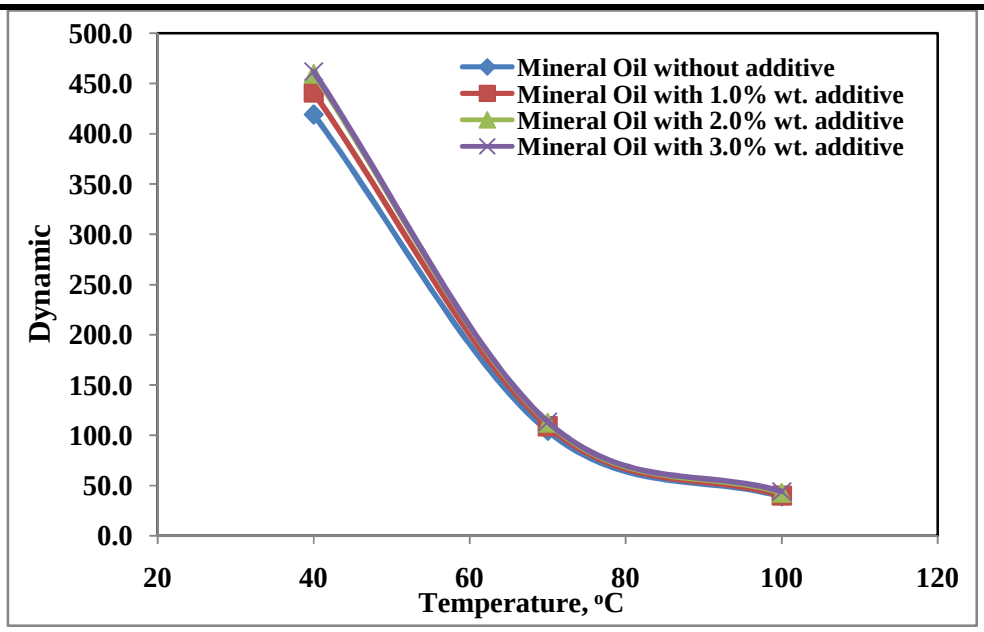

Fig.4: Measurement of dynamic viscosity for mineral base oil blank and different additives concentration of poly-aromatic cationic surfactant on it versus different temperatures.

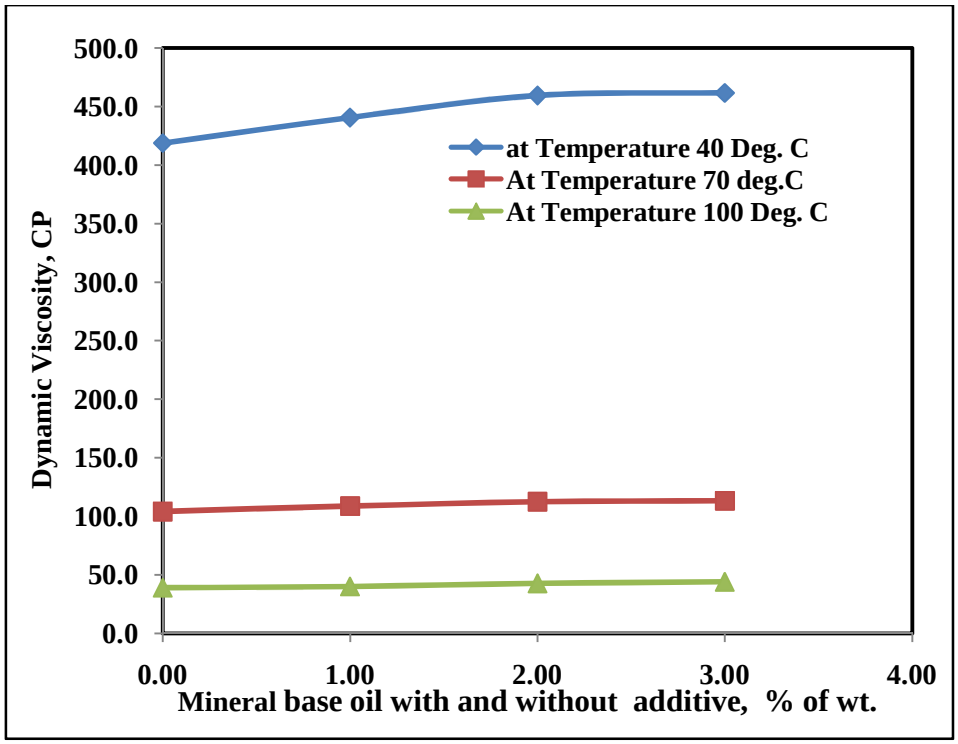

Fig. 5: Measurement of dynamic viscosity for Mineral Base Oil versus different additives concentration of poly-aromatic cationic surfactant at different temperature.

https://dx.doi.org/10.22161/ijaers/3.11.26 *ISSN: 2349-6495(P) | 2456-1908(O)*

Table.2: Predict of viscosity value at different temperature from 40 to 170°C For Mineral base Oil without additive calculated with using Exponential Trendline option.

An Equation for the variation of liquid viscosity with temperature : $\mu = C\, e^{b/T}$						
Temperature T,	Average Viscosity measured **μ,**	Empirical Constant **b**	Empirical Constant **C**	**b/T**	**Predict Viscosity, μ,**	**% Error**
°C	**cp**	value	value	value	**cp**	
40	**418.84**	158.125211	8.0394943	3.953130	**418.840**	**0.00**
50	**???**			3.162504	**189.969**	
60	**???**			2.635420	**112.143**	
70	**104.20**			2.258932	**76.960**	**-0.27**
80	**???**			1.976565	**58.028**	
90	**???**			1.756947	**46.586**	
100	**39.08**			1.581252	**39.080**	**0.00**
110	**???**			1.437502	**33.847**	
120	**???**			1.317710	**30.026**	
130	**???**			1.216348	**27.132**	
140	**???**			1.129466	**24.874**	
150	**???**			1.054168	**23.070**	
160	**???**			0.988283	**21.599**	
170	**???**			0.930148	**20.379**	

In addition **Tables 3, 4 and 5** illustrated that Predict of viscosity value at different temperature from 40°C to 170°C for Mineral base Oil with D-1.0; D-2.0 and D-3.0% wt. additive of poly-aromatic Cationic Surfactant.

Table.3: Predict of viscosity value at different temperature from 40°C to 170°C For mineral base Oil with D-1.0% wt. additive of poly-aromatic Cationic Surfactantcalculated with using Exponential Trendline option.

An Equation for the variation of liquid viscosity with temperature : $\mu = C\, e^{b/T}$						
Temperature T,	Average Viscosity measured **μ,**	Empirical Constant	Empirical Constant	**b/T**	**Predict Viscosity, μ,**	**% Error**
°C	**cp**	value	value	value	**cp**	
40	**440.69**	**159.764448**	**8.1191907**	3.994111	**440.690**	0.00
50	**???**			3.195289	**198.248**	
60	**???**			2.662741	**116.393**	
70	**108.93**			2.282349	**79.565**	-0.29
80	**???**			1.997056	**59.817**	
90	**???**			1.775161	**47.913**	
100	**40.12**			1.597644	**40.120**	0.00
110	**???**			1.452404	**34.696**	
120	**???**			1.33137	**30.741**	
130	**???**			1.228957	**27.749**	
140	**???**			1.141175	**25.417**	
150	**???**			1.065096	**23.555**	
160	**???**			0.998528	**22.038**	
170	**???**			0.939791	**20.781**	

https://dx.doi.org/10.22161/ijaers/3.11.26 *ISSN: 2349-6495(P) | 2456-1908(O)*

Table.4: Predict of viscosity value at different temperature from 40°C to 170°C for mineral base Oil with D-2.0% wt. additive of poly-aromatic Cationic Surfactant calculated with using Exponential Trendline option.

An Equation for the variation of liquid viscosity with temperature : $\mu = C\, e^{b/T}$						
Temperature T,	Average Viscosity measured **μ,**	Empirical Constant	Empirical Constant	**b/T**	**Predict Viscosity, μ,**	**% Error**
°C	**cp**	value	value	value	**cp**	
40	**459.45**	**158.186059**	**8.80555121**	3.954652	**459.450**	0.00
50	**???**			3.163722	**208.325**	
60	**???**			2.636435	**122.954**	
70	**112.58**			2.259801	**84.367**	-0.28
80	**???**			1.977326	**63.606**	
90	**???**			1.757623	**51.060**	
100	**42.83**			1.581861	**42.830**	0.00
110	**???**			1.438055	**37.093**	
120	**???**			1.318217	**32.904**	
130	**???**			1.216816	**29.731**	
140	**???**			1.129901	**27.256**	
150	**???**			1.054574	**25.278**	
160	**???**			0.988663	**23.666**	
170	**???**			0.930506	**22.329**	

Table.5: Predict of viscosity value at different temperature from 40°C to 170°C For Gear Oil with D-3.0% by wt. additive of poly-aromatic Cationic Surfactant calculated with using exponential Trendline option.

An Equation for the variation of liquid viscosity with temperature : $\mu = C\, e^{b/T}$						
Temperature T,	Average Viscosity measured **μ,**	Empirical Constant	Empirical Constant	**b/T**	**Predict Viscosity, μ,**	**% Error**
°C	**cp**	value	value	value	**cp**	
40	**461.74**	**156.539251**	**9.2213429**	3.913481	**461.740**	0.00
50	**???**			3.130785	**211.095**	
60	**???**			2.608988	**125.275**	
70	**113.35**			2.236275	**86.297**	-0.24
80	**???**			1.956741	**65.252**	
90	**???**			1.739325	**52.502**	
100	**44.12**			1.565393	**44.120**	0.00
110	**???**			1.423084	**38.268**	
120	**???**			1.304494	**33.988**	
130	**???**			1.204148	**30.743**	
140	**???**			1.118138	**28.210**	
150	**???**			1.043595	**26.183**	
160	**???**			0.97837	**24.530**	
170	**???**			0.920819	**23.158**	

https://dx.doi.org/10.22161/ijaers/3.11.26 *ISSN: 2349-6495(P) | 2456-1908(O)*

Also, a comprehensive dynamic viscosity study has been carried out for three ternary mixtures composed of poly-aromatic cationic surfactant concentration at different temperatures range from 40°C to 170°C with applied of three types of regression exponential, polynomial and power Trendline options using excel program. From these results during applied of their types, it should be typical result representations by used the power regression.

Table 6 shows that Trendline options of Exponential, Polynomial and Power in case of mineral base oil (Blank Sample), and at different concentration additives of Poly-aromatic Cationic Surfactant.**Fig. 6** illustrated that Relation between dynamic viscosity values measured and Predicted at different temperature for gear oil (blank sample) and with additives of Poly-aromatic Cationic Surfactant concentration by using the power regression type (Typical Values).

The experimental viscosity data obtain in this study have been used in order to evaluate the performance of three types from Trendline option (regression types) such as exponential, polynomial and power regression types mathematic modelling from applied with used of Excel software, applicable to gear oil blank and different additives concentrations of poly-aromatic Cationic Surfactant. The evaluation of these mathematic models shows the typical or best results for this modelling are obtained the power regression type for totally typical predictive of dynamic viscosity at certain temperature as we need to know.

Table.6: Trendline options of Exponential, Polynomial and Power in case of mineral base Oil (Blank Sample), and at different concentration additives of Poly-aromatic Cationic Surfactant.

Mineral base oil (Blank Sample)			
Trendline Options	**Exponential**	**Polynomial**	**Power**
Fitting Equation	$Y=1901.4\ e^{-0.040X}$	$Y= 0.1386\ X^2 – 25.736\ X + 1226.5$	$Y=6\ E+06\ X^{-2.579}$
Error	$R^2= 0.9901$	$R^2 =1.0000$	$R^2=0.9992$
D-1.0% by wt. of Poly-aromatic Cationic Surfactant			
Trendline Options	**Exponential**	**Polynomial**	**Power**
Fitting Equation	$Y=2037.6\ e^{-0.040\ X}$	$Y=0.1461\ X^2 – 27.128\ X + 1292.1$	$Y=7\ E+06\ X^{-2.605}$
Error	$R^2= 0.9909$	$R^2= 1.0000$	$R^2=0.9990$
D-2.0% by wt. of Poly-aromatic Cationic Surfactant			
Trendline Options	**Exponential**	**Polynomial**	**Power**
Fitting Equation	$Y=2076.8\ e^{-0.040\ X}$	$Y=0.1540\ X^2 – 28.497\ X + 1353$	$Y=6\ E+06\ X^{-2.583}$
Error	$R^2=0.9887$	$R^2= 1.0000$	$R^2=0.9996$
D-3.0% by wt. of Poly-aromatic Cationic Surfactant			
Trendline Options	**Exponential**	**Polynomial**	**Power**
Fitting Equation	$Y=2045.9\ e^{-0.039X}$	$Y=0.1551\ X^2 – 28.673\ X + 1360.5$	$Y=6\ E+06\ X^{-2.558}$
Error	$R^2= 0.9873$	$R^2= 1.0000$	$R^2=0.9998$

https://dx.doi.org/10.22161/ijaers/3.11.26 *ISSN: 2349-6495(P) | 2456-1908(O)*

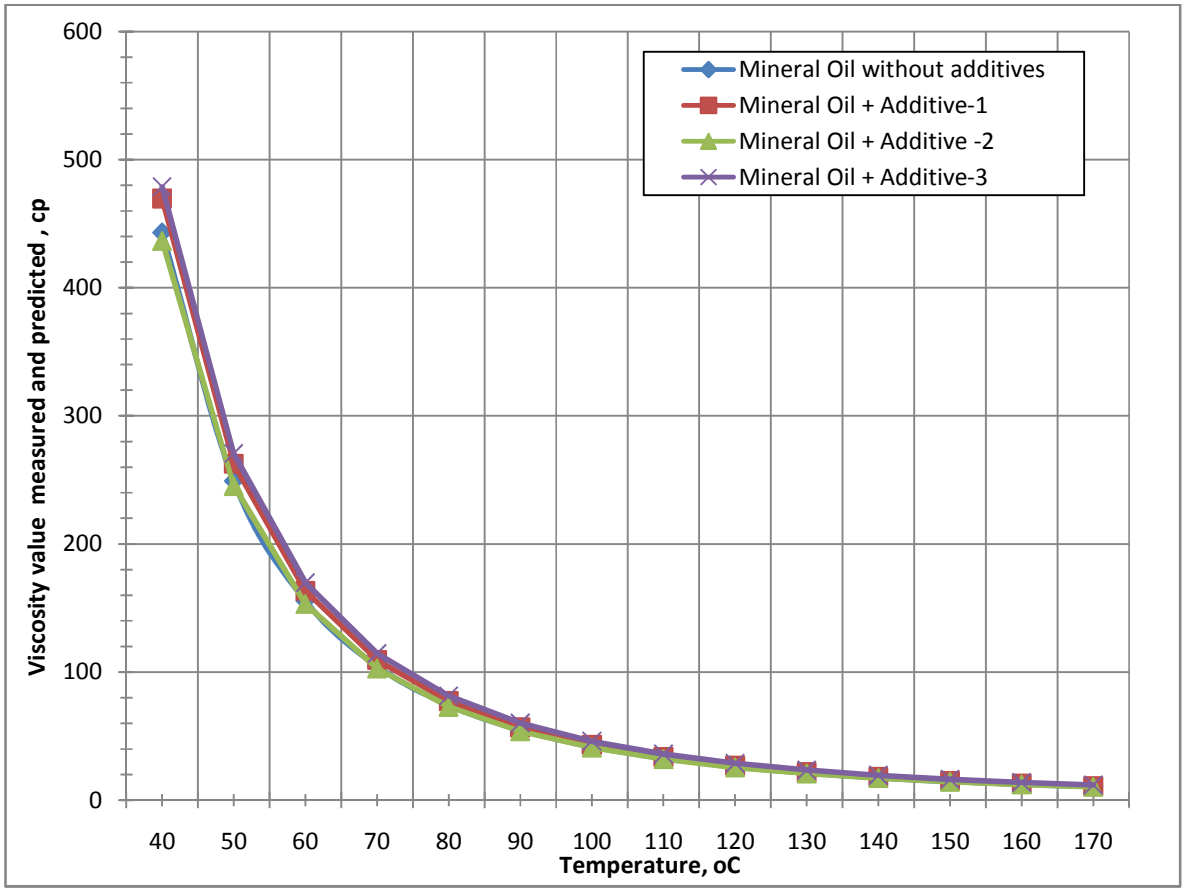

Fig. 6: Relation between dynamic viscosity value measured and Predicted at diferent temperatures for mineral base oil (blank sample) and with additives of Poly-aromatic Cationic Surfactant concentation by using the power regression type (Typical Values).

VII. CONCLUSION

The evaluation of this optimization shows that the best results for different this ternary system are obtained with the Trendline Options group. In spite of their mathematical simplicity, these viscosity approaches have a physical and theoretical background and related to characteristic parameters and properties of pure compounds, making these Prediction formals totally typical predictive for different mixtures.

In spite the studied Trendline Options(regression types) is only simple representationof some petroleum distillation cuts, the obtained results further show the capabilities ofthese viscosity approaches to real petroleum fluids and close to the experimental uncertainty (±2%) for the studied Trendline Options system.

REFERENCES

[1] Noura Al Mehbad1, A. M. A. Omar, (2014): *Journal of Surface Engineered Materials and Advanced Technology*, 4, PP 33-40

[2] Noura Al Mehbad1, A. M. A. Omar, (2014): "Preparation Of Polymeric Alcohol For Waste Petroleum Products By Phase Transfer Catalysis," *International Journal of modern organic*.2(3), pp251-261

[3] Jukic, A.; Rogosic, M.; Vidovic, E.; Janovic, Z. (2007): "Ter-polymerization Kinetics of Methyl Methacrylate or Styrene/Dodecyl Methacrylate/ Octa-decyl Methacrylate Systems. Polym. Int., 56, 112.

[4] Bielmeier, E.; Camera, F.; Neveu, C. D. (2003): "A New Breed of Viscosity Index Improvers," Croatian Society for Fuels and Lubricants Symposium Proceedings, Croatian Engineers Association, XXXVI, Symposium Lubricants.

https://dx.doi.org/10.22161/ijaers/3.11.26 *ISSN: 2349-6495(P) | 2456-1908(O)*

[5] El-Abbas Moustafa et.al: "Preparation and Application of Surfactants for Enhanced Oil Recovery (EOR)," preparation and Testing of Surface Active Agents, Study the Effect of prepared surfactants on oil recovery, and feasibility study, project during 1990-1993, supported from Ministry of Scientific Research, Cairo-Egypt.

[6] IvanaS.oljicJerbic, JelenaParlovVukovic and Ante Jukic (2012): "Production and Application Properties of Dispersive Viscosity Index Improvers," Ind. Eng. Chem. Res., 51, PP 11914−11923.

[7] Akhmedov, A. I.; Ibragimova, R. I. 1991: "Butyl methacrylate-Styrene Copolymers as VI Improvers for Ester Oils." Chem. Technol. Fuels Oils, 27, 160.

[8] Kang-Min Jung, Byung-Hee Chun, Sun Hee Park, Chang Hun Lee, Sung Hyun Kim (2011): "Synthesis of Methacrylate Copolymers and Their Effects as Pour Point Depressants for Lubricant Oil," Journal of Applied Polymer Science, Vol. 120, PP 2579–2586.

[9] Jukic, A.; Tomasek, L. J.; Janovic, Z. (2005): "Polyolefin and Poly-Alkyl Methacrylate Mixed Additives as Mineral Lubricating Oil Rheology Modifiers," Lubr. Sci., 17, 431.

[10] Jukic, A.; Rogosic, M.; Vidovic, E.; Janovic, Z. (2007): "Ter-polymerization Kinetics of Methyl Methacrylate or Styrene/Dodecyl Methacrylate/ Octadecyl Methacrylate Systems. Polym. Int., 56, 112.

[11] Aldajah, S.; Ajayi, O. O.; Fenske, G. R.; Goldblat, I. L. (2007): "Effect of exhaust gas recirculation (EGR) contamination of diesel engine oil on wear," Wear J., 263, 93.

[12] Ana Paula Pena Almeida, Ana Paula Lelis Rodrigues de Oliveira, Cynthia D'ÁvilaCarvalhoErbetta, Ricardo Geraldo de Sousa, Roberto Fernando de Souza Freitas, Maria Elisa ScarpelliRibeiro e Silva (2014): "Rheological Study of Polymers Used as Viscosity Index Improvers for Automotive Lubricant Oils," Journal of Modern Physics, 5, PP 1085-1093.

[13] Stephen Childress, (2008): Stephen Childress" An Introduction to Theoretical Fluid Dynamics," February 12, J. of Chemistry, 2 (3), pp. 251-261.

Appendix A:

We have some tables for prediction of viscosity value at different temperatures for mineral base oil (Blank Sample), and variation of concentrations of poly-aromatic cationic surfactant of 1.0%, 2.0% and 3.0% by wt. with used three methods from trend-line options for regression typeseither polynomial, power or exponential modelling calculations for the viscosity predict at any certain temperature but the typical predicted dynamic viscosity has been obtained from applied of power regression type in case of this study. Table A-1 shows that Predicted viscosity for Gear Oil (Blank sample) and with additives 1.0, 2.0 and 3.0% by wt. of Poly-aromatic Cationic Surfactant by using the typical results from applied Trendline option of **Power** Regression and general R- squared values.

Table.A-1: Predicted viscosity for mineral baseoil (Blank sample) and with additives 1.0, 2.0 and 3.0% by wt. of Poly-aromatic Cationic Surfactant by using the best result from applied Trendline option of Power Regression and general R- squared values.

Set -3a	**Mineral baseoil (Blank Sample) at 40 to 150°C.**											
Trend-line Power	**$Y= 6E+06\ X^{-2.579}$**					**for Predict of viscosity**						
$\mu_p=C\ T^b$			**C =**	**6E+06**		**b=**	**-2.579**		**General R^2=**		**0.9992**	
Temperature, °C	**40**	**50**	**60**	**70**	**80**	**90**	**100**	**110**	**120**	**130**	**140**	**150**
Average Viscosity, μ, cp	**418.84**	**???**	**???**	**104.20**	**???**	**???**	**39.08**	**???**	**???**	**???**	**???**	**???**
Predicted Viscosity,μ_p, cp	**443.04**	**249.18**	**155.70**	**104.63**	74.15	54.72	41.70	32.61	26.06	21.20	17.51	14.66
Error, %	0.06			0.00			0.07					

https://dx.doi.org/10.22161/ijaers/3.11.26 *ISSN: 2349-6495(P) | 2456-1908(O)*

Set -3b	**Mineral base oil with D-1.0% by wt. additive of Poly-aromatic Cationic Surfactant at 40 to 150°C.**											
Trend-line Power	**$Y= 7E+06\ X^{-2.605}$**					**for Predict of viscosity**						
$\mu_p=C\ T^b$			**C =**	**7E+06**			**b=**	**-2.605**		**General R^2=**	**0.9990**	
Temperature, °C	**40**	**50**	**60**	**70**	**80**	**90**	**100**	**110**	**120**	**130**	**140**	**150**
Average Viscosity, μ, cp	**440.69**	**???**	**???**	**108.93**	**???**	**???**	**40.12**	**???**	**???**	**???**	**???**	**???**
Predicted Viscosity,μ_p, cp	**469.60**	**262.59**	**163.31**	**109.30**	**77.19**	**56.79**	**43.16**	**33.67**	**26.84**	**21.79**	**17.97**	**15.01**
Error, %	-0.01			0.05			-0.01					

Set -3c	**Mineral base oil with D-2.0% by wt. additive of Poly-aromatic Cationic Surfactant at 40 to 150°C.**											
Trend-line Power	**$Y= 6E+06\ X^{-2.583}$**					**for Predict of viscosity**						
$\mu_p=C\ T^b$			**C =**	**6E+06**			**b=**	**-2.583**		**General R^2=**	**0.9996**	
Temperature, °C	**40**	**50**	**60**	**70**	**80**	**90**	**100**	**110**	**120**	**130**	**140**	**150**
Average Viscosity, μ, cp	**459.45**	**???**	**???**	**112.58**	**???**	**???**	**42.83**	**???**	**???**	**???**	**???**	**???**
Predicted Viscosity,μ_p, cp	**436.55**	**245.31**	**153.17**	**102.86**	**72.86**	**53.75**	**40.94**	**32.01**	**25.56**	**20.79**	**17.17**	**14.37**
Error, %	0.05			0.09			0.04					

Set -3d	**Mineral base oil with D-3.0% by wt. additive of Poly-aromatic Cationic Surfactant at 40 to 150°C**											
Trend-line Power	**$Y= 6E+06\ X^{-2.583}$**					**for Predict of viscosity**						
$\mu_p=C\ T^b$			**C =**	**6E+06**			**b=**	**-2.558**		**General R^2=**	**0.9998**	
Temperature, °C	**40**	**50**	**60**	**70**	**80**	**90**	**100**	**110**	**120**	**130**	**140**	**150**
Average Viscosity, μ, cp	**461.74**	**???**	**???**	**113.35**	**???**	**???**	**44.12**	**???**	**???**	**???**	**???**	**???**
Predicted Viscosity,μ_p, cp	**478.72**	**270.51**	**169.68**	**114.39**	**81.29**	**60.14**	**45.94**	**36.00**	**28.81**	**23.48**	**19.42**	**16.28**
Error, %	0.04			0.01			0.04					

International Journal of Advanced Engineering Research and Science (IJAERS) *[Vol-3, Issue-11, Nov- 2016]*
https://dx.doi.org/10.22161/ijaers/3.11.27 *ISSN: 2349-6495(P) | 2456-1908(O)*

A Survey On Outlier Detection Methods In Spatio-Temporal Datasets

M L Prasanthi[1], A Krishna Chaitanya[2], Dr.N Sambasiva Rao[3]

[1]Assistant Professor in Information Technology, BVRITH College of Engineering for Women, Hyderabad, JNTUH, India.
[2]Assistant Professor in Information Technology,Institute of Aeronautical Engineering, Hyderabad, JNTUH, India.
[3]Professor in Computer Science and Engineering, SRIT for Women, Warangal, JNTUH, India.

Abstract*—Outlier mining has many applications in the real world, such as Weather forecasting, Traffic management, Forest fire, and crop sciences. Extending these applications to Satellites, sensor networks, RFID technology, GPS and telecommunication systems which have become centers for gathering of large sources of data, several interesting facts from Spatio temporal datasets can be extracted. This paper summarizes recent works on the different outlier detection methods which are suitable to detect outliers from Spatio temporal datasets.*

Keywords—spatio temporal data, outlier detection.

I. INTRODUCTION

Outlier detection is a emerging field, which has lot of significance due to the increasing amount of spatio-temporal data available, and the need to understand and interpret it. A spatiotemporal object can be defined as an object that has at least one spatial and one temporal property. The spatial properties are location and geometry of the object. The temporal property is timestamp or time interval for which the object is valid. The spatio-temporal object usually contains spatial, temporal and thematic or non-spatial attributes. Examples of such objects are moving car, forest fire, and earth quake. Spatiotemporal data sets essentially capture changing values of spatial and thematic attributes over a period of time. An event in a spatio temporal dataset describes a spatial and temporal phenomenon that may happens at a certain time t and location x. Examples of event types are earth quake, hurricanes, road traffic jam and road accidents. In real world many of these events interact with each other and exhibit spatial and temporal patterns which may help to understand the physical phenomenon behind them. Therefore, it is very important to identify efficiently the spatial and temporal features of these events and their relationships from large spatio temporal datasets of a given application domain.

Spatio-temporal data mining is the discovery of interesting spatial patterns from data over time using data mining techniques on spatially and temporally distributed data. One such pattern is a spatio-temporal outlier. A spatio-temporal outlier is a spatio-temporal object whose thematic (non-spatial and non-temporal) attributes are significantly different from those of other objects in its spatial and temporal neighborhoods.

This paper is organized as follows section 2 emphasis on classification of outlier detection. Section 3 focuses on taxonomy of approaches to collect Spatio-temporal data. Section 4 summarizes various algorithms to detect outliers from multivariate spatio temporal data

II. CLASSIFICATION OF OUTLIER DETECTION METHODS

The most significant approaches for outlier detection are included in Figure1:

1) Distribution-based approaches that make use of standard statistical distribution to model the data declaring as outliers the objectsthat deviate from the model.

2) Depth-based techniques which are based on computational geometry and compute different layers of convex hulls declaring as outliers the objects belonging to the outer layers

3) Distance-based approaches which compute the proportion of database objects that are at specified distance from a target object

4) Density-based approaches which assign a weight to each sample based on their local neighborhood density.

https://dx.doi.org/10.22161/ijaers/3.11.27 *ISSN: 2349-6495(P) | 2456-1908(O)*

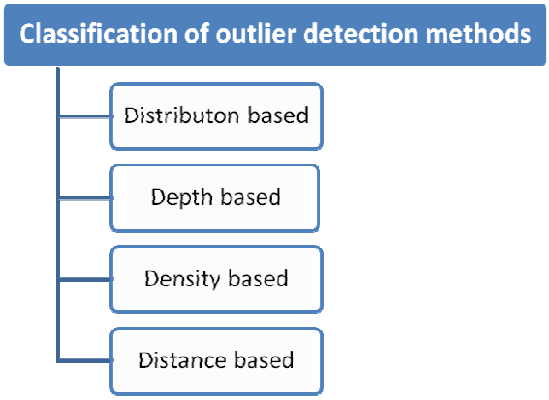

Fig.1: Classification of outlier detection methods

A different classification is based on the outlier detection output and divides into: Labeling and Scoring techniques. Labeling methods partition the data into two non-overlapping sets (outliers and non-outliers) and scoring methods offer a ranking list by assigning to each datum a factor reflecting its degree of outlierness. These former methods exploit a hard decision about the sets, the latter ones deal with a sort of soft decision about the membership of each datum to the set.

Another way of classifying Outlier detection methods can be divided between univariate methods, proposed in earlier works in this field, and multivariate methods that usually form most of the current body of research.

Another fundamental taxonomy of outlier detection methods is between parametric (statistical) methods and nonparametric methods that are model-free (e.g., see (Williams et al., 2002)).

Statistical parametric methods either assume a known underlying distribution of the observations or, at least, they are based on statistical estimates of unknown distribution parameters. These methods considers outliers as those observations that deviate from the model assumptions. They are often unsuitable for high-dimensional data sets and for arbitrary data sets without prior knowledge of the underlying data distribution. Within the class of non-parametric outlier detection methods one can set apart the data-mining methods, also called distance-based methods. These methods are usually based on local distance measures and are capable of handling large databases .

Another related class of methods consists of detection techniques for spatial outliers. These methods search for extreme observations or local instabilities with respect to neighboring values, although these observations may not be significantly different from the entire population.

Univariate Statistical Methods: Most of the earliest univariate methods for outlier detection rely on the assumption of an underlying known distribution of the data, which is assumed to be identically and independently distributed .Moreover, many discordance tests for detecting univariate outliers further assume that the distribution parameters and the type of expected outliers are also known (Barnett and Lewis, 1994). Needless to say, in real world data-mining applications these assumptions are often violated. A central assumption in statistical-based methods for outlier detection, is a generating model that allows a small number of observations to be randomly sampled from distributions G1,. . . , Gk, differing from the target distribution F, which is often taken to be a normal distribution N ¡ µ, σ2 ¢ (see (Ferguson, 1961; David, 1979; Barnett and Lewis, 1994; Gather, 1989; Davies and Gather, 1993)). The outlier identification problem is then translated to the problem of identifying those observations that lie in a so-called outlier region.

III. TAXONOMY OF APPROACHES TO COLLECT SPATIO-TEMPORAL DATA

Two approaches are used to collect spatio temporal data.

1. Lagrangian approach
2. Eularian approach.

1. Lagrangian approach:

The Lagrangian approach is individual-based and entails tracking a specific individual. Figure 2 below, shows classification of various technologies used in lagrangian approach. The technologies used for the Lagrangian modeling are, on the other hand invasive, in form of a mark or device which is fitted on the object. They are designed specifically to retrieve specific spatio-temporal data type with high quality.

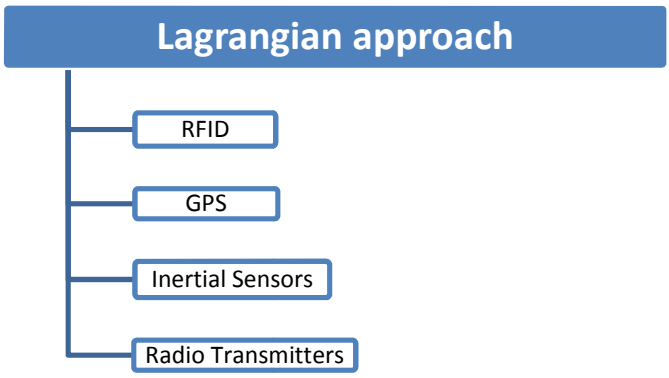

Fig.2: Lagrangian approach

https://dx.doi.org/10.22161/ijaers/3.11.27 *ISSN: 2349-6495(P) | 2456-1908(O)*

Eulerian approach:

The Eulerian approach is place-based and deals with the probability of presence of an individual or a group in a place and the change of this occurrence over time. Figure3 shows classification of various technologes used in Eularian approach. Various types of data can be retrieved from sensor technologies used for the Eulerian modeling, these data are subject to error and noise.

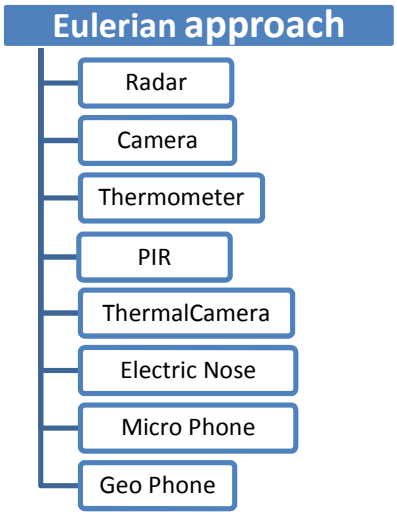

Fig.3: Eulerian approach

IV. OUTLIER DETECTION METHODS SUITABLE TO MULTIVARIATE SPATIO TEMPORAL DATA

Spatiotemporal data mining is used in various applications domains like Meterology,crop sciences,Forestry,Medicine,Geo physics, ecology, Transportation.Outlier detection in spatio temporal data patterns used to identify interesting abnormal patterns in huge datasets . some of such interesting patterns are detecting tropicalcyclonic paths, patterns of growing cancer cells in the cancer data of a patient in different time intervals.

In anomaly detection we also have the additional problem of identifying what is an anomaly in the domain: this is especially hard when dealing with multivariate data, because characterizing anomalies involving multiple features may not be intuitive and in most cases visualization approaches can't be used with high dimensionality. Finally, in multivariate data some features may not be available as frequently as others due to coming from different sources, leading to missing data concentrated in some features. The strategies for dealing with missing data in multivariate sets need to account for correlation between features.

Dataset composed of many correlated attributes or features are common in real world application. Traditional time series anomaly detection algorithms such as CUSUM or STCOD analyze only one feature of the dataset.While many anomalies may be detected by analyzing a single feature, other anomalies might affect multiple features without being evident in a single one. In this situation the analysis must be performed on multiple features at once. Univariate analysis also does not account for the possibility of features being correlated to each other; this information could be used, for example, to predict the behavior of a feature by analyzing other correlated features. Secondly, multivariate data is often heterogeneous; when types of features are different the analysis needs to rely on techniques that are general enough to be applicable to every data type involved. Other than the data type, different features may be differently distributed, or have different semantic (for example only positive are meaningful, only integer etc.).The survey of outlier detection algorithm shows that no algorithm can guarantee all our desired properties when applied to multivariate spatiotemporal data.

This paper summarizes few outlier detection approches used to identify outlier patterns from different multivariate spatio temporal datasets of various domains.

a) ST-SNN Algorithm:

K.P. Agrawal, Sanjay Garg and Pinkal Patel suggested Spatio-Temporal Shared Nearest Neighbor (ST-SNN) clustering approach, SNN which is based on the Shared Nearest Neighbor Similarity and modified version of existing density based clustering approach. It focuses on the clustering technique to detect outliers, which works well for high dimensional, arbitrary shaped, size and different density dataset and it is capable to handle high dimensional spatio-temporal data having different sizes and densities and also identifies arbitrary shaped clusters.

They experimented the algorithm on spatio-temporal dataset containing NDVI (Normalized difference vegetation index)values for different states in India. These NDVI values shows low vegetation when values are between 0.1 and 0.3 and shows high vegetation when values are between 0.8 and 1. Dataset has the columns: Grid code for each grid, Latitude of the grid, Longitude of the grid, state, City and 23 columns for NDVI values, where each column contains 16 days composite NDVI values.

In particular, algorithm first finds k-nearest neighbors for each data objects and then, as in SNN clustering approach, shared nearest neighbors are found between the pairs of points in terms of how many nearest neighbors the two points share. Using ST-SNN clustering, core points are

https://dx.doi.org/10.22161/ijaers/3.11.27 *ISSN: 2349-6495(P) | 2456-1908(O)*

identified in spatiotemporal data and clusters are created around the core points. The use of Shared Nearest Neighbor approach solves the problems with variable density and the unreliability of distance measure in high dimensions, while the use of core points handles problems with shape and size. The average runtime complexity of ST-SNN outlier detection algorithm is O (n2), where n is the number of objects in the dataset. The space complexity of the algorithm is also O (n2), since we need to store k-nearest neighbors which takes O (k*n) space and shared nearest neighbors similarity matrix which takes O(n2)

b) MUSTF Algorithm:

Gianluca Goffredi proposed a new algorithm "Multivariate Spatio-Temporal Anomaly Detection using Fisher's method(MuSTF) " to detect outliers in mobile network.MuSTF algorithm proved in detecting anomalies in the same data. Another particularly important improvement of MuSTF is the shorter delay in detection: our algorithm is able to detect the same anomaly several hours sooner than the state-of-the-art algorithms. Finally, MuSTF performance is less sensitive to small changes in the user-set parameters than other state-of-the-art algorithm, which relieves the user from having to discover the best settings to find acceptable results. We also showed how MuSTF is able to identify the spatial cluster that is involved in the anomaly, distinguishing clusters of nodes that belong to areas with different behavior even when close to each other.

c) COVSRE Method:

Alka Bhushan , Monir H. Sharker, Hassan A. Karimi suggested a statistical outlier detection method COVSRE(covariance free squared reconstruction error) which is suitable for spatio temporal datastreams. It uses the concept of incremental Principal component Analysis. The dataset used in their method is the air quality index (AQI) dataset which is publicly available from central Environmental Protection Agency (EPA) repository in USA (EPA, 2011).

EPA has placed sensors to measure pollutants across locations all over USA. The data is collected on hourly basis. Each sensor measures air pollutants at regular intervals and sends the measurement to the central data repository. AQI measures the quality of air which is computed based on the quantity of pollutants measured at each location at each given instance. From amongst 3000 sensors, 81 sensors from one geographically chosen area are selected for the experiments. The computational time to detect outliers using COVSRE method is O(nk).

For spatial applications, however, these global forms can only detect outliers in a non-spatial manner. This can result in false positive detections, such as when an observation's spatial neighbors are similar, or false negative detections such as when its spatial neighbors are dissimilar. To avoid mis-classifications, we demonstrate that a local adaptation of various global methods can be used to detect multivariate spatial outliers. In particular, we account for local spatial effects via the use of geographically weighted data with either Mahalanobis distances or principal components analysis. Detection performance is assessed using simulated data as well as freshwater chemistry data collected over all of Great Britain. Results clearly show value in both geographically weighted methods to outlier detection.

Derya Birant, Alp Kut proposed a new approach to find Spatio temporal outliers in large databases, the approach uses a 3-step algorithm constitutes clustering, checking spatial neighbors to identify spatial outliers, and checking temporal neighbors to identify spatio-temporal outliers.

d) ROSE(Rough Outlier set Extraction) Algorithm:

Alessia Albanese, Sankar K. Pal, and Alfredo Petrosino proposed a new rough set based approach called ROSE (Rough outlier set exraction) to detect spatiotemporal outliers. This method uses a new set called Kernel set as input instead of the universe, which is derived from universe U and detects outliers with low computational time.

e) Multi scale approach to detect spatio temporal outliers:

Tao Cheng ,Zhilin LiA used a multiscale approach to detect spatio temporal outliers ,where the detection process constitutes four steps classification, aggregation, comparision, and verification. The dataset used is Ameland, a barrier island in the north of the Netherlands, was chosen as a case study area. The process of coast change involves the erosion and accumulation of sediments along the coast, which is scale-dependent in space and time. It can be monitored through the observation of annual changes of landscape units such as foreshore, beach and foredune. The data set we used covers part of the island. The DEMs of six consecutive years (from 1989-1995) is displayed in Figure 2. It is hard to identify the outliers in the images displayed in Figure 2. The purpose of our experiment is to use the multiscale approach to detect the outliers in these six year DEMs.

V. CONCLUSION

The Spatio temporal outlier detection is very much essential to find out the noise in dataset. These outliers must be checked whether they are true or false outliers since the elimination of false outliers may affect the final analysis

https://dx.doi.org/10.22161/ijaers/3.11.27 *ISSN: 2349-6495(P) | 2456-1908(O)*

results and the presence of true outliers also makes confusion. In any datamining process the elimination of inconsistent values or outliers itself makes the process easier for further analysis and in spatial datamining it is very much essential since abundant data is involved in the processing. This paper discusses the approaches, methods and some algorithms used for outlier detection in spatio temporal data streams.

REFERENCES

[1] K.P. Agrawal, Sanjay Garg andPinkal Patel "Spatio-Temporal Outlier Detection Technique" IJCSC Vol 6 Number 2 April - Sep 2015

[2] Raymond T. Ng and Jiawei Han, CLARANS: A Method for Clustering Objects for Spatial Data Mining 2002.
Alka Bhushan , Monir H. Sharker, Hassan A. Karimi "INCREMENTAL PRINCIPAL COMPONENT ANALYSIS BASED OUTLIER DETECTION METHODS FOR SPATIOTEMPORAL DATA STREAMS"
Remote Sensing and Spatial Information Sciences, Volume II-4/W2, 2015 International Workshop on Spatiotemporal Computing, 13–15 July 2015.

[3] Derya Birant, Alp Kut "Spatio-Temporal Outlier Detection in Large Databases" Journal of Computing and Information Technology - CIT 14, 2006.

[4] Tao Cheng Zhilin Li "A MULTISCALE APPROACH TO DETECT SPATIAL-TEMPORAL OUTLIERS".

[5] Paul Harris Chris Brunsdon, Martin Charlton, Steve Juggins, Annemarie Clarke "Multivariate Spatial Outlier Detection Using Robust Geographically Weighted Methods".

[6] Gianluca Goffredi "MULTIVARIATE SPATIO-TEMPORAL ANOMALY DETECTION IN A MOBILE NETWORK" 2014-2015.

[7] V. Barnett and T. Lewis 1994 "Outliers in Statistical Data," John Wiley & Sons.

[8] P. Burge and J. Shaw-Taylor 1997 "Detecting Cellular Fraud Using Adaptive Prototypes," Proc. AI Approaches to Fraud Detection and Risk Management, pp. 9-13.

[9] T. Cover and J.A. Thomas 1991 "Elements of Information Theory," Wiley-International.

[10] T. Fawcett and F. Provost 1999 "Activity Monitoring: Noticing Interesting Changes in Behavior," Proc. ACM-SIGKDD Int'l Conf. Knowledge Discovery and Data Mining, pp. 53-62.

[11] S.B. Guthery, "Partition Regression 1974," J. Am. Statistical Assoc., vol. 69, no. 348, pp. 945-947.

[12] D.M. Hawkins 1976 "Point Estimation of Parameters of Piecewise Regression Models," J Royal Statistical Soc. Series C, vol. 25, no. 1, pp. 51-57.

[13] M. Huskova, 1993 "Nonparametric Procedures for Detecting a Change in Simple Linear Regression Models," Applied Change Point Problems in Statistics.

[14] G. Kitagawa and W. Gersch 1996 "Smoothness Priors Analysis of Time Series," Lecture Notes in Statistics, vol. 116, Springer-Verlag.

[15] E.M. Knorr and R.T. Ng 1998 "Algorithms for Mining Distance-Based Outliers in Large Data Sets," Proc. 24th Very Large Data Bases Conf.,pp. 392-403.

[16] U. Murad and G. Pinkas 1999 "Unsupervised Profiling for Identifying Superimposed Fraud," Proc. Third European Conf. Principles and Practice of Knowledge Discovery in Databases, pp. 251-261.

[17] R.M. Neal and G.E. Hinton 1993 "A View of the EM Algorithm that Justifies Incremental, Sparse, and Other Variants".

[18] T. Ozaki and G. Kitagawa 1995 "A Method for Time Series Analysis," Asakura Shoten, (in Japanese).

[19] J. Rissanen 1996 "Fisher Information and Stochastic Complexity," IEEE Trans. Information Theory, vol. 42, no. 1, pp. 40-47.

[20] K. Yamanishi, J. Takeuchi, G. Williams, and P. Milne May 2004 "Online Unsupervised Outlier Detection Using Finite Mixtures with Discounting Learning Algorithms," Data Mining and Knowledge Discovery J., vol. 8, no. 3, pp. 275-300.

[21] K. Yamanishi and J. Takeuchi 2001 "Discovering Outlier Filtering Rules from Unlabeled Data," Proc. Fourth Workshop Knowledge Discovery and Data Mining, pp. 389-394.

[22] K. Yamanishi and J. Takeuchi 2002 "A Unifying Approach to Detecting Outliers and Change-Points from Nonstationary Data," Proc of the Eighth ACM SIGKDD Int'l Conf. Knowledge Discovery and Data Mining.

[23] B.K. Yi, N.D. Sidiropoulos, T. Johnson, H.V. Jagadish, C. Faloutsos, and A. Biliris 2000 "Online Data Mining for Co-Evolving Time Sequences" Proc. 16th Int'l Conf. Data Eng.

https://dx.doi.org/10.22161/ijaers/3.11.28 *ISSN: 2349-6495(P) | 2456-1908(O)*

Noise Suppression in Images by Median Filter

Dontabhaktuni Jayakumar, Neelapala Saisruthi, Laiphangbam Renita Devi

Assistant professor Department of ECE, Holy Mary Institute of Technology and Science, Hyderabad, India

Abstract— *A new and efficient algorithm for high-density salt and pepper noise removal in images and videos is proposed. In the transmission of images over channels, images are corrupted by salt and pepper noise, due to faulty communications. Salt and Pepper noise is also referred to as Impulse noise. The objective of filtering is to remove the impulses so that the noise free image is fully recovered with minimum signal distortion. Noise removal can be achieved, by using a number of existing linear filtering techniques. We will deal with the images corrupted by salt-and-pepper noise in which the noisy pixels can take only the maximum or minimum values (i.e. 0 or 255 for 8-bit grayscale images).*

Keywords— About five key words in alphabetical order, separated by comma.

I. INTRODUCTION

1.1 Introduction to project

In image processing it is usually necessary to perform high degree of noise reduction in an image before performing higher-level processing steps, such as edge detection. The median filter is a non-linear digital filtering technique, often used to remove noise from images or other signals. The idea is to examine a sample of the input and decide if it is representative of the signal. This is performed using a window consisting of an odd number of samples. The values in the window are sorted into numerical order; the median value, the sample in the center of the window, is selected as the output. The oldest sample is discarded, a new sample acquired, and the calculation repeats.

Median filtering is a common step in image processing. It is particularly useful to reduce speckle noise and salt and pepper noise. Its edge-preserving nature makes it useful in cases where edge blurring is undesirable Image synthesis is the process of creating new images from some form of image description. The kinds of images that are typically synthesized include as follows.

1.1.1 Noise

In common use, the word noise means unwanted sound or noise pollution. In electronics noise can refer to the electronic signal corresponding to acoustic noise (in an audio system) or the electronic signal corresponding to the (visual) noise commonly seen as 'snow' on a degraded television or video image. In signal processing or computing it can be considered data without meaning that is, data that is not being used to transmit a signal, but is simply produced as an unwanted by-product of other activities. In Information Theory, however, noise is still considered to be information. In a broader sense, film grain or even advertisements in web pages can be considered noise. Noise can block, distort, or change the meaning of a message in both human and electronic communication.

In many of these areas, the special case of thermal noise arises, which sets a fundamental lower limit to what can be measured or signaled and is related to basic physical processes at the molecular level described by well-known simple formulae.

1.1.2 Salt and Pepper Noise

Another common form of noise is data drop-out noise (commonly referred to as intensity spikes, speckle or salt and pepper noise). Here, the noise is caused by errors in the data transmission. The corrupted pixels are either set to the maximum value (which looks like snow in the image) or have single bits flipped over. In some cases, single pixels are set alternatively to zero or to the maximum value, giving the image a `salt and pepper' like appearance. Unaffected pixels always remain unchanged. The noise is usually quantified by the percentage of pixels which are corrupted.

In the following examples, images have been corrupted with various kinds and amounts of drop-out noise. In, pixels have been set to 0 or 255 with probability p=1%. In pixel bits were flipped with p=3%, and in 5% of the pixels (whose locations are chosen at random) are set to the maximum value, producing the snowy appearance.

For this kind of noise, conventional low pass filtering, *e.g.* mean filtering or Gaussian smoothing is relatively unsuccessful because the corrupted pixel value can vary significantly from the original and therefore the mean can be significantly different from the true value. Median filter removes drop-out noise more efficiently and at the same time preserves the edges and small details in the image better. Conservative smoothing can be used to obtain a result which preserves a great deal of high frequency detail, but is only effective at reducing low levels of noise.

1.1.3 Median Filter

The Common Names are Median filtering, Rank filtering. The median filter is normally used to reduce noise in an

https://dx.doi.org/10.22161/ijaers/3.11.28 *ISSN: 2349-6495(P) | 2456-1908(O)*

image, somewhat like the mean filter. However, it often does a better job than the mean filter of preserving useful detail in the image.

How Median filter works

Like the mean filter, the median filter considers each pixel in the image in turn and looks at its nearby neighbours to decide whether or not it is representative of its surroundings. Instead of simply replacing the pixel value with the mean of neighbouring pixel values, it replaces it with the median of those values. The median is calculated by first sorting all the pixel values from the surrounding neighbourhood into numerical order and then replacing the pixel being considered with the middle pixel value. (If the neighborhood under consideration contains an even number of pixels, the average of the two middle pixel values is used.) Figure 1.1 illustrates an example calculation.

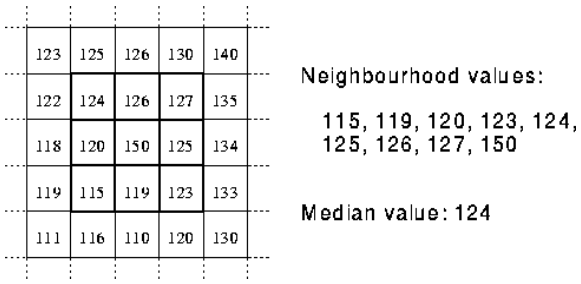

Fig.1.1: Calculating the median value of a pixel neighborhood.

As can be seen the central pixel value of 150 is rather unrepresentative of the surrounding pixels and is replaced with the median value 124. A 3×3 square neighborhood is used here and larger neighborhoods will produce more severe smoothing.

1.1.4 Mean Filter

The Common Names are Mean filtering, Smoothing, Averaging, Box filtering. Mean filtering is a simple, intuitive and easy to implement method of smoothing images, *i.e.* reducing the amount of intensity variation between one pixel and the next. It is often used to reduce noise in images.

How mean filter works

The idea of mean filtering is simply to replace each pixel value in an image with the mean (`average') value of its neighbours, including itself. This has the effect of eliminating pixel values which are unrepresentative of their surroundings. Mean filtering is usually thought of as a convolution filter. Like other convolutions it is based around a kernel, which represents the shape and size of the neighbourhood to be sampled when calculating the mean. Often a 3×3 square kernel is used, as shown in Figure 1.1, although larger kernels (*e.g.* 5×5 squares) can be used for more severe smoothing. (Note that a small kernel can be applied more than once in order to produce a similar - but not identical - effect as a single pass with a large kernel.)

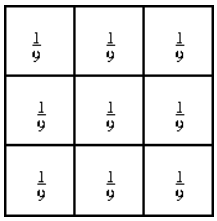

Fig.1.2: 3×3 averaging kernel often used in mean filtering

Computing the straightforward convolution of an image with this kernel carries out the mean filtering process.

1.1.5 Adaptive Median Filter

Comparing with Standard median filtering the Adaptive median filtering is an advanced method. Which pixels in an image have been affected by impulse noise can be determined by using spatial processing. AMF performs in the image by comparing each pixel with its surrounding neighbor pixels to classify pixels as noise. The neighborhood pixel of the size is adjustable, as well as for the comparison the threshold is adjustable. A pixel is not structurally aligned with those pixels to which it is similar, as well as pixel that is Different from a majority of its neighbors can be treated as impulse noise. The median pixel value of the pixels in the neighborhood can be replaced in the place of noise pixels that have passed the noise labeling test.

1.1.6 Unsymmetric Trimmed Median Filter

In this UTMF, the selected window elements are arranged in either increasing or decreasing order. Then the pixel values 0's and 255's in the image (i.e., the pixel values responsible for the salt and pepper noise) are removed from the image. Then the median value of the remaining pixels is taken. This median value is used to replace the noisy pixel. This filter is called trimmed median filter because the pixel values 0's and 255's are removed from the selected window.

1.1.7 Proposed Algorithm

The proposed Modified Decision Based Unsymmetrical Trimmed Median Filter (MDBUTMF) algorithm processes the Corrupted images by first detecting the impulse noise. The processing pixel is checked whether it is noisy or noisy free. That is, if the processing pixel lies between maximum and minimum gray level values then it is noise free pixel, it is left unchanged. If the processing pixel takes the maximum or minimum gray level then it is noisy pixel which is processed by MDBUTMF.

1.2 Introduction to VLSI

1.2.1 Digital Design

Prompted by the development of new types of sophisticated field-programmable devices (FPDs), the process of designing digital hardware has changed

https://dx.doi.org/10.22161/ijaers/3.11.28 *ISSN: 2349-6495(P) | 2456-1908(O)*

dramatically over the past few years. Unlike previous generations of technology, in which board-level designs included large numbers of SSI chips containing basic gates, virtually every digital design produced today consists mostly of high-density devices. This applies not only to custom devices like processors and memory, but also for logic circuits such as state machine controllers, counters, registers, and decoders. When such circuits are destined for high-volume systems they have been integrated into high-density gate arrays. However, gate array NRE costs often are too expensive and gate arrays take too long to manufacture to be viable for prototyping or other low-volume scenarios. For these reasons, most prototypes, and also many production designs are now built using FPD s. The most compelling advantages of FPDs are instant manufacturing turnaround, low start-up costs, low financial risk and (since programming is done by the end user) ease of design changes. The market for FPDs has grown dramatically over the past decade to the point where there is now a wide assortment of devices to choose from. A designer today faces a daunting task to research different types of chips, understand what they can best be used for, choose a particular manufacturer's product, learn the intricacies of vendor-specific software and then design the hardware. Not only the sheer number of FPDs available exacerbates confusion for designers, but also by the complexity of the more sophisticated devices. The purpose of this paper is to provide an overview of the architecture of the various types of FPDs. The emphasis is on devices with relatively high logic capacity; all of the most important commercial products are discussed.

1.2.2 Overview of Commercially Available FPDs

This section provides many examples of commercial FPD products. SPLDs are first discussed briefly, and then details are given for all of the most important CPLDs and FPGAs. The reader who is interested in more details on the commercial products is encouraged to contact the manufacturers, or their distributors, for the latest data sheets.

Commercially Available CPLDs

As stated earlier, CPLDs consist of multiple SPLD-like blocks on a single chip. However, CPLD products are much more sophisticated than SPLDs, even at the level of their basic SPLD-like blocks. In this section, CPLDs are discussed in detail, first by surveying the available commercial products and then by discussing the types of applications for which CPLDs are best suited. Sufficient details are presented to allow a comparison between the various competing products, with more attention being paid to devices that we believe are in more widespread use than others.

Commercially Available FPGAs

As one of the largest growing segments of the semiconductor industry, the FPGA market-place is volatile. As such, the pool of companies involved changes rapidly and it is somewhat difficult to say which products will be the most significant when the industry reaches a stable state. For this reason, and to provide a more focused discussion, we will not mention all of the FPGA manufacturers that currently exist, but will instead focus on those companies whose products are in widespread use at this time. In describing each device we will list its capacity, nominally in 2-input NAND gates as given by the vendor. Gate count is an especially contentious issue in the FPGA industry, and so the numbers given in this paper for all manufacturers should not be taken too seriously. Wags have taken to calling them "dog" gates, in reference to the traditional ratio between human and dog years. There are two basic categories of FPGAs on the market today 1. SRAM-based FPGAs and 2. antifuse-based FPGAs. In the first category, Xilinx and Altera are the leading manufacturers in terms of number of users, with the major competitor being AT&T. For antifuse-based products, Actel, Quick logic and Cypress, and Xilinx offer competing products.

1.2.3 Needs for FPGA

Because they offer high speeds and a range of capacities, FPGAs are useful for a very wide assortment of applications, from implementing random glue logic to prototyping small gate arrays. One of the most common uses in industry at this time, and a strong reason for the large growth of the FPGA market, is the conversion of designs that consist of multiple SPLDs into a smaller number of FPGAs. FPGAs can realize reasonably complex designs, such as graphics controller, LAN controllers, UARTs, cache control, and many others. As a general rule-of-thumb, circuits that can exploit wide AND/OR gates, and do not need a very large number of flip-flops are good candidates for implementation in FPGAs. A significant advantage of FPGAs is that they provide simple design changes through re-programming (all commercial FPGA products are re-programmable). Within system programmable FPGAs it is even possible to re-configure hardware (an example might be to change a protocol for a communications circuit) without power-down.

Designs often partition naturally into the SPLD-like blocks in a FPGA. The result is more predictable speed-performance than would be the case if a design were split into many small pieces and then those pieces were mapped into different areas of the chip. Predictability of circuit implementation is one of the strongest advantages of FPGA architectures.

https://dx.doi.org/10.22161/ijaers/3.11.28 ISSN: 2349-6495(P) | 2456-1908(O)

II. LITERATURE SURVEY

In this section, we have gone through detail literature reviews of impulse noise removal on the reported recent articles and critically studied their performances through computer simulation. In traditional median filtering called standard median filter (SMF), the filtering operation is performed across to each pixel without considering whether it is uncorrupted. So, the image details, contributed by the uncorrupted pixels are also subjected to filtering and as a result the image details are lost in the restored version. To overcome this problem, an impulse noise detection mechanism is applied prior to the image filtering. A Dynamic Adaptive Median Filter (DAMF) was proposed for removing high density salt and pepper noise. The filter is dynamic in nature as it decides the window size for the test pixel locally before filtering during run time and is adaptive due to the selection of a proper window size. The progressive switching median filter (PSMF) was proposed which achieves the detection and removal of impulse noise in two separate stages. In first stage, it applies impulse detector and then the noise filter is applied progressively in iterative manners in second stage. In this method, impulse pixels located in the middle of large noise blotches can also be properly detected and filtered. The performance of this method is not good for very highly corrupted image.

Nonlinear filters such as adaptive median filter (AMF) can be used for discriminating corrupted and uncorrupted pixels and then apply the filtering technique. Noisy pixels will be replaced by the median value, and uncorrupted pixels will be left unchanged. An efficient decision-based algorithm (DBA) was proposed using a fixed window size of , where the corrupted pixels are replaced by either the median pixel or neighborhood pixels. It shows promising results, a smooth transition between the pixels is lost with lower processing time which degrades the visual quality of the image.

A novel improved median filtering (NIMF) algorithm is proposed for removal of highly corrupted with salt-and-pepper noise from images. Firstly all the pixels are classified into signal pixels and noisy pixels by using the Max-Min noise detector. The noisy pixels are then separated into three classes, which are low-density, moderate density, and high-density noises, based on the local statistic information. Finally, the weighted 8-neighborhoodsimilarity function filter, the median filter and the 4-neighborhood mean filter are adopted to remove the noises for the low, moderate and high level cases, respectively.

A Tolerance based Arithmetic Mean Filtering Technique (TSAMFT) is proposed to remove salt and pepper noise from corrupted images. Arithmetic Mean filtering technique is modified by the introduction of two additional features. In the first phase, to calculate the Arithmetic Mean, only the unaffected pixels are considered. In the second phase, a Tolerance value has been used for the replacement of the pixels. This proposed technique provides much better results than that of the existing mean and median filtering techniques.

A modified decision based unsymmetrical trimmed median filter (MDBUTMF) algorithm is proposed for the restoration of gray scale, and color images that are highly corrupted by salt and pepper noise. The proposed algorithm replaces the noisy pixel by trimmed median value when other pixel values, 0's and 255's are present in the selected window and when all the pixel values are 0's and 255's then the noise pixel is replaced by mean value of all the elements present in the selected window. When this algorithm tested against different gray scale and color images, it gives better Peak Signal-to-Noise Ratio (PSNR) and Image Enhancement Factor (IEF).

Existing System

Median filters are known for their capability to remove impulse noise without damaging the edges i.e., to preserve the edges. The main drawback of a standard median filter (SMF) is that it is effective only for low noise densities. At high noise densities, SMFs often exhibit blurring for large window sizes.

Proposed System

Adaptive Median is a "decision-based" filter known as (MDBUT median filter) that first identifies possible noisy pixels and then replaces them using the median filter or its variants, while leaving all other pixels unchanged. This filter is good at detecting noise even at a high noise level.

III. SOFTWARE AND HARDWARE DESIGN

3.1 Introduction

Digital images play a very important part both in applications such as television magnetic resonance imaging computer tomography as well as in field of science and technology such as geographical information system and astronomy. Sets of data collected by image sensors and other devices are generally contaminated by noise .Also noise can introduced due to transmission errors and compression. Hence denoising is often a necessary and first step to be performed before image data is analyzed and processed. An efficient denoising technique must be applied to compensate for such data corruption. Noise is generally modeled as Gaussian noise (Normal), Uniform noise and Impulse noise (salt and pepper noise). The impulse noise is of two types, Fixed valued and random valued. The fixed valued impulse noise is also known as salt and pepper noise which can have value either 0 or 255. Here 0 represent complete black and 255 represent complete white on gray scale image. The random valued impulse noise can have any

https://dx.doi.org/10.22161/ijaers/3.11.28 *ISSN: 2349-6495(P) | 2456-1908(O)*

value between 0 and 255; hence its removal is very important and difficult. Image de-noising is an important pre-processing step for image analysis. It refers to the task of recovering a good estimate of the true image from a degraded observation without altering and changing useful structure in the image such as discontinuities and edges. Image denoising still remains an important challenge for researchers because denoising process removes noise but introduces artifacts and also causes blurring.

Several nonlinear filters have been proposed for restoration of images contaminated by salt and pepper noise. Among these standard median filter has been established as reliable method to remove the salt and pepper noise without damaging the edge details. However, the major drawback of standard Median Filter (MF) is that the filter is effective only at low noise densities. When the noise level is over 50% the edge details of the original image will not be preserved by standard median filter. Adaptive Median Filter (AMF) performs well at low noise densities. But at high noise densities the window size has to be increased which may lead to blurring the image. In switching median filter, the decision is based on a pre-defined threshold value. The major drawback of this method is that defining a robust decision is difficult. Also these filters will not take into account the local features. As a result of which details and edges may not be recovered satisfactorily, especially when the noise level is high.

To overcome the above drawback, Decision Based Algorithm (DBA) is proposed. In this, image is de noised by using a window. If the processing pixel value is 0 or 255 it is processed or else it is left unchanged. At high noise density the median value will be 0 or 255 which is noisy. In such case, neighboring pixel is used for replacement. This repeated replacement of neighboring pixel produces streaking effect. In order to avoid this drawback, Decision Based Un symmetric Trimmed Median Filter (DBUTMF) is proposed. At high noise densities, if the selected window contains all 0's or 255's or both then, trimmed median value cannot be obtained. So this algorithm does not give better results at very high noise density that is at 80% to 90%. The proposed Modified Decision Based Unsymmetric Trimmed Median Filter (MDBUTMF) algorithm removes this drawback at high noise density and gives better Peak Signal-to-Noise Ratio (PSNR) and Image Enhancement Factor (IEF) values than the existing algorithm.

The proposed Modified Decision Based Unsymmetric Trimmed Median Filter (MDBUTMF) algorithm processes the corrupted images by first detecting the impulse noise. The processing pixel is checked whether it is noisy or noisy free. That is, if the processing pixel lies between maximum and minimum gray level values then it is noise free pixel, it is left unchanged. If the processing pixel takes the maximum or minimum gray level then it is noisy pixel which is processed by MDBUTMF. In many practical cases of image processing, only a noisy image is available. This circumstance is known as the blind condition. Many denoising methods usually require the exact value of the noise distribution as an essential filter parameter. So, the noise estimation methods in the spatial domain use the variance or standard deviation to estimate the actual added noise distribution. But it is found that the mean deviation provides better results than the variance or standard deviation to estimate the noise distribution. The advantage of this approach is that the mean deviation is actually more efficient than the standard deviation in practical situations. The standard deviation emphasizes a larger deviation; squaring the values makes each unit of distance from the mean exponentially (rather than additively) larger. The larger deviation will cause overestimation or underestimation of the noise. So, we assume that use of the mean deviation may contribute to more accurate noise estimation. Keeping these points in view, the authors have used the mean deviation parameter in deciding the noise pixel and replaced the central pixel by its mean deviation instead of its mean. The steps in the proposed MDBUTMF algorithm are given below.

3.2 Algorithm

Step 1 The MDBUTM Filter selects a 2D-window of size 3×3. The center pixel in the selected window is the processing pixel and it is denoted as Pij . It is given in Fig.3.1. The neighboring pixels of the processing pixel are present in the directions NW, N, NE, W, E, SW, S, and SE. The positions of these directions are (i-1,j-1), (i-1,j), (i-1,j+1), (i,j-1), (i,j+1), (i+1,j-1), (i+1,j) and (i+1,j+1) respectively. The directions are clearly mentioned in the following Fig.3.1. The X-axis is considered for 'i' and Y-axis is considered for 'j'.

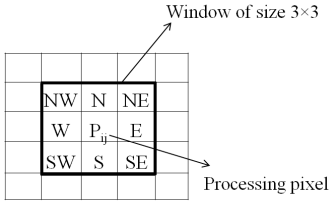

Fig.3.1: Pixel 2D-window of size 3×3

Step 2 If then is an uncorrupted pixel and its value is left unchanged.

Step 3 If or then is a corrupted pixel then two cases are possible as given in Case i) and ii).

Case i) If the selected window contains all the elements as 0's and 255's. Then replacewith the mean of the element of window.

Case ii) If the selected window contains not all elements as 0's and 255's. Then eliminate255's and 0's and find

https://dx.doi.org/10.22161/ijaers/3.11.28 *ISSN: 2349-6495(P) | 2456-1908(O)*

the median value of the remaining elements. Replace with the median value.

Step 4 Repeat steps 1 to 3 until all the pixels in the entire image is processed.

The pictorial representation of each case of the proposed algorithm is shown in below flow chart.Each and every pixel of the image is checked for the presence of salt and pepper noise. Different cases are illustrated below. If the processing pixel is noisy and all other pixel values are either 0's or 255's is illustrated in Case i). If the processing pixel is noisy pixel that is 0 or 255 is illustrated in Case ii). If the processing pixel is not noisy pixel and its value lies between 0 and 255 is illustrated in Case iii).

Case i) If the selected window contains salt/pepper noise as processing pixel (i.e., 255/0 pixel value) and neighboring pixel values contains all pixels that adds salt and pepper noise to the image

where "255" is processing pixel, i.e., .

Since all the elements surrounding are 0's and 255's.If one takes the median value it will be either 0 or 255 which is again noisy. To solve this problem, the mean of the selected window is found and the processing pixel is replaced by the mean value. Here the mean value is 170. Replace the processing pixel by 170.

Case ii) If the selected window contains salt or pepper noise as processing pixel (i.e., 255/0 pixel value) and neighboring pixel values contains some pixels that adds salt (i.e., 255 pixel value) and pepper noise to the image

where "0" is processing pixel, i.e., .

Now eliminate the salt and pepper noise from the selected window. That is, elimination of 0's and 255's. The 1-D array of the above matrix is [78 90 0 120 0 255 97 255 73]. After elimination of 0's and 255's the pixel values in the selected window will be [78 90 120 97 73]. Here the median value is 90. Hence, replace the processing pixel by 90.

Case iii) If the selected window contains a noise free pixel as a processing pixel, it does not require further processing. For example, if the processing pixel is 90 then it is noise free pixel

where "90" is processing pixel, i.e., .

Since "90" is a noise free pixel it does not require further processing.

Process Flow Chart of MDBUTMF

In this process we consider 0 to 15 values as 0 i.e papper noise and 230 to 255 values as 255 i.e salt noise.

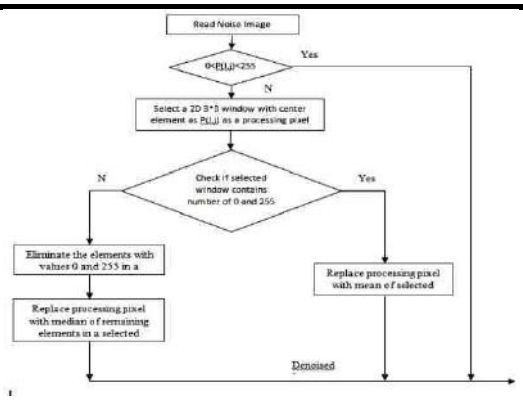

Fig.3.2: Flow chart of MDBUTMF

The above figure 3.2 indicates flow chart of MDBUTMF. It represents the process flow of a MDBUTMF and the process steps as shown below.

Step 1 Read a Noisy image.

Step 2 Check the each pixel value (P(i,j)) is in between 0 to 255 or not.

Step 3 If the pixel value is in between 0 to 255 then we consider it as a de noise value so we can take this as output.

Step 4 If the pixel value is 0 or 255 then select a 2D 3*3 window and keep that pixel value in center of the window and take the neighbor values also.

Step 5 we can check the number of 0's and number of 255's in that window.

Step 6 Check if the number of 0's or 255's are greater than 4 then we have to calculate Mean value by taking all pixel values from that window and keep that mean value in center and we consider it as a de noise value.

Step 7 Check if the number of 0's or 255's are less than 4 then we have to calculate Median value by taking all pixel values from that window and keep that median value in center and we consider it as a de noise value.

Step 8 Repeat the process from Step 2 to Step 7 for each pixel in a noisy image and take the output pixel values

3.3 Block Diagram

The below figure 3.3 represents the block diagram of Noise removal and its having main parameters Input Noisy Image, Xilinx Platform Studio, FPGA and Visual Basic.

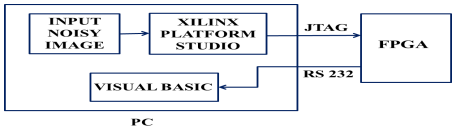

Fig.3.3: Block Diagram of Noise removal

- Input Noise Image block contains Noisy image and applied to Xilinx Platform Studio.
- We should upload header file of an image in Xilinx Platform Studio and we can write the

https://dx.doi.org/10.22161/ijaers/3.11.28 *ISSN: 2349-6495(P) | 2456-1908(O)*

code for removing the noise in System C Language.

- Now we can dump these program to FPGA processor through JTAG cable.
- FPGA Processor do the preprocessing and gives the output i.e de noisy image to the Visual Basic through serial communication by using RS232 cable.
- In the Visual Basic we can see the input and output images along with the corresponding pixel values.

Internal Process of Noise removal

The above figure 3.4 represents internal process of noise removal and the process as follows.

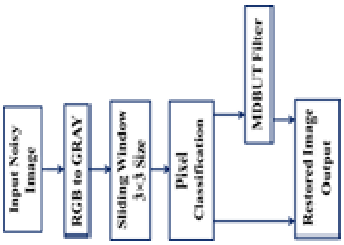

Fig.3.4: Internal Process of Noise removal

- Take the input noisy image. The image having three individual values for R,G and B.
- So we need to convert this RGB value to Gray value because its having only one value and we easily process by single value.
- After that we need to do pixel classification so we came to know noisy pixel values and de noisy pixel value.
- We can apply the noisy pixel value to MDBUT Filter, It process the noisy pixel value and give the de noisy pixel value.
- We can take de noisy pixel value and consider it as output. We consider these de noisy pixel values as output image.

3.4 Design

There are different ways to include processors inside Xilinx FPGA for System-on-a-Chip (SoC) PowerPC hard processor core, or Xilinx MicroBlaze soft processor core, or user-defined soft processor core in VHDL/Verilog. In this work, The 32-bit MicroBlaze processor is chosen because of the flexibility. The user can tailor the processor with or without advance features, based on the budget of hardware. The advance features include memory management unit, floating processing unit, hardware multiplier, hardware divider, instruction and data cache links etc. The architecture overview of the system is shown in Figure 2. It can be seen that there are two different buses (i.e., processor local bus (PLB) and fast simplex link (FSL bus) used in the system [5-6]. PLB follows IBM core connect bus architecture, which supports high bandwidth master and slave devices, provides up to 128- bit data bus, up to 64-bit address bus and centralized bus Arbitration. It is a type of shared bus. Besides the access overhead, PLB potentially has the risk of hardware/software incoherent due to bus arbitration. On the other hand, FSL supports point-to-point unidirectional communication. A pair of FSL buses (from processor to peripheral and from peripheral to processor) can form a dedicated high speed bus without arbitration mechanism. Xilinx provides C and assembly language support for easy access. Therefore, most of peripherals are connected to the processor through PLB; the DWT coprocessor is connected through FSL instead.

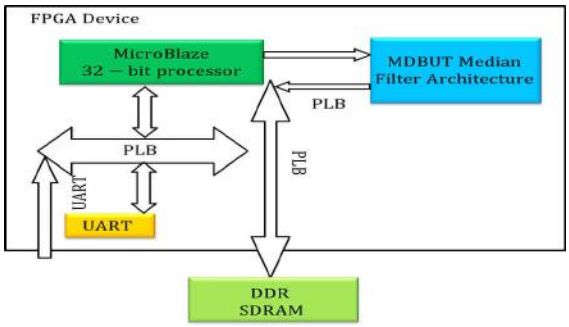

Fig.3.5: System Overview

The current system offers several methods for distributing the data. These methods are a UART, and VGA, and Ethernet controllers. The UART is used for providing an interface to a host computer, allowing user interaction with the system and facilitating data transfer. The VGA core produces a standalone real-time display. The Ethernet connection allows a convenient way to export the data for use and analysis on other systems. In our work, to validate the DWT coprocessor, an image data stream is formed using VISUAL BASIC, then transmitted from the host computer to FPGA board through UART port.

In terms of its instruction-set architecture, MicroBlaze is very similar to the RISC-based DLX architecture described in a popular computer architecture book by Patterson and Hennessy. With few exceptions, the MicroBlaze can issue a new instruction every cycle, maintaining single-cycle throughput under most circumstances.

The MicroBlaze has a versatile interconnect system to support a variety of embedded applications. MicroBlaze's primary I/O bus, the Core Connect PLB bus, is a traditional system-memory mapped transaction bus with master/slave capability. A newer version of the MicroBlaze, supported in both Spartan-6 and Virtex-6 implementations, as well as the 7-Series, supports the

https://dx.doi.org/10.22161/ijaers/3.11.28 *ISSN: 2349-6495(P) | 2456-1908(O)*

AXI specification. The majority of vendor-supplied and third-party IP interface to PLB directly (or through an PLB to OPB bus bridge.) For access to local-memory (FPGA BRAM), MicroBlaze uses a dedicated LMB bus, which reduces loading on the other buses. User-defined coprocessors are supported through a dedicated FIFO-style connection called FSL (Fast Simplex Link). The coprocessor(s) interface can accelerate computationally intensive algorithms by offloading parts or the entirety of the computation to a user-designed hardware module.

IV. SOFTWARE AND HARDWARE SPECIFICATIONS

4.1 Software Specifications

1. XILINX Platform Studio
2. MATLAB
3. Visual Basic

4.1.1 XILINX Platform Studio

The Xilinx Platform Studio (XPS) is the development environment or GUI used for designing the hardware portion of your embedded processor system. Xilinx Embedded Development Kit (EDK) is an integrated software tool suite for developing embedded systems with Xilinx MicroBlaze and PowerPC CPUs. EDK includes a variety of tools and applications to assist the designer to develop an embedded system right from the hardware creation to final implementation of the system on an FPGA. System design consists of the creation of the hardware and software components of the embedded processor system and the creation of a verification component is optional.

A Typical embedded system design project involves hardware platform creation, hardware platform verification (simulation), software platform creation, software application creation, and software verification. Base System Builder is the wizard that is used to automatically generate a hardware platform according to the user specifications that is defined by the MHS (Microprocessor Hardware Specification) file. The MHS file defines the system architecture, peripherals and embedded processors]. The Platform Generation tool creates the hardware platform using the MHS file as input. The software plat defined by MSS (Microprocessor Software Specification) file which defines driver and library customization parameters for peripherals, processor customization parameters, standard 110 devices, interrupt handler routines, and other software related routines. The MSS file is an input to the Library Generator tool for customization of drivers, libraries and interrupts handlers.

Algorithm Mapping

The FPGA implementation is divided into blocks, each block implementing a separate portion of the algorithm. This approach allowed for concurrent development and for testing of individual blocks. The inbuilt finite state machine (FSM) controls each block. In addition, a high-level FSM controls the interaction of the blocks. Each computational block is implemented in C and checked for proper functionality with simulators (ISE Simulator) The Algorithm primarily consists on mapping low-level operations like local filters. Conceptually, each pixel in the output image is produced by sliding an N×N window over the input image and computing an operation according to the input pixels under the window and the chosen window operator. The result is a pixel value that is assigned to the center of the window in the output image as shown below in Figure 4.4.

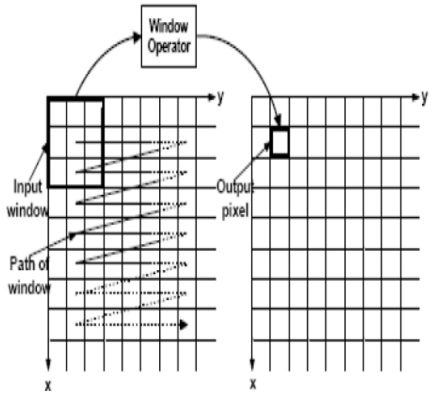

Fig.4.5: Mapping the window operation

For processing purposes, the straightforward approach is to store the entire input image into a frame buffer, accessing the neighborhood pixels and applying the function as needed to produce the output image. If processing of the video stream is required N×N pixel values are needed to perform the calculations each time the window is moved and each pixel in the image is read up to N×N times. Memory bandwidth constraints make obtaining all these pixels each clock cycle impossible. Input data from the previous N-1 rows can be cached using a shift register (or circular memory buffer) for when the window is scanned along subsequent lines.

Instead of sliding the window across the image, the above implementation now feeds the image through the window. Introducing the row buffer data structures adds additional complications. With the use of both caching and pipelining there needs to be a mechanism for adding to the row buffer and for flushing the pipeline. This is required when operating on video data, due to the horizontal blanking between lines and the vertical blanking between frames. If either the buffer or the pipeline operated during the blanking periods the results for following pixels would be incorrect due to invalid data being written to them. This requires us to stop entering data into the row buffers and to stall the pipeline while a blanking period occurs.

https://dx.doi.org/10.22161/ijaers/3.11.28 *ISSN: 2349-6495(P) | 2456-1908(O)*

A better option is to replicate the edge pixels of the closest border. Such image padding can be considered as a special case of pipeline priming. When a new frame is received the first line is pre-loaded into the row buffer the required number of times for the given window size. Before processing a new row the first pixels are also pre-loaded the required number of times, as is the last pixel of the line and the last line with the implementation of the Row Buffers for Window Operations.

Memory Interfacing and C Compiler

Because the Spartan 3E FPGA that is used in the design does not have enough internal RAM for image storage, the processing blocks were interfaced with five on-board 256K×36-bit pipelined DDRAM devices. To reduce the hardware computation time, each sub-block can read and write within the same clock cycle; each sub-block was connected to two memory chips while active. Typically, a computational block reads its inputs from one memory and writes its outputs to another. It is also necessary to control/arbitrate the FPGA internal block RAM, which is used for storage of computed thresholds and other parameters. The memory interface provides the computational blocks with a common interface and hides some of the complex details.

C Compiler

Xilinx MicroBlaze Processor Supports Linux and C-to-FPGA Acceleration embedded systems can be developed to create hardware accelerated, single-chip applications that take advantage of the MicroBlaze processor features and C-to-hardware acceleration for complex, performance-critical applications. The addition of memory management to the MicroBlaze processor provides embedded systems designers with a powerful new alternative for hardware-accelerated embedded systems. By offloading critical C-language processes to dedicated hardware coprocessors, the system as a whole can operate at a slower clock speed, consume less power and yet provide vastly more processing performance than would be possible using a discrete processor.

Using the automated C-to-hardware compiler tools and interactive optimizers, performance gains well in excess of 100X over software-only approaches, in applications that include image processing, DSP and secure communications have been reported. The MicroBlaze configurable soft processor includes configurable coprocessor capabilities through its high-performance Fast Simplex Link (FSL) accelerator interface. The compiler automatically parallelizes and pipelines C-language algorithm and generates FSL interfaces, with little or no need for hardware design experience or hardware description language (HDL) coding. The automatic C-to-HDL capabilities of MicroBlaze dramatically accelerate system design.

Program Files

Input Files

1. MHS File

The Microprocessor Hardware Specification (MHS) file defines the hardware component. The MHS file serves as an input to the Platform Generator (Platgen) tool. An MHS file defines the configuration of the embedded processor system, and includes the following

- Bus architecture
- Peripherals
- Processor
- System Connectivity

2. MSS File

The Microprocessor Software Specification (MSS) is used as an input file to the Library Generator (Libgen). The MSS file contains directives for customizing OSs, libraries, and drivers.

3. UCF File

The User Constraints File (UCF) specifies timing and placement constraints for the FPGA Design.

Output Files

1. Block Memory Map

A BMM file is a text file that has syntactic descriptions of how individual Block RAMs constitute a contiguous logical data space. When updating the FPGA bitstream with memory initialization data, the Data2Mem utility uses the BMM file to direct the translation of data into the proper initialization form. This file is generated by the Platform Generator (Platgen) and updated with physical location information by the Bitstream Generator tool.

2. ELF File

The Executable and Linkable Format (ELF) is a common standard in computing. An executable or executable file, in computer science, is a file whose contents are meant to be interpreted as a program by a computer. Most often, they contain the binary representation of machine instructions of a specific processor, but can also contain an intermediate form that requires the services of an interpreter to be run.

V. SOFTWARE TESTING AND RESULTS

5.1 Image to Text Conversion

The below process indicates image to header file conversion and each step as shown in the below.

Step 1 The below figure 5.1 indicates the Creation of main page for image browsing and header file. Here we can create two rectangle boxes foe image browsing and header file creation and take one square box also for displaying the selected image.

https://dx.doi.org/10.22161/ijaers/3.11.28 *ISSN: 2349-6495(P) | 2456-1908(O)*

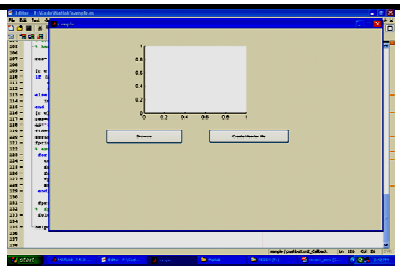

Fig.5.1 : Creation of main page for image browsing and header file

Step2 The below figure 5.2 indicates browse an image from the location where the image is existing. By clicking on browse button we can open an image.

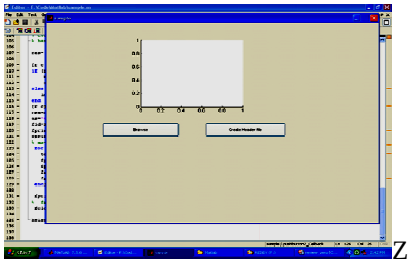

Z

Fig.5.2: Browse an Image

Step3 Figure 5.3 indicates showing a selected image. After browsing an image its displayed on the square box in main page.

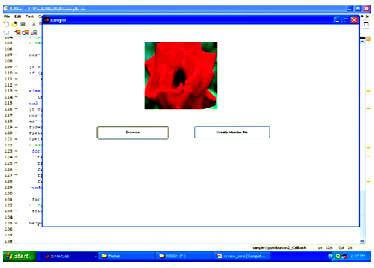

Fig.5.3: Showing a selected image

Step4 The below figure 5.3 indicates the Header file creation. After selecting the image we can click on the create header file button then it will create header file for that image and showing one dialog box saying that file created successfully after that we need to click on OK button which is showing in dialog box.

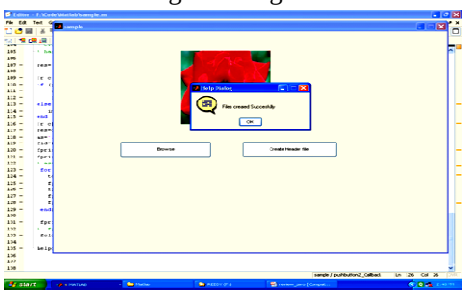

Fig.5.4: Header file creation

Step5 The below figure 5.5 indicates showing pixel values of a selected image. Its represents individual pixel value of an image.

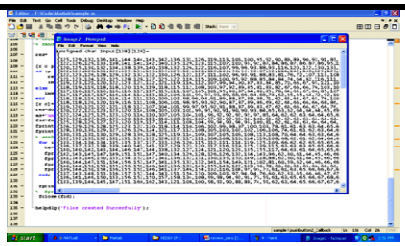

Fig.5.5: Showing pixel values of a selected image

5.2 Simulation Results

Experiments are performed on gray level images to verify the proposed method. These images are represented by 8 bits/pixel and size is 128 x 128. Image used for experiments are shown in below figure 5.6.

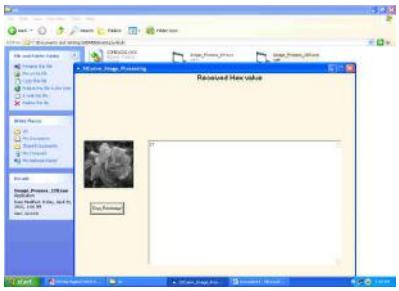

Fig.5.6: Input image

The above figure 5.6 represents input noisy along with pixel values and the below figure 5.7 indicates output image along with pixel values.The measurands used for proposed method are as follows

The entropy (E) is defined as where s is the set of processed coefficients and p (e) is the probability of processed coefficients. By using entropy, number of bits required for compressed image is calculated. An often used global objective quality measure is the mean square error (MSE) defined as Where, nxm is the number of total pixels. p(i,j) and p(i,j)' are the pixel values in the original and reconstructed image.

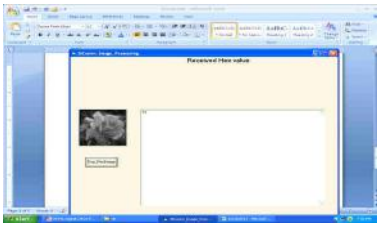

Fig.5.7: Output image

The synthesis report is below

The above figure 5.8 represents Synthesis report having the information about how many registers we are using and number of inputs etc.The Quantitative performance of the proposed algorithm is evaluated based on Peak signal to noise ratio (PSNR) ,Mean Square Error (MSE) and Image Enhancement Factor (IEF) which is given in equations 1 and 2 respectively.

https://dx.doi.org/10.22161/ijaers/3.11.28 *ISSN: 2349-6495(P) | 2456-1908(O)*

$$MSE = \frac{1}{MN}\sum_{i=1}^{M}\sum_{j=1}^{N}\left(X_{ij} - R_{ij}\right)^2 \quad \text{…. (1)}$$

Where

$$PSNR = 10\log_{10}\left(\frac{255^2}{MSE}\right) \quad \text{… (2)}$$

Where x refers to Original image, R denotes restored image, M x N is the size of Processed image.

VI. CONCLUSION

In this paper, a new algorithm (MDBUTMF) is proposed which gives better performance in comparison with MF, AMF and other existing noise removal algorithms in terms of Peak signal to noise ratio (PSNR) and Image Enhancement Factor (IEF). The performance of the algorithm has been tested at low, medium and high noise densities on both gray-scale and color images. Even at high noise density levels the MDBUTMF gives better results in comparison with other existing algorithms. Both visual and quantitative results are demonstrated. The proposed algorithm is effective for salt and pepper noise removal in images at high noise densities.

In this paper, a We have presented an alternative implementation of median filtering for arbitrarily large windows. The architecture is immune to changes in window size, the area being determined solely by the bit width. This allows for a flexible window-size that can change from one calculation to another and we finally presented the results which are implemented on the Spartan-3 EDK evolution board.

6.1 Future Scope

In the Transmission of Videos over channel, Video frames are corrupted by salt and pepper noise (Impulse Noise), due to faulty communication systems. With this project we can implement a better filtering technique that makes the noisy video frames to noise free video frames. Median filters are the best known nonlinear digital filters based on order statistics to solve the present problem in videos. Median filters are known for their capability to remove salt and pepper noise and preserves the shape. The noise detection process to discriminate between uncorrupted pixels and the corrupted pixels prior to applying non-linear filtering is highly desirable to protect the signal details of uncorrupted pixels. We proposed A Modified Decision Based Unsymmetrical Trimmed Median filter (MDBUTM) algorithm for the restoration of gray scale, and color video frames that are highly corrupted by salt and pepper noise.

REFERENCES

[1] J. Astola and P. Kuosmaneen, Fundamentals of Nonlinear Digital Filtering. Boca Raton, FL CRC, 1997.

[2] H. Hwang and R. A. Hadded, “Adaptive median filter New algorithms and results,” IEEE Trans. Image Process., vol. 4, no. 4, pp. 499–502, Apr. 1995.

[3] S. Zhang and M. A. Karim, “A new impulse detector for switching median filters,” IEEE Signal Process. Lett., vol. 9, no. 11, pp. 360–363,Nov. 2002.

[4] P. E. Ng and K. K. Ma, “A switching median filter with boundary discriminative noise detection for extremely corrupted images,” IEEE Trans. Image Process., vol. 15, no. 6, pp. 1506–1516, Jun. 2006.

[5] K. S. Srinivasan and D. Ebenezer, “A new fast and efficient decision based algorithm for removal of high density impulse noise,” IEEE Signal Process. Lett., vol. 14, no. 3, pp. 189–192, Mar. 2007.

[6] V. Jayaraj and D. Ebenezer, “A new switching-based median filtering scheme and algorithm for removal of high-density salt and pepper noise in image,” EURASIP J. Adv. Signal Process, 2010.

[7] K. Aiswarya, V. Jayaraj, and D. Ebenezer, “A new and efficient algorithm for the removal of high density salt and pepper noise in images and videos,” in Second Int. Conf. Computer Modeling and Simulation,2010, pp. 409–413.

[8] G. Eason, B. Noble, and I. N. Sneddon, “On certain integrals of Lipschitz-Hankel type involving products of Bessel functions,” Phil. Trans. Roy. Soc. London, vol. A247, pp. 529–551, April 1955. *(references)*

[9] J. Clerk Maxwell, A Treatise on Electricity and Magnetism, 3rd ed., vol. 2. Oxford: Clarendon, 1892, pp.68–73.

[10] I. S. Jacobs and C. P. Bean, “Fine particles, thin films and exchange anisotropy,” in Magnetism, vol. III, G. T. Rado and H. Suhl, Eds. New York: Academic, 1963, pp. 271–350.

[11] K. Elissa, “Title of paper if known,” unpublished.

[12] R. Nicole, “Title of paper with only first word capitalized,” J. Name Stand. Abbrev. in press.

https://dx.doi.org/10.22161/ijaers/3.11.29 *ISSN: 2349-6495(P) | 2456-1908(O)*

Electrochemical Behavior of Cu-Al-Ni Alloy in Simulated Body Fluids

Rabab M. El-Sherif

Chemistry Department, Faculty of Science, Cairo University, Gamaa Street, 12613 Giza, Egypt.

Abstract— *The electrochemical comparative studies between, Cu-Al-Ni alloy as a non-precious casting alloy and a pure Ti as a common biomaterial were investigated in simulated body fluid (SBF). The aim of the work was to evaluate the corrosion resistivity of these alloys in the simulated body fluids, using electrochemical impedance spectroscopy (EIS) and potentiodynamic polarization measurements. The surface morphology of the alloys was examined via the scanning electron microscopy. This comparison was focused on the effect of the solution chemistry and immersion time on the passivity of the alloys. The influence of albumin, as a model protein, and a fluoride ion with its simulated dose in a human body, on both biomaterials was investigated. The Albumin has enhanced the corrosion resistance of both samples. On the contrary, fluoride ion increased their corrosion rate in all the tested solutions. The electrochemical behavior of Ti has shown a higher transfer resistance and a lower capacitance compared with the copper alloy. However, the resistivity of both materials increased with immersion time in the different solutions.*

Keywords— Biomaterials, Corrosion, Cu-Al-Ni alloy, impedance, Polarization, SEM.

I. INTRODUCTION

Titanium and its alloys have been widely used in the last decades as biocompatible materials for dental implants, orthopedic implants and medical devices [1-5]. This is due to a passive film formation on their surface, consisting mainly of amorphous titanium dioxide (TiO_2), which is responsible for their biocompatibility and corrosion resistance in several media, including the human body environment [6, 7]. A contact between the metallic implant and the living tissues takes place through the oxide layer on the implant surface during the osseointegration process [8].

Nowadays in the prosthetic dentistry field “non precious” alloys (Ni and Co based) substitutes the much more expensive precious metal alloys (Pt, Au, Pd and Ti) [8]. Copper-based alloys have been used in many practical applications because of their good corrosion resistance, and excellent physical properties [9-11]. The addition of aluminum to Cu-based alloys increases its corrosion resistance while the presence of nickel is essential in the passivation of Cu-Ni alloys. The passivation of the alloy is attributed to the greater affinity of aluminum toward oxygen than copper and a considerable stability of Al_2O_3 than Cu_2O in neutral solutions [12, 13]. Different corrosion studies of aluminum bronze in artificial saliva, acidic and saline solutions showed that 0.9% saline solution is more corrosive than artificial saliva [14]. Also, ‘passivation’ was observed in artificial saliva and Na_2S solutions, but not in citric acid or KCl solutions [15]. One of the main challenging issues that faces the casting non-precious alloys is the release of elements into the body over the short-term (days) and long term (months) during corrosion[16-22]. For some metals and alloys, elemental release during corrosion can be affected significantly by biological environments in vitro and in vivo, and specifically in the presence of proteins [23]. In vitro, proteins show an increase of the corrosion rate of some alloys and pure metals such as stainless steel, copper, nickel and titanium [24, 25]. However, few studies have considered the effects of proteins on the elemental release from dental casting alloys. Liu [26] has found that the corrosion resistance in simulated body fluid (SBF) + 1 g/L albumin is almost twice that in SBF alone. The electrochemical behavior of WE43 alloy in SBF in the absence and presence of 40 g/L albumin was investigated by Retting [27, 28].

In the present work, it is aimed to assess the influence of the simulated body fluid in the presence of albumin, as a model protein, and a fluoride ion with its simulated dose in a human body on the passivation and dissolution behavior of Cu-Al-Ni and Ti metal at about 37 ˚C. The study is furthermore aimed to improve knowledge of the nature of the formed passive films in these systems by comparing the behavior of Cu-Al-Ni as a non-precious low cost alloy with titanium, using potentiodynamic, electrochemical impedance spectroscopy techniques and scanning electron microscopy.

II. EXPERIMENTAL

2.1 Materials and solutions

Two samples of pure titanium (99.99%) and Cu-Al-Ni alloy with composition of wt. %; 9.71 Al, 5.03 Ni, 3.05 Fe, 1.06 Mn, 0.02 Si, 0.02 Sn, and 81.11 Cu were used in this study. The electrodes were supplied in the form of

https://dx.doi.org/10.22161/ijaers/3.11.29 *ISSN: 2349-6495(P) | 2456-1908(O)*

cylindrical rods from Johnson and Malthey (England) with exposed surface area of 0.4 and 0.5cm^2 for titanium and Cu-Al-Ni alloy, respectively. The electrodes surfaces were successively polished with finer grades of emery paper (600–1200 grade) to obtain a mirror-like image. A conventional three-electrode cell was used with a saturated calomel reference electrode (SCE) (E_{SCE} = 0.242 V vs. NHE) and a rectangular platinum sheet as counter electrode. The experiments were carried out using three simulated body solutions: naturally aerated aqueous simulated body fluid (SBF) (NaCl 8.74 g/l, $NaHCO_3$ 0.35 g/l, Na_2HPO_4 0.06 g/l, NaH_2PO_4 0.06 g/l, PH 7.4), SBF with 0.5 g/l albumin and SBF with 4.4 mg/l KF (simulated dose in the human body) in order to analyze the influence of fluoride ion and albumin on the electrochemical behavior of the biomaterials .The solutions were prepared from Analytical grade reagents and triply distilled water. Temperature of the solutions was kept out ± 37 ^oC and pH 7.4 (human body conditions).

2.2 Electrochemical Techniques

All the electrochemical measurements, including open-circuit potential E_{oc}, potentiodynamic and electrochemical impedance spectroscopy (EIS) were carried out using the electrochemical workstation IM6e Zahner-electrik GmbH (Mebtechnik, Kronach, Germany) provided with Thales software. Open-circuit potential measurements, E_{oc}, for each material were measured on a freshly polished sample, in naturally aerated aqueous solutions without stirring, for 24 h. Potentiodynamic polarization tests were performed after one hour of immersion in the tested solutions. The cathodic and anodic polarization scans were carried out at 2 mVs^{-1} scan rate vs. SCE. Electrochemical impedance spectroscopy (EIS) measurements were studied at the open-circuit potential. The impedance spectra were acquired in the frequency range from 0.1 Hz up to 10 kHz with a perturbation signal of 10 mV. EIS plots were obtained after the specimens were immersed in the test solution for different time immersion up to 24 h. SEM micrographs were conducted using a JEOL JXA-840 A electron probe micro analyzer. The experiments were always carried out at 37 ^oC, unless otherwise stated.

III. RESULTS AND DISCUSSION

3.1 Open-circuit potential analyses

The open-circuit potential (E_{oc}) of pure Ti and Cu–Al-Ni alloy was followed over a period of 24 h in three media, simulated body fluid (SBF), SBF+ Albumin and SBF+ KF. The results were presented in Figs. 1, 2. E_{oc} changed towards more positive potentials during the first hour of electrode immersion in different solutions. After that, E_{oc} changed slowly until it reached a quasi-stationary state after three hours. No significant change occurred after that. This indicated that a spontaneously passive film is formed with time on both Cu-Al-Ni and pure Ti surfaces. The addition of fluoride ion shifted the potential towards more negative values in both samples. This is because; fluoride addition to the solution made Ti potential more active and enhanced its corrosion. In other words, fluoride ion affected the electrochemical activity of Ti [29-31].

On the other hand, adding albumin to the SBF solution shifted the potential towards more positive values for both samples (Cf. Figs. 1, 2). It is known that a layer of adsorbed proteins is formed immediately on the dental implant surface after being into the oral cavity, which enhances the biocompatibility of the implant. Therefore, the naturally contained proteins in the human saliva may play an important role in the corrosion resistance of dental implant materials, e.g. Ti and Ti-based alloys. The presence of protein (bovine albumin) in phosphate buffered saline (PBS) increased the corrosion resistance of Ti–6Al–4V, but decreased that of Ti–13Nb–13Zr and Ti–6Al–7Nb [32, 33]. Obviously, the presence of proteins, albumin would affect the corrosion resistance of titanium alloys.

3.2 Potentiodynamic polarization

Figs. 3, 4 showed the potentiodynamic polarization curves of Ti and Cu-Al-Ni alloy in the three solutions: SBF, SBF+ KF and SBF+ Albumin respectively. The polarization curves of Cu-Al-Ni revealed an active-to-passive transition behavior in all the tested solutions, whereas Ti showed a totally passive behavior. The passivation and corrosion behavior of the Cu-Al-Ni alloy could be explained on the basis of the data reported on Cu and cast nickel-aluminum bronze [34-37]. The copper dissolution reaction represented the major anodic process. Whereas, the cathodic reaction was mainly due to oxygen reduction, as seen in the following equation:

$$O_2 + 2H_2O + 4e^- \rightarrow 4OH^- \quad [E^o = 0.401 \text{ V vs. SHE}] \quad (1)$$

The corrosion resistance of the Cu-Al-Ni alloy was mainly due to the duplex nature of the protective layer containing both Cu_2O and Al_2O_3 [38].

On adding albumin to the solution, the cathodic current density was significantly decreased. All the corrosion parameters were estimated and presented in Tables 1, 2. Since the albumin isoelectric point is known to be 4.9 [39], so it was expected that albumin is negatively charged at the pH of the tested solutions (pH7.4). As the alloy surface was polarized in the positive direction where electron depletion was created, the adsorption of negatively charged species of albumin on the electrode surface was detected.

On the contrary, addition of fluoride ion increased the corrosion current density significantly and shifted the

https://dx.doi.org/10.22161/ijaers/3.11.29 *ISSN: 2349-6495(P) | 2456-1908(O)*

corrosion potential to more negative direction (cf. Tables 1, 2). The increase of the current density in the presence of fluoride ion could be explained by the dissolution of the protective oxide film. The structure of oxide layer may be affected by the fluoride ion and become more porous, which leads to a decrease in its resistance. Generally, the effect of fluoride ion depends on its concentration and the solution pH [40].

3.3 Electrochemical impedance spectroscopy measurements

Impedance spectra of pure Ti and Cu-Al-Ni alloy at different immersion times in SBF, SBF+ Albumin and SBF + KF solutions were represented as Bode plots, in Fig. 5 (a, b, c) and Fig. 6 (a, b, c) respectively. The presence of additional time constants in the impedance spectra at different frequency range was predicted from the phase angle, Θ. It is usually more preferable to use Bode plots format as, it presents all experimental data over the entire frequency domain [41].

After one hour of immersion, both of the tested samples exhibited low impedance values. The total impedance was considerably increased with immersion time. However, no significant change in the behavior was observed after 24 h. This trend could be due to the surface full coverage with spontaneous oxide layers [42]. The broadening of the Bode plots spectra and the increase of the phase angle with immersion time indicated a decrease in the corrosion rate of the alloys. The increase in the charge transfer resistance of the surface oxide film reflected the improvements of the corrosion resistance of the alloy with the immersion time [43]. The Bode plots in the frequency domain 0.1 Hz up to 10 kHz showed two time constants with a phase angle close to 80^o for pure Ti and 70^o for Cu-Al-Ni alloy. The relation between the frequency (log f) and the impedance (log |Z|) was observed to be a linear one with a slope near to 1. After 24 h of immersion, the phase angle of Ti remained near 80^o even at low frequencies, and 70^o for the copper alloy. This indicated a near-capacitive response for both samples. However, the alloys immersed for 24 h in SBF solution showed two time constants spectra with a bi-layered surface corresponding to an inner layer and an outer one.

The equivalent circuit shown in Fig. 7 was the best fitting for all the experimental data. Where, R_s, CPE_1 and R_1 are the solution resistance, a constant- phase element corresponding to the double layer capacitance and the charge transfer resistance, respectively. CPE_2 and R_2 assigned the electrical elements of the outer layer. The electrode impedance, Z, was expressed as follows:

$$Z = Rs + [Rct/ \{1 + (2 \pi f R_{ct} C_{dl})^{\alpha}\}] \quad (2)$$

Where α is an empirical parameter ($0 \leq \alpha \leq 1$) and f is the frequency in Hz. This formula considered the deviation from the ideal RC-behavior due to surface inhomogeneties, roughness effects, and different compositions of surface layers [44, 45]. The observed first time constant at low frequency range was due to the presence of an inhomogeneous passive film [46].

It can be noted from Tables 3-8 that the capacitance decreased, in almost all cases, with the immersion time and (α) values were close to 1, so CPE showed an almost pure capacitive behavior. The increase of the film resistance R_2 with immersion time reflected a formation of a spontaneously oxide film on both cu-alloy and Ti metal as can be seen from Fig. 8 a, b. The impedance values for Ti showed better corrosion resistance than that of Cu-Ni-Al alloy in all the studied simulated body fluids. On the other hand, the copper alloy showed a remarkably high corrosion resistance, which was essentially due to the presence of a protective layer of duplex nature, containing both Cu_2O and Al_2O_3 [38, 47-48]. The inner layer was an Al-rich barrier layer which prevents a Copper dissolution from the alloy surface. The outer layer was a porous Cu-rich consisting mainly of Cu_2O passive film [38, 49]. This result was confirmed by EDX [50], where the surface showed a higher concentration of Cu and also a lower concentration of Ni due to Ni diffusion in the inner barrier layer. Al was involved in the compact inner layer and its concentration on the surface is slightly lower than the bulk. The duplex barrier layer hindered the ionic transport and consequently increased the corrosion resistance [48, 51].

In both samples, the effect of time on the resistance and capacitance depended on the solution chemistry. With respect to the influence of albumin, it increased the charge transfer resistance and the outer layer resistance of titanium and copper alloy and slightly decreased the capacitance. This was mainly due to the blocking effect of the organic molecule and the adsorption effect [46]. R_2 values of Ti increased from 592.2 kΩ cm^2 in SBF solution to 1080 kΩ cm^2 in SBF + Albumin and from 168.5 kΩ cm^2 to 292 kΩ cm^2 for the copper alloy. On contrary was the effect of KF, as it decreased significantly the impedance resistance of both samples with respect to SBF solutions (cf. Tables 3, 4, 6 and 8). The presence of the fluoride ion in the solution may affect the nature of the oxide layer and change it to a porous structure that leads to a decrease in its resistance and increase in its capacitance [52- 54].

3.4. Morphology

Fig. 8 (a-h) showed the surface morphology of Cu-Ni-Al and Ti in SBF, SBF+KF and SBF + Albumin respectively. A significant improvement of the surface morphology due to the film formation was observed in the presence of albumin in both samples (Fig.8 d, h). On the other hand, a higher dissolution and roughness of the surface was assigned in the presence of KF (Fig. 8 c, g). The sample surface became denser and the flawed regions were repaired in the presence of albumin**.** This behavior

https://dx.doi.org/10.22161/ijaers/3.11.29 *ISSN: 2349-6495(P) | 2456-1908(O)*

confirmed well the polarization and impedance measurements.

IV. CONCLUSIONS

-The electrochemical behavior Cu-Ni-Al alloy and Ti metal was investigated in simulated body fluids at the human body temperature 37 ˚C.

-The remarkably high corrosion resistance of Cu-Ni-Al was essentially due to the presence of a protective layer of duplex nature containing both Cu_2O and Al_2O_3**.**

-The effect of time on the resistance and capacitance behavior of both samples depended on the solution chemistry**.**

-The influence of albumin as a model protein in the simulated body fluid enhanced the impedance performance of both materials.

-Addition of fluoride ion to the simulated body fluid increased the corrosion current density of Ti and copper alloy.

-The corrosion resistance of both alloys has been improved with the immersion time.

-The scanning electron microscopy confirmed well the electrochemical techniques results

- Cu-Ni-Al alloy could be considered as a promising non-precious casting alloy that has a considerable high corrosion resistance in simulated body fluids.

REFERENCES

[1] Z. Cai, T. Shafer, I. Watanabe, M.E. Nunn, T. Okabe, Electrochemical characterization of cast titanium alloys, Biomaterials, vol. 24, pp. 213-218, 2003.

[2] D.w. Shoesmith, J.J. Noël, Corrosion of titanium and its alloys, in Shreir's Corrosion Fourth Edition, Volume 3, Academic Press, New York, 2010, p. 2042.

[3] A.C. Vieira, A.R. Ribeiro, L.A. Rocha, J.P. Celis, Influence of pH and corrosion inhibitors on the tribocorrosion of titanium in artificial saliva, Wear, vol. 261, pp. 994–1001, 2006.

[4] A. Abdal-Hay, A.S. Hamdy, K.A. Khalil, J.H. Lim, A novel simple one-step air jet spinning approach for deposition of poly(vinyl acetate)/hydroxyapatite composite nanofibers on Ti implants, Mater. Sci. Eng. C. 49 pp. 681–690, 2015.

[5] N. Horasawa, T. Yamashita, S. Uehara, N. Udagawa, High-performance scaffolds on titanium surfaces: Osteoblast differentiation and mineralization promoted by a globular fibrinogen layer through cell-autonomous BMP signaling, Mater. Sci. Eng. C. 46 pp. 86–96, 2015.

[6] S. Tamilselvi, V. Raman, N. Rajendran, Corrosion behavior of Ti– 6Al–7Nb and Ti–6Al–4V ELI alloys in the simulated body fluid solution by electrochemical impedance spectroscopy, Electrochim. Acta, vol. 52, pp. 839-846, 2006.

[7] M. Geetha, U. Kamachi Mudali, A.K. Gogia, R. Asokamani, Baldev Raj, Influence of microstructure and alloying elements on corrosion behavior of Ti-13Nb-13Zr alloy, Corros. Sci. vol. 46, pp. 877-892, 2004.

[8] F. Toumelin-Chemia, F. Rouelle, G. Burdairon, Corrosive properties of fluoride-containing odontologic gels against titanium, J. Dentistry, vol. 24, pp. 109-115 , 1996.

[9] E.A. Ashour, B.G. Ateya, Electrochemical behavior of a copper–aluminum alloy in concentrated alkaline solutions, Electrochim. Acta, vol. 42, pp. 243-250, 1997.

[10] X.Z. Zhou, C.P. Deng, Y.C. Su, Comparative study on the electrochemical performance of the Cu–30Ni and Cu–20Zn–10Ni alloys, J. Alloys Compd. Vol.49, pp. 92-97, 2010.

[11] Lj. Alijnovi´ c, S. Gudi´ c, M. ˇSmith, Inhibition of CuNi10Fe corrosion in seawater by sodium-diethyl-dithiocarbamate: an electrochemical and analytical study, J. Appl. Electrochem. Vol. 309, pp. 973-979, 2000.

[12] M. Gojic, L. Vrsalovic, S. Kozuh, A. Kneissl, I. Anzel, S. Gudic, B. Kosec, M. Kliskic, Electrochemical and microstructural study of Cu–Al–Ni shape memory alloy, J. Alloys Compounds vol. 509, pp. 9782-9790, 2011.

[13] J.C. Scully, The Fundamentals of Corrosion, Pergamon Press, Oxford, 1990.

[14] B.I. Johansson, L.C. Lucas, J.E. Lemons, Corrosion of copper, nickel, and gold dental casting alloys: an in vitro and in vivo study, J. Biomed. Mater. Res. 23(Suppl. A3), pp. 349-361, 1989.

[15] A.C. Guastaldi, Comparative evaluation of in vitro tarnish corrosion changes of non-precious dental alloys a function of time and storage solutions. Ph.D. Thesis, S˜ao Paulo: School of Engineering, University of S˜ao Paulo; 1987.

[16] D. Brune, Metal release from dental biomaterials, Biomaterials, vol. 7, pp. 163-175, 1986.

[17] D. Brune, Mechanisms and kinetics of metal release from dental alloys, Int Endod J. vol. 21, pp. 135-142, 1988.

[18] J.C. Wataha, R.G. Craig, C.T. Hanks, The release of elements of dental casting alloys into cell-culture medium, J. Dent. Res. Vol. 70, pp. 1014, 1991.

[19] J.D. Bumgardner, L.C. Lucas, Corrosion and cell culture evaluations of nickel-chromium dental casting alloys, J. Appl. Biomater. Vol. 5, pp. 203-213,1994.

[20] R.L.W. Messer, L.C. Lucas, Cytotoxicity evaluations of ions released from nickel-chromium

https://dx.doi.org/10.22161/ijaers/3.11.29 *ISSN: 2349-6495(P) | 2456-1908(O)*

dental alloys, J. Dent. Res. Vol. 75, pp. 255,1996 Abstract No. 1902.

[21] J.G. Gerstorfer, K.H. Sauer, K. PaÈssler, Ion release for Ni-Cr-Mo and Co- Cr-Mo casting alloys, Int. J. Prosthodont. Vol. 4, pp. 152-158 , 1991.

[22] J.S. Covington, M.A. McBride, W.F. Slagle, A.L. Disney, Quantitization of nickel and beryllium leakage from base metal casting alloys, J. Prosthet. Dent. Vol. 54, pp. 127-136, 1985.

[23] S.A. Brown, L.J. Farnsworth, K. Merritt, T.D. Crowe, In vitro and in vivo metal ion release, J. Biomed. Mater. Res, vol. 22, pp. 321-328, 1988.

[24] D.D. Zabel, S.A. Brown, K. Merritt, J.H. Payer, AES (auger electron spectroscopy) of stainless steel corroded in saline, in serum and in vivo, J. Biomed. Mater. Res, vol. 22, pp. 31-44 , 1988.

[25] G.C.F. Clark, D.F. Williams, The effects of proteins on metallic corrosion, J. Biomed. Mater. Res, vol. 16, pp. 125-134, 1982.

[26] C.L. Liu, Y.C. Xin, X.B. Tian, P.L. Chu, Degradation susceptibility of surgical magnesium alloy in artificial albumin-containing biological fluid, Journal of Materials Research, 22(2007) 1806-1814.

[27] R. Rettig, S. Virtanen, Time-dependent electrochemical characterization of the corrosion of a magnesium rare-earth alloy in simulated body fluids, Journal of Biomedial Materials Research, vol. 85, pp. 167-175, 2008.

[28] R. Rettig, S. Virtanen, Composition of corrosion layers on a magnesium rare earth alloy in simulated body fluids, Journal of Biomedial Materials Research, vol. 88, pp. 359-369, 2009.

[29] B.I. Johansson, B. Bergman, Corrosion of titanium and amalgam couples: effect of fluoride, area size, surface preparation and fabrication procedures, Dent. Mater. Vol. 11, pp. 41-46, 1995.

[30] F. Di Carlo, L.F. Ronconi, G. Gambarini, M. Andreasi Bassi, M. Quaranta, The influence of fluorides on the electrochemical interaction between titanium and amalgam couples, J. Dent. Res, vol. 80, pp. 663, 2001, (abstract no. 1096)

[31] R.W. Schutz, D.E. Thomas, Corrosion of titanium and titanium alloys, Metals handbook, vol. 13, 9th ed. Metals Park, OH: American Society for Metal (ASM) International, 1987, 669-706.

[32] M.A. Khan, R.L. Williams, D.F. Williams, Conjoint corrosion and wear in Ti alloys, Biomaterials, vol. 20, pp. 765-772, 1999.

[33] M.A. Khan, R.L. Williams, D.F. Williams DF, The corrosion behavior of Ti-6Al-4V, Ti-6Al-7Nb and Ti-13Nb-13Zr in protein solutions, Biomaterials, vol. 20, pp. 631-637, 1999.

[34] G. Kear, B.D. Barker, K.R. Stokes, F.C. Walsh, Electrochemical Corrosion Behaviour of 90-10 Cu-Ni Alloy in Chloride-Based Electrolytes, J. Appl. Electrochem. Vol. 34, pp. 659-669, 2004.

[35] J.C. Scully, The Fundamentals of Corrosion, Pergamon Press, Oxford, 1990.

[36] C. Deslouis, B. Tribollet, G. Mengoli, M.M. Musiani, Electrochemical behavior of copper in neutral aerated chloride solution. I. Steady-state investigation, J. Appl. Electrochim. Vol. 18, pp. 374-383, 1988.

[37] G. Kear, B.D. Barker, F.C. Walsh, Electrochemical corrosion of unalloyed copper in chloride media-a critical review, Corros. Sci. vol. 46, pp. 109-135, 2004.

[38] J.A. Wharton, R.C. Barik, G. Kear, R.J.K. Wood, K.R. Stokes, F.C. Walsh, The corrosion of nickel–aluminum bronze in seawater, Corros. Sci. vol. 47, pp. 3336-3367, 2005.

[39] M.A. Khan, R.L. Williams, D.F. Williams, Biomaterials, vol. 20, pp. 631–637, 1999.

[40] V. Zwilling , M. Aucouturier , E. Darque-Ceretti, Anodic oxidation of titanium and TA6V alloy in chromic media. An electrochemical approach, Electrochim. Acta, vol. 45, pp. 921-929 , 1999.

[41] M. Metikos-Hukovic, A. Kwokal, J. Piljac, The influence of niobium and vanadium on passivity of titanium-based implants in physiological solution, Biomaterials vol. 24, pp. 3765-775 , 2003.

[42] S. Tamilselvi, V. Raman, N. Rajendran, Corrosion behaviour of Ti-6Al-7Nb and Ti-6Al-4V ELI alloys in the simulated body fluid solution by electrochemical impedance spectroscopy, Electrochim. Acta, vol. 52, pp. 839-846, 2006.

[43] W.A. Badawy, S.S. El-Egamy, K.M. Ismail, Comparative study of tantalum and titanium passive films by electrochemical impedance spectroscopy, Br. Corr. J. vol. 28, pp. 133-136, 1993.

[44] K. Hladky, L.M. Calow, J.L. Dawson, Corrosion Rates from Impedance Measurements: An Introduction, Br. Corr. J. vol. 15, pp. 20-25, 1980.

[45] J. Hitzig, J. Titz, K. Juettner, W.J. Lorenz, E. Schmidt, Frequency response analysis of the Ag/Ag^{+} system: a partially active electrode approach, Electrochim. Acta, vol. 29, pp. 287-296 , 1984.

[46] A. Igual-Muñoz, S. Mischler, Interactive Effects of Albumin and Phosphate Ions on the Corrosion of CoCrMo Implant Alloy, Journal of the Electrochemical Society, vol. 154, pp. C562–C570, 2007.

[47] W.A. Badawy, F.M. Al-Kharafi, A.S. El-Azab, Electrochemical behavior and corrosion inhibition of

https://dx.doi.org/10.22161/ijaers/3.11.29 *ISSN: 2349-6495(P) | 2456-1908(O)*

Al, Al-6061 and Al-Cu in neutral aqueous solutions, Corros. Sci. vol. 41, pp. 709-727, 1999.

[48] W.A. Badawy, M. El-Rabiee, N.H. Hilal, H. Nady, Effect of nickel content on the electrochemical behavior of Cu-Al-Ni alloys in chloride free neutral solutions, Electrochim. Acta, vol. 56, pp. 913-918, 2010.

[49] W.A. Badawy, M. El-Rabiee, N.H. Hilal, H. Nady, Electrochemical behavior of Mg and some Mg alloys in aqueous solutions of different pH, Electrochim. Acta, vol. 55, pp. 1880-1887, 2010.

[50] H. Nady , N.H. Helal , M.M. El-Rabiee , W.A. Badawy, The role of Ni content on the stability of Cu-Al-Ni ternary alloy in neutral chloride solutions, Materials Chemistry and Physics, vol. 134, pp. 945-950, 2012.

[51] A. Schussler, H.E. Exner, The corrosion of nickel-aluminum bronzes in seawater-I. Protective layer formation and the passivation mechanism, Corros. Sci. vol. 34, pp. 1793-1802, 1993.

[52] N. Schiff, B. Grosgogeat, M. Lissac, F. Dalard, Biomaterials, vol. 23, pp. 1995, 2002.

[53] L. Reclaru, J.-M. Meyer, Biomaterials vol. 19, pp. 85, 1998.

[54] S.B. Basame, H.S. White, J. Electrochem. Soc. Vol. 147, pp. 1376, 2000.

HIGHLIGHTS

- Cu-Ni-Al alloy could be considered as a promising non-precious casting alloy that has a considerable high corrosion resistance in simulated body fluids.
- The considerable corrosion resistance of Cu-Al-Ni is due to a protective layer of duplex nature containing both Cu_2O and Al_2O_3.
- The presence of albumin as a model protein enhanced the impedance performance of the tested materials
- The fluoride ion addition increased the corrosion current density of the tested samples.
- The corrosion resistance of the alloys increased with immersion time.

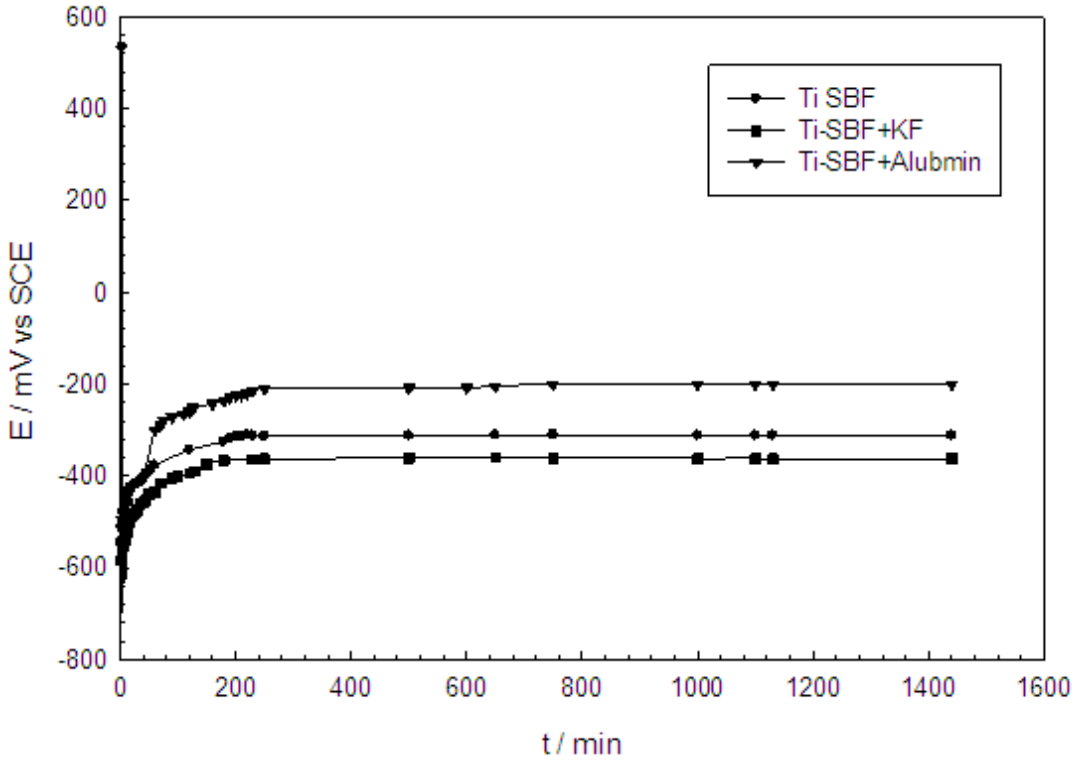

Fig. 1: Open-Circuit potential vs. time profile for pure Ti in SBF, SBF+ Albumin and SBF+ KF at 37°C.

https://dx.doi.org/10.22161/ijaers/3.11.29 *ISSN: 2349-6495(P) | 2456-1908(O)*

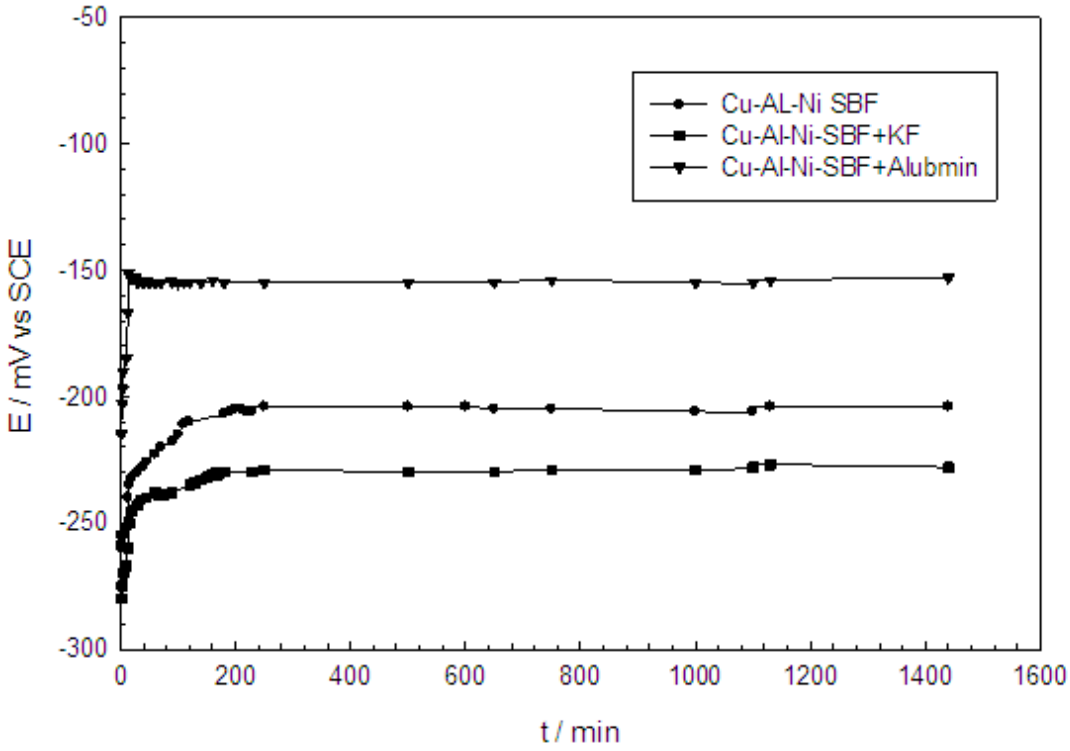

Fig. 2: Open-Circuit potential vs. time profile for Cu-Al-Ni in SBF, SBF+ Albumin and SBF+ KF at 37°C.

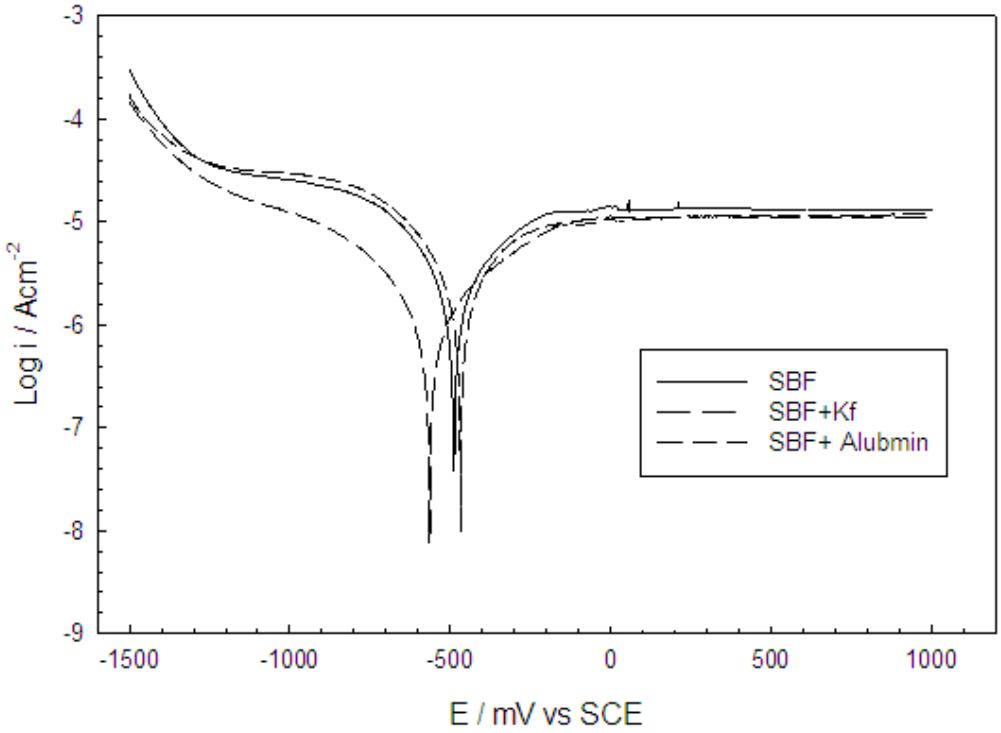

Fig. 3: Potentiodynamic polarization curves for Ti in SBF, SBF+ Albumin and SBF+ KF at 37°C.

https://dx.doi.org/10.22161/ijaers/3.11.29 ISSN: 2349-6495(P) | 2456-1908(O)

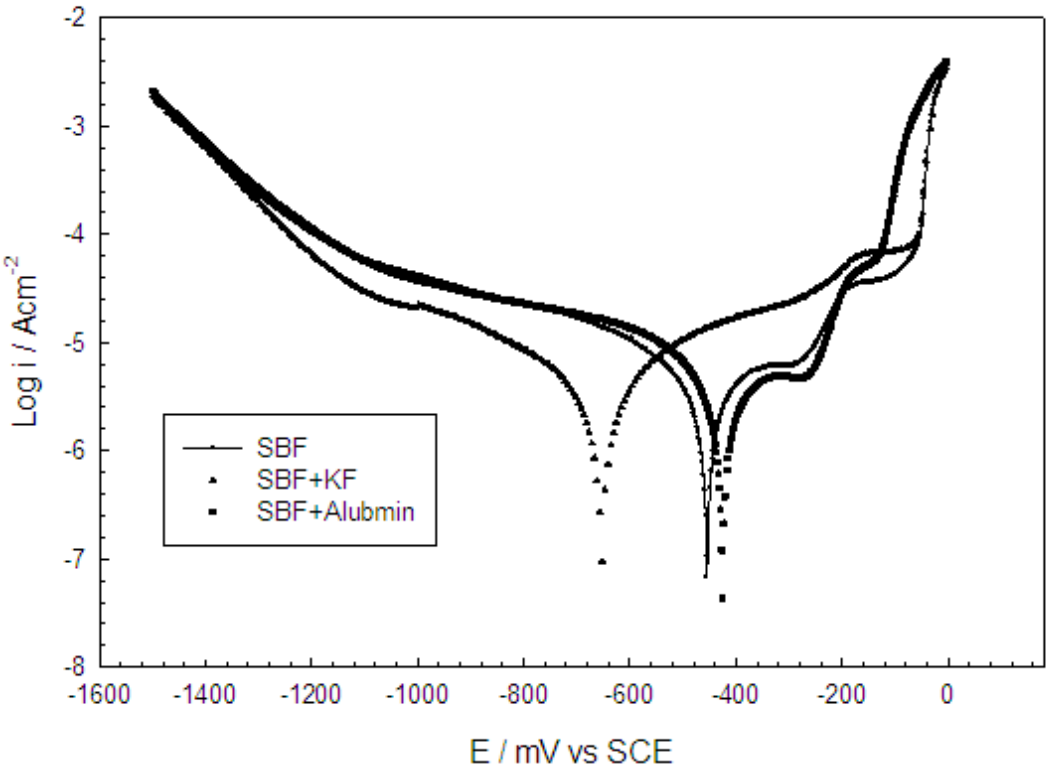

Fig. 4: Potentiodynamic polarization curves for Cu-Al-Ni in SBF, SBF+ Albumin and SBF+ KF at 37°C.

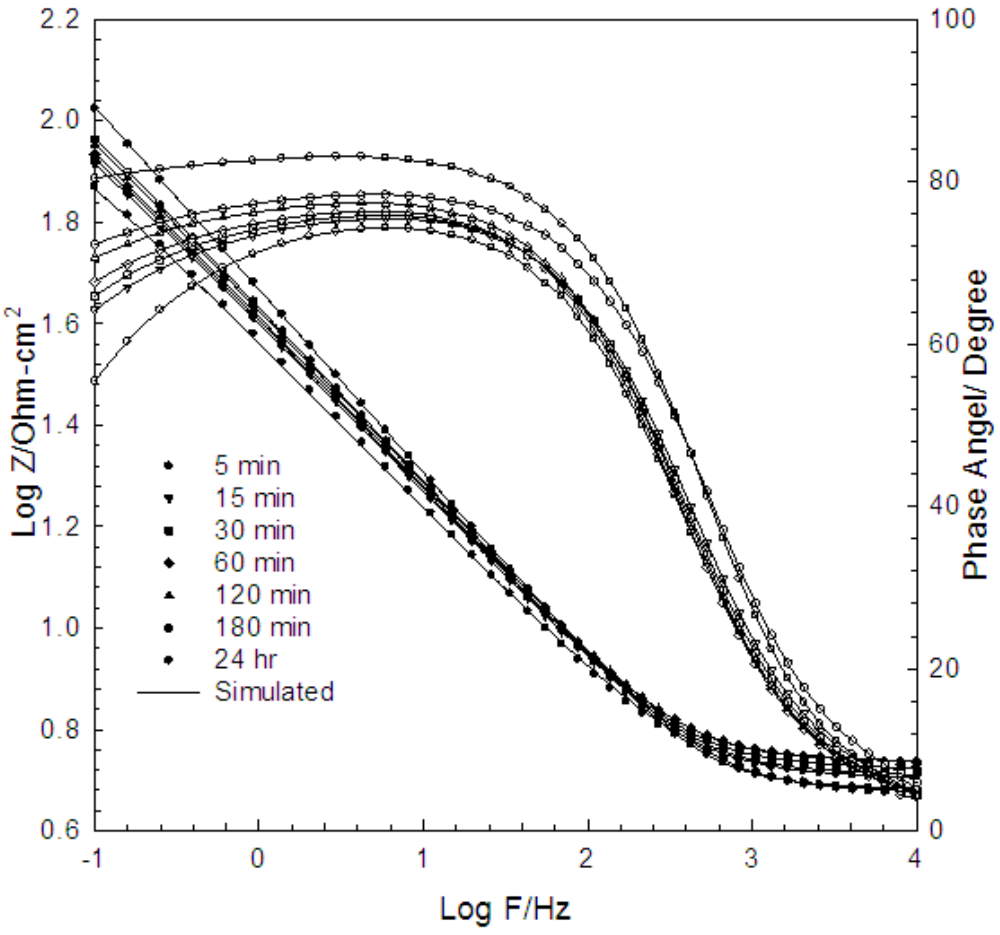

Fig. 5(a): Bode plots of Ti as a function of immersion time at 37°C in SBF solution

https://dx.doi.org/10.22161/ijaers/3.11.29 ISSN: 2349-6495(P) | 2456-1908(O)

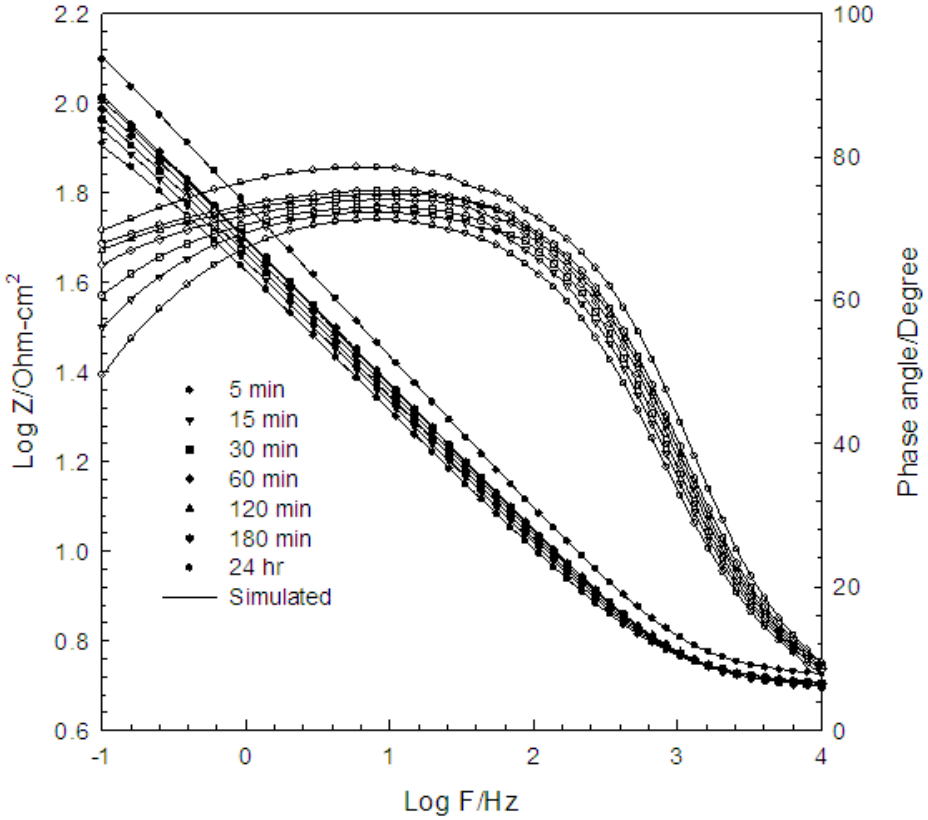

Fig. 5 (b): Bode plots of Ti as a function of immersion time at 37^{o}C in SBF +Albumin

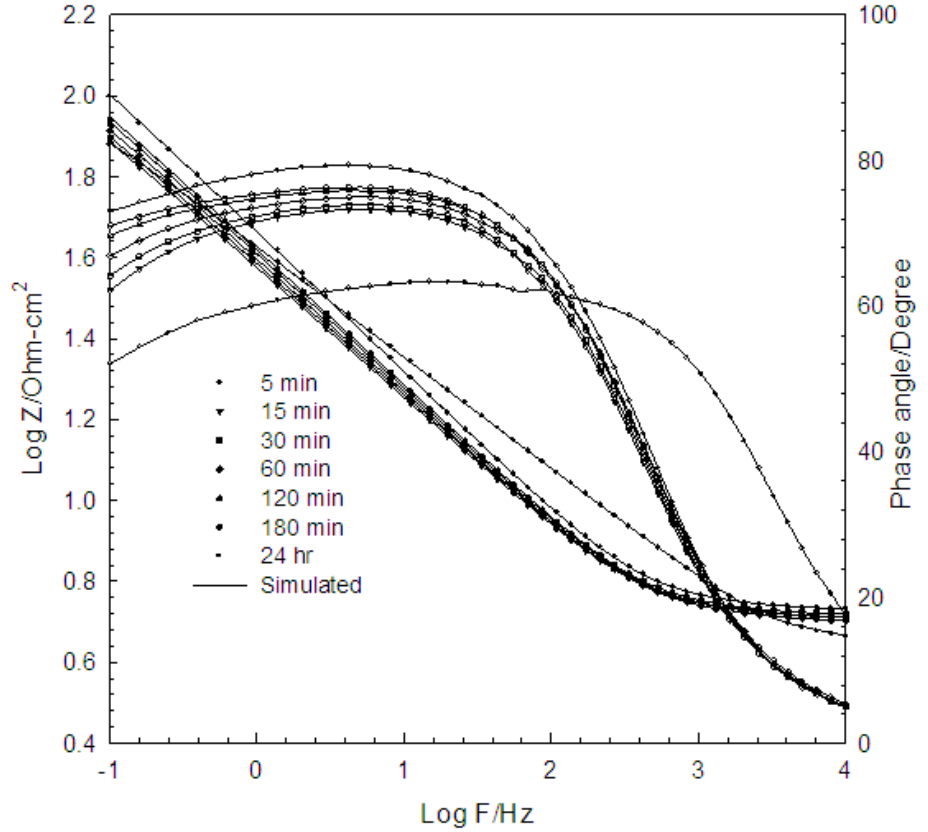

Fig. 5 (c): Bode plots of Ti as a function of immersion time at 37^{o}C in SBF +KF

https://dx.doi.org/10.22161/ijaers/3.11.29 ISSN: 2349-6495(P) | 2456-1908(O)

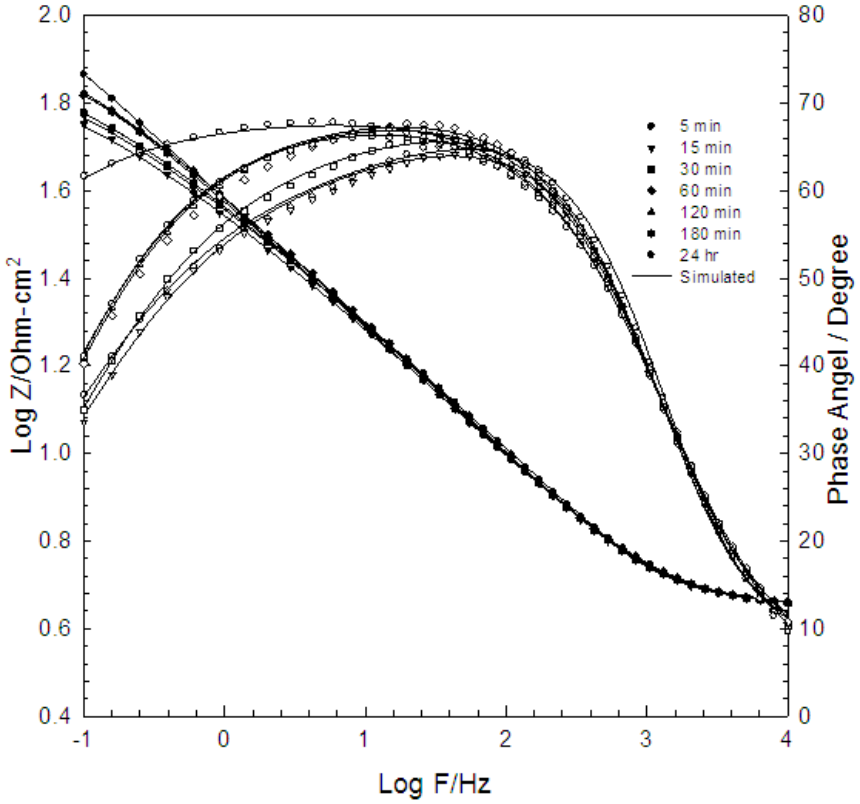

Fig. 6 (a): Bode plots of Cu-Al-Ni as a function of immersion time at 37^{o}C in SBF solution

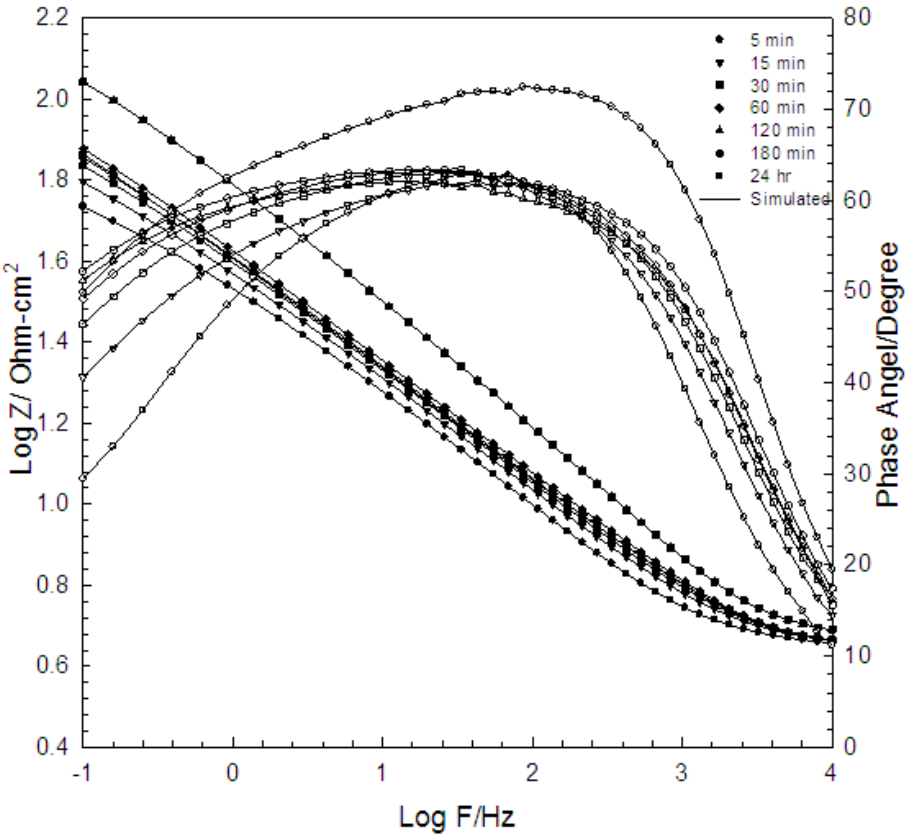

Fig. 6 (b): Bode plots of Cu-Al-Ni as a function of immersion time at 37^{o}C in SBF +Albumin

https://dx.doi.org/10.22161/ijaers/3.11.29 ISSN: 2349-6495(P) | 2456-1908(O)

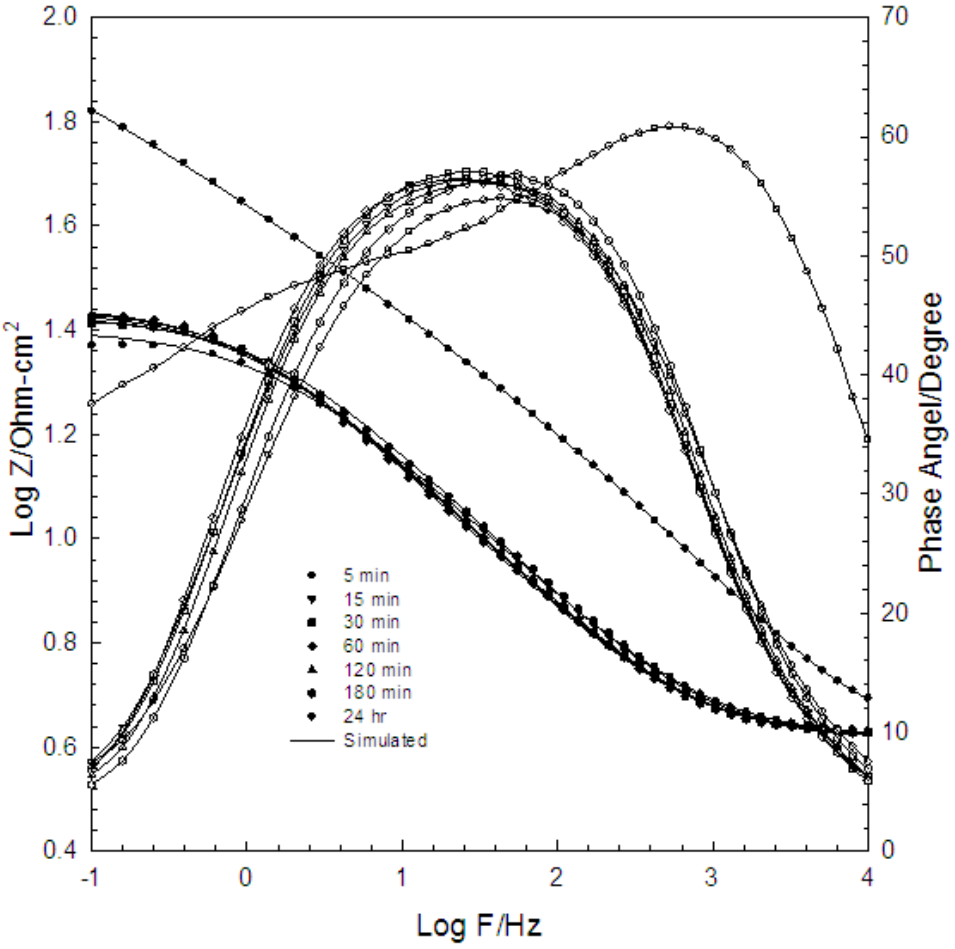

Fig. 6 c Bode plots of Cu-Al-Ni as a function of immersion time at 37^{o}C in SBF +KF

Fig. 7

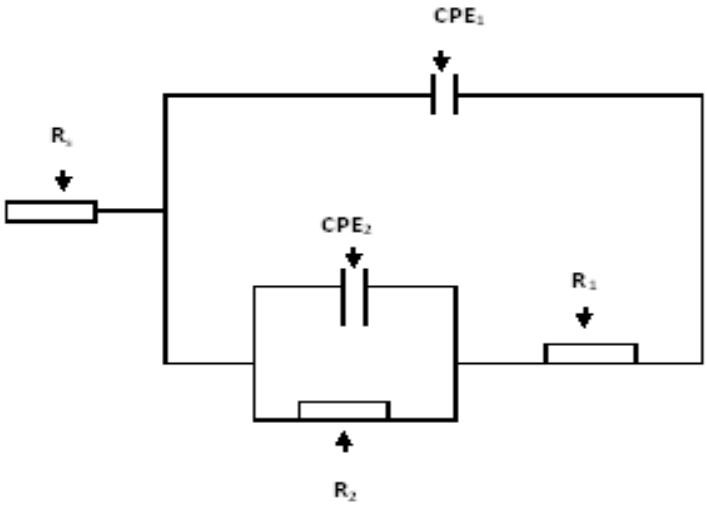

Fig. 7: The equivalent circuit

https://dx.doi.org/10.22161/ijaers/3.11.29 ISSN: 2349-6495(P) | 2456-1908(O)

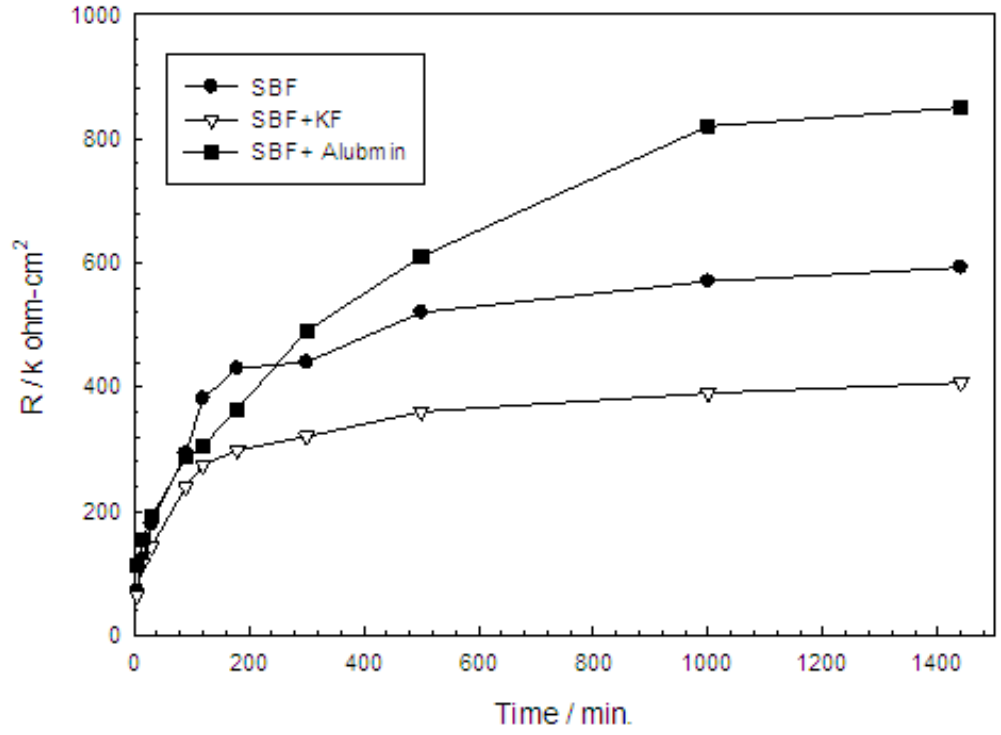

Fig. 8 (a): Change of the impedance with immersion time for Ti in different simulated body fluids

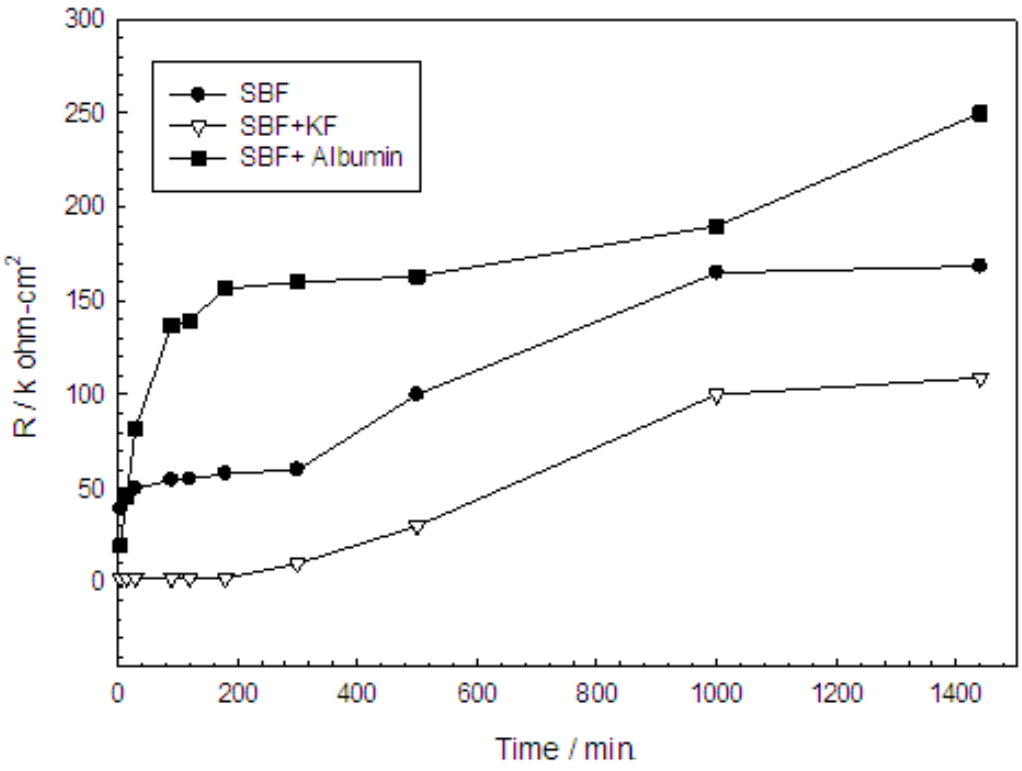

Fig. 8 (b): Change of the impedance with immersion time for Cu-Al-Ni in different simulated body fluids

https://dx.doi.org/10.22161/ijaers/3.11.29 *ISSN: 2349-6495(P) | 2456-1908(O)*

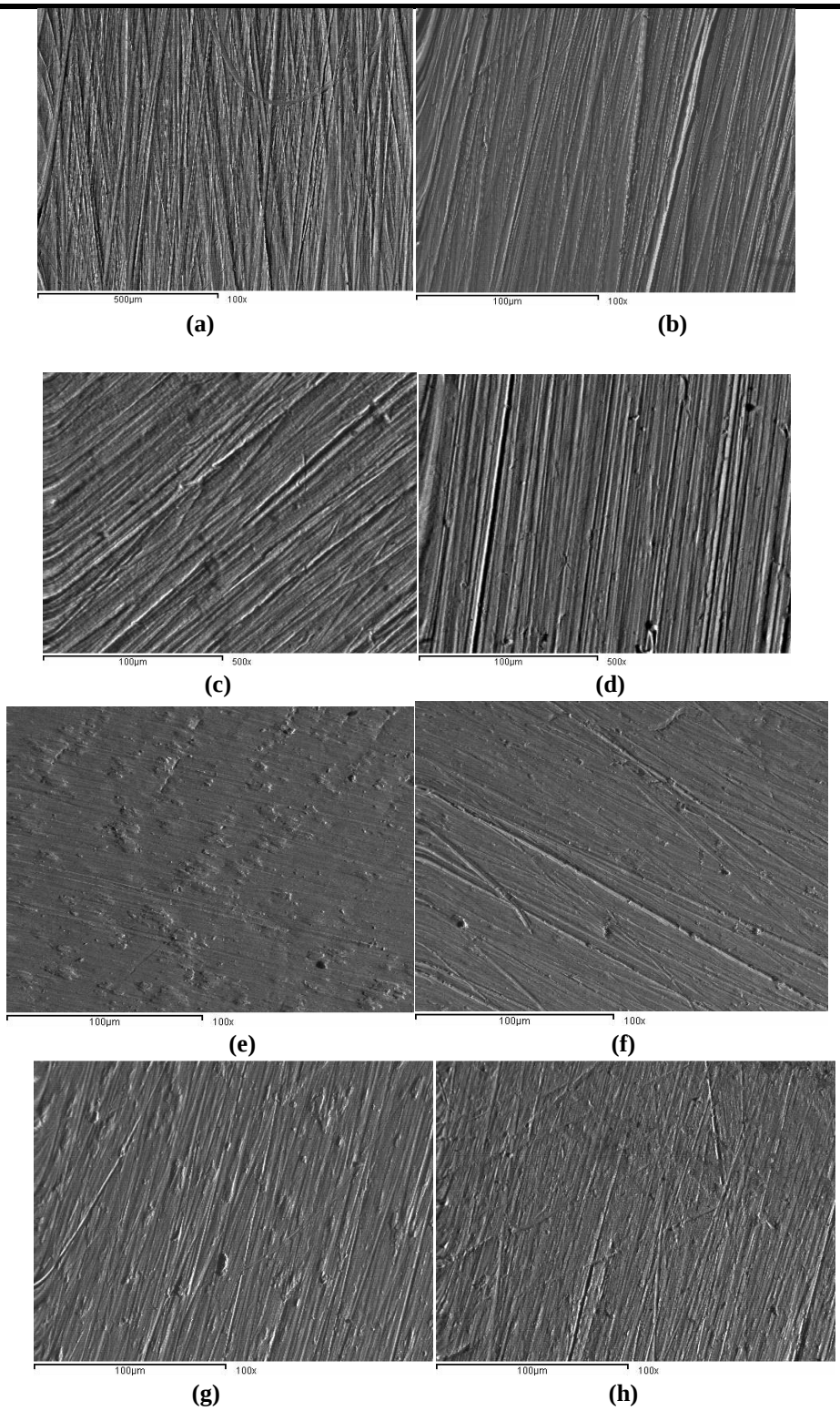

Fig. 9: Scanning electron microscopic images of samples after potentiodynamic testing;
a) Polished Cu-Ni-Al, b) Cu-Al-Ni in SBF, c) Cu-Al-Ni in SBF + KF, d) Cu-Al-Ni in SBF + Albumin, e) Polished Ti, f) Ti in SBF, g) Ti in SBF +KF, h) Ti in SBF + Albumin.

https://dx.doi.org/10.22161/ijaers/3.11.29 *ISSN: 2349-6495(P) | 2456-1908(O)*

Table.1: Potentiodynamic corrosion data of Ti in SBF, SBF+KF and SBF+ Albumin solutions.

Medium	E_{corr} (mV)	i_{corr} (μA cm^{-2})	Ba (mVdecade^{-1})	Bc (mVdecade^{-1})
SBF	**-487.9**	**3.2**	**542**	**-626**
SBF+KF	**-563.4**	**5.0**	**617**	**-554**
SBF+Albumin	**-466.8**	**1.8**	**1220**	**-525**

Table.2: Potentiodynamic corrosion data of Cu-Al-Ni in SBF, SBF+KF and SBF+ Albumin solutions

Medium	E_{corr} (mV)	i_{corr} (μA cm^{-2})	Ba (mVdecade^{-1})	Bc (mVdecade^{-1})
SBF	-454	0.22	124	-754
SBF+ KF	-653	6.22	605	-511
SBF+Albumin	-425	0.062	86.5	-523

Table.3: Impedance parameters of Ti in SBF

Time/min.	R_s/ Ω	CPE_1/μF cm^{-2}	α_1	R_1/kΩ cm^2	CPE_2/μF cm^{-2}	α_2	R_2/kΩ cm^2
5	59.0	5.025	0.79	0.015	2.30	0.91	71.84
15	58.7	4.74	0.79	0.015	2.24	0.94	122.1
30	58.5	4.55	0.79	0.015	2.11	0.95	179.4
90	58.3	4.37	0.78	0.016	2.04	0.97	292.9
120	57.8	4.22	0.81	0.018	1.96	0.98	380.8
180	55.7	4.37	0.86	0.021	1.77	0.99	429.6
24 hr.	64.0	3.45	0.86	0.022	1.29	0.93	592.2

Table.4: Impedance parameters of Ti in SBF + KF

Time/min.	R_s/ Ω	CPE_1/μF cm^{-2}	α_1	R_1/kΩ cm^2	CPE_2/μF cm^{-2}	α_2	R_2/kΩ cm^2
5	45.5	3.5	0.71	0.061	0.42	0.99	65.2
15	64.5	10.2	0.82	0.075	1.78	0.99	116.2
30	64.9	10.0	0.83	0.076	1.77	0.99	142.8
90	64.5	9.75	0.84	0.075	1.76	0.99	238.7
120	65.1	9.72	0.84	0.075	1.76	0.99	274.8
180	68.0	9.50	0.85	0.077	1.75	0.99	297.5
24 hr.	74.0	8.60	0.87	0.088	1.62	0.99	406.8

Table.5: Impedance parameters of Ti in SBF + Albumin

Time/min.	R_s/ Ω	CPE_1/μF cm^{-2}	α_1	R_1/kΩ cm^2	CPE_2/μF cm^{-2}	α_2	R_2/kΩ cm^2
5	**59.7**	**4.175**	**0.81**	**0.0036**	**8.75**	**0.86**	**112.5**
15	**59.8**	**3.75**	**0.78**	**0.0064**	**8.50**	**0.92**	**154.8**
30	**64.1**	**3.95**	**0.78**	**0.0068**	**8.43**	**0.93**	**190.5**
90	**74.5**	**3.85**	**0.80**	**0.0064**	**8.08**	**0.93**	**286.7**
120	**70.8**	**3.87**	**0.81**	**0.0060**	**7.97**	**0.94**	**305.4**
180	**50.5**	**3.97**	**0.83**	**0.0048**	**7.67**	**0.92**	**364.0**
24 hr.	**52.5**	**4.20**	**0.93**	**0.0036**	**7.60**	**0.92**	**850.0**

https://dx.doi.org/10.22161/ijaers/3.11.29 *ISSN: 2349-6495(P) | 2456-1908(O)*

Table.6: Impedance parameters of Cu-Al-Ni in SBF

Time/min.	*R_s/ Ω*	*CPE_1/μF cm^{-2}*	*α_1*	*R_1/kΩ cm^2*	*CPE_2/μF cm^{-2}*	*α_2*	*R_2/kΩ cm^2*
5	*38.3*	*3.04*	*0.66*	*0.017*	*2.46*	*0.98*	*39.1*
15	*38.1*	*2.50*	*0.65*	*0.017*	*1.57*	*0.95*	*45.0*
30	*37.6*	*2.32*	*0.66*	*0.017*	*1.34*	*0.92*	*50.0*
90	*37.2*	*2.18*	*0.67*	*0.016*	*1.12*	*0.92*	*54.5*
120	*37.7*	*2.25*	*0.67*	*0.015*	*1.14*	*0.90*	*55.0*
180	*37.1*	*2.14*	*0.68*	*0.014*	*1.06*	*0.92*	*58.0*
24 hr.	*37.1*	*2.12*	*0.68*	*0.014*	*1.04*	*0.95*	*168.5*

Table.7: Impedance parameters of Cu-Al-Ni in SBF+ Albumin

Time/min.	**R_s/ Ω**	**CPE_1/μF cm^{-2}**	**α_1**	**R_1/kΩ cm^2**	**CPE_2/μF cm^{-2}**	**α_2**	**R_2/kΩ cm^2**
5	**35.6**	**2.07**	**0.63**	**0.0125**	**3.50**	**0.96**	**19.5**
15	**36.1**	**2.13**	**0.63**	**0.0120**	**3.68**	**0.93**	**46.1**
30	**36.3**	**2.10**	**0.65**	**0.0115**	**3.70**	**0.92**	**82.3**
90	**37.5**	**2.04**	**0.68**	**0.0105**	**3.58**	**0.87**	**136.8**
120	**38.1**	**2.04**	**0.68**	**0.0095**	**3.54**	**0.86**	**139.5**
180	**39.5**	**2.07**	**0.69**	**0.0065**	**2.40**	**0.83**	**156.6**
24 hr	**40.7**	**2.12**	**0.70**	**0.0050**	**3.53**	**0.83**	**250.0**

Table 8: Impedance parameters of Cu-Al-Ni in SBF + KF

Time/min.	**R_s/ Ω**	**CPE_1/μF cm^{-2}**	**α_1**	**R_1/kΩ cm^2**	**CPE_2/μF cm^{-2}**	**α_2**	**R_2/kΩ cm^2**
5	32.3	2.13	0.61	0.0045	7.46	0.77	1.97
15	32.7	2.28	0.65	0.0040	8.94	0.77	2.44
30	33.4	2.28	0.67	0.0035	9.24	0.77	2.45
90	33.7	2.19	0.69	0.0030	9.00	0.76	2.20
120	33.6	2.15	0.69	0.0025	8.80	0.76	2.30
180	34.1	1.99	0.65	0.0025	7.80	0.78	2.25
24 hr	36.9	0.594	0.55	0.0030	0.864	0.93	109.0

International Journal of Advanced Engineering Research and Science (IJAERS) *[Vol-3, Issue-11, Nov- 2016]*
https://dx.doi.org/10.22161/ijaers/3.11.30 *ISSN: 2349-6495(P) | 2456-1908(O)*

Fatigue Crack Growth Life Prediction of 6061 Al-Alloy under Load Ratio Effect by Using ANFIS

J. R. Mohanty

Department of Mechanical Engineering, Veer Surendra Sai University, Burla, Sambalpur 768018, India

Abstract*—Fatigue crack growth under constant amplitude loading for a particular material strongly depends on load ratio (R). The prediction of fatigue crack growth life under such situation through deterministic approach is a tedious task. Application of artificial intelligence methods is more encouraging in those complex situations. In the present work a novel soft-computing approach i.e. adaptive neuro-fuzzy technique (ANFIS) has been applied to predict fatigue life of 6061 (AA 6061) aluminum alloy under the influence of load ratio. It has been observed that the ANFIS model predict the fatigue life of the alloy reasonably well with percentage deviation of –0.024 and prediction ratio of 1.025.*

Keywords*—Adaptive neuro-fuzzy inference system (ANFIS); fatigue crack growth rate (FCGR); root mean squre error (RMSE); prediction ratio.

I. INTRODUCTION

Fatigue failure is an important mode of failure which occurs in almost all engineering structures/components. There are several approaches such as fail-safe, safe-life and damage tolerant approaches in fatigue literature to deal with the fatigue phenomena. Out of those, the damage tolerant approach is one of the modern approaches based on fracture mechanics principle which mainly correlate fatigue crack growth with life (i.e. No. of cycle to failure) of the specimen. In this approach the crack growth rate (da/dN) is correlated with different material parameters and above all the crack driving forces to determine fatigue life of the computing is a good alternative for handling those complex problems as it is tolerant of imprecision, uncertainty and partial truth. As such, different soft-computing methods such as, artificial neural network (ANN), genetic algorithm (GA), fuzzy logic and adaptive neuro-fuzzy inference system (ANFIS) are being used in various fields including fatigue [9-12]. However, the prediction of fatigue life considering load ratio effect using ANFIS is rare in fatigue literature. Therefore, in the present work an attempt has been made to evaluate the constant amplitude fatigue life of 6061 aluminum alloy under load ratio effect by using components. It can be represented by the functional form as:

$$\frac{da}{dN} = f(\Delta K, K_{\max}, R, E.....) \quad (1)$$

Based on this, several deterministic models [1-4] have been proposed till date to predict fatigue crack growth life to schedule inspection intervals for repairing/replacement of the components to avoid untimely catastrophic failures. However, the fatigue life prediction from those models suffers from several drawbacks. One of the major drawbacks is that the calculation of fatigue life from any prediction model involves complicated numerical integration schemes. Further, to formulate a fatigue model, several coupon tests are required which are not only costly but time consuming. In order to avoid those shortcomings, recently the researchers are taking the help of different computational techniques to predict fatigue crack growth life.

Fatigue crack growth under constant amplitude loading for a particular material strongly depends on load ratio (R) which is the ratio of minimum load ($P_{\min}$) to maximum load ($P_{\max}$). It has tremendous effect on fatigue crack growth. Some fatigue experts [5-8] have investigated its effect on fatigue crack growth and also proposed different empirical and semi-empirical models to evaluate fatigue life. However, problems associated with fatigue are difficult to solve using conventional mathematical models because of non-linearity, noise, cost, time constraint and above all the associated micro-mechanisms. Hence, soft-ANFIS technique. It has been observed that the proposed soft-computing technique predicts the fatigue life reasonable well with percentage deviation of –0.024 and prediction ratio of 1.025.

II. EXPERIMENTATION AND DATA PREPARATION

Fatigue crack growth experiment

The material under investigation was 6061 aluminum alloy received in T6 heat treated condition from rolled palte of 15 mm thickness. It was supplied by HINDALCO Industries

https://dx.doi.org/10.22161/ijaers/3.11.30 *ISSN: 2349-6495(P) | 2456-1908(O)*

Ltd., Hirakud, Distt. Sambalpur (Odisha), India. The chemical composition of the alloy as certified by the supplier is given in Tables 1.

Table.1: Chemical Composition of 6061 T6 Al-alloy

Elem-ents	Cu	Mg	Mn	Fe	Si	Cr	Al
Wt. %	0.15 – 0.4	0.8– 1.1	0.14 max	<0.02	0.3-0.7	0.04 - 0.35	Bal

The compact tension (CT) specimens for fatigue crack growth rate (FCGR) determination were machined in the longitudinal direction with notch perpendicular to rolling direction as per ASTM E-647-99 standard [13] as shown in Fig. 1. Both the sides of the specimen were mirror polished in order to facilitate the observation of crack growth. The FCGR (d*a*/d*N*) tests were conducted on as-received condition of AA 6061 T6 alloy as per ASTM E647 standard on a servo-hydraulic test machine (*Instron*-8502) having a load capacity of 250 kN in air at room temperature.

Initially, the specimens were fatigue pre-cracked under mode-I loading with a sinusoidal waveform up to a crack length to width (*a*/*w*) ratio of 0.3 under given loading conditions (frequency: 6Hz; load ratio: 0.1). Then the specimens were subjected to FCGR tests under constant amplitude technique (i.e. Δ*K* increasing) maintaining different load ratios (*R*) of 0, 0.2, 0.4, 0.5, 0.6, 0.8 respectively separately and the test data were recorded. The crack growth was monitored with the help of a COD gauge mounted on the face of the machined notch.

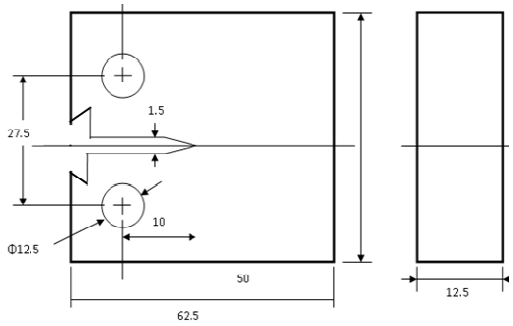

Fig. 1: Compact tension (CT) specimen geometry

Crack growth rate determination

After the fatigue crack growth rate tests, raw *a* – *N* laboratory data were obtained under each load ratio which usually contained much scatter. In order to smoothen the test data and to determine the fatigue crack growth rate, the following procedures were adopted by applying the concept of authors' previously proposed exponential [14]. The experimental *a* – *N* data were fitted with the following exponential equation as per the previous model.

$$a_j = a_i e^{m_{ij}(N_j - N_i)} \quad (2)$$

$$m_{ij} = \frac{\ln\left(\frac{a_j}{a_i}\right)}{\left(N_j - N_i\right)} \quad (3)$$

where, a_i and a_j = crack length in i^{th} step and j^{th} step in 'mm' respectively,

N_i and N_j = No. of cycles in i^{th} step and j^{th} step respectively,

m_{ij}= specific growth rate in the interval *i*-*j*,

i = No. of experimental steps, and $j = i+1$

The values of specific growth rate 'm_{ij}' were calculated according to the equation (3) and subsequently refined by curve fitting with calculated *a* values (i.e. crack lengths from initial to final with an increment of 0.005mm). The smoothened values of the number of cycles were calculated in the excel sheet from the refined 'm_{ij}' values as per the following equation.

$$N_j = \frac{\ln\left(\frac{a_j}{a_i}\right)}{m_{ij}} + N_i \quad (4)$$

Then the crack growth rates (d*a*/d*N*) were determined directly from the above calculated values of '*N*' as follows:

$$\frac{da}{dN} = \frac{\left(a_j - a_i\right)}{\left(N_j - N_i\right)} \quad (5)$$

The superimposed crack length (*a*) vs. number of cycle (*N*) and the corresponding log (d*a*/d*N*) vs. log (Δ*K*) curves at different load ratios were plotted in Figs. 2 and 3 respectively.

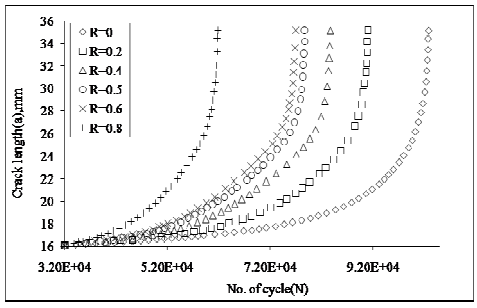

Fig. 2: Comparison of a–N curves for different load ratios

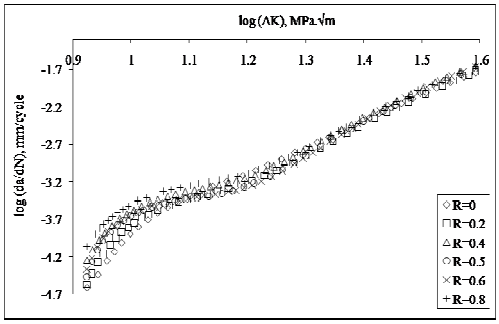

Fig. 3: Comparison of log (da/dN) – log (ΔK) for different load ratios

https://dx.doi.org/10.22161/ijaers/3.11.30 *ISSN: 2349-6495(P) | 2456-1908(O)*

III. ANFIS: METHODOLOGY

The fuzzy inference system (FIS) is generally used as a suitable tool for approximating ill-defined nonlinear functions. It can implement qualitative aspects of human knowledge and reasoning by using following four functional components as shown in Fig. 4.

- A rule base containing a number of fuzzy if-then rules.
- A decision-making unit as the inference engine.
- A fuzzification interface which transforms crisp inputs to linguistic variables.
- A defuzzification interface converting fuzzy outputs to crisp outputs.

Adaptive neuro-fuzzy inference system (ANFIS) is an integrated system of artificial neural network (ANN) and fuzzy inference system (FIS) and utilizes the advantages of both. ANFIS is a class of adaptive networks, whose membership function parameters are tuned (adjusted) using either a back-propagation algorithm or hybrid algorithm based on a combination of back-propagation and least squares estimate (LSE). In the present investigation, type-3 ANFIS [15] topology based on first-order Takagi-Sugeno (TSK) [16] if-then rules has been used.

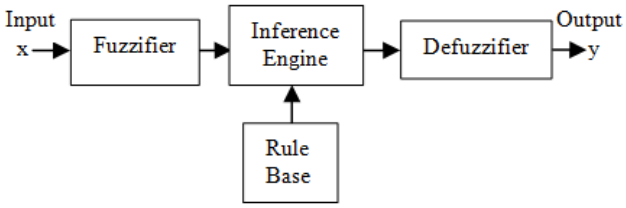

Fig. 4: Fuzzy Inference System

The structure of proposed ANFIS model consists of a number of interconnected fixed and adjustable nodes corresponding to first-order TSK fuzzy model as shown in Fig. 5. It is composed of five layers having three inputs and one output. Bell-shaped membership function has been chosen for the present investigation because it is the best membership function type [17]. A hybrid-learning algorithm is applied to adapt the premise and consequent parameters to optimize the network. Heuristic rules are used to guarantee fast convergence.

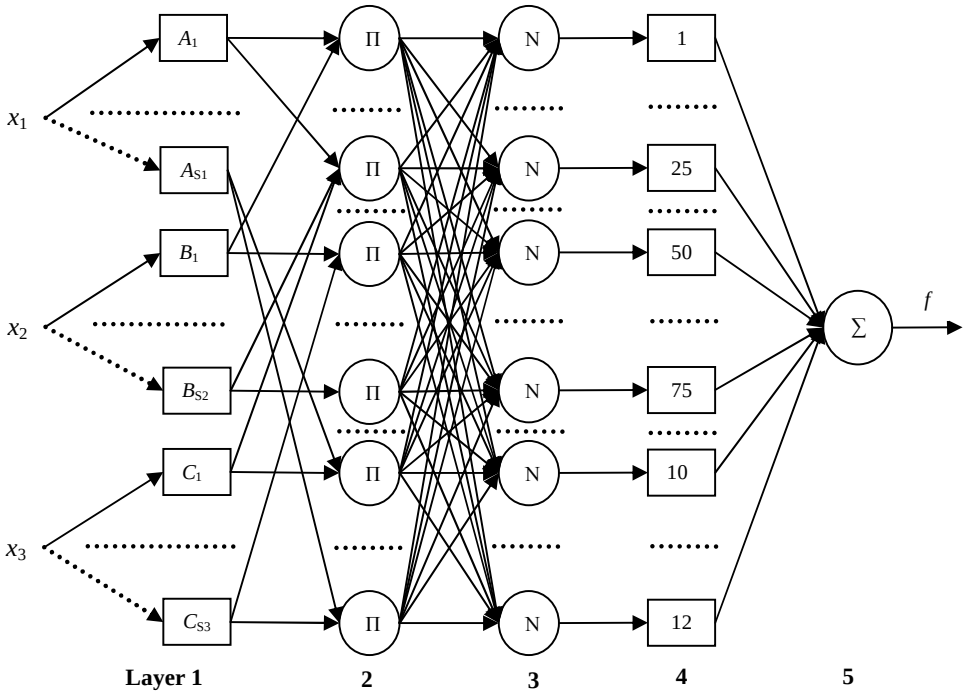

Fig. 5: Structure of the ANFIS model

IV. APPLICATION DESIGN

It is known that fatigue crack growth life decreases as load ratio increases [18]. Accordingly, the maximum stress intensity factor (K_{max}), and the stress intensity factor range (ΔK) are also affected by load ratio. Therefore, during model formulation load ratio (R), maximum stress intensity factor (K_{max}), and stress intensity factor range (ΔK) were selected as linguistic input variables whereas, crack growth rate (da/dN) was taken as output variable. A set of linguistic rules formulated in the "If-Then" form were derived from expert observation and experimentation.

The experimental data base consisted of six sets of fatigue crack growth data having load ratios (R) of 0, 0.2, 0.4, 0.5, 0.6 and 0.8. Each set for a particular load ratio contained

https://dx.doi.org/10.22161/ijaers/3.11.30 *ISSN: 2349-6495(P) | 2456-1908(O)*

approximately 300 data of both K_{max} and ΔK along with their corresponding da/dN (calculated as per the procedure mentioned earlier). The model was applied to simulate the crack growth rate of an unknown input/output data set for load ratio of 0.5 as validation set (VS) by constructing a training set (TS) with five known input/output data sets for load ratios (R) of 0, 0.2, 0.4, 0.6 and 0.8.

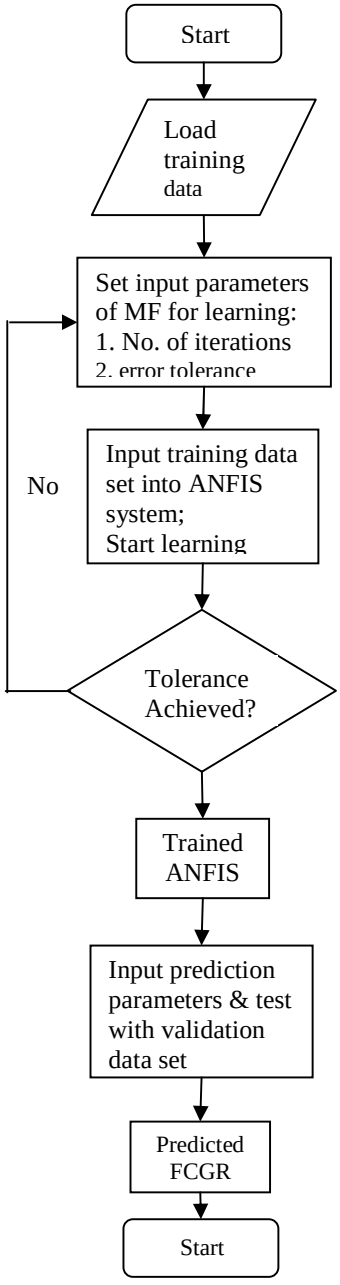

Fig. 6: Flow chart of ANFIS hybrid learning algorithm

Fig. 6 shows the flow chart of ANFIS hybrid learning algorithm. Before applying ANFIS model, the pre-processing of experimental data is essential in order to achieve optimum modeling results. The input variables i.e. load ratios (R), maximum stress intensity factor (K_{max}) and stress intensity factor range (ΔK) were normalized in such a way that their maximum values were normalized to unity. The crack growth rate (da/dN), which constituted the system output, was also normalized in similar manner. The numbers of membership functions (MF) were chosen to be 5-5-5 corresponding to the inputs R, K_{max} and ΔK respectively.

The $5\times5\times5=125$ fuzzy '*if-then*' rules constituted in which fuzzy variables were connected by T-norm (fuzzy AND) operators. The adjustment of premise and consequent parameters was made in batch mode based on the hybrid-learning algorithm. The model was trained for 4000 epochs until the given tolerance was achieved.

Table 2 summarizes all the characteristics of ANFIS network used during training. As per Fig. 5, layer 1 had 15 (5×3) nodes with 45 parameters. Layers 2, 3 and 4 had 125 (5^3) nodes each with 500 parameters associated in layer 4.

Table 2: Characteristics of the ANFIS network

Type of membership function	Generalized bell
Number of input nodes (n)	3
Number of fuzzy partitions of each variable (p)	5
Total number of membership functions	15
Number of rules (p^n)	125
Total number of nodes	394
Total number of parameters	545
Number of epochs	4000
Step size for parameter adaptation	0.01

The model performances during training and testing were verified by computing root mean square error (RMSE); coefficient of determination (R^2) and mean percent error (MPE) defined by the following equations:

$$RMSE = \left((1/p) \sum_{i=1}^{p} |t_i - o_i| \right)^{1/2} \quad (6)$$

$$R^2 = 1 - \left(\frac{\sum_{i=1}^{p} (t_i - o_i)^2}{\sum_{i=1}^{p} (o_i)^2} \right) \quad (7)$$

https://dx.doi.org/10.22161/ijaers/3.11.30 *ISSN: 2349-6495(P) | 2456-1908(O)*

$$MPE = \frac{1}{p}\sum_{i=1}^{p}\left(\frac{t_i - o_i}{t_i}\times 100\right) \quad (8)$$

where'*t*' is the target value, '*o*' is the output value, and '*p*' is the number of data items.

The model was trained and tested by using MATLAB with Fuzzy Logic Toolbox. The performance of the model during training and testing was verified through three statistical indices (Eqs. 6 to 8) and presented in Table 3.

Table: 3 Performance of ANFIS model

During training RMSE	R^2	MPE	During testing RMSE	R^2	MPE	Comp-utat-ional Time (Min.)
0.0012 7	0.9985	0.2758	0.0129	0.9986	0.7796	384

V. DISCUSSION

As observed from the performance table, the MPE and RMSE values for the training data were negligible in both the cases. MPE values for testing were found to be slightly higher than those for training. The coefficient of determination was found to be close to 1.0 during training. However, its value for testing was slightly less than unity. Based on the above statistical performances, the trained ANFIS model was tested for load ratio of 0.5. The predicted crack growth rates curve (for R=0.5) obtained from ANFIS model has been compared with experimental results in Fig. 7 and found to be in good agreement.

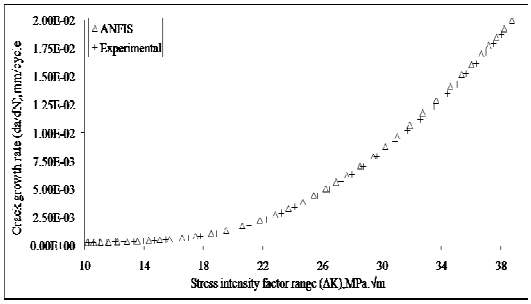

Fig. 7: Comparison of da/dN–ΔK curves for R=0.5

The numbers of cycles (fatigue life) have been calculated as per the following equation.

$$N_{i+1} = \frac{a_{i+1} - a_i}{da/dN} + N_i \quad (9)$$

The predicted (ANFIS) numbers of cycles are presented along with experimental results in Table 4 for quantitative comparison. The crack length vs. number of cycle (a~N) curve has been plotted in Fig. 8.

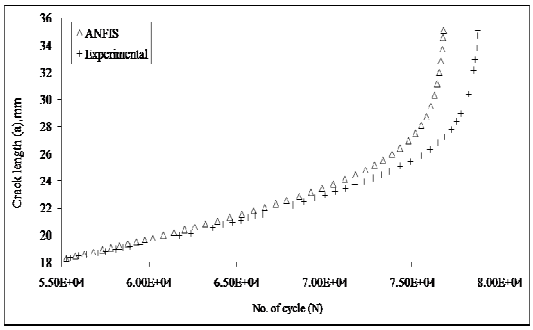

Fig.8: Comparison of predicted (ANFIS) and experimental crack length with number of cycle

The performance of the model was evaluated by comparing the prediction results with the experimental findings by the following criteria:

- Percentage deviation of predicted life from the experimental life i.e. $\% Dev = \frac{predicted - Experimental}{Experimental}\times 100$
- Prediction ratio which is defined as the ratio of actual life (i.e. experimental) to predicted life i.e. Prediction ratio, $P_r = \frac{actual}{predicted}$
- Error bands i.e. the scatter of the predicted life in either side of the experimental life within certain error limits.

Performance of the model result from first two criteria has been presented in Table 4.

Table.4: Prediction results of the model

Fatigue life ($\times 10^3$ cycle) ANFIS	Fatigue life ($\times 10^3$ cycle) Experimental	% Deviation ANFIS	Prediction ratio ANFIS
76.826	78.783	–0.024	1.025

It is observed that the ANFIS model prediction is reasonable in comparison to experimental findings as far as prediction of fatigue life is concerned. Further, the prediction ratio is approximately 1.0, which is adequate and also acceptable [19]. Fig. 9 illustrates the performance of the alloy evaluated graphically under the third criteria. It is observed that the scatter of the predicted life is within ± 0.025%.

https://dx.doi.org/10.22161/ijaers/3.11.30 *ISSN: 2349-6495(P) | 2456-1908(O)*

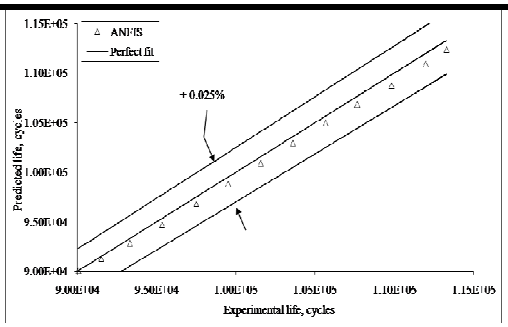

Fig. 9: Error band scatter of predicted lives for R = 0.5

VI. CONCLUSION

The focus of this work was to develop an ANFIS model in order to predict crack growth rate and in turn the fatigue life of 6061 Al alloy under the effect of load ratio. It has been observed that the predicted fatigue life from ANFIS model is 76.826×10^3 cycles whereas from experimental result it is 78.783×10^3 cycle. As far as performance of the model is concerned the percentage deviation of predicted fatigue life from the experimental result is –0.024 whereas the prediction ratio is 1.025. It can be concluded that the adaptive neuro-fuzzy technique (ANFIS) can be reasonably applied to predict the fatigue life under constant amplitude loading taking into account the load ratio effect.

REFERENCES

[1] P. C. Paris, and F. Erdogan, "A critical analysis of crack Propagation law," J. Basic Eng., vol. 85, pp. 528–534, 1963.

[2] R. G. Forman, V. E. Kearney, and R. M. Engle, "Numerical analysis of crack Propagation in cyclic-loaded structures," J. Basic Eng., vol. 89, pp. 459–464, 1967.

[3] K. Walker, "The effect of stress ratio during crack propagation and fatigue for 2024-T3 and 7075-T6 aluminum," ASTM STP, vol. 462, pp. 1–14, 1970.

[4] D. Kujawski, "A new $(\Delta K+ K_{max})^{05}$ driving force parameter for crack growth in aluminum alloys," Int. J. Fat., vol. 23, pp. 733–740, 2001.

[5] D. Kujawski, "Enhanced model of partial crack closure for correlation of R- ratio effects in aluminum alloys," Int. J. Fat., vol. 23, pp. 95-102, 2001.

[6] X. Huang, and T. Moan, "Improved modeling of the effect of R-ratio on crack growth Rate," Int. J. Fat., vol. 29, pp. 591-602, 2007.

[7] S. B. Singh, and R. Kumar, "Experimental Observations of Fatigue Crack Growth in IS-1020 Steel under Constant Amplitude Loading," Int. J.Pres.Ves. Piping, vol. 53, pp. 217-227, 1993.

[8] R. Kumar, "Investigation of Fatigue Crack Growth Under constant Amplitude Loading," Int. J.Pres.Ves. Piping, vol. 41, pp. 179-192, 1990.

[9] J. A. Lee, D.P. Almond, and B. Harris, "The use of neural networks for the prediction of fatigue lives of composite materials." Compos. Part A: Appl. Sci. Manufact., vol. 30, pp. 1159-1169, 1999.

[10] T. T. Pleune, and O. K. Chopra, "Using artificial neural networks to predict the fatigue life of carbon and low-alloy steels," Nucl. Eng. Des., vol. 197, pp. 1–12, 2000.

[11] R. M. V. Pidaparti, and M. J. Palakal, "Neural Network Approach to Fatigue Crack-Growth Predictions under Aircraft Spectrum Loadings," J. Aircraft, vol. 32, no. 4, pp. 825-831, 1995.

[12] A. Fotovati, and T. Goswami, "Prediction of elevated temperature fatigue crack growth rates in Ti-6Al-4V alloy – neural network approach," Maters. Eng. Des., vol. 25, pp. 547-554, 2004.

[13] Anon, "Standard test method for measurement of fatigue crack growth rates," ASTM E-647, In: ASTM Book of Standard, ASTM, Philadelphia, vol. 03.01, pp. 899– 926, 1996.

[14] J. R. Mohanty, B. B. Verma, and P. K. Ray, "Prediction of fatigue crack growth and residual life using an exponential model: Part I (constant amplitude loading)," Int. J. Fat., vol. 31, pp. 418-424, 2009.

[15] J. S. R. Jang, "ANFIS: Adaptive-network-based fuzzy inference system," IEEE Trans. on Syst. Man Cyber., vol. 23, no. 3, pp. 665-685, 1993.

[16] T. Takagi, and M. Sugeno, "Fuzzy identification of systems and its applications to modeling and control," IEEE Trans. on Syst. Man Cyber., vol. 15, pp. 116–132, 1985.

[17] M. A. Jarrah, Y. Al-Assaf, and H. El Kadi, "Neuro-fuzzy modeling of fatigue life prediction of unidirectional glass fiber / epoxy composite laminates," J. Comput. Mats., vol. 36, no. 6, pp. 685–699, 2002.

[18] S. B. Singh, and R. Kumar, "Experimental Observations of Fatigue Crack Growth in IS-1020 Steel under Constant Amplitude Loading," Int. J. Pres. Ves. Piping, vol. 53, pp. 217-227, 1993.

[19] P. Heuler, and W. Schuetz, "Assessment of concepts for fatigue crack initiation and propagation life prediction," Z. Werkstofftech vol. 17, pp. 397-405, 1986.

https://dx.doi.org/10.22161/ijaers/3.11.31 *ISSN: 2349-6495(P) | 2456-1908(O)*

An Application of Distributional Two Dimensional Fourier-Mellin Transform

V. D. Sharma[1], P. D. Dolas[2]

[1]HOD, Department of Mathematics, Arts, Commerce & Science College, Kiran Nagar, Amravati, Maharashtra, India
[2]Department of Mathematics, Dr. Rajendra Gode Institute of Technology & Research, Amravati, Maharashtra, India.

Abstract— *Integral transforms are linear continuous operators with their inverses, transforming a class of functions to another class of functions or sequences. They provide powerful operational methods for solving initial value problems and initial-boundary value problems for linear differential and integral equations. With ever greater demand for mathematical methods to provide a both theory and applications for science and engineering, the utility and interest of integral transforms seems more clearly established than ever. In spite of the fact that integral transforms have many mathematical and physical applications, their use is still predominant in advanced study and research.*

Keeping these features in mind in this paper we provide the solution of differential equation for the distributional two dimensional Fourier-Mellin transform of the type $P\left(\Lambda^*_{t,l,x,y}\right) u(t,l,x,y) = f(t,l,x,y)$ *and* $P\left(D_{t,l,x,y}\right)u(t,l,x,y) = f(t,l,x,y)$ *using the differential operator* $\Lambda_{t,l,x,y}$ *and* $\Lambda^*_{t,l,x,y}$.

Keywords— Adjoint operator, Fourier Transform, Generalized function, Mellin Transform, Two Dimensional Fourier-Mellin Transform.

I. INTRODUCTION

Characteristically, one uses the integral transformation as mathematical or physical tool to alter the problems into one that can be solved. Integral transforms are linear continuous operators with their inverses, transforming a class of functions to another class of functions or sequences. The concept of integral transform originated from Fourier integral formula. It is composed of four objects & defined as

$$F(s) = \int_{t_1}^{t_2} f(t)\ K(t,s)\ dt$$

There are two functions ($F(s)$ as output, $f(t)$ as input) that changes depending on problem and two objects which are remain same for a transform irrespective of input function ($K(t,s)$ as kernel, interval). Kernels are different for different type of transforms. They operate on function in much the same way as (certain) matrices do on vectors [2]. Integral Transform methods providing unifying mathematical approach to the study of electrical, network, devices for energy conversion and control, antennas and other component of electrical system [3]. Integral transforms transform a class of differential equations into a class of algebraic equations; the algebraic equations can be solved easily. So, we can easily find the solutions of those differential equations, this is the most useful significance of integral transforms. These are also providing powerful operational methods for solving initial value problems and initial-boundary value problems for linear differential and integral equations [1]. These are equally applied to the subject of electrical communication by wire or optical fibers, to wireless radio propagation [3]. This is a key point because it provides a way to understand exactly what an integral transform does. The integral transforms provide both theory and applications for science and engineering. Integral Transform methods are at the heart of engineering curriculum. In spite all that things their uses are still predominant in advanced study and research. So, these integral transforms are attracting to all researchers, since, their fabulous work and applications in almost all fields. In the present paper, we have focused on applications of Distributional Two Dimensional Fourier-Mellin Transform to differential equations. For this purpose, we have putting the following definitions which are already defined in our previous papers [4,7,8,9] as-

1.1. The Test Function space $FM_{a,b,c,d,\alpha}$

Let I be the open set in $R_+ \times R_+$ and E_+ denotes the class of infinitely differentiable function defined on$I$, the space $FM_{a,b,c,d,\alpha}$ is given by

$$FM_{a,b,c,d,\alpha} = \{\emptyset : \emptyset \in E_+ / \ \gamma_{a,b,c,d,k,r,h,g.q,j}\emptyset(t,l,x,y)$$
$$= \sup_{I_1}\left|t^k l^r \xi_{a,b}(x) x^{h+1} \eta_{c,d}(y) y^{g+1} D_t^q D_x^h D_l^j D_y^g \emptyset(t,l,x,y)\right|$$
$$< C\ A^k\ k^{k\alpha} \qquad k,r,h,g,g,q,j = 0,1,2,3 \ldots\ldots\ldots \quad (1.1.1)$$

Where, the constant C, A depending on testing function space$\emptyset$.

1.2. Two Dimensional Distributional Fourier-Mellin Transform of Generalized function in $FM^*_{a,b,c,d,\alpha}$

The Two Dimensional Distributional Fourier-Mellin Transform is defined as-

$$FM\{f(t,l,x,y)\} = F(s,u,p,v)$$
$$= \langle f(t,l,x,y), e^{-i(st+ul)} x^{p-1} y^{v-1} \rangle \qquad (1.2.1)$$

https://dx.doi.org/10.22161/ijaers/3.11.31 *ISSN: 2349-6495(P) | 2456-1908(O)*

Where for each fixed $x(0 < x < \infty), y(0 < y < \infty), t(0 < t < \infty)$ and $l(0 < l < \infty)$.

The R.H.S. of (2.1) has sense of an application of $f(t,l,x,y) \in FM^*_{a,b,c,d,\alpha}$ to $e^{-i(st+ul)}x^{p-1}y^{v-1} \in FM_{a,b,c,d,\alpha}$.

In the present paper, we have defined the differential operator$\Lambda_{t,l,x,y}$, its adjoint operator$\Lambda^*_{t,l,x,y}$. Using this differential operator in the given paper we have present an application of Two Dimensional Fourier-Mellin Transform to differential equations. The notation and terminology are given as per A.H. Zemanian [5, 6].

II. AN APPLICATION OF DISTRIBUTIONAL TWO DIMENSIONAL FOURIER-MELLIN TRANSFORM

The kernel of Distribution Two Dimensional Fourier-Mellin Transform

$$K(t,l,x,y,s,u,p,v) = e^{-i(st+ul)}x^{p-1}y^{v-1}$$
$$= e^{-ist}e^{-iul}x^{p-1}y^{v-1}$$

Now differentiate above term w.r.t. t, l, x and$y$, we get

$$D_tD_lD_xD_y\ K(t,l,x,y,s,u,p,v) =$$
$$(-is)e^{-ist}(-iu)e^{-iul}(p-1)x^{p-2}(v-1)y^{v-2}$$
$$= (is)(iu)(p-1)(v-1)e^{-ist}e^{-iul}x^{p-2}y^{v-2}$$
$$D_tD_lD_xD_y\ K(t,l,x,y,s,u,p,v) = -su(p-1)(v-1)e^{-ist}e^{-iul}x^{p-2}y^{v-2}$$

Now multiplying both side by xy, we get

$$xyD_tD_lD_xD_y\ K(t,l,x,y,s,u,p,v) = -su(p-1)(v-1)e^{-ist}e^{-iul}x^{p-1}y^{v-1} =$$
$$-su(p-1)(v-1)K(t,l,x,y,s,u,p,v)$$

Now we construct an operator

$$\Lambda_{t,l,x,y} = xyD_tD_lD_xD_y - su(p-1)(v-1)$$

Where, $D_t = \frac{d}{dt}, D_l = \frac{d}{dl}, D_x = \frac{d}{dx}, D_y = \frac{d}{dy}$

$$\Lambda_{t,l,x,y}\ K(t,l,x,y,s,u,p,v) = [xyD_tD_lD_xD_y - su(p-1)(v-1)]K(t,l,x,y,s,u,p,v) =$$
$$xyD_tD_lD_xD_yK(t,l,x,y,s,u,p,v) - su(p-1)(v-1)K(t,l,x,y,s,u,p,v) =$$
$$-su(p-1)(v-1)K(t,l,x,y,s,u,p,v) - su(p-1)(v-1)K(t,l,x,y,s,u,p,v)\Lambda_{t,l,x,y}\ K(t,l,x,y,s,u,p,v) =$$
$$-2su(p-1)(v-1)K(t,l,x,y,s,u,p,v)$$

Now Consider-

$$\Lambda_{t,l,x,y}\ K(t,l,x,y,s,u,p,v) = (C_0)\ K(t,l,x,y,s,u,p,v)$$

Where, $C_0 = -2su(p-1)(v-1)$

Continuing in this way we get

$$\Lambda^2_{t,l,x,y}\ K(t,l,x,y,s,u,p,v) = (C_0)^{\,2}K(t,l,x,y,s,u,p,v)$$
$$\Lambda^3_{t,l,x,y}\ K(t,l,x,y,s,u,p,v) = (C_0)^{\,3}K(t,l,x,y,s,u,p,v)$$
$$\Lambda^4_{t,l,x,y}\ K(t,l,x,y,s,u,p,v) = (C_0)^{\,4}K(t,l,x,y,s,u,p,v)$$

…… and so on

$$\Lambda^k_{t,l,x,y}\ K(t,l,x,y,s,u,p,v) = (C_0)^{\,k}K(t,l,x,y,s,u,p,v)$$
$$= (-2su(p-1)(v-1))^{\,k}K(t,l,x,y,s,u,p,v)$$

Since, the operator $\Lambda^k_{t,l,x,y}\ K(t,l,x,y,s,u,p,v) = (-2su(p-1)(v-1))^{\,k}K(t,l,x,y,s,u,p,v)$ is obviously linear and continuous, we have

$$FM\{\Lambda^k_{t,l,x,y}\ K(t,l,x,y,s,u,p,v)\} =$$
$$\langle\Lambda^k_{t,l,x,y}\ f(t,l,x,y), K(t,l,x,y,s,u,p,v)\rangle$$
$$=$$
$$\langle f(t,l,x,y), \Lambda^k_{t,l,x,y}K(t,l,x,y,s,u,p,v)\rangle FM\{\Lambda^k_{t,l,x,y}\ K(t,l,x,y,s,u,p,v)\}$$
$$\langle f(t,l,x,y), (-2su(p-1)(v-1))^{\,k}\ K(t,l,x,y,s,u,p,v)\rangle$$

For all $f \in FM^*_{a,b,c,d,\alpha}$.

III. ADJOINT OPERATOR

We have define an operator $\Lambda^*_{tl.,x,y}: FM^*_{a,b,c,d,\alpha} \to FM_{a,b,c,d,\alpha}$ using the relation

$$\langle\Lambda^*_{t,l,x,y}\ f(t,l,x,y), \emptyset(t,l,x,y)\rangle =$$
$$\langle f(t,l,x,y), \Lambda_{t,l,x,y}\emptyset(t,l,x,y)\ \rangle$$

For all $f \in FM^*_{a,b,c,d,\alpha}$ and $\emptyset \in FM_{a,b,c,d,\alpha}$. The operator $\Lambda^*_{t,l,x,y}$ is called the adjoint operator of$\Lambda_{t,l,x,y}$.For each $k = 1,2,3, \ldots\ldots\ldots$ we can easily get-$\langle\left(\Lambda^*_{t,l,x,y}\right)^k f(t,l,x,y), \emptyset(t,l,x,y)\rangle =$
$\langle f(t,l,x,y), \Lambda^k_{t,l,x,y}\emptyset(t,l,x,y)\rangle$ It can be easily shown that if f is regular distribution generated by an element in$FM_{a,b,c,d,\alpha}$. Then,$\Lambda^*_{t,l,x,y}\ f = \Lambda_{t,l,x,y}\ f$,

For each $k = 1,2,3 \ldots\ldots\ldots$

We have-$\langle\left(\Lambda^*_{t,l,x,y}\right)^k f(t,l,x,y), K(t,l,x,y,s,u,p,v)\rangle =$
$\langle f(t,l,x,y), \Lambda^k_{t,l,x,y}K(t,l,x,y,s,u,p,v)\rangle =$
$\langle f(t,l,x,y), (-2su(p-1)(v-1))^{\,k}\ K(t,l,x,y,s,u,p,v)\rangle$
$= \langle f(t,l,x,y), (C_0)^{\,k}\ K(t,l,x,y,s,u,p,v)\ \rangle$
$\langle\left(\Lambda^*_{t,l,x,y}\right)^k f(t,l,x,y), K(t,l,x,y,s,u,p,v)\rangle =$
$(C_0)^{\,k}\ \langle f(t,l,x,y), K(t,l,x,y,s,u,p,v)\ \rangle FM\left\{\left(\Lambda^*_{t,l,x,y}\right)^k f(t,l,x,y)\right\}$
$(C_0)^{\,k}\ FM\{f(t,l,x,y)\}$ For all $f \in FM^*_{a,b,c,d,\alpha}$.

IV. AN APPLICATION OF THE TWO DIMENSIONAL FOURIER-MELLIN TRANSFORM TO DIFFERENTIAL EQUATION

4.1 SOLUTION OF $P\left(\Lambda^*_{t,l,x,y}\right)u(t,l,x,y) = f(t,l,x,y)$

Consider the Differential equation as

$$P\left(\Lambda^*_{t,l,x,y}\right)u(t,l,x,y) = f(t,l,x,y) \qquad (4.1.1)$$

Where, $f \in FM^*_{a,b,c,d,\alpha}$ and P is any polynomial of degree m. Suppose that the equation (4.1.1) possesses the solution$u$. Applying Two Dimensional Fourier-Mellin Transform to (4.1.1) we get-

$$FM\{P\left(\Lambda^*_{t,l,x,y}\right)u\} = FM\{f\}\ P(-2su(p-1)(v-1))FM\{u(t,l,x,y)\} = FM\{f(t,l,x,y)\}$$

{Since by using $\left\{\left(\Lambda^*_{t,l,x,y}\right)^k f(t,l,x,y)\right\} = [-2su(p-1)(v-1)]^{\,k}\ FM\{f(t,l,x,y)\}$

https://dx.doi.org/10.22161/ijaers/3.11.31 *ISSN: 2349-6495(P) | 2456-1908(O)*

$P(C_0)FM\{u\} = FM\{f\}$ (4.1.2)

If we further assume that the polynomial P is such that for $\in > 0$. $|P(C_0)| < \in \neq 0$

For $s > 0, u > 0, p > 0, v > 0$ (4.1.3)

Then under this assumption (4.1.2) gives-

$FM(u) = [P(-2su(p-1)(v-1))]^{-1} FM(f)$ (4.1.4)

Applying the inversion of Two Dimensional Fourier-Mellin Transform we get

$u = FM^{-1}\left\{\frac{FM(f)}{P[-2su(p-1)(v-1)]}\right\}$

$u = FM^{-1}\left\{\frac{FM(f)}{P(C_0)}\right\}$ (4.1.5)

4.2 SOLUTION OF DIFFERENTIAL EQUATION

$P\left(D_{t,l,x,y}\right)u(t,l,x,y) = f(t,l,x,y)$

Consider the differential equation

$P\left(D_{t,l,x,y}\right)u(t,l,x,y) = f(t,l,x,y)$ (4.2.1)

When $f \in FM^*_{a,b,c,d,\alpha}$ and

$P\left(D_{t,l,x,y}\right) = \sum_{\substack{|\alpha|\leq m \\ |\beta|\leq n \\ |\gamma|\leq m' \\ |\delta|\leq n'}} a_\alpha D_t^\alpha a_\beta D_l^\beta a_\gamma D_x^\gamma a_\delta D_y^\delta$ is a linear differential operator of order m, n, m', n' with constant coefficients $a_\alpha, a_\beta, a_\gamma, a_\delta$ respectively. Suppose that the equation (4.2.1) possesses a solution u. Applying Two Dimensional Fourier-Mellin Transform to (4.2.1) and using we get

$xy\ D_t^q D_l^h D_x^j D_y^g\ K(t,l,x,y,s,u,p,v) =$

$(-is)^q(-iu)^q(p-1)^j(v-1)^g e^{-i(st+ul)} x^{p-1} y^{v-1} =$

$(-is)^q(-iu)^q(p-1)^j(v-1)^g K(t,l,x,y,s,u,p,v) xy\ D_t^q D_l^h D_x^j D_y^g\ K(t,l,x,y,s,u,p,v) =$

$(-1)^{q+h}\ (is)^q(iu)^q(p-1)^j(v-1)^g K(t,l,x,y,s,u,p,v)$ We have,

$FM\{P\left(D_{t,l,x,y}\right)u(t,l,x,y)\} = FM\{f(t,l,x,y)\}$ (4.2.2)

We can reform them to the Two Dimensional Fourier-Mellin Transform and hence we get

$P[xy\ D_t^q D_l^h D_x^j D_y^g\ K(t,l,x,y,s,u,p,v)]\ FM(u) = FM(f)$ (4.2.3)

Under the assumption that the polynomial P is such that

$P[xy\ D_t^q D_l^h D_x^j D_y^g\ K(t,l,x,y,s,u,p,v)] < \epsilon$

for $\epsilon > 0 \in R^n$

Using (4.2.3)

$FM(u) =$

$P[xy\ D_t^q D_l^h D_x^j D_y^g\ K(t,l,x,y,s,u,p,v)]^{-1}\ FM(f)$Applying the inversion of Two Dimensional Fourier-Mellin Transform to above equation, we have

$$u = [FM]^{-1}\left\{\frac{FM(f)}{P[xy\ D_t^q D_l^h D_x^j D_y^g\ K(t,l,x,y,s,u,p,v)]}\right\}$$

V. CONCLUSION

In this paper we have given an application of Distributional Two Dimensional Fourier-Mellin transform to differential equation by introducing new operator of $\Lambda_{t,l,x,y}$ and its adjoint operator$\Lambda^*_{t,l,x,y}$.

REFERENCES

[1] Lokenath Debnath and Dambaru Bhatta, Integral Transforms and their Applications, Chapman and Hall/CRC Taylor and Francis Group Boca Raton London, New York, 2007.

[2] J. Berian James: The Integral Transform for you & me, Royal Observatory Edinburgh Institute for Astronomy, March 2008.

[3] Ronald N. Bracewell: The Fourier Transform and its Applications, Third Edition, McGraw-Hill International Edition, 2000.

[4] V.D. Sharma, P.D. Dolas: Inversion formula for Two Dimensional Generalized Fourier-Mellin Transform & its applications, Int. Jr. of Advanced Scientific and Technical Research, December 2011, Issue 1, Vol. 2.

[5] A. H. Zemanian, "Generalized integral t ransform," Inter science publisher, New York, 1968.

[6] A. H. Zemanian, "Distribut ion theory and t ransform analysis," McGraw Hill, New York, 1965.

[7] V.D. Sharma, P.D. Dolas: Convolution Theorem for Two Dimensional Fourier-Mellin Transform, International Journal of Research in Engineering and Applied Sciences, Vol. 6, Issue 3 (March, 2016).

[8] V.D. Sharma, P.D. Dolas: Representation Theorem For The Distributional Two Dimensional Fourier-Mellin Transform, International Journal of Mathematical Archive-5(9), 2014, 258-262.

[9] V.D. Sharma, A. N. Rangari: An application of Generalized Fourier-Finite Mellin Transform, International Journal of Innovative Research in Science, Engineering and Technology, Vol. 5, Issue 1, January 2016.

[10] V.D. Sharma, P.D. Dolas: Adjoint Operators of Two Dimensional Fourier-Mellin Transform, International Journal Of Pure And Applied Research In Engineering And Technology, 2016; Volume 4 (9): 64-70.

https://dx.doi.org/10.22161/ijaers/3.11.32 *ISSN: 2349-6495(P) | 2456-1908(O)*

Low Power Explicit Pulse Triggered Flip-Flop Design Based On A Pass Transistor

Amruta S. Vibhandik, Prof. P. V. Baviskar, Prof. K.N. Pawar

Abstract— *In VLSI system design, power consumption is the ambitious issue for the past respective years. Advanced IC fabrication technology grants the use of nano scaled devices, so the power dissipation becomes major problem in the designing of VLSI chips. In this paper we present, a low-power flip-flop (FF) design featuring an explicit type pulse-triggered structure and a modified true single phase clock latch based on a signal feed-through scheme using pass transistor. The offered design successfully figure out the long discharging path problem in conventional explicit type pulse-triggered FF (P-FF) designs and achieves better power performance by consuming low power. The proposed design also significantly reduces delay time, set-up time and hold time. Simulation results based on TMC 180nm CMOS technology reveal that the proposed design features the best power and delay performance in several FF designs under comparison.*

Keywords—Flip-Flop, low power consumption, pulse triggered, high-speed.

I. INTRODUCTION

Flipflops are the memory element of sequential circuit. Flip-flop are the basic storage elements that stores logical state of one or more input data signals in response to a clock pulse. They are fundamental building blocks of electronic system used extensively in all kinds of digital designs. Most digital designs nowadays often adopt intensive pipelining techniques and hire many flip-flop rich modules such as register file, shift register. Flip-flop is one of the most power consuming element in VLSI system. Generally it accounts 30%-60% of the total power dissipation in a system. So that it is necessary to work with such a flip-flop which consumes less power in overall system design [1], [2].

There are primarily two types of flip-flop. First one is the conventional flip-flop and another one is the pulse triggered flip-flop. Conventional flip-flop consist of two stages, one is the master and another one is slave. Master is activated when positive edge is triggered and slave is activated when negative edge is triggered. Conventional flip-flop such as master-slave flip-flop, sense amplifier based flip-flop are characterized by their hard edge property positive set-up time which causes. Large D-to-Q delay. On the other hand, Pulse-triggered FF (P-FF), because of its single-latch structure, is more popular than the conventional master–slave based FFs in high-speed applications. Besides the speed advantage, its simple circuitry is also beneficial to lowering the power consumption of the overall system. Pulse triggered flip-flop are characterized by their soft edge property negative set-up time which reduces D-to-Q delay. A P-FF which reduces two stages of conventional flip-flop into one stage, consists of a pulse generator for strobe signals and a latch for data storage. Since only one latch is needed, a P-FF is simpler in circuit complexity. This allows higher toggle rate for high-speed operations [3]–[8].

Depending on the method of pulse generation, pulse triggered flip-flop can be classified as implicit or explicit P-FF. In an implicit P-FF, the pulse generator is the part of the latch design and pulse signals are generate inside the flip-flop. In an explicit P-FF, pulse generator and latch are separate. Pulse signals are externally generate in the explicit P-FF. In this brief, we present a novel low-power explicit P-FF design based on a pass transistor. Observing the delay discrepancy in latching data “1” and “0,” the design reduces longer delay time by feeding the input signal directly to an internal node of the latch design to speed up the data transition. This is done by introducing a simple pass transistor for extra signal driving. When it is combined with the pulse generator, it forms a new P-FF design with increased speed performance Flip-flops are the memory element of sequential circuit. Flip-flop are the basic storage elements that stores logical state of one or more input data signals in response to a clock pulse. They are fundamental building blocks of electronic system used extensively in all kinds of digital designs. Most digital designs nowadays often adopt intensive pipelining techniques and employ many flip-flop rich modules such as register file, shift register. Flip-flop is one of the most power consuming element in VLSI system. Generally it accounts 30%-60% of the total power dissipation in a system. So that it is necessary to work with such a flip-flop which consumes less power in overall system design [1], [2].

II. LITERATURE SURVEY

H. Kawaguchi and Takayasu Sakurai worked on - A Reduced Clock-Swing Flip-Flop (RCSFF) for 63% Power Reduction [1] in May 1998. He proposed a reduced clock swing flip-flop (RCSFF) which is composed of a reduced swing clock driver with a special extra flip-flop which personifies current cut-off mechanism. The RCSFF can reduce one-third clock system power as compared to the other traditional flip-flops. This power improvement is obtained by reducing clock the swing down to 1V. Fabian

https://dx.doi.org/10.22161/ijaers/3.11.32 *ISSN: 2349-6495(P) | 2456-1908(O)*

Klass, Ashutosh Das and Gin Yee worked on - A New Family of Semi dynamic and Dynamic Flip-Flops with Embedded Logic for High-Performance Processors [2] in May 1999 to introduce a new family of semidynamic and dynamic edge triggered flip-flops which are compatible for high performance microprocessor design. James Tschanz, Siva Narendra, Vivek De, Zhanping Chen, Shekhar Borkar and Manoj Sachdev worked on - Comparative Delay and Energy of Single Edge-Triggered & Dual Edge-Triggered Pulsed Flip-Flops for High Performance Microprocessors [3] in May 2001. In this paper, different types of single edge-triggered flip flops, including static and semi dynamic along with both explicit as well as implicit pulse generation, are compared and studied. Bai-Sun Kong, Young-Hyun Jun and Sam-Soo Kim have worked on Conditional- Capture Flip-Flop (CDFF) for Statistical Power Reduction [4] in Aug 2001 to prove that the proposed design attains power reduction by eliminating redundant transitions of internal nodes. This paper provides the analysis of conventional high-performance flip-flops such as transmission-gate flip-flops (TGFFs), hybrid latch-flip-flops (HLFFs), semi-dynamic flip-flops (SDFFs), and sense amplifier-based flip-flops (SAFFs). The simulation results of this paper indicates that the proposed Conditional-Capture flip-flop achieves power savings up to 60% while the single-ended structure provides the power savings up to 69%, as compared to conventional flip-flops. Peiyi Zhao, Tarek K. Darwish has been worked on High-Performance and Low-Power Conditional Discharge (CDFF) Flip-Flop [5] in May 2004. In this paper, a modern conditional discharge flip-flop (CDFF) based on a conditional discharge technology is introduced. The offered CDFF not only reduces the internal switching activities of flip flops, but also generates less glitches at the output of flip flop, during maintaining the negative setup time and small to delay characteristics. With a data switching activity of 37%, the proposed conditional discharge flip flop can save up to 40% of the energy with the same speed that for the fastest pulsed flip-flops. Ying-Haw Shuu, Ming- Chang Sun, and Wu-Shhiung Feng, presents the paper XNOR-Based Double-Edge-Triggered Flip-Flop for Two-Phase Pipelines [6] in Feb 2006. In this paper a new designed DET-FF depending on an alternative XNOR gate is offered. Hamid Mahmmodi, Matthew Cooke, Vishy Tirumallashetty have proposed Ultra Low-Power Clocking Scheme Using Energy Recovery and Clock Gating [7]. This paper is introduced in Dec 2008. In this paper, four energy recovery clocked flip flops that are enable energy recovery from the clock network leading substantial energy savings, are introduced. The simulation results of the proposed flip-flop shows that a power reduces of 90% on the clock-tree and total power savings of up to 85% compared to the same implementation using the conventional square-wave clocking scheme and flip flops. Peiyi Zhaoo, and Zhoongfeng Wang worked on Design of Sequential Elements for Low Power Clocking System [8] in May 2011. With this proposed design the number of local clocked transistors can be effectively reduced to 40%. A 25% reduction of clock driving power has been attained. S.Esmaeilli, and Glenn E.R. Cowan workout A Low- Swing Differential Conditional Capturing Flip-Flop for LC Resonant Clock Distribution Networks [9] – This paper introduced in June 2012. Y.T. Hwang, J.F. Lin, and M.H. Sheu, go with Low power P-FF design with conditional pulse enhancement scheme [10] in Feb 2012. The maximum power saving of proposed FF is up to 40%. Majid Rahimi Nezhad, Mohsen Saneei presents the paper on Low-Power Pulsed Triggered Flip-Flop with New Explicit Pulse in 250-nm CMOS Technology [12]. Simulation outcomes of proposed flip-flop show that, for 50% data activity, power consumption is less than 7% to 30% lower than other flip-flops.

III. PROPOSED EXPLICIT P-FF DESIGN BASED ON A PASS TRANSISTOR

A. Conventional Explicit P-FF Designs

Generally implicit P-FFs are more power economical than explicit P-FF. Even so, they suffer from a longer discharging path inducing inferior timing characteristics. On the other hand, explicit pulse generation consumes more power than implicit pulse generation but the logic separation from the latch design establishes a unique speed advantage. Power consumption and the complexity of circuit of explicit flip-flop can be greatly brought down if one pulse generator is share a group of FFs (e.g., an *n*-bit register). In this paper, we are focusing explicit type P-FF designs only.

In this, we studied first some conventional explicit P-FF designs which are used as the reference designs in later performance comparisons.

1. EP-DCO- explicit Data closed to output Flip-Flop

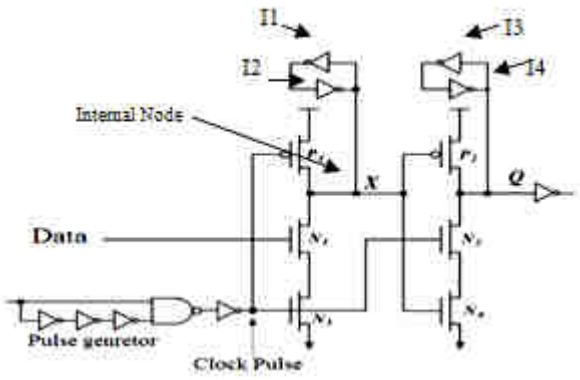

Fig.1: ep-DCO

Fig.1 shows data closed to output flip-flop design [7]. It consists of pulse generator of a three inverters connected to a NAND gate a semidynamic true-single-phase-clock (TSPC) structured latch design. In this explicit P-FF design,

https://dx.doi.org/10.22161/ijaers/3.11.32 *ISSN: 2349-6495(P) | 2456-1908(O)*

inverters I3 and I4 are used to latch data, and coupling circuit consisting inverters I1 and I2 used to hold the internal node *X*. Back-to-back end connected inverters i.e. I1 and I2 are act as a Keeper Logic. The delay of three inverters determines the pulse width of ep-DCO flip-flop. The serious drawback of ep-DCO P-FF is that in presence of static input '1', the internal node X is dropped off on every rising edge of the clock. This problem leads to large switching power dissipation. To get over this problem, some techniques such as conditional capture, conditional precharge, conditional discharge, and conditional pulse enhancement scheme have been proposed [4][7][9].

2. CDFF- conditional discharged flip-flop

Fig.2 shows a conditional discharged flip-flop design (CDFF) [4].To overcome the problem of continuous discharging of internal node X and large switching power dissipation in ep-DCO, CDFF is introduced.

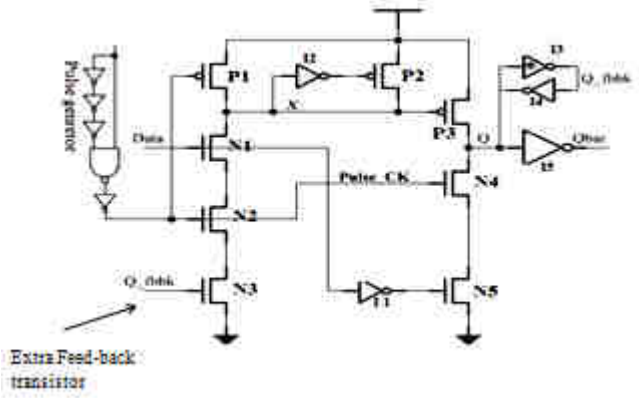

Fig.2: CDFF

In this, an extra n-MOS transistor MN3 controlled by the output signal Q-feedback is hired so that no discharge occurs at static input data "1." In addition, to simplify the circuit, the keeper logic at the internal node *X* is replaced with an inverter plus a pull-up p-MOS transistor only. But in CDFF, since discharging path consists of 3 stacked transistors MN1 to MN3, it face worst case delay. Therefore CDFF has longer data-to-Q (D-to-Q) delay.

3. MHLFF- modified hybrid latch flip-flop

Fig.3 shows modified hybrid latch flip-flop design. This is modified version of simple hybrid latch flip-flop. MHLFF uses static latch in which keeper logic at internal node X is removed. In this design, a weak pull-up transistor MP1 controlled by the output signal Q is used to maintain level of internal node X when Q equals to 0.

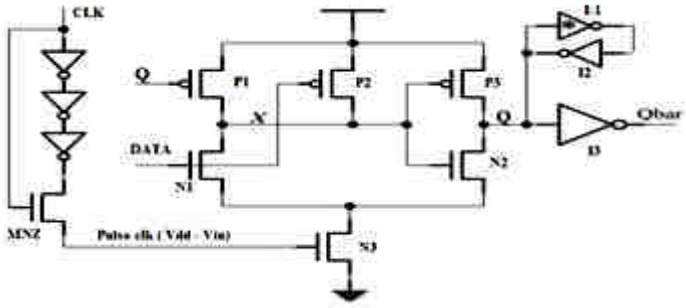

Fig.3: MHLFF

Though its circuitry is simple, it has two drawbacks. First one is it exhibits a longer D-to-Q delay during 0 to 1 transitions because node X is not pre-discharged. Another drawback of MHLFF is that node X becomes floating when output Q and input data both are equal to 1 and its value may drift causing excess DC power [6].

B. Proposed P-FF Design

Remembering the above four techniques, they all meet the same worst case timing occurring at 0 to 1 data transitions. The proposed design using a signal feed-through technique is introduced to improve this delay.

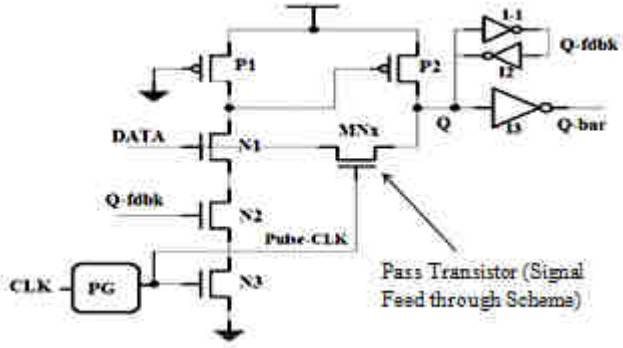

Fig.4: Proposed flip-flop

The proposed design acquires a static latch structure and a conditional discharge scheme to avoid surplus switching at an internal node X.

There are three major conflicts that makes the proposed design unique and distinct from the previous designs.

1. Addition of Pull-up pMOS transistor -

In proposed flip-flop, a weak pull-up pMOS transistor MP1 with gate connected to the ground is added in the first phase. This gives rise to a pseudo-nMOS logic style design. Pseudo nMOS transistor reduces number of devices and wiring complexity. The charge keeper circuit for the internal node can be saved due to the addition of pull-up pMOS transistor. With the circuit simplicity, this approach also keep down the load capacitance of node *X* [14], [15].

2. Pass Transistor MNx -

The extra component a pass transistor MNx controlled by the pulse clock is included in the proposed flip-flop design due to which input data can drive node Q of the latch

https://dx.doi.org/10.22161/ijaers/3.11.32 *ISSN: 2349-6495(P) | 2456-1908(O)*

directly (signal feed-through scheme). This pass transistor MNx provides a discharging path. The pass transistor MNx is thus played twofold role, i.e., providing extra driving to node Q during 0 to 1 data transitions, and discharging node Q during "1" to "0" data transitions. Since input data can be drive directly to output through pass transistor, it reduces data transition delay.

3. Removal of Pull-down network –

Third, the pull-down network of the second stage inverter is completely removed in the proposed flip-flop design. Hence circuit complexity and layout area of proposed design is reduced. This proposed design actually improves the "0" to "1" delay and thus reduces the disparity between the rise time and the fall time delays.

In proposed design, when a clock pulse gets in, if no data transition occurs, i.e., the input data and node Q are at the same level, current passes through the pass transistor MNx, which keeps the input stage of the FF from any driving effort. At the same time, the input data and the output feedback Q_fdbk are complementary signal levels and the pull-down path of node *X* is off. Consequently, it leads in no signal switching occurs in any internal nodes. When a "0" to "1" data transition occurs, node *X* is discharged to turn on transistor MP2, which then pulls node Q high. With the signal feedthrough scheme, a boost can be obtained from the input source through the pass transistor MNx and the delay can be greatly sawed-off. When a "1" to "0" data transition occurs, transistor MNx is also turned on by the clock pulse and node Q is discharged by the input stage through this route. Unlike the case of "0" to "1" data transition, the input source bears the sole discharging responsibility. The loading effect to the input source is not significant because MNx is turned on for only a short time slot.

IV. SIMULATION RESULT

The performance of the proposed P-FF design is done through post-layout simulations. The proposed designs is compared with three explicit type P-FF designs. A conventional CMOS NAND-logic-based pulse generator design with a three-stage inverter chain is used for all P-FF designs except the MHLFF design, which employs its own pulse generation circuitry.

Table.1: Comparison Table

Type of Explicit Flip-Flop	Average power Dissipation (µW)	D-to-Q Delay (pSec)	No. of Transistors	Set-up Time (nSec)	Hold Time (nSec)
EPDCO	17.43	128.83	24	-0.0014	5
CDFF	16.83	121.32	26	10.13	20
MHLFF	17.92	156.30	19	0.167	10.1
Proposed FF	**14.57**	**111.67**	**20**	**0.10**	**0.131**

The target technology is the TSMC 180-nm CMOS process. Since pulse width design is essential to the correctness of data capture as well as the power consumption [10]–[13], the transistors of the pulse generator logic are sized for a design spec of 120 ps in pulse width in the TT case. The sizing also assures that the pulse generators can function properly in all process corners. With regard the latch structures, each P-FF design is individually optimized subject to the product of power and D-to-Q delay i.e. input to output delay. To mimic the signal rise and fall time delays, input signals are generated through buffers. Since the proposed design using signal feed through scheme requires direct output driving from the input source, for fair comparisons the power consumption of the data input buffer (an inverter) is included. The operating condition used in simulations is 500 MHz/1.8 V. The comparison is done regarding power consumption, delay, set-up time and hold time of the system.

A. Power Consumption of Flip-Flop Design

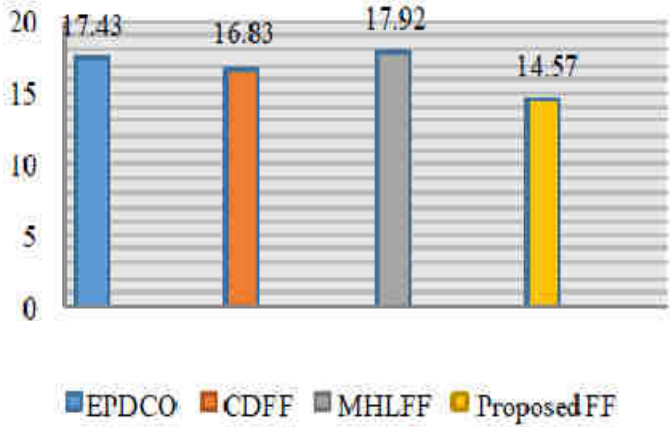

Graph.1: Average Power Calculation of Diff. Flip-Flop in Micro Watt

Since the proposed design uses less number of transistors, it has the smallest layout area. This is mainly because of the signal feed-through scheme, which largely reduces the transistor sizes on the discharging path. In terms of power behavior, the proposed design is the most efficient than the existing flip-flop designs. The given figure shows graphical representation of average power calculation of different flip-flops in microwatt.

B. Timing Parameters of Flip-Flop Design

https://dx.doi.org/10.22161/ijaers/3.11.32 *ISSN: 2349-6495(P) | 2456-1908(O)*

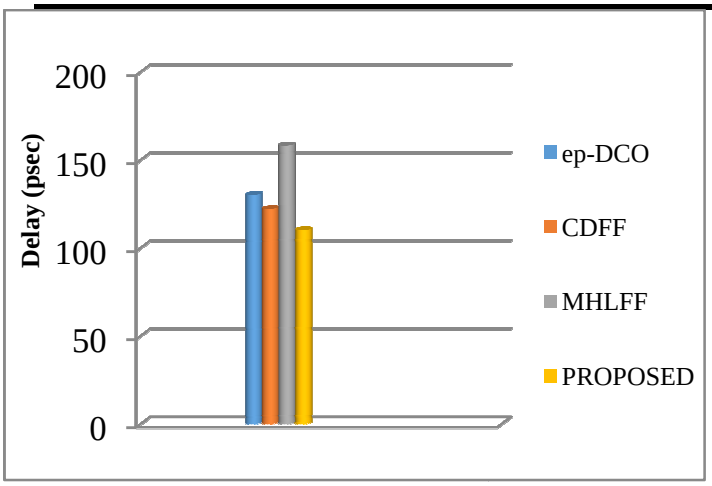

Graph.2: Delay Calculation of Diff. Flip-Flop in picoSec

After the analysis of power performances, we then examine the timing parameters of these FF designs. In order to function correctly, the edge triggered flip-flop requires the input to be stable for some time before the clock's active edge. This period is the set-up time. Given a sufficient setup time, the hold time is measured. Flip-flop design requires the state of the input to be held for some time after the clock edge. The time after the clock edge that the input has to remain stable is called hold time. In terms of set-up time and hold time, the proposed design is the most efficient than the existing flip-flop designs.

V. CONCLUSION

In this Paper, the several Flip flop designs like ep-DCO, CDFF, MHLLF & Proposed new P-FF are discussed. In this brief, we have presented a novel P-FF design by applying a modified TSPC latch structure integrating a mixed design significant style consisting of a pass transistor with p-seudo-nMOS logic. The key idea has been to provide a signal feed scheme through from input source to the internal node of the latch, which would be reduces the extra transition time and enhance both power and speed performance of flip flop. Extensive simulations have been conducted which supports the claim of the proposed design in various performance aspects. Simulation results indicate that proposed flip-flop design improves power performance and significantly reduces D to Q delay, set-up time and hold time.

REFERENCES

[1] H. Kawaguchi and T. Sakurai, ―A reduced clock-swing flip-flop (RCSFF) or 63% power reduction, *IEEE JSolid-State Circuits*, vol.33, no.5, pp.807, May 1998.

[2] F. Klass, C. Amir, A. Das, K. Aingaran, C. Truong, R.Wang, A. Mehta, R. Heald, and G. Yee, ―A new family of semidynamic and dynamic flip-flops with embedded logic for high-performance processors, *IEEE J. Solid-State Circuits*, vol. 34, no. 5, pp. 712–716, May 1999.

[3] J.Tschanz S. Narendra,, Chen, S. Borkar, M. Sachdev ―Comparative delay and energy of single edge-triggered and dual edge triggered P-FF for high-performance microprocessors, in *Proc. ISPLED*, 2001, pp.207–212.

[4] B. Kong, S. Kim, and Y. Jun, ―Conditional-capture flip-flop for statistical power reduction, *IEEE J. Solid-State Circuits*, vol. 36, pp. 1263–1271, Aug. 2001.

[5] P. Zhao, T. Darwish, and M. Bayoumi, ―High-performance and low power conditional discharge flip-flop, *IEEE Trans. Very Large Scale Integr. (VLSI) Syst.*, vol. 12, no. 5, pp. 477–484, May 2004.

[6] Y.-H. Shu, S. Tenqchen, M.-C. Sun, and W.-S. Feng, ―XNOR-based double- edge-triggered flip-flop for two-phase pipelines, *IEEE Trans. Circuits Syst. II, Exp. Briefs*, vol. 53, no. 2, pp. 138–142, Feb 2006.

[7] H. Mahmoodi, V. Tirumalashetty, M. Cooke, and K. Roy, ―Ultra low power clocking scheme using energy recovery and clock gating, *IEEE Trans. Very Large Scale Integr. (VLSI) Syst.*, vol. 17, pp. 33–44, Jan 2009.

[8] P. Zhao, J. McNeely, W. Kaung, N. Wang, and Z. Wang, ―Design of sequential elements for low power clocking system, *IEEE Trans. Very Large Scale Integr. (VLSI) Syst.*, to be published.

[9] Seyed E. Esmaeili, Asim J. Al-Kahlili, and Glenn E. R. Cowan worked on ―Low-Swing Differential Conditional Capturing Flip-Flop for LC Resonant Clock Distribution Networks *IEEE Trans. Very Large Scale Integr. (VLSI) Syst.*, vol. 20, no. 8, August 2012.

[10] Y.T. Hwang, J.F. Lin, and M.H. Sheu, ―Low power pulse triggered flip-flop design with conditional pulse enhancement scheme, *IEEE Trans. Very Large Scale Integration. (VLSI) Syst.*, vol. 20, no. 2, pp. 361–366, Feb. 2012.

[11] K. Chen, ―A 77% energy saving 22-transistor single phase clocking D flip-flop with adoptive-coupling configuration in 40 nm CMOS, in Proc. IEEE Int. Solid-State Circuits Conf., Nov. 2011, pp. 338–339.

[12] Majid Rahimi Nezhad, ―Low-Power Pulsed Triggered Flip-Flop with New Explicit Pulse in 250-nm CMOS Technology in Proc. IEEE Int. Solid-State Circuits Conf., Feb.2011-2012, pp. 688–693.

[13] H. Partovi, R. Burd, U. Salim, F.Weber, L. DiGregorio, and D. Draper, ―Flow-through latch and edge-triggered flip-flop hybrid elements, Sin Proc. IEEE Int. Solid-State Circuits Conf., Feb. 1996,pp. 138–139.

[14] M. Alioto, E. Consoli, and G. Palumbo, ―Analysis and comparison in the energy-delay-area domain of nanometer CMOS flip-flops: Part I - methodology and design strategies, *IEEE Trans. Very Large Scale Integr. (VLSI) Syst.*, vol. 19, no. 5, pp. 725–736, May 2011.

https://dx.doi.org/10.22161/ijaers/3.11.32 *ISSN: 2349-6495(P) | 2456-1908(O)*

[15] M. Alioto, E. Consoli and G. Palumbo, ― Analysis and comparison in the energy-delay-area domain of nanometer CMOS flip-flops: Part II - results and figures of merit, *IEEE Trans. Very Large Scale Integr. (VLSI) Syst.*, vol. 19, no. 5, pp. 737–750, May 2011.

Amruta Vibhandik is Post-Graduate student in the Department of Electronics Engineering at S.S.V.P.S. College of Engineering Dhule.

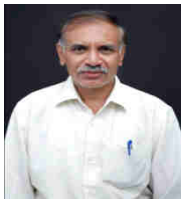

Prof. **P. V. Baviskar** is presently working as Associate Professor in the Department of Electronics Engineering at S.S.V.P.S. College of Engineering Dhule. He has 26 yrs. of teaching experience in the academic field.

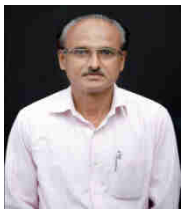

Prof. **K. N. Pawar** is presently working as Associate Professor and Head of the Department of Electronics Engineering at S.S.V.P.S. College of Engineering Dhule. He has 32 yrs. of teaching experience in the academic field.

https://dx.doi.org/10.22161/ijaers/3.11.33 ISSN: 2349-6495(P) | 2456-1908(O)

Designing and Manufacturing of Bamboo Processing Machine

Kalayu Mekonen Abate, Mohammed Irfaan

Lecturer, Department of Mechanical Engineering, Adigrat University, Ethiopia

Abstract— *This document describes about designing and manufacturing of bamboo processing machine having three functions, namely; splitting, grinding and sanding bamboo surfaces. It helps to avoid a tedious and time taking manual bamboo processing. Three people can work at the same time when a need arise. It is designed considering safety factors and ergonomic considerations. The machine is robust in design having low sound, and good aesthetic so as to look attractive and durable while giving service. Designing and fabricating such type of machine is important so as to save money and it avoids from buying individual machine.*

For the purpose of convenience, focusing on the need assessment of the project, developers are using exploratory research method. Exploratory research made by conducting focus group interviews to get detail information. Developers used four data gathering techniques (tools), namely; oral questions, direct observation, document analysis and questionnaires (closed and open questionnaires) to understand current problems of bamboo processing activities and for the need of this machine.

After the quantitative and qualitative data are gathered from those sources developersreached at conclusion to designed and manufactured bamboo processing machine as a solution to facilitate bamboo products. The findings indicate that, there is lack of bamboo processing machine and having high demand of it.

In general, according to the newly designed and manufactured bamboo processing machine, it can perform manual splitting, grinding bamboo knots and sanding bamboo surfaces. For the future it can create job opportunity to the society.

Keywords—Designing, Manufacturing, bamboo processing, splitting and grinding knots, all cost are in Birr (Ethiopian currency).

I. INTRODUCTION

1.1 Background

Machinery from various sources has become operational in recent years for the primary processing of bamboo by bamboo processing machine (BPM). The main requirement is for an optimal configuration of machinery with adequate performance and productivity in a cost effective manner to process bamboo culms to slivers and slats for different applications.

In Ethiopia, from time to time forests are destructing in rural areas, if this continuous in the same manner; there will be change to bad weather conditions. Even though forests are declining, on the other hand, our country has good bamboo substituting resources, so it is better to use bamboo substituting wood forests. Bamboo is a renewable plant belonging to grass and its growing rate is faster than wood. Now a day's our government also focused on bamboo plants and initiating investors to invest in the area to process bamboo for different uses, this project will contribute significant role for the improvement of bamboo products since wood lumber is expensive and also forests are declining, many SMEs emerge to use bamboo for different furniture makings. Thus, this Bamboo Processing Machine will help them for facilitating and improving their productivity.

The International Network for Bamboo develops, provides and promote appropriate technologies and other solutions to benefit people and the environment [1].

Bamboo is one of the oldest building materials used by mankind the bamboo Culm, or stem, has been made into an extended diversity of products ranging from domestic household products to industrial applications. Examples of bamboo products are food containers, skewers, chopsticks, handicrafts, toys, furniture, flooring, pulp and paper, boats, charcoal, musical instruments and weapons [2].

In Asia, bamboo is quite common for bridges, scaffolding and housing, but it is usually a temporary exterior structural material. In many overly populated regions of the tropics, certain bamboos supply the one suitable material that is sufficiently cheap and plentiful to meet the extensive need for economical housing. Bamboo shoots are an important source of food, and a delicacy in Asia. In addition to its more common applications, bamboo has other uses, from skyscraper scaffolding and phonograph needles to slide rules, skins of airplanes, and diesel fuels [3]. Extractives from various parts of the plant have been used for hair and skin ointment, medicine for asthma, eyewash, potions for lovers and poison for rivals. Bamboo

https://dx.doi.org/10.22161/ijaers/3.11.33 ISSN: 2349-6495(P) | 2456-1908(O)

ashes are used to polish jewels and manufacture electrical batteries. It has been used in bicycles, dirigibles, windmills, scales, retaining walls, ropes, cables and filament in the first light bulb. Indeed, bamboo has many applications beyond imagination. Its uses are broad and plentiful. With the advancement of science and technology and the tight supply of timber, new methods are needed for the processing of bamboo to make it more durable and more usable in terms of building materials. Studies have been done on the basic properties, and processing bamboo into various kinds of composite products. More studies are needed to aid and promote its application in the modern world.

Machinery from various sources has become operational in recent years for the primary processing of bamboo. The base requirement is for an optimal configuration of machinery with adequate performance and productivity in a cost effective manner to process bamboo culms to slivers and slats for different applications [5].

1.1.1 Processing Characteristics of Bamboo

Because of the special structure of bamboo, the processing and utilization methods for bamboo plants have their own characteristics that are different with woody plants. They are as follows:

(1) Bamboo stems are small in diameter, hollow inside, thin in wall, large in taper, and different in component between inner, middle and outer layers. The diameter of most of Phyllostachyspubescent, which is larger in diameter among bamboo plants, ranges from 70 mm to 100 mm with average wall thickness less than 10 mm. A few of bamboo species are small in diameter ranging from 30 mm to 50 mm with mean wall thickness 4 – 6 mm. (2) Most of bamboo products can be manufactured with machines, but a few procedures or products can't avoid of handwork.

Consequently, the production rate of bamboo industry is several times even ten times less than that of wood industry.

(3) Because the outer skin and inner players of a bamboo Culm can't be wetted by adhesive, the very portion that can be used is mainly the middle portion of bamboo wall. So the utilization percent of bamboo is much lower, ranging from 20% to 50% of volume or weight.

(4) Bamboo is difficult to be dealt like wood, which can be manufactured into boards or blocks of large size. It is usually machined into strips of 20 mm to 30 mm wide by 5 mm to 8 mm thick that can't be used directly.

(5) The difference, not only in structure but also in chemical composition, between bamboo and wood is obvious because bamboo contains much more nutrition substances such as hemicelluloses, starch, protein, sugar etc. As a result, bamboo products have lower resistance against insects and fungi.

1.1.2 Importance of Bamboo in Ethiopia

Although bamboo is not an integral part of the economy of Ethiopia, it plays a very important role socially, economically and ecologically in areas where it occurs naturally and where it is planted. Both the highland and lowland bamboos are such a versatile type of resources that they can be used in many ways. Their paramount importance and multifaceted use in different parts of the country are reported.

Bamboo is the main material for the construction of houses, animal sheds, fences and beehives at Asossa Zone and in different parts of Ethiopia [6, 7]. In the case of towns, some people are using bamboo's furniture due to less cost than wood products. Some people are producing bamboo furniture for their source of income. Even though, using bamboo products are increasing time to time in Ethiopia, quality of bamboo product's surface finish is poor being manual worked. The researchers initiated to design and fabricate this bamboo processing machine in order to solve the existing problem of poor quality bamboo products.

1.2 Statement of the problem

Processing bamboo is a tedious, manual task or Bamboo processing by hand is a time consuming and difficult process. Using a short local machete (heavy knife), workers in Ethiopia hack away the protruding nodes of the bamboo, and rub the silica away with rough hand tools. However, their imprecise and irregular methods are crude and extremely time-consuming. The surface of bamboo is naturally coated with protective silica, giving it its sheen (shine). The silica must also be filed away in order to prepare its surface for texturing and for receiving paint. .

The main problems are poor quality surface finish of bamboo and the exhausting manual task of bamboo processing activities.

1.3 Objective

1.3.1 General Objectives

The general objective of this project is:

- To design and manufacture bamboo processing machine that can manual splitting, bamboo knot, grinding and polishing bamboo surfaces.

1.3.2 Specific Objectives

The following are the specific objectives of the project:

- To design machine elements.
- To design and manufacture bamboo splitter.
- To fabricate different machine parts like shaft, pulley, and the like.
- To reduce cost by using local available materials. It is beneficial being creating local market.
- To adapt technology.
- To transfer technology to SMEs.
- To develop designing and manufacturing skills.
- To manufacture from locally available materials.

https://dx.doi.org/10.22161/ijaers/3.11.33 *ISSN: 2349-6495(P) | 2456-1908(O)*

- To substitute other import bamboo machines. This is beneficial to save foreign exchange currency.

II. METHODOLOGY

2.1 Material

For the purpose of convenience, focusing on the need assessment of the project, developers are using exploratory research method. Exploratory research might involve a literature search or conducting focus group interviews. The exploration of new phenomena can help the researcher's need for better understanding and test the feasibility of a more extensive study, or determine the best methods to be used in a subsequent study. For these reasons, exploratory research is broad in focus and provides definite answers to specific research issues. The objective of exploratory research is to identify key issues and key variables. Developers used four data gathering techniques to understand current problems of bamboo processing and for the need of this machine; the researchers collected data by interviewing, direct observation, document analysis and questionnaires (closed and open questionnaires). The interview will be from different private sectors and customers. The documents which are analyzed for the project are internet, and many types of reports and researches about bamboo processing machine.

After the quantitative and qualitative data are gathered from those sources developers designed and manufactured bamboo processing machine as a solution to facilitate bamboo products and to avoid exhausting and time consuming of grinding or polishing activities.

2.2 Target Groups

The target group is, for those who are working directly on bamboo furniture for unskilled, semi-skilled and technically trained persons and who will be worked on bamboo furniture makings.

2.3 Sample and Sampling Technique

Sampling involves selecting relatively small number of elements from the large defined group of elements and expecting that the information gathered from small group allow generalization to be made about the larger group of population. (Research method for construction 3rd edition)

The sampling units are the defined target population elements available for selection during the sampling process. In this research, Adama Town bamboo furniture workers are selected purposely as the total population since the result can be considered for the whole bamboo workers in the country.

A total of 20 numbers of bamboo workers are selected from the population of 40 number of bamboo workers including SMEs at Adama Town that are currently working in the field of bamboo furniture makings.

The reason why Adama Town is selected for this study is because the town is near to the university and due to limited budget; the researchers couldn't include other places. The sampling is selected by using systematic random sampling method. The sample ratio can give sufficient information because it is taken 50% out of total population.

III. DESIGN ASPECTS

3.1 General Considerations in Machine Design

- Type of load and stresses caused by the load.
- Motion of the parts or kinematics of the machine.
- Selection of materials.
- Form and size of the parts and
- Use of standard parts and safety operations, etc.

This newly designs of bamboo processing machine focus on three functions that can grind, polish and manual splitting of bamboo. Starting from the idea of design principles and functional requirements the researchers designed the parts of the machine based on the design procedures.

3.2 Designing Power

There are two types of electrical motors, namely alternative current motor (AC) and direct current (DC). Developers selected AC motor for bamboo processing machine having 220 to 380V considering functional requirements and the availability of Ethiopian Electrical power so as to get more energy and to work for 8 hours continuously.

The power is designed based on the required functions by referring wood work machines and estimating the required force for operating grinding and polishing of bamboo and it is calculated based on the following steps using standard table of (ISO V belt products of Goodyear). The power selected for this project is 1.5Kw.

a. Determine appropriate service factor

A belt drive is designed based on the design power, which is the modified required power. The modification factor is called the service factor. The service factor depends on hours of running, type of shock load expected and nature of duty.

Proper service is determined based on intermittent, normal or continuous services, from standard table. The service factor, 1.2 is selected (Engineering data for v-belts and wedge belts) for normal service, i.e., daily service 6 to 16 hours.

b. Multiply the Absorbed Power by the service factor to get Design Power.

Required motor power = 1.5kw (by referring other related machines, E.g. Wood machines)

Service factor = 1.2

Design power = 1.2 x 1.5

= 1.8 kW but from standard table of V belt products 1.90 Kw is selected.

https://dx.doi.org/10.22161/ijaers/3.11.33 *ISSN: 2349-6495(P) | 2456-1908(O)*

Table.3.1: SPZ section – drives selections, drive speeds and kilowatts per belt (From power transmission products of hand book)

Speed ratio	Pulley datum diameters in mm		Driver 1440 rev/min		E in Kw
	Driver, R	Driven, N	Driven in rev/min	MC in	Kw
1.33	**75**	**100**	**1084**	**1.90**	**1.60**
2.06	60	125	698	1.27	0.95
2.07	63	132	694	1.41	1.09
2.07	67	140	696	1.58	1.27
2.08	56	118	691	1.10	0.77
2.08	170	355	692	5.83	5.57
2.09	71	150	688	1.76	1.45

IV. DESIGN OF SHAFT

Shaft is a basic, important and very common machine element. It is a rotating member used for the transmission of power. It is designed to perform a specific task in this machine. A pulley is mounted on it to receive motion from motor through belt and then the shaft rotates. This rotational movement of shaft performs grinding and polishing activities of bamboo.

4.1 Material Selection for the Shaft

Most shafts are made from steel, either low- or medium-carbon. However, high quality alloy steel, usually heat treated, may be chosen for critical applications. Other metals, e.g. brass, stainless steel or aluminium, may be used where corrosion is a problem or lightness is required.

4.2 Functional Requirements of the Shaft

The main function of shaft is to transmit power. Since the shaft is subjected to high torque, it may be bent. Therefore, the shaft must be strong, wear resistant, tough and ductile.

4.3 Material's Priorities Requirement of the Shaft

To satisfy the functional requirement of shaft, the material should be chosen require the following:

- ✓ The material should have better yield strength and tensile strength.
- ✓ The material to be selected requires higher young modules value.
- ✓ Should be tough enough, machine able and light in weight.

To select the material for the shaft, the following candidate materials are listed:

- ❖ Annealed SAE 1020
- ❖ SAE 1010
- ❖ W-100 of SAE 1045
- ❖ SAE 1040

Table.4.1: Application of digital logic method (Machine Design)

Property	Decision No.									
	1	2	3	4	5	6	7	8	9	10
Density	1	1	1	1						
Modules of elasticity	0				1	1	1			
Toughness		0			0			1		
Tensile strength			0			0			1	
Yield strength				0			0		0	1

Table.4.2: weight factor for the shaft (Machine Design)

Property	Positive decision	Weight factor
Density	4	0.4
Modules of elasticity	3	0.3
Toughness	1	0.1
Tensile strength	1	0.1
Total	10	1.0

https://dx.doi.org/10.22161/ijaers/3.11.33 ISSN: 2349-6495(P) | 2456-1908(O)

Table.4.3: Candidate material for shaft (A Text of Machine Design)

Material	Density kg/m^3	Modules of Elasticity (Mpa)	Toughness (Mpa)	Tensile strength (Mpa)	Yield strength (Mpa)
Annelid SAE 1020	7680	207	25	380	207
SAE 1010	7680	207	28	325	180
W-1000 of SAE 1045	7680	207	8	825	614
SAE 1040	7680	207	33	621	414

Table.4.4: Decision matrix for shaft (Machine Design)

Material	Density kg/m^3	Modules of Elasticity (MPa)	Toughness (MPa)	Ultimate Tensile strength (MPa)	Yield strength (MPa)
Annelid SAE 1020	7680	207	25	380	207
SAE 1010	7680	207	28	325	180
W-1000 of SAE 1045	7680	207	8	825	614
SAE 1040	7680	207	33	621	414

Table.4.5: Normalized outcome for shaft (Machine Design)

Material	Density kg/m^3	Modules of Elasticity (Mpa)	Toughness (Mpa)	Ultimate Tensile strength (Mpa)	Yield strength (Mpa)
Annelid SAE 1020	100	100	75.75	45.9	33.7
SAE 1010	100	100	84.85	39.25	29.3
W-1000 of SAE 1045	100	100	24	100	100

Table.4. 6: value outcome (Machine Design)

Material	Density X0.4	Modules of Elasticity X0.3	Toughness X0.1	Ultimate Tensile strength X0.1	Yield strength X0.1
Annelid SAE 1020	40	30	7.575	4.59	3.37
SAE 1010	40	30	8.485	3.925	2.93
W-1000 of SAE 1045	40	30	2.4	10	10
SAE 1040	40	30	10	7.5	6.74

Table.4.7: Overall satisfaction (Machine Design)

Annelid SAE 1020	85.535
SAE 1010	85.34
W-1000 of SAE 1045	92.4
SAE 1040	94.24

https://dx.doi.org/10.22161/ijaers/3.11.33 *ISSN: 2349-6495(P) | 2456-1908(O)*

The result should shows that on the bases of allocated weighting factor SAE 1040 gives the highest overall satisfaction among these materials. Therefore, this material is preferable for the production shaft (suitable material selected for the shaft is SAE 1040 for designing).

V. COST ANALYSIS

5.1Theory of Economic Consideration

It is important that the designer develops skills in estimating costs of designs in order to secure the most economic features. This entails being aware of the breakdown of products costs and the various cost stages that exists in an organization. These have to be broken down in to individual units to calculate the overall cost of the product. For most purposes of calculating costs however, it would be extremely difficult and time consuming to put together these individual costs which are:-

- Material cost
- Labor cost
- Overhead cost

Material costs plus labour costs in unit cost of manufacture; the overhead cost is the cost of preparation of the component.

5.2 Economics of Design

The following considerations high lights some of the methods by which thoughtful design may reduce the overall product least.

- Economic choice of production technique
- Economic choice of material
- Economic choice of design form
- Avoiding material wastage
- Avoiding excessive machining and close tolerance
- Consideration for size and product
- Efficient use of standard components and bought-items.
- Designing to aid packaging
- Using computer-aided techniques.

Design and manufacture a product according to a certain specification by minimizing total cost and maximizing efficiency of the product or machine to meet service requirements is only one aspect of production. Since economics is one of the most important aspects of any manufacturing operation, So that the product successfully marked and the cost must be competitive with similar products in the market place. Based on these the design and manufacture of certain bamboo processing machine analysis should be done in order to be competitive. The cost minimizing and maximizing efficiency of product or machine is the main objective of our project. In this project the total cost consists of material cost, tooling cost, labour cost, fixed cost and capital cost.

5.2.1 Labour Cost

According to the information obtained from different machine shops that are available at Adama city, a single beginner machinist is paid at least about 1400 birr per month. Assuming that developers each paid **5.8** birr/hr.

Table.5.1: Labor cost

Duties	No. of people engage	Total time	cost
Cutting aluminum ingot ϕ100mm, ϕ75mm using power hack saw	1	1/4 hr	1.45birr
machining Pulley ϕ100mm *60mm using lathe machine	1	3hrs	17.4birr
machining Pulley ϕ75mm *40mm using lathe machine	1	3hrs	17.4birr
Cutting round bar for shaft ϕ30 using power hack saw	1	¼ hr	1.45birr
Machining round bar for shaft ϕ30mm using lathe machine	1	5hrs	29 birr
Cutting angle iron for table	1	1.5 hrs	8.7 birr
welding angle iron for table	2	3hrs	34.8 birr
Thread making for end shaft	1	3hrs	17.4birr
Lay out & making hole for motor seating and bearing- house seating	2	1hr	11.6 birr
Cutting round road rollers using power hack aw	1	1hr	5.8 birr
Machining round road rollers	2	2hrs	23.2 birr
Making blades (splitters)	2	8hrs	92.8 birr
Tensioner for sand belt	4	2hrs	46.4 birr

https://dx.doi.org/10.22161/ijaers/3.11.33 *ISSN: 2349-6495(P) | 2456-1908(O)*

Total	**33 hrs**	**307.4birr**

5.2.2 Material cost

Material cost: - material cost consumes in order to produce each part is composed of different areas each component with these materials cost is listed as follows. Note that in this case it is roughly calculated value of each component. Since the detail is time taking and too much to show each calculation.

Table.5.2: Material cost (From current Adama town market price)

No	Item	Specification	Amount		Unit price (birr)	Total cost (birr)
			Unit	Quantity		
1	Sheet metal	1000 x 2000X1.5	Pcs	01	900	900
2	Aluminium ingot	Φ100mmx500mm	pcs	01	4000	4000
3	Aluminium ingot	Φ75mmx500mm	Pcs	01	3000	3000
4	Screws	Φ4mm	pkt	01	75	75
7	Paint brush	2 ½ inch	pcs	02	15	30
8	Wood Sand paper	Coarse	meter	04	20	80
9	Anti-rust	Grey	litter	01	68	68
10	Mild steel Round bar	Φ40x700mm	pcs	01	600	600
11	Chip wood	122*244*8mm	pcs	01	120	120
12	Electrode	E6013,Φ2.5	pkt	01	150	150
13	Drill bit	Φ4mm	pcs	06	08	48
14	Drill bit	Φ5mm	pcs	04	08	32
15	Drill bit	Φ6mm	pcs	02	08	16
16	Drill bit	Φ7mm	pcs	02	15	30
17	Drill bit	Φ8mm	pcs	02	15	30
20	grinding disc	180x22x6	pcs	02	32	64
21	Sheet metal	1700x620*4mm	pcs	01	2000	312
22	cutting disk	180x22x3	pcs	05	28	140
24	Glue	Tiger	Lit	01	80	80
25	hack saw blade	Sweden	pcs	04	25	100
27	Angle iron	40 x 40 x 3mm	pcs	01	300	300
28	Flat iron	40*4*6000	pcs	02	300	600
					Total cost	**10,175** ETB

5.2.3 Operation Cost

It is composed of handling, machining, and tool changing and tooling cost, handling time in minute to load and unload the work piece obtained from time table.

Start and stop ----------0.08min
Change speed----------0.04min
Engage speed----------0.05min
Inspect dimension with micrometre----------0.30min
Clean the machine----------0.50min
Load and unload----------0.40min

Total = 1.1 min

Let the cost for 60 min = 5 .8 birr, therefore,
Handling cost = 1.1*5.8/60 = **1.06** birr per min.

https://dx.doi.org/10.22161/ijaers/3.11.33 *ISSN: 2349-6495(P) | 2456-1908(O)*

5.2.4 Cost of Standard Materials

The cost of standard materials according to current market price, here are listed below in the following table.

Table.5.3: Cost of standard materials(From current market of price Adama town)

No.	Item	Specification	Unit	Quantity	Unit cost		Total cost	
					Birr	Cent	Birr	Cent
1	Bolt and nut	M6	Pc	6	3	50	21	00
2	Bolt and nut	M8	Pc	14	3	00	42	00
3	Bolt and nut	M10	Pc	4	4	00	16	00
4	Bolt and nut	M12	Pc	16	5	oo	80	00
5	Bolt and nut	M16	Pc	2	7	00	14	00
6	Bush Bearing	Dia. 30 mm	Pc	2	350	00	700	00
7	Ball Bearing	Dia. 25 mm	Pc	2	70	00	140	00
8	Electrode	Dia.2.5	Pack	1	120	00	120	00
9	Grinding disc	5 x 180	Pc	2	75	00	150	00
10	Cutting disc	3 x 180	Pc	1	75	00	75	00
11	Breaker	16A	PC	1	80	00	80	80
12	Cable	2.5 x 3	Meter	3	45	00	135	00
13	V belt	A 1425	PC	1	34	00	34	00
						Total	**1607.00**	

Standard material cost----------1607 birr
Total material cost----------10175 birr
Total operation cost----------1.06 birr
Total labor cost----------307.4 birr

Total = **12,090.46** birr

5.2.5 Fixed Cost

Fixed cost is the money that is paid for administration works.

Fixed cost is about ten percent of the sum of material costs and labour cost.

Material cost = 10175 birr and labour cost = 307.4 birr.

The sum of material cost and labour cost is 10482.4birr and fixed cost is 10% of these costs, i.e., Fixed cost = (10482.4*10) / 100 = **1048.24 birr**

5.2.6 Machine Depreciation

Many assets like machinery and equipment have a limited life span and even if that life span is many years, the asset will eventually reach the end of the life. Over the courses of machine's life span, it gradually decreases value and approaches its bottom end value as it becomes worn out or out dated. The percentage of the machine worn out each year is referred to as machine depreciation.

Machine depreciation cost is the cost of oil, grease and simple maintenance etc. This is estimated 20% of the fixed cost that is equal to **209.65** birr.

Total production cost (T_p)

T_p = material cost + Labour cost + Fixed cost + Cost of machine depreciation + standard material cost and tooling cost.

= 10,175 birr + 307.4 birr +**1048.24** birr + **104.824** birr +1607 birr

T_p =**13,242.46 birr**. This cost is good according to the current market price.

VI. CONCLUSION AND RECOMMENDATIONS

6.1 CONCLUSION

The demand of this machine is higher and it is the time to response for the bamboo furniture workers' problem. It can solve the exhausting manual bamboo processing tasks and saves time, it can also facilitate products. This bamboo processing machine has three functions, namely, manual splitting, bamboo knot grinding and sanding the splitter bamboo. Since wood resources are declining, and their products are very expensive comparatively with bamboo, it is preferable to use bamboo furniture's.

Our country has good bamboo resources, but can't get economic advantages from the resources because there was no trend of usage of bamboo furniture's widely. So it

https://dx.doi.org/10.22161/ijaers/3.11.33 *ISSN: 2349-6495(P) | 2456-1908(O)*

is better to use bamboo for furniture's makings so as to reduce deforestation of wood plants. Since the main function of this machine is to process bamboo for bamboo furniture workers it can facilitate productivity and it increases quality as well. As it is well known one of the major problems in our country is forest declining but by nature bamboo is fast growing and renewable plant which belongs to grass which can substitute woods for furniture making. Because of the declining of forest and to solve the problems of bamboo workers, developers intended to design and manufacture bamboo processing machine.

The machine can perform the following activities:

- Grinding bamboo knots.
- Polishing bamboo surfaces into the required thickness.
- Split into the required divisions manually.

The machine can split up to the diameter of 100 mm in to the required divisions within one minute up to the length of 120 centimetres with average human push force 250N. The machine can reduce the time taking of bamboo processing for the operations of splitting, sanding of bamboo knot and polishing bamboo surfaces. This machine has the following advantages:

- Manufactured from local materials
- Easy to assemble and disassemble.
- It does not need highly skilled man.
- Convenient for transportation.
- Low in cost and easy to maintain.
- Having three functions leads not to buy three different machines, this helps to save time and money.
- It can create job opportunity.
- The machine has another advantage which is the bamboo grinding disc can be replaced by metal grinding disc or it can be replaced by cutter.

It can be easily manufactured and distributed to various areas of our country and easily adapted as technology transfer to SMEs.

REFERENCES

[1] M., K.C. Khoo, 2004, **The proceedings of 7th World Bamboo Congress**, New Delhi.

[2] M.A. Nor Azah, 2006, **Prashant Bamboo Machine Sales Corporation**, Nagpur (India).

[3] Abd.Latif, and 1991, **Carbohydrates in some natural stand bamboos.**

[4] EFAP. 1993**. Ethiopian Forestry Action program, vol. II.**

[5] SeyoumKelemwork February, 2008, **Testing of Two Ethiopian Bamboo Species**

[6] Zhang Qisheng, 2004, **Bamboo processing Machine, China**

[7] EnsermuKelbessa and TamratBekele, 2009, A **socio-Economic Case Study of the Bamboo sector in Ethiopia.**

https://dx.doi.org/10.22161/ijaers/3.11.34 ISSN: 2349-6495(P) | 2456-1908(O)

Applications of Renewable Energy Sources in the World and the EU with a Particular Focus on Solar Energy

Isak Karabegovic

Department of Technical faculty, University of Bihać, Bosnia and Herzegovina

Abstract— *This Energy stability and security in the world have become important issues in almost every country. These are very important for the economic, social and economic development of each country. Getting energy is crucial for the development of any country, whether it comes to its industry or the economy. The paper presents the development and implementation of renewable energy sources, such as wind-power, solar energy, small hydro and biomass, both in the world and the EU. It elaborates and portrays an increasing trend of renewable energy sources in the total share of energy production, with the trend of reducing fossil fuels in energy production. The paper shows the trend of investments in renewable energy sources, with the trend of opening work posts and employment of workers who are working on the implementation of renewable energy sources, with a special emphasis on solar energy. We analyze the capacity to generate solar energy in the world for the period 2005-2015, as well as in the countries in which solar energy is used the most.*

Keywords— energy, renewable energy sources, solar energy, hydropower, wind energy, biomass

I. INTRODUCTION

The use of fossil fuels in the world resulted in an increase in carbon dioxide and other greenhouse gases. The effects of climate changes are already noticeable, so that we are witnessing the melting of glaciers, the polar ice and permafrost, as well as an increase in sea level - in other words, the change in the ecosystem. All these are the consequences of fossil fuels use in the world. All of humanity, i. e. governments of almost all countries, are obliged to seriously consider and make policy about the development and replacement of fossil fuels with renewable energy sources [1,2,4,6,7,8,10,11,12,13,16,21,22,23,36-39]. Nowadays, energy evolution is the most ambitious in the world, because it increases the renewable energy power generation. Energy efficiency measures are being introduced all over the world to reduce energy consumption to the lowest possible level with the same efficiency that we have had so far. World Energy Strategy to 2050 is such that renewable energy sources have the largest share of energy production. Renewable energy sources include: biomass (bio-fuels, bio-gas), hydro-power solar photovoltaic energy, solar thermal energy, wind-power, geothermal energy, sea energy (tides, waves and sea currents) [13,41,42]. Which of renewable energy sources should be used in a particular country depends on geographical situation of that particular country and its natural resources.

II. THE APPLICATION OF RENEWABLE ENERGY SOURCES IN THE WORLD

Currently, the world obtains most of its energy mainly from non-renewable energy sources, mainly fossil fuels – coal, oil and natural gas. The renewable energy sources produce far smaller share of power, while the smallest part of energy is produced by the nuclear fuel. The increase in the application of renewable energy sources will eliminate all negative consequences of the use of fossil fuels for energy production. In this way, climate issues and problems regarding the eco-system in the world will disappear, and we will receive energy from renewable sources, i. e. clean energy [14-38]. If you look at the use of all energy sources from 1860 (Figure II), you will notice three waves of fossil fuels: coal, oil and natural gas.

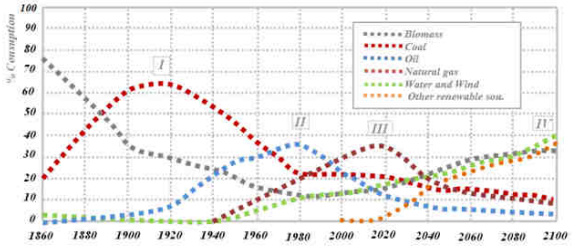

Fig. 1: The need for renewable energy sources and the "FOUR WAVES" scenario of fossil and renewable energy sources [1,2]

Figure 1 shows the „FOUR WAVES" scenario of fossil and renewable energy sources. The first wave of fossil fuels (Figure 1) is carbon in the period from1900-1930,

https://dx.doi.org/10.22161/ijaers/3.11.34 *ISSN: 2349-6495(P) | 2456-1908(O)*

the second wave was related to oil in the period from 1960 to 1990, and the third wave of fossil fuels is now dominant, and it is estimated its period will last from 2000-2030. According to the global energy scenario shown in Figure I on the use of renewable energy sources, it is estimated that the fourth wave will be the wave of renewable energy sources of the future and its onset is expected around 2080. The share of individual energy sources in the world's global final energy consumption in 2014 is shown in Figure 2. As it can be concluded from Figure 2, the largest share of energy sources in the world's global final energy consumption is from fossil fuels 78.3%, followed by renewable sources of energy 19.2% and nuclear energy 2.5%, which is in accordance with a comprehensive global energy scenario of renewable energy sources implementation for the period 1930-2090 [1-3].

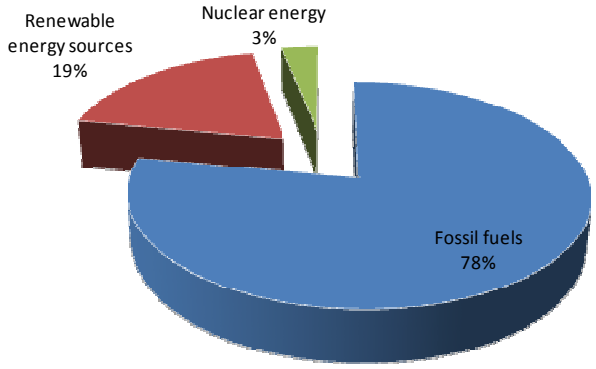

Fig. 2: The percentage of all energy sources in the global final energy consumption in the world in 2014 [6,43-45]

Renewable sources increase the sustainability of the power system in cases of a possible energy crisis, when it comes to power generation, which today is dependent on the delivery of coal, gas and oil. In order to gain a picture of energy production from renewable sources in the world, we display the capacity of energy production in the world in 2015 in Figure 3.

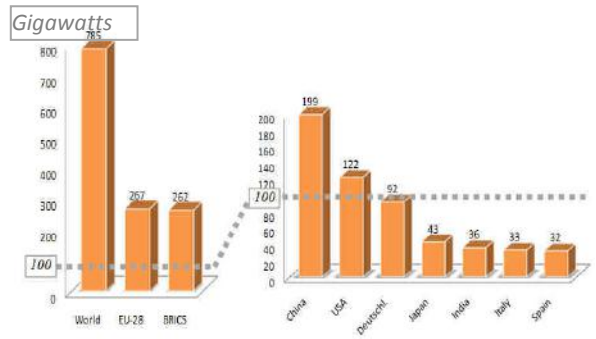

Fig. 3: The capacity of producing energy from renewable energy sources in the world, the EU-28, BRICS (Brazil, Russia, India and China) and seven top countries in late 2015 [6]

The analysis of Figure 3. shows that 785 GW of energy power in the world is produced from renewable energy sources, out of which 267 GW was produced by EU-28, and the countries BRICS (Brazil, Russia, India and China) produced 262 GW of energy power in 2015. If you perform an analysis of energy production from renewable energy sources by countries in the world, we see that China is number one with 199 GW of produced energy power. China is followed then by the USA, Germany, Japan, India, Italy and Spain. In the world nowadays, large investments will lead to greater participation of renewable energy sources in energy production; 286 billion dollars was invested in 2015. Investments in renewable energy sources in the world have resulted in job creation. Depending on the renewable energy sources and technologies in which that particular type of energy is applied, investments are not proportionate to the workplace, so that some renewable source of energy involves far more employees than other renewable energy sources, as shown in Figure 4.

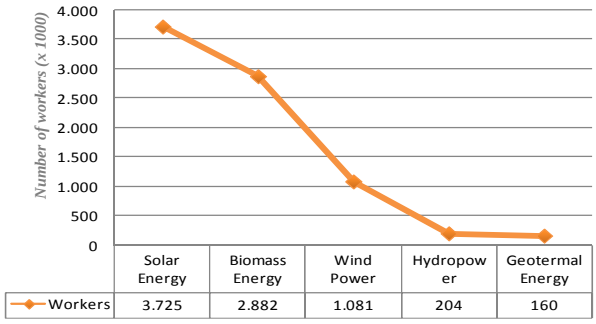

When it comes to production from renewable sources, 8.1 million employees was hired in the world in 2015, of which the energy obtained by means of solar radiation is number one when it comes to the number of employees with 3,725,000 workers, as shown in Figure 4. The second place goes to the production of energy from biomass, where 2,882,000 employees is hired; the third place goes to wind energy with 1.081 million working places; fourth is hydropower (SHP) with 204,000 employees; and the last is geothermal energy with 160,000 employees in 2015.

III. THE USE OF SOLAR ENERGY IN THE WORLD AND THE EUROPEAN UNION

The sun is a renewable and unlimited source of energy and can be directly converted – into thermal energy, which is used for heating, hot water, as well as electricity obtained from the photo-voltage system. On the earth's surface comes 7,500 times more energy per year than the total annual energy consumption from all primary sources. Solar energy is a renewable and unlimited source of energy, and it can be directly converted into solar photovoltaic energy and solar thermal energy [3,4,14-35].

https://dx.doi.org/10.22161/ijaers/3.11.34 *ISSN: 2349-6495(P) | 2456-1908(O)*

This paper analyzes both of these. Figure 5 shows the energy production in the world with the help of photo-voltage cells in the period 2005 - 2015.

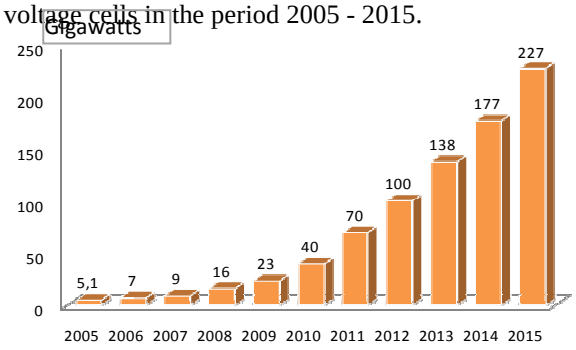

Fig. 5: Energy production (using solar cells PV) in the world from 2005 – 2015 [6-13]

As shown in Figure 5, energy production using solar cells (PV) in the world is increasing each year, i. e. has a growing trend, so that it reached 227 GW in 2015. It is expected that the growing trend will continue in the future, as it comes to the development of new technologies allowing ever greater use of energy generation with solar cells PV.

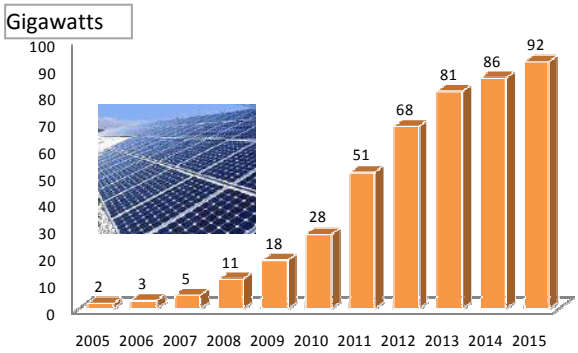

Fig. 6: Energy production (using solar cells PV) in the EU from 2005 – 2015

When it comes to the European Union, energy production using solar cells (PV) is increasing each year. In 2015, energy production using solar cells in the EU has reached 92 GW, which is 40.52% of the world energy production. The trend of energy production using solar cells will increase in the future.

Fig. 7: Energy production (using solar cells PV) in the world intop five countries from 2005-2015

Figure 7. shows energy production using solar cells (PV) in five countries in the world that produce the most energy of this kind. In the period 2005-2015, we see that energy production in Germany, China, Japan, USA and Italy is increasing each year. Figure 8. is an overview of capacities of energy production in each of the countries.

Fig. 8: Energy production (using solar cells PV) in top ten countries in the world in 2015 [5,6]

As can be inferred from Figure 8, the first country in the world in energy production using solar cells in 2015 was China with about 45 GW, which increased its production by 15.2 GW compared to 2014 (in 2014, Germany was number one). China is followed by Germany with a production of about 41 GW, and then come following countries: Japan, USA, Italy, England, France, Spain, India and Australia with about 5 GW of energy produced using solar cells. Lately, solar power plants for electricity production are being opened in the world, and the capacities of producing electricity using solar power plants are shown in Figure 9.

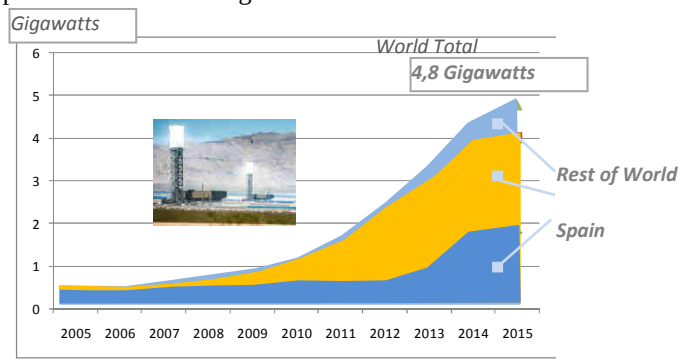

Fig. 9: Production of solar (CSP, known as STE) electrical energy in the world from 2005-2015 [2,6]

Electricity production in solar power plants has suddenly begun to increase from 2008, so that the capacity worldwide reached 4.8 gigawatts in 2015. As it can be seen from Figure 8, it is the most produced in Spain and the USA. The largest solar power plant in the world is to be built in the Mojave Desert in California, which will have a capacity of 1,000 MW and will cost six billion dollars. The largest solar power plants in the world are: Ivanpah 392MW (California), Perovo 100MW (Ukraine), Sarnia 92 MW (Canada), Montalto di Castro 84 MW (Italy), Finsterwalde 83 MW (Germany), Ohotnikovo 80 MW (Ukraine) Senftengerg 78 MW (Germany), Lieberose 71 MW (Germany), Ravingo 70 MW (Italy), Olmedilla de Alarcon 60 MW (Spain) and Boulder City 56 MW (USA). Many energy experts believe that solar energy is the only renewable energy source that has

Gigawatts44,2

https://dx.doi.org/10.22161/ijaers/3.11.34 *ISSN: 2349-6495(P) | 2456-1908(O)*

enough potential to replace fossil fuels as the dominant energy source in coming years. Quite a few of the countries is seriously considering solar energy and are investing large amounts of money in various projects, mainly solar plants for electricity generation.

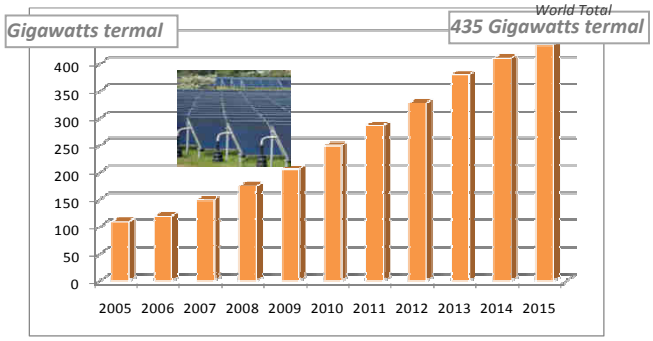

Fig. 10: Solar water heating of global capacities in the worldfrom 2005-2015 [1,7,42]

The capacity of production of solar thermal energy increases each year from 2005-2015, as shown in the diagram 10. In 2015, it reached a record production of 435 Gigawatts-thermal. The development of technology leads to increased production of this type of energy, because the sun is one of the best examples of renewable energy sources.

IV. CONCLUSION

Analysis the application of renewable energy sources in the world, with special emphasis on renewable sources of energy, we can conclude that fossil fuels occupy the first three places in the production of energy in the world in the last fifteen years: coal, oil and natural gas; then renewable energy; and in last place is obtaining energy from nuclear fuel. In the world, energy assessment in the global final energy consumption is as follows: 78.3% of the fossil fuels, 19.2% of renewable energy sources and nuclear energy 2.5% in 2014. In 2015, 785 GW of energy was produced from renewable energy sources: 267 GW in the EU, 262 GW in the countries of BRICS (Brazil, Russia, India and China), and the first in energy production from renewable energy sources is China, which produced 199 GW of energy in 2015. Energy production (using solar cells PV) in the world is continuously increasing every year in the world and the European Union, so that it reached 227 GW in 2015 in the world and 92GW in the European Union. China is number one country in the world in energy production using solar cells and it produced about 45 GW of energy in 2015. Germany is number one country in the EU with 41GW of energy. Electricity production (CSP known as STE) in the world has reached 4.8GWh. In 2015, 8.1 million employees work in the production of energy from renewable energy sources (also including the creation of plants for energy production), of which: 3,725,000 employees work in solar energy; 2,882,000 employees work in energy from biomass; 1,081. 000 work in wind energy; 204,000 employees work in small hydropower; and 160,000 employees work in geothermal energy. We note that solar energy employs most workers. We expect wider use of renewable energy sources in total energy production in the world and the EU in the coming period, and the development of new technologies will speed up the replacement of fossil fuels with renewable energy sources.

REFERENCES

[1] Isak Karabegović**,** V.Doleček, (2013), Current state and prospects for renewable energy sources with a special emphasis onpotential of solar energy in the world, europe and bosnia and herzegovina, Contemporary Materials (Renewable Energy Sources), Vol. IV. No. 2. 2013,Banjaluka, Bosnia and Hercegovina, ISSN 1986-8677: pp. 171-179.

[2] Vlatko Doleček, Isak Karabegović, (2015),Renewable energy sources in Bosnia and Herzegovina: situation and perspectives ,Contemporary Materials (Renewable Energy Sources), Vol. IV. No. 2., Banjaluka, Bosnia and Hercegovina, ISSN 1986-8677: pp. 152 - 163.

[3] Agrafiotis, C. (2005). "Solar water splitting for hydrogen production with monolithic reactors". Solar Energy 79 (4): 409–421

[4] Anderson, Lorraine (1994). Cooking with Sunshine (The Complete Guide to Solar Cuisine with 150 Easy Sun-Cooked Recipes), Marlowe & Company. ISBN 156924300X

[5] Richards, B.S. ; Schäfer, A.I. (2009) Renewable Energy Powered Water Treatment Systems,Chapter in: Escobar, I.C. ; Schäfer, A.I. (Eds.) (2009) Sustainable Water for the Future – Waterversus Desalination, Sustainability Science and Engineering: Defining Principles, Series Editor Abraham M.A., Elsevier, pp.353-374.

[6] Renewable 2016. Global Status Report, Paris: REN21 Secretariat, 2016.

[7] Renewable 2015. Global Status Report, Paris: REN21 Secretariat, 2015.

[8] Renewable 2014. Global Status Report, Paris: REN21 Secretariat, 2014.

[9] Renewable 2013. Global Status Report, Paris: REN21 Secretariat , 2013.

[10] Renewable 2012. Global Status Report, Paris: REN21 Secretariat, 2012.

[11] Renewable 2010. Global Status Report, Paris: REN21 Secretariat, 2010.

https://dx.doi.org/10.22161/ijaers/3.11.34 *ISSN: 2349-6495(P) | 2456-1908(O)*

[12] Renewable 2005 Global Status Report, DC:Worldwatch Institute. Washington, 2005.
[13] Global Trends in Renewable Energy Investment 2014, Frankfurt School-UNEP Centre/BNEF. 2014.
[14] Vanek F., Albright L., Angenent L. (2012) Energy Systems Engineering: Evaluation and Implementation, Conveo Publisher Service, New York.
[15] Daniels, Farrington (1964). Direct Use of the Sun's Energy, Ballantine Books. ISBN 0345259386
[16] Halacy, Daniel (1973). The Coming Age of Solar Energy, Harper and Row. ISBN 0380002337
[17] Karan, Kaul (2001). "Row Orientation Affects Fruit Yield in Field-Grown Okra". Journal of Sustainable Agriculture 17 (2/3): pp.169–174.
[18] Leon, M. (2007). "Mathematical modeling and thermal performance analysis of unglazed transpired solar collectors". Solar Energy 81 (1):pp. 62–75.
[19] Lieth, Helmut; Whittaker, Robert (1975). Primary Productivity of the Biosphere, Springer-Verlag1. ISBN 0387070834
[20] Meier, Anton (2005). "Solar chemical reactor technology for industrial production of lime". Solar Energy 80 (10): pp.1355–1362.
[21] Mills, David (2004). "Advances in solar thermal electricity technology". Solar Energy 76 (1-3):pp. 19–31.
[22] Müller, Reto (2007). "Band-approximated radiative heat transfer analysis of a solar chemical reactor for the thermal dissociation of zinc oxide". Solar Energy 81 (10): pp.1285–1294.
[23] Vlatko Doleček,Isak Karabegović, (2013), Renewable Energy Sources of Bosnia and Hercegovina:State and Perspektives,8th International Conference on Renewable Energy and Energy Efficiency, Montenegrin Academy of Sciences and Arts,7.Oktober 2013,Podgorica,Montenegro,2013.
[24] Igor Raguzin,(2011),Model analize troškova i doboti uporabe biomase u proizvodnji električne energije,Magistarski rad, Strojarski fakultet Slavonski Brod.
[25] Šljivac,D. Šimić Z. (2009)Obnovljivi izvori energije, AWERES, FER, Zagreb.
[26] Miloš Banjac,(2012) Obnovljivi izvori energije u Srbiji, SREM,Ruma.
[27] Union of Concerned Scientists (1999) Benefits of Renewable Energy Use.
[28] [28] Granić G., Željko M., (2008) Studija energetskog sektora u BiH. Modul 1, 2, 3, 4, 5, 6, 7, 8, 9, 10, Sarajevo.
[29] Armstrong J., Hamrin J. (2013) What are "Renewable Resources"?, Chapter 1: Renewable Energy Overview, Cost-Effectiveness of Renewable Energy, Organization of American States.
[30] Hondge B.K. (2010) Alternative Energy Systems and Applications, Mississippi State University.
[31] Buhrke T., Wengenmayr R. (2012) Erneuerbare Energie: Kozepte fur die Energiewende, Wiley-VCH Verlag GmbH, Weinheim.
[32] Ministero dello Sviluppo Economico (2012) Izvještaj o analizi stanja okolišnih tehnologija i obnovljivih izvora energije u BiH, Sarajevo.
[33] European commission, Directorate-General for Energy and Transport: (2001) COM 2001/77/EC Direktive on Electricity production from Reoewable Energy Sources.
[34] International Energy Agency (IEA), Head of Publications Service, 9 rue de la Fédération, 75739 Paris Cedex 15, France. (www.worldenergyoutlook.org/media/weowebsite/2008.../WEO2006)
[35] World Small Hydropower Development Report 2013, Published in 2013 by United Nations Industrial Development Organization and International Center on Small Hydro Power,2013.
[36] AEBIOM,EuropeAn Bioenergx Outlook,2014.
[37] AEBIOM, Annual Report,2013.
[38] http://en.wikipedia.org/wiki/Renewable_energy(4.9. 2016.
[39] http://www.obnovljivi.com/geotermalna-energija/67-iskoristavanje-geotermalne-energije-energetici;(4.9.2016.)
[40] http://www.wbdg.org (5. 9. 2016.)
[41] http://www.inhabitat.com (18. 9. 2016.)
[42] http://www.q-solar.com (18. 9. 2016.)
[43] http://www.klubmamut-wordpress.com(20. 9. 2016.)
[44] http://www.bpz.hr (25. 0. 2016.)
[45] http://www.intrade.co.ba (27. 9. 2016.)

International Journal of Advanced Engineering Research and Science (IJAERS) *[Vol-3, Issue-11, Nov- 2016]*
https://dx.doi.org/10.22161/ijaers/3.11.35 *ISSN: 2349-6495(P) | 2456-1908(O)*

Automobile Vibration and their Control

Mr. Nitesh Kumar Dixit[1], Dr. Kamal J Rangra[2]

[1]Dept. of ECE, VGU, Jaipur, Rajasthan, India
[2]Chief Scientist and Professor AcSIR, Sensors & Nano-technology Group, SDA , (CSIR-CEERI), Pilani (Raj), India

Abstract— *The vibration is harmful noise for every moving machine. This paper describes vibration general sources. The paper also describes automobile vibration and their elimination. As researches found the frequencies of different domestics vibration sources is varies between 4 Hz to 220 Hz and in automobile it nearly about 30 Hz. This paper also describes the vibration absorbers for automobile application.*

Keywords—Noise, Vibration Sources, automobile, Vibration Absorber.

I. INTRODUCTION

Vibration, means oscillation which generates noise, it has three main categories: seismic vibrations, acoustic vibrations and, free and forces vibration [1].

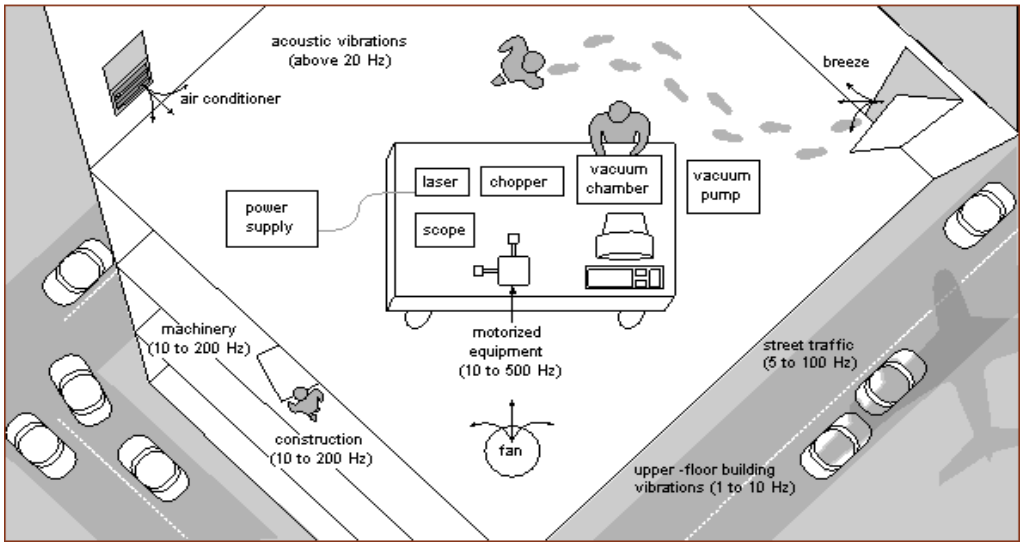

Periodic vibration comes through continuously running vibration system. Random vibrations generates through from unpredictable sources like car component vibrations [3]. The frequency range has been found from 4-400 Hz of most of vibrations for various applications and also mentioned in below Table I and II [4].

TABLE I. VIBRATION SOURCES AND THEIR FREQUENCIES

Type	**Frequency(Hz)**	**Amplitude**
Air Compressors	4 – 20	10^{-2} in
Handling Equipment	5 – 40	10^{-3} in
Pumps (Vacuum, comp or non-comp fluids)	5 – 25	10^{-3} in
Building Services	7 – 40	10^{-4} in
Foot Traffic	0.5 – 6	10^{-5} in
Acoustics (B)	100 – 10000	10^{-2} to 10^{-4} in
Air currents	Labs can vary depending on class	Not applicable
Punch Presses	Up to 20	10^{-2} to 10^{-5} in
Transformers	50 – 400	10^{-4} to 10^{-5} in
Elevators	Up to 40	10^{-3} to 10^{-5} in
Building Motion	46/Height in meters,	0.1 in

Vibrations sources are bottom traffic, wind blowing the structure, vehicular traffic, and construction aeration fans etc. the lots of the seismic vibration sources that generate also generate acoustic vibrations. The effects of air pressure measure through it [2]. The forces functional straightforwardly to the load on the functioning outside; they are directly coupled mechanically to the tentative setup.

II. IDENTIFICATION OF VIBRATION SOURCES

Vibrations are either random or periodic, in around environment vibration sources shows in figure 1.

https://dx.doi.org/10.22161/ijaers/3.11.35 *ISSN: 2349-6495(P) | 2456-1908(O)*

	Horizontal	
Building Pressure Waves	1 – 5	10^{-5} in
Railroad	5 - 20	±0.15g
Highway Traffic	5 - 100	±0.001g

TABLE II. VIBRATION SOURCES AND THEIR FREQUENCIES

Vibration source	**Acceleration (m/s2)**	**Frequency (Hz)**
Drilling machine	0.93	178
Lathe machine	1.36	68
Bearing test bed	10.57	200
Refrigerator	0.14	110
Washing machine	0.82	62
Cloth dryer	4.21	59
Microwave oven	0.49	40
A/C compressor	2.14	59
Car engine	0.56	30
Truck engine	1.98	37

III. AUTOMOBILE VIBRATIONS AND THEIR CHARACTERISTICS

There are two major reasons for generation of car vibration like, first reason Engine vibration and Second if an axle gets bent. Other reasons like Brake Trouble, Wobbly Wheels, and Tire Problems etc.

The automobile vibrations are classified according to when they occur[6] as shown in figure 2:

(1) Vehicle speed sensitive – This noise direct proportion to vehicle speed and only occurs at certain speeds.

(2) Acceleration/deceleration sensitive -- This noise depends on change in vehicle speed.

(3) Engine speed sensitive -- This vibration is generates through engine speed. The vibration is also direct proportion to engine rpm [7].

(4) Suspension Vibration - It occurs when suspension has problem in the driveline or chassis.

(5) Speed Sensitive Vibrations: At speeds above 45 to 50 mph most of wheel facing imbalance problems that are causes of speed sensitive vibration. A back-and-forth shimmy wheels are dynamically imbalanced. Whereas a sawtooth design wheels are also produce vibrations and also speed sensitive [8].

(6) Driveshaft Vibrations: That's reason also produce vibration.

(7) Resonance: It generally produced by exhaust system.

(8) Broken engine mountings: Engine mounting materials are hard rubber-like objects which hold and fix whole engine at their position and also preventing metals rubbing to each other. The vibration generates when mounting broken.

(9) Random – This vibration comes through random sources of Car body and also comes through road. They generates through loose shock absorbers, ball joints, spring mounts, stabilizer bars, control arm bushings, etc. Loose/broken ball joints and Brakes: These are loose or broken that generates vibrations [9].

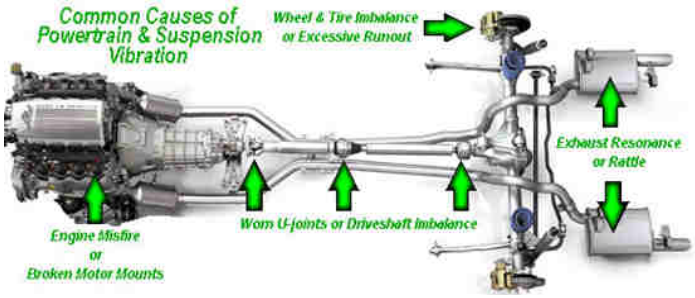

Fig.2: Automobile vibration

Automobile vibrations and sources are shown in Table III.

TABLE III. CAR VIBRATION DATA (1000CC)

Vibration location	**Acceleration (m/s^2)**	**Frequency (Hz)**	**Amplitude (µm)**
Engine	1.23	30.5	33.5
Radiator	0.16	29.5	4.66
Headlight	0.23	29.5	6.64
Bonnet	0.18	29.5	5.18
Dashboard	0.04	30	1.07
Roof	0.26	29.5	7.54

IV. MOUNTING SYSTEM

The vibration frequency range is varies from 4Hz to 100 Hz, it is necessary to make an isolation system that can attenuate all dynamic vibration inputs [10]. There are two factors to be considered before making a isolation system:

•The severity of the environment - it's the primary factor for determining the level of isolation which is required.

•The sensitivity of the application -it's also the primary factor for determining the stiffness and internal damping features.

The mountings absorbs/reduces/cancels the vibrations produced by vehicles or their components. There is some impotence of anti vibration mountings like Noise of the running engine is attenuated, which helps for smooth working. And improve the all over functionality of vehicle. The some harmful noise generates when engine runs that is known as annoying noise, the isolators can used to minimize this potentially noise [11].

It is necessary to consider high vertical stationary & shock load in compression when anti vibration system going to design. The design may be combination of sheet metal components, ferrous or non-ferrous castings with

https://dx.doi.org/10.22161/ijaers/3.11.35 *ISSN: 2349-6495(P) | 2456-1908(O)*

nuts, bolts, etc. The heavy load or metallic part should be mounting on high grade cushion like neoprene rubber and low carbon steel should use for rusting. It is also necessary to fitted at specific location to optimal vibration isolation.

There are some selection criteria for selection perfect anti vibration mountings like first it observe the material which used, Load bearing capacity of the mountings, shock absorption and deflection characteristics of the mountings.

The deadly accident will occurs when no mounting of engine. The engine mounts basically consists two steel plates with tightly sealed in engine body that easily absorbs the vibrations. The thick rubber cushion is applied in between the two steel plates that absorb most of the vibrations from the engine. In other word engine mounts also the backbone of automobile, it has lot of advantages like it ensure stable running of engine, Provides high isolation value in the horizontal shear direction, protects other components of vehicle from vibrations etc. There are some mountings explained in next and shown in figure 3.

(a) Cushion Mountings: This usually used for diesel gen sets, Compressors, Cooling Systems hydraulic systems and pumps. The cushion foot mounting is high performing anti-vibration mountings that can be easily installed on various machines and also use as friction pads are in combinations in the mounts. Special quality rubber is used as raw material like Natural Rubber, SBR, EPDM, Neoprene, Silicone etc..

The Absorb shock, Isolate vibrations and noise reduction are the main function of cushion mounting. They are available in several of dimension with high resistance for surface abrasion, operating condition and with chemicals. They have highly dynamic stiffness rate and easy to install and also have easy to maintains as shown in figure 3 (a).

(b) O Mounting: The O mountings are also eliminating vibrations produced by running engines. The cylinder shapes makes it a powerful shock absorber. The high grade steel is used for manufacturing of O mountings. It has cylindrical shaped with rubber affixed around it. The main purpose of this mounting in air conditioners, compressors, generator sets etc. The selection criteria same as of other mounting has.

(c) Rectangular Mounting: Rectangular mountings are type of rubber mountings. It is used for fixing engines. A Vehicle suspension springs and acoustic chambers are designed using rectangular mounting. The layered structure increase the load capacity of rectangular mounting. Most of these mountings are manufactured with fine quality metals preferably Steel and high grade rubbers are used to manufacture this. The result of apply this to performing at the optimum level, gives Longer life of equipment, Increased production capacity and Reduction in maintenance costs as shown in figure 3 (b).

(d) U Mountings: It is special kind of rubber mounting that having high shear strength. It absorbs shock resistance in lateral and vertical direction. This is used in electronics apparatuses, electrically controlled panels, suspending light components, and high speed motor resistance to grease, lubricants, surface abrasion wear, sunlight and UV rays etc as shown in figure 3 (b).

a) Cushion Mountings

b) Rectangular Mounting

c) U Mount

Fig.3: Different types of Automobile Mounting

https://dx.doi.org/10.22161/ijaers/3.11.35 *ISSN: 2349-6495(P) | 2456-1908(O)*

V. AUTOMOBILE INTELLEGENT ANTIVIBRATION SYSTEM

There are some major components are applied to absorb the vibration. In below figure 4 some major points show where absorber applied. Some of intelligent components that also generate vibration wave in anti-phase to other excitation with same amplitude that cancel generate vibration [12] as shown in figure 5.

(1) Backrest vibration absorber:

It is necessary to make contoured are easily and effectively accomplished. Most of people 50% suffer form of back pain and many of complaint related to poor seat design.

The main Purpose is to maintain for a stable posture muscles. Air spring system gives more comfortable design. The design is like scissors that control sleeve lever at 3 to 7 bar working pressure and also gives adjustable seat height. The air medium is optimized suspension and damping performance.

(2) Steering wheel vibration absorber:

The propeller shaft is way to transmitted vibration which generated by rear wheel drive to rear axle. The propeller shaft bearing stabilize the shaft in static for every dynamic operation and also control topple motion of shaft to minimize the vibration.

(3) Hydraulic absorbers:

The main work of hydraulic absorbers is to reduce structure-born vibration that generated by engine. The elastomer spring applied with hydro bushing that use for this work. Hydro bushings do isolation against vibration.

(4) Brake vibration absorbers:

The brake calipers and serves is used to reduce brake vibration and also reduce flexural vibrations.

(5) Active Absorbers:

The main purpose is to cancel out the vibration that generates through engine and other components. The general work to generate a anti signal of vibration that equal and opposite. It has mainly four components actuator, control unit, power amplifier and sensors. The sensors used for measure the vibration. This information gives to control unit that is generally electronic circuits, which gives signal to amplifier that generate opposite signal. This generated signal gives to actuator to generate opposite power and vibrate chassis. This process canceled the vibration.

(6) Internal tube vibration absorbers

In hollow drive shafts a internal tube is used, that pressed into shaft of a front wheel drive and reduce vibration.

(7) Torsional vibration absorbers

The engine's torsional vibration can be reduced by torsional vibration absorber. They are generally installed at the transmission outlet.

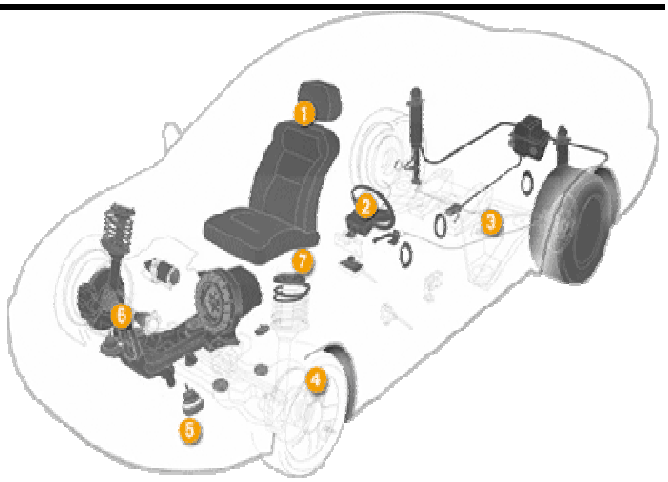

Fig.4: Intellegent Antivibration System

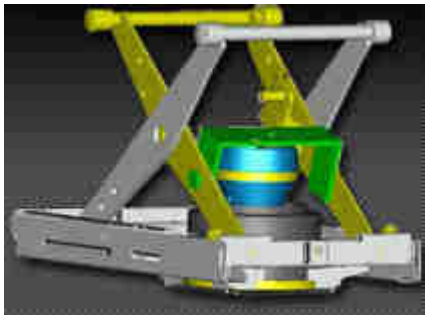

a) Backrest vibration absorber

b) Intermediate propeller shaft bearing

c) Hydraulic absorbers

https://dx.doi.org/10.22161/ijaers/3.11.35 *ISSN: 2349-6495(P) | 2456-1908(O)*

d) Car hydromounts

e) Commercial vehicle engine mount

f) Brake vibration absorber

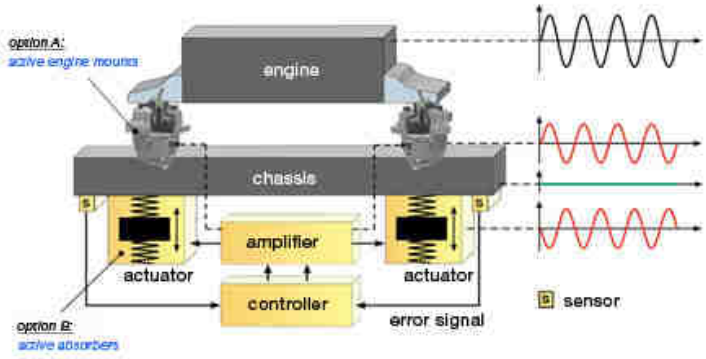

g) Active Absorber

h) Internal tube vibration absorber

i) torsional vibration absorber

Fig.5: Components of Intellegent Antivibration System

VI. CONCLUSION

The paper explained the different types of vibration sources and their frequency in domestics. This paper also explained the vibration absorber / isolation system. In automobile intelligent anti vibration system explained for comfort driving

.

ACKNOWLEDGMENT

I thank to Dr. Kamal J Rangra for their kind guidance. Also thankful to VGU, jaipur to their support.

REFERENCES

[1] W. Thomson, Theory of Vibrations With Applications, Second Edition, Prentice-Hall, New Jersey, 1981.

[2] W. Seto, Mechanical Vibrations, McGraw-Hill, New York, 1964.

[3] W. Fackler, Equivalence Techniques for Vibration Testing, SVM-9, The Shock and Vibration Information Center, Naval Research Laboratory, United States Department of Defense, Washington D.C., 1972.

[4] Gao, R. and Cui, Y. (2005) Vibration Based Sensor Powering for Manufacturing Process Monitoring. Transactions of the North American Manufacturing Research Institution, Society of Manufacturing Engineers, 33, 335-342.

[5] Beeby, S.P., Tudor, M.J. and White, N.M. (2006) Energy Harvesting Vibration Sources for Microsystems Applications.Measurement Science and Technology, 17, R175-R195. http://dx.doi.org/10.1088/0957-0233/17/12/r01

https://dx.doi.org/10.22161/ijaers/3.11.35 *ISSN: 2349-6495(P) | 2456-1908(O)*

[6] Raju.S, ARAI Pune, Workshop on Noise, vibration and harshness for automotive engineering, 2004, 123-139.
[7] Herman V Auleraer, Noise and vibration characteristics of low emission vehicles. Keynote paper, 51-62.
[8] Karanath N.V. and Raju .S, Investigation of relation between stationary and pass by noise for new in use vehicle, SAE paper No. 2005-26-051. ARAI Pune, 623-629.
[9] Gabiniemic J, Gatt J,Cerrato G. – Jay (Tecumesh products research laboratory) Automatic detection of BSR events. (Magna Automotive Testing).
[10] J. S. Sui, C. Hoppe, J. Hirshey, "Powertrain Mounting Design Principles to Achieve Optimum Vibration Isolation with Demonstration Tools," SAE Technical Paper Series 2003-01-1476.
[11] A. Geisberger, A. Khajepour, F. Golnaraghi, "Non-linear Modeling of Hydraulic Mounts: Theory and Experiment," Journal of Sound and vibration (2002) 249(2), 371-397.
[12] http://www.contitech.de/pages

International Journal of Advanced Engineering Research and Science (IJAERS) [Vol-3, Issue-11, Nov- 2016]
https://dx.doi.org/10.22161/ijaers/3.11.36 *ISSN: 2349-6495(P) | 2456-1908(O)*

Health Impact and Medicinal Properties of Nutritionally Edible Milky Mushroom (*Calocybe Indica*)

Anju R.P[1], Dr. Mary Ukkuru.P[2]

[1]Guest faculty NSS College for Women, Neeramankara, Kerala, India
[2]Professor & Head, department of Home Science, KAU, Vellayani, Kerala, India

Abstract*—Dietary mushrooms are considered as valuable health foods since they are known for rich proteinacious food, it consists of about 75 per cent proteins and are low in calories, fat, fatty acids, vitamins and minerals. Mushrooms as functional foods are used as nutrient supplements to enhance immunity in the form of tablets. Calocybe indica is an indigenous popular edible mushroom, having a variety of secondary metabolites such as phenolic compounds, terpenes and steroids possibly involved in their medicinal effects and nutritive value. Result of the present supplementation study revealed that milky mushroom is highly suitable and beneficial for promoting and maintaining health. Blood profile of the subjects showed a significant decrease in blood sugar, blood cholesterol and blood pressure levels in the subjects*

Keywords—Calocybe indica, medicine, food, properties.

I. INTRODUCTION

Mushrooms now increasingly recognized because they correct diet, controls and modulates many functions of human body and consequently participates in the maintenance of state of good health, necessary to reduce the risk of many diseases. Modern pharmacological research confirms large parts of traditional knowledge regarding the medicinal effects of mushrooms due to their antifungal, antibacterial, antioxidant and antiviral properties, besides used as functional foods. *Calocybe indica*, popularly known as milky mushroom or summer mushroom, is a relatively new introduction from India to the world of mushroom growers.

Calocybe indica P&C is one of the promising mushrooms cultivated in summer introduced by Purkayastha and Chandra in 1974. The name is derived from the ancient Greek terms kalos means“pretty” and cubos “head”. In Orissa it is known as *dudha chhatu* and in some places they are called *kuduk*. Around nine species of *Calocybe* are found in neotropical regions. Being low in fat and devoid of cholesterol, mushrooms make an ideal diet for the heart patients. Mushrooms are low in calorie: high in protein, with no starch and sugars, and are called the diabetics delight.

Mushrooms are low calorie food with very little fat which is free of cholesterol and rich in linoleic acid. Pushpa and Purushothama (2010) reported that *C.indica* is rich in protein and fiber with low fat content, which make the mushroom as a low energy, healthy food stuff. They were also of the opinion that milky mushroom can also be used as protein supplementary diet. Digestibility of milky mushroom protein is 72-83 per cent.

II. MATERIALS AND METHODS

Selection of subjects and experimental design

Medicinal value of *calocybe indica* was investigated by conducting supplementation study conducted on human volunteers as case study. A list of hyperglycemic, hyperlipidemic and hypertensive subjects were identified through the preliminary screening among the subjects with the above three disease conditions residing in Trivandrum by the interviewer. From among the above list, person under medication and subjects with co-morbidities were deleted. For each disease condition two subjects with similar clinical parameters were selected.

After selection, preliminary information’s regarding their medical history, socio economic background, dietary and life style pattern were collected through a suitably structured pre tested questionnaire. The socio economic profile of the subjects such as socioeconomic status, religion and family background in general has a very distinct part to play in determining attitude and food consumption, health and behavioral pattern of the individual.

Details on the medical history of the subjects, food consumption pattern, use of medicines, other personal habits, blood profile and blood pressure of the respondents were estimated.

https://dx.doi.org/10.22161/ijaers/3.11.36 ISSN: 2349-6495(P) | 2456-1908(O)

Anthropometric measurements relevant to the study include height, weight, waist and hip circumference. The waist hip ratio is a simple method for distinguishing between fatness in the lower trunk and upper trunk. Waist hip ratio (WHR) of >1.0 for men and >0.85 for women is often referred to as gynoid obesity, on assessing the anthropometric measurements, all the subjects does not follow ideal body weight and were at risk and prone to develop lifestyle diseases.

Preparation of mushroom sample

Milky mushroom (*Calocybe indica*) cultivated on paddy straw will be selected for the study. Milky mushroom was sun dried, powdered in a grinder and sieved using a fine mesh of about 10x size. Dried mushroom powder was packed in five gram sachet for supplementation to the respondents selected for the case study. Impact of the mushroom supplement on the subjects was monitored initially and after supplementation.

Monitoring indicators

Blood pressure, blood sugar, lipid profile, general health and morbidity of the subjects.

Diet and feeding

Various recipes were standardized in the laboratory incorporating mushroom supplement, in order to ensure the prompt inclusion of the supplement in the diet of the respondents. Recipes standardized with mushroom powder were commonly consumed popular breakfast dishes like dosa, idly, chapathy etc. Apart from the above other dishes like chutney powder, mixing the powder with rice, curd and black tea were also tested. It was observed that mushroom powder incorporation neither alter the texture nor the acceptability of the preparation.

Mushroom supplement was distributed to the subjects for consumption for a period up to three months. Subjects were given five g sachet of mushroom supplement distributed on a weekly basis. Investigator made a good rapport among the respondents and ensured the incorporation of supplement daily in their diet. Investigator has made interaction with the respondents personally and through telephone to know whether the subjects were consuming the supplement regularly. The supplementation study continued for three months. Two of the subjects discontinued the trial. Feeding trial over a given period of time is considered as the most reliable method to determine the impact of the food. The feeding experiment was conducted for a period of three months to assess the efficacy of mushroom powder on hyperglycemia, hyperlipidemic and hypertension. Blood profile of the subjects recorded before the introduction of the supplement and after 45th and 90th day of supplementation.

III. RESULTS AND DISCUSSION

Impact of the mushroom supplement on the blood sugar levels

Both the subjects were willingly participated in the mushroom supplementation study and were not taking any oral hypoglycemic agents for controlling the disease. The result revealed that initial value obtained for fasting blood glucose of subject A and B were 135 mg/dl and 165 mg/dl respectively. After supplementation 45 days for both the subjects the level has reduced to 128 mg/dl. At the end of the 90 th day, fasting blood sugar level was 112 mg/dl and 98 mg/dl respectively. A steady decline was observed in the two subjects studied with regard to fasting blood sugar levels.

Impact of the mushroom supplement on the cholesterol levels

Both the hyper cholesterolemic subjects were interestingly participated in the feeding experiment and were not on medication. Direct monitoring was done by the investigator. The result showed that value obtained for fasting blood cholesterol level initially 231 mg/dl and 240 mg/dl for subject A and subject B respectively. In 45 th day of supplementation there is no decrease in the cholesterol level in subject A while subject B showed reduced level to 225 mg/dl. At the end of 90 th day of supplementation the cholesterol level reduced to 223 mg/dl and 178 mg/dl for subject A and B respectively. Result revealed remarkable decline in the cholesterol level of the subjects selected for the study.

Impact of mushroom supplement on the blood pressure levels

Subjects under study were not on any medication for controlling hypertension. The result showed that initially the value obtained for blood pressure level of subject A and B were found to be 170/100 mm Hg and 140/100 mm Hg respectively. After 45 th days of supplementation subject A shows reduction in blood pressure level to 150/90 mm Hg but in subject B slight increase in the level was observed to 150/100 mm Hg. When monitored after 90 days of supplementation there was steady decline in the case of subject A to 80/100 mm Hg and 120/80 mm Hg in subject B

Table.1: Mean basal characteristics of subjects selected for the study

https://dx.doi.org/10.22161/ijaers/3.11.36 ISSN: 2349-6495(P) | 2456-1908(O)

Basal characteristics	Diabetic		Hypercholesterolemic		Hypertensive	
	SubjecA	Subject B	SubjecA	SubjectB	SubjecA	Subject B
Height	154	160	155	155	175	155
Weight	79	76	65	65	78	60
Waist circumference	45	46	42	43	40	46
Hip circumference	47	49	45	47	41	48
BMI	25.64	23.87	20.96	20.96	22.28	25
Waist hip ratio	0.95	0.93	0.93	0.91	0.97	0.95

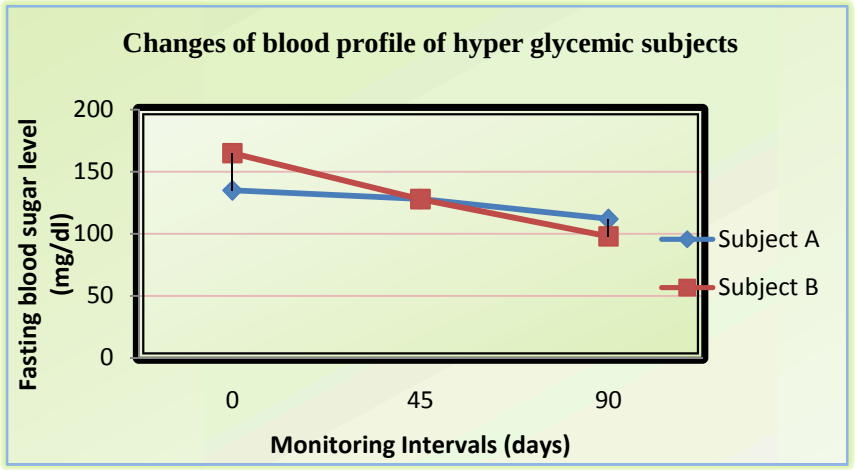

Fig.1

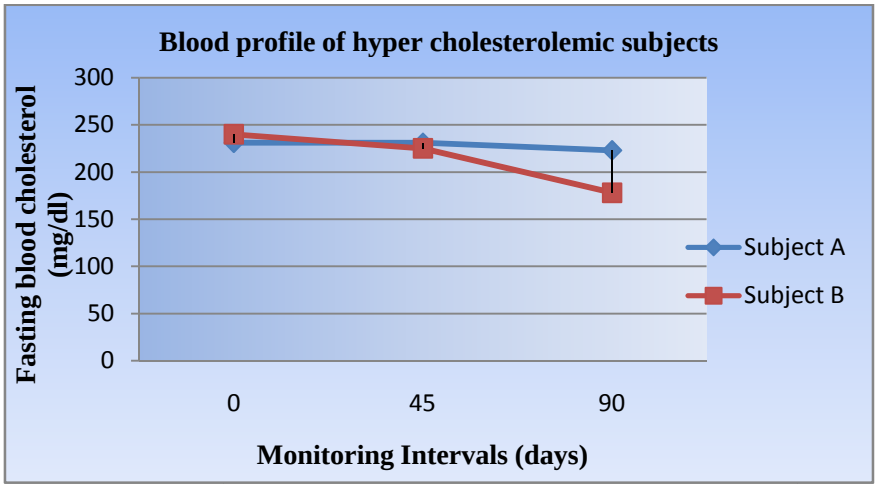

Fig.2

IV. CONCLUSIONS

Overall, the result revealed that incorporation of mushroom supplement was able to reduce blood sugar and blood cholesterol to a considerable level. Hypertension was also found to control to some extent. Further research is necessary so as to get more data for generating concrete assign.

REFERENCES

[1] Purkayastha R.P and Chandra A. 1974. New species of edible mushroom from India. Trans Brit *Mycol* p.415-418

[2] Pushpa, H and Purushothama 2010. Nutritional analysis of wild and cultivated edible medicinal mushrooms World J. of *Diary & Food Scie*.5 (2):140-144.

International Journal of Advanced Engineering Research and Science (IJAERS) [Vol-3, Issue-11, Nov- 2016]
https://dx.doi.org/10.22161/ijaers/3.11.37 *ISSN: 2349-6495(P) | 2456-1908(O)*

Novel and Efficient approach for Duplicate Record Detection

Mrs. D. V. LalitaParameswari.[1], K. Mounika[2]

[1]Sr. Asst. Professor, Dept. of CSE, GNITS, Hyderabad, India
[2] M. Tech Student, Dept. of CSE, GNITS, Hyderabad, India

Abstract*—Similarity check of real world entities is a necessary factor in these days which is named as Data Replica Detection. Time is an critical factor today in tracking Data Replica Detection for large data sets, without having impact over quality of Dataset. In this system primarily introduce two Data Replica Detection algorithms, where in these contribute enhanced procedural standards in finding Data Replication at limited execution periods. This system contribute better improvised state of time than conventional techniques. We propose two Data duplicate record detection algorithms namely progressive sorted neighbourhood method (PSNM), which performs best on small and almost clean datasets, progressive blocking (PB), and parallel sorted neighbourhood method which performs best on large and very grimy datasets. Both enhance the efficiency of duplicate detection even on very large datasets.*

Keywords*— *Data cleaning, Duplicate detection, Entity Resolution, Progressiveness.

I. INTRODUCTION

Now-a-days, Databases play a primary role in IT situated economy. Many industries as well as systems rely on the accuracy of databases to carry out operations. As a result, the worth of the data will be saved in the databases; can have significant price suggestions to a system that relies on data to operate and perform business. In an error-free system with exactly clean data, the construction of a comprehensive view of the information contains linking -- in relational phrases, joining-- two or more tables on their key fields. Unfortunately, information most commonly needs a unique, world identifier that may permit such an Operation. Furthermore, the information is neither cautiously controlled for outstanding nor defined in a consistent means throughout distinctive data sources. [2]Accordingly, information quality is frequently compromised by using many causes, together with knowledge entry errors (e.g., studet as an alternative of student), missing integrity constraints (e.g., enabling entries), and more than one conventions for recording information To make things poorer, in independently managed databases not most effective the values, but the constitution, semantics and underlying assumptions about the data could vary as well. The Progressive techniques may method larger dataset in brief span of time and also the quality of knowledge is additionally smart relatively. The Progressive duplicate detection makes it totally different from the normal approach by yielding additional advanced results throughout the first termination; the algorithms of duplicate detection additionally compute the duplicates at a virtually constant frequency however the progressive algorithms increase the time because it finds out the duplicates at the first stage itself. The proposed system enhances the strength of duplicate detection even on very massive datasets. The parameterization complexness for duplicate detection is created comfortable generally and contributes to the event of additional user interactive applications.

II. LITERATURE SURVEY

The sorted Neighborhood process depends on the assumption that replica records can be close in the sorted record, and accordingly shall be when compared for the duration of the merge step. The effectiveness of the sorted neighborhood strategy is totally dependent upon the contrast key that's selected to sort the records. Typically, no single key shall be plenty to sort the documents in this sort of approach that all the matching files may also be detected. If the error in a file occurs within the unique discipline or element of the subject that's the fundamental a part of the sorting key, there's a very small probability that the file will turn out to be practically an identical record after sorting. [4]To expand the quantity of identical records merged, Herna´ndez and Stolfo carried out a approach for executing a couple of independent runs of the Sorted-Neighborhood Method by means of using yet another sorting key and a slightly small window every time. This process is known as the multi-pass technique. This method is similar in spirit to the multiple-run blocking approach described above. Each impartial run produces a collection of pairs of documents that can be merged. The final outcomes, including the transitive closure of the files matched in extraordinary passes, are due to this fact computed.

https://dx.doi.org/10.22161/ijaers/3.11.37 *ISSN: 2349-6495(P) | 2456-1908(O)*

A. Map-Reduce Algorithm

A map reduced algorithm was introduced which has high affability for scheduling about responsibilities for dynamic load balancing. [6]The author Oktie, presents the Stringer framework that gives an evaluation arrangement to understanding what hindrances remain towards the objective of really flexible as well as broadly useful duplication recognition calculations. Few unrestrained bunch algorithms are assessed for copy discovery by broad examinations over totally different arrangements of string information with numerous attributes. A theme was introduced to combine multisource data. The results from the preliminary examinations are according that was taken from four card inventory databases that rescale to over ten million records are according within the paper.

B. Sorted Neighborhood Method with Map-Reduce

This method introduces new approaches reduce time.

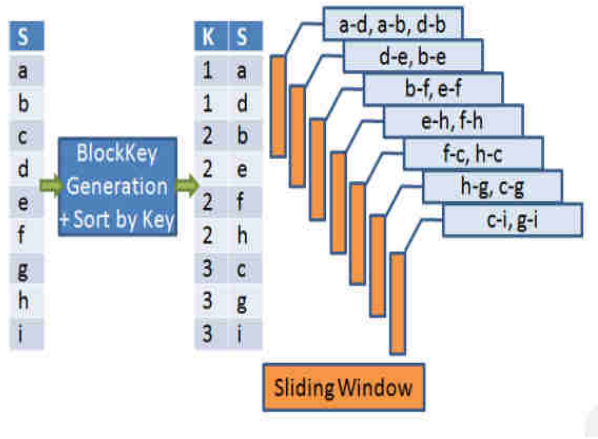

Fig.1: Example Execution of SNM

Sorted Neighborhood Method (SNM) is a popular blocking approach that works as follows;

A blocking key K is determined for each of n entities. Generally the concatenated prefixes of a few attributes form the blocking key. Afterwards the entities are sorted with the aid of this blocking key. A window of a fixed size w is then forward over the sorted records & in each step all entities within the window, i.e., entities inside a distance of w−1, are when put next. Above figure shows a SNM example execution for a window size of w = 3. This is the time consuming process.

C. Incremental Adaptive SNM

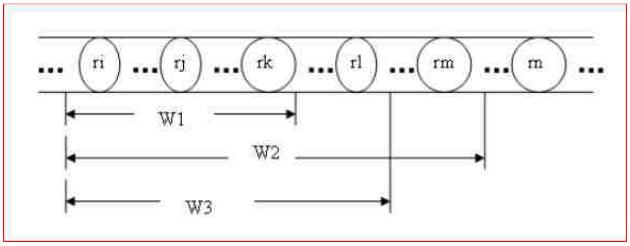

Fig.2: Incremental Adaptive SNM

The fundamental thought is to measure whether records in a small neighborhood are close or sparse and if there are rooms to develop/shrink within the window, and then the window size is extended or decreased dynamically. In order to measure the record distribution within a window, it appears as if we need to measure the distances between all of the records within the window. If the distance between the primary and final record satisfies dist(r1,rw1), the place φ is the distance threshold. This distance indicates that files within the present window are virtually every other, so there's still room to enlarge the window size to find more abilities duplicate records. In any other case the window must be retrenched.

III. FRAMEWORK

A. Duplicate Detection Architecture

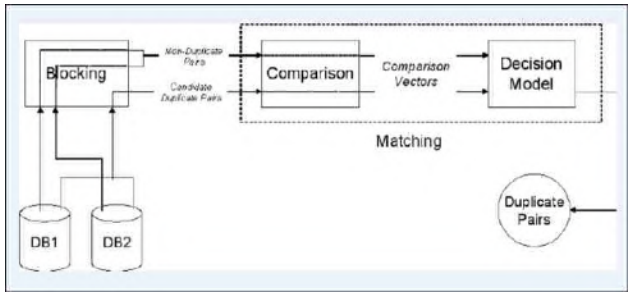

Fig.3: Duplicate Detection System

For instance, if we take an online shopping database, in that numbers of catalogues are there and number of employees is enter the data into the database. So, there is possible to enter the same data number of times. That is referred as duplicate data. If this duplicate data is increased in the database then there is no space for other information means here reduces the storage space of the database. This is the major problem of duplicate data. To overcome this problem, there are various approaches but those are not efficient as well as they are time consuming approaches. In fig3, first the complete data has to be collected from databases. After that, our system need to select pairs of data and compare those pairs. Which pairs are duplicates those duplicates are clustered into a group. Like this system can detect and remove the duplicate data. The main objective of this paper is to detect duplicate data and count the duplicates in the large datasets within the less time. For that in this paper, we propose two new methods to detect the duplicate data as well as count the duplicates in the complete dataset as a parallel. Those two algorithms are;

1. Progressive Sorted Neighborhood Method (PSNM)
2. Progressive Blocking (PB)

And these two are generalized by the existing sorted neighborhood method. In existing method we got the good quality duplicate data but it is very time consuming.

https://dx.doi.org/10.22161/ijaers/3.11.37 *ISSN: 2349-6495(P) | 2456-1908(O)*

Hence, this paper introduce the two progressive and parallel methods. These two are detect the duplicates within in the milliseconds.

B. Sorting Key Selection

In this project we are sorting the dataset by using the magpie sorting. In these sorting methods, we need to select the sorting key to sort the dataset through that key. Importance of this sorting key is, we are mostly applying these two algorithms on the large datasets means those are in thousands and lakh of records are stored in the dataset. But, sometimes user needs deduplication and detect the duplicate count on only particular data. This type of situations, we need a sorting. Without sorting key it is difficult to sort the data from dataset.

For selecting the sorting we propose an Attribute Concurrency method. Through this method we can select the best key for sorting. An attribute concurrency method works based on the multi-pass execution method. This multi-pass method executes the multiple keys in each pass. Attribute Concurrency method we apply to the progressive sorted neighborhood method as well as progressive blocking.

C. Progressive Sorted Neighborhood Method (PSNM)

The algorithm takes five input parameters: D is a reference to the data, which has not been loaded from disk yet. The sorting key K defines the attribute or attributes combination that should be used in the sorting step. W specifies the maximum window size, which corresponds to the window size of the traditional sorted neighborhood method. When using early termination, this parameter can be set to an optimistically high default value. Parameter I defines the enlargement interval for the progressive iterations. For now, assume it has the default value 1. The last parameter N specifies the number of records in the dataset. This number can be gleaned in the sorting step, but we list it as a parameter for presentation purposes. Progressive Sorted Neighborhood Require: dataset reference D, sorting key K, window size W, enlargement interval size I, number of records N

Step 1: procedure PSNM(D, K, W, I, N)
Step 2: pSize← calcPartitionSize(D)
Step 3: pNum←[N/pSize-W + 1)]
Step 4: array order size N as Integer
Step 5: array recs size pSize as Record
Step 6: order ←sortProgressive(D, K, I, pSize, pNum)
Step 7: for currentI← 2 to[W/I]do
Step 8: for currentP ←1 to pNum do
Step 9: recs← loadPartition(D, currentP)
Step 10: for dist belongs to range(currentI, I, W) do
Step 11: for i ←0 to |recs|_ dist do
Step 12: pair←<recs[i], recs[i + dist]>
Step 13: if compare(pair) then
Step 14: emit(pair)
Step 15: lookAhead(pair)

D.Progressive Blocking

The algorithm accepts five input parameters: The dataset reference D specifies the dataset to be cleaned and the key attribute or key attribute combination K defines the sorting. The parameter R limits the maximum block range, which is the maximum rank-distance of two blocks in a block pair, and S specifies the size of the blocks. Finally, N is the size of the input dataset.

Progressive Blocking Require: dataset reference D, key attribute K, maximum block range R, block size S and record number N.

Step 1: procedure PB(D, K, R, S, N)
Step 2: pSize ← calcPartitionSize(D)
Step 3: bPerP ← [pSize/S]
Step 4: bNum ← [N/S]
Step 5: pNum ← [bNum/bPerP]
Step 6: array order size N as Integer
Step 7: array blocks size bPerP as <Integer; Record[]>
Step 8: priority queue bPairs as <Integer; Integer; Integer>
Step 9: bPairs←{<1,1,->, . . . ,<bNum, bNum,->}
Step 10:order ←sortProgressive(D, K, S, bPerP, bPairs)
Step 11: for i ←0 to pNum - 1 do
Step 12: pBPs ← get(bPairs, i . bPerP, (i+1) . bPerP)
Step 13: blocks ← loadBlocks(pBPs, S, order)
Step 14: compare(blocks, pBPs, order)
Step 15: while bPairs is not empty do
Step 16: pBPs← {}
Step 17: bestBPs← takeBest([bPerP/4], bPairs, R)
Step 18: for bestBP € bestBPs do
Step 19: if bestBP[1] − bestBP[0] < R then
Step 20: pBPs← pBPs U extend(bestBP)
Step 21: blocks ←loadBlocks(pBPs, S, order)
Step 22: compare(blocks, pBPs, order)
Step 23: bPairs ←bPairs U pBPs
Step 24: procedure compare(blocks, pBPs, order)
Step 25: for pBP € pBPs do
Step 26: <dPairs,cNum> comp(pBP, blocks, order)
Step 27: emit(dPairs)
Step 28: pBP[2] ←|dPairs|/ cNum

E.Parallel Sorted Neighborhood Method

In particular, introduced a two phase parallel SNM, which executes a traditional SNM on balanced, overlapping partitions. Here, we can instead use our PSNM to progressively find duplicates in parallel. By using this method duplicate detection to deliver results even faster compare to progressive sorted neighborhood method and progressive blocking.

F. Magpie Sorting:

The sorting of records may be a block preprocessing step that we are able to already use to (progressively) execute

https://dx.doi.org/10.22161/ijaers/3.11.37 *ISSN: 2349-6495(P) | 2456-1908(O)*

some initial comparisons. Magpie Sort may be a naive algorithm that works the same as Selection Sort. The name of this algorithmic rule is impressed by the larcenous bird that collects beautiful things whereas only being able to hold a few of them directly. Magpie Sort repeatedly iterates overall records to search out the presently top-x smallest ones. Thereby, it inserts each record into a sorted buffer of length x. whether the buffer is full; every new inserted record displaces the biggest record from the list. Each iteration the final order are often supplemented by following top x records from the buffer. A record that has been emitted once won't be emitted once more. In fact, Magpie Sort integrates the complete first progressive iteration of PSNM. Overall, this sorting method generates only a small overhead, as a result of the algorithmic rule needs to repeat over the complete dataset anyway whenever a partition has to be read from disk.

G. Attribute Concurrency Method:

The best key for locating the duplicate is usually hard to identify. Selecting good keys can increase the progressiveness. Multi-pass execution will be applied for progressive SNM. Key separation isn't required in PB algorithmic rule. Here all the records are taken and checked as a parallel processes so as to reduce average execution time. The records are kept in multiple resources when splitting. The intermediate duplication results are intimated instantly when found in any resources and came back to the most application. Therefore the time consumption is reduced. Resource consumption is same as existing system however the information is kept in multiple RESOURCE memories.

IV. EXPERIMENTAL RESULTS

In this system consider some datasets (DBLP,CD DATASETS) which is in different formats like xml ,csv etc. To detect the duplicates and duplicate count in the dataset, first select the sorting key and then give the 'title', 'author', and some attributes in the dataset are the sorting keys. After that choose window size or block size. Finally implements PSNM, PB& PARALLEL SNM.

The below screen shows that the duplicate count and duplicate data in the dataset;

The below screen shows that the normal execution or processing time of the algorithms;

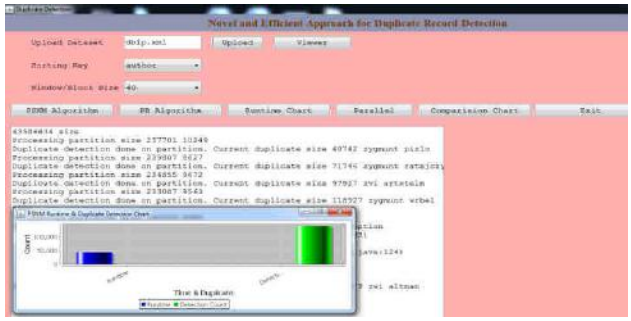

The below screens shows that, the comparison between the normal processing time and parallel processing time of the algorithms;

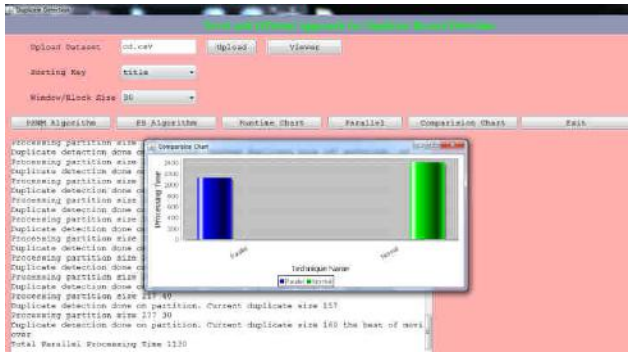

The below graph shows that,the no of duplicates in CD dataset the keyword "Title", It shows the no of duplicates and processing time with in a window in all the methods.

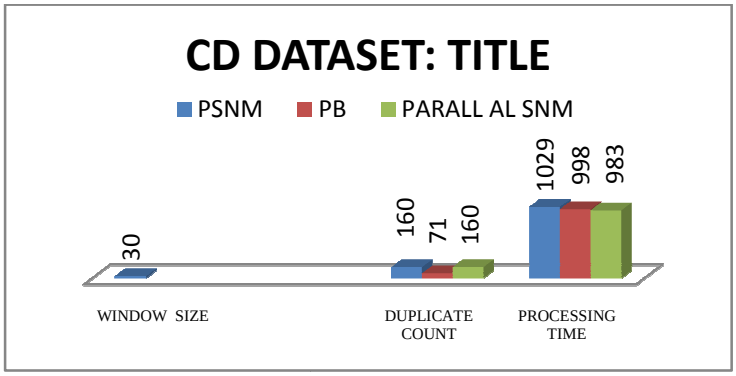

Three approaches will give the results varying the window sizes will get the duplicate count and processing time as shown below,

https://dx.doi.org/10.22161/ijaers/3.11.37 *ISSN: 2349-6495(P) | 2456-1908(O)*

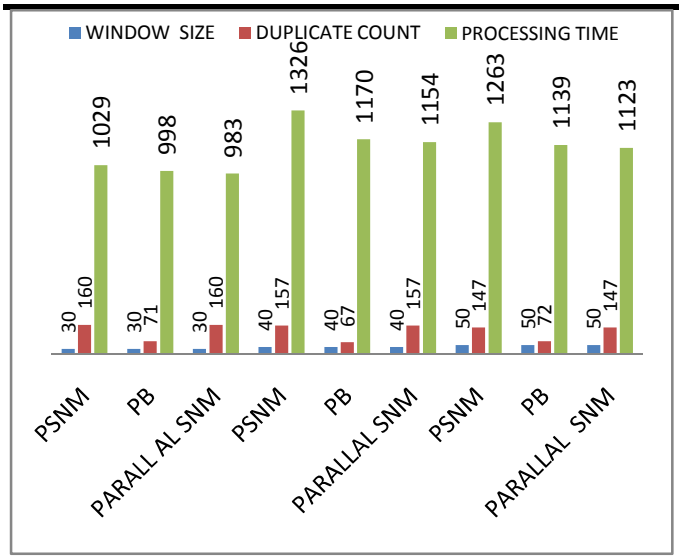

From above results it can prove that proposed algorithms are time efficient and scalable approaches. Parallel SNM will take less time to compare with PSNM and PB.

V. CONCLUSION

In this paper, introduced two methods named, Progressive SNM, progressive blocking and parallel SNM which improve the efficiency of duplicate detection. By this efficiency that time will be reduced for duplicate detection. These two algorithms are generalized by the traditional sorted neighborhood method only. Using these two algorithms reduced the processing time of duplicate detection as well as increased performance. Parallel SNM achieves the better processing time and duplicate count accurately compare to PSNM and PB. In future work, implementing of all the time factors and methods to improve the performance in parallel approach.

REFERENCES

[1] Papenbrock T., Heise A. and Naumann F. (2015), „Progressive duplicate detection", Proc. IEEE Trans. Know. Data Eng., vol. 27, No. 5, pp. 1316-1329.

[2] Whang S. E., Marmaros D., Molina H. (2012),„Pay-as-you-go entity resoln", IEEE Trans. Know. Data Eng., vol. No 25.5, pp. 1111–1124.

[3] Draisbach U, Naumann F, Szott S, Wonneberg O. (2012),„Adaptive windows for duplicate detection", Proc. IEEE 28th Int. Conf. Data Eng., pp. 1073-1083.

[4] Draisbach U. and Naumann F. (2011), „A generalization of blocking and windowingalgorithms for duplicate detection",Proc. Int. Conf. Data Knowl. Eng., pp. 18-24.

[5] Hassanzadeh O., Chiang F., Lee H.C., Miller R. J. (2009), „Framework for Evaluating Clustering Algorithms in Duplicate Detection",Proc. Very Large Databases Endowment, Vol. 2, pp.1282-1293.

[6] A. K. Elmagarmid, P. G. Ipeirotis, and V. S. Verykios, "Duplicate record detection: A survey," IEEE Trans. Knowl. Data Eng., vol. 19, no. 1, pp. 1–16, Jan. 2007.

[7] H. B. Newcombe and J. M. Kennedy, "Record linkage: Making maximum use of the discriminating power of identifying information," Commun. ACM, vol. 5, no. 11, pp. 563–566, 1962.

[8] M. A. Hernandez and S. J. Stolfo, "Real-world data is dirty: Data cleansing and the merge/purge problem," Data Mining Knowl. Discovery, vol. 2, no. 1, pp. 9–37, 1998.

[9] O. Benjelloun, H. Garcia-Molina, D. Menestrina, Q. Su, S. E. Whang, and J. Widom, ―Swoosh: a generic approach to entity resolution,‖ VLDB Journal.

[10] R. Baxter, P. Christen, and T. Churches, ―A comparison of fast blocking methods for record linkage,‖ in Proceedings of the ACM SIGKDD Workshop on Data Cleaning, Record Linkage, and Object Consolidation, 2003, pp. 25–27.

International Journal of Advanced Engineering Research and Science (IJAERS) [Vol-3, Issue-11, Nov- 2016]
https://dx.doi.org/10.22161/ijaers/3.11.38 *ISSN: 2349-6495(P) | 2456-1908(O)*

An Estimation of Discomfort Indices in Qena City, Upper Egypt

Abdel Galeil A Hassan[1], Kassem Kh. O[2]

Physics Department, Faculty of Science, South Valley University, P. O. 83523, Qena, Egypt

Abstract*—Wind chill index WCI and temperature humidity index THI, are calculated in Qena during the period 2001-2014 using hourly data of temperature, relative humidity and wind speed collected in weather research station located in south valley university at Qena. Results of WCI indicate that the winter months are cool, while, summer months are hot. The middle of spring and autumn is pleasant. Results of THI indicate that Winter, spring and autumn months are comfortable or partially comfortable or quite comfortable. While, summer months are not comfortable due to hot and humid weather. Annual mean values of WCI indicate that Qena weather was pleasant during the period from 2001 to 2014, except the two years 2003 and 2012 was worm. The mean value of the total period indicates that the atmosphere of Qena is pleasant. the THI mean value of the study period as well as the average yearly values are located in the category 100%are quite comfortable.*

***Keywords*— Discomfort index, Wind chill index, Hathor, Dendara, Qena.**

I. INTRODUCTION

Heat stress is becoming increasingly appreciated because of its influence on living matter . Heat stress is caused by a combination of environmental factors (temperature, relative humidity, solar radiation, air movement, and precipitation). Many indices combining different environmental factors to represent the level of heat stress. These indices have been proposed by several studies [1, 2, 3 and 4]. However, their use is limited by poor availability of data.

A temperature humidity index (THI) is a single value representing the combined effects of air temperature and humidity associated with the level of thermal stress . it was originally called the discomfort index. [5]. This index was empirically obtained by experimentally subjecting a sample of people to varying temperature and humidity and polling them as to the discomfort they felt. The results were tabulated as numbers a legend indicating the degree of discomfort that a majority of people would feel in various ranges of values [6]

THI has been developed as a weather safety index to monitor and reduce heat stress related losses. Different animal species and human have different sensitivities to ambient temperature and the amount of moisture in the air. The main factor in human discomfort is the thermal component of environmental conditions and was calculated by many indices taking into consideration air temperature, relative humidity and wind speed [7,8, 9, 10, and 11].

The values of the discomfort index DI have been recorded in the past through limited studies. In Thessaloniki, Greece, [12] found that most people uncomfortable when DI was greater than 24. In Mexico, United States, [13] found that most people experienced the sense of discomfort when DI reached 24.

Qena city (26^{o} $16^{\backslash}$ N, 32^{o} $75^{\backslash}$ E) is the capital of the province (population - 2,000,000) located about 60 km north of Luxor. It is most famous for its proximity to the archeological site of Dendera. Dendera is few kilometers to the west of Qena city. The main attraction of Dendera is the temple dedicated to Hathor goddess of love, music and dancing. Visitors to Luxor may visit the famous Temple of Hathor at Dendera. In a taxi, the trip takes about 1 hour from Luxor. In addition, Qena city owes its modern prosperity to the opening of the Wadi Qena towards the Red Sea, which is a major traffic route between Upper Egypt and the Red Sea, will assuredly pass through this city. Climate of Qena is very hot, dry in summer and cold in winter [14], [15] , [16]. It rarely rains. Also it receives a large quantity of solar radiation especially in summer. Hopefully we could quantify discomfort indices, where no studies have been conducted before to estimate these indices in Qena city. This study is an attempt to start bridging this gap in Qena, it is very important and benefit study for inhabitants and tourists as well.

Aim of the present work is to quantify Wind Chill Index WCI and Temperature Humidity Index THI in Qena over the period (2001 – 2014).

II. MATERIALS AND METHODOLOGY

The hourly data of temperature, relative humidity and wind speed for fourteen years used in this investigation were procured from Qena Meteorological Agency station.

https://dx.doi.org/10.22161/ijaers/3.11.38 *ISSN: 2349-6495(P) | 2456-1908(O)*

Wind Chill Index, (WCI), the cooling sensation caused by the combined effect of temperature and wind, was computed using the chill index of Sipple and Passel (1945) [17] given by,

$$WCI = \left(10\sqrt{V} + 10.45 - V\right)\left(33 - T_a\right) \quad (1)$$

Where V is the wind speed in meters per second and T_a is the atmospheric temperature in C^0

The Temperature-Humidity Index (THI_1) was calculated for each hour using the formula developed by Kibler (1964) [18],

$$THI_1 = 1.8 \times T_a - \left(1 - RH\right)\left(T_a - 14.3\right) + 32 \quad (2)$$

Where Ta = average ambient temperature in C^0
RH = average relative humidity as a fraction of the unit.

The Temperature-Humidity Index (THI_2) was also calculated for each hour using formula developed by NOAA (1979) [19] as follows,

$$THI_2 = (1.8 \times Ta + 32) - (0.55 - 0.55 \times RH) \times [(1.8 \times Ta + 32) - 58] \quad (3)$$

Where Ta = average ambient temperature in C^0.
RH = average relative humidity.

Significance of both of Wind-Chill Index (WCI) and temperature humidity index THI are shown in Table (1) and Table (2) [5, 20]

Table.1: Significance of Wind –Chill index WCI

WCI value	Human/animal and plant feeling
< 50	hot
50 – 100	worm
101 – 200	pleasant
201 – 400	cool
401 – 600	very cool
601 – 800	cold
801-1000	very cold
> 1000	bitter cold

Table .2: Significance of temperature humidity index THI

THI value	Human/animal and plant feeling
> 80	100% are not comfortable.
75 – 80	50% are not comfortable due to hot and humid weather.
65 – 75	100%are quite comfortable.
60 – 65	50% are partially comfortable.
< 60	Almost 100% are comfortable due to cold and dry weather.

III. RESULTS AND DISCUSSION

3.1 Monthly variation of wind chill index WCI

During all the same months of the study period, the WCI is computed using equation (1). The number of days and its percentage for each Human/animal and plant feeling category of WCI are considered and is shown in Table (3). From this Table, it is obvious that: almost all summer season (June, July and August) is characterized by hot days with day's percentage ranges from 95% to 99%, while, 73% - 85% of winter (Dec., Jan., and Feb.) days are cool. Spring season is characterized by, 50% cool in March, 40% pleasant in April and 64% hot in May. In Autumn season, 68% of September days are hot, 46% of October days are pleasant, and 52% of Nov. are cool. Very cold and bitter cold categories are not recorded in Qena city. Cold days are ranged from 2% to 4% during winter season.

Fig. (1) and Table (4) represent monthly variation of average, maximum and minimum of WCI in Qena during the period 2001-2014. We can notice that the categories cold, very cold and bitter cold are not recorded during all the period of study. The cool category is recorded during all winter months as well as two months, March and Nov. Pleasant category is recorded during two months, April and October. These two months represent mid spring and mid autumn, respectively. Warm category is not recorded, while the hot category is recorded during five months including summer months, (Jun., Jul., and August) and other two months (May and Sept). May represents the end of spring and Sept. represents the beginning of autumn.

https://dx.doi.org/10.22161/ijaers/3.11.38 *ISSN: 2349-6495(P) | 2456-1908(O)*

Table .3: Monthly variation of wind chill index WCI for different human/animal and plant feeling categories in Qena during the period 2001-2014.

Categories	Jan	Feb	Mar	Apr	May	Jun	Jul	Aug	Sept	Oct.	Nov.	Dec.	Feeling
<50	0	0	12	83	277	369	431	428	287	76	2	0	hot
	0%	0%	3%	20%	64%	95%	99%	99%	68%	18%	0%	0%	
50-100	1	4	21	88	84	20	2	5	94	141	11	2	Warm
	0%	1%	5%	21%	19%	5%	0%	1%	22%	32%	3%	0%	
101-200	13	52	161	166	70	1	1	1	31	198	185	33	Pleasant
	3%	13%	37%	40%	16%	0%	0%	0%	7%	46%	44%	8%	
201-400	362	287	219	83	3	0	0	0	8	18	219	370	Cool
	83%	73%	50%	20%	1%	0%	0%	0%	2%	4%	52%	85%	
401-600	54	47	20	0	0	0	0	0	0	1	3	27	very cool
	12%	12%	5%	0%	0%	0%	0%	0%	0%	0%	1%	6%	
601-800	3	4	0	0	0	0	0	0	0	0	0	2	Cold
	1%	1%	0%	0%	0%	0%	0%	0%	0%	0%	0%	0%	
801-1000	1	1	1	0	0	0	0	0	0	0	0	0	very cold
	0%	0%	0%	0%	0%	0%	0%	0%	0%	0%	0%	0%	
>1000	0	0	0	0	0	0	0	0	0	0	0	0	bitter cold
	0%	0%	0%	0%	0%	0%	0%	0%	0%	0%	0%	0%	
Total No	434	395	434	420	434	420	434	434	420	434	420	434	

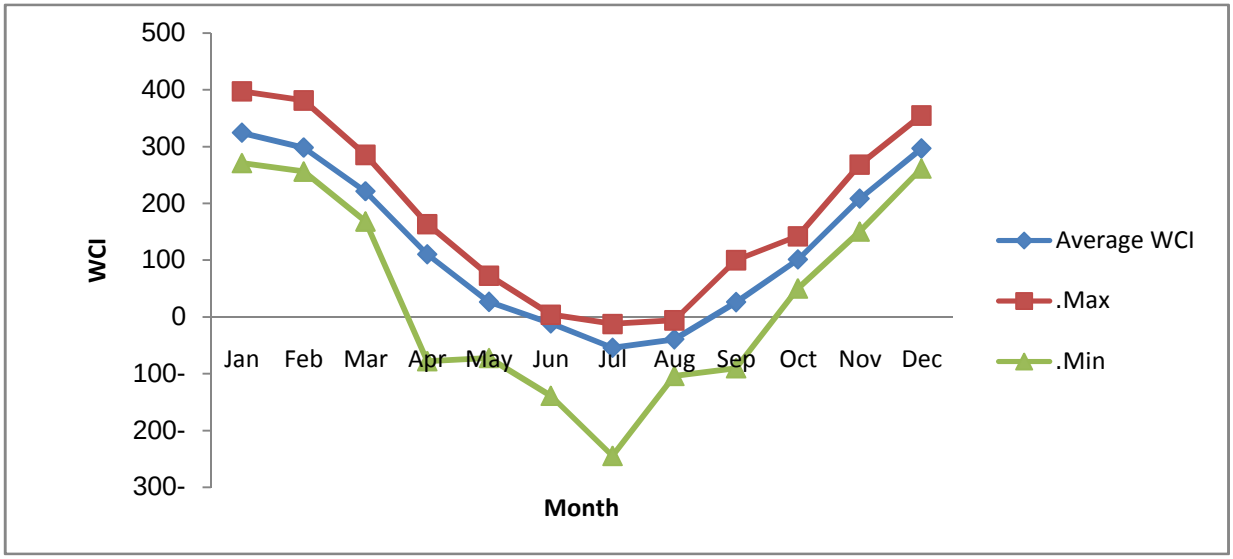

Fig.1: Monthly average, maximum and minimum of WCI in Qena during the period 2001-2014.

3.2 Monthly variation of temperature humidity index THI

The calculations of the Temperature-Humidity Index THI_1 by Kibler method (eq. 2) are considered. The results are tabulated by different THI_1 categories according to Table (2) to represent the THI_1 monthly variations. The corresponding numbers of days and its percentages for each category of THI_1 are shown in Table (5). It is obvious that:

- Summer days for all months are found almost in the category: (*50% are not comfortable due to hot and humid weather)* with percentage ranges from 81% - 88%.
- The days of winter months are mainly located in two categories: (*Almost 100% are comfortable due to cold and dry weather*) and (*50% are partially comfortable*).
- In spring season, the category (*100% are quite comfortable*) is recorded where its percentages is 57% in March, 90% in April and 62% in May.
- Autumn season days are almost found in two categories: (*50% are not comfortable due to hot and humid weather*) and (*100% are quite comfortable*). 73% of total days of Sept is found in the category

https://dx.doi.org/10.22161/ijaers/3.11.38 *ISSN: 2349-6495(P) | 2456-1908(O)*

(*50% are not comfortable due to hot and humid weather*) while, 85% and 58% of total days in Oct. and Nov. are in the category (*100% are quite comfortable*). It is noticed that, as stated before, Sept. weather is partially similar to summer weather, while, Nov. weather is similar to that of winter months. weather is partially similar to summer weather, while, Nov. weather is similar to that of winter months.

Table (6) shows THI_2 calculation by the formula by NOOA (1979). It could be seen that the days percentages for the different THI_2 categories are almost the same as found by THI_1 calculated by Kibler's formula, where, it differs only by 1-2% in some months. So, one could conveniently represent the other. This result is found also in Nigeria (16)..

Fig. (2) and Table (7) represent the monthly variations of average, maximum and minimum of $THI_{1,2}$ in Qena during the period 2001-2014. It is clear that the figure is reciprocal form of the Fig. (1) and that the feeling conditions during different months in Table (6) confirms that in Table (4). Where, winter , spring and autumn months are comfortable or partially comfortable or quite comfortable. While, summer months are not comfortable due to hot and humid weather.

Table.4: Monthly average, maximum and minimum of WCI in Qena during the period 2001-2014.

Month	Average WCI	Max.	Min.	Feeling
Jan	**324**	**397**	**271**	**cool**
Feb	**298**	**381**	**256**	**cool**
Mar	**221**	**285**	**168**	**cool**
Apr	**110**	**164**	**-78**	**pleasant**
May	**26**	**73**	**-72**	**hot**
Jun	**-12**	**4**	**-139**	**hot**
Jul	**-54**	**-12**	**-245**	**hot**
Aug	**-39**	**-6**	**-104**	**hot**
Sep	**26**	**100**	**-90**	**hot**
Oct	**101**	**142**	**50**	**pleasant**
Nov	**208**	**268**	**150**	**cool**
Dec	**297**	**355**	**261**	**cool**

Table.5: Monthly variation of temperature-humidity index (Kibler) different categories in Qena during the period 2001-2014

Categories	Jan	Feb	Mar	Apr	May	Jun	Jul	Aug	Seb.	Oct.	Nov.	Dec.	Feeling
>80	**0**	**0**	**0**	**3**	**6**	**14**	**63**	**49**	**4**	**4**	**0**	**0**	**100% are not comfortable**
	0%	**0%**	**0%**	**1%**	**1%**	**4%**	**15%**	**11%**	**1%**	**1%**	**0%**	**0%**	
75-80	**0**	**1**	**5**	**31**	**158**	**339**	**371**	**384**	**305**	**59**	**4**	**1**	**50% are not comfortable**
	0%	**0%**	**1%**	**7%**	**36%**	**81%**	**85%**	**88%**	**73%**	**14%**	**1%**	**0%**	
65-75	**10**	**70**	**249**	**377**	**270**	**37**	**0**	**1**	**103**	**371**	**242**	**41**	**100%are quite comfortable**
	2%	**18%**	**57%**	**90%**	**62%**	**9%**	**0%**	**0%**	**25%**	**85%**	**58%**	**9%**	
60-65	**71**	**20**	**168**	**9**	**0**	**0**	**0**	**0**	**1**	**0**	**165**	**177**	**50% are partially comfortable.**
	16%	**52%4**	**39%**	**2%**	**0%**	**0%**	**0%**	**0%**	**0%**	**0%**	**39%**	**41%**	
<60	**353**	**120**	**12**	**0**	**0**	**0**	**0**	**0**	**7**	**0**	**9**	**215**	**Almost 100% are comfortable**
	81%	**30%**	**3%**	**0%**	**0%**	**0%**	**0%**	**0%**	**2%**	**0%**	**2%**	**50%**	
Total No	**434**	**395**	**434**	**420**	**434**	**390**	**434**	**434**	**420**	**434**	**420**	**434**	

https://dx.doi.org/10.22161/ijaers/3.11.38 ISSN: 2349-6495(P) | 2456-1908(O)

Table.6: Monthly variation of temperature-humidity index (NOOA) for different categories in Qena during the period 2001-2014

Categories	Jan	Feb	Mar	Apr	May	Jun	Jul	Aug	Sept.	Oct.	Nov.	Dec.	Feeling
>80	0 0%	00 %	0 0%	3 1%	8 2%	21 5%	74 17%	58 13%	6 1%	4 1%	0 0%	0 0%	100% are not comfortable
75-80	0 0%	1 0%	6 0%	35 8%	171 39%	338 87%	360 83%	375 86%	316 75%	69 16%	4 1%	1 0%	50% are not comfortable
65-75	11 3%	71 18%	255 59%	374 89%	255 59%	31 8%	0 0%	1 0%	90 21%	361 83%	245 58%	42 10%	100% are quite comfortable
60-65	74 17%	211 53%	161 37%	8 2%	0 0%	0 0%	0 0%	0 0%	1 0%	0 0%	162 39%	182 42%	50% are partially comfortable.
<60	349 80%	112 28%	12 3%	0 0%	0 0%	0 0%	0 0%	0 0%	7 2%	0 0%	9 2%	209 48%	Almost 100% are comfortable
Total No.	434	395	434	420	434	390	434	434	420	434	420	434	

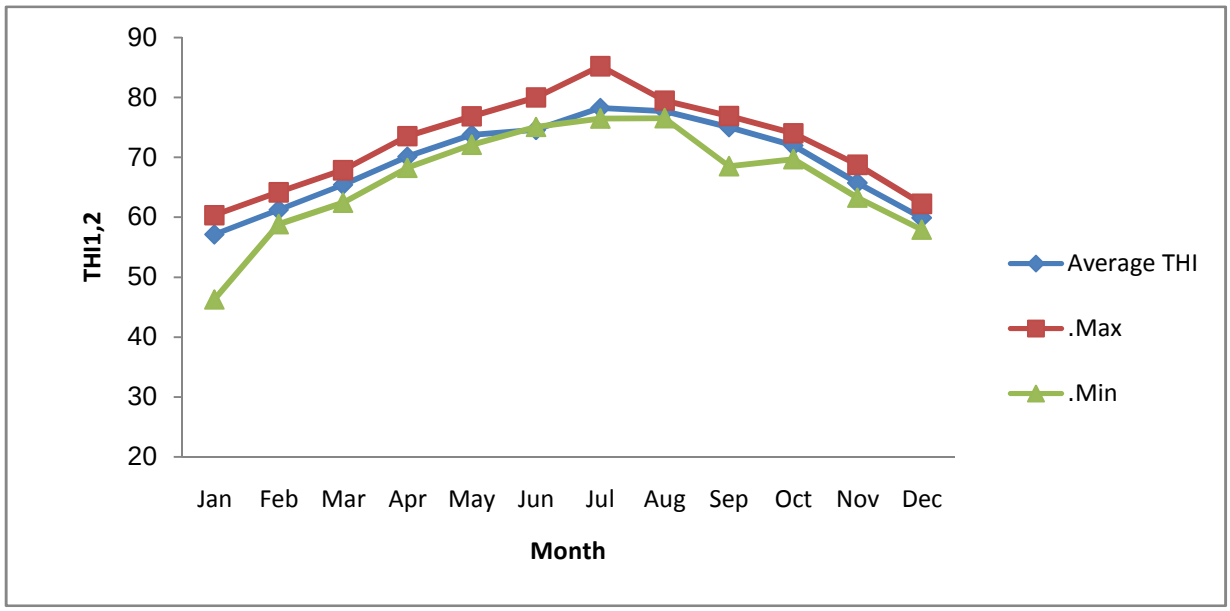

Fig.2: monthly average, maximum and minimum of $THI_{1,2}$ in Qena during the period 2001-2014.

Table.7: Monthly average, maximum and minimum of $THI_{1,2}$ in Qena during the period 2001-2014.

Month	Average THI	Max.	Min.	Feeling
Jan	57	60	46	Almost 100% are comfortable
Feb	61	64	59	50% are partially comfortable.
Mar	65	68	62	50% are partially comfortable.
Apr	70	74	68	100% are quite comfortable
May	74	77	72	100% are quite comfortable
Jun	75	80	75	50% are not comfortable due to hot and humid weather.

https://dx.doi.org/10.22161/ijaers/3.11.38 *ISSN: 2349-6495(P) | 2456-1908(O)*

Jul	**78**	**85**	**76**	**50% are not comfortable due to hot and humid weather.**
Aug	**78**	**79**	**77**	**50% are not comfortable due to hot and humid weather.**
Sep	**75**	**77**	**69**	**50% are not comfortable due to hot and humid weather.**
Oct	**72**	**74**	**70**	**100% are quite comfortable**
Nov	**66**	**69**	**63**	**100% are quite comfortable**
Dec	**60**	**62**	**58**	**50% are partially comfortable.**

3.3 Annual variations of $THI_{1,2}$ and WCI

Fig. (3) shows annual variation sof THI1,2 and WCI during the period of study. It could be seen that there is no remarkable variation in the annual values of THI1,2 . The mean value of THI1,2 ,during the study period, is 69 with standard deviation of 0.61. These value is located in the range of (65 – 75) which indicates that (100% are quite comfortable).

In the same time, obvious fluctuation is found in WCI with mean value of 123 and standard deviation 20. This value is in the category Pleasant. It is found that, during the fourteen years, from 2001 to 2014, there are seven years have mean values less than the total mean, these years are 2001, 2002, 2003, 2010, 2012, 2013 and 2014. While the rest seven years have mean values more than the total mean value.

Annual mean values of WCI, during the fourteen years from 2001 to 2014, indicate that Qena weather was pleasant except the two years 2003 and 2012 were worm. The mean value of the total period,123, indicates that the atmosphere of Qena is pleasant. This result is confirmed by THI1,2 annual mean values. Where, the THI1,2 mean value of the study period as well as the average yearly values are located in the category 100% are quite comfortable.

IV. CONCLUSION

In this study, both Temperature - Humidity Index THI and Wind Chill Index WCI are calculated in Qena during the period 2001-2014. Monthly and annual variations have been discussed. Results of WCI indicate that winter months are cool, while, summer months are hot. The middle of spring and autumn is pleasant. THI is calculated by Kibler formula and NOOA formula, The two methods lead to the same results. Results of monthly average variation of THI indicate that winter , spring and autumn months are comfortable or partially comfortable or quite comfortable. While, summer months are not comfortable due to hot and humid weather. Annual mean values of WCI indicate that Qena weather during the period of study was pleasant except the two years 2003 and 2012 was worm. The mean value of the total period indicates that the atmosphere of Qena is pleasant. the THI mean value of the study period as well as the average yearly values are located in the category 100%are quite comfortable. The monthly variation of WCI is a mirror image of that of THI. This study encourages tourists to visit the temple of Hathor at Dendara, specially during winter , spring and autumn seasons.

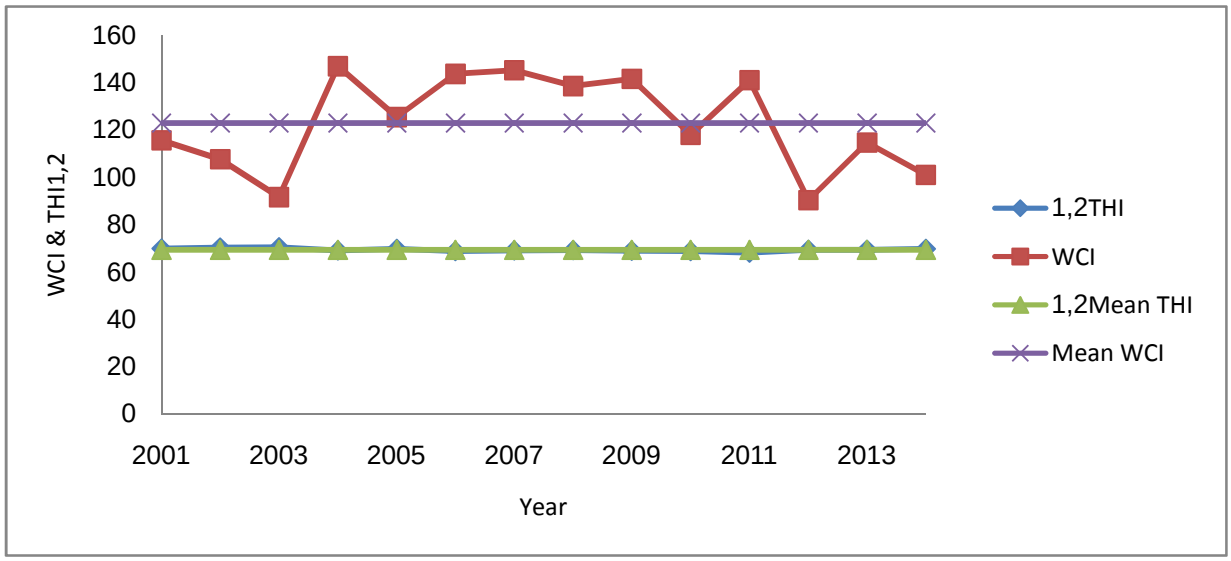

Fig.3: Annual variation of $THI_{1,2}$ and WCI in Qena during the period 2001-2014.

https://dx.doi.org/10.22161/ijaers/3.11.38 *ISSN: 2349-6495(P) | 2456-1908(O)*

REFERENCES

[1] J. Bohmanova,I. Misztal, and J. B. Cole (2007) "Temperature-Humidity Indices as Indicators of Milk Production Losses due to Heat Stress". Dairy Sci. 90:1947–1956

[2] A. Marc, E. Konstantinos, D.Konstantinos, and M. John-Alexander (2010) "Applying Thermal Comfort Indices to Investigate Aspects of the Climate in Greece". International Review of Chemical Engineering, **2**, 204-209

[3] S. Robaa, (2011)" Effect of Urbanization and Industrialization Processes on Outdoor Thermal Human Comfort in Egypt". Atmospheric and Climate Sciences, **1**, 100-112.

[4] S. Robaa (2003) "Thermal Human Comfort in Egypt". International Journal of Meteorology, 283, 359-371.

[5] A.A Musari, O.A. Sojobi, O.A Abatan and A.I Egunjobi. (2015)" An estimation of thermal comfort index in North-central region of Nigeria" IOSR Journal of Applied Physics Volume 7, Issue 1 Ver. I (Jan.-Feb. 2015), PP 60-66

[6] F. E. Bair, and J. A. Ruffner, Eds., (1977)" The Weather Almanac 2d ed". Avon Books, 728 pp.

[7] E.C. Thom, (1959)" The discomfort index. Weather wise"' 12: 57–60.

[8] R. G. Steadman,. (1971)" Indices of wind chill of clothed persons" J. Appl. Meteorol. 10:674–683.

[9] ISO. (1983). ISO 7730: Moderate thermal environments- Determination of the PVI and PPD indices and specification of the conditions of thermal comfort. International Organization of Standardization, Geneva.

[10] A. Matzarakis, and H. Mayer (1996)" Another kind of environmental stress: thermal stress. NEWSLETTERS No. 18, 7–10. WHO Collaborating Centre for Air Quality Management and Air Pollution Control.

[11] S.Becker, O. Potchter, and Y.Yaakov (2003). "Calculated and observed human thermal sensation in an extremely hot and dry climate" Energy and Buildings, 35, 747–756.

[12] V.E. Angouridakis, and T.J. Makrogiannis (1982)"The discomfort index in THESSALONIKI, GREECE" International Journal of biometeorology .V26, Issue 1 pp 53-59

[13] E. Jauregui, and C. Soto, (1963)" Wet-bulb temperature and discomfort index areal distribution in Mexico" International Journal of Biometeorology, Volume 11, Issue 1, pp 21-28.

[14] Kh. O. Kassem.(2014) "Long Range Transport Contribution to PM10 Concentrations in a Subtropical City (Qena/Egypt)" World Environment 2014, 4(1): 1-13. DOI: 10.5923/j.env.20140401.01

[15] A. I. El-Tantawy, (1969). "On the cyclogenesis and structure of spring desert depressions in subtropical Africa. Egyptian Meteorological Authority (EMA), Meteorological " Research Bulletin, vol. 69, pp. 68–107.

[16] M. El-Nouby Adam (2013)" Suspended Particulates Concentration (PM10) under Unstable Atmospheric Conditions over Subtropical Urban Area (Qena, Egypt)" Advances in Meteorology. http://dx.doi.org/10.1155/2013/457181

[17] P. Sipple , and .Passel, (1945)" Measurement of dry atmospheric Cooling In subfreezing temperatures" Proc. Amer. Phil. Soc., 89: 177-199.

[18] H. H. Kibler (1964)" Thermal Effects Of Various Temperature- Humidity Combinations On Holstein Cattle As Measured By Eight Physiological Responses. Missouri Agricultural Experiment, Exp. Stn Res. Bull. 862, Mt Vernon. Environmental Physiology and Shelter Engineering, LXVII

[19] NOAA (1976)" Livestock hot weather stress. Kansas City" M.O Open Man Lett C- 31-76.

[20] M. O. Adeniyi (2009)" Determination of Heat Stress Index In The Tropical Urban Area Of Ibadan, Southwest Nigeria" International Journal Of Natural and Applied Sciences, 5(3): 235-243.